Proceedings

RF expo EAST

October 29-31, 1991
Orlando Resort
Orlando, Florida

Sponsored by
RF design
Magazine

Proceedings

RF expo
EAST

October 29-31, 1991
Orlando Resort
Orlando, Florida

RF design
6300 S. Syracuse Way
Suite 650
Englewood, Colorado 80111

TABLE OF CONTENTS

The papers contained in these Proceedings represent the views of the authors and/or their employers, and have been presented by them as original works. While an attempt has been made to assure accuracy, Cardiff Publishing Company and *RF Design* will not be responsible for any copyright, trademark or patent infringement that may be contained in these papers.

State-of-the-Art Nonlinear CAD for Microwave/RF Circuit Design

Jason Gerber, Leong F. Mah, Chao-Ren Chang,
Murat Eron* and Anthony Kwan

Compact Software, Inc.
483 McLean Blvd. & 18th Ave.
Paterson, NJ 07504

*M/A-Com Inc.
GMIC Operations
Semiconductor Division
80 Cambridge Ave.
Burlington, MA 01903

Introduction

The need for nonlinear CAD in high-frequency circuit design has increased tremendously in the last decade. SPICE, and its derivatives, were virtually the only nonlinear circuit analysis programs commercially available five years ago. Today we also have harmonic balance based programs and SPICE-enhanced mixed mode simulators. These programs are suited for different applications based on the frequency range and whether the circuit is analog, digital or mixed. This paper focuses on the state-or-the-art in the harmonic balance set of simulators, since these simulators perform more efficiently and accurately in high-frequency problems. Some aspects of the Spice-based simulators are discussed as well as other methods for nonlinear circuit analysis.

The goal of nonlinear circuit CAD is straightforward. It is to reduce fabrication and engineering costs by meeting design goals in the first fabrication pass. This will only occur with accurate models of circuit components, efficient simulation of practical-sized circuits, and with designers who understand the limits of both the simulation and fabrication process used. MMIC requires first-pass success to be cost effective and hybrid designs greatly benefit from first-pass success. The designer must understand the limits and configurations of linear and nonlinear models; for example, two microstrip line tees close together may violate the accuracy of the tee model. Spurious coupling effect within an enclosure is another example that the designer must recognize because most circuit simulators cannot predict it. Full EM field simulators can determine these modes, but most are not efficient enough to be used on an interactive design basis.

As systems become more complex, full nonlinear modeling of interaction between sub-systems becomes important. The ability to efficiently handle wide separation of frequency components, from kHz to GHz, within a system was not possible until recently. Multichip MMIC circuits containing sub-systems of amplifiers, mixers, switches and phase shifters can be simulated and optimized together as one system. This development advances circuit simulation to accurate system simulation without the need to make overly restrictive assumptions on the sub-systems.

The topical outline of this paper identifies recent advances in nonlinear harmonic balance CAD which are critical to the usefulness of nonlinear CAD as a design tool. These topics are:

- analytic Jacobian calculation
- sparse Jacobian methods
- nonlinear noise analysis
- statistical analysis
- broadband optimization
- multitone analysis
- oscillator analysis
- pulse and transient analysis
- improvement of analysis convergence
- analysis of circuits with bifurcations

In addition to these topics, some background material is presented to classify the methods of nonlinear analysis and state the harmonic balance problem. All of these topics have been presented previously within the literature, but they are collected here with an emphasis on practical applications rather than mathematics.

Simulation Methods

Two most popular methods that solve nonlinear circuit analysis problems are direct integration, as used in SPICE, and the harmonic balance method. Although both have good points and bad points, neither can be used alone for all problems. Table 1 classifies these methods, along with others, in the domain that the linear and nonlinear elements are calculated. Each of these methods will be discussed briefly.

Pure Time-Domain Methods

The direct integration method (referred here as the SPICE method) solves a set of coupled nonlinear differential equations using brute force integration [1]. Special time step selection and convergence methods are used to improve the robustness of the simulators. This allows SPICE to handle highly nonlinear circuits that are excited by arbitrary waveform sources. SPICE allows transient analysis of a circuit. All other methods presented here are meant for stead-state analysis, although some can handle special-case transient analysis. Oscillator start-up analysis and non-periodic responses (chaotic) can be analyzed effectively in the time-domain.

Attempts to solve for the steady-state solution directly with time-domain methods have been made without much success. The shooting method searches for the set of initial conditions that produce a steady-state response. The circuit equations have to be solved over the fundamental period in order to determine if the initial conditions did indeed produce a steady-state response. At the end of each period, a Newton based optimizer, or some other nonlinear minimizer, is used to determine a new set of initial conditions so the next iteration yields a steady-state response. Much time is used each iteration to compute the single period response so success has only been marginal. Another approach has been to compute the state of the circuit at a number of time instants and extrapolate from these points the set of initial conditions that result in the steady-state response. Again, only marginal success has been met.

There are three main difficulties with time-domain methods that have not been successfully solved. The first is the long analysis time required to compute circuits with long time constants. This occurs when the circuit is high Q, has long transmission lines, or contains frequency components that differ by an order of magnitude or more as in mixers and intermodulation problems. The time required to allow the transients to die out can be on the order of a few fundamental periods to several tens of periods, depending on the Q of the circuit. If two tones are exciting the circuit and the difference between them is small, then the analysis must take place for at least the period of the difference. However, the time step must be small enough to accurately represent the exciting tones, so the number of time steps becomes very large. The long execution times necessary for these types of analysis preclude SPICE based simulators from being used for many RF and microwave circuits.

A second difficulty is that the linear elements must be computed in the time-domain. All elements that exhibit dispersion (such as microstrip transmission lines and discontinuities) are only computable, and measurable, in the frequency-domain. This leads to simplified models for many linear components that could be determined accurately in the frequency-domain. For much RF work, quasi-static approximations can be used to form an equivalent circuit of the element in terms of basic electrical components, but this introduces large, complex networks that slow execution time. Some work has been performed to Fourier transform the frequency-domain response into a type of impulse response and then form the convolution integral to evaluate the time-domain response. This approach is computationally expensive and has not been demonstrated for problems of practical size.

Finally, the third difficulty is more of a post-processing issue rather than basic limitations. Obtaining nonlinear frequency-domain quantities from time-domain simulators has been a difficult task. Responses such as power gain, return loss and efficiency are not readily computed by SPICE programs and therefore require computation by the user. It seems that significant progress could be made in this area, since it does not require complex mathematics, but software vendors have not acted to remedy the problem.

Hybrid Time-Domain/Frequency-Domain Methods

The hybrid methods are classified according to the domain the error function is formed from; that is, if convergence is determined from the errors in the frequency-domain, the method is called harmonic balance [2]; if it is determined from the errors in the time-domain, the method is called sample balance. Harmonic balance programs are commercially available from vendors such as Compact Software [59], Hewlett Packard and EEsof with their respective products Microwave Harmonica, MDS and Libra. Harmonic balance methods will be discussed here, but sample balance has very similar characteristics.

Given the fundamental frequencies of the analysis, a set of harmonically related frequencies can be generated according to a pre-defined harmonic-selection algorithm which is only dependent on the order of desired nonlinearity from the user. Since harmonic balance use the Fourier series to transform between the frequency and time-domains, the infinite summations must be truncated for use on a

computer. For example, if the circuit is excited by a single tone, a user can select the number of harmonics to be included in the analysis. If a two-tone test is performed, the user can select the order of the intermodulation products that will be considered in the analysis, and so on. In harmonic balance, the linear components are computed in the frequency-domain at all harmonically related frequencies within the analysis. This allows the linear network to use the most accurate models of high frequency circuit components available. Dispersive and lossy transmission lines, coupled transmission lines and discontinuities can be accurately modelled using microwave linear analysis software. Analysis of the linear components in the frequency-domain is one of the main advantages over time-domain methods. The nonlinear components are defined in the time-domain so that the same models used in SPICE can be used in the hybrid methods.

Formally, harmonic balance is a nodal analysis of the voltages and currents at each node in the circuit. Since high frequency circuits generally consist of few nonlinear devices interconnected with many linear components, a nodal analysis for the whole circuit leads to sparse matrices that require special handling. The method usually employed is to gather all the linear components into a single sub-network and the nonlinear components into a second sub-network, as in Figure 1. A set of wires connect the two netwoks. The linear sub-network is then dense and easier to handle. The set of harmonic balance equations are then confined to the interface between the two sub-networks. This method is known as piecewise harmonic balance and is applied in all commercial harmonic balance simulators.

The harmonic balance method is intrinsically steady-state because of the use of Fourier series. Start-up and transient analysis are not possible in the same sense of a time-domain analysis. Special cases can be configured by exciting the circuit with a periodic square wave or a periodic pulse train. Under certain conditions, these can simulate a step and impulse response, respectively. The square and pulse waves are formed using a set of sinusoids of proper amplitude and phase. The waves have high harmonic content for accuracy, so the harmonic order of the analysis must be high.

Since the steady-state solution is determined, both time-domain and frequency-domain quantities are readily available. Gain, return loss, efficiency, spectral purity, etc. are easily computed frequency-domain quantities while voltage, current and power waveforms are determined by inverse transforms.

Pure Frequency-Domain Methods

In the pure frequency-domain methods the nonlinear devices are computed in the frequency-domain. This is accomplished by writing the nonlinear model equations as power series. The first series used was the Volterra series which was limited to small nonlinearities due to its complexity. Volterra series greater than third order are very difficult to determine and were limited to single variables, making FET simulations inaccurate over broad operating regions. Generalized power series [3] were introduced as the expansion of an operator using a basis function in order to facilitate high order nonlinearities, but determination of the basis coefficients was still a problem. Arithmetic operator methods (AOM) [4] simplified both problems of Volterra and generalized power series methods by composing the four basic operators as spectral transform matrix operations. All other functions (e.g. tanh(x)) are composed of expansions on the four basic operations. This greatly simplified the determination of general nonlinear modeling using more than one control variable.

The advantages of AOM over harmonic balance are significant. Firstly, AOM can perform multitone analysis efficiently because multi-dimensional Fourier transforms are not needed, as in harmonic balance. Analyses generally require that exact derivatives of the nonlinear devices be known for efficiency and improved convergence. AOM produce derivatives more easily than the time-domain SPICE models. However, the restricted modeling capability limits the frequency-domain method in today's commercial application.

A large disadvantage of the hybrid and frequency-domain methods is the large amount of computer memory that is required for large circuits or circuit with many frequency components. Memory upwards of 48MB is needed just for the derivative matrix when a circuit of 20 FETs is analyzed under large-signal two-tone excitation with 5th order intermodulation products are considered. This number increases dramatically when three tones are present. Sparse matrix techniques for the derivative matrix greatly reduce this, but are not always useful in highly nonlinear conditions.

The Harmonic Balance Problem

Harmonic balance analysis combines the efficiency of frequency-domain analysis of linear circuit elements and the accurate time-domain analysis of nonlinear devices. This hybrid technique is based on an algorithm to enforce the equality between the time-domain and frequency-domain independent variables at the domain interface.

Full Analysis

Consider a typical nonlinear circuit consisting of nonlinear devices (e.g. FET, diodes, etc.) which are interconnected with linear elements (e.g. transmission lines, inductors, capcitors, etc.), biased by some external DC sources, and driven into its devices' nonlinear operating range by some external signal generators operating at possibly non-harmonically related frequencies.

Note that a typical nonlinear device is modeled by a time-domain intrinsic model packaged with a linear frequency-domain parasitic network. The intrinsic nodes of the model are the nodes where the time-domain model is connected to its frequency-domain parasitic network. The nodes where the frequency-domain parasitic network connects to the external circuit are known as the extrinsic nodes.

Since the harmonic balance technique requires access to intrinsic ports of the nonlinear devices, the ports of the driving sources (signal generators and DC biases) and the output ports, therefore, an augmented port admittance matrix is required.

The augmented port admittance matrix (herein referred to as [Y]) consists of all the linear elements in the circuit, including the parasitics of the nonlinear device, augmented by the admittances of the external driving sources as shown in Figure 1 (note that an output port with Z_O impedance termination can be treated as a 0-volt signal generator in series with Z_O internal impedance).

In a one-tone harmonic balance analysis, all the frequencies present in the nonlinear circuit must be harmonically related. If we chose the Kth harmonic (of the fundamental) to be the highest frequency of interest, then, from sampling theorem, the minimum number of time samples needed for waveform reconstruction without aliasing is

$$N = 2K + 1 \qquad (1)$$

$$w = [k\ w_0] \qquad k = 1...K \qquad (2)$$

Because N > K, computation time is considerably reduced if the nonlinear state-variables chosen are in the frequency-domain.

If D is the number of nonlinear devices, ND is the total number of nonlinear device ports, and S is the number of DC sources plus signal generators, then for each device, the instantaneous voltage and current at the intrinsic device port are given by

$$v_d = f_d\left(x_d(t), \frac{dx_d(t)}{dt}, \ldots, \frac{d^n x_d(t)}{dt^n}, x_d(t-\tau) \right) \qquad (3)$$

$$i_d = g_d\left(x_d(t), \frac{dx_d(t)}{dt}, \ldots, \frac{d^n x_d(t)}{dt^n}, x_d(t-\tau) \right) \qquad (4)$$

where d = 1,2,...,D

x_d, v_d, i_d, are the set of state-variables, intrinsic port voltages, and intrinsic currents for device d respectively, and f_d and g_d are the set of nonlinear time-domain equations for device d.

Given the spectral components of the state-variables $X_d(k)$, in steady-state, the time-domain state-variables are given by

$$x_d(t) = \mathrm{Re}\left\{ \sum_{k=-K}^{K} X_d(k)\, e^{jkw_0 t} \right\} \qquad (5)$$

where w_0 is fundamental angular frequency.

Since $x_d(t)$ is real, and therefore $X_d(-k) = X_d^*(k)$, then

$$x_d(t) = x_d(0) + 2\mathrm{Re}\left\{ \sum_{k=1}^{K} X_d(k)\, e^{jkw_0 t} \right\} \qquad (6)$$

Given (3) and (4), the spectral components of $I_d(k)$ and $V_d(k)$ of device d are computed from their respective waveforms by the following equations:

$$I_d(k) = \sum_{t=0}^{N} i_d(t)\ e^{-jkw_0 t} \qquad (7)$$

$$V_d(k) = \sum_{t=0}^{N} v_d(t)\ e^{-jkw_0 t} \tag{8}$$

If I_{nl} and V_{nl} are the vectors device spectral currents and voltages at the linear-nonlinear interface, then we can represent I_{nl} and V_{nl} in a compact notation:

$$I_{nl}(X) = [I_1(X_1), I_2(X_2), \ldots, I_{ND}(X_{ND})]^T \tag{9}$$

$$V_{nl}(X) = [V_1(X_1), V_2(X_2), \ldots, V_{ND}(X_{ND})]^T \tag{10}$$

On the linear subnetwork portion, the currents into the linear subnetwork, I_{ln}, is computed as follows:

$$I_{ln}(X) = Y\ V(X) + J_s \tag{11}$$

where $V(X) = [V_{nl}(X), V_s]$, and V_s and J_s are the voltage and current source vectors respectively.

Note that I_{ln} are the currents into the linear network, and I_{nl} are the currents into the nonlinear devices.

Since the harmonic currents at the linear and nonlinear sides are of opposite directions, by Kirchhoff's current law, they should sum to zero at every harmonic if convergence is achieved. This is the harmonic balance error:

$$E(X) = [E_1(X_1), E_2(X_2), \ldots, E_{ND}(X_{ND})]^T \tag{12}$$

$$= I_{nl}(X) + I_{ln}(X) \tag{13}$$

$$= I_{nl}(X) + Y\ V(X) + J_s \tag{14}$$

Therefore, the harmonic balance problem is to find a set of state-variables X such that $E(X) = 0$.

Solving Methods

Since X is complex, therefore, E(X) is a set of complex functions. However, in practice, X is normally decomposed into $X_r = \mathrm{Re}\{X\}$ and $X_i = \mathrm{Im}\{X\}$ real variables. Hence, the total number of unknown variables is ND * (2K + 1) variables.

In practice, E(X) will not be zero, and therefore, solving the system of equations $E(X) = 0$ problem is similar to minimizing E(X). A large number of system solving algorithms can be used. Some of these algorithms are robust, but slow, while others offer superior speed but do not have good convergence properties. The following sections investigate the properties of some of these methods.

Gradient Method

The Newton-Raphson method is well-known for its quadratic convergence if the starting point is close enough to the final solution.

$$X^{n+1} = X^n - J(X^n)^{-1} E(X^n) \tag{15}$$

To improve convergence, especially for highly nonlinear circuits, a damping factor d can be applied. Hence, the above equation becomes

$$X^{n+1} = X^n - d\ J(X^n)^{-1} E(X^n) \tag{16}$$

Since numerical gradient computation is time consuming, a new class of algorithms, known as quasi-Newton, were developed to reduce the time in computing the Jacobian. One such method is the quasi-Newton with Powell-Broyden update algorithm yields satisfactory results for most classes of circuits. The Broyden update algorithm approximates the Jacobian by

$$B^n(X^n) = J^n(X^n) \tag{17}$$

and

$$B^{n+1} = B^n + \frac{(y^n - B^n s^n)(s^n)^T}{(s^n)^T s^n} \tag{18}$$

where

$$s^n = X^{n+1} - X^n \tag{19}$$

$$y^n = E(X^{n+1}) - E(X^n) \tag{20}$$

As evident in the equations above, updating B involves three matrix multiplications, three matrix subractions, one matrix addition and one scalar division. Hence, a quasi-Newton method with Broyden's update formula is more efficient than a conventional Newton-Raphson method.

The Newton-Raphson (quasi-Newton) method gives good performance, but fails to converge when starting point is not close enough to the solution. One strategy to provide the Newton-Raphson method with a good starting point is to use the results of DC analysis. From experiments, this strategy helps convergence for most classes of circuits.

The main disadvantage of Newton-Raphson method is the case when the Jacobian is singular, and therefore, no solution exists.

Analytic Jacobian Calculation

The process of calculating the Jacobian numerically is inefficient and generally inaccurate when the error functions are not sensitive to the parameters.

Analytical Jacobian evaluation [5,6] can be computed if the gradients of v(t) and i(t) in (3) and (4) can be found analytically. That is, if the partial derivatives of **f** and **g** with respect to the state-variables and time-derivatives y_m are available, where

$$y_m = \frac{d^m x}{dt^m}$$

then, we get the Fourier coefficients $C_{m,k}$ and $D_{m,k}$ of the voltage and current derivatives with respect to y_m:

$$\frac{\partial f}{\partial y_m} = \sum_{k=-K}^{K} C_{m,k}\, e^{jkw_0 t} \qquad (21)$$

$$\frac{\partial g}{\partial y_m} = \sum_{k=-K}^{K} D_{m,k}\, e^{jkw_0 t} \qquad (22)$$

Given these Fourier coefficients, we can readily calculate the Jacobian by expressing (21) and (22) in frequency-domain. Using chain-rule on the equations, we get [5,6]

$$\frac{\partial F_k}{\partial X_s} = \sum_{m=0}^{n} (jsw_0)^m C_{m,k-s} \qquad (23)$$

$$\frac{\partial G_k}{\partial X_s} = \sum_{m=0}^{n} (jsw_0)^m D_{m,k-s} \qquad (24)$$

These analytic derivatives can then be applied to (14) to obtain an analytic Jacobian. This idea can be extended to handle situations whereby a mixture of nonlinear devices with and without analytic derivatives can be present in the circuit.

Continuation Method

Continuation method transforms the $E(X) = 0$ problem to an auxiliary problem of the form $F(X,n) = 0$ [7,8], where n is called the continuation parameter. This method gives a solution to the original problem by the assumption that if $F(X^0, n=0) = 0$ is known, then $F(X, n=1) = E(X)$. Since $F(X^0, 0) = 0$ exists, the $F(X,n)$ nonlinear problem is very well conditioned because the continuation parameter n can be made small enough to make the solution close enough to the previous solution.

For example, in electrical circuits, X^0 is the set of state-variables of the DC analysis and the continuation parameter n can be view as the increasing power of the driving source such that $n=1$ is the desired driving power level.

This search method is numerically intense and therefore, extremely slow. Other variations to the above auxiliary equation are the natural embedding and artificial embedding strategies. They provide alternatives to the continuation problem when the Jacobian becomes singular. These description of these methods can be found in the references, and will not be described any further here.

Relaxation Method

The general idea of the relaxation method is to find a nonlinear vector operator F [6] such that the update of X is an iterative procedure as:

$$X^{n+1} = F(X^n) \qquad (25)$$

Like any iterative method, relaxation methods typically offer fast computation speed but suffer from poor convergence properties. To help improve convergence, the update procedure of (25) can be modified with the following popular formula [9]:

$$X^{n+1} = P^n\, F(X^n) + (I - P^n)\, X^n \qquad (26)$$

where I is the identity matrix and P^n is a diagonal matrix of conversion parameters at iteration n.

Multitone Analysis

The harmonic balance method for analyzing single-tone periodic signals can easily be extended to represent quasi-periodic signals with N exciting tones. Hence, Eqn (5) becomes

$$x(t) = Re\left\{ \sum_{k=-K}^{K} X(k)\, e^{\left(j \sum_{n=1}^{N} k_n w_n t \right)} \right\} \qquad (27)$$

where w_n is the fundamental of the nth exciting tone and K is the maximum number of unique frequencies used.

For example, in a mixer circuit where w_1 and w_2 are the LO and RF exciting tones,

$$x(t) = Re\left\{ \sum_{k=-K}^{K} X(k)\, e^{j(n_1 w_1 + n_2 w_2)t} \right\} \qquad \text{where } \sum_{i=1}^{N} |n_i| \le K \qquad (28)$$

One way to solve the multitone quasi-periodic problem in (27) is by replacing the quasi-periodic case with a strictly periodic one and choosing the greatest common divisor of all the exciting tones to be the fundamental. The harmonic balance method can then be applied in a straight forward manner. However, this approach is impractical when the "fundamental" is extremely small, resulting is very high sampling rate, and hence impractical.

Alternatively, the Almost-periodic Fourier Transform (APFT) [10,11] can be applied to solve circuits operating in the quasi-periodic regime. This method employs the technique of selecting sampling time points randomly from a time interval larger than the period of the smallest nonzero frequency, subject to the condition that the row vectors of the Fourier transform matrix are orthogonal.

The advantage of this method is that it uses the theoretical minimum number of sampling points, and the algorithm of sampling time point selection is independent of the number of exciting tones.

The obvious drawback of APFT is the time penalty in using a conventional Fourier transform instead of a FFT. Another disadvantge is the selected random time points may not correspond to the frequencies of interest, and consequently resulting in incorrect representation of the spectrum.

A more efficient and practical method for solving the quasi-periodic problem is the multidimensional FFT [5]. Since multidimensional FFT ensures orthogonality between frequencies, it can correctly handle multitone quasi-periodic problems whereby the tones can be very close together. In addition, computation time is independent of the values of frequencies used. Another advantage is that multidimensional FFT ensures sampling time points directly correspond to the frequencies used.

Spectral Patterns For Mixer And Intermodulation Analysis

Consider a circuit excited by two tones, namely f1 and f2. The choice of frequencies used in the analysis depends on the nature of the problem that exist.

When the strength of one signal is much greater than the other, using a mixer spectrum is appropriate. For example, a mixer circuit usually uses a strong LO signal to mix with a weak RF signal to produce a fairly strong IF signal. The spectrum is typically bands of LO harmonics with weaker sidebands at each LO harmonic. The strength of sidebands decrease as the order of sidebands increase, and therefore can be neglected.

On the contrary, a intermodulation spectrum is ideal when both both signals are of almost or equal in strength. This is because the higher order sidebands strength are strong and cannot be neglected.

Two-Tone Mixer Case

Consider the case where the power in one signal dominates. Let this signal be f_{LO} and the weaker signal be f_{RF}. If the number of LO harmonics is N_{LO} and the number of sidebands is N_{SB}, then the mixer spectrum is calculated from the following set of equations [12]:

$$f_k = |n_1 f_{LO} + n_2 (f_{RF} - f_{LO})| \qquad (29)$$

$$[f_k],\ 0 \le |n_1 + n_2| \le N_{LO} \text{ and } 0 \le |n_2| \le N_{SB}$$

The total number of frequencies in this spectrum is $N_{LO}(2N_{SB} + 1) + N_{SB}$. Figure 2 illustrates the mixer spectrum. Note the repeated pattern of sidebands around each LO harmonic.

Two-Tone Intermodulation Case

If the two signals are of comparable power, a different spectrum is used to compute intermodulation products. If the frequencies are given as f_{RF1} and f_{RF2} and the intermodulation order is N_{IMD}, then the spectrum is given as [12]:

$$f_k = |n_1 f_{RF1} + n_2 f_{RF2}| \qquad (30)$$

$$[f_k],\ 0 \le |n_1| + |n_2| \le N_{IMD}$$

The total number of frequencies in this spectrum is $N_{IMD}(N_{IMD} + 1)$. Figure 3 illustrates the intermodulation spectrum. An example with 5th-order intermodulation products generates 30 frequencies.

Three-Tone Mixer Case

The three-tone mixer spectrum is made up of several LO harmonics, each flanked by intermodulation products of the two given RF frequencies. This spectrum can be veiwed at two independent RF signals superimposed on the LO pump. If the number of LO harmonics is N_{LO} and the intermodulation order of the RF signals is N_{IMD}, then the mixer spectrum is calculated from the following equations [13]:

$$f_k = |n_1 f_{LO} + n_2 (f_{RF1} - f_{LO}) + n_3 (f_{RF2} - f_{LO})| \qquad (31)$$

$$[f_k],\ 0 \le |n_1 + n_2 + n_3| \le N_{LO} \text{ and } 0 \le |n_2 + n_3| \le N_{IMD}$$

The total number of frequencies is $N_{LO} + N_{IMD}(N_{IMD} + 1)(2N_{LO} + 1)$. For example, a problem with 3 LO harmonics and 3rd-order intermodulation generates a spectrum of 87 frequencies. Figure 4 illustrates a spectrum of third-order intermodulation with one LO harmonic.

Three-Tone Intermodulation Case

The three-tone intermodulation case is a straightforward extension of the two-tone case. This spectrum is:

$$f_k = |n_1 f_{RF1} + n_2 f_{RF2} + n_3 f_{RF3}| \qquad (32)$$

$$[f_k],\ 0 \le |n_1| + |n_2| + |n_3| \le N_{IMD}$$

The total number of frequencies is $N_{IMD} + N_{IMD}(N_{IMD} + 1)(2N_{IMD} + 1)/3$. For example, a spectrum with 5th-order intermodulation products consists of 115 frequencies.

Frequency Conversion Analysis Method

Frequency conversion analysis is a technique for approximating the solution of a nonlinear mixer circuit [6]. This concept employs some nonlinear subnetworks P and Q to replace all the nonlinear devices in the mixer circuit so that the voltage and current computations at the linear-nonlinear interface involve only matrix operations.

Consider the waveform of a weak RF signal mixing with a strong LO signal

$$x(t) = \tilde{x}(t) + \mathrm{Re}\left\{ \sum_k \Delta X_k \, e^{j(w_R + kw_0)t} \right\} \qquad (33)$$

where w_0 and w_r are the angular frequencies of the LO and RF respectively, $x^{\sim}(t)$ is the waveform due to the LO drive. The voltages and currents at the linear-nonlinear interface are similar (x replaced by v and i).

If we linearize (33) around $x^{\sim}(t)$ we get:

$$v(t) = f(\tilde{x}(t)) + \mathrm{Re}\left\{ \sum_k \Delta X_k \, e^{j(w_R + kw_0)t} \right\} f'(\tilde{x}(t)) \qquad (34)$$

Comparing (34) with the v(t) expression of (33), we get the voltage and current relationships

$$\Delta V = P \Delta X$$
$$\Delta I = Q \Delta X \qquad (35)$$

The conversion matrices P and Q are defined by [6] as:

$$P \equiv [P_{k,s-k}]$$
$$Q \equiv [Q_{k,s-k}] \qquad (36)$$

and the square matrices of size ND are:

$$P_{k,p} = \sum_{m=0}^{n} \{j(w_r + kw_0)\}^m C_{m,p}$$

$$Q_{k,p} = \sum_{m=0}^{n} \{j(w_r + kw_0)\}^m D_{m,p} \qquad (37)$$

Note that these equations are similar to the derivative matrices of (23) and (24) and are readily available after performing a harmonic balance analysis.

If P and Q are nonsingular, then we get the impedance and admittance conversion matrices by:

$$\Delta V = PQ^{-1}\Delta I = Z_C\Delta I$$

$$\Delta I = QP^{-1}\Delta I = Y_C\Delta V$$

With this result, we can compute mixer performance of multi-tone RF signals without a full multi-tone analysis. Of course the signals must be of low power or the results will be erroneous. The dynamic range and other high power results can only be computed with a full analysis. However, we will find later that these conversion matrices are needed for nonlinear noise analysis.

Sparse Jacobian Matrix Methods

Obtaining higher accuracy by using harmonic balance method to solve nonlinear equations usually requires many iterations during the nonlinear solving procedure, and the number of iterations required closely depends on the iterative methods used. Newton's method is frequently used in nonlinear circuit analysis to minimize the objective function because of its asymptotic rate of convergence. However, evaluation of the whole Jacobian can be time consuming. The size of the Jacobian matrix depends on the number of unknowns of the system evaluated. For a circuit with several nonlinear devices and multitone excitations, a large number of unknowns may be required for solving the system, and both the computation time and memory required for the Jacobian matrix calculations may significantly degrade the circuit simulation efficiency.

Since, in many circuit analysis, extreme power levels are not of major concern, using special sparse matrix technique by setting some predetermined elements of the matrix to be zero is a good compromise among power-handling, convergence speed, and memory occupation. One extreme approximation has been used for the Jacobian matrix is the block Newton method [14]. In that approximation, nonzero elements are assumed in the diagonal blocks of the matrix only, where the matrix is in a frequency-oriented permutation (i.e., all elements at the same frequency are grouped in the same block). The basic assumptions for this approximation are that the input power level is not very high and, for most microwave nonlinear analog circuits, the values of those derivatives in the diagonal blocks are larger than those values in the off-diagonal blocks. Compared with the full Jacobian technique for a large nonlinear system, both the memory occupation and the matrix calculation time using the block Newton method are negligible. Therefore, this approach is very useful for the small signal circuit analysis.

A compromise between the Newton and the block Newton methods is to make some necessary arrangements on the frequency sequence and expand the nonzero elements by including wider bandwidth with the diagonal blocks [15]. As in the block Newton method, the nonzero elements are predetermined, and a specific sparse matrix solver is used rather than a general purpose solver. The result is a good tradeoff between speed and dynamic range. The width of the diagonal blocks used is controlled by a number called the "sparsity parameter". This sparse matrix structure and sparsity parameter are depicted in Figure 5.

In a general purpose nonlinear circuit simulator, a mixed type of dense and sparse matrix solver for the Jacobian matrix calculation is necessary. Dynamic switching between these two methods and some other techniques (e.g. chord method and back-tracking technique) can form a powerful error minimization algorithm. Criteria used to determine the sparsity parameter is generally as follows: The block Newton method (sparsity parameter = 0) is always tried first since this is the fastest Jacobian to evaluate. If the rate of convergence is not satisfactory, then the sparsity parameter is increased. The rate of convergence is tested at each iteration. Once the sparsity parameter is greater than a certain level, the dense Jacobian is used because the efficiency of computing and inverting the sparse Jacobian has degraded to the point where it is compatible to the dense Jacobian.

To illustrate the type of circuit complexity that a sparse Jacobian allows, consider the receiver front end of Figure 6. This circuit contains a low-noise amplifier providing 25dB gain, a balanced diode mixer and three stages of 10dB gain blocks. With dynamic switching of the sparsity parameter, this circuit analyzes efficiently to produce sub-system-level computations. Output such as total conversion loss over frequency and compression of the system are shown in Figures 7 and 8 respectively.

Oscillator Analysis

One approach to free-running oscillator analysis is to use the harmonic balance equations developed for the circuit and to include the oscillation frequency as an additional optimization variable. Generally, one of the variables that would be used as an optimization variable in examining a non-autonomous circuit is eliminated, for

example, by setting the phase of a voltage or current to zero. Usually, with this approach, the simulated results tend to converge to a degenerate solution [18] (i.e. all currents equal to zero is also a solution of Kirchhoff's current law), or else the initial setting of the oscillating frequency must be very close to the final result. However, the degenerate solution can be avoided by incorporating additional criteria in the system objective function. This was done by many researchers in different approaches [19, 20, 21]. In this section, a new free-running oscillator analysis algorithm is presented. This algorithm is based on the conventional harmonic balance method and suited to large signal oscillator analysis. Basically, the algorithm can be divided into two steps: search and analysis. In the search mode, an external test source is connected to an oscillator circuit to inject AC power and forces all the state variable values away from the degenerate solutions. The steady-state solutions of the search mode is treated as the initial guess of the second step-the analysis mode. In the analysis mode, the system equation is solved using a modified harmonic balance method, in which the oscillating frequency is used as an independent variable and the system error function is modified to incorporate an additional criteria which is an extension of the original Kurokawa oscillation condition [22].

Search Mode

The method used in the search mode of the oscillator analysis is to inject an external AC source into the oscillator circuit and find the steady-state condition using harmonic balance. By sweeping the injected frequency and power and examining both the magnitude and phase of the injected current, the oscillating condition of the circuit can be determined.

The basic idea used in this method can be explained starting from the Kurokawa oscillation condition. As shown in Figure 9, an oscillator circuit can be represented as an one-port circuit, where, Y is the input admittance of the one-port network, and Y_{load} and Y_{osc} are the equivalence admittances of the load element and the "oscillator circuit", respectively. For a steady-state free-running oscillator, the oscillation condition for the circuit in Figure 9 is that [23]

$$Y(w) = Y_{OSC}(w) + Y_{LOAD}(w) = 0 \tag{38}$$

where w is the radian frequency. (38) applies to each frequency component. If K different AC frequency components are present in the circuit, (1) can be represented as

$$Y_k = \mathrm{Re}\{Y_k\} + j\,\mathrm{Im}\{Y_k\} = 0, \quad k = 1,2,...,K \tag{39}$$

where, k indicates that the admittance Y_k is evaluated at the radian frequency w_k. If i(t) and v(t) in Figure 9 are represented as summations of different frequency components in the frequency-domain and I_k and V_k are the phasor representations of i(t) and v(t) at w_k respectively, then the input admittance Y_k evaluated at the radian frequency w_k is

$$Y_k = \frac{I_k}{V_k} \tag{40}$$

Consequently, (39) and (40) imply that [23]

$$\mathrm{Re}\{I_k\} = \mathrm{Im}\{I_k\} = 0, \qquad k = 1,2,...,K \tag{41}$$

and

$$|V_k| \neq 0 \qquad k = 1,2,...,K \tag{42}$$

(41) and (42) can be described as follows: If the voltage magnitude of the injected test source of Figure 9 is large enough and the current magnitude of the test source under the harmonic balance condition is zero, then the circuit is in oscillation condition. Using this method, we can simply inject an external AC source to any port of the test circuit. By sweeping the frequency and power of the external source and monitoring the injected current value, the oscillation condition of the test circuit can be determined.

(41) and (42) are for the general case. As a matter of fact, they can be simplified for k = 1 only, since, for a general nonlinear oscillator circuit, $|V_1| \neq 0$ normally implies that $|V_k| \neq 0$ (k = 2,3,...,K) and, using software techniques, it is very easy to always set $|I_k| = 0$ (k = 2,3,...,K).

For efficient search of the frequency and power of the external injected source, the following algorithm for the searching process can be used:

1) Set the external power to be constant and at low level.

2) Sweep the frequency of the external source until Im{I_1} is close to zero and Re{I_1} is negative.

3) Increase the power of the external source stepwise and track the frequency until both Re{I_1} and Im{I_1} are close to zero.

With this search method, highly accurate circuit analysis results may be obtained if both Re{I_1} and Im{I_1} are reduced to very small values. However, this may require a large number of iterations. Instead, a near target solution (about 0.1% error) is often good enough as an initial guess for the analysis mode which is described in the next section. In the analysis mode, the external injected source is excluded and a modified harmonic balance technique is used to get an accurate circuit analysis result.

Analysis Mode

The most efficient way to solve the nonlinear system equations is to cast the problem into the minimization of an objective function and to use Newton's method to iteratively obtain the zero of this function. In general, the iterative process of Newton's method can be represented as

$$\mathbf{X}^{n+1} = \mathbf{X}^n - \mathbf{J}(\mathbf{X}^n)^{-1}\mathbf{E}(\mathbf{X}^n) \tag{43}$$

where $\mathbf{x}^n$ is the independent state variable vector at the n-th iteration; **E** is the error function vector; and **J** is the Jacobian matrix of **E**.

As mentioned in previous sections, for non-autonomous circuit analysis, vector **x** is composed of the state variables (e.g. device port voltages) and vector **E** is composed of the elements of the system errors (e.g. corresponding port current errors). For oscillator circuit analysis, the structure of the vector **x** is changed with the oscillating frequency f_1 is an additional variable. Here the imaginary part of the fundamental voltage of the first state variable in vector **x** is replaced by f_1 (and so the phases of the harmonic state variable voltages are referred to the phase of the voltage of the first state variable):

$$\mathbf{X} = [V_{1,1,r},\ f_1,\ V_{2,1,r},\ V_{2,1,i},\ \cdots\cdots V_{p,q,r},\ V_{p,q,i},\ \cdots\ \cdots\ ] \tag{44}$$

where, $V_{p,q,r}$ and $V_{p,q,i}$ represent the real and imaginary part of the voltage of p-th state variable at radian frequency w_q. Likewise, for eliminating the degenerate solution using Newton's method to solve the nonlinear system equation, the error function vector **E** in (43) is reconstructed by replacing all the error function elements at the fundamental frequency $I_{p,1} = I_{p,1,r} + jI_{p,1,i}$ with $I_{p,1}/V_a$:

$$\mathbf{E} = \left[\mathrm{Re}\left\{\frac{I_{1,1}}{V_a}\right\},\ \mathrm{Im}\left\{\frac{I_{1,1}}{V_a}\right\},\ \mathrm{Re}\left\{\frac{I_{2,1}}{V_a}\right\},\ \cdots\cdots,\ I_{1,2,r},\ I_{1,2,i},\ I_{2,2,r},\ \cdots\cdots \right] \tag{45}$$

where V_a is defined as the product of all the state variables at the fundamental frequency, i.e., if there are P state variables in the circuit analyzed, then

$$V_a = \prod_{p=1}^{P} V_{p,1} \tag{46}$$

Solving the modified nonlinear system equations for oscillator analysis can definitely exclude the degenerated solution. With the initial guess acquired from the search method mentioned above, convergence is also good. The method for the formulation of the Jacobian matrix which is required for the Newton's method is similar to the techniques used for the non-autonomous circuit analysis and is described in [23]. This algorithm is also suitable for the simulation of self-oscillating mixer circuits.

Example

Here is an example of FET oscillator used to demonstrate how the technique in Microwave Harmonica works. The schematic is shown in Figure 10. After running both the search and the analysis modes, results show that the oscillating frequency of this circuit is 4.86793GHz and the fundamental output power is 13.157dBm. Some simulated results are shown in Figure 11.

Noise Analysis

Noise analysis of nonlinear circuits has been covered as it applies to mixers. Held and Kerr [24] presented the method for Schottky diode mixers and Rizzoli [25] extended the results to FET and HEMT mixers and is the basis of the discussion given here. As of October, 1990, nonlinear noise analysis has not been implemented in commercial simulators, but probably will be in a short matter of time.

Noise analysis proceeds similar to the generalized frequency-conversion problem where a small RF signal is injected into the nonlinear network operating under sinusoidal steady-state and the resulting perturbation is analyzed. In the noise analysis, the injected noise signals are statistical in nature and may be correlated, making the analysis much more difficult than the previous frequency-conversion problem. The goal of the analysis is to compute the noise power delivered to the IF load. Noise contributions arise from the shot noise of the nonlinear network and the thermal noise of the linear network. The shot noise is partly correlated while the thermal noise is uncorrelated and independent of the shot noise. Therefore the noise power contributions from these two sources superimpose at the load.

The mechanism that is responsible for the noise power at the IF load is as follows. At the DC bias point of the device, the nonlinear noise sidebands are uncorrelated and are dependent on the bias point. When the devices are pumped by the LO, the nonlinear noise sidebands are modulated accordingly and are partly correlated because each sideband is a combination of the the original uncorrelated DC sidebands. During mixing, each sideband generates a correlated component in the vicinity of the IF. To determine the correct nonlinear noise power contribution, the correlation of the sidebands must be considered in the analysis. Similarly, contributions to the noise power at the IF load are made by the thermal noise generated by the linear network through frequency conversion in the mixer. The thermal noise is not dependent on the LO excitation and because it is uncorrelated, its noise power contribution is additive.

In FETs flicker (1/f) noise is a significant noise source at frequencies below a few megahertz. This can be modeled by an additional noise source at the FET gate and including this source in the corelation matrix of the FET. Empirical expressions for the flicker noise exist in the literature [26].

The noise figure is found from the noise power delivered to the IF load by

$$F(w_{IF}) = \frac{2\pi\, dN(w_{IF})}{K_B T_0 G(w_{RF}) dw} \tag{47}$$

where $dN(w_{IF})$ is the average noise power between w_{IF} and $w_{IF} + dw$, K_B is Boltzmann's constant, T_0 is the reference temperature, 290K, and G is the conversion gain between the RF signal and the IF. Conversion gain is computed by the standard harmonic balance analysis.

The calculation of dN is done by the following equation where the intermediate steps are given in [5, 25].

$$dN(w_{IF}) = R_{IF}\sum_{p} T_{0p} C_L(w_{IF} + p\, w_0)\, T_{0p}^{*} + R_{IF}\sum_{p,q} T_{0p}\left[\sum_{s} H_{p-s} C_{dc}(w_{IF} + s\, w_0) H_{s-q}\right] T_{0q}^{*} \tag{48}$$

R_{IF} is the IF load resistance, T_{0p} is the conversion matrix from the p'th sideband to the IF, C_L is the correlation matrix of the linear network, C_{dc} is the correlation matrix of the nonlinear network at the dc operating point, and H represents the Fourier components of the waveform modulating the nonlinear noise sources. The interpretation of this equation is as follows. The first term represents the noise power contribution of the linear network. Each noise sideband in the analysis is frequency converted by the T matrix to the IF sideband and summed. The noise power contribution to the total noise power, dN, is additive because the linear network noise is uncorrelated with the nonlinear noise. The second term represents the noise power contribution from the nonlinear devices. The noise correlation matrix evaluated at the instantaneous operating point, C_{dc} , is modulated by the LO waveform to generate noise components at each sideband s. A portion of these noise sidebands are then frequency-converted to the IF sideband by the sideband conversion matrix T. These two contributions make up the total noise power.

Another noise contributor not in (48) is that noise injected from the local oscillator. The LO noise can be accounted if the statistical properties are known. An additional term would be added to (48) since the injected noise is additive [25].

The noise correlation matrix for diodes and FETs can be found in the literature [24,27]. The commonly known FET correlation matrix that originated from [27] is given as:

$$C_{dc}(w) = \frac{2}{\pi} K_B\, T\, dw \begin{bmatrix} \frac{w^2 C_{gs}^2}{g_m} R & -jwC_{gs}\sqrt{PRC} \\ jwC_{gs}\sqrt{PRC} & g_m P \end{bmatrix} \tag{49}$$

where the gate and drain noise parameters, R and P, and the correlation coefficient C are functions of the device structure and bias point. This noise model does not

include the gate noise or flicker noise. Expressions for these contributions can be found in [26] and [28].

An application taken from [25] of the noise analysis with the simplified FET noise model appears below. The mixer of Figure 12 is a simple single-ended, single gate FET that was not designed for low noise. Results of simulated noise figure, conversion gain and measured noise figure are shown in Figure 13 as a function of LO power. Good agreement is obtained, even with the simplified noise model, because the gate noise contribution is small compared to the total noise figure of the mixer. The flicker noise contribution is also small because the IF is 800MHz; well above the flicker corner frequency. The FET is biased near pinchoff, which is close to the bias point for minimum noise. As the LO power is increased, the operating point of the FET changes accordingly to larger drain currents and becomes noisier. At very low LO power, the conversion gain drops and the noise figure rises. This is consistent with measurements.

Transient Analysis

The problem of transient analysis has intrinsically been a time-domain problem. Simulating transients is a natural result of the solution of the differential equations with arbitraty initial conditions. Again, simulation in the time-domain poses problems of accuracy with high-speed circuits, especially switching circuits whose harmonic content is high. Characterization of lossy, dispersive components is typically only available in the frequency-domain. For this reason, we present an investigation of transient analysis in the frequency-domain. In our reference to transient analysis, we also cover waveform excitation that is generally descibed in the time-domain, e.g. square-wave, pulse, triangle-wave, etc., and modulated carrier waves.

Because the harmonic balance method uses the Fourier series to represent signals, any desired excitation can be decomposed into a set of complex sinusoidal sources:

$$m(t) = \sum_{k_m=-N}^{N} S_k \, e^{jkw_m t} \qquad (50)$$

where N is the number of harmonics. Of course, the excitation must be periodic. Consider a circuit excited with a square wave of 50% duty cycle. If the portion of the response due to the transition relaxes between the edge conditions, then this will be the transient response [29]. Therefore, the fundamental period of the square wave must be greater than twice the transient response time. This may lead to very long square waves in order to simulate the step response of a circuit.

Note that this analysis is only an approximation to the true transient analysis. The transients will generally contain frequencies that are not harmonically related to the fundamental of the excitation. Also, in some circuits, subharmonics may be present which are not accounted for.

The periodic response of other wave shapes can also be determined. In fact, arbitrary wave shapes can be accomodated by Fourier transforming the wave into the frequency-domain and assigning a set of sinusoidal sources the values of the complex coefficients. For wave shapes containing abrupt edges, such as the square wave, a large number of harmonics are needed to portray the wave accurately. For instance, 30 to 40 harmonics are adequate for most square wave applications. Other wave shapes that are of interest are the rectangular pulse (a square wave with low duty cycle), the triangular wave and the sawtooth wave. For these shapes, the Fourier series is known and the previously mentioned Fourier transform can be avoided. The wave shapes are built-in to some harmonic balance simulators including Microwave Harmonica.

An example illustrating pulse excitation is shown in Figure 14. The circuit is a buffer-receiver circuit excited by a periodic pulse train of 10% duty cycle whose period is 5nsec. A total of 50 harmonics were used for the simulation. The transmission medium between the buffer and receiver is a lossy, dispersive coupled microstrip line with nonlinear terminations on the coupled ports. The buffer and receiver consist of bipolar darlington pairs with a constant power gain of 11db from DC to 4GHz. Voltage waveforms are shown at various points of interest in the circuit. Note the significant amount of coupling in the parallel strip. The impedance mismatch of the channel with the receiver causes significant reflections of the pulse. The dispersive nature of the channel is evident by the spreading of the pulse shape at the receiver. The spreading is also caused by the even-odd mode velocities supported by the structure which becomes multi-modal when more coupled lines are present.

The large number of harmonics required in the analysis makes the Jacobian of the harmonic balance equations very large. For the example shown with 50 harmonics and 10 nonlinear device ports (4 bipolar transistors and 2 diodes), the number of unknowns is 1010 and a dense Jacobian occupies 7.78Mbytes of double precision memory. Using sparse Jacobian techniques, this problem required a sparsity parameter of 1 and the Jacobian occupied 0.69Mbytes. The required CPU time for the LU decomposition operation is dramatically reduced by more than an order of magnitude.

Modulated RF carriers can also be analyzed with similar techniques. If the modulation is represented by equation Tran1, and the carrier is a single-tone signal:

$$c(t) = 2\mathrm{Re}\{V_c\, e^{jw_c t}\} \tag{51}$$

Then the ideally modulated carrier is:

$$w(t) = c(t)\ m(t) = 2\mathrm{Re}\left\{\sum_{k_m=-N}^{N} V_c S_{k_m}\, e^{j(w_c + k_m w_m)t}\right\} \tag{52}$$

This signal contains two fundamental frequency components (wc, wm), therefore the analysis can proceed as a standard two-tone problem with the analysis spectrum modified. The new spectrum contains the frequecies:

$$[f_k],\ k_c w_c + k_m w_m \quad \text{subject to } 0 \le |k_c| \le M \text{ and } 0 \le |k_m| \le N \tag{53}$$

where M is the number of carrier harmonics. This signal is the ideal double-sideband AM modulated signal.

The number of harmonics used in the modulating signal strongly affects the size of the harmonic balance problem. For example, if N=50 then 101 sources are required for the excitation source. If four carrier harmonics are used for the analysis, then a total of 909 spectral lines are needed in the analysis. With just a few nonlinear devices, several thousand unknowns are present in the problem. Sparse Jacobian techniques are therefore required to make modulation analysis possible.

As an example, [29] presents a microwave amplifier excited by a 10GHz sinusoid modulated by a 30% duty square wave of period 100nsec. With N=50 and M=4, the required memory for the full Jacobian is 26.5Mbytes. The memory for a sparse Jacobian suitable for analysis to saturation is 0.52Mbytes. The amplifier topology is shown in Figure 15. Note the radial stubs which all but prevent accurate analysis in the time-domain. Details of the power envelopes of the input and output waveforms are shown in Figure 16 for input powers of 15.5dBm (1dB compression) and 19.3dBm (saturation).

Nonlinear Modeling Issues

Accurate representation of the active devices is critical for the simulation results to match measurements. A brief overview of the extensive work performed in device modeling, as it applies to high frequency devices, will be given in this section. It will concentrate mainly on MESFET models and mention some of the important models still missing from simulators.

Active device models come in three flavors: Curve-fit, empirical and physics-based. The first two types are based on equivalent circuits comprised of linear and bias-dependent components. The third is a mixture of the intrinsic model, whose terminal characteristics are computed directly, and an equivalent circuit extrinsic parasitic topology. Curve-fit models are generally accurate only when used within the neighborhood of the conditions used to characterize the model. Once outside this range, performance can be erroneous. Additionally, if a high order polynomial, for instance, is used then the response between measured data points can also be erratic. Arbitrary curve-fitting expressions and procedures are therefore seldom used for simulation. Two of the more reliable expressions for the MESFET channel current have been used by Maas [30] and more popularly, by Curtice [31]. Note that these functions are of low order. Another disadvantage of curve-fit models is that the coefficients cannot usually be related directly to the measurements; that is, they have little or no physical bearing.

Empirical models are derived from simplified, physics-based semiconductor equations and from behavioral characteristics of measurements. These models offer the advantages of being well behaved outside the neighborhood of the measurements and many of the model coefficients can be directly related to measurements. Many models can also be written in terms of physical geometries and dopings of the device, though the accuracy is often comprimized. Most of the device models available in commercial simulators are empirical.

Physics-based models offer the ability to simulate devices from the process level [32, 33, 34]. The input to these models are the geometrical properties like gate width, gate to drain spacing, gate finger layout, doping profile, etc.. The model response is computed by solving a set of basic semiconductor equations subject to the boundry conditions imposed based on the geometrical data, doping data and applied potentials. The set of equations include Poisson's equation, usually in two-dimensions, and the current continuity equation [35]. Because this set must be solved for each voltage point present in the device terminal waveforms, execution times are very long. Some workers have developed means of determining the equivalent circuit model parameters over a given bias range which can subsequently be used in the circuit simulation via a table look-up procedure [32]. This method provides an effective means of simulation while making a small compromise on the physics-based model's accuracy. Although the physics-based models are dependent on the true physical parameters of the device, the accuracy is similar to equivalent circuit models. Physical models are best used for determining process variation effects and proper statistical analysis [36].

Diode Models

Models for p-n and Schottky junctions have been very stable for quite some time. The models incorporated in the original SPICE simulators are still used today. These were derived from fundamental semiconductor physics and have proven to be accurate into the Terahertz region. The determination of model parameters for diodes is a fairly simple task compared to three terminal devices. Parameters such as reverse saturation current, ideality factor and breakdown voltage can be measured directly on I-V tracers. Capacitances can be measured by C-V meters or S-parameters and fit to the model.

Other diode types have not seen such successful implementation. Varactor diodes, although a key component in RF and microwave designs, have only been simulated by modifying the diode capacitance exponent. This does not accurately model effects like the rapid decrease in capacitance at punch-through [37]. Step-recovery diodes are another widely used device for frequency multiplication whose model has not been implemented in simulators. PIN diodes are yet another, although the dispersive characteristics are a problem for models described in the time-domain.

Bipolar Transistor Models

The Gummel-Poon bipolar model has dominated simulation of BJT circuits. It is available in all major SPICE and harmonic balance simulators. Minor modifications have been made for high frequency simulations. These are mostly for better modeling of the distributed base and parasitic extrinsic elements [38]. The determination of the Gummel-Poon model parameters is not an easy task. Although parameter determination by specialized measurements [39] has been proven to work for devices to the VHF range, higher frequency devices do not always behave as if each model component is independent. As will be discussed in the next section, the DC model cannot be treated independent of the AC model. Because the model is not "perfect", the DC and AC components are not decoupled. This becomes especially evident at high frequencies. Although BJTs are typically used only up to 6GHz, the use of heterojunction bipolar transistors (HBTs) at much higher frequencies will bear evidence to this. There has been some work [40, 41, 47] based on optimization methods to fit the model parameters by considering the DC and AC responses simultaneously.

MESFET Models

In contrast to diode and BJT models, there are a number of MESFET models that are used in simulators and the field is still evolving. The Curtice quadratic model [42] was one of the improvements over the SPICE 2 JFET model that was popularly accepted although it has since been superceeded. The Materka-Kacprzak [43] was later modified by Rizzoli to better model subtle DC characteristics and appears today as one of the best MESFET models available. Curtice [31] introduced a new channel current expression that is based on a polynomial curve fit on the gate voltage but is modified by the drain voltage to account for the change in pinchoff voltage with Vds. Breakdown effects were also added for high power applications. This has popularly become known as the Curtice cubic model since the polynomial is cubic. Statz et. al. [44] introduced new channel current and capacitance expressions for increased accuracy and symmetric drain-source characteristics. McCamant et. al. [45] modified the Statz expression to better model current near pinchoff, at high current levels and small-signal output conductance. This model became popularly known as the TOM model (Triquint's Own Model). This handful

represents the MESFET models available in most high-frequency-oriented circuit simulators.

Two significant problems that most of these models share is the incorrect output conductance observed at frequencies greater than 10MHz and modelling gate-drain breakdown effects. To alleviate the first problem, a series R-C pair is connected to the intrinsic drain-source of the FET. Resistance, labelled Rdsd in Figure 17, increases the output conductance to match it at high frequencies. The capacitance Cdsd is a large value that basically prevents DC current in Rdsd. Using this patch, modeled S22 of the device matches measured better, but fails when considered over the full bias range of the device. Rdsd can be made bias dependent, but this adds another nonlinear component and more complexity that is more of a "quick fix" than a real solution. The second significant problem is the breakdown model of the FET. Breakdown equations presented above are either exponentials or a simple resistance. Model parameter values for breakdown can be taken directly from DC measurements which indicate that it has an exponential characteristic with a very high ideality factor compared to a junction diode (e.g. the ideality factor for a quality diode is approximately 1.5 and for breakdown is approximately 40 to 60). The behavior of breakdown at high frequencies, however, may not be so straightforward. It is observed by comparing simulations with measurements that the voltage at which breakdown occurs at high frequencies is higher than that measured at DC. This indicates there are some time delay mechanisms at work that have not yet been identified.

Parameter extraction of the linear equivalent circuit has reached a high level of accuracy for wafer-probed and chip devices. The method of "peeling away" layers of parasitics to reveal the intrinsic FET was developed by Dambrine et. al. [46]. Since this method is analytic and not based on any optimization it is both fast, accurate and consistent over a broad frequency range. Using this data at a number of bias points, cuves of the bias dependant model components can be obtained (e.g. Cgs vs. Vgs and Vds). The expressions given above for each model component can then be fit to these curves. Most of the individual model parameters can be determined by intercept points, slopes, etc. or by simple curve fitting and optimization routines. The channel current expression can be fit to the bias data by optimization. This approach treats each component of the FET model independently in a decoupled fashion. Such an approach may not be reliable [47] since parameters determined at DC, for example, may not be suitable at high frequencies. A simple example illustrates the concept: Suppose the channel current, I_{ds}, is determined from the DC I-V curves. The high frequency transconductance is the derivative of the channel current with respect to the gate-source voltage, $g_m = dI_{ds}/dV_{gs}$. Since g_m can also be determined by the linear extraction method, the two values should be the same. Typically they are not. The question then becomes which g_m to use. If the high frequency g_m is used in the optimization to determine I_{ds}, then DC I_{ds} will be in error. Likewise if I_{ds} is determined from DC measurements, then high frequency g_m is in error. Another way of stating this problem is to ask whether the large-signal bias-dependent model reduces to the small-signal equivalent circuit at low power levels. This implies that not only derivatives of the channel current must be correct, but all bias-dependent components must reduce to their small-signal values. To encourage the channel current to reduce properly, Golio et. al. [48] uses a weighted combination of the g_m and g_{ds} (output conductance) from high frequency S-parameter measurements and I_{ds} from DC measurements in their optimization with good results. Obviously, there must be some tradeoff between fit to DC measurements and fit to high frequency measurements.

A second method of extraction considers the DC model components and AC model components simultaneously [41, 47]. Here not only can the DC and high frequency component of the channel current be considered coupled, but all model components may be considered. Therefore forward conduction of the gate-source and gate-drain diodes may be considered as well a the extrinsic model parameters. In this method, a larger set of data is used that consist of DC and S-parameter measurement at multiple bias points and frequencies. This large set of data improve the uniqueness of the solution [47] that plagues optimization problems. Breaking the optimization into multiple stages [40, 41] also helps in obtaining physically meaningful parameter values. Practical examples of this extraction with simulation results and measurements can be found in [49, 50, 51].

Finally a third MESFET extraction method considers large-signal harmonic power data. The previous method considers only data based on small-signal quantities, such as S-parameters, which is determined by the reactive model components and first derivatives of the current sources. No attention is given to the higher-order derivatives that determine the harmonic response as well as the intermodulation response. Bandler [52] proposed to use the harmonic output power data along with

S-parameter measurements and DC I-V data. His success was good, but the time of the optimization only becomes practical when analytic adjoint methods are used to compute derivatives. This makes it difficult to incorporate many models. Regardless, this method is able to determine model parameters that govern high-order effects in MESFETs. Other work that investigates high-order effects of the channel current that is not based on large-scale optimization is Maas and Neilsen [30]. In this work the derivatives of Ids with respect to gate-source voltage are compared to measured DC derivatives. It was noted that the Curtice cubic model does not correctly portray derivatives above first order, but other models were not examined. It has been our experience that the modified Materka-Kacprzak model can follow the DC derivatives to at least fourth-order. More work is needed in this area since extraction based on measured DC derivatives is much more efficient than large-scale optimization procedures.

Methods of Improving Convergence

Improving the convergence properties of nonlinear circuits has been a popular topic since pre-SPICE days. Three methods were mentions in the harmonic balance section of this paper: Analytic Jacobian, Newton damping factors and continuation methods. Two more topics are presented here that further improve convergence and are relatively new.

Parametric Modeling

The Newton-Raphson update method uses the Taylor series to expand the harmonic balance error system and truncates the series after the linear term. In highly nonlinear systems the higher-order terms can dominate and successive locally linear approximations may not converge to the root. Continuation methods and small damping factors may not improve the situation. Circuits where diodes are heavily forward driven are good examples and, in fact, the diode expressions in FETs and BJTs are often the culprits that limit convergence. If the highly nonlinear diode conduction current could be re-formulated such that it is a linear function of the state variable, then it is resonable to assume convergence should improve. Indeed this is the basis of parametric modeling. Since FETs and BJTs contain diodes, they too can be reformulated in terms of the new diode state variable and receive improved convergence characteristics.

Consider the well-known diode equation:

$$i(t) = I_s\,(e^{\alpha v_j(t)} - 1) \tag{54}$$

From [53] the state variable becomes a fictitous quantity that is identical to the junction voltage below some threshold. Imposing the restriction that the diode current and voltage and their derivatives must be continuous, the new expressions are:

$$v(t) = \begin{cases} V_1 + \dfrac{1}{\alpha}\ln(1 + \alpha(x(t) - V_1)) \\ \\ x(t) \end{cases} \tag{55}$$

$$i(t) = \begin{cases} I_s\, e^{\alpha V_1}(1 + \alpha\,[x(t) - V_1]) - I_s \\ \\ I_s(e^{\alpha v_j(t)} - 1) \end{cases} \tag{56}$$

where the threshold, V_1, is determined by setting the derivative of (54) with respect to V_j, to one. The other nonlinear diode components (e.g. diffusion capacitance) use the diode voltage. Since reverse breakdown is also a highly nonlinear effect, it too can use its own parametric model variable. A numerical example will be discussed in the next section.

Norm Reducing Methods

Most harmonic balance implementations determine the criteria for convergence using the l_2 (Euclidean) norm. That is, from equation 1.1-14, $||\mathbf{E}||_2 < \text{tol.}$ where tol is the maximum allowed error. Some update schemes require that

$$||\mathbf{E}||_2^{(n)} < ||\mathbf{E}||_2^{(n-1)} \tag{57}$$

where n is the iteration number. The problem is that the direction of the update in multi-dimensional space may not coincide with the steepest-descent direction and may be skewed as much as 90 degrees [54] in which (57) becomes difficult to satisfy. In cases where the Jacobian as large non-symmetric off-diagonal terms, the skew is generally 90 degrees. This happens often with nonreciprocal gain elements such as FETs and BJT's [29] and worsens with cascaded stages. If the Jacobian is computed numerically, the skew may even be greater in which case no degree of damping will satisfy (57). A different norm, proposed by Yeager [54] and first implemented into

the harmonic balance method by Rizzoli [29] helps alleviate this problem by aligning the steepest-descent and Newton-update directions is:

$$\| E(X^{n+1}) \|_{NU} = \| J(X^n)^{-1} E(X^{n+1}) \|_{L2} \tag{58}$$

This norm is termed the NU norm for Newton-update. The salient feature of the NU norm is that the residual errors are weighted by the inverse Jacobian which tends to emphasis particular elements in the state variable vector according to their distance from the solution point. In this way, the state variables that are furthest from the solution point are updated according to their relative sensitivity. The damping factor can then be chosen to satisfy (57) by methods such as parabolic minimum.

An example to illustrate parametric modeling and norm reduction is taken from [29]. Here, a three FET distributed amplifier is excited by three tones at increasing power but without source stepping (that is, all harmonics are reset to zero at each new power). The small-signal gain of the amplifier is 5dB and has a 1dB compression point of 20dBm output power. The analysis was carried out with an intermodulation order of four. Reference [55] can be viewed for the schematic, if desired. Figure 18 illustrates the number of iteration neccessary for adequate convergence for combinations of parametric modeling, norm reduction and conventional modeling. Note the tremendous increase in power-handling capabilities with both parametric modeling and norm reduction. For this case input powers of 100dBm are possible to analyze. This clearly illustrates the improved convergence capabilities that are desired for simulation and optimization discussed next.

Circuit Optimization

Circuit optimization, as used here, is the problem of finding the values of a chosen set of circuit components to satisfy a desired set of circuit responses. The topology and choice of circuit components is determined by the designer and not the optimization program. With this in mind, let us define the values of the set of circuit component as **P** and the desired set of circuit responses as **RD**. In a nonlinear frequency-domain analysis, the circuit responses typically consist of network parameters such as transducer gain, return loss, spectral purity, etc., but can also be other specialized responses such as harmonic matching. An error vector can then be formulated as the difference between the computed response, RC, and the desired response, **RD**. If the function is an inequality, e.g. gain > 10db, then no contribution is made when the inequality is satisfied. The error vector **G**, also known as the design criteria, is defined as follows:

$$G_i(P) = w_i (RD_i - RC_i(P)) \tag{59}$$

Where w_i is the weight assigned to the i'th design criteria.

There are two different approaches taken in nonlinear optimization problems. The original approach by Rizzoli [2] solves the circuit state variable unknowns **X** simultaneously with the circuit component values **P**. This will be called *Combined Optimization*. The second approach decouples the state variables and circuit variables and will be called *Decoupled Optimization*.

Combined Optimization

In the combined optimization approach, the harmonic state variables *and* circuit component values form the vector of unknowns to be found. The criteria imposed are the solution of the harmonic balance equations *and* satisfaction of the design criteria. The problem can then be stated as:

$$F_{OB}(X,P) = \left\{ \| E(X,P) \|^p + \sum_i G_i(X,P)^p \right\}^{1/p} \tag{60}$$

where $||*||$ is the norm. Because this system is generally not square (the number of circuit variables usually is not equal to the number of design criteria) equation (60) is minimized by a suitable minimization routine, such as Quasi-Newton minimization. In contrast to a system solving routine as Newton-Raphson, minimization is generally very slow to converge because the number of unknowns is large. The derivatives of F_{ob} are required and are generally computed by numerical perturbations, making each iteration expensive. There have been methods proposed in the literature [5] to make the derivative calculations analytic using adjoint techniques, but these have not been implemented in commercially available simulators.

Note that equation (60) is formulated at a single frequency spectra rather than over a bandwidth as in linear circuit optimization. The state variable vector X contains

the state variables for one analysis spectrum. The specification of design criteria over a frequency bandwith (or power band, bias range, etc.) is not computationally feasible with the combined optimization approach. This limitation is one of the major drawbacks of this approach.

There are, however, some unique qualities of the combined optimization that are not available in regular analysis or decoupled optimization. These include analysis of circuits exhibiting bifurcations, and optimization of oscillators. Because the design criteria is coupled with the system state variables, restrictions can be placed on the system to move the state from one numerically stable solution to a different one, if it exists. As referenced in [6], a parametric frequency divider has several numeric solutions. These solutions were obtained by imposing the design criteria of improved efficiency and starting from the previous solution. This result could not be obtained by regular analysis of the circuit without proper starting conditions. Although the combined optimization technique cannot find all valid numerical solutions without the designer having knowledge of the circuit, it does provide a tool which allows analysis of circuits with bifurcations.

Decoupled Optimization

Decoupled optimization treats the circuit optimization problem separate from the harmonic balance analysis. In this method, the optimization of a nonlinear circuit proceeds analagous to that of linear circuit optimization. That is, the optimizer determines new values of the circuit components P and then analyzes the circuit with P. The solution of the harmonic balance equations becomes a nonlinear sub-problem to the optimization. Needless to say, the optimization is heavily dependent on the convergence of the harmonic balance problem. If the harmonic balance problem fails to converge, the optimization will terminate or, perhaps, try another step. The methods used in the previous section on improving convergence are needed to make the decoupled optimization method feasible for a wide variety of circuits.

The least-pth objective function used for decoupled optimization is:

$$F_{OB}(P)=\begin{cases}\left\{\sum_{i,f}^{+} G_{i,f}(X(P),P)^{p}\right\}^{1/p} \\ \\ -\left\{\sum_{i,f} -G_{i,f}(X(P),P)^{-p}\right\}^{-1/p}\end{cases} \qquad (61)$$

where G_{max} as the maximum error in G and + indicates that only positive errors are summed. The derivatives of (61) can be computed in a pure analytic form using adjoint techniques [55, 56], but it is usually more practical to compute them in a semi-analytic form as done in Microwave Harmonica. The derivative of (61) is

$$\frac{dF_{OB}}{dP_j}=\left(\sum_{i,f}(G_{i,f})^{p}\right)^{\frac{1-p}{p}}\left(\sum_{i,f}(G_{i,f})^{p-1}\frac{dG_{i,f}}{dP_j}\right) \qquad (62)$$

$$\frac{dG_{i,f}}{dP_j}=\frac{\partial G_{i,f}}{\partial P_j}-\frac{\partial G_{i,f}}{\partial X}J^{-1}\frac{\partial E}{\partial P_j} \qquad (63)$$

In (63), all terms except J are determined numerically, but in such a way that is efficient. Several partial results can be computed at the solution of the regular harmonic balance computation to make the numerical derivatives efficient.

Notice that the outer summation of (61) is over the set of frequency spectra. This is possible in decoupled optimization because the optimizer does not care about the system state variables and therefore the number of unknowns is very small compared to the combined optimization problem. In fact, the error vector G and the derivative matrix of G can be formulated at each frequency spectra independently of all other frequency spectra. Therefore optimization of the design criteria can take place over arbitrary frequency bands. Actually, each frequency band can have a set of design criteria independent of other frequency bands. This may be extended to power bands and bias ranges, if desired. The architecture of decoupled optimization forms a power tool in the design of arbitrary nonlinear circuits.

The advantages of decoupled optimization are clear, but this method cannot be used for all nonlinear circuit optimization probelms. It is best suited for non-autonomous (forced) circuits that are not dependent on bifurcations for their normal mode of operation. This includes a wide range of circuits such as amplifiers, mixers, frequency multipliers, etc.. The optimization of oscillators using search and analysis

methods presented in a preceeding section have not been investigated. It would appear feasible based on the robustness of the oscillator analysis. If the optimizer were constrained to take small steps at each iteration so the analysis mode could be used, then the efficiency would be improved.

For an example of decoupled optimization, consider the single FET mixer schematically shown in Figure 19. This basic circuit was initially designed for the input matching section to be alternating capacitances and inductances of 1pF and 1nH respectively. These were transformed to microstrip line components of open stubs for the capacitances and high impedance series lines for the inductances at 8GHz. The output filter was simply a low-pass design for the IF frequency of 500MHz. The circuit was then optimized using a Quasi-Newton gradient minimizer with the parameters marked by an arrow being allowed to vary. The design criteria was given as the following:

From 3GHz to 10GHz:	Conversion Gain > 10dB	weight = 10
	LO Power at IF Port < -20dBm	weight = 1
	Return Loss of LO > 15dB	weight = 1
	Return Loss of RF > 15dB	weight = 1

The gradient optimizer was allowed to continue untill it could not improve. The original and optimized response is shown in Figure 20. Notice that not all design criteria were met, but this is due to the simple topology. Because the design criteria were too demanding for this circuit, the same problem would not work in the combined optimization method where both the design criteria and harmonic balance error must be met for a valid result. Even for this very rough initial design, the outcome with decoupled optimization is very good.

Other types of optimization can be used with the decoupled method. For example, optimization using a gaussian random optimization routine was used with the initial point being the solution of the gradient optimizer. The routine was allowed to execute for 100 trials and the best result is also shown in Figure 20. Although this type of optimization takes considerable CPU time, it has the capability of getting out of local minima in which a gradient optimizer may become trapped. For this problem, the random optimizer took 150 CPU minutes on a Sun SparcStation1.

Conclusion

In summary this paper touches many topics that have improved harmonic-balance based nonlinear CAD over the past four years. These improvements in solution methods, modeling and convergence and new techniques in multi-tone analysis, noise analysis, optimization and oscillator analysis have brought a set of tools to the fingertips of RF and microwave circuit designers that allow active circuit design before any breadboarding is done. Although not yet complete or as efficient as possible, these tools give designers the ability to say "what if" and have results very quickly at a low cost. As the nonlinear models improve and linear models account for various modal and coupling effects, the results of computer simulations will become more relied upon as necessary design aids.

In closing, it would be worthwhile to mention the areas that are still elusive to harmonic balance thechniques. The first is statistical yield and design centering. Although this topic has received some investigation [57], very little work has been done to determine the effectiveness of statistical nonlinear equivalent circuit models. Investigations into the physical geometrical properties are usually more worthwhile.

The analysis of circuits containing large numbers of nonlinear devices (e.g. greater than 100 FETs) under multi-tone excitation currently requires tremendous amounts of memory and CPU time. As microwave circuits become more complex and digital/analog circuits increase clocking speeds, this limitaion will become more restrictive.

Methods are not available to systematically identify modes of circuit operation. This means finding the stable states given a circuit and excitations. Some basic nonlinear circuits [58] undergo bifucations when a critical power is reached an begin sub-harmonic generation. Circuits may exhibit a series of bifurcations that eventually lead to chaotic (non-periodic) behavior. Currently, there is no method to determine the conditions that bifurcations occur, or given the conditions, determine the stable states. A similar issue is: given a numerically stable solution, is this solution physically stable? Rizzoli [6] has done significant work on this subject, but as yet this work has not been incorporated into a commercial simulator.

Finally, the tools presented deal with the analysis and optimization of nonlinear circuits but not with the design and systhesis. This is generally a much more difficult problem, but several tools are available as design aids and/or synthesis of linear networks. A set of design aids for various nonlinear circuits would be helpful.

Acknowledgements

The authors would like to thank Professor Vittorio Rizzoli for allowing us to use his extensive published work as the basis for this paper.

References

[1] L. W. Nagel, "SPICE2: A Computer Program to Simulate Semiconductor Circuits," Electronic Research Laboratory, University of California-Berkeley, Memo ERL-M520, 1975.

[2] V. Rizzoli, A. Lipparini, E. Marazzi, "A General-Purpose Program for Nonlinear Microwave Circuit Design", pg. 762-770, IEEE Trans. On Microwave Theory Tech., Vol. MTT-31 No. 9, September 1983.

[3] G. W. Rhyne, M. B. Steer and B. D. Bates, "Frequency Domain Nonlinear Analysis Using Generalized Power Series," IEEE Trans. on Microwave Theory and Tech., vol. MTT-36, pp. 379-387, Feb. 1988.

[4] C.-R. Chang and M. B. Steer, "Frequency-Domain Nonlinear Microwave Circuit Simulation Using the Arithmetic Operator Method," IEEE Trans. on Microwave Theory and Tech., vol. MTT-38, pp. 1139-1143, Aug. 1990.

[5] V. Rizzoli, C.Cecchetti, A. Lipparini, and F. Mastri, "General-Purpose Harmonic Balance Analysis of Nonlinear Microwave Circuits Under Multitone Excitation", pg. 1650-1660, IEEE Trans. On Microwave Theory Tech., Vol. MTT-36 No. 12, December 1988.

[6] V. Rizzoli, and A. Neri, "State of the Art and Present Trends in Nonlinear Microwave Microwave CAD Techniques", pg. 343-365, IEEE Trans. On Microwave Theory Tech., Vol. MTT-36 No. 2, February 1988.

[7] L.O Chua and A. Ushida, "A switching-parameter algorithm for finding multiple solutions of nonlinear resistive circuits", pg. 215-239, International Journal Circuit Theory and Appl. Vol. 4, 1976.

[8] D. Hente and R.H. Jansen, "Frequency-domain continuation method for the analysis and stability investigation of nonlinear microwave circuits", pg. 351-366, IEE Proceedings, Vol. 133, Pt. H, No. 5, October 1986.

[9] R.G. Hicks and P.J. Khan, "Numerical Analysis of Nonlinear Solid-State Device Excitation In Microwave Circuits", pg. 251-259, IEEE Trans. On Microwave Theory Tech., Vol. MTT-30, March 1982.

[10] K.S. Kundert, G. Sorkin, and A. Sangiovanni-Vincentelli, "An Almost-Periodic Fourier Transform for use with Harmonic Balance", pg. 717-720, IEEE MTT-S Int. Microwave Symp. Dig., June 1987.

[11] K.S. Kundert, G. Sorkin, and A. Sangiovanni-Vincentelli, "Applying Harmonic Balance to Almost-Periodic Circuits", pg. 366-378, IEEE Trans. On Microwave Theory Tech., Vol. MTT-36 No. 2, February 1988.

[12] V. Rizzoli, C. Cecchetti and A. Lipparini, "A General-Pupose Program for the Analysis of Nonlinear Microwave Circuits Under Multitone Excitation by Multidimensional Fourier Transform," 17th European Microwave Conf. Dig., pp. 635-640, Sept. 1987.

[13] V. Rizzoli et. al., "Intermodulation Analysis of Microwave Mixers by a Sparse-Matrix Method Coupled with the Piecewise Harmonic-Balance Technique,"20th European Microwave Conf. Dig., pp. 189-194, Sept. 1990.

[14] C.R. Chang, P.L. Heron, and M.B. Steer, "Harmonic balance and frequency-domain simulation of nonlinear microwave circuits using the block Newton method," IEEE Trans. Microwave Theory Tech., pp. 431-434, Apr. 1990.

[15] V. Rizzoli, F. Mastri, F. Sgallari, and V. Frontini, "The exploitation of sparse-matrix techniques in conjunction with the piecewise harmonic-balance method for nonlinear microwave circuit analysis," in 1990 IEEE MTT-S Int. Microwave Symp. Dig., pp. 1295-1298, May 1990.

[16] S. Hamilton, "Microwave oscillator circuits," Microwave Journal, pp. 63-84, Apr. 1978.

[17] R.J. Trew, "Design theory for broad-band YIG-tuned FET oscillators," IEEE Trans. Microwave Theory Tech., vol. MTT-27, pp. 8-14, Jan. 1979.

[18] R.J. Gilmore and M.B. Steer, "Nonlinear circuit analysis using the method of harmonic balance - a review of the art: part II, Advanced concepts," Int. J. of Microwave and Millimeter Wave CAE, vol. 1, pp. 159-180, Apr. 1991.

[19] F. Sterzer, "Analysis of GaAs tunnel diode oscillators," IEEE Trans. Electron Devices, vol. ED-12, pp. 242-245, May 1965.

[20] K. Solbach, "Simulation study of harmonic oscillators," IEEE Trans. Microwave Theory Tech., vol. MTT-30, pp. 1233-1237, Aug. 1982.

[21] B.D. Bates and P.J. Khan, "Stability of multifrequency negative-resistance oscillators," IEEE Trans. Microwave Theory Tech., vol. MTT-32, pp. 1310-1318, Oct. 1984.

[22] K. Kurokawa, "Some basic characteristics of broadband negative resistance oscillator circuits," Bell System Tech. J., vol. 48, pp. 1937-1955, July 1969.

[23] C.R. Chang, Computer-Aided Analysis of Nonlinear Microwave Analog Circuits using Frequency-Domain Spectral Balance, CCSP, Dept. of Electrical and Computer Engineering, NCSU, 1990.

[24] D. N. Held and A. R. Kerr, "Conversion Loss and Noise of Microwave and Millimeter-Wave Mixers: Parts 1 and 2: Theory and Experiment," IEEE Trans. Microwave Theory Tech., vol. MTT-26, pp. 49-61, Feb. 1978.

[25] V. Rizzoli, F. Mastri and C. Cecchetti, "Computer-Aided Noise Analysis of MESFET and HEMT Mixers," IEEE Trans. Microwave Theory Tech., vol. MTT-37, pp.1401-1410, Sept. 1989.

[26] R. A. Pucel, "A Model for Flicker Noise in MESFETs," MIMIC Report MIM-1-9-91, Jan. 1991.

[27] H. Statz, H. Haus, R. A. Pucel, "Noise Characteristics of Gallium Arsenide Field-Effect Transistors," IEEE Trans. Electron Devices, vol. ED-21, pp. 549-562, Sept. 1974.

[28] U. L. Rohde, "Enhanced Microwave Discontinuity and Noise Models for Linear Simulators," to be published.

[29] V. Rizzoli et. al., "State-of-the-Art Harmonic-Balance Simulation of Forced Nonlinear Microwave Circuits by the Piecewise Technique," to be published.

[30] S. A. Maas and D. Neilson, "Modeling MESFETs for Intermodulation Analysis of Mixers and Amplifiers," 1990 IEEE Microwave Theory Tech. Symp. Dig., pp 1291-1294.

[31] W. R. Curtice and M. Ettenberg, "A Nonlinear GaAs FET Model for Use in the Design of Output Circuits for Power Amplifiers," IEEE Trans. Microwave Theory Tech., vol. MTT-33, pp. 1383-1393, Dec. 1985.

[32] M. A. Khatibzadeh and R. J. Trew, "A Large-Signal, Analytic Model for the GaAs MESFET," IEEE Trans. Microwave Theory Tech., vol. MTT-36, pp. 231-238, Feb. 1990.

[33] R. R. Pantoja et. al., "A Large-Signal Physical MESFET Model for CAD and its Applications," 1989 IEEE Microwave Theory Tech. Symp. Dig., pp 573-576.

[34] W. R. Curtice, "Intrinsic GaAs MESFET Equivalent Circuit Models Generated from Two-Dimensional Simulations," IEEE Trans. CAD, vol. 8, no. 4, pp. 395-402, April 1989.

[35] T. M. Barton and C. M. Snowden, "Two-Dimensional Numerical Simulation of Trapping Phenomena in the Substrate of GaAs MESFETs," IEEE Trans. Electron Devices, vol. ED-37, no. 6, pp. 1409-1415, June 1990.

[36] J. W. Bandler, Q. J. Zhang and Q. Cai, "Nonlinear Circuit Optimization with Dynamically Integrated Physical Device Models," 1990 IEEE Microwave Theory Tech. Symp. Dig., pp. 303-306.

[37] E. Reese and J. M. Beall, "Optimized X & Ku Band GaAs MMIC Varactor Tuned FET Oscillators," 1988 IEEE Microwave Theory Tech. Symp. Dig., Session Q1.

[38] H. Cho and D. E. Burk, "A Simple Model for Distributed Base Impedance with AC Verification using S-parameter Measurements," 1990 IEEE Bipolar and Circuits Technology Meeting, pp. 106-109.

[39] I. E. Getreu, Modeling the Bipolar Transistor, Tektronics, Inc., Beaverton, OR, 1976.

[40] J. A. Seitchik, C. F. Machala and P. Yang, "The Determination of SPICE Gummel-Poon Parameters by a Merged Optimization-Extraction Technique," 1989 IEEE Bipolar and Circuits Technology Meeting, pp. 275-278.

[41] Compact Scout User's Manual, Compact Software Inc., Paterson, NJ 07504, 1991.

[42] W. R. Curtice, "A MESFET Model for Use in the Design of GaAs Integrated Circuits," IEEE Trans. Microwave Theory Tech., vol. MTT-28, no. 5, pp. 448-456, May 1980.

[43] A. Materka and T. Kacprzak, "Computer Calculation of Large-Signal GaAs FET Amplifier Characteristics," IEEE Trans. Microwave Theory Tech., vol. MTT-33, no. 2, pp. 129-135, Feb. 1985.

[44] H. Statz et. al., "GaAs FET Device and Circuit Simulation in SPICE," IEEE Trans. Electron Devices, vol. ED-34, no. 2, pp. 160-169, Feb. 1987.

[45] A. McCamant, G. D. McCormack and D. H. Smith, "An Improved GaAs MESFET Model for SPICE," IEEE Trans. Microwave Theory Tech., vol. MTT-38, no. 6, pp. 822-824, June 1990.

[46] G. Dambrine et. al., "A New Method for Determining the FET Small-Signal Equivalent Circuit,"IEEE Trans. Microwave Theory Tech., vol. MTT-36, no. 7, pp. 1151-1159, July 1988.

[47] J. W. Bandler et. al., "Integrated Model Parameter Extraction Using Large-Scale Optimization Concepts," IEEE Trans. Microwave Theory Tech., vol. MTT-36, no. 12, pp. 1629-1638, Dec. 1988.

[48] M. Miller et. al., "Choosing an Optimum Large-Signal Model for GaAs MESFETs and HEMTs," 1990 IEEE Microwave Theory Tech. Symp. Dig., pp. 1279-1282.

[49] J. Gerber and R. Gilmore, "Active Device Parameter Extraction for Oscillator Simulation," 1989 WESCON Conference Record, pp. 83-87.

[50] M. Eron, J. Gerber, L. Mah and W. Tompkins, "MESFET Model Extraction and Verification Techniques for Nonlinear CAD Applications," 1990 Asia-Pacific Microwave Conference, pp. 321-324.

[51] M. Eron and J. Gerber, "Simulation and Modeling Techniques Applied to an Optimum 18.5GHz DRO Design," 1991 RF Expo West, pp. 429-435.

[52] J. W. Bandler et. al., "Efficient Large-Signal FET Parameter Extraction Using Harmonics," 1989 IEEE Microwave Theory Tech. Symp. Dig., pp. 577-580.

[53] V. Rizzoli, F. Mastri and C. Cecchetti, "A Highly Efficient p-n Junction Model for use in Harmonic-Balance Simulation," 19th European Microwave Conf. Dig., pp. 979-984, Sept. 1989.

[54] H. R. Yeager and R. W. Dutton, "Improvement in Norm-Reducing Newton Methods for Circuit Simulation," IEEE Trans. CAD, vol. 8, no. 5, pp. 538-546, May 1989.

[55] V. Rizzoli, A. Costanzo and C. Cecchetti, "Numerical Optimization of Broadband Nonlinear Microwave Circuits," 1990 IEEE Microwave Theory Tech. Symp. Dig., pp. 335-338.

[56] J. W. Bandler, Q. J. Zhang and R. Biernacki, "A Unified Theory for Frequency-Domain Simulation and Sensitivity Analysis of Linear and Nonlinear Circuits," IEEE Trans. Microwave Theory Tech., vol. MTT-36, no. 12, pp. 1661-1668, Dec 1988.

[57] J.W. Bandler et. al., "Statistical Modeling of MESFETs," 1991 IEEE Microwave Theory Tech. Symp. Dig., pp. 87-90.

[58] M. I. Sobhy, N. A. Butcher and A. A. A. Nasser, "Chaotic Behaviour of Microwave Circuits," 19th European Microwave Conf. Dig., pp. 363-368, 1989.

[59] Microwave Harmonica User's Manual, Compact Software, Inc. 483 McLean Blvd, Paterson, NJ 07504.

[60] V. Rizzoli et. al., "Pulsed-RF and Transient Analysis of Nonlinear Microwave Circuits by Harmonic-Balance Techniques," 1991 IEEE Microwave Theory Tech. Symp. Dig., pp. 607-610.

Linear Component Calculation	Nonlinear Component Calculation: Time Domain	Nonlinear Component Calculation: Frequency Domain
Time Domain	Direct Integration Shooting Methods Extrapolation Methods	
Frequency Domain	Harmonic Balance Sample Balance	Volterra Series Generalized Power Series Arithmetic Operator Method

Table 1. Nonlinear analysis types arranged by domain.

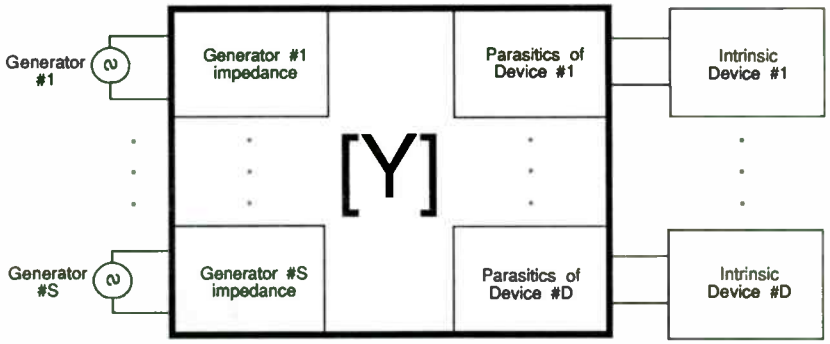

Figure 1. Augmented Port Admittance Matrix [Y]

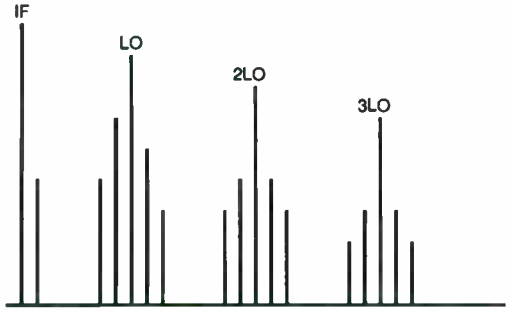

Figure 2. 2-tone Mixer Spectrum
(3 LO harmonics, 2 sidebands)

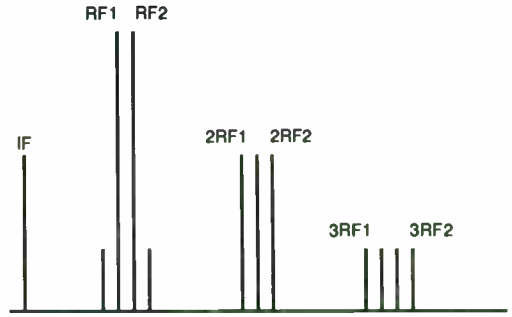

Figure 3. 2-tone Intermodulation Spectrum
(3rd Order Intermodulation)

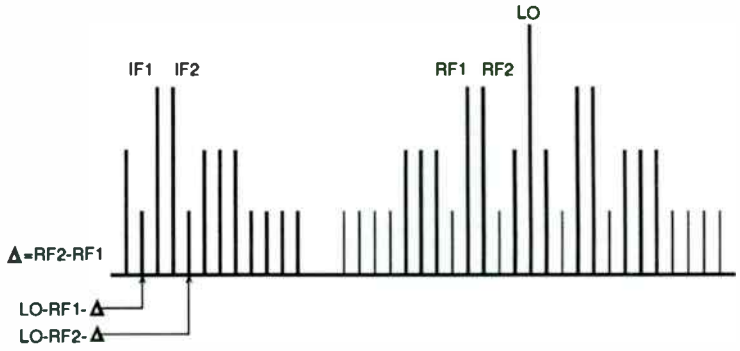

Figure 4. 3-tone Mixer Spectrum
(1 LO harmonic, 3rd Order Intermodulation)

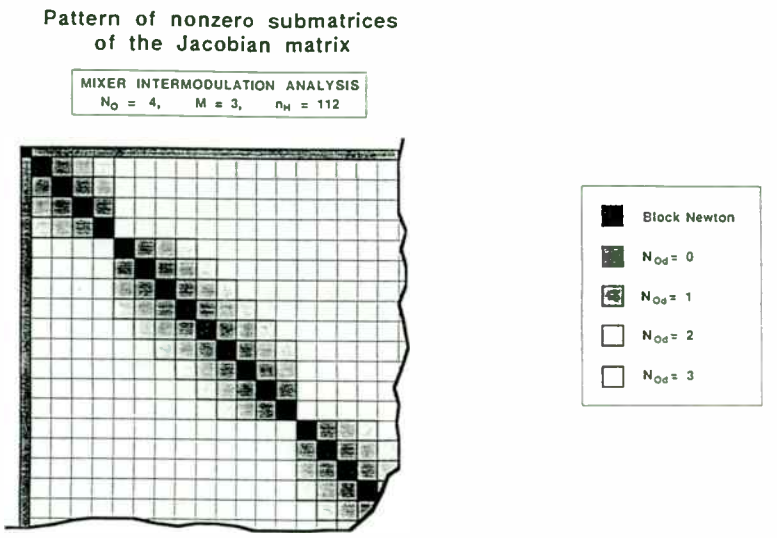

Figure 5. Sparse Jacobian Structure. Nod is the block with of the diagonal.

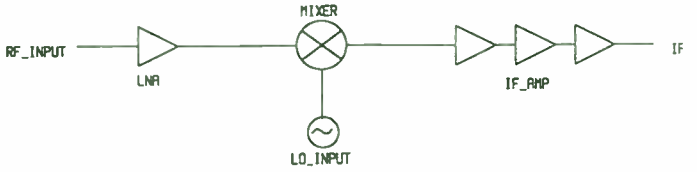

Figure 6. Block diagram of receiver front-end. This circuit is analyzed with two-tone mixer analysis.

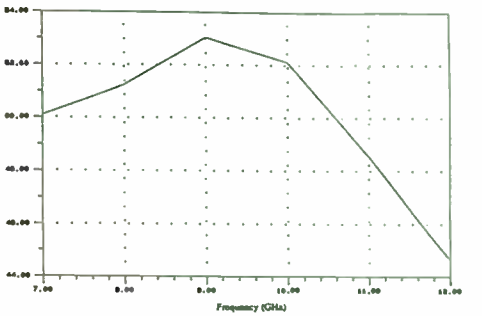

Figure 7. Frequency sweep of front-end showing conversion gain.

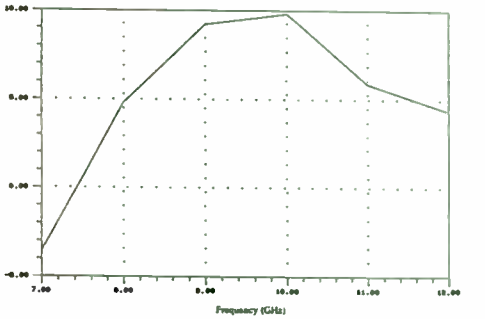

Figure 8. Power sweep of input RF signal showing compression of conversion gain.

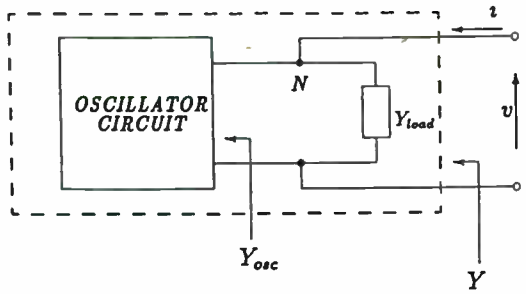

Figure 9. One-port equivalent circuit of an oscillator circuit.

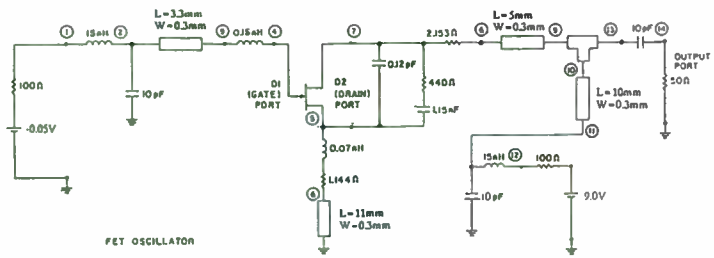

Figure 10. FET oscillator circuit topology.

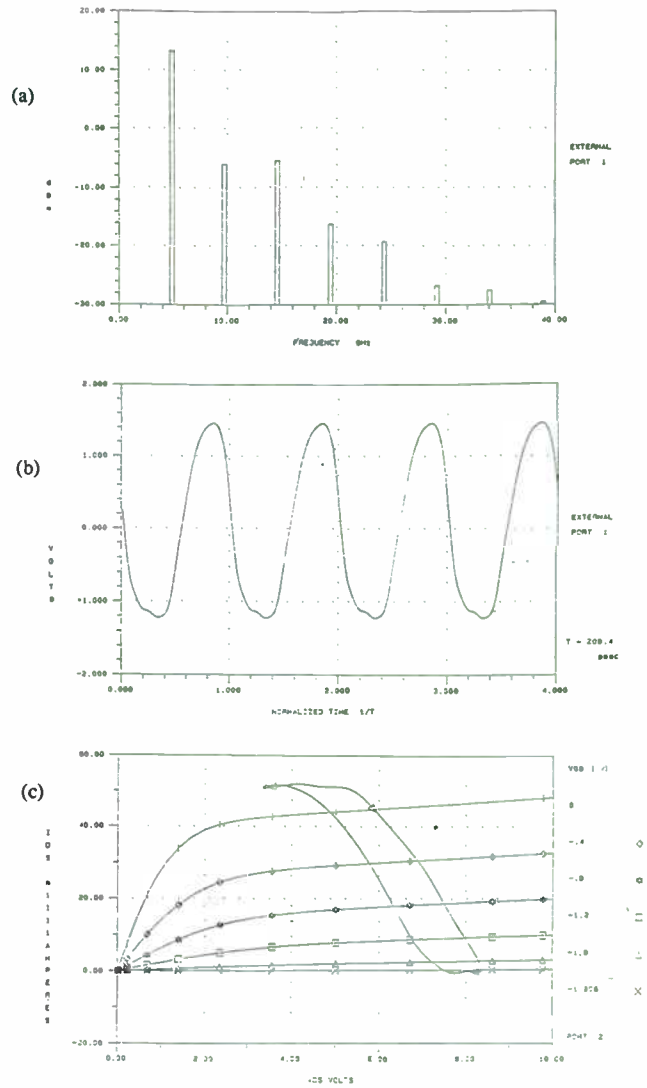

Figure 11. Output of oscillator: (a) Output power spectrum, (b) voltage waveform across load, (c) phase plane of FET.

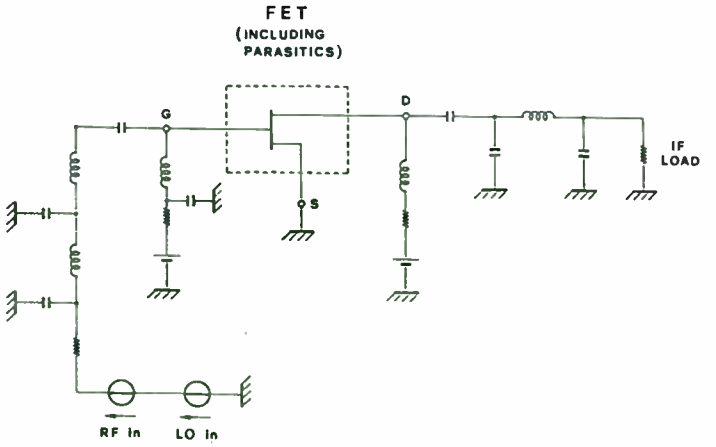

Figure 12. FET mixer topology (from[25]).

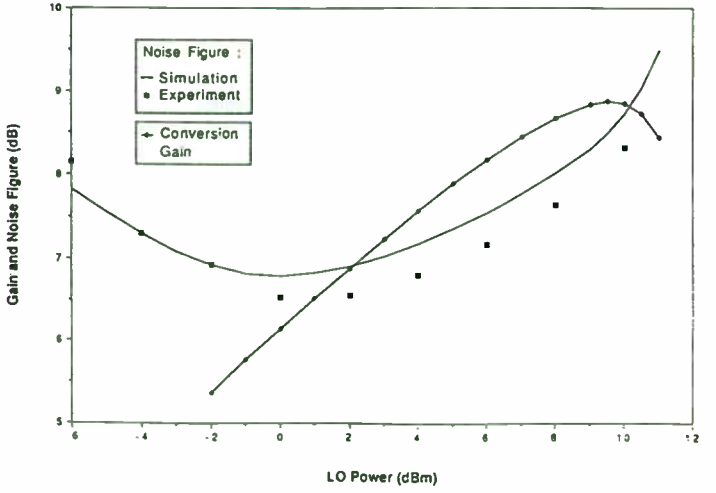

Figure 13. Conversion gain and noise figure of mixer as a function of LO drive (from [25]).

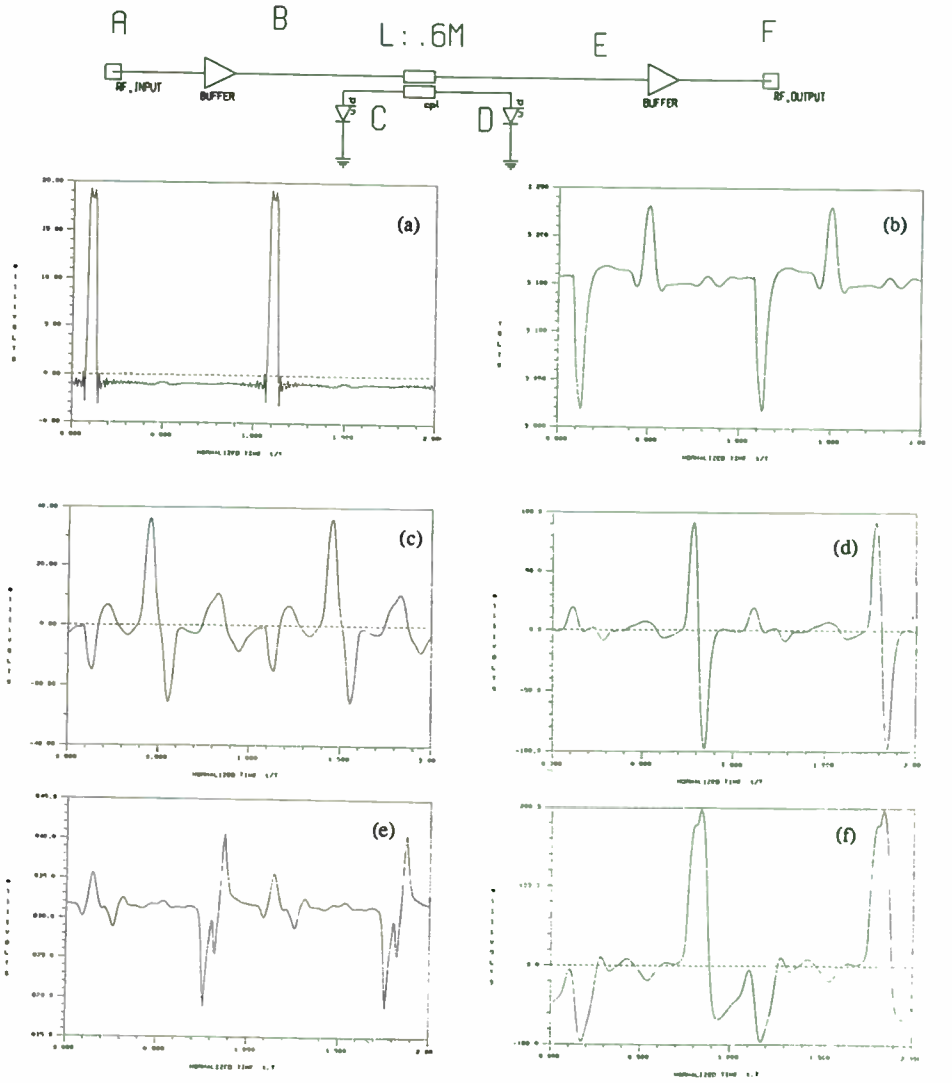

Figure 14. Buffered line driver excited with a pulse train whose period is 5 nS. Voltage waveforms at key circuit points marked by letters on schematic. Structure is 60 cm long, lossy and dispersive.

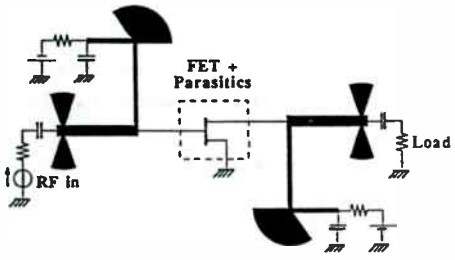

Figure 15. FET amplifier topology (from [60]).

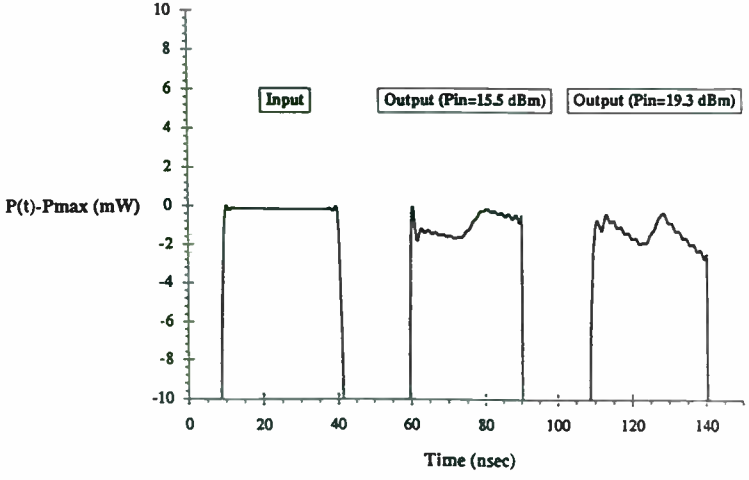

Figure 16. Output power envelopes of modulated RF pulse for 15.5dBm input power and 19.3dBm input power.

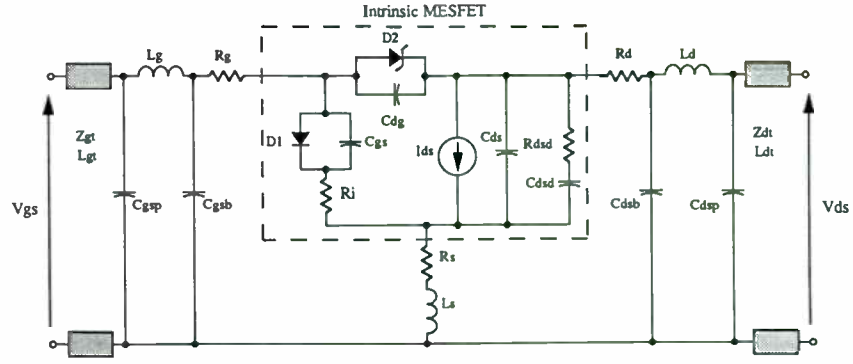

Figure 17. Equivalent MESFET model of intrinsic device embedded in chip and package parasitics.

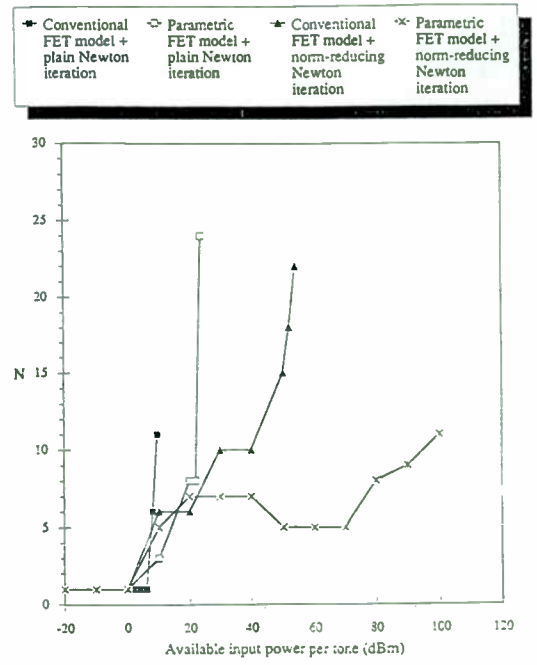

Figure 18. Iteration number vs. input power per tone into a distributed amplifier (from [29]).

Figure 19. Single FET mixer topology used in the broadband optimization.

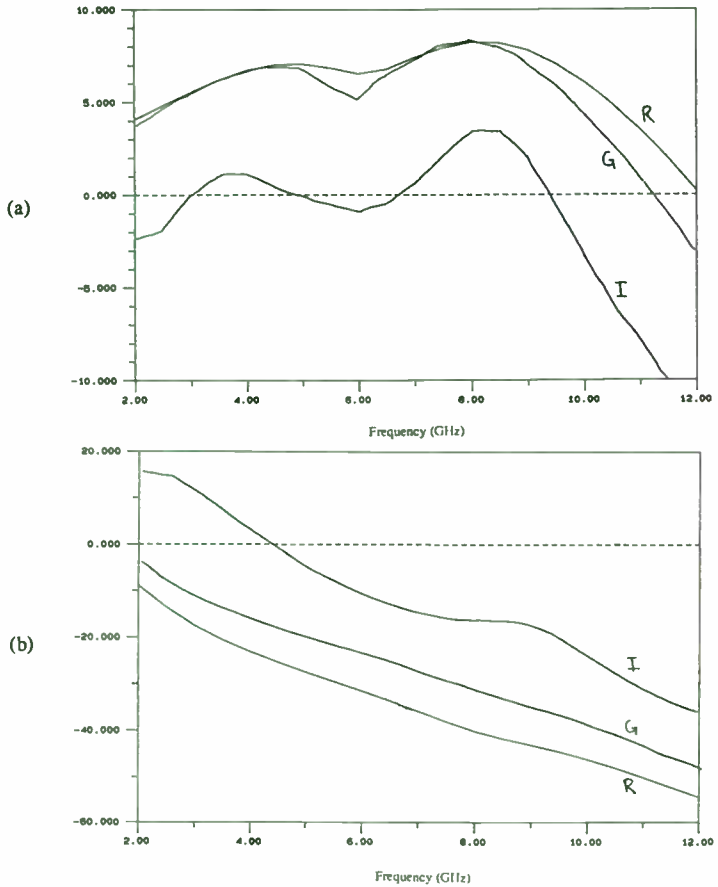

Figure 20. Initial design, Gradient optimized, and Random optimized response. (a) Conversion gain (dB (b) LO power at IF port (dBm).

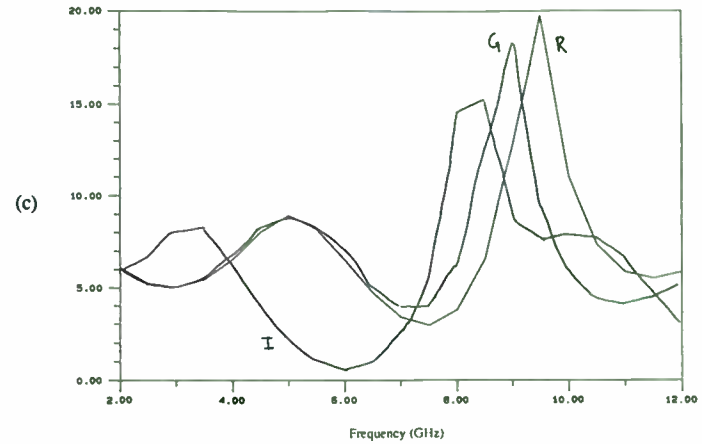

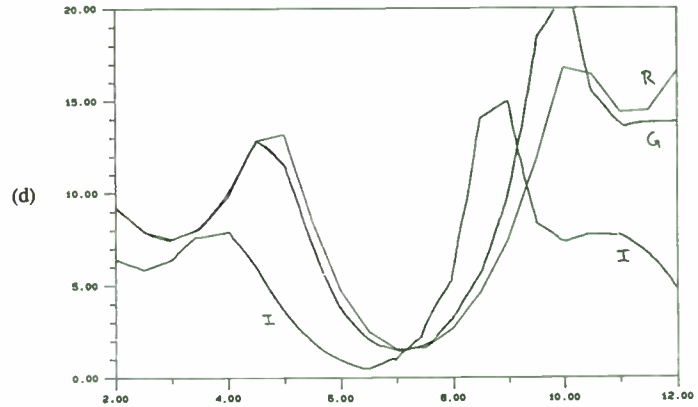

Figure 20 con't. (c) RF return loss (dB). (d) LO return loss (dB).

NEW NONLINEAR NOISE MODEL FOR MESFETs INCLUDING MM-WAVE APPLICATIONS

Ulrich L. Rohde and Raymond S. Pengelly
Compact Software, Inc.
483 McLean Boulevard
Paterson, New Jersey, 07504, USA

Abstract

This paper shows a linearized time-domain approach for calculating the dynamic elements of the hybrid Pi, MesFET model. These elements in the traditional linear model have been used to calculate the noise correlation matrix. The model then supplies the required four-noise parameters: F_{min}, G_{opt}, and R_n. A novel enhancement to the basic equivalent circuit guarantees its use into the MM-wave area. This enhancement consists of an additional time delay in the drain source conductance G_{ds}. This approach has been incorporated into a simulator for the purpose of verification.

I. Introduction

Noise analysis of linear circuit has been available ever since the introduction of the noise correlation matrix [1]. The noise theory for linear circuit is now well understood and implemented. In the practical world, we are dealing with circuits which require nonlinear analysis. Typical cases are the combination of amplifiers, mixers, and oscillators in subsystems. The present day harmonic balance programs are beginning to have noise analysis capabilities under large signal conditions. This is done at the expense of slow computation and occasional difficulties with conversions. The calculation of the Jacobian matrix and necessary Fourier transformations are both time consuming and can be mathematically unstable. The approach shown in this application uses a combination of a linear program and a nonlinear model. It can be extended to be used in HB-programs. By calculating the nonlinear behavior of the element of a GasFET model, depending on the terminal voltage, the element values of the FET equivalent circuit are a function of the large signal drive level. A variety of papers [2, 3, 4] already have dealt with noise analysis in nonlinear circuits, but have only addressed the noise analysis at the lower frequency range and did not have the ability to determine the noise correlation coefficients for external use. The influence of flicker noise and gate noise was not considered.

II. Obtaining a Model

In many cased the manufacturer does not supply the actual hybrid Pi model for the FET chip but provides a set of S-parameters for the chip as a function of bias. The traditional approach for obtaining the equivalent circuit is to use a dedicated fitting program or a linear simulator for the purpose of fitting S-parameters calculated from a hybrid Pi model to the measured S-parameters. In practice, it turns out that the fitting to the S-parameters alone is insufficient and that the additional constraint, fitting it to the measured stability factor K and the maximum available gain (MAG) is also necessary. The advantage of this method is that the values of the element determined for the equivalent circuit are realistic and are not just the result of an optimization procedure. An additional sanity check can be done by determining the minimum noise figure Fmin from the calculation of the input circuit of the hybrid Pi model, and comparing this to the measured minimum noise figure at a particular frequency. This approach has been quite successful up to 26 GHz. Figures 1-4 show the result of such fittings. Above 26 GHz, and well into the MM-wave area, $MAG(Y_{22})$ shows an increase in value which cannot be modeled with the traditional equivalent circuit. In order to make provision for this effect, an additional delay similar to the one G_{ds} used in describing G_m has to be introduced to RDS which then allows to describe this phenomenon sufficiently accurate. Fig. 5 shows calculated and modeled response as verification, and Fig. 6 shows the enhanced e.g. circuit.

The output of the curve fitting program, including those enhancements, then results in an equivalent "noisy" intrinsic chip FET which can be used as the basis for determining the 4-noise parameters (F_{min}, G_{opt}, and R_n). Using the conventions by Statz, Haus, and Pucel [5], the noise correlation matrix does not consider the flicker noise contribution, which has been added to the actual implementation. In taking those parameter values, the FET description shown in Table 1 allows to compute the small signal noise performance of Figures 7, 8.

These are the starting conditions for the noise modeling.

III. Large Signal Approach

A nonlinear large-signal model of the FET will be used with practical circuitry to predict its performance. The validity of this model was established by its success in predicting the large-signal mixing and oscillating performance of an FET embedded in an actual circuit [6].

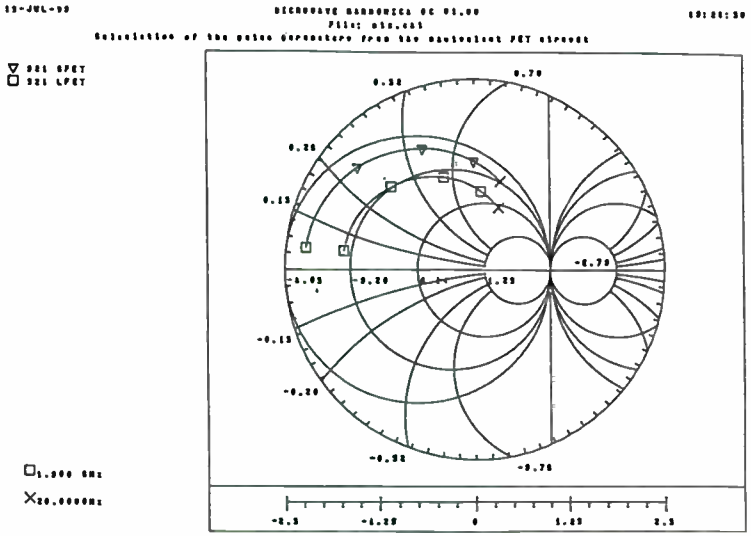

Figure 1

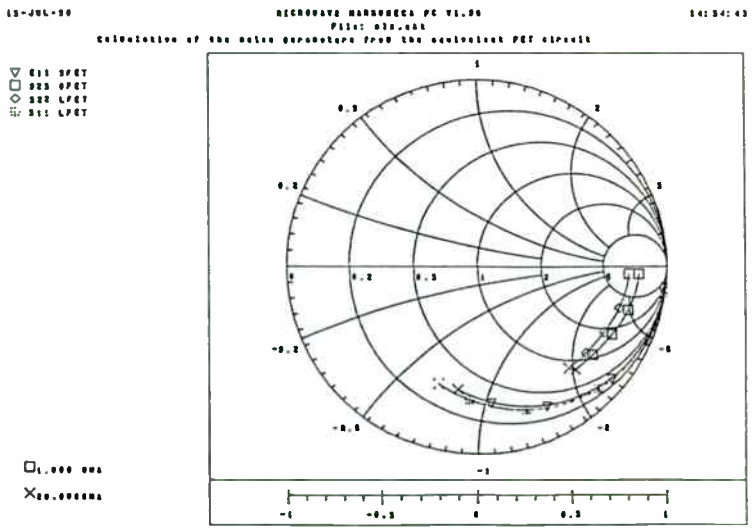

Figure 2

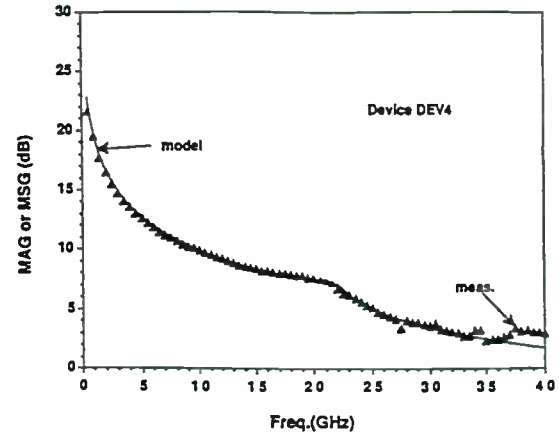

Fig. 3 Measured and Modeled MAG/MSG

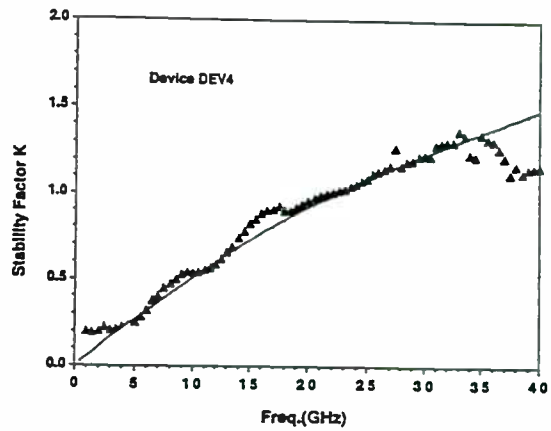

Fig. 4 Measured and Modeled Stability Factor

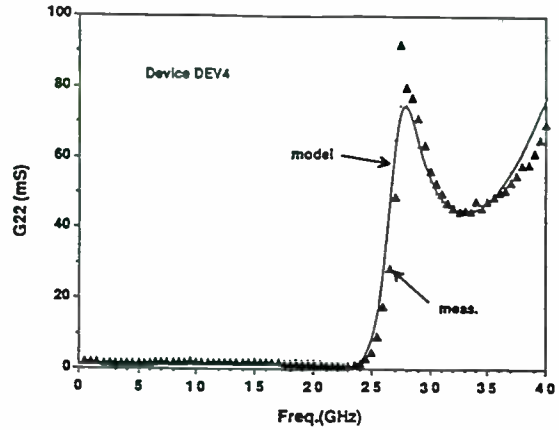

Fig. 5 Measured and Modeled Real Part of Y_{22}

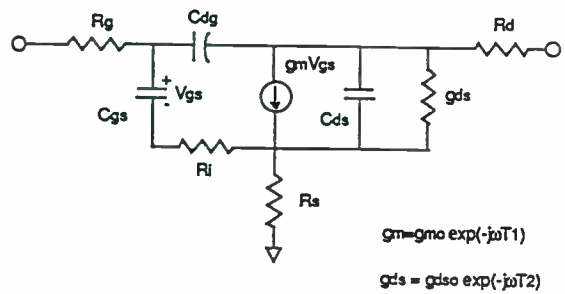

Fig. 6 New Linear Model of the FET Including Time Delay Factor in Output Conductance

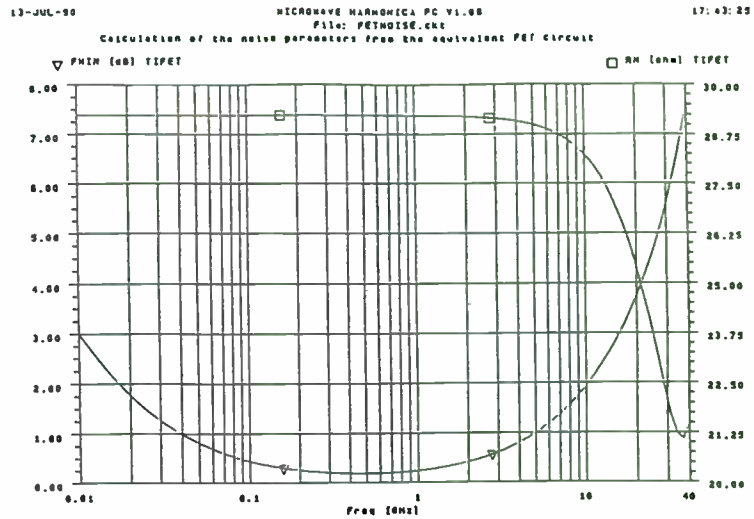

Figure 7

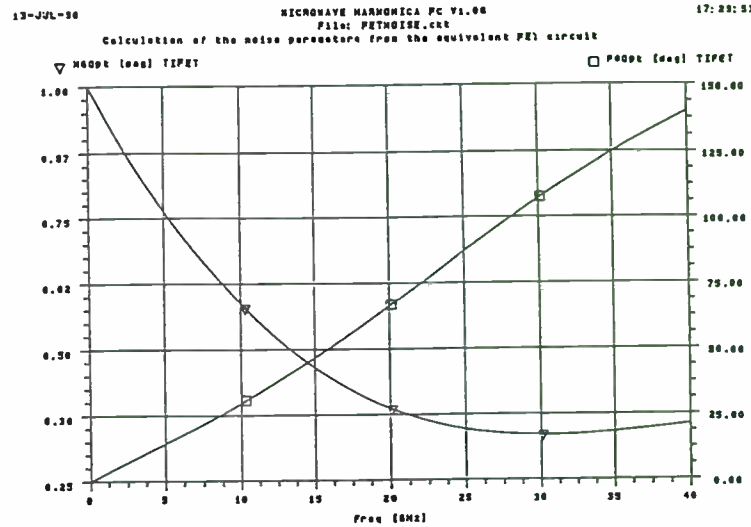

Figure 8

```
MICROWAVE HARMONICA PC V1.06  13-JUL-90  17:14:55  File: FETNOISE.ckt

 ********************************************************
 * TEXAS INSTRUMENTS INTERDIGITAL FET MODEL             *
 * WIDTH NORMALIZED TO 300 MICRONS (0.5 um gate length) *
 ********************************************************
21.63
 BLK
   FET 1 2 0 G=(.045*Z) CGS=(.3PF*Z) T=3E-12 CDG=(.02PF*Z) TJ=25CEL
+  CDS=(.125PF*Z) RG=(4/Z) RI=(4/Z) RS=(3.5/Z) RD=(3.8/Z) LS=.02NH
+  GDS=(.0029*Z) NRG=.3 NCG=.1 FC=10MHZ nfac=.5 TEMPC  TDS=3PS LD=.3NH
* fet drain pad
   TRL 2 3 W=2.9MIL P=.8MIL SUB1
 TIFET: 2POR 1 3
 END
 *
 FREQ
 STEP .1GHZ 40GHZ .2GHZ
 END
 *
 OUT
  PRI tifet s
 END
  *
data
sub1:as h=6mil er=12.9 metl=au 5um tand=0.0004
TEMPC: DTC
end
```

Table 1

The first step in this procedure is to establish the nonlinear behavior of the circuit and to obtain the correlation between it and the FET equivalent circuit. To do this, the FET is represented in terms of its equivalent circuit, as shown in Fig. 9. Under large-signal operation, the element values of the FET equivalent circuit vary with time because at large drive-levels they become dependent on terminal voltages. We may consider two of the terminal voltages to be independent and choose the set V_{gs} and V_{ds}, V_{gs} being the voltage across the gate capacitance and V_{ds} that across the drain conductance. If we restrict our interest to the signal frequency and ignore the effects due to higher harmonic components, these voltages can be written as

$$V_{gs} = V_{gso} + v_{gs} \cos(\omega t + \phi)$$
$$V_{ds} = V_{dso} + v_{ds} \cos \omega t \qquad (1)$$

where V_{gso} and V_{dso} are the dc bias voltages, v_{gs} and v_{ds} the amplitudes of signal frequency components, and ϕ the phase difference between the gate and drain voltages. The equivalent circuit for the signal frequency can now be expressed as a function of the following parameters, which are independent of time : V_{gso}, V_{dso}, v_{gs}, v_{ds}, ω, and ϕ.

To avoid unnecessary complexity of calculations, we limit the nonlinear behavior to five elements, gate forward conductance, G_{gf}, gate capacitance C_{gs}, gate charging resistance R_i, transconductance, g_m, and drain conductance G_d. This is justifiable. Here G_{gf} represents the effect of the forward-rectified current across the gate junction under large-signal operation. No voltage dependence was assumed for the parasitic elements, that is, the lead inductances (L_g, L_d, L_s) and contact resistance R_g, R_d, R_s). Also ignored was the small voltage dependence of the drain channel capacitance C_{ds} and feedback capacitance C_{dg} because of their small values.

Expressions for g_m and G_d

Transconductance g_m and drain conductance G_d are defined as

$$g_m = \left(\frac{i_{ds}}{v_{gs}}\right)_{V_{ds}=0} \quad G_d = \left(\frac{i_{ds}}{v_{ds}}\right)_{V_{gs}=0} \qquad (2)$$

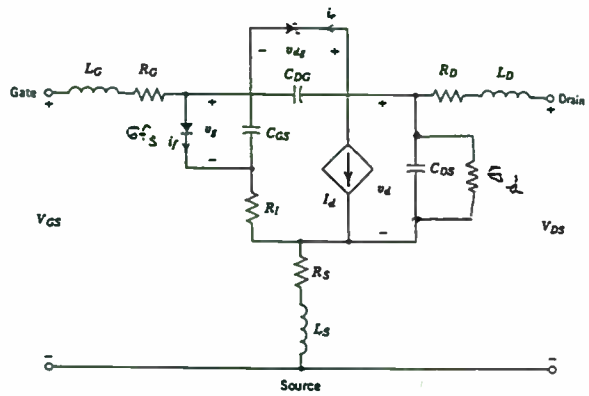

Figure 9

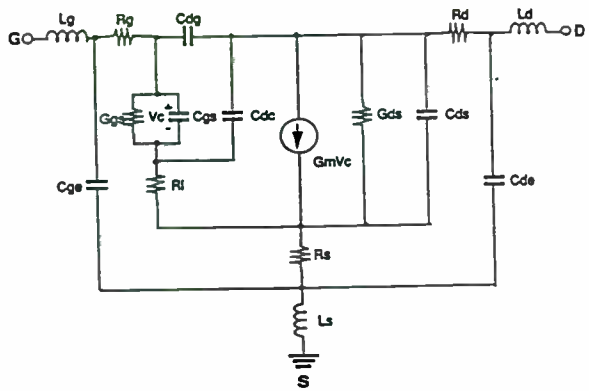

Figure 10

where i_{ds} is the RF drain current amplitude. The instantaneous drain current can be written in terms of g_m and G_d as

$$I_{ds}(t) = I_{dso} + g_m v_{gs} \cos(\omega t + \phi) + G_d v_{ds} \cos \omega t \qquad (3)$$

where i_{ds} is the dc drain current. This this expression linear superposition of the dc and RF/IF currents is assumed.

Now, if we have a function that can simulate the nonlinear dependence of the drain current I_{ds} on V_{gs} and V_{ds}, as

$$I_{ds} = I_{ds}(V_{gs}, V_{ds}) \qquad (4)$$

then under large-signal conditions, the instantaneous current $I_{ds}(t)$ can be obtained by inserting (1) into (4) by multiplying sin ωt by (3) and integrating over a complete period, g_m is obtained as

$$g_m = -\frac{\omega}{\pi v_{gs} \sin \phi} \int_0^{2\pi/\omega} I_{ds} \sin \omega t \, dt \qquad (5)$$

Similarly G_d is obtained as

$$G_d = \frac{\omega}{\pi v_{gs} \sin \phi} \int_0^{2\pi/\omega} I_{ds} \sin(\omega t + \phi) \, dt \qquad (6)$$

Equations (5) and (6) are now functions of RF amplitudes V_{gs} and V_{ds}, as well as of bias voltages V_{gso} and V_{dso}. We turn now to a more detailed discussion of the nonlinear relation (4).

The functional relation $I_{ds}(V_{gs}, V_{ds})$ was established empirically by simulating the dc I-V characteristics by a nonlinear function given by

$$I_{ds}(V_{ds},V_{gs}) = I_{d1}I_{d2}$$

$$I_{d1} = \frac{1}{k}\left\{1 + \frac{V'_{gs}}{V_p} - \frac{1}{m} + \frac{1}{m}\exp\left[-m\left(1 + \frac{V'_{gs}}{V_p}\right)\right]\right\}$$

$$I_{d2} = I_{dsp}\left\{1 - \exp\left[\frac{-V_{ds}}{V_{dss}} - a\left(\frac{V_{ds}}{V_{dss}}\right)^2 - b\left(\frac{V_{ds}}{V_{dss}}\right)^3\right]\right\}$$

$$k = 1 - \frac{1}{m}[1 - \exp(-m)]$$

$$V_p = V_{po} + pV_{ds} + V_\phi$$

$$V'_{gs} = V_{gs} - V_\phi$$

where V_{po} (>0) = pinch–off voltage at $V_{ds} \approx 0$

V_{dss} = drain current saturation voltage

V_ϕ = built–in potential of the Schottky barier

I_{dsp} = drain current when $V_{gs} = V_\phi$ (7)

and a, b, m and p are fitting factors that can be varied from device to device.

Nonlinear Expressions for C_{gs}, G_{gf}, and R_i

Although the gate junction is also a function of V_{gs} and V_{ds}, we assume here that it can be approximated by a Schottky barrier diode between gate and source, with V_{gs} as the sole voltage parameter. Gate capacitance C'_{gs} and forward gate current i_{gf} can be found from Schottky barrier theory as

$$C'_{gs} = \frac{C'_{gso}}{\sqrt{1 - V_{gs}/V_\phi}} \quad (-V_p \le V_{gs}) \tag{8}$$

or

$$C'_{gs} = \frac{C'_{gso}}{\sqrt{1 + V_p/V_\phi}} \quad (-V_p \ge V_{gs}) \tag{9}$$

$$i_{gf} = i_s \exp(\alpha V_{gs} - 1) \tag{10}$$

where C'_{gso} is the zero-bias gate capacitance, i_s the saturation current of the

Schottky barrier, and $\alpha = q/nkT$.

When V_{gs} varies according to (7), the effective gate capacitance C_{gs} and gate forward conductance G_{gf} for the signal frequency are obtained from (8)-(10) as

$$C_{gs} = \frac{1}{\pi v_{gs}} \int_0^{2\pi} \left(\int^{v_{gs}} C'_{gs} dv\right) \cos \omega t \, d(\omega t) \tag{11}$$

$$G_{gf} = 2i_s \exp(\alpha V_{gso}) \frac{I_1(\alpha v_{gs})}{v_{gs}} \tag{12}$$

where $I_1(x)$ is the modified Bessel function of the first order.

The gate-charging resistance Ri was assumed to vary in such a way that the charging time consistent was invariant, with bias.

$$R_i C_{gs} = \tau_i \text{ (constant)} \tag{13}$$

Thus all nonlinear element values of the equivalent circuit can be expressed in terms of terminal RF amplitudes and their relative phase. One may now determine more precisely all the values by an iteration method such as follows.

First, starting values for v_{gs} and the equivalent-circuit parameters are assumed. For the latter, small-signal values based on measured S parameters are suitable. With these parameters specified, the output voltage v_{ds} and its phase can be calculated in a straightforward manner. With the resultant value of v_{ds} , ϕ , and the initially assumed V_{gs}, the "first-cut" evaluation of the equivalent-circuit elements can be made with the help of (5), (6), and (11)-(13). The procedure above is then repeated, each time using the most recently evaluated values of v_{ds}, ϕ, and v_{gs}, until convergence is obtained. The process converges when successive iterations reproduce the equivalent circuit parameters to within some specified error.

Fig.10 shows the complete equivalent circuit diagram for the FET including all parasitics. The values for previously computed elements are being used, and the values in the noise correlation matrix

$$C^{Y}(\omega) = 4KT\Delta f \begin{bmatrix} \frac{\omega^2 C_g^2}{g_m} R & -j\omega C_g \sqrt{PRC} \\ j\omega C_g \sqrt{PRC} & g_m P \end{bmatrix} \qquad (14)$$

taken from [5] get substituted. This new noise correlation matrix is the basis for computing the noise of the nonlinear circuit. Fig. 11 shows a comparison of the small and large signal noise parameters as calculated from the previous expressions. The abbreviation S-FET refers to the small signal operation, while L-FET refers to the large signal operation. Figures 11 and 12 show the comparison of the large signal and small signal noise parameters of the FET chip.

These evaluations assume that the FET is pumped at the gate input as shown in Fig. 13. Another interesting application is applying the local oscillator at the drain electrode similar to the older Doherty plate modulation. Figure 14 shows the noise figure under the same working conditions for gate and drain pumping. The plot for drain pumping is labeled as M-FET.

Verification

Both a mixer and an oscillator were used for verification purposes. A standard single gate mixer was used consistent with the publication of Rizzoli [2]. The previously mentioned Fig. 13 shows the actual circuit diagram and Fig. 15 compares conversion gain and noise figure between measured and predicted results.

A modified Leeson model was used for the calculation of the phase noise of the oscillator, and Fig. 16 show the relationship between measured and predicted results.

Summary

By enhancing the equivalent circuit of a linear active device like a MesFET, even inside a linear program, it is possible to actually predict its performance under large signal conditions, provided that single-tone analysis is done. This means that the RF level is significantly below the LO drive

The same principle can be applied for an oscillator. An additional benefit from this is that the inherent noise analysis capability permits to

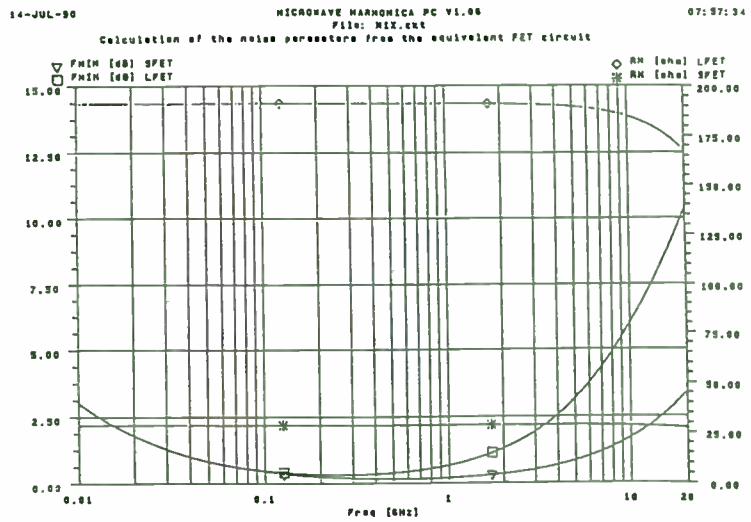

Figure 11

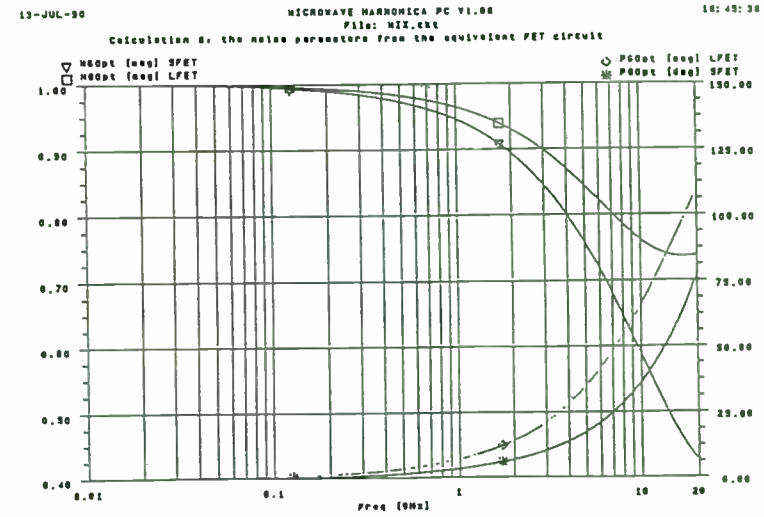

Figure 12

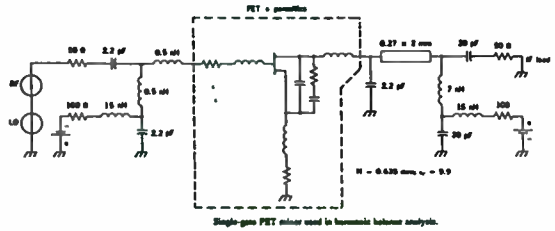

Figure 13

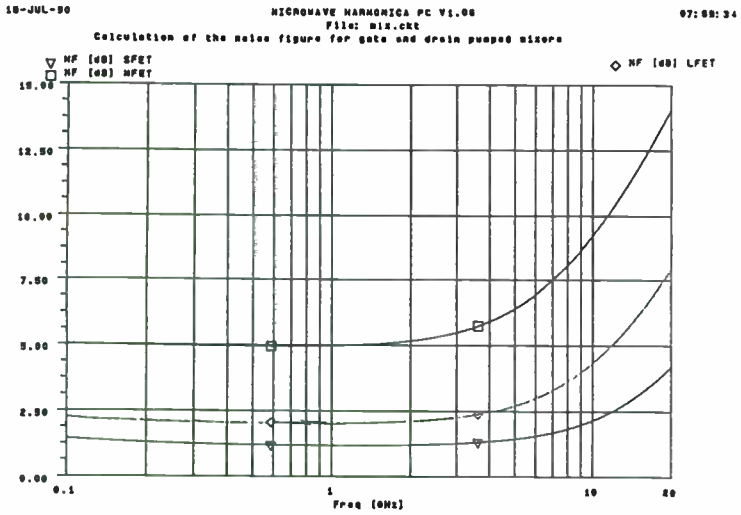

Figure 14

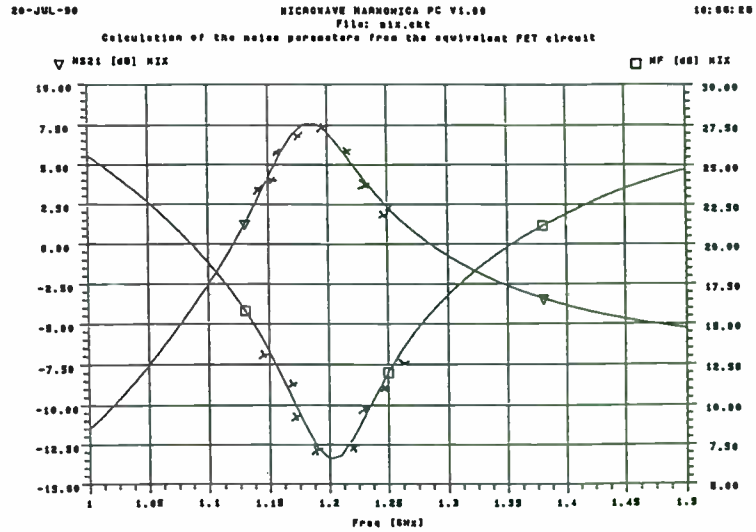

Figure 15

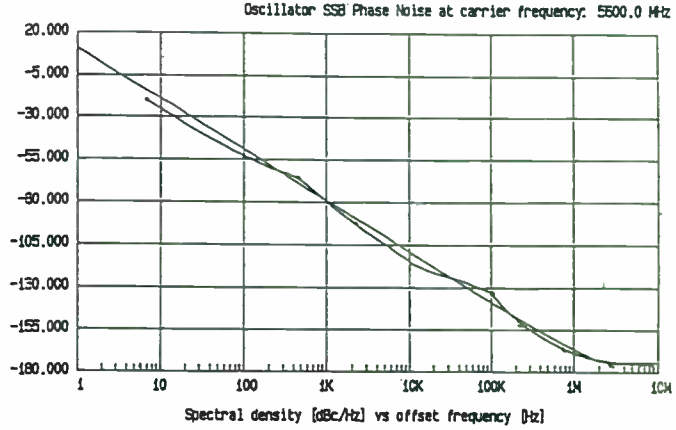

Figure 16

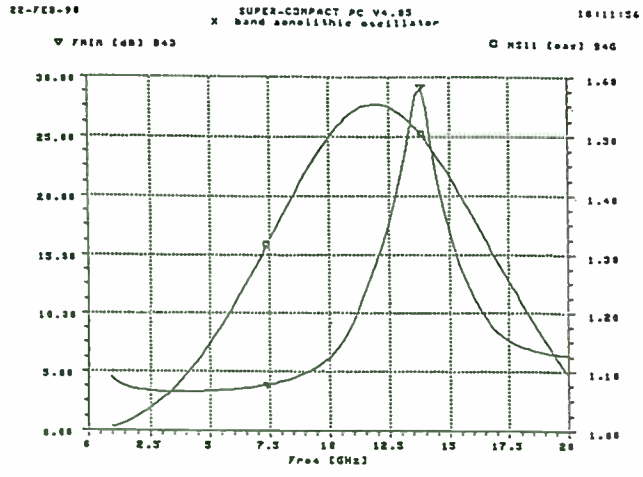

Figure 17

predict and allows to optimize a noise matching condition, even for oscillators. As figure 17 shows, the noise figure at the operating point, as an oscillator, has increased to 30 dB because the matching was done for best output power and not lowest phase noise. A re-design would have allowed an improvement of 30 dB in the signal to noise ratio.

By introducing a time-domain model which is linearized and assumes the time average values for the parameter of the equivalent circuit, the approach is probably sufficiently accurate predict the noise performance of a mixer and an oscillator, the working conditions apply to the fundamental frequencies. The next step is to introduce general purpose time domain model. The parameters extraction capacities for this purpose has to be enhanced before this is possible [7].

An additional side benefit of this method is the ability to optimize the phase noise of an oscillator by matching it to the best condition for low noise operation rather than highest loop gain. Initial tests have shown that an improvement up to 30 dB in the signal to noise ratio is possible.

References

[1] H. Hillibrand and P.H. Russer, "*An Efficient Method for Computer Aided Noise Analysis of Linear Amplifier Networks*, " IEEEE Trans. on Circuits and Systems, pp. 235-238 (April 1976).

[2] V. Rizzoli, F. Mastri and C. Cecchetti, "*Computer Aided Noise Analysis of MESFET and HEMT Mixers*" in IEEE Trans. Microwave Theory Tech., vol. MTT-37, 1989, pp. 1401-1410

[3] S. Heinen, R. Stahlmann, N. Haensel, S. Kosslowski, J. Kunisch, N.H.L. Koster and I. Wolff, "*Noise Analysis of Nonlinear Microwave Circuits*, Department of Electrical Engineering and Sonderforschungsbereich 254 Duisburg University, Bismarckstr. 69, D-4100 Duisburg West Germany.

[4] S. A. Mass, *Nonlinear Microwave Circuits*. Norwood, MA: Artech House, 1988

[5] R. A. Pucel, H. A. Haus, and H. Statz, "Signal and Noise Properties of GaAs FETs," *Advances in Electronics and Electron Physics*, V.38, Academic Press, New York (1975) pp. 195-265.

[6] G. D. Vendelin, A.M. Pavio, U.L. Rohde, *Microwave Circuit Design Using Linear and Nonlinear Techniques*, John Wiley & Sons, Inc., New York, 1990

[7] R. A. Pucel, W. Struble, Research Division, Raytheon Co., Lexington MA *"Proposed Models for the Noise Performance of the GaAs FET and the BiasTemperature Dependence of the Small-Signal Equivalent Circuit Parameters of the FET and Other MMIC Components,"* February 20, 1989.

Use of Yield Optimization Methods For Desensitization of Circuit Performance

Tianrong Zhang
Compact Software Inc. Paterson NJ
Murat Eron
M/A-COM, GMIC Operation, Burlington MA

ABSTRACT

Customarily designers put a large premium on getting the most performance out of their circuits. There may be times when that may not be the most desirable situation. In fact, if building enough parts that meet a given specification is of any concern then the designer should also be concerned with sensitivity of the final design performance to parameter variations, tolerance, and inaccurate modeling or measurement. It will be demonstrated how the newly developed design yield optimization methods can be used to render the circuit performance immune to variations and uncertainties in critical circuit parameters. A high performance RF amplifier design example is chosen where expected yield improvements of 100% is accomplished by desensitizing the design to known transistor parameter variations.

INTRODUCTION

Yield can be a consideration even when mass production of a circuit is not contemplated. Realizability is a requirement even when only a single part is to be produced. Typical circuit (performance) analysis and optimization methods offer very little clue about the possible sensitivity of the performance to variations and uncertainties of various design parameters. These uncertainties may arise as a result of poor process control, normal device-to device variations, and uncertainty of the CAD models used in the design.

As a first step, one needs to be able to calculate expected design yield for a given set of parameter tolerance [Ref.1]. This may not be very straightforward since the necessary data is very rarely available from manufacturers or foundries. It gets even more complicated for active devices. They are typically modeled with the use of a large number of parameters that need to be extracted from measurements and/or physical considerations. For sensitivity or yield analysis, statistics of these parameters also need to be known. This usually involves characterization of a large number of parts by the manufacturer and close monitoring of process parameters by the foundries.

Statistics of a set of parameters include means, distributions and more importantly for active devices, the correlations between the parameters. For a given manufacturing process, there are usually very few basic parameters that can be considered completely independent of each other. Since most of the circuit/device parameter variations are a result of fluctuations of these primary parameters, the disturbances of the circuit/device parameters may be strongly correlated and this needs to be

considered for accurate estimation of yield and/or sensitivities.

DESIGN AND SPECIFICATIONS

The design requirement was for a low noise amplifier for a cellular base station operating in the 1800Mhz band [Fig.1]. The performance requirements are shown in Table I. These specifications are somewhat contradictory and the most important specifications were the noise figure and the gain flatness. The design was also to be based on Siemens MESFET CFY25 due to other considerations. Even though this device had the required noise performance (FMIN=0.6db at 2Ghz) it was obvious that gain spec could not be met with a single device. More critically, it was extremely difficult to come up with a single ended configuration that could meet both the NF and VSWR requirements.

After much trial with various other topologies a balanced configuration was chosen which had the best chance of meeting the opposing performance requirements. Due to relatively narrow band of operation multiple section matching networks were avoided to simplify the design, biasing and manufacturing on standard alumina substrate.

Microstrip branchline couplers were used for input and output power splitting/combining. Two two-stage sections were combined this way, which included four transistors and a stabilizing shunt resistor. The resulting design had a minimum number of components and after final optimization the nominal response was within specification (see Fig.2).

STATISTICAL MODELING

The design procedure up to this point was mostly concerned with achieving the best nominal performance. Since some of the specs were only narrowly met, there was some concern about the sensitivity and realizability of this circuit. Most of the variation was expected to originate from the transistors, so all other circuit parameters were assumed to have zero tolerance. Since full statistical model of the device was not available, we assumed typical variations for the transistor parameters. These variations reflect a well controlled manufacturing process where FET channel doping variation is under 3%. Assuming this to be the major source of disturbance, all model parameter variations and their correlations were estimated using a physics-based device simulator. The nominal values of the equivalent small-signal model were determined from measured/published S-parameters.

Only small-signal model parameter variations that could not be estimated or modeled were those of the noise parameters. The published noise parameters were fitted to a broad-band noise model that is available in Super Compact. This enabled a very compact description of the full linear behavior of the transistor. Variations in the range of 10%

percent were assigned to all the noise parameters which includes typical measurement repeatability, inaccuracy, and device-to-device variation. The noise parameters were also considered to be statistically independent of each other.

YIELD ANALYSIS AND DESENSITIZATION RESULTS

A traditional Monte-Carlo statistical analysis was carried out on the performance optimized LNA design. The yield window was set by the NF, stability, gain, gainflatness, and VSWR requirements across the 1710-1785 Mhz band. For the given set of correlated statistical parameters the design yield was estimated to be 48%. It was also observed that most of the yield loss was attributable to out of spec gain flatness in-band stability and VSWR.

A yield optimization was carried out on the same circuit. It is important here to note that a full simulation based on Monte-Carlo yield optimization would have resulted in excessive CPU times and it would be impractical to do this for any type of circuit of realistic complexity. Response surface modeling [Ref.2 and Ref.3] employed in Super-Compact reduces the required number of full simulations dramatically. This method is based on fitting the circuit response as a function of all of the statistical and optimizable parameters (note that not all optimizable parameters are statistical and vice versa) to a multi-dimensional polynomial and then using this function for each iteration in the analysis optimization loop.

Aside from the small penalty paid in the initial setup and some sacrifice in the accuracy, the resulting model of the circuit response is much faster to calculate which reduces the overall CPU requirement dramatically.

For our example a total of 10 designables circuit parameters were subjected to design centering. These included transmission line lengths, capacitors, and resistors. The final yield after the optimization was up to 96.7%. This represents almost a 100% increase in the number of "good" circuits. Because the use of response modeling method, there are only 307 circuit simulations are needed during the yield optimization. This takes about 22 minutes CPU time on MV3500 computer. To achieve the same results without response model, over 30000 circuit simulations needed. This makes exact yield optimization almost impossible in practical sense. The nominal values of optimizable parameters before and after design centering are shown in Table 2.

DISCUSSION AND CONCLUSION

This increase in the design yield was achieves with only minor modifications of the design parameters. The largest parameter variation was about 5% and the design yield showed negligible or no sensitivity to half of the parameters included in the design centering. This means that the number

of potential good parts is doubled without any change in the topology, number and quality of the components used, or a major re-work of the artwork. Only a minor tuning of the designable parameters in essence desensitized the circuit performance (with only a negligible compromise of the theoretical optimum nominal performance, see Fig.3) to unavoidable or costly to control tolerances of the used parts or processes.

In conclusion, recent improvements in simulators have made it possible to carry out realistic and meaningful yield analysis and optimization of circuits of any complexity so that producibility issues can be addressed at the design stage where it is much more economical to do so.

REFERENCES

[1] J.W.Bandler and S.H.Chen, "Circuit optimization: the state of the art", IEEE Trans. Microwave Theory Tech., Vol. MTT-36,1988.

[2] P.Cox, P.Yang, S.S.Manhant-Shetti, and P.Chatterjee, "Statistical modeling for efficient parametric yield estimation of MOS VLSI circuits," IEEE Trans. Electron Devices, Vol. ED-32, pp 471-478, Feb. 1985.

[3] K.K.Low and S.W.Director, "An Efficient Methodology for Building Macromodels of IC Fabrication Processes", IEEE Trans. on Computer-aided Design. Vol.8, No. 12, pp. 1299-1313, Dec. 1989.

TABLE I

Circuit	Frequency Range	Performance	Specification
BAL_LNA	1710Mhz-1785Mhz	MS21	> 25.50 DB
		MS21	> 29.50 DB
		MS11	< -17.69 DB
		MS22	< -13.98 DB
		NF	< 1.55 DB
SING_LNA	1690Mhz-1820Mhz	MS11	< 0.00 DB

- Performance specifications for the low noise amplifier in the example.

TABLE II

Optimizable Parameters	Before Opt.	After Opt.
C1	0.80607 PF	0.82285 PF
P1	1.0103 CM	1.0223 CM
P2	1.9019 CM	2.0000 CM
C2	6.1130 PF	6.1555 PF
P3	0.31444 CM	0.32916 CM
R1	125.61 OH	126.23 OH
L1	5.0751 NH	5.0482 NH
P4	0.60343 CM	0.54514 CM
P5	1.1714 CM	1.2183 CM
C3	1.0165 PF	1.0207 PF

- Circuit optimizable parameters before and after yield optimization.

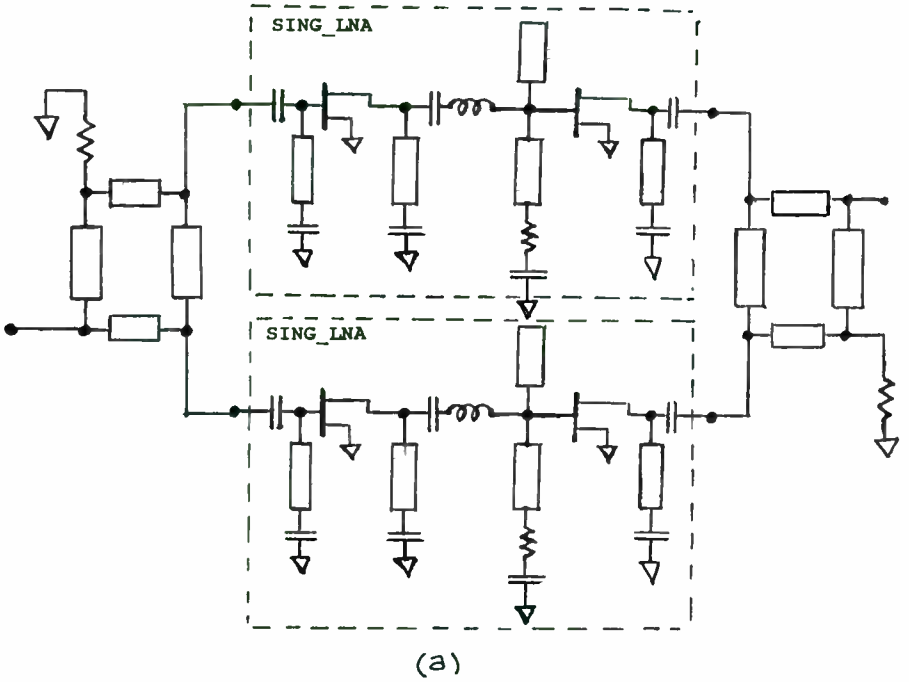

(a)

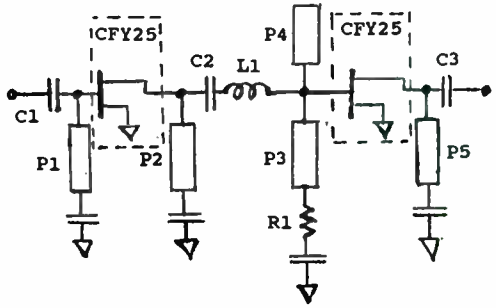

(b)

Fig.1(a) Schematic of circuit BAL_LNA, the low noise amplifier in the example.

(b) Schematic of subcircuit SING_LNA. C1-C3, P1-P5 and R1, L1 are optimizable parameters. Here letter C stands for capacitance, P for physical length of transmission line, R is resistance and L is inductance. Statistical variables have not been shown on the plot. They are the internal parameters inside the model CFY25.

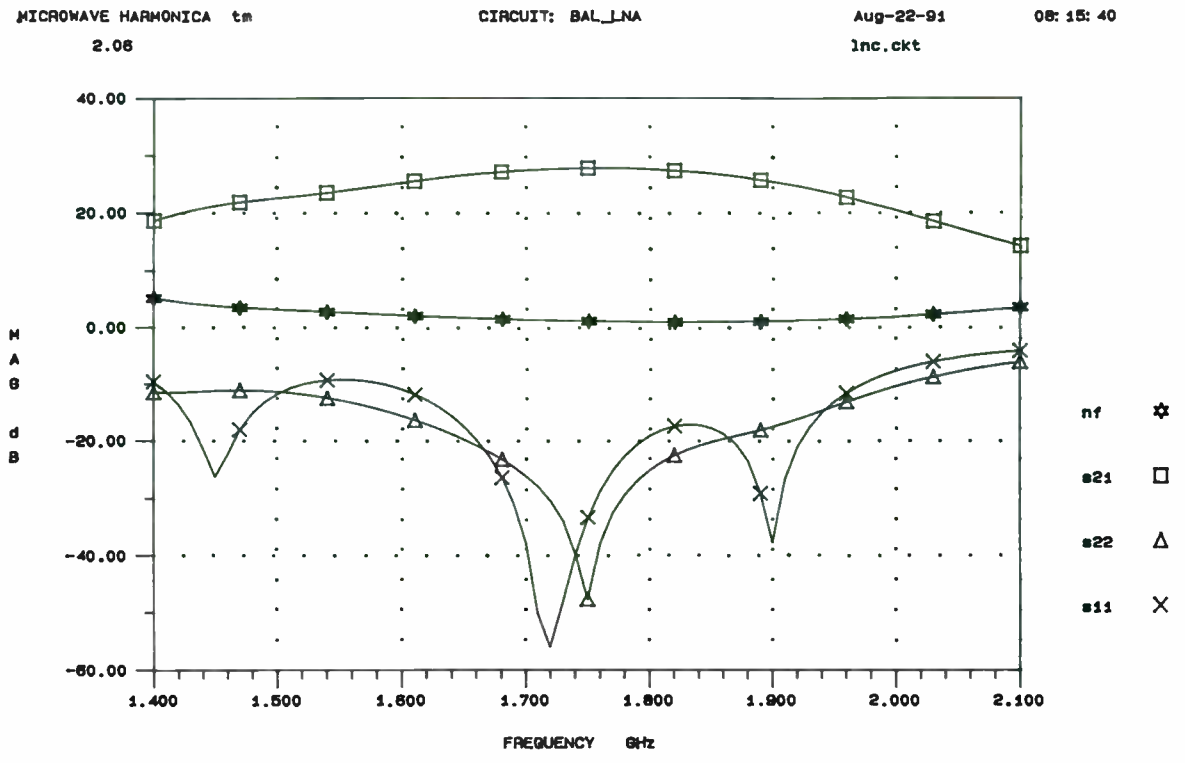

Fig.2 Nominal circuit performance before yield optimization.

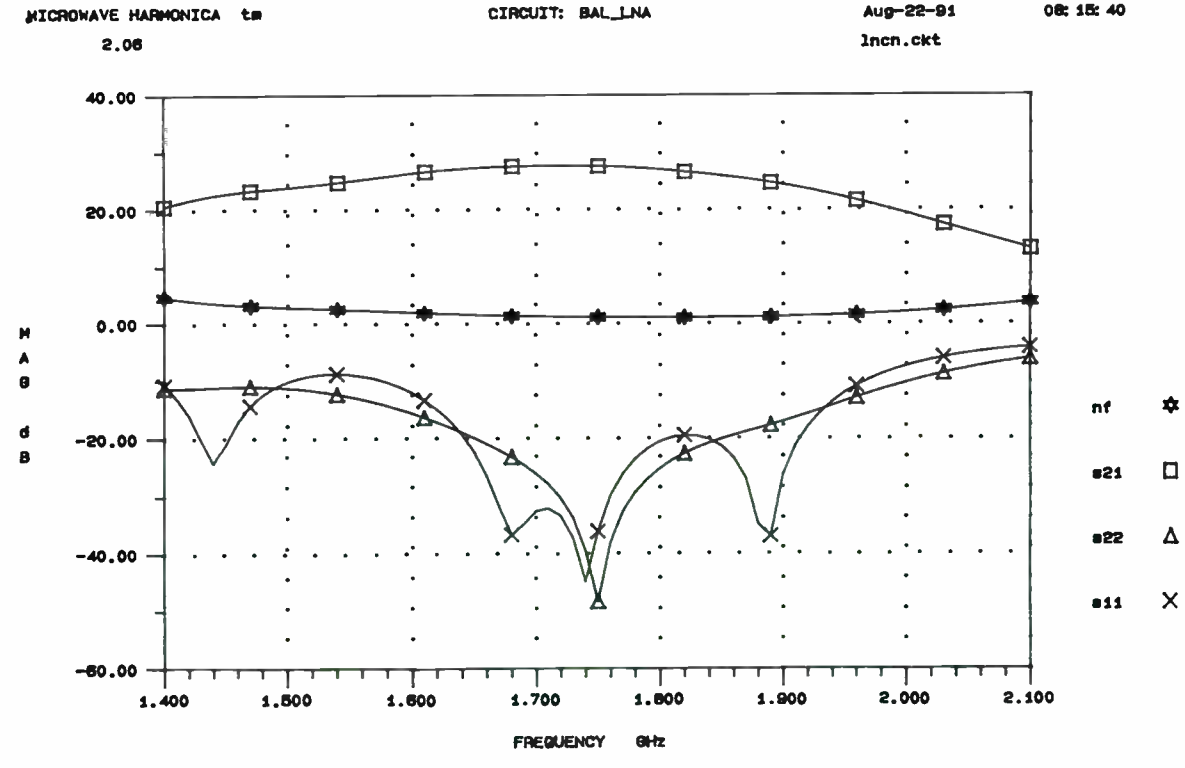

Fig.3 Nominal circuit performance after yield optimization.

System Simulation for RF and Microwave Communications Applications.

Raymond S. Pengelly and Ross G. Hicks,
Compact Software, Inc.,
483 McLean Boulevard,
Paterson, NJ, 07504, USA

Introduction

Recently, commercial system simulators have become available which allow system engineers unprecedented general access to relatively powerful CAD tools that address the problems of analyzing and optimizing subsystems and systems at the 'black box' level. This paper will refer specifically to two available simulators, Microwave Success from Compact Software and OmniSys from EEsof. After a description of the requirements for and the computations available from such simulators, two design examples are given - the first is that of a C-Band satellite TVRO double downconverter and the second is a complete digital terrestrial radio link.

Features of System Simulators

In the following we consider the general features of system simulators available today. The simulators described essentially calculate parameters in the frequency domain. A summary of the system simulator features are contained in Table 1.

1) *Definition of Component Parameters*

Unlike linear and nonlinear circuit simulators which analyze circuits on an element by element basis in a detailed manner, system simulators calculate the results of cascading and/or 'paralleling' linear and nonlinear 'black boxes' at the component level. These black boxes include amplifiers, mixers, oscillators, filters, path loss and antennas. It is possible, using 'frameworks' and databases to "link" the results of changes in component designs (using linear or nonlinear simulators) to the effects those changes have on system performance - an example of this is given later.

System simulators use the well known 'nodal' interconnection technique to define the system under investigation. Component parameters can be input to the simulator using either schematic capture and editing or netlist entry and editing. Schematic capture is to be preferred since it gives the user an easy-to-understand pictorial representation of the system, can be easily edited, is available for later documentation processes and allows the passage of information from one design engineer or department to another in an efficient and accurate way. An example of a schematic is that of the C-Band TVRO double downconverter produced using the Serenade schematic editor from Compact Software (Figure 1). The simplest component descriptions are those which are essentially frequency independent - whether the component definitions are entered via a schematic or a netlist. Such descriptions are usually ample for preliminary designs such as those required for development proposals. For example, an amplifier may be described by its gain, MS21=30dB; its noise figure, NF=3dB and its -1dB gain compression value, P1dB=20dBm. In this case other usual parameters are considered to be perfect - for example, the input and output VSWRs are 1:1, the reverse transmission coefficient is zero and the phase shift of the transmitted signal is zero degrees. Normally the simulator will assume that the output third order intercept point of the amplifier is related to the 1 dB gain compression point e.g. 10 dBm above the output gain compression point. Otherwise the user can define the third order intercept point related to the 1 dB compression point. It is more likely that the user will define the small and large signal parameters of the component in terms of s-parameters.

In some cases the simulator allows the use of 'generic' components such as filters. For example, a Chebyschev filter may be defined as :-

CBPF 1 2 N=7 RIP=0.25dB Fl=1GHz FU=1.5GHz QU=200

where a prototype filter having 7 sections, with 0.25 dB equi-ripple in the passband has a 0.25 dB bandwidth of 500 MHz centered at 1.25 GHz. The elements of the filter have unloaded quality factors of 200.

Mixers are defined using their usual properties such as conversion loss, noise figure etc.. In particular, types of mixers, such as single-ended, balanced, double-balanced and image rejection, can be defined. Spurious responses of the mixer can

be defined using a spurious signal table. Local oscillators are defined using frequency, power and close-to-carrier phase noise components.

Generally components will be defined in a complex manner. The required parameters can be supplied, via a components library or database, by the user, from manufacturers' supplied data or from the software vendor.

2) *Definition of Signal Sources*

Just as connecting signal sources to hardware in the laboratory is required to measure system performance it is necessary to supply a number of signal sources in a system simulation. These signal sources can be single carriers, multiple carriers, swept carriers and modulated sources or combinations of them. Complex modulations can be provided as well as standard forms such as single sideband AM, suppressed carrier AM, FM, QAM etc.. An example of a complex waveform is the NTSC color test pattern of Figure 2. In general, modulating waveforms can be

defined using equations or time samples. Demodulation can either be perfect (ideal AM, FM, QAM etc..) or in some cases can be produced by using defined components. Other detection techniques include log video and limiting (refs. 1 and 2).

3) *Definition of Output Parameters*

The system parameters that need to be calculated and displayed are defined either before or after the simulations. On Microwave Success, the required parameters are generally defined after calculations of the system using a "report writer". In OmniSys, the required parameters are defined before the calculations. The advantage of the former approach is that no further editing or calculations are needed if other displayed parameters are required. The types of tabular and/or graphical outputs available include single sweeps, e.g. the gain of the system as a function of frequency; dual sweeps e.g. the gain of the system as a function of frequency as a function of the gain of an amplifier in that system.

Budget analysis of systems is one of the most useful features of the simulators whereby the contributions of individual components to overall system performance can be calculated. This is particularly useful in investigating the changes in performance of a system as a function of parameters such as temperature etc.. (so called "what-if" analysis).

The nonlinear performance of a system can be broadly divided into two areas - one involving considerations of compression and dynamic range calculations, the other involving more detailed calculations of multitone, intermodulation and cross-modulation performances.

4) *How system simulators work*

The majority of calculations performed by commercial system simulators occur in the frequency domain and where necessary transformations are performed between the time domain and the frequency domain. In Microwave Success, for example, no assumptions are made about the reflection coefficients or reverse transmission coefficients of the 'black boxes' when calculating cascaded noise figures. In some cases, to ease calculation complexity, assumptions are made about the nonlinear properties of black boxes. For example, if two input tones are input into a system, the first nonlinear components will generate harmonics and intermodulation products. The largest of these resultant signals is used in the following nonlinear components for further computations whilst leaving the smaller level signals to be computed using the 'linear' parameters of the system. It is important that system simulators can cope with multichannel situations such as that found in multichannel receivers, phased-array T/R systems (such as electronically steered satellite multi-spot beams) and feedback/AGC loops.

Some Examples of Using System Simulators

Two examples are given in this paper of using system simulator CAD tools. The first is a C-band TVRO double downconverter whose schematic is shown in Figure 1 and the second is a C-band digital terrestrial radio link.

1) *C-Band TVRO Receiver*

The C-band TVRO receiver consists of two major sections - the so-called outdoor unit (ODU) which consists of a 2 meter diameter parabolic dish antenna, a low-noise front-end receiver with RF filtering, low noise GaAs FET amplifier, balanced mixer and IF amplifier. Following a long coaxial cable, at the 1st IF of approximately 1 GHz into the house, a TV top indoor unit (IDU) contains a band-defining filter, amplifier, balanced mixer and 2nd IF filtering and amplification at 300 MHz. Both LO's are defined in terms of power as well as close to carrier phase noise. Usually, in order to produce more constant signal-to-noise ratios at the TV, an AGC amplifier is contained in the IDU. In this example, AGC has not been included. With a low-noise front-end amplifier in the ODU having a gain of 15 dB followed by a diode mixer with a noise figure of 8 dB, the overall receiver noise figure was 4 dB. This noise figure does not allow a sufficient C/N ratio in all weather conditions. Increasing the gain of the front-end amplifier to 25 dB (Figure 3) results in an overall noise figure of 2.5 dB in the center channel of the TVRO unit corresponding to a carrier frequency of 3.95 GHz. At this gain the overall compression characteristics of the receiver, shown in Figure 4, give a 1 dB compression point of -47 dBm. This is well above the levels of likely received signal strengths into the ODU. The signal levels at which the system components compress can be investigated by using budget analysis. The results of this analysis are given in Figure 5(a) and (b) for two conditions - one where the carrier level is at -70 dBm and one where it is at -30 dBm. Clearly compression is mainly produced by the second amplifier in the IDU.

The overall performance of the receiver to modulated carriers can be calculated. For example, when the 3.85 GHz carrier is modulated with an NTSC six color burst test pattern, the simulator translates the time domain information (at video) into frequency domain information, calculates the effects of the components in the system on the frequency spectrum of the signal and then converts the resultant information back to the time domain using Fast Fourier Transforms.

Figure 6(a) shows the effect of the receiver on the NTSC waveform whilst Figure 6(b) shows the corresponding effect in the frequency domain where the 2nd IF modulated output carrier before demodulation is displayed.

A useful application of system simulation is in its use for optimization of the system performance and the sensitivity of the system to component performance variations. An example of this is to 'link' a circuit simulator with a system simulator. In Figure 7, for example, the linear circuit simulator, SuperCompact, is operating concurrently with Microwave Success under Windows 3.0 on a personal computer. When a transmission line matching element is identified and changed in the design of the front-end low-noise amplifier of the TVRO receiver, the effect of that component change on the overall performance of the TVRO system can be 'rippled' through to the system simulator.

2) *C-Band Digital Terrestrial Radio Link*

The schematic for this example is shown in Figure 8. The radio link uses eudo-random bit sequences modulated onto a C-band carrier using quadrature amplitude modulation (QAM). The transmitter takes a signal centered at 300 MHz and upconverts it to 3700 MHz, then amplifies the signal to 2 watts before it is transmitted from a 4 meter diameter dish antenna. The QAM modulation is provided by a .WFM datafile that defines the I and Q bit sequences in the time domain within a 32 microsecond window. The receiver consists of band-defining filters, amplifiers, double-balanced mixer and synchronous QAM demodulator. The antenna was a 3 meter dish followed by a low noise amplifier. Figure 9 shows the overall gain budget for the complete link where the path length was 64 km.. Figure 10 (a) and (b) show the noise figure and signal-to-noise ratio budgets for the complete link. Figures 11(a) and (b) display the spectrum prior to the receiver demodulator as well as the output from the I channel of the receiver demodulator. Note the noise on the signal - clearly the signal level is such that the pseudo-random bit sequence can be cleanly extracted in the following signal processing. An important parameter in communications systems is the performance changes as a function of temperature. By defining relationships between black box parameters and temperature (e.g. gain, noise figure and 1 dB compression point) the performance of the complete system can be determined (each black box can have individual temperatures defined as well). This data can be available in the form of either equations relating parameters to temperature or measured data in datafiles. Figure 12(a) and (b) show, for example, the compression characteristics of the complete radio link at the two temperatures of zero and + 100 degrees Celsius.

Conclusions

Although commercially available system simulators are not as mature as linear and nonlinear CAD tools, they already enable subsystem and system design engineers to efficiently calculate parameters of interest. System design accuracy and productivity are considerably improved particularly when systems comparison, optimization and yield analysis are included.

References

1. Microwave Success, Users' Reference Manual, Volume 2, 1990, Compact Software, Inc., Paterson, NJ, USA

2. OmniSys, Applications Manual, 1990, EEsof, Inc., Westlake Village, CA, USA

Trademarks

TABLE 1 **Some of the Characteristics of System CAD Tools**

Components	Sources	Calculations
One Ports	Single Carriers	Gain
Two Ports	Multicarriers	Noise Figure
Multiports	Swept Frequency	Signal/Noise ratio
Mixers	AM	Compression
Filters	FM	Intercept points
Oscillators	PM	Return losses
Path Length	Digital	Group Delay
Multipath	Temperature	AM to PM conversion
	Swept Power	Amp. and phase differences

Displays	Facilities
Single Sweep	Analysis
Dual Sweep	Optimization
Budget	Yield analysis
Multitone	Links to other simulators
Waveform	and databases
Spectrum	
Tabular	

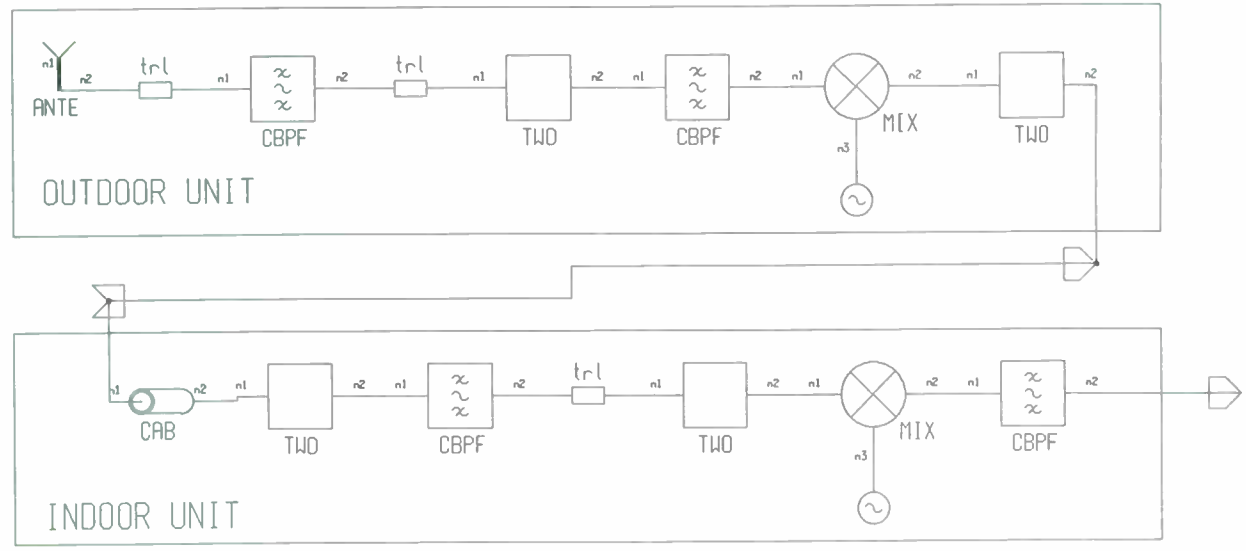

Figure 1. C-Band TVRO Double Downconverter Schematic

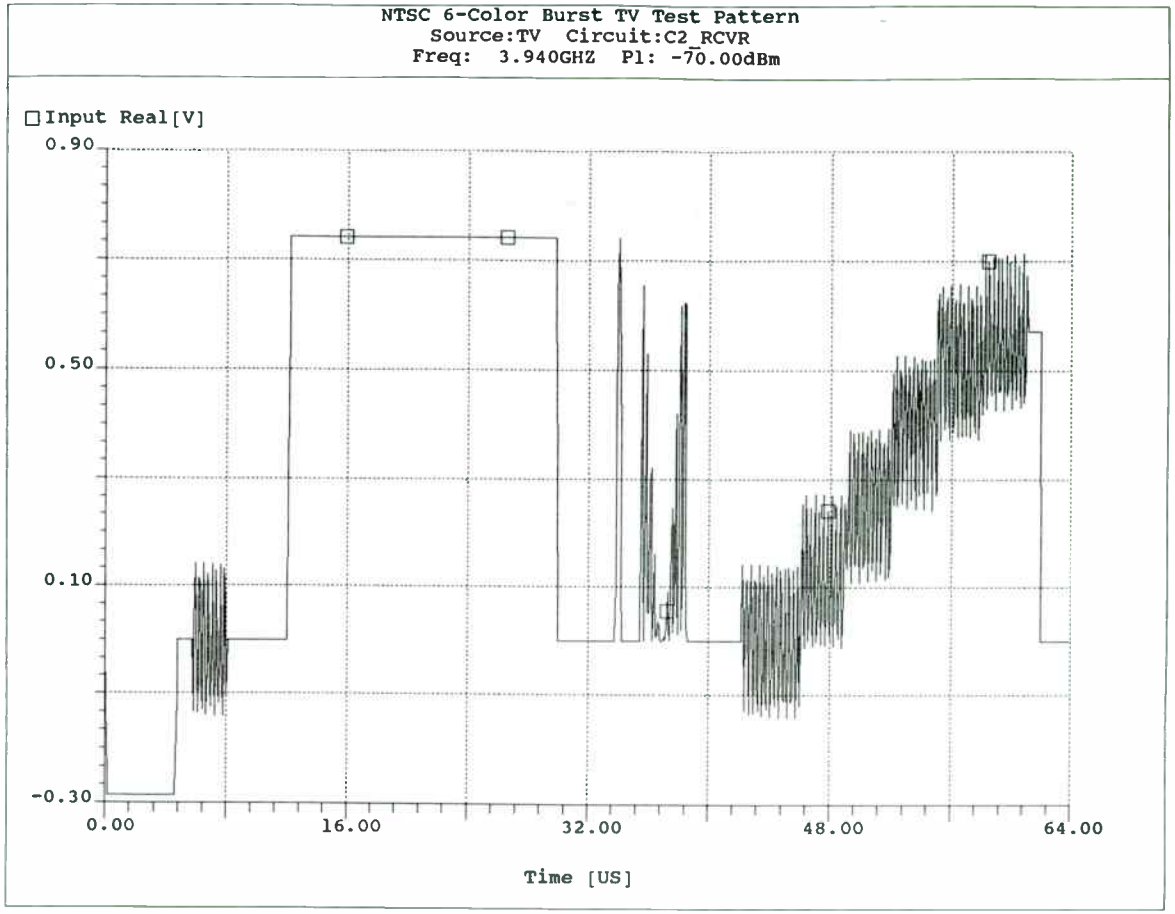

Figure 2. **NTSC 6-Color Burst TV Test Pattern**

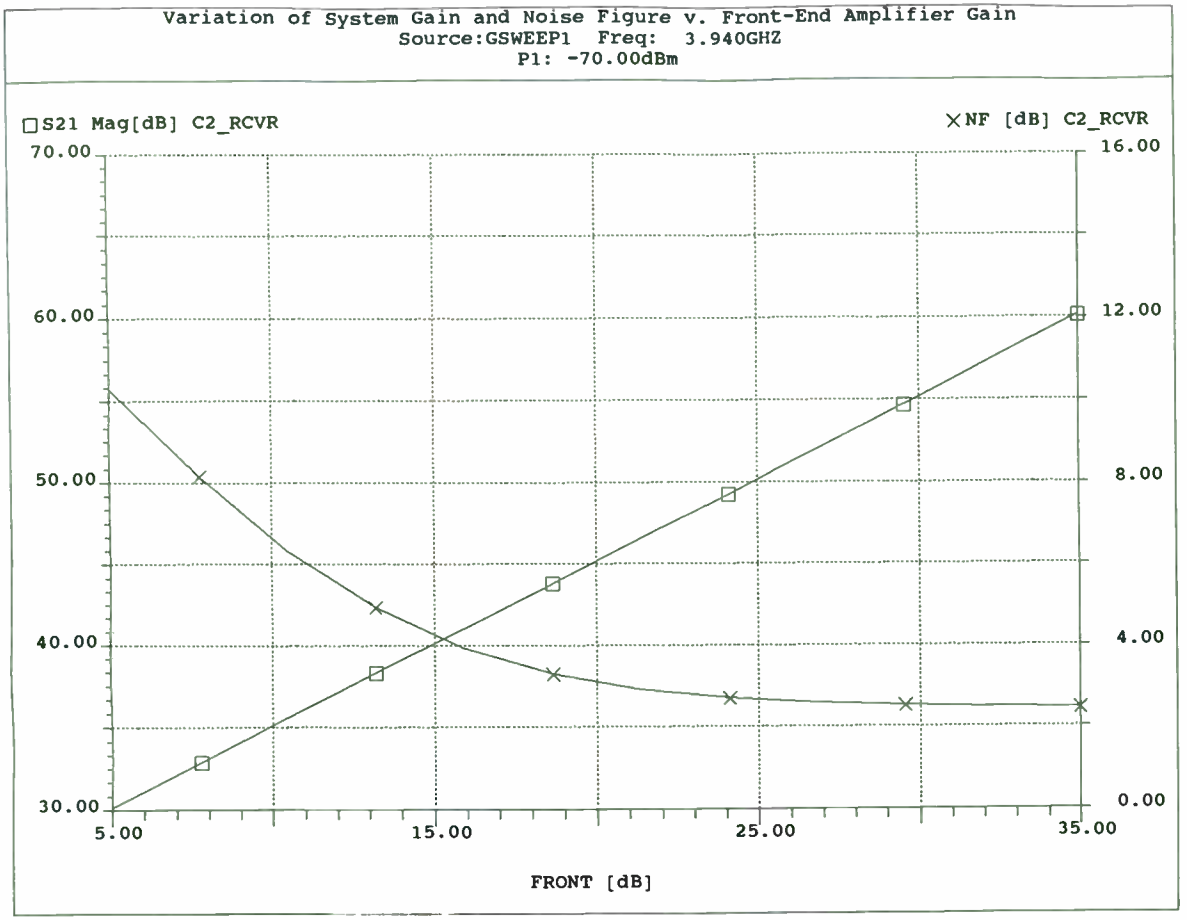

Figure 3. **Variation in System Gain and Noise Figure versus Front-End Amplifier Gain**

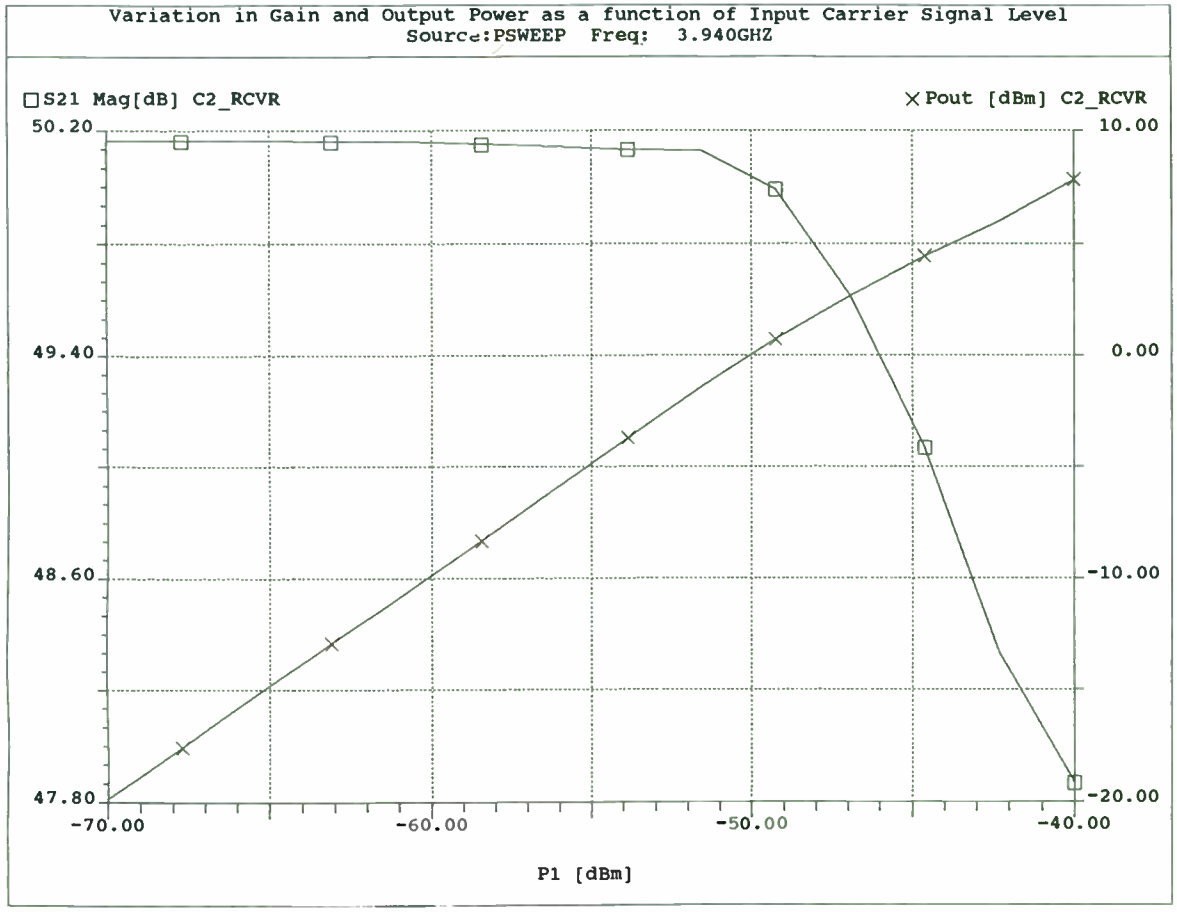

Figure 4. **Variation in Gain and Output Power as a Function of Input Carrier Signal Level**

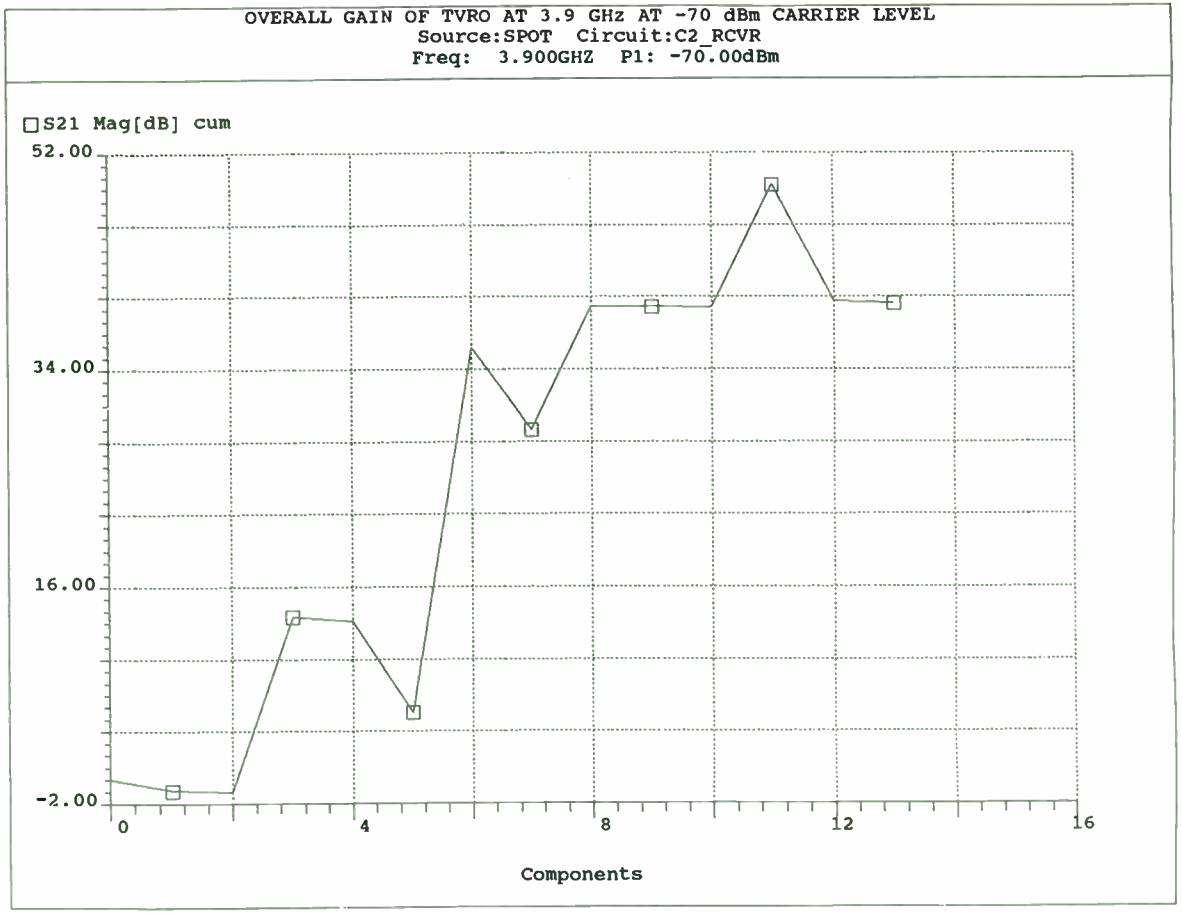

Figure 5(a). Overall Gain of TVRO at 3.9 GHz at -70 dBm Input Carrier Level

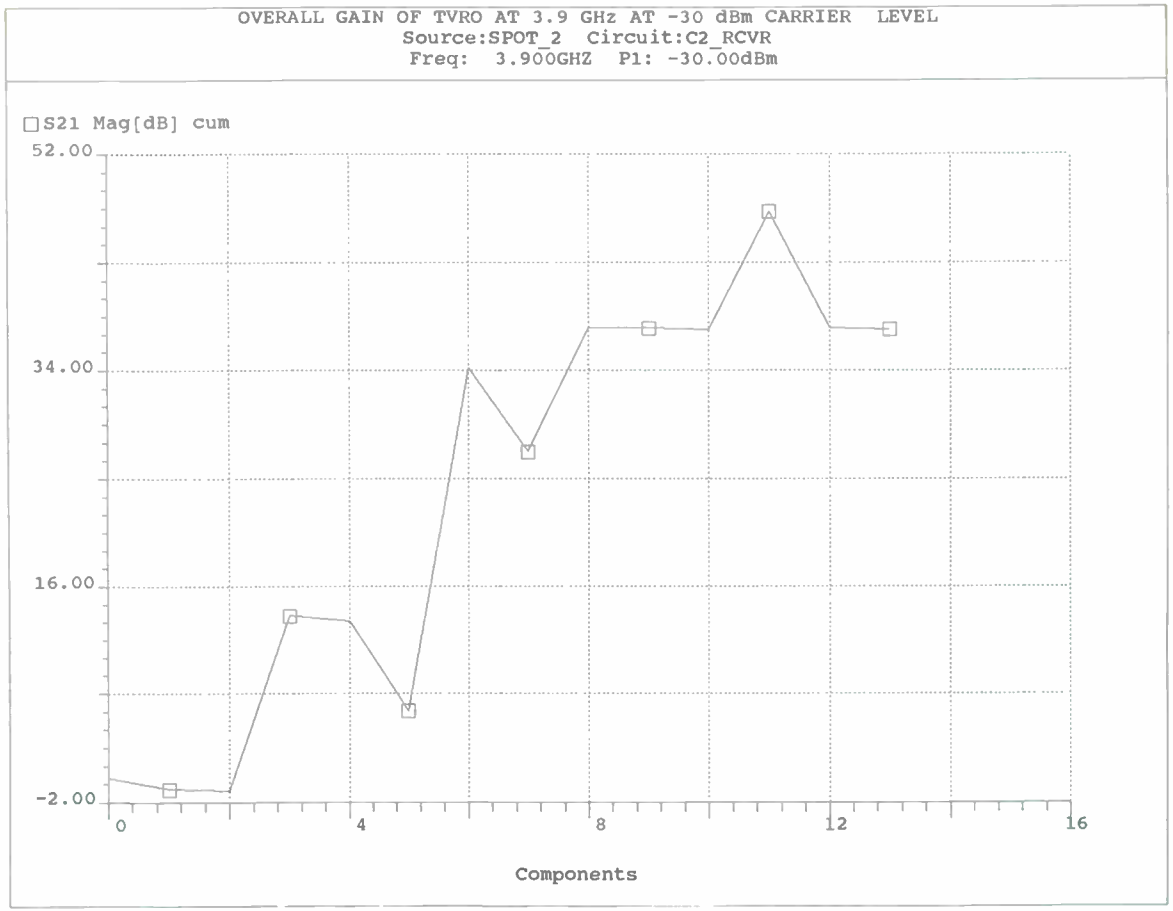

Figure 5(b). Overall Gain of TVRO at 3.9 GHz at -30 dBm Input Carrier Level

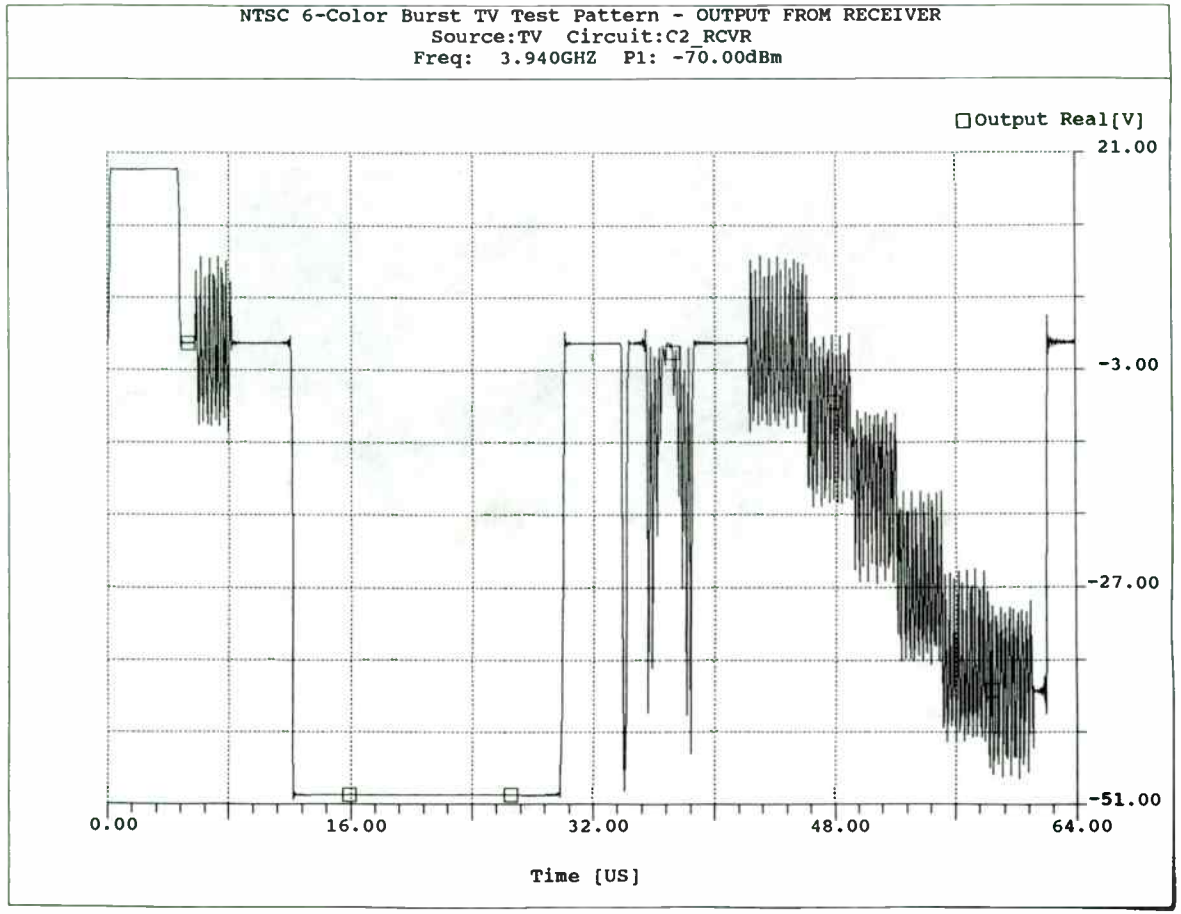

Figure 6(a). Color Burst Test Pattern after Demodulation

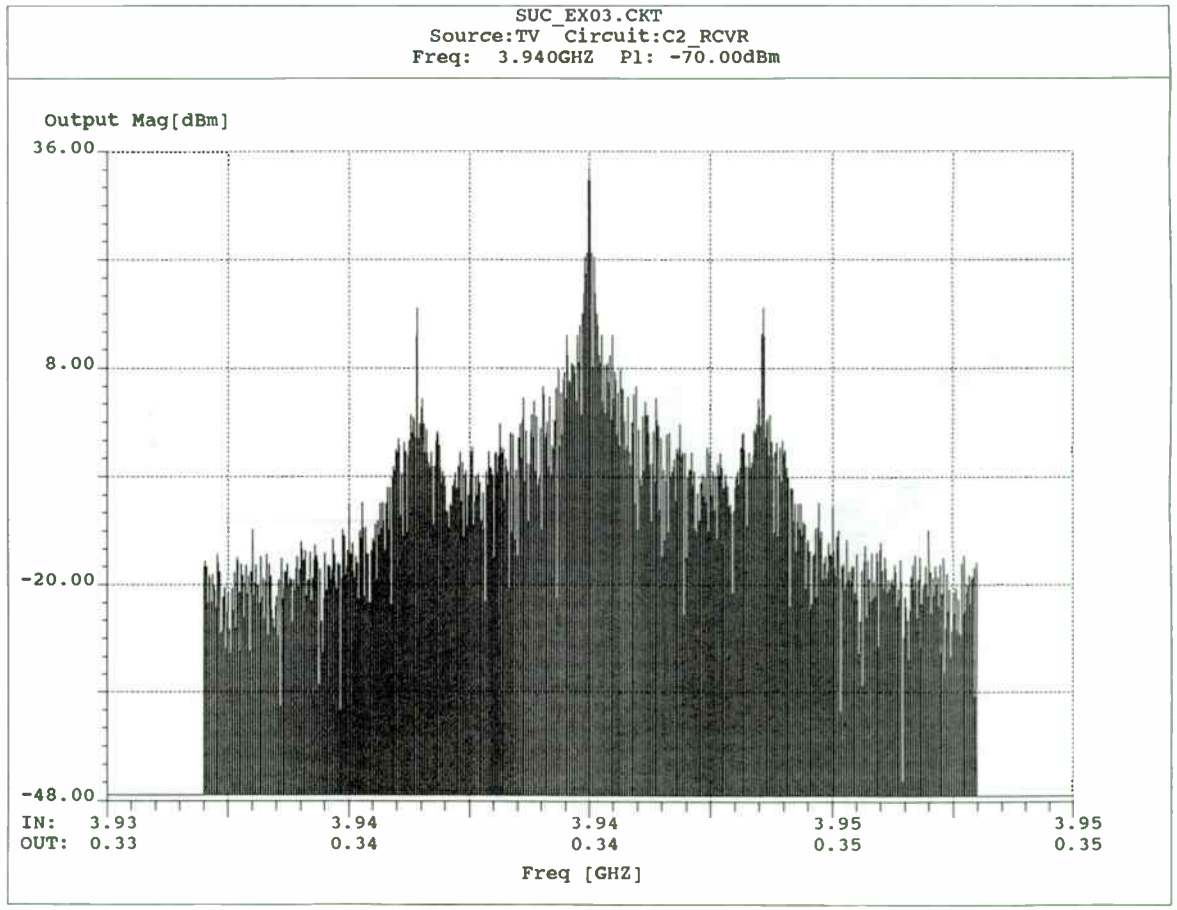

Figure 6(b). Color Burst Test Pattern Spectrum prior to Demodulation

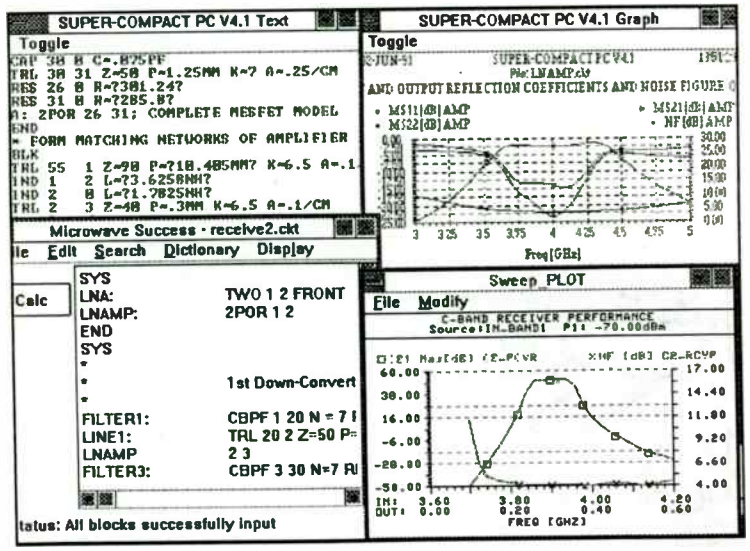

Figure 7. **Microwave Success and SuperCompact running concurrently within Windows 3.0**

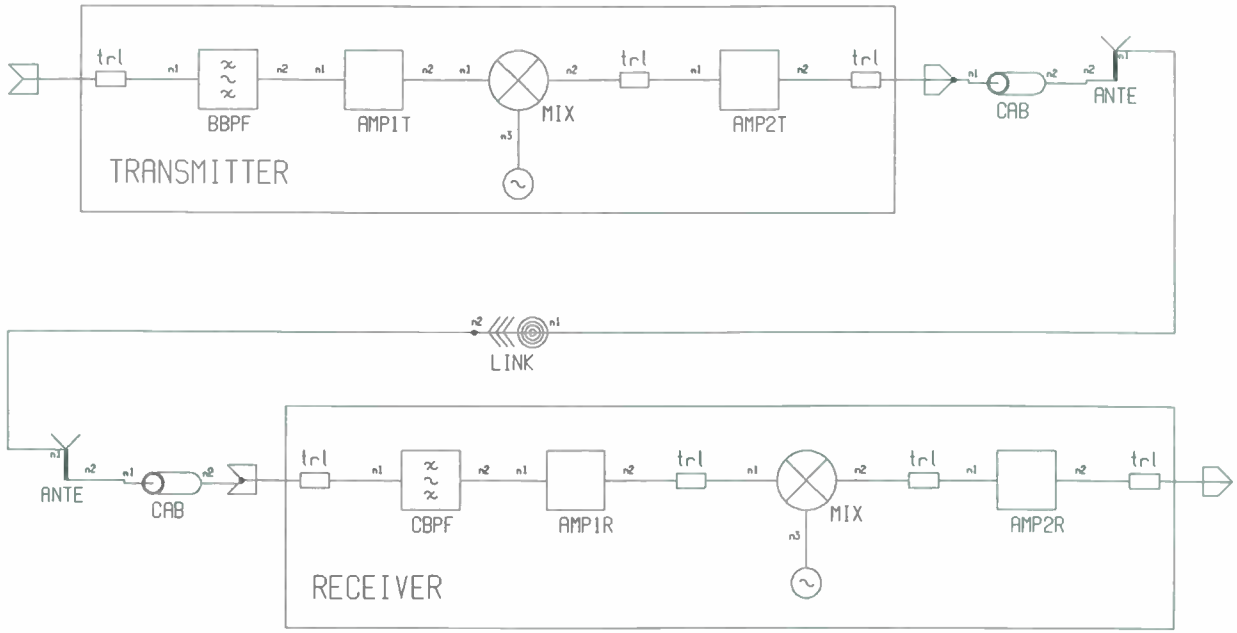

Figure 8. C-Band Digital Terrestrial Radio Link Schematic

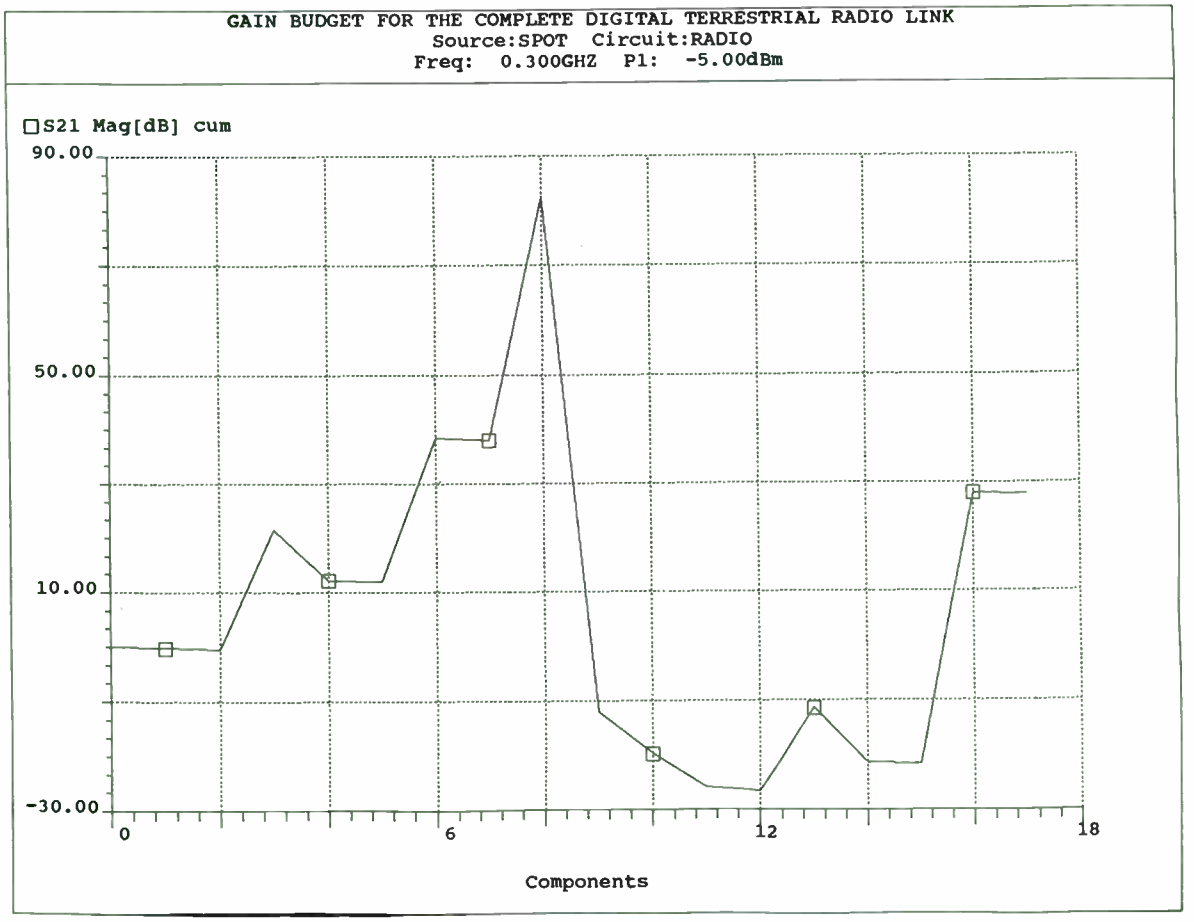

Figure 9. Gain Budget for the complete terrestrial radio link

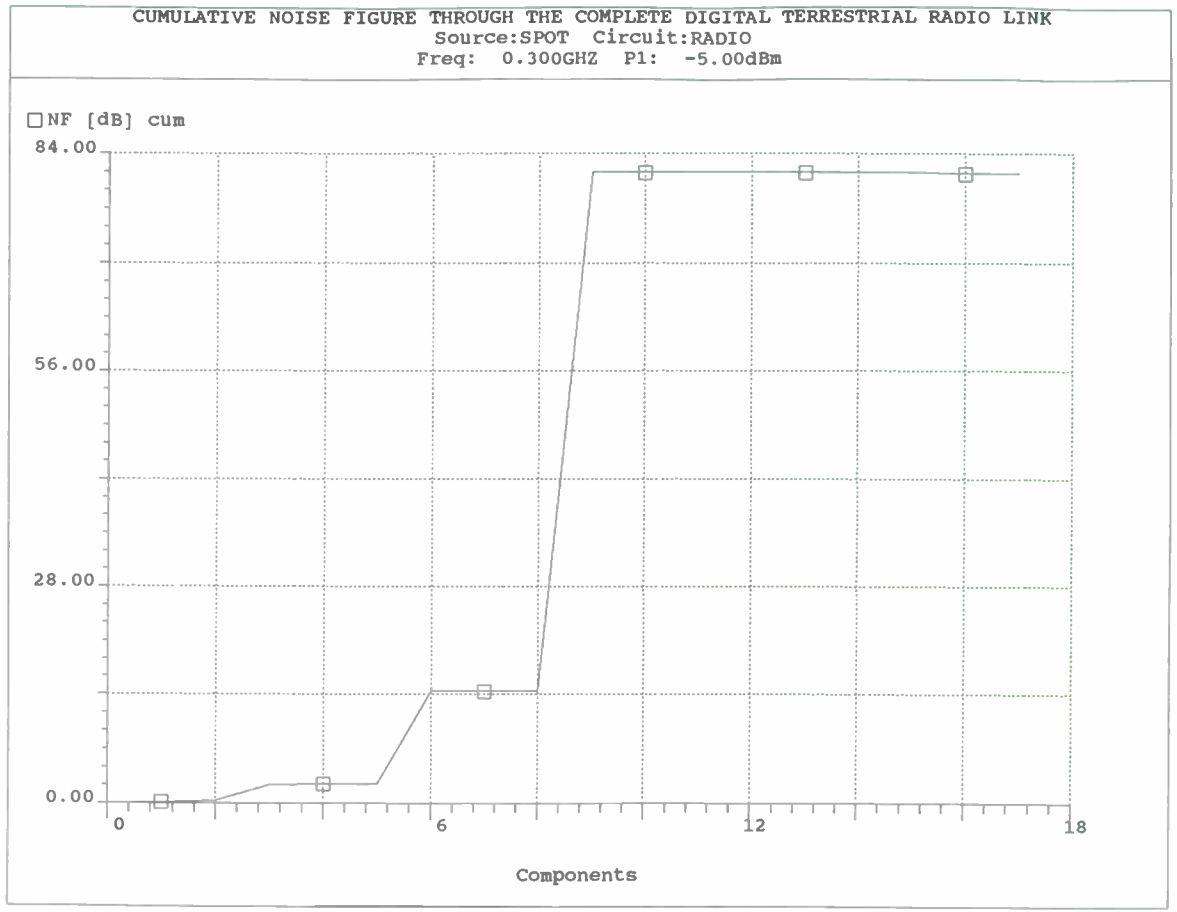

Figure 10(a). Cumulative Noise Figure through the Radio Link

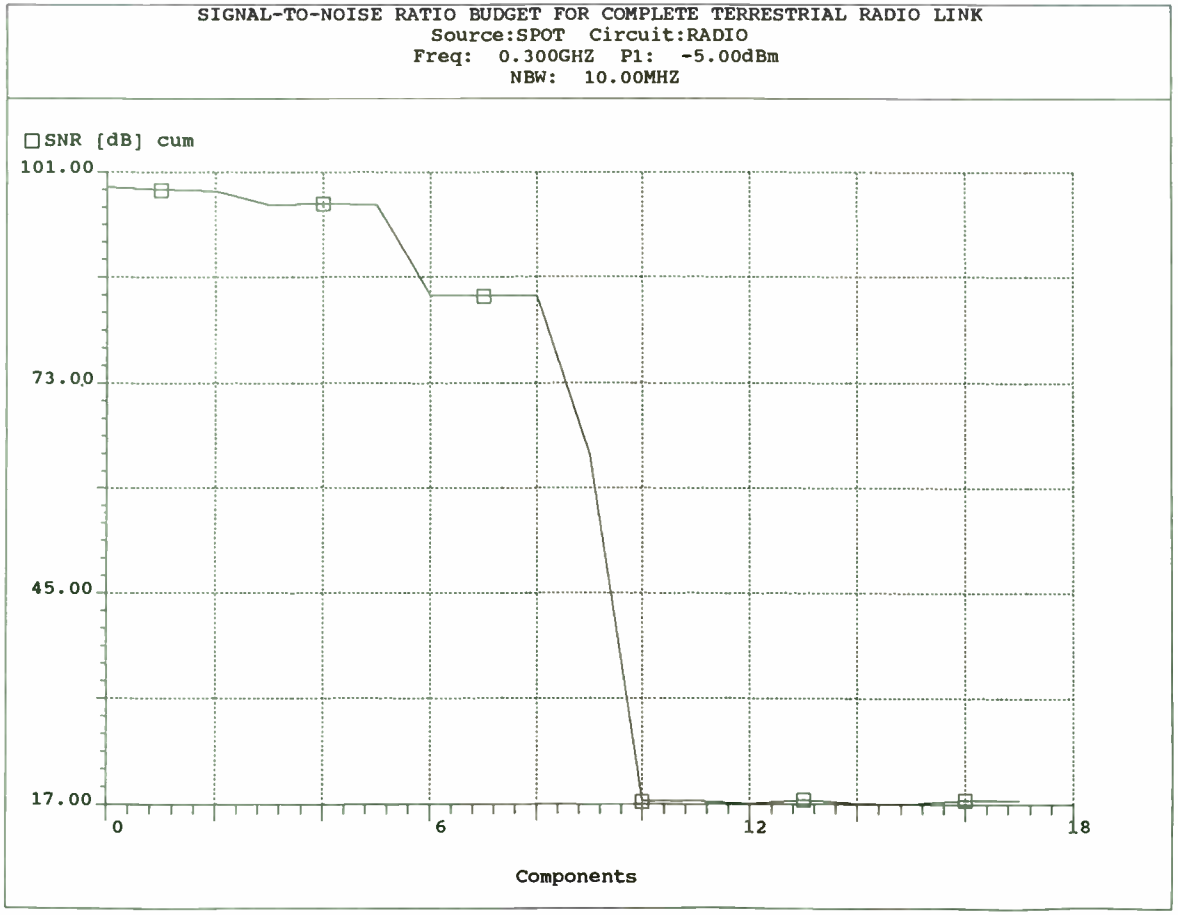

Figure 10(b). Signal-to-noise Ratio Budget through the Radio Link

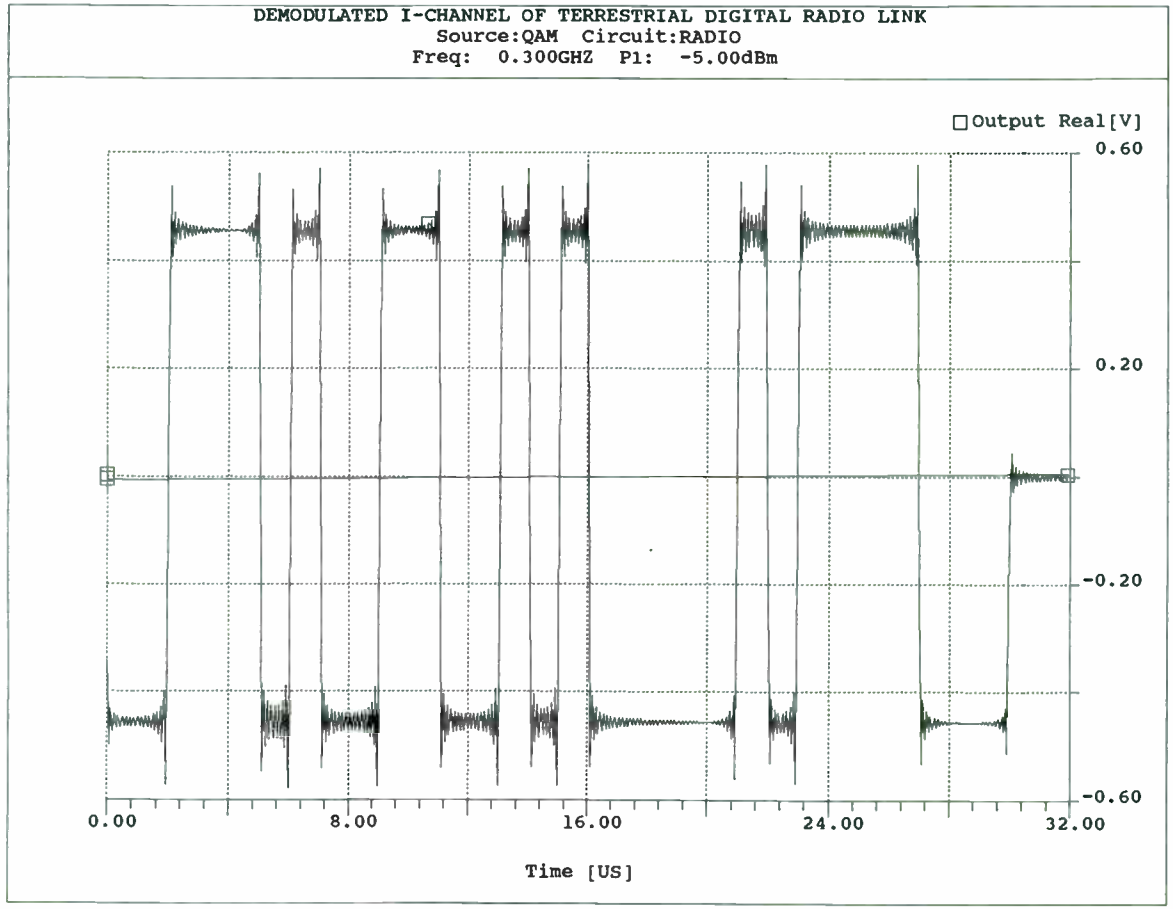

Figure 11(a). Demodulated Bit Sequence in I-Channel of Radio Link

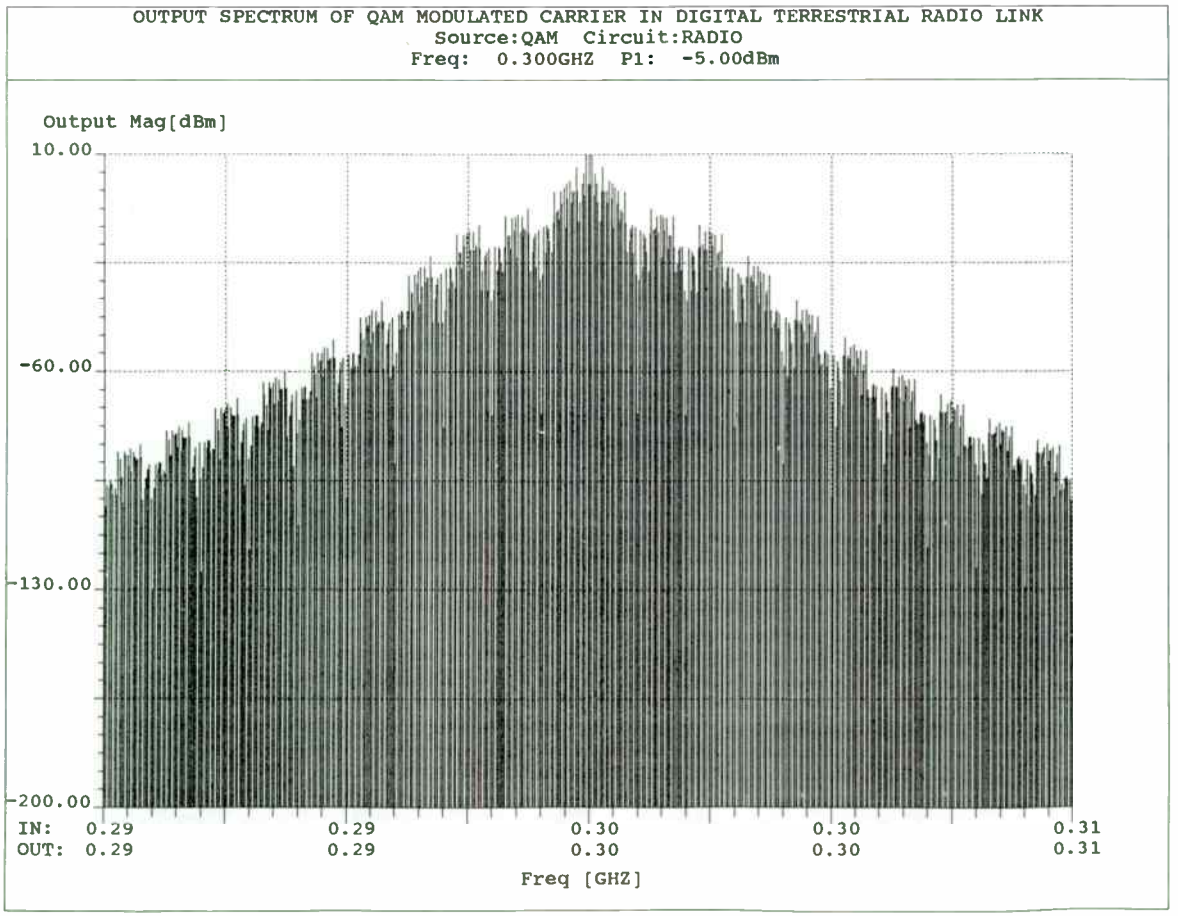

Figure 11(b). Output Spectrum of QAM Modulated Carrier

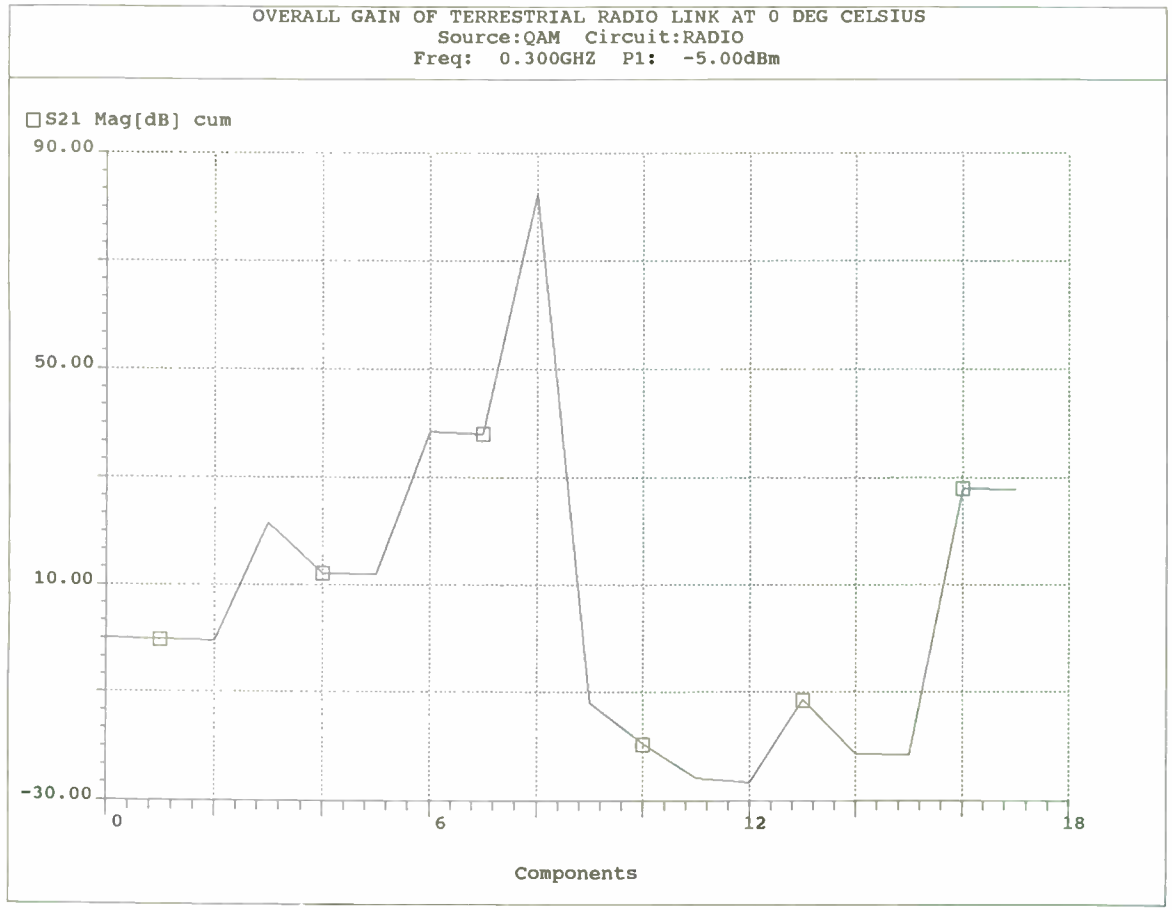

Figure 12(a). **Overall Gain of System at Zero Degrees Celsius**

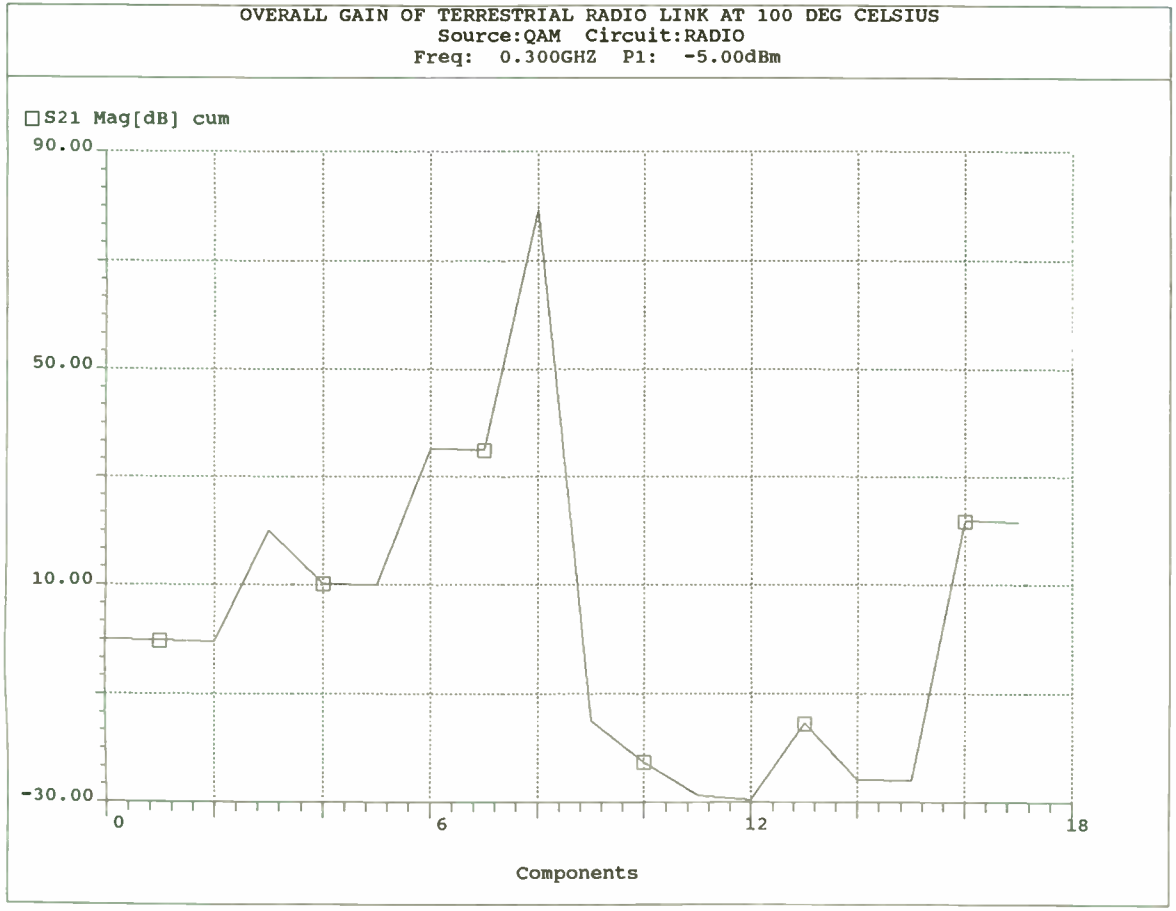

Figure 12(b). Overall Gain of System at 100 Degrees Celsius

EM Theory-Based Analysis of Passive Microstrip RF Components on Single and Multiple Metallization Layers

A. HILL, J. BURKE, K. KOTAPALLI
Compact Software Inc.
483 McLean Blvd
Paterson, NJ 07504

ABSTRACT

This paper describes an application as well as the theoretical foundation of the electromagnetic simulator, COMPACT EXPLORER™, which allows the analysis of predominantly planar, arbitrarily shaped microstrip circuits. Multiple substrate and metallization layers can be handled by the program and results are computed in terms of scattering parameters of passive multiport circuits. Due to the rigorous formulation of the underlying integral equation approach, COMPACT EXPLORER™ can be applied to RF as well as microwave circuits. As an example the analysis of a miniaturized hairpin resonator filter is demonstrated for application in the L band.

Introduction

In the past, design formulas for standard microstrip components have been used for the analysis and synthesis of microstrip circuits at RF and microwave frequencies. Typically the microstrip circuit is subdivided into functional blocks for which design equations are readily available. Representative components include single and coupled transmission line sections, L-bends, tee junctions, crosses and vias. The performance of the entire circuit is obtained by cascading the individual functional blocks. This technique yields accurate results if there is insignificant electromagnetic interaction between the various functional components. With the increase in circuit complexity, the cascading of circuit components may lead to unsatisfactory results due to inter-element coupling. In addition, the need for new component geometries requires the availabily of a general purpose electromagnetic solver that does not impose restrictions on component geometry.

A number of fullwave electromagnetic techniques have been developed in the past for the characterization of planar microstrip discontinuities [1-10]. The analytical foundation of most solvers is based on the electric field integral equation approach which formulates the electric field in terms of the unknown current on the metallization. A moment method procedure is used for the solution of the integral equation. Some techniques have been extended to allow vertical metal sections to be included in the analysis. The fact that planar geometries and a limited number of vertical geometries can be handled lead to the notion of "2.5D simulator".

Theory

COMPACT EXPLORER™ analyses predominantly planar structures within an enclosure. Figure 1 shows the general geometry of interest. The circuit housing is filled with an arbitrary number of homogeneous substrate layers. Metallization can be positioned

between any two layers and circuit ports are required to be defined at the location of a side wall. Transitions between various metallization layers are realized in terms of vertical strip line sections and vias. Loss mechanisms in the form of dielectric, magnetic and metallization loss are included in the formulation.

The total electric field on the microstrip metallization can be written as

$$\vec{E}^{tot}(x,y,z) = \vec{E}^{inc}(x,y,z) + \vec{E}^{scat}(x,y,z) \qquad (1)$$

where

$$\vec{E}^{scat}(x,y,z) = \iiint \overline{\overline{G}}(x|x',y|y',z|z') \cdot \vec{J}(x',y',z')\, dV' \qquad (2)$$

and E^{inc} is the incident electric field. E^{tot} is determined from the boundary conditions on the conductor surface. In equation (2), G represents the Dyadic Green's function associated with the multi-layered geometry [11]and J represents the volume current within the microstrip housing. The method of moments [12] is used to solve equation (1) for the unknown current distribution. The current is expanded using a known set of basis functions. The basis functions are roof top functions for the planar metallization and pulse functions for the vias. Equation (1) is tested using Galerkin's method and Parseval's theorem resulting in the linear system of equations

$$[V] = [Z]\,[I] \qquad (3)$$

The elements in the Z-matrix can be evaluated using a two dimensional discrete fast Fourier transform. An efficient technique for the evaluation of these elements has been published previously [10]. The unknown current distribution is found by solving equation (3). After determining the current, S-parameters can be found. The application of fast Fourier transforms leads to a considerable reduction of computation times. However, the technique requires the geometries to fit on a rectangular grid. Therefore, structures that do not conform to a manhatten type geometry need to be approximated by staircases.

COMPACT EXPLORER™ includes a feature which allows the deembedding of the port discontinuity in the computed S-parameters. This situation is similar to an actual measurement procedure where the effects of the fixture and connectors need to be removed from the measured results. COMPACT EXPLORER™ utilizes two through standards for the computation of the effect at the port discontinuities and subsequently deembeds the circuit with respect to a user definable reference plane. [13].

Example

The technological trend towards the full utilization of the L band for mobile radio communication has been recognized recently [14]. This requires the development of new filter components. Hairpin resonators have been used successfully as filter elements at microwave frequencies. However, the size of these filters in the L-band are too large making their use impractical. A miniaturized hairpin resonator has been suggested [14,15] that is half the size of conventional hairpin resonators. Filters incorporating the new resonator have been successfully

used in receiver front ends resulting in good characteristics such as low noise and high image suppression.

Figure 2 shows the schematic of a miniaturized hairpin resonator. The advantages of this resonator compared to conventional hairpin resonators are:

1) small size, with no Q-value degradation
2) expansion of the applicable frequency range
3) easy adjustment of the resonant frequency

Figure 3 shows the schematic of the hairpin filter as it was drawn using the layout editor of MICROWAVE EXPLORER™. The filter was enclosed in a shielding box of dimensions 16.383mm by 15.621mm by 7.62mm in the x, y and z direction, respectively. The dimensions for the resonator were chosen to be (see Figure 2): L_h = 10.287mm, L_d = 4.953mm, W_s = 1.143mm, L_p = 4.572mm, W_c = 0.381mm, S = 0.381mm. The substrate was 1.27mm in height and had a dielectric constant of 10.5. The separation between the two resonators was 1.143mm.

The response of the filter was analyzed using both a circuit simulator and an electromagnetics simulator. Results from SUPER-COMPACT™ and MICROWAVE EXPLORER™ are illustrated in Figure 4 for the frequency range of 1.25GHz to 2.75GHz. According to the results obtained from MICROWAVE EXPLORER™, the filter has a center frequency of 1.92GHz and a bandwidth of about 54MHz. SUPER COMPACT™ predicted a center frequency of 1.98GHz and a bandwidth of about 80MHz. The compactness of the resonators suggests to model the entire structure, under consideration of all element interactions. This approach is used for the electromagnetic simulator but not for the circuit simulator, which results in the different circuit response as shown in Figure 4. The circuit elements used in SUPER-COMPACT™ were right angle bends, tee junctions, open ends, various single and one coupled transmission line section. MICROWAVE EXPLORER™ subdivided the structure into 554 elements and required an analysis time of 2 minutes per frequency on an Apollo dn10k computer. SUPER-COMPACT™ ran on a 386 PC and took several seconds to analyse the structure for the entire spectrum.

Acknowledgement

Thanks are due to Mr. Hiroyuki Yabuki from Matsushita and Mr. Ray Pengelly from Compact Software for providing data on the miniaturized hairpin filter.

References

(1) R.H. Jansen, "The Spectral-Domain Approach for Microwave Integrated Circuits", IEEE Trans. on Microwave Theory and Tech., October 1985.

(2) W. Wertgen, R.H. Jansen, "Novel Green's Function Database Technique for the Efficient Full-Wave Analysis of Complex Irregular (M)MIC Structures", 19th European Microwave Converence, 1989.

(3) R.W. Jackson, "Full-Wave, Finite Element Analysis of Irregular Microstrip Discontinuities", IEEE Trans. on Microwave Theory and Tech., January 1989.

(4) J.R. Mosig, "Arbitrarily Shaped Microstrip Structures and their Analysis with a Mixed Potential Integral Equation", IEEE Trans. on Microwave Theory and Tech., October 1985.

(5) P.B. Katehi, Alexopoulos N.G., "Frequency - Dependent Characteristics of Microstrip Discontinuities in Millimeter Wave Integrated Circuits", IEEE Trans. on Microwave Theory and Tech., October 1985

(6) L.P. Dunleavy, P.B. Katehi, "A Generalized Method for Analyzing Shielded thin Microstrip Discontinuities", IEEE Trans on Microwave Theory and Tech., December 1988.

(7) D.J. Wu, D.C. Chang, B.L. Brim, "Accurate Numerical Modeling of Microstrip Junctions and Discontinuities", Microwave and Millimeter-Wave Computer-Aided Engineering, January 1991.

(8) J.C. Rautio, R.F. Harrington, "An Electromagnetic Time-harmonic Analysis of Shielded Microstrip Circuits", IEEE Trans. on Microwave Theory and Tech., August 1987.

(9) A. Skrivervik, J.R. Mosig,"Equivalent Circuits of Microstrip Discontinuities including Radiation Effects", IEEE MTT-S, 1989.

(10) A. Hill, V.K. Tripathi, "An efficient Algorithm for the 3D Analysis of Passive Microstrip Components and Discontinuities for Microwave and Millimeter Wave Integrated Circuits", IEEE Trans. on Microwave Theory and Tech., January 1991.

[11] T. Itoh, "Spectral Domain Immitance Approach for Dispersion Characteristics of Generalized Printed Transmission Line," IEEE Trans. Microwave Theory Tech., Vol. July 1986.

(12) R.F. Harrington, "Time-Harmonic Electromagnetic Fields," McGraw-Hill, 1961.

[13] A. Hill, "Analysis of Multiple Coupled Microstrip Discontinuities for Microwave and Millimeter Wave Discontinuities", IEEE Intern. Microwave Symposium, June 1991.

[14] M. Sagawa, K. Takahashi, M. Makimoto, "Miniaturized Hairpin Resonator Filters and Their Application to Receiver Front-End MIC's", IEEE Trans. Microwave Theory Tech., December 1989.

[15] H. Yabuki, M. Sagawa, M. Makimoto, "Voltage Controlled Push-Push Oscillators Using Miniaturized Hairpin Resonators", IEEE Intern. Microwave Symposium, June 1991.

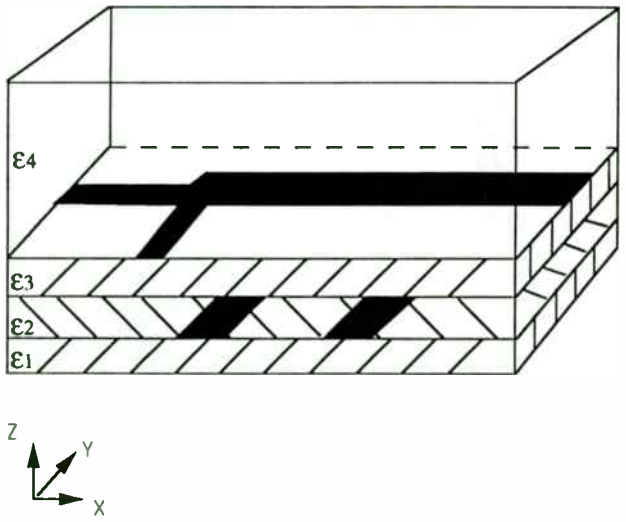

Figure 1: Compact Explorer Can Analyze a General Multilayered Microstrip Circuit

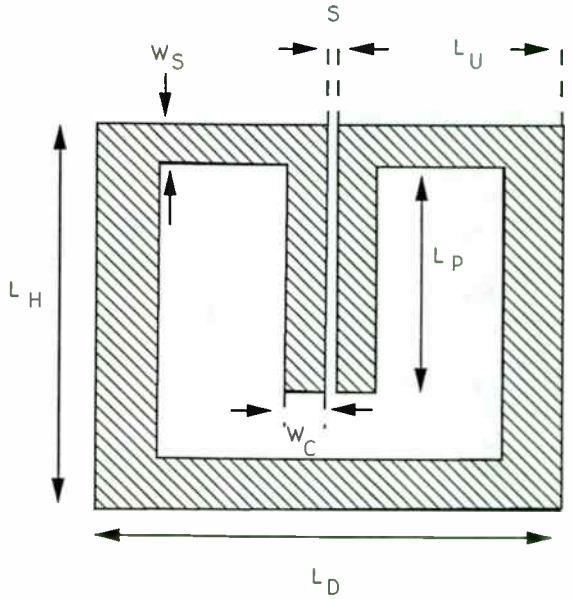

Figure 2: Miniaturized Hairpin Resonator

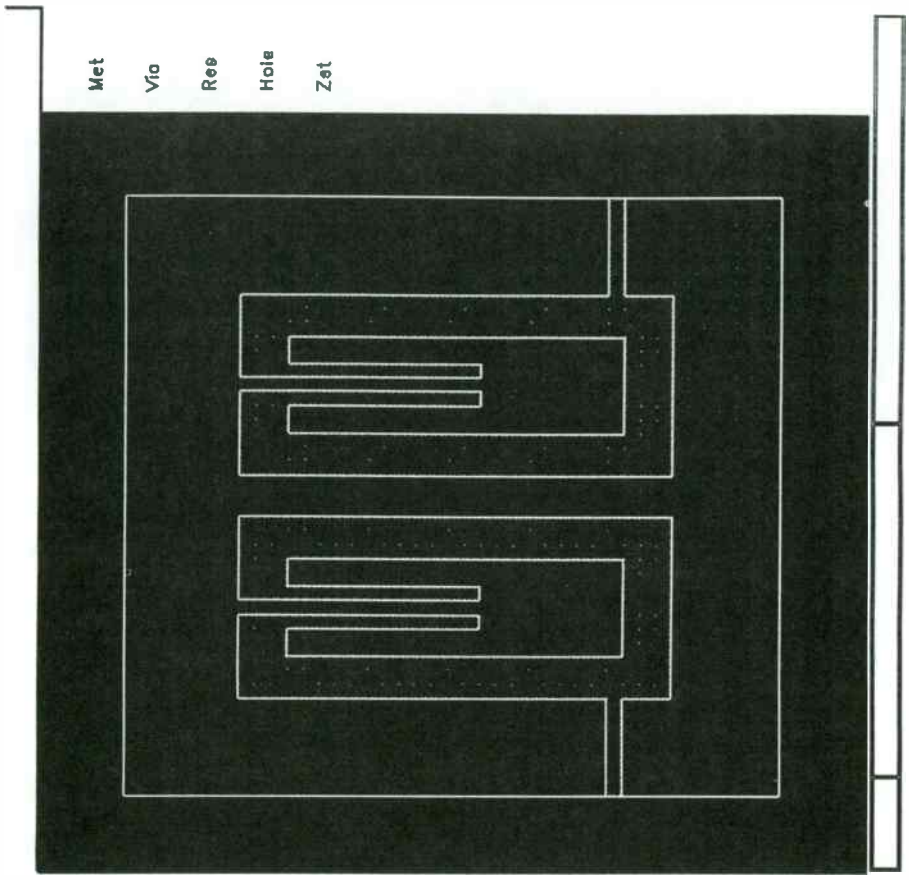

Figure 3: Hairpin Filter Generated with EXPLORER'S Layout Editor

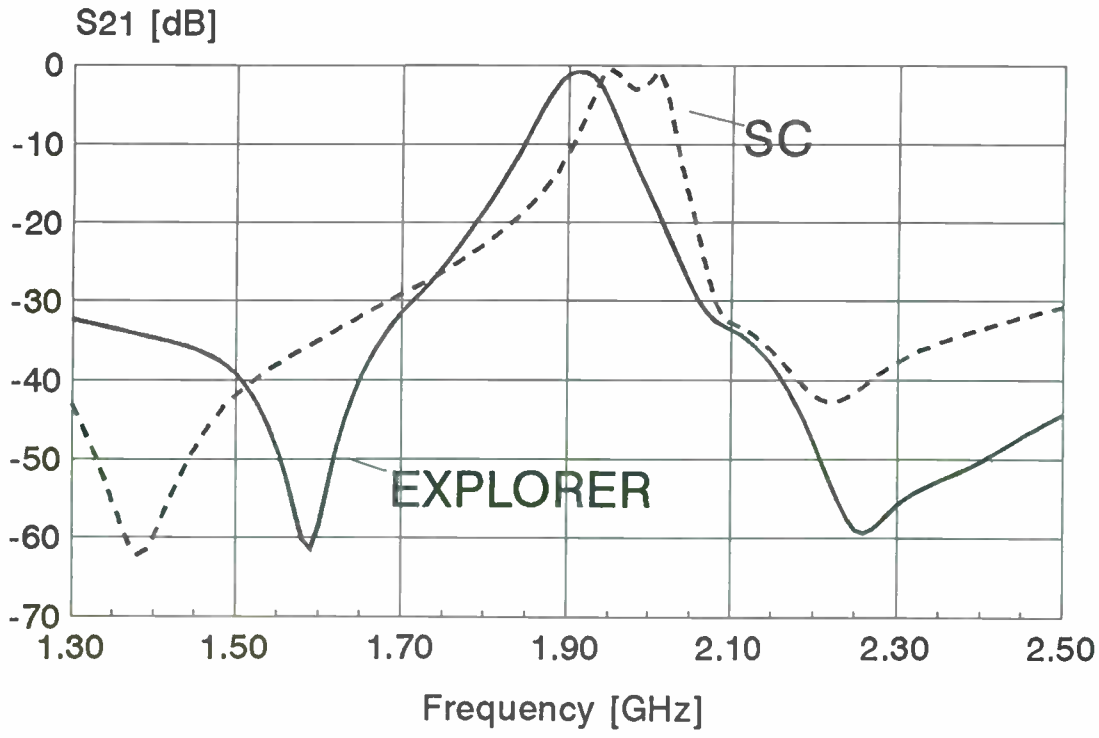

Figure 4: Comparison of results obtained from the circuit simulator and electromagnetic simulator

A Unified Look at Spurious Performance of
Multiple Conversion Receiving and Transmitting Systems

Richard C. Webb
Webb Laboratories
139 E. Capitol Drive Suite 4
Hartland, Wisconsin 53029

Abstract

While spurious behavior of mixers is generally well-understood, system architectures, especially those involving a number of frequency conversions, are often defined without full anticipation of undesired tuned and coincident responses or outputs. Different classes of receive and transmit products are discussed, and a nomenclature is proposed for quick identification of spurious product type and origin.

The Transmit Mixer

A transmit frequency conversion is one in which signals of known frequency are applied to the LO and either RF or IF ports of a mixer. Each transmit mixing process results in a single desired output as well as an infinite sum of primary and higher order spurious outputs.

In the exciter, the converter may be arranged such that the variable signal is injected as a local oscillator or as a lower level IF or RF input. In the first case, leakage of the local oscillator exists throughout the LO band, while the single frequency input may reach the output as a fixed lower level signal. In the alternate case, the variable signal is applied to the input port and the single tone serves as the LO. It must be pointed out that practical mixers display limiting in the LO port. That is, signals entering the local oscillator port undergo limiting prior to the classical frequency conversion. Thus, signals possessing important amplitude related information are necessarily applied to the IF or RF ports of the mixer.

Mixer Behavior with Spurious Inputs

Figure 1 depicts a typical mixer with inputs F_r and F_l applied to the RF and LO ports respectively. The are an infinite number of output terms at frequencies given by

$$F_o = \pm mF_r \pm nF_l$$

Spurs in RF or IF Input

There are two considerations regarding the introduction of additional signals to a mixer input port. In the first case, one adds a discrete term (spectral line) to the 'linear' mixer input (RF or IF port). In this instance, it may be assumed that the mixer transfer function is quasi-linear. That is, the addition of additional discrete terms at the mixer input will result in independent families of spurious outputs, assuming the mixer is operated at fairly low levels. Under these conditions, phase and/or amplitude modulation intrinsic to the input signals is well-preserved. At higher drive levels, however, crossmodulation will result.

Spurs in LO Input

A more interesting case involves the introduction of additional spectra into the LO port of a mixer. The LO port of a practical mixer acts as a limiter prior to the mixing process. Hence, one may apply classical limiter theory to LO input spectra prior to performing spurious calculations. There are several interesting cases. Figure 2 represents a phase (or frequency) modulated signal. Application of this signal as a local oscillator provides

some interesting results. Regarding the desired and image outputs (the primary 1 x 1 tones), the phase modulation present on the LO source is applied directly to each. Output products of input order **m** and LO order 1 also receive the phase modulation of the LO signal. Output products of LO order **n** greater than unity likewise possess the phase modulation of the LO, but in addition display phase (frequency) deviation increased linearly by the order **n**. In other words, an **m** x **n** output will display the PM (FM) of the local oscillator, with deviation multiplied by **n** (modulation sidebands enhanced by 20log[**n**] dB in low deviation (linear FM) cases).

A second case of interest involves amplitude modulation present on the LO input. A hard limiter will remove all AM from a signal, and will leave in its place a purely phase modulated signal. Figure 3 depicts AM and limited AM (now PM) signals in the frequency domain. In general, an AM signal with a small modulation index, applied to a hard limiter will see its AM sidebands replaced by PM (FM) sidebands, with sideband level reduced by 3 dB. Practically, a mixer LO port approximates a hard limiter quite well. Reference 1 discusses signal limiting in general.

A third case is represented in Figure 4. Here, an unrelated signal is summed into the LO. That is, the main LO signal is accompanied by a significantly smaller term, possibly the result of leakage or due to some frequency synthesizer imperfection. The limiting action of the LO port will convert the signal, originally offset from the main LO signal by $\pm\Delta f$ and smaller than the main signal by A dB, to phase modulation with sidebands each offset by $\pm\Delta f$ and each 6 dB below the level of the original extraneous tone.

Spurious Outputs

Intrinsic to each conversion are two families of spurious products. *Tuned* outputs exist as a result of particular LO and input (RF or IF) frequencies. They are the classical primary and higher order sum and difference terms, and are called *tuned* outputs because their existence results from simple imposition of the input frequencies. That is, the desired output frequency results from adjustment of the LO or input frequency (usually the other remains fixed). Once the two applied frequencies are imposed, the tuned spurious spectrum results. *In general, tuned outputs differ in frequency from that of the desired output.*

Crossover, or *coincident*, products are outputs that are, by definition, equal in frequency to the desired transmit frequency. In a single mixing process, crossovers may not be removed by filtering, whereas tuned output amplitudes are subject to filtering.

The Transmit Tuned Output

The tuned output is the easiest spurious product to understand and predict. Application of signals to the input and LO ports of a mixer results in an infinite number of outputs at frequencies F_O

$$F_O = \pm mF_I \pm nF_I$$

where F_I and F_I are the mixer input and local oscillator frequencies, respectively. Figure 5 presents typical tuned spurious outputs. When tuned for a desired output frequency of 35 MHz (LO at 45.7 MHz), the *transmit image* exists at 56.4 MHz. While the desired output is derived by subtracting the two input frequencies, the image coexists due to a similar addition.

An example of an in-band tuned output is the +2 by +1 tone at 67.1 MHz. And, a typical out-of-band output at 102.1 MHz is the result of a similar +1 by +2 conversion. Tuned outputs are subject to removal or attenuation via filtering.

The Transmit Crossover Output

The transmit crossover output coincides precisely with the desired output. As such, *the crossover output cannot be removed by filtering*. The crossover output is identically equal in frequency to the desired output at some in-band frequency. In the architecture of Figure 6, a coincident output exists at 37.45 MHz. The desired output is -1 by +1 in nature. That is, the 37.45 MHz output signal results from a mixing process in which the 10.7 MHz input frequency is subtracted from the corresponding LO frequency of 48.15 MHz. A -10 by +3 crossover exists as shown. For the ordering of frequencies in this example, crossover frequencies result for any **m** and **n** as

$$F_r = F_i \ (n \pm m) \ / \ (1 \pm n)$$

where F_i is the input frequency, and **m** and **n** are the integral multipliers of the input and LO frequencies, respectively. For any $m \geq 0$ and $n \geq 0$, there is a crossover output if the resulting F_r falls within the output band.

The Receive Mixer

Each receive mixing process results in a single desired response as well as an infinite sum of primary and higher order spurious responses. Intrinsic to each frequency conversion are two families of spurious products. *Crossover*, or *coincident*, products are responses that are, by definition, equal in frequency to the desired receive frequency. *Tuned* responses, on the other hand, exist as a result of a particular local oscillator frequency, and are in general different in frequency from the desired receive input. *In a single mixing process, crossovers may not be removed by filtering, whereas tuned products are subject to preselection.* Figure 7 displays a typical receiver frequency conversion. A signal in the 30 to 88 MHz band is converted to an intermediate frequency (IF) of 10.7 MHz by mixing with a high side local oscillator (LO) equal in frequency to the sum of the desired frequency and 10.7 MHz.

The primary mixer response in the example of Figure 7 is obtained by subtracting the frequency of the desired signal from the frequency of the LO. In practice, a processor of some kind is attached to the IF port of the mixer, and the goal is to shift, or convert, the signal of interest to the IF without distortion. To receive a signal at 32.1 MHz, for example, the LO would be set to 42.8 MHz. Then, any information entering the RF port of the mixer at 30 MHz would experience a shift in frequency by the amount of the LO frequency, or 42.8 MHz. In this instance, the IF response is known as a -1 by +1 product, as the 10.7 MHz IF results from subtracting the desired input frequency from the established LO frequency. It is important to note that while the signal of interest appears to have been ideally shifted to the IF frequency, any spectrum of information associated with the input signal is inverted in the mixing process. This phenomenon is associated with the subtractive nature of this particular conversion, and can be easily confirmed by perturbing the input frequency slightly. An increase in the input frequency will result in a corresponding decrease in the IF. The implications of such a frequency inversion are beyond the scope of this article. Suffice it to say that modern signal processing techniques can easily accommodate the flipped spectrum, but must clearly be planned in advance.

The Receive Tuned Response

The receive tuned response is analogous to the transmit tuned output. The tuned response may be anywhere in-band, or even out of band. Figure 7 depicts a frequency scheme similar to the exciter configuration of Figure 5. As an example, the desired frequency of 35 MHz is converted to the IF by virtue of an LO at 45.7 MHz. The desired response is the LO frequency less the input frequency. A type of tuned response of

paramount interest is the *image response*. *The image response is undesired primary response for the specified IF frequency and the imposed LO frequency*. In Figure 7, the image response occurs at 56.4 MHz. In this example, the image lies within the band of interest, but this is not necessarily the case for all frequency conversion arrangements.

An example of a higher order in-band response occurs at 72.6 MHz. With the LO at 45.7 MHz, an input at 72.6 MHz can arrive at the 10.7 MHz IF via a -3 by +5 conversion. Similarly, a signal exterior to the desired 30 to 88 MHz band may result in an IF response. An input at 102.1 MHz can produce a strong +1 by -2 IF response if not remove by preselection. The tuned response can, at least in principle, be removed or attenuated by suitable filtering. Out-of-band inputs can theoretically be eliminated by preselection. In-band spurious responses, particularly in wideband systems, are often reduced by switched bandpass filter arrangements or through the use of tracking bandpass filters. The preferred filtering approach is determined by the precise frequency scheme and the degree of needed product suppression. *Judicious specification of the frequency conversion architecture must be viewed as a necessary precursor to discussions involving filtering requirements.*

The Receive Crossover Response

It is often assumed that received information is converted in frequency without distortion. While such an assumption is sometimes acceptable, there are instances in which the signal can suffer distortion even in the absence of other interfering frequencies. The *crossover*, or *coincident*, response is intrinsic to any given frequency conversion scheme. In the arrangement of Figure 8, a crossover exists for a received frequency of 32.1 MHz. The desired, or primary, 10.7 MHz response is due simply to the subtraction of the 32.1 MHz input from the imposed 42.8 MHz LO. Note, however, that +3 times the 32.1 MHz input summed with -2 times the 42.8 MHz LO also yields 10.7 MHz. The significance of this spurious relationship is quite profound. Simply stated, specification of the frequency scheme alone resulted in the crossover at 32.1 MHz. Any attempt to receive at 32.1 MHz will result in the superposition of a higher order response in the IF. The degree to which the spurious response is suppressed below the desired response is intrinsic to the mixer itself. *As crossover responses* coincide *with the desired response, they can never be filtered out*. The system engineer must plan in advance for crossovers and must be careful not to underestimate their prevalence in the design phase.

In the receiver example of Figure 8, or in any single receive conversion in which the IF frequency is obtained by subtracting the RF frequency from the LO frequency, the crossover frequencies are given by

$$F_r = F_i \ (n \pm 1) \ / \ (m - n)$$

where F_i is the IF frequency, and **m** and **n** are the integral multipliers of the RF and LO frequencies, respectively. For any $m \geq 0$ and $n \geq 0$ ($m \neq n$), there is a crossover response if the resulting F_r falls within the receive band.

Multiple Frequency Conversions

Multiple frequency conversion architectures likewise display the imperfections of both coincident and tuned spurious phenomena. In addition, a system of N conversions reveals an additional N-1 classes of each of these general categories. These response [output] varieties behave identically to the single conversion families with the major exception that all products, including crossovers, become subject to frequency filtering in general.

Multiple conversion arrangements aside for a moment, even a single frequency conversion may represent more to worry about than first meets the eye. While transmit schemes can be as troublesome as receive conversion processes, attention here will focus on receiver-oriented spurious products, or responses.

Figure 9 illustrates a typical first downconversion for a UHF radio. The receive band of 225 to 400 MHz is converted to a 70 MHz first IF by mixing with a low side local oscillator spanning 155 to 330 MHz. There are two types of spurious responses for such an arrangement. The first type, often overlooked in system definition, is the *crossover*, or *coincident*, response. Unanticipated crossovers have been the death of otherwise well planned systems more than once. In the example, a crossover exists at 280 MHz. Tuning the converter to 280 MHz, by definition, requires setting the LO to 210 MHz. The 70 MHz IF is simply the difference between the RF and LO frequencies. Of note is the fact that the 70 MHz IF frequency can likewise be obtained by subtracting twice the RF frequency from three times the LO frequency. This coincidence, shown mathematically in Figure 9, represents a response that cannot be filtered away. By definition, the coincident spur frequency and the receive frequency are equal. Crossover locations and amplitudes must be taken into account in the early stages of system conception.

A more commonly understood class of response is the *tuned product*. The tuned spur is a frequency, in general different from the receive frequency, at which an IF response may occur. In Figure 5, with the receiver tuned to 225 MHz (LO frequency of 155 MHz), there is a tuned response at 395 MHz. Three times the 155 MHz LO frequency, minus the 395 MHz tuned spur frequency, yields the 70 MHz IF. Tuned products can in general be filtered out.

Two additional classes of spurious products exist in a dual conversion scheme as shown in Figure 10. Here there are two crossover classes. In the first (Class 2RC11), the crossover, in the first IF, coincides exactly with the first IF frequency. In the second (2RC10), the crossover response can occur with an offset IF frequency. In the example, a crossover occurs at 281.45 MHz via a first IF at 71.45 MHz. By definition, the first IF remains at 70 MHz for the desired signal. *Higher classes of coincident responses or outputs are subject to filtering within IFs, but not at the front end of the receiver or the output of the exciter.* The class designation introduced here, summarized in Appendix A, greatly facilitates understanding of spurious characteristics in both receiving and transmitting systems. In this example, the first character (2) specifies a dual conversion in general. The second character (R) indicates a receive system. The third character (C or T) informs that the product of interest is a crossover or tuned product. There remain as many characters, each either 0 or 1, as there are frequency conversions in the system.

Figure 10 likewise illustrates higher classes of tuned products. As is the case with crossovers, IF filtering can impact the overall level of the product.

Figure 11 illustrates a typical triple conversion receive architecture. This system tunes the 30 to 1200 MHz band by initially upconverting the input to a narrowband 2500 MHz first IF. The corresponding high side first LO falls in the 2530 to 3700 MHz band. A tracking bandpass filter is employed as a preselector. The 2500 MHz first IF is converted to a 160 MHz second IF via a second LO at 2660 MHz, and is ultimately reduced to baseband at 21.4 MHz. Narrowband fixed bandpass filters are used in the two IFs. As might be expected, the overall spurious computation, including the effects of practical fixed and voltage-tuned filters, can be overwhelming.

Figure 12 depicts a partial ***SysCad*** printout of tuned products for the triple conversion receiver tuned to 880 MHz. The desired response (3RT111) arrives at the 21.4 MHz IF by repeated conversion to the nominal IF frequencies. *Tuning* the system to a particular frequency implies only that the first LO be set to some corresponding frequency. In this example, the first LO is set at 3380 MHz, thereby shifting the frequency of the input to that of the 2500 MHz first IF. Subsequently, by virtue of mixing with the 2660 MHz second LO, the signal of interest coincides with the nominal 160 MHz second IF. A final frequency conversion locates the desired input at precisely 21.4 MHz.

It is important to note that while the desired response relies on one of the two primary modes of each mixer, many classes of compound responses exist in a system of the complexity shown in Figure 11. The following table provides some examples of other classes of triple conversion tuned responses. Bold faced frequencies coincide with the respective nominal IF frequencies.

Spur Freq	Class	1st IF	2nd IF
819.0667	3RT000	2457.2000	202.8000
940.0000	3RT001	2820.0000	***160.0000***
625.0000	3RT011	***2500.0000***	***160.0000***
880.0000	3RT100	880.0000	20.0000
880.0000	3RT111	***2500.0000***	***160.0000***

The input at 819.0667 MHz results in a final 21.4 MHz response via a +3X0/-1X+1/+1X-1 process. Both related IF frequencies result away from the nominal band centers. The 940 MHz response (+3X0/+1X-1/-1X+1) enters the last mixer at 160 MHz, and therefore must be removed by filtering before the first conversion (preselection) or in the first IF. The 625 MHz response (+4X0/-1X+1/-1X+1) is due only to the 4X0 behavior of the first mixer, and may only be filtered in the preselector. The 3RT100 class 880 MHz response (+1X0/-3X+1/-8X+1) is also a 3RC100 crossover. Finally, the desired 3RT111 880 MHz response, also a crossover by definition, causes a response in the 21.4 MHz third IF (baseband) by passing directly through the various nominal IF frequencies (-1X+1/-1X+1/-1X+1).

Summary

Spurious performance of systems employing a single receive or transmit frequency conversion, while simple in concept, is often misunderstood. In particular, the crossover, or coincident, class of spurious products is easily overlooked, and is often solely responsible for incapacitation of key band segments or channels. Multiple conversion systems represent a greatly aggravated spurious environment for the system engineer. Understanding the nature of compound spurious phenomena, in particular the locations of all crossover and tuned responses and outputs, is paramount to the successful realization of modern wideband receiving and transmitting hardware.

Appendix A

Spurious Product Class Identification

Spurious class nomenclature is due to Webb Laboratories and is provided to ease understanding and recognition of spur families and types:

First Character

Integer	Number of Frequency Conversions

Second Character

R	Receive Process
T	Transmit (Excite) Process

Third Character

0	Spur Frequency Unequal to First Receive Mixer Input Frequency, or First Transmit Mixer Output Frequency
1	Spur Frequency Equal to First Receive Mixer Input Frequency, or First Transmit Mixer Output Frequency

Fourth Character

0	Spur Frequency Unequal to Second Receive Mixer Input Frequency, or Second Transmit Mixer Output Frequency
1	Spur Frequency Equal to Second Receive Mixer Input Frequency, or Second Transmit Mixer Output Frequency

Fifth Character

0	Spur Frequency Unequal to Third Receive Mixer Input Frequency, or Third Transmit Mixer Output Frequency
1	Spur Frequency Equal to Third Receive Mixer Input Frequency, or Third Transmit Mixer Output Frequency

.
.
.

REFERENCES

1. S. F. George and J. W. Wood, *Ideal Limiting*, Part 1 (Washington, D.C.: U.S. Naval Research Laboratory, AD 266069, October 2, 1961).

2. V. Manassewitch, *Frequency Synthesizers - Theory and Design*, Wiley - Interscience, New York, 1987, pp. 71-83.

3. R. C. Webb, "Optimize Multiple Conversions by Controlling Spurs," *Microwaves & RF*, August 1991, pp. 140-148.

4. *SysCad 5.0 User's Manual*, Webb Laboratories, Hartland, Chapters 5 and 7.

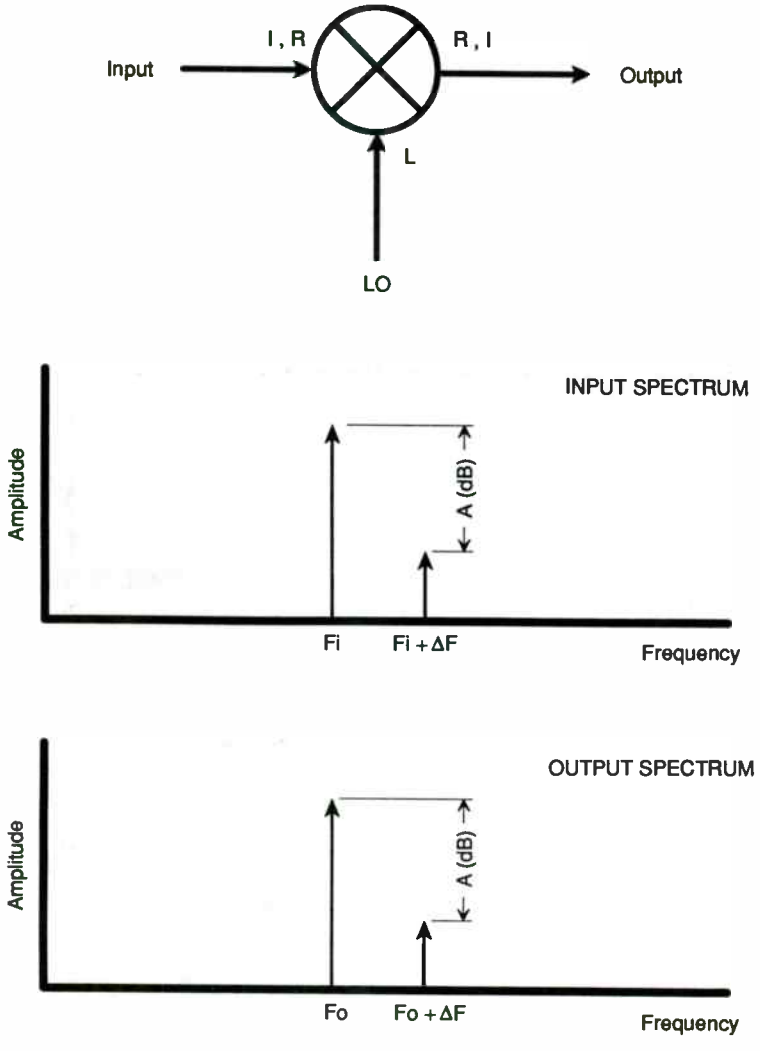

Figure 1 - Spurious Inputs to RF or IF Mixer Port

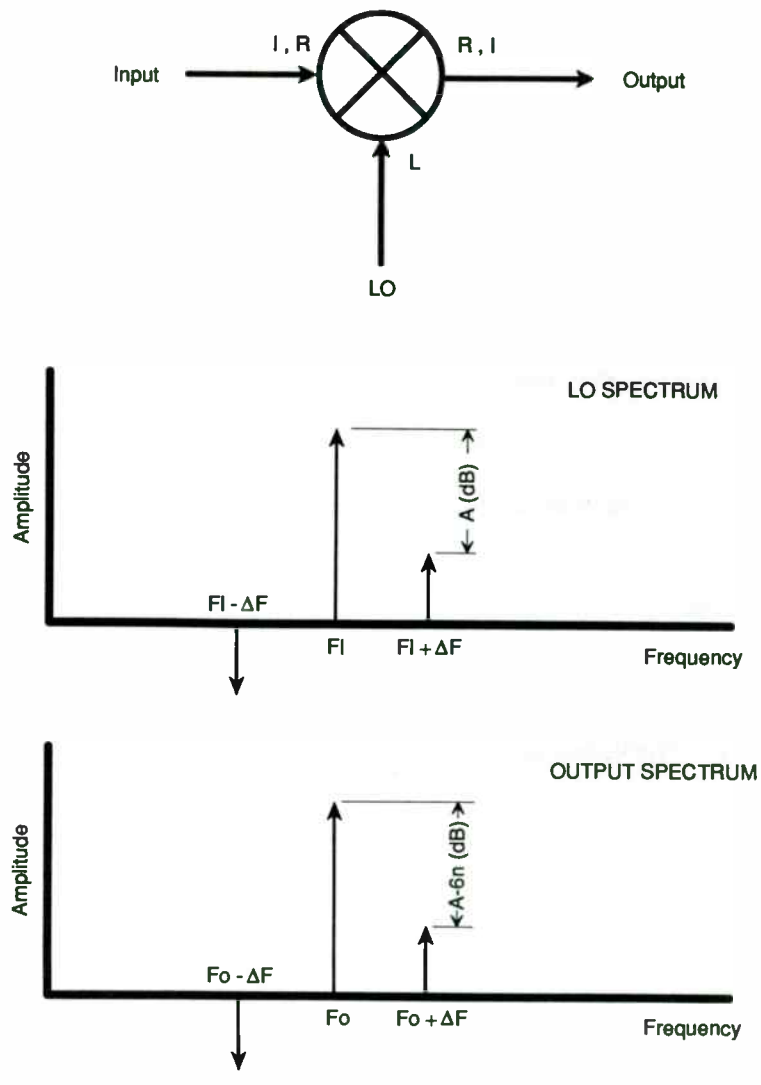

Figure 2 - Phase (Frequency) Modulation on LO Signal

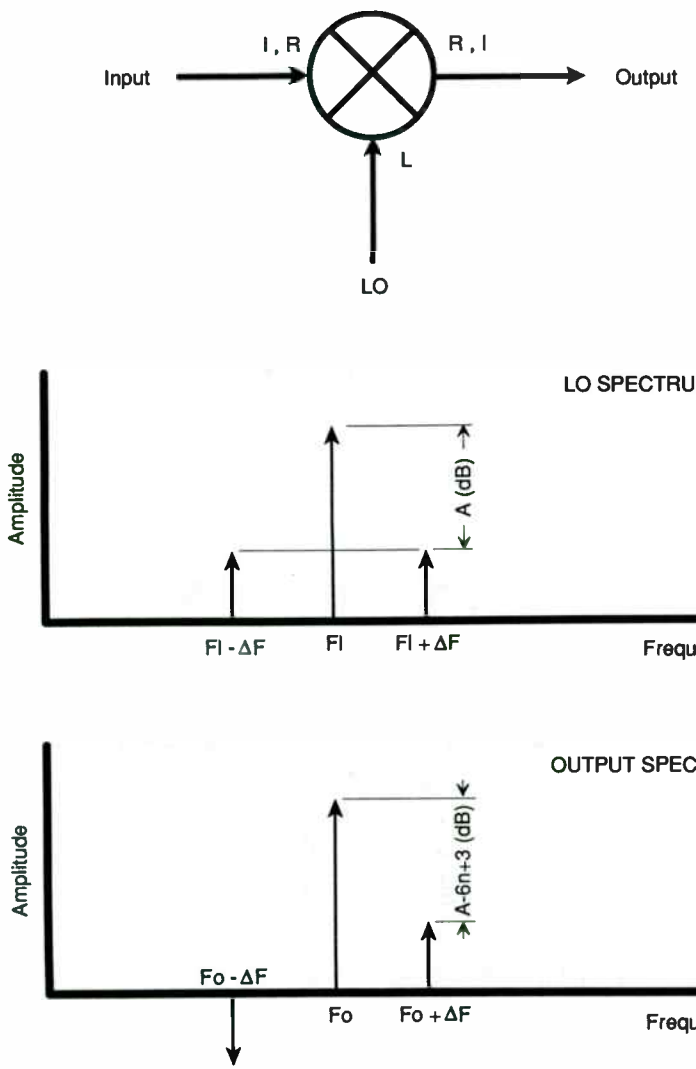

Figure 3 - Amplitude Modulation on LO Signal

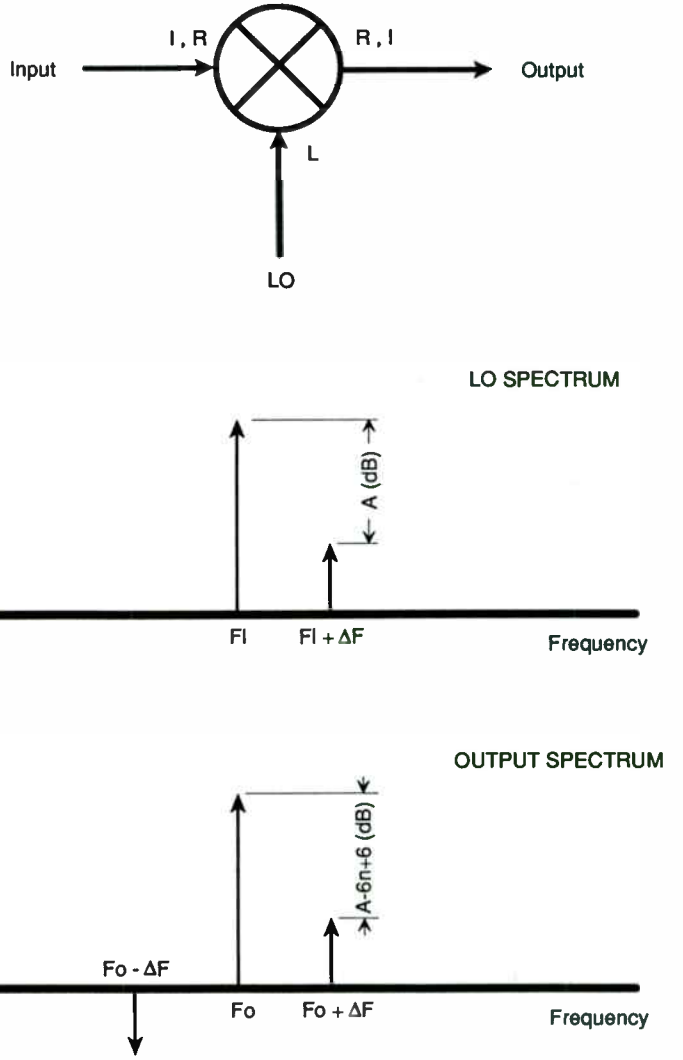

Figure 4 - Spurious Tone Summed with LO Signal

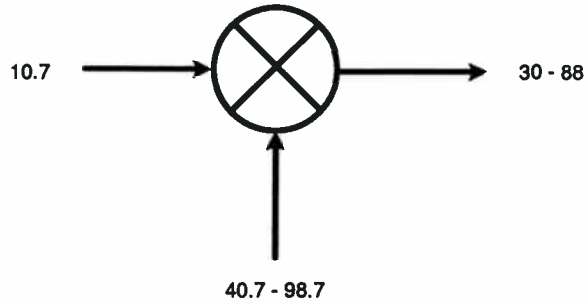

Fr 30 - 88 MHz
Fl 40.7 - 98.7 MHz
Fi 10.7 MHz

Desired Output: Fr = Fl - Fi

Typical Tuned Outputs when tuned to 35 MHz:

Desired:	-1 (10.7) +1 (45.7)	=	35
Image in Band:	+1 (10.7) +1 (45.7)	=	56.4
Higher Order in band:	+2 (10.7) +1 (45.7)	=	67.1
Out of Band:	+1 (10.7) +2 (45.7)	=	102.1

Figure 5 - Typical Exciter Upconverter - Tuned Outputs

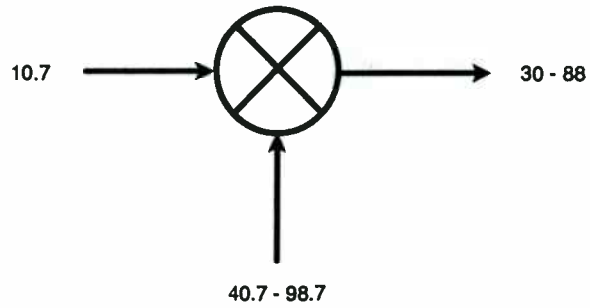

Fr 30 - 88 MHz
Fl 40.7 - 98.7 MHz
Fi 10.7 MHz

Desired Output: Fr = Fl - Fi

Typical Crossover (Coincident) Output at 37.45 MHz:

Desired:	-1 (10.7) +1 (48.15)	=	37.45
Crossover:	-10 (10.7) +3 (48.15)	=	37.45

Figure 6 - Typical Exciter Upconverter - Crossover Outputs

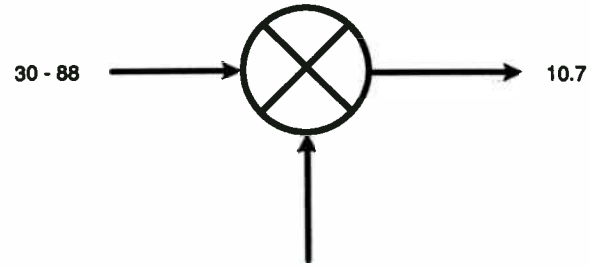

Fr 30 - 88 MHz
Fl 40.7 - 98.7 MHz
Fi 10.7 MHz

Desired Response: Fi = Fl - Fr

Typical Tuned Responses when tuned to 35 MHz:

Desired:	-1 (35.0)	+1 (45.7)	=	10.7
Image in Band:	+1 (56.4)	-1 (45.7)	=	10.7
Higher Order in Band:	-3 (72.6)	+5 (45.7)	=	10.7
Out of Band:	+1 (102.1)	-2 (45.7)	=	10.7

Figure 7 - Typical Receiver Downconverter - Tuned Responses

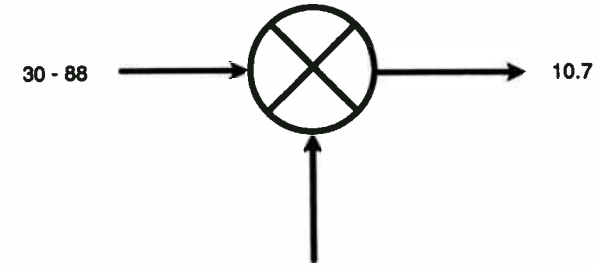

Fr 30 - 88 MHz
Fl 40.7 - 98.7 MHz
Fi 10.7 MHz

Desired Response: Fi = Fl - Fr

Typical Crossover (Coincident) Response at 32.1 MHz:

Desired:	-1 (32.1)	+1 (42.8)	=	10.7
Crossover:	+3 (32.1)	-2 (42.8)	=	10.7

Figure 8 - Typical Receiver Downconverter - Crossover Response

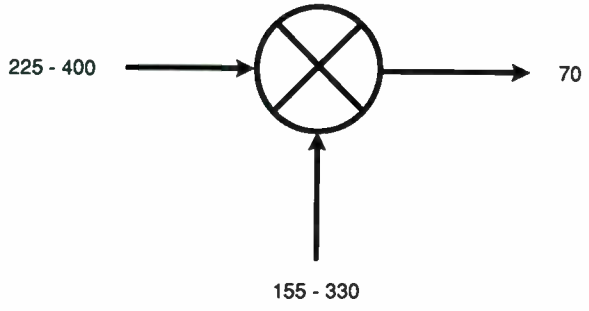

Fr 225 - 400 MHz
Fl 155 - 330 MHz
Fi 70 MHz

Desired Response: Fi = Fr - Fl

Typical Crossover (Coincident) Response at 280 MHz:

Desired:	+1 (280) -1 (210) = 70	Class	1RC1
Crossover:	-2 (280) +3 (210) = 70	Class	1RC1

Typical Tuned Response (Receiver Tuned to 225 MHz : Spur at 395 MHz):

Desired:	+1 (225) -1 (155) = 70	Class	1RT1
Spurious Response:	-1 (395) +3 (155) = 70	Class	1RT0

Figure 9 - Typical Receiver Downconverter

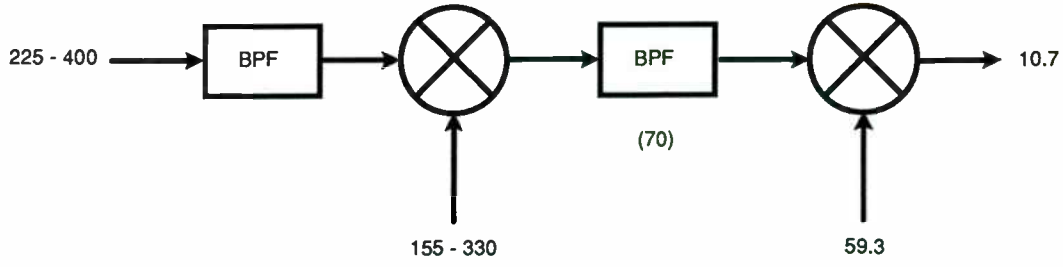

Desired Response: FI2 = FR - FL1 - FL2

Typical Crossover (Coincident) Responses:

Desired:	+1 [+1 (280) -1 (210)] -1 (59.3) = 10.7	I1s = 70	Class	2RC11
Crossover:	+1 [-2 (280) +3 (210)] -1 (59.3) = 10.7	I1s = 70	Class	2RC11
Desired:	+1 [+1 (281.45) -1 (211.45)] -1 (59.3) = 10.7	I1s = 70	Class	2RC11
Crossover:	-4 [-2 (281.45) +3 (211.45)] +5 (59.3) = 10.7	I1s = 71.45	Class	2RC10

Typical Tuned Responses (Receiver Tuned to 300 MHz : FL1 at 230 MHz):

Desired:	+1 [+1 (300) -1 (230)] -1 (59.3) = 10.7	I1s = 70	Class	2RT11
Tuned Response:	+1 [+2 (265) -2 (230)] -1 (59.3) = 10.7	I1s = 70	Class	2RT01
Tuned Response:	-3 [+1 (305.5) -1 (230)] +4 (59.3) = 10.7	I1s = 75.5	Class	2RT00
Tuned Response:	+4 [+2 (268.4) -2 (230)] -5 (59.3) = 10.7	I1s = 76.8	Class	2RT00

Figure 10 - Typical Dual Conversion Receive Downconverter

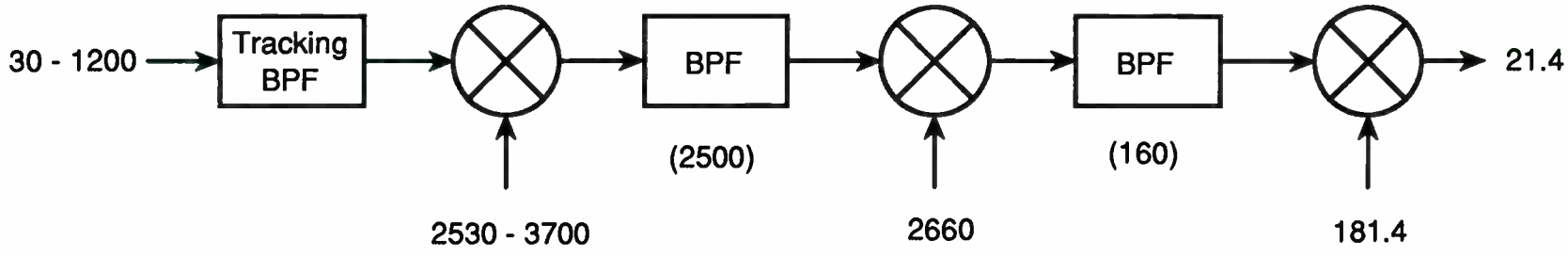

Figure 11 - Typical Multioctave EW Receiver Frequency Architecture

SysCad Version 5.0 S/N 13686 Copyright(c) Webb Laboratories 1985-1991 All Rights Reserved 8-21-91

Rcv Freq	Spur Freq	1st LO	1st IF	2nd IF	M1	N1	M2	N2	M3	N3	Mx1	Mx2	Mx3	Pre	F1	F2	Rej	Class
880.0000	2820.0000	3380.0000	2820.0000	160.0000	+1	+0	+1	-1	-1	+1	24	0	0	26	46	0	96	3RT001
880.0000	2457.2000	3380.0000	2457.2000	202.8000	+1	+0	-1	+1	+1	-1	24	0	0	23	0	44	91	3RT000
880.0000	2500.0000	3380.0000	2500.0000	160.0000	+1	+0	-1	+1	-1	+1	24	0	0	23	0	0	47	3RT011
880.0000	1250.0000	3380.0000	2500.0000	160.0000	+2	+0	-1	+1	-1	+1	73	0	0	4	0	0	77	3RT011
880.0000	940.0000	3380.0000	2820.0000	160.0000	+3	+0	+1	-1	-1	+1	67	0	0	0	46	0	113	3RT001
880.0000	819.0667	3380.0000	2457.2000	202.8000	+3	+0	-1	+1	+1	-1	67	0	0	0	0	44	111	3RT000
880.0000	833.3333	3380.0000	2500.0000	160.0000	+3	+0	-1	+1	-1	+1	67	0	0	0	0	0	67	3RT011
880.0000	625.0000	3380.0000	2500.0000	160.0000	+4	+0	-1	+1	-1	+1	86	0	0	3	0	0	89	3RT011
880.0000	500.0000	3380.0000	2500.0000	160.0000	+5	+0	-1	+1	-1	+1	90	0	0	11	0	0	101	3RT011
880.0000	2820.0000	3380.0000	2820.0000	160.0000	+1	+0	+1	-1	-1	+1	24	0	0	26	46	0	96	3RT001
880.0000	2457.2000	3380.0000	2457.2000	202.8000	+1	+0	-1	+1	+1	-1	24	0	0	23	0	44	91	3RT000
880.0000	2500.0000	3380.0000	2500.0000	160.0000	+1	+0	-1	+1	-1	+1	24	0	0	23	0	0	47	3RT011
880.0000	1250.0000	3380.0000	2500.0000	160.0000	+2	+0	-1	+1	-1	+1	73	0	0	4	0	0	77	3RT011
880.0000	940.0000	3380.0000	2820.0000	160.0000	+3	+0	+1	-1	-1	+1	67	0	0	0	46	0	113	3RT001
880.0000	819.0667	3380.0000	2457.2000	202.8000	+3	+0	-1	+1	+1	-1	67	0	0	0	0	44	111	3RT000
880.0000	833.3333	3380.0000	2500.0000	160.0000	+3	+0	-1	+1	-1	+1	67	0	0	0	0	0	67	3RT011
880.0000	625.0000	3380.0000	2500.0000	160.0000	+4	+0	-1	+1	-1	+1	86	0	0	3	0	0	89	3RT011
880.0000	500.0000	3380.0000	2500.0000	160.0000	+5	+0	-1	+1	-1	+1	90	0	0	11	0	0	101	3RT011
880.0000	6200.0000	3380.0000	2820.0000	160.0000	+1	-1	+1	-1	-1	+1	0	0	0	41	46	0	87	3RT001
880.0000	5837.2000	3380.0000	2457.2000	202.8000	+1	-1	-1	+1	+1	-1	0	0	0	40	0	44	84	3RT000
880.0000	5880.0000	3380.0000	2500.0000	160.0000	+1	-1	-1	+1	-1	+1	0	0	0	40	0	0	40	3RT011
880.0000	5960.0000	3380.0000	2580.0000	160.0000	+1	-1	-2	+2	-1	+1	0	74	0	40	2	0	117	3RT001
880.0000	2940.0000	3380.0000	2500.0000	160.0000	+2	-1	-1	+1	-1	+1	73	0	0	27	0	0	100	3RT011
880.0000	1960.0000	3380.0000	2500.0000	160.0000	+3	-1	-1	+1	-1	+1	64	0	0	17	0	0	81	3RT011
880.0000	1470.0000	3380.0000	2500.0000	160.0000	+4	-1	-1	+1	-1	+1	90	0	0	9	0	0	99	3RT011
880.0000	517.2000	3380.0000	2862.8000	202.8000	-1	+1	+1	-1	+1	-1	0	0	0	10	50	44	105	3RT000
880.0000	560.0000	3380.0000	2820.0000	160.0000	-1	+1	+1	-1	-1	+1	0	0	0	7	46	0	53	3RT001
880.0000	922.8000	3380.0000	2457.2000	202.8000	-1	+1	-1	+1	+1	-1	0	0	0	0	0	44	44	3RT000
880.0000	880.0000	3380.0000	2500.0000	160.0000	-1	+1	-1	+1	-1	+1	0	0	0	0	0	0	0	3RT111
880.0000	912.1000	3380.0000	2467.9000	192.1000	-1	+1	-1	+1	+2	-2	0	0	74	0	0	40	114	3RT000
880.0000	848.0667	3380.0000	2531.9333	128.0667	-1	+1	-1	+1	+3	-2	0	0	69	0	0	43	112	3RT000
880.0000	890.7000	3380.0000	2489.3000	170.7000	-1	+1	-1	+1	-2	+2	0	0	74	0	0	22	96	3RT000
880.0000	833.8000	3380.0000	2546.2000	113.8000	-1	+1	-1	+1	-3	+2	0	0	69	0	0	51	120	3RT000
880.0000	640.0000	3380.0000	2740.0000	160.0000	-1	+1	+2	-2	-1	+1	0	74	0	3	36	0	113	3RT001
880.0000	821.4000	3380.0000	2558.6000	202.8000	-1	+1	-2	+2	+1	-1	0	74	0	0	0	44	118	3RT000
880.0000	800.0000	3380.0000	2580.0000	160.0000	-1	+1	-2	+2	-1	+1	0	74	0	0	2	0	76	3RT001
880.0000	440.0000	3380.0000	2500.0000	160.0000	-2	+1	-1	+1	-1	+1	73	0	0	14	0	0	87	3RT011
880.0000	293.3333	3380.0000	2500.0000	160.0000	-3	+1	-1	+1	-1	+1	64	0	0	24	0	0	88	3RT011
880.0000	220.0000	3380.0000	2500.0000	160.0000	-4	+1	-1	+1	-1	+1	90	0	0	30	0	0	120	3RT011
880.0000	9260.0000	3380.0000	2500.0000	160.0000	+1	-2	-1	+1	-1	+1	35	0	0	48	0	0	83	3RT011
880.0000	4630.0000	3380.0000	2500.0000	160.0000	+2	-2	-1	+1	-1	+1	74	0	0	35	0	0	109	3RT011
880.0000	3086.6667	3380.0000	2500.0000	160.0000	+3	-2	-1	+1	-1	+1	69	0	0	28	0	0	97	3RT011
880.0000	3940.0000	3380.0000	2820.0000	160.0000	-1	+2	+1	-1	-1	+1	35	0	0	32	46	0	114	3RT001
880.0000	4302.8000	3380.0000	2457.2000	202.8000	-1	+2	-1	+1	+1	-1	35	0	0	34	0	44	114	3RT000
880.0000	4260.0000	3380.0000	2500.0000	160.0000	-1	+2	-1	+1	-1	+1	35	0	0	34	0	0	69	3RT011
880.0000	2130.0000	3380.0000	2500.0000	160.0000	-2	+2	-1	+1	-1	+1	74	0	0	19	0	0	93	3RT011
880.0000	1313.3333	3380.0000	2820.0000	160.0000	-3	+2	+1	-1	-1	+1	69	0	0	5	46	0	120	3RT001
880.0000	1420.0000	3380.0000	2500.0000	160.0000	-3	+2	-1	+1	-1	+1	69	0	0	8	0	0	77	3RT011
880.0000	12960.0000	3380.0000	2820.0000	160.0000	+1	-3	+1	-1	-1	+1	13	0	0	54	46	0	113	3RT001
880.0000	12597.2000	3380.0000	2457.2000	202.8000	+1	-3	-1	+1	+1	-1	13	0	0	53	0	44	111	3RT000
880.0000	12640.0000	3380.0000	2500.0000	160.0000	+1	-3	-1	+1	-1	+1	13	0	0	53	0	0	66	3RT011
880.0000	6320.0000	3380.0000	2500.0000	160.0000	+2	-3	-1	+1	-1	+1	70	0	0	41	0	0	111	3RT011
880.0000	7320.0000	3380.0000	2820.0000	160.0000	-1	+3	+1	-1	-1	+1	13	0	0	44	46	0	103	3RT001
880.0000	7682.8000	3380.0000	2457.2000	202.8000	-1	+3	-1	+1	+1	-1	13	0	0	45	0	44	102	3RT000
880.0000	7640.0000	3380.0000	2500.0000	160.0000	-1	+3	-1	+1	-1	+1	13	0	0	45	0	0	58	3RT011
880.0000	3820.0000	3380.0000	2500.0000	160.0000	-2	+3	-1	+1	-1	+1	70	0	0	32	0	0	102	3RT011
880.0000	16020.0000	3380.0000	2500.0000	160.0000	+1	-4	-1	+1	-1	+1	40	0	0	58	0	0	98	3RT011
880.0000	11020.0000	3380.0000	2500.0000	160.0000	-1	+4	-1	+1	-1	+1	40	0	0	51	0	0	91	3RT011

Figure 12 - Partial SysCad Tuned Response Printout for Triple Conversion Receiver

Specifying Local Oscillator Phase Noise Performance: How Good is Good Enough?

Robert Gilmore

Qualcomm, Inc.
10555 Sorrento Valley Road
San Diego, CA 92121
(619) 587 - 1121

Abstract

Definitive criteria are provided for specifying local oscillator phase noise performance for use in communication systems. In the absence of such criteria, many oscillators tend to be either under or over-specified. The emphasis is on digital modulation and demodulation, but analog communications are also considered. LO phase noise is analyzed for loss in demodulator performance, and also for impact on the modulation process. The results may be used to select an appropriate oscillator, or to tailor the noise characteristics of a frequency synthesizer design.

I. Introduction

The systems designer must consider the effects of local oscillator phase noise when planning a communication system. The effect of imperfect local oscillators is to degrade both the demodulation and modulation processes. The extent of the degradation depends upon the characteristics of the phase noise, and also upon the particular modulation type selected. It will be shown that LO phase noise may degrade a system in three major ways: a coherence error, a signal loss due to PM spreading, and an additive noise effect. The coherence error applies only to coherent digital demodulators. The other two effects apply to most receivers, but it will be shown that coherent BPSK is largely immune to the additive noise effect.

The paper begins with a description of pertinent concepts and definitions. The performance loss due to phase noise is described in general, and then specifically applied to the following demodulators: analog FM, non-coherent FSK, coherent BPSK, QPSK, OQPSK, and MSK, and differential PSK. Since phase noise may be specified either in the frequency or the time domain, some results are provided both in terms of frequency and time domain criteria. The emphasis is not upon the source of noise in oscillators, but rather upon the performance loss attributable to phase noise.

II. Definitions and Concepts

i. Fourier frequency

The frequency difference between a specific frequency component and the fundamental frequency (ie., the carrier) of a signal.

ii. $S_\phi(f)$

The one-sided spectral density of the phase fluctuations. Phase fluctuations are due to noise, instability, and modulation. The range of Fourier frequency f is from zero to infinity, and the dimensions are radians^2/Hz. $S_\phi(f)$ involves no power measurement of the signal - it is not a *power* spectral density which would be measured in Watts/Hz. In practice, $S_\phi(f)$ is measured by passing the signal through a phase detector and measuring the power spectral density at the detector output. (see Ref. 4)

iii. $\mathcal{L}(f)$

The normalized frequency domain representation of phase fluctuations. It is the ratio of the power spectral density in one phase modulation sideband, referred to the carrier frequency on a spectral density basis, to the total signal power, at Fourier frequency f. The units are 1/Hz. The frequency ranges from $-f_o$ to $+\infty$, where f_o is the carrier frequency. $\mathcal{L}(f)$ is a 2-sided spectral density. For small angles ϕ (see Ref. 3),

$$\mathcal{L}(f) = S_\phi(f)/2 \qquad (1)$$

iv. $S_y(f)$

The spectral density of frequency fluctuations. In practice, $S_y(f)$ is measured by applying the signal to an FM detector and measuring the resulting spectral density. The dimensions are (fractional frequency)^2/Hz, or 1/Hz. The range of f is from zero to infinity. Since the random process $S_\phi(f)$ is differentiated to yield Sy(f) ,

$$S_y(f) = \left(\frac{f}{f_o}\right)^2 S_\phi(f) \qquad (2)$$

where f_o is the carrier frequency.

v. Allan (or Pairwise) variance $\sigma^2(2,\tau)$

The instantaneous frequency of an oscillator is not observable since any measurement technique requires a finite time interval to be performed. We define $\bar{y}_k$ as a normalized frequency measurement over the gate time τ. Note that

$$\bar{y}_k = \frac{\phi(t_k+\tau) - \phi(t_k)}{2\Pi f_o \tau} \qquad (3)$$

Due to the random phase fluctuations of real oscillators, repeated measurements of $\bar{y}_k$ yield different results. The variance of this statistical process provides a time-domain measure of instability over τ. Assuming that the $\bar{y}_k$ have zero mean, the true variance is equal to

$$\sigma^2[\bar{y}_k] = \langle \bar{y}_k^{\,2} \rangle \qquad (4)$$

where the bracket <> indicates a statistical average calculated over an infinite number of samples at a given time t_k. The Allan or pairwise variance is defined as:

$$\sigma_y^{\,2}(\tau) = \frac{1}{2}\langle (\bar{y}_2 - \bar{y}_1)^2 \rangle \qquad (5)$$

y_1 and y_2 are two adjacent samples taken τ seconds apart, hence *pairwise* variance. A practical measurement technique which involves M individual normalized frequency measurements $y_k = f_k/f_o$ results in the following widely accepted estimate of the Allan variance:

$$\sigma_y^{\,2}(\tau) = \frac{1}{2(M-1)} \sum_{k=1}^{M-1} (\bar{y}_{k+1} - \bar{y}_k)^2 \qquad (6)$$

vi. Power Low Noise Processes

Power low noise processes are models of oscillator noise that result in a particular slope of the spectral density verses frequency. The following table summarizes the five commonly identified power law noise processes, detailing their frequency behavior and Allan variance. (see Ref. 4)

Process Name	S_ϕ proportional to	S_y proportional to	$\sigma_y^2(\tau)$ Allan Variance
Random-walk FM	f^{-4}	f^{-2}	$\frac{3f_n}{(2\pi\tau f_o)^2}$
Flicker FM	f^{-3}	f^{-1}	$\frac{1.038 + 3\ln(\omega_n\tau)}{(2\pi\tau f_o)^2}$
White FM	f^{-2}	flat	$\frac{1}{2\tau f_o^2}$
Flicker øM	f^{-1}	f	$\frac{2\ln 2}{f_o^2}$
White øM	flat	f^2	$\frac{(2\pi)^2\tau}{6f_o^2}$

Table I: Power Low Noise Processes

In the table above, $f_n = \omega_n/2\pi$ is the measurement system 3 dB bandwidth (the measurement should be within 3 dB from DC to f_n).

vii. One-sided vs. Two-Sided Spectral Densities

By convention, noise processes are defined as one-sided spectral densities, and on a per-Hz of bandwidth density basis. The total mean-square fluctuation of frequency is given by (Ref. 3):

$$\text{Total Variance} = \int_0^\infty S_y(f)\,df \tag{7}$$

In contrast, two-sided spectral densities are defined such that the range of integration is from -∞ to +∞. The total variance of frequency fluctuations is given by

$$\int_{-\infty}^{\infty} S_{2\text{-sided}}\,df = 2\int_0^\infty S_{2\text{-sided}}\,df = \int_0^\infty S_{1\text{-sided}}\,df \tag{8}$$

In terms of $\mathcal{L}(f)$, a good approximation for the signals under discussion is

$$\mathcal{L}(-f) = \mathcal{L}(f) \tag{9}$$

However, for special cases of pure PM or FM, as well as correlated combinations of AM and PM, the RF spectral density of the signal is not symmetrical. For pure AM, the power spectral density is strictly symmetrical.

viii. The Relationship Between Phase Noise and Thermal Noise Density

Phase noise and thermal noise (i.e., AWGN) have important similarities and equally important differences. The similarites permit the system designer to add phase noise and thermal noise densities. A common way to ensure that phase noise will not impact system performance is to specify the phase noise density to be x dB (typically 20 dB) below the receive thermal noise density. The differences must be considered, however, in an accurate calculation of performance loss due to phase noise.

The major difference is that phase noise is a small angle random phase modulation of the received signal itself. In this regard, phase noise is more of a multiplicative effect than an additive process. The random PM process responsible for phase noise spreads the signal energy, and therefore reduces the signal power which carries useful information. Fortunately, this reduction in signal power is usually small. It is important to understand that phase noise is not added to the received signal, it is actually derived from the received signal by PM spreading.

When a carrier with a pedestal of pure phase noise power is downconverted to baseband I and Q channels, the phase noise appears primarily in the Q channel (assuming small angle phase modulation). This will be shown in this section. Noncoherent demodulators, which cannot distinguish between received phases, cannot benefit from this phenomena. Coherent modulation with information in the I channel only, such as coherent BPSK, are tolerant of LO phase noise because of this effect.

We now discuss the similarities between phase noise and AWGN. Consider superposed double-sideband thermal noise with total power $2N_o$ added to a carrier. Robins has shown (Ref. 6) that the DSB noise power may be represented as 4 sidebands, upper and lower pure AM sidebands and upper and lower pure PM sidebands, each with power $N_o/2$. Therefore, narrowband AWGN is a composite of $\frac{1}{2}$ AM and $\frac{1}{2}$ PM noise processes.

This result is consistent with the familiar results of signal-to-noise ratios in bandpass limiters. As the input signal-to-noise ratio of a bandpass limiter is varied, the asymptotes of the output SNR are well documented (Ref. 2):

$$\frac{(S/N)_{out}}{(S/N)_{in}} \to 2 \quad (+3\text{ dB}) \text{ as } (S/N)_{in} \to \infty \tag{10}$$

$$\frac{(S/N)_{out}}{(S/N)_{in}} \to \frac{\pi}{4} \quad (-1.05\text{ dB}) \text{ as } (S/N)_{in} \to 0$$

The +3 dB asymptotic increase in SNR for large input SNR's is due to the limiter suppression of the AM component of the additive noise. *The remaining noise is the PM component, and accounts for precisely $\frac{1}{2}$ of the input narrowband noise).*

The fact that additive narrow-band thermal noise may be represented as half AM and half PM is important to a discussion of the effect of phase noise on communications system performance. Phase noise effects system performance in three major ways - it degrades the coherence of the demodulation process, it reduces the signal power due to PM spreading, and it *adds noise.* Unlike thermal noise, additive phase noise due to local oscillators is typically non-white. However, the fact that additive thermal noise may be considered to be half phase noise implies that LO phase noise degrades the signal-to-noise ratio of a communications system as does thermal noise. The fact that LO phase noise is not flat, though, significantly complicates the calculation of performance degradation for this effect in contrast with additive white Gaussian noise (AWGN).

Additional insight may be gained by considering the narrowband noise representation:

$$n(t) = x(t)\cos\omega_o t + y(t)\sin\omega_o t \quad (11)$$

where $\overline{x^2(t)} = \overline{y^2(t)} = \overline{n^2(t)} = N_o$

In polar coordinates,

$$n(t) = r(t)\cos[\omega_o t + \theta(t)] \quad (12)$$

where r(t) is Rayleigh distributed $0 \le r(t) \le \infty$

$\theta(t)$ is uniformly distributed $0 \le \theta(t) \le 2\pi$

This form shows the AM and PM portions of narrowband noise. If this noise process is downconverted to baseband using in-phase and quadrature local oscillators, the baseband portions of the I and Q downconverted outputs are

$$I(t) = \frac{r(t)}{2}\cos[\theta(t)] \quad (13)$$

$$Q(t) = \frac{-r(t)}{2}\sin[\theta(t)] \quad (14)$$

which are noise components each having equal power and $\theta(t)$ varying from 0 to 2π.

If a carrier is inserted into equation 30 the result is:

$$n(t) = [x(t) + A]\cos\omega_o t + y(t)\sin\omega_o t = r(t)\cos[\omega_o t + \theta(t)] \quad (15)$$

where r(t) is Rician distributed $0 \le r(t) \le \infty$ and $\theta(t)$ is an angle modulation process symmetrically distributed about 0° phase. In this case $\theta(t)$ is measured relative to the carrier. For small $\theta(t)$,

$$I(t) \approx \frac{r(t)}{2}\left(1 + \frac{\theta^2}{2}\right) \approx \frac{r(t)}{2} \quad (16)$$

$$Q(t) \approx \frac{-r(t)}{2}\theta(t) \quad (17)$$

The baseband I component contains primarily AM noise, and the Q component contains AM and PM noise. Therefore, the hard-limited Q channel provides a measure of the phase noise $2\mathcal{L}(f) \approx S_\theta(f)$ of an oscillator. In the case of a carrier with pure phase noise, most of the downconverted phase noise appears in the Q channel if the small angle assumption is valid.

III. General Formulation of the Problem

There are three major sources of communication system performance degradation due to LO phase noise:

1. Coherence or correlation error
2. Signal loss due to PM spreading
3. Additive noise effect

The degradation in signal to noise ratio is calculated for each effect (at the nominal receiver SNR in thermal noise) and the results are added in dB. There is also a small effect of phase noise on the demodulator bit timing loop, but this is shown to negligible in general in Ref. 7 (p. 260).

Coherence error applies to coherent demodulation only. Noise in the demodulator carrier tracking loop (i.e., phase estimation loop) causes a phase error which results in a loss in BER performance. The usual assumption is that the bandwidth of the phase estimation loop is small in comparison with the data rate. The resultant phase error may then be considered as constant during each bit interval. In an M-ary transmission with M > 2, this effect also produces interchannel interference. Demodulator phase error causes a cross coupling between, for example, the two orthogonal channels of a QPSK transmission. Coherence loss and interchannel interference will be discussed in detail in the following section.

The third effect is the increase in received noise floor due to the LO noise characteristics. LO noise is integrated in the detection bandwidth and added to integrated thermal noise:

$$\text{Total Noise Power} = \int_0^B N_{LO}\,df + \int_0^B N_o\,df \quad (18)$$

where N_{LO} is the one-sided noise spectral density due to the LO and N_o is the one-sided thermal noise spectral density. From section II – x,

$$\mathcal{L}(f) = \frac{N_{LO}(f)}{C} \quad (19)$$

where C is the LO carrier power. The degraded signal-to-noise ratio in the detection bandwidth is then given by

$$SNR = \left[\int_0^B 2\mathcal{L}(f)\,df + \int_0^B \frac{N_o(f)}{C}\,df\right]^{-1} \quad (20)$$

where C is the LO carrier power.

A convenient way to evaluate the contribution of LO phase noise to total noise density is to plot the normalized phase noise density $\mathcal{L}(f)$ in dBc/Hz on the same plot as $\int_0^B 2\mathcal{L}(f)\,df$ in dBc. The lower integration limit is the phase estimation loop noise bandwidth for the case of coherent demodulation. This is because the phase tracking loop removes phase fluctuations within this frequency region (resulting in coherence error, as described in the following section). In the case of non-coherent demodulation, some high-pass lower limit is generally assumed (perhaps on the order of 1 Hz). An example is shown in Fig 1. Such a plot is easy to create using a computer spreadsheet program. Measured or predicted phase noise data is entered manually in one column, numerically integrated in another column, and both columns are plotted. 3 dB must be added to phase noise data measured on a spectrum analyzer to yield $2\mathcal{L}(f)$. Other spectrum analyzer corrections must usually be applied as well to correct for averaging in LOG mode, and for the envelope detector response to noise.

The integrated phase noise in dBc is compared with the signal-to-noise ratio at a particular frequency. In a digital communication system, the integrated phase noise is compared with E_b/N_o at f = bit rate. Note that

$$\frac{E_b}{N_o} = \frac{P_s \times R^{-1}}{N_o} = \frac{P_s}{N_o R} \qquad \text{dBc in BW} = R \quad (21)$$

where R = bit rate and N_o is assumed to be white. Therefore, E_b/N_o is the total signal power to $\int_0^B N_o\,df$ ratio, where thermal noise is integrated over a bandwidth equal to the bit rate. The

integrated phase noise may be compared directly with E_b/N_o at f = R.

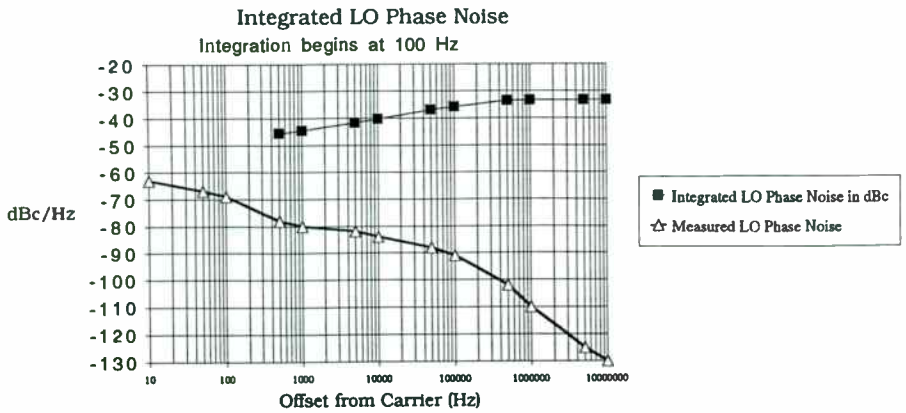

Figure 1: Example LO Phase Noise and Integrated Phase Noise Plot

Consider a 100 Kb/sec received signal data rate, and a nominal receiver operating E_b/N_o of 10 dB. Using the LO depicted in Fig 1, the integrated phase noise at 100 Kb/sec is -36 dBc. The integrated phase noise is 26 dB below thermal noise at the operating point. Summing a noise power X with a noise power X - ΔN dB yields a noise power X + Δ where

$$\Delta\,dB = 10\log\left[1 + 10^{-\Delta N/10}\right] \qquad (22)$$

For ΔN = 26 dB, Δ dB = 0.025. At this operating point, the LO phase noise degrades the received E_b/N_o by 0.025 dB. For convenience, Equation 41 is plotted in Figure 2.

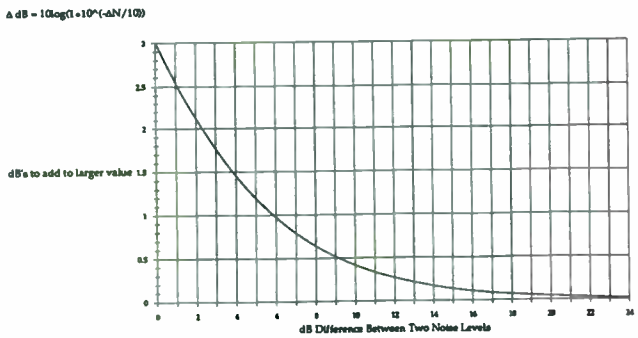

Figure 2: Addition of Two Noise Levels

This technique is straightforward, and added to the signal loss and coherence error effects provides a reasonable estimate of performance loss due to phase noise. For better accuracy though, each modulation type must be treated as a special case. The performance impact on specific modulation types is discussed in Section V.

IV. Coherence or Correlation Error

One effect of LO phase noise on coherent demodulation is that it causes a noisy estimate of phase. (Ref. 6). This results in a coherence or correlation performance degradation. This effect is also caused by additive thermal noise, and the phase noise contribution must be considered relative to thermal noise. Since phase noise tends to increase rapidly at small frequency offsets (typically f^{-3} behavior), phase noise may dominate over AWGN in the frequency region defined by the bandwidth of the phase estimation loop. In the case of M-ary transmissions where M > 2, coherence error results in inter-channel interference between the M-ary channels. The SNR degradation due to coherence error is added in dB to the degradation caused by the additive noise effect. The coherence error effect does not apply to non-coherent demodulators.

Coherent demodulation is performed by correlating the received signal with a phase reference derived by the phase estimation loop. If the bandwidth of the phase estimation loop could be made arbitrarily narrow, the phase noise and thermal noise jitter of the phase reference would be made negligible. System considerations, however, make this impractical. These include frequency instabilities, acquisition bandwidth requirements, and phase/frequency tracking requirements (due to doppler, etc.).

The bandwidth of the phase estimation loop is assumed to be small relative to the bit rate. The resultant phase error may be considered constant during each bit interval. The bit error probability is calculated by averaging the probability of error conditional on phase P(E|ø) over the density function of the phase estimation error ø.

Noise in the phase estimation loop causes a voltage correlation loss of cos(ø) for a phase estimation error ø. This is the total degradation for coherent FSK (orthogonal signalling) and BPSK (antipodal signalling). For QPSK (4-ary orthogonal signalling) interchannel interference proportional to sin(ø) is caused by cross coupling between the ideally orthogonal signal components. During each QPSK symbol interval one channel has destructive cross-coupling interference while the other channel has constructive interference. The conditional probability of bit error P(E|ø) is the arithmetic mean of the error performances for destructive and constructive interference. The coherence error and cross-coupling are shown graphically in Figure 3.

a. BPSK b. QPSK

Figure 3: Coherence Error for BPSK and QPSK

Offset QPSK and MSK signalling will also be considered for performance loss due to coherence error. In offset QPSK, the bit transitions for one channel are staggered to occur at the center of the bit duration for the other channel. This avoids the possibility of 180° transitions, which cause the envelope of filtered QPSK to momentarily go to zero. When a bit transition occurs in offset QPSK, the cross coupling changes sign at midbit of the other channel, so the interference during the first half of the bit interval is cancelled by interference of the opposite polarity during the second half of the bit. Therefore, $P(E|\phi)$ has a correlation loss of $\cos(\phi)$ when a bit transition takes place. If no transition occurs, the situation is identical to QPSK. $P(E|\phi)$ is therefore equal to the average of the performance for BPSK and QPSK given a probability of bit transition of $\frac{1}{2}$ (i.e., random data). The analysis of correlation error for MSK signalling is significantly more complicated, and the results will be quoted from Matyas in Ref. 5.

In summary, the probability of error conditional upon the phase estimation error ϕ is:

$$P_F(E|\phi) = Q\left[\sqrt{\frac{E_b}{N_o}}\cos\phi\right] \quad \text{for FSK} \tag{23}$$

$$P_B(E|\phi) = Q\left[\sqrt{\frac{2E_b}{N_o}}\cos\phi\right] \quad \text{for BPSK} \tag{24}$$

$$P_Q(E|\phi) = \frac{1}{2}\,Q\left[\sqrt{\frac{2E_b}{N_o}}(\cos\phi+\sin\phi)\right] + \frac{1}{2}\,Q\left[\sqrt{\frac{2E_b}{N_o}}(\cos\phi-\sin\phi)\right] \quad \text{for QPSK} \tag{25}$$

$$P_{OQ}(E|\phi) = \frac{1}{2}P_B(E|\phi) + \frac{1}{2}P_Q(E|\phi) \quad \text{for OQPSK} \tag{26}$$

The probability density function for the phase estimation error ϕ given a first-order PLL is given by Viterbi (Ref. 12, p. 90):

$$P(\phi) = \frac{\exp(\alpha\cos\phi)}{2\pi\, I_o(\alpha)} \quad -\pi \le \phi \le \pi \tag{27}$$

where α is the SNR of the phase reference in the phase estimation loop bandwidth:

$$\alpha = \frac{A^2}{N_o B_L} = (\text{phase error variance})^{-1} \tag{28}$$

I_o is the zeroth-order modified Bessel function. This is also a close approximation to $P(\phi)$ for a second-order PLL for large α (Ref. 12, p. 111).

The degraded probability of error is given by:

$$P(e) = \int_{-\pi}^{\pi} P(E,\phi)\,d\phi \tag{29}$$

where $P(E,\phi) = P(E|\phi)\,P(\phi)$

The detection loss in dB is plotted vs. the SNR of the phase reference at E_b/N_o = 7 dB in Figure 4, where SNR = 10 log (α) dB.

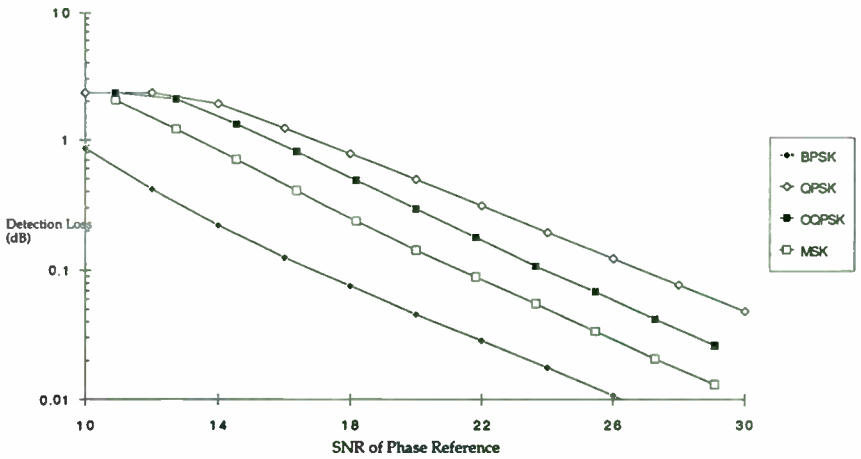

Figure 10: Detection Loss in dB vs. SNR of Phase Reference at E_b/N_o = 7 dB

Fig 4 may be used to establish the performance loss due to coherence error based on the SNR in the phase estimation loop bandwidth. It may also assist in the selection of the phase estimation loop bandwidth. The SNR in the loop bandwidth is given by

$$SNR = \left[\int_0^{B_L} 2\mathcal{S}(f)\,df + \int_0^{B_L}\frac{N_o}{C}\,df\right]^{-1} \tag{30}$$

where B_L is the loop noise bandwidth, and N_o is the thermal noise spectral density.

V. Specific Cases

i. Analog FM

A frequency modulated carrier is described by

$$f_c(t) = A_c\cos\left[\omega_c t + 2\pi f_d\int^t m(\tau)\,d\tau\right] \tag{31}$$

where f_d is the frequency deviation.

The FM demodulater is shown in Figure 5.

Figure 5: FM Demodulator

The limiter strips off AM noise, so that all noise in the demodulation process (either thermal, or due to LO phase noise) is PM. With AWGN only through the demodulator, the output power is given as

$$S_n(f) = \left(\frac{k_D}{2\pi A_c}\right)^2 \cdot (2\pi f)^2 N_o = \frac{k_D^2}{A_c^2} N_o f^2 \quad \text{for } |f| < B_p/2 \qquad (32)$$

$$= 0 \quad \text{elsewhere}$$

This noise spectrum at the discriminator output is plotted in Figure 6.

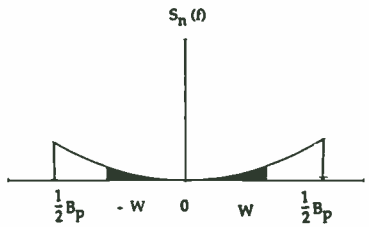

Figure 6: Noise Spectrum at FM Discriminator Output

Low frequency message signals are clearly subjected to lower noise levels than are high frequency signals. The output noise power after the postdetection filter is

$$P_N = \frac{k_D^2}{A_c^2} N_o \int_{-W}^{W} f^2 \, df = \frac{2 k_D^2 N_o W^3}{3 A_c^2} = \frac{k_D^2 W^3}{3}\left(\frac{N_o}{C}\right)_t \qquad (33)$$

where $(N_o/C)_t$ is the thermal noise to carrier power ratio.

The benefit of the postdetection lowpass filter is obvious. The predetection filter bandwidth B_p is greater than 2W. The output SNR is improved by the postdetection LPF of bandwidth W, which reduces the noise power but has no effect upon the signal. In practice, W must be somewhat greater than the signal bandwidth to prevent signal distortion. Note also that the output noise is inversely proportional to the carrier power $C = A_c^2/2$. As the carrier increases, the noise power drops. This is the well known FM "noise quieting" effect.

The FM detector's response to noise shown in Figure 6 shows the reason for the use of pre-emphasis and de-emphasis in FM systems. If higher frequencies are emphasized at the transmitter, they may be de-emphasized at the receiver prior to detection. The received noise at these higher frequencies is therefore reduced, compensating for the detector's parabolic sensitivity vs. frequency. If $H_{DE}(f)$ is the frequency response of the deemphasis filter, the output noise power is given by

$$N_D = \int_{-W}^{W} |H_{DE}(f)|^2 S_n(f) \, df \qquad (34)$$

where $S_n(f)$ is the input noise spectral density.

Now consider the effects of LO phase noise on the demodulation process. Two of the degradations described in Section III apply: signal loss due to PM spreading, and the additive noise effect. As described in Section III, LO phase noise is a random phase modulation of the signal itself, and therefore decreases the received signal power by the power in the phase noise sidebands. With the received signal power normalized to unity, the degraded signal power due to LO phase noise is:

$$P_D = 1 - \int_0^{\infty} S_\phi(f) \, df \qquad (35)$$

10 log (P_D) therefore gives this degradation in dB.

The second degradation is the added noise due to the LO in the region $0 \le f \le W$. The degradation due to this noise power being x dB below thermal noise is given in Figure 2 for C/N_o values above the FM threshold. The requirement that phase noise power be a factor x below thermal power can be stated as

$$\int_0^W 2\wp(f) f^2 \, df \le \frac{1}{x}\left(\frac{N_o}{C}\right)_t \frac{W^3}{3} \qquad (36)$$

The right side of Eq. 36 is from Eq. 33. The discriminator constant k_D is taken to be unity, since it applies equally to both sides of Eq. 36. In practice, the integral on the left is evaluated from some highpass cutoff frequency f_h rather than 0. If a de-emphasis filter is used at the receiver, then Eq. 36 is modified as follows:

$$\int_{f_h}^{W} |H_{DE}(f)|^2 2\wp(f) f^2 df \le \frac{1}{x}\left(\frac{N_o}{C}\right)_t \int_{f_h}^{W} |H_{DE}(f)|^2 f^2 df \qquad (37)$$

ii. Non-Coherent FSK

Coherent detection of FSK is rarely used in practice since it only yields approximately 1 dB of performance improvement over non-coherent detection. We therefore focus on non-coherently detected FSK.

Figure 7 is a block diagram for the MFSK demodulator.

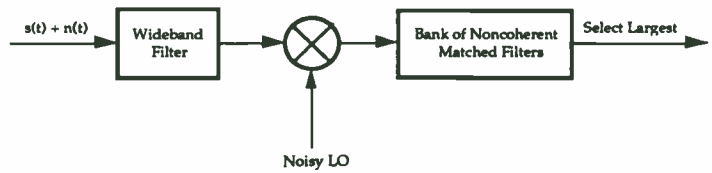

Figure 7: Noncoherent MFSK Demodulator

The matched filters each have a $\sin(\pi fT)/\pi fT$ response, where T is the bit duration. It is assumed that the transmitted signal is mixed down to the matched filter at zero Hz using an LO disturbed by the random phase modulation $\phi(t)$, having spectral density $S_\phi(f)$. The filters are spaced at the tone spacing f_s. Since the demodulator does not estimate received phase, the energy output of the correct filter must involve both the I and Q channels:

$$Y^2 = I^2 + Q^2$$

With the non-degraded correct filter output normalized to unity, the correct filter output power is given by (Ref. 13):

$$\overline{Y^2} = 1 - \sigma_\phi^2 + \int_0^\infty S_\phi(f)\left[\frac{\sin(\pi fT)}{\pi fT}\right] df$$

$$= 1 - \int_0^\infty S_\phi(f)\,df + \int_0^\infty S_\phi(f)\left[\frac{\sin(\pi fT)}{\pi fT}\right]^2 df$$

$$= 1 - \int_0^\infty \left[1 - \left(\frac{\sin(\pi fT)}{\pi fT}\right)^2\right] S_\phi(f)\,df \qquad (38)$$

For tones with orthogonal spacing $f_s = n/T$, the incorrect (noise only) filter outputs are given by

$$\overline{Y_N^2} = \int_0^\infty S_\phi(f)\left[\frac{\sin\pi(f - f_s)T}{\pi(f - f_s)T}\right]^2 df \qquad (39)$$

The correct filter output is equal to the uncorrupted signal power, minus the power in the phase noise sidebands, plus the power recovered in the filter. The incorrect filter outputs are simply the spectrum of the random phase process passed through the linear matched filters. For other than binary FSK, the noise contributions of each of the incorrect matched filters must be summed up. Each component is calculated by replacing f_s by nf_s in Eq. 39.

The resulting SNR is, where N = thermal noise power,

$$SNR = \frac{S \cdot \overline{Y^2}}{N + S \cdot \overline{Y_N^2}} = \frac{S \cdot \overline{Y^2}}{N\left(1 + \frac{S}{N} \cdot \overline{Y_N^2}\right)}$$

$$= \frac{S}{N} \cdot \frac{\overline{Y^2}}{1 + \frac{S}{N} \cdot \overline{Y_N^2}} \qquad (40)$$

The integrals in equations 38 and 39 may be evaluated numerically, and the degradation to the SNR in thermal noise is given by Eq. 40.

Charles Wheatley (Ref. 13) has analyzed the degraded signal power given by Eq. 38 for the case where

$$S\phi_i(f) = \frac{k_i}{f^i} \qquad i = 0,1,2,3 \qquad (41)$$

That is, the power low processes that typically describe oscillator phase noise. He also provides approximate expressions for the loss factors $(1 - \overline{Y^2})$ in terms of the Allan variances of these processes, which were given in Section II – vi. The results are summarized in Table 2. Note that

$$\overline{Y^2} = 1 - \int_{f_1}^{f_2}\left[1 - \left(\frac{\sin(\pi fT)}{\pi fT}\right)^2\right]\frac{k_i}{f^i}\,df \qquad i = 0,1,2,... \qquad (42)$$

Although the results in Table 2 are precise only for non-coherent FSK, they are useful in assessing the relative impact of phase noise in general. If the coefficients $k_0 - k_3$ are known, or Allan variance measurements are available, the results provide a quick, relative measure of phase noise impact.

Notes:

f_1 = lower integration limit
f_2 = upper integration limit
T = bit duration
f_o = center frequency

Phase Noise $S_\phi(f)$	$\overline{Y^2}$	$1 - \overline{Y^2}$ in terms of Allan variance
k_0	$1 - k_0 f_2$	$\frac{(2\pi f_o T)^2}{3}\sigma_y^2(\tau)$
k_1/f	$1 - k_1\left[\ln(2\pi f_2 T) + 0.23\right]$	$\frac{(2\pi f_o T)^2}{3}\sigma_y^2(\tau)$
k_2/f^2	$1 - \frac{\pi^2 k_2 T}{3}$	$\frac{(2\pi f_o T)^2}{6}\sigma_y^2(\tau)$
k_3/f^3	$1 - \frac{k_3\pi^2 T^2}{3}\left[\ln(2\pi f_1 T)^{-1}\right]$	$\frac{(2\pi f_o T)^2 \ln\left[(2\pi f_1 T)^{-1}\right]}{24\ln(2)}\sigma_y^2(\tau)$

Table 2: Signal Degradation for Integrate and Dump Matched Filters

Note that the signal degradation in dB is given by $10 \log\left(\overline{Y^2}\right)$

iii. Coherent Demodulation of BPSK

The coherent BPSK demodulator is quite tolerant of local oscillator phase noise. Since BPSK is an antipodal waveform, the coherence loss due to phase reference SNR is significantly less than for M-ary PSK with M > 2. Another important consideration is that BPSK contains no information in the Q channel (the binary data is transmitted in phase with the carrier). It was shown in Section II-viii that for a small angle phase noise process, downconverted phase noise appears primarily in the Q channel. Therefore, BPSK does not have the additive noise degradation described in Section III. Most of the phase noise is orthogonal to the modulation,

and is not seen by the demodulator. Since the phase estimation loop processes both the I and Q channels, the coherence loss effect is properly described in Section IV.

The SNR performance degradation due to phase noise is the sum in dB of the coherence loss defined in Section IV, plus the loss in signal power due to the PM spreading effect:

$$10 \log\left(1 - \int_0^\infty S_\phi(f)\, df\right) \text{dB}.$$

iv. Coherent Demodulation of QPSK, OQPSK, MSK

Unlike the case of BPSK, each of these coherent demodulators processes information in both the I and Q channels. The SNR performance degradation due to LO phase noise is the sum in dB of the coherence loss, the PM spreading loss, and the additive noise loss. The LO phase noise spectrum is integrated as described in Section III, and found to be a factor x below the thermal noise power:

$$\int_{B_L}^{1/T} 2\,\mathcal{L}(f)\, df \le \frac{1}{x}\left(\frac{N_0}{C}\right)\frac{1}{T} \qquad (43)$$

where B_L is the phase estimation loop BW and T is the bit rate. The loss associated with a noise floor 10log(x) below thermal noise is derived from Figure 2. This is added to the coherence loss in dB from Section IV, plus the PM spreading loss $10 \log\left(1 - \int_0^\infty S_\phi(f)\, df\right)$ dB.

v. Differential BPSK

Differential demodulation of PSK is typically used for low bit rate transmissions, which would require excellent LO phase noise close to the carrier for coherent demodulators. For example, a coherent demodulator for 100 bps would have a phase estimation loop bandwidth of 10 Hz or less. The phase noise within 10 Hz of the carrier would have to be low enough to assure coherence. The differential PSK demodulator measures the phase difference between two successive received bits rather than comparing each received bit with a derived phase reference. The resulting loss in bit error rate performance may be justified by the relaxed requirements upon LO phase noise.

Robins (Ref. 7) has shown that the differential phase detector has a sinusoidal sensitivity to noise. The integrated phase jitter variance is given by

$$\overline{\Delta\phi^2} = \int_0^{\frac{1}{T}} 2\left(\frac{N_0}{C}\right)_t \sin^2(\pi f T)\, df \qquad \text{thermal noise} \qquad (44)$$

$$= \int_0^{\frac{1}{T}} 2\,\mathcal{L}(f) \sin^2(\pi f T)\, df \qquad \text{LO phase noise} \qquad (45)$$

where T is the bit duration. The sensitivity of the differential phase detector to phase noise is shown in Figure 8. Note the suppresion of the effect of phase noise at frequencies below the bit rate.

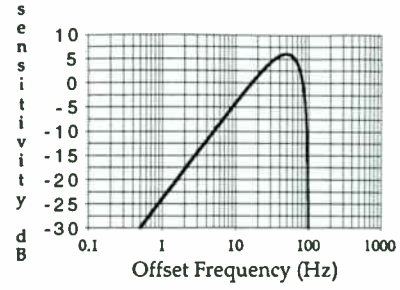

Figure 8 Differential BPSK Sensitivity to Phase Noise (100 bps)

For the case of white noise

$$\overline{\Delta\phi^2} = 2\left(\frac{N_0}{C}\right) \int_0^{\frac{1}{T}} \sin^2(\pi f T)\, df = \left(\frac{N_0}{C}\right)\frac{1}{T} \qquad (46)$$

Although the noise sensitivity has a $\sin^2(\pi f T)$ dependence on f, the integrated phase jitter variance for a *white noise* input may be calculated assuming the demodulator characteristic is flat from 0 – 1/T. For the phase noise contribution to be a factor x below thermal noise:

$$\int_0^{\frac{1}{T}} 2\,\mathcal{L}(f) \sin^2(\pi f T)\, df \le \frac{1}{x}\left(\frac{N_0}{C}\right)\frac{1}{T} \qquad (47)$$

Should the phase noise function not be well behaved in the neighborhood of 0 Hz, the lower integration limit may be taken as some low high-pass cutoff frequency f_h (a highpass filter of cut-off frequency ~ 1 Hz will have minimal impact on the demodulator).

The degradation due to phase noise is the loss due to the LO noise power 10log(x) dB below thermal noise as given in Figure 2, plus the loss in signal power due to the PM spreading effect: $10 \log\left(1 - \int_0^\infty S_\phi(f) df\right)$ dB. The LO noise power is computed using Equation 47.

VI. Effects on the Modulation Process

The signal loss due to PM spreading and the additive noise effect described in Section III apply to the modulator as well as the demodulator. The signal loss due to PM spreading at the modulator, $1 - \int_0^\infty S_\phi(f)\, df$, is not recoverable. The noise floor added by phase noise also cannot be improved by subsequent processing. It is interesting to note that a hard limiter placed after the upconverter has no effect upon pure phase noise. Therefore, the same performance criteria must be applied to the modulator LOs as well as those in the receiver. When computing the performance due to LO phase noise, the effects of all local oscillators in the system must be considered. These include the LOs in the transmitter, those in the receiver, and the LOs in any repeaters in the link.

VII. Conclusion

Criteria have been provided to calculate the effects of phase noise on communications

system performance. The precise degradation has been given for non-coherent FSK, and techniques for calculating the effect on other modulation types have been described. A remaining task is to derive the precise analytical solution for these other modulation types.

Some tests for an adequate phase noise spectrum have been described which are relatively easy to perform. If the Allan variance or power-law process coefficients are known for an oscillator, the effect upon the signal assuming an ideal integrate and dump matched filter can be quickly derived from Table 2. This may be done for a quick check whether or not a particular LO is a concern. The phase noise integration technique described in Section III can be implemented quickly using a spreadsheet program, and gives an indication of the relative severity of the phase noise issue. Although somewhat more time consuming, summing each of the effects of coherence error, signal loss due to PM spreading, and the additive noise effect described in Sections III and IV provide an accurate prediction of performance with imperfect local oscillators.

VIII. Acknowledgement

The author wishes to thank Richard Kornfeld and Dr. Charles E. Wheatley III of QUALCOMM, Inc. for invaluable discussions on this topic, and the preparation of the plots in Section IV. Tremendous thanks are also due to Susana Anaya of QUALCOMM, Inc. for the preparation of the manuscript.

References

1. J. A. Barnes, et al, "Characterization of Frequency Stability," *IEEE Transactions on Instrumentation and Measurement*, Vol. IM-20, No. 2, May 1971, pp. 105-120
2. W. B. Davenport, "Signal-to-Noise Ratios on Band-Pass Limiters," *Journal of Applied Physics*, Vol. 24, No. 6, June 1953.
3. D. Halford, J. Shoaf, and A. S. Risley, "Spectral Density Analysis: Frequency Domain Specification and Measurement of Signal Stability," *Proceedings of the 27th Annual Symposium on Frequency Control, U. S. Army Electronics Command*, Fort Monmouth, New Jersey, June 1973, 11 pages
4. D. A. Howe, "Frequency Domain Stability Measurements: A Tutorial Introduction," Nat. Bur. Stand. (U.S.) Tech Note 679, March 1976, 27 pages
5. R. Matyas, "Effect of Noisy Phase References on Coherent Detection of FFSK Signals," *IEEE Transactions on Communications*, Vol. Com-26, N, June 1978, pp. 807-815
6. S. A. Rhodes, "Effect of Noisy Phase Reference on Coherent Detection of Offset-QSPK Signals," *IEEE Transactions on Communications*, Vol. Com-22, No. 8, Aug 1974, pp. 807-815
7. W. P. Robins, *Phase Noises in Signal Sources (Theory and Applications)*. IEE Telecommunications Series 9, Peter Peregrinus Ltd., London, UK., 1982
8. J. Rutman, "Characterization of Phase and Frequency Instabilities in Precision Frequency Sources: Fifteen Years of Progress," *Proceedings of the IEEE*, Vol. 66, No. 9, Sept 1978, pp. 1048-1075
9. J. H. Shoaf, D. Halford, and A. S. Risley, "Frequency Stability Specification and Measurement: High Frequency and Microwave Signals," Nat. Bur. Stand. (U.S.) Tech Note 632, Jan 1973, 70 pages
10. M. Schwartz, *Information Transmission, Modulation, and Noise*. McGraw-Hill, New York, N.Y., 1970
11. B. Sklar, *Digital Communications Fundamentals and Applications*. Prentice Hall, Englewood Cliffs, New Jersey, 1988
12. A. J. Viterbi, *Principals of Coherent Communication*. McGraw-Hill, New York, N.Y., 1966
13. C. E. Wheatley III, private notes.
14. J. M. Wozencraft and I. M. Jacobs, *Principals of Communication Engineering*. John Wiley & Sons, Inc., New York, N.Y., 1965
15. R. E. Ziemer and W. H. Tranter, *Systems, Modulation, and Noise*. Houghton Mifflin, Co., Boston. 1976

RECEIVING SUBSYSTEM RADIO FREQUENCY (RF)/INTERMEDIATE FREQUENCY (IF) DESIGN METHODOLOGY

by

John Summerville
AIL Systems Inc.
Melville, New York 11746

ABSTRACT

A systematic approach to microwave multioctave receiving subsystem design and implementation is discussed. The major factors are addressed that must be considered in selecting a cost-effective, reproducible receiver [radio frequency (RF) input to preprocessed intermediate frequency (IF) output(s)].

The design methodology being illustrated begins with a set of comprehensive but realistic performance requirements assumed to have been derived from an overall analysis of mission needs. The specifications addressed include: (1) RF range; (2) instantaneous bandwidth and band breaks; (3) dynamic range [including noise figure, sensitivity, large signal handling capability (instantaneous and total)], spurious responses; (4) tuning speed. (5) IF output characteristics; (6) reliability and maintainability; (7) mechanical and thermal considerations, including technology types and integration levels; and (8) cost (acquisition and life cycle).

Logical procedures, including trade-offs, are outlined to derive a design from the given performance criteria. The following aspects are considered: architecture; frequency conversion plan; preselection and filtering; gain-loss distribution; RF/IF "on-line" and "off-line" [local oscillators (LO's), built in test (BIT), and calibration (CAL)] circuitry; functional partitioning; make-or-buy considerations; and the designer's relationship with vendors.

INTRODUCTION

The dilemma facing today's receiver designer is how to address seemingly diametrically opposed requirements. Namely, give greater capability for the customer's money in smaller, more reliable, and easily maintainable systems. Microwave engineers tend to view designs from a purely technical vantage point and strive to achieve the best performance possible. In doing so, other important concerns such as cost (point of diminishing returns), size, weight, power, reliability, maintainability, and producibility may not be equally considered.

The designer must offer a cost-effective solution for real-time requirements yet allow for future growth. This requires an understanding by the designer of the mission requirements (not necessarily the same as the specification) and a cultivated rapport with the customer. The true cost of ownership considers not only acquisition but life cycle costs (LCC's) as well. A generally accepted estimate is that the LCC of a typical military system is 10 times the acquisition cost. This fact emphasizes the importance of reliability and maintainability in the design equation and the merit of considering nonrecurring investments that can be amortized over the life of the equipment.

Modern military hardware needs are, therefore, best met by the use of flexible architectures — modular plug-in construction with provisions for growth ports. Designs must be adaptable to multiple platforms and readily integrable with other systems. This allows growth by serial addition and the form-fit-function replacement of subassemblies as technology improves and performance requirements change [Preplanned Product Improvement (P^3I)].

A design methodology is outlined that illustrates a step-by-step approach to receiver implementation and provides insight into factors that must be considered early in the design phase. The objective is to converge on low risk, reproducible hardware that meets the intent of the customer's requirements in a cost-effective manner and anticipates the customer's future needs.

TECHNICAL DISCUSSION

Receiver as Part of the Overall System

Figure 1 shows the function of the receiver within a typical system. The antenna couples electromagnetic signals from free space into the receiver which then provides the gain, frequency conversion, and filtering required before converting the resultant IF signals into detected video representations suitable for digitizing.

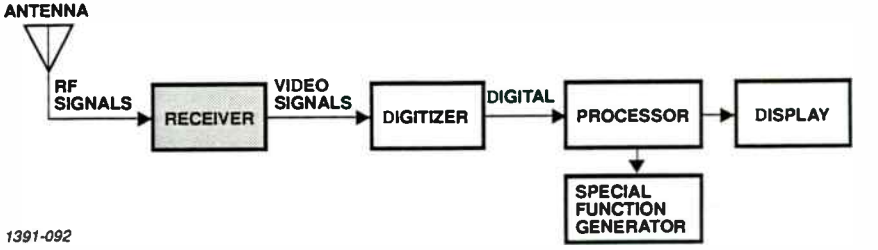

Figure 1. Basic Elements of a Receiving System

Receiver Subsystem Specification

Table 1 represents typical performance requirements for a military receiver. It describes a 3-channel receiver covering the standard Electronic Warfare (EW) range of 2 – 18 GHz. It is assumed that system level analysis has been done and has considered the mission-oriented criteria of sensitivity, spectral and spacial coverage, direction finding (DF) accuracy, processing requirements, ambiguity resolution, dense signal environment operation, and flexibility. Obviously, mission requirements encompass many other important considerations, most notably encoding accuracies and resolutions for key parameters such as: frequency, time of arrival (TOA), amplitude, pulse width (PW), and angle of arrival (AOA). These are primarily a function of the design of the digitizer and processor (parameter encoder) and will not be addressed as part of the receiver subsystem.

Table 1. Receiver Specifications

PARAMETER	REQUIREMENT
Frequency/Bands	2 - 6 GHz, 6 - 18 GHz
Noise Figure	9.5 dB
Bandwidth (Instantaneous)	500 MHz
Configuration	3 channels
Predetected IF Output	2 - 2.5 GHz
Dynamic Range [1]	
Frequency Encoding	60 dB
Parameter Encoding	50 dB
M X N Spurious	50 dB
Two-Tone (Second and Third Order), Second and Third Harmonic	40 dB
Image Rejection	50 dB
Tuning Step Size	250 MHz for Receiver 25 MHz for IF CAL
Tuning Time	1 msec
BIT/FIT Requirements	Fault Isolation to Shop Replaceable Unit (SRU) Level

Note: (1) The dynamic range referred to is instantaneous. A 90 dB overall range is achieved with a 40 dB gain step - 10 dB overlap. This is discussed in the Dynamic Range Overview section of this paper.

Design Flow Steps

Receiver design is a logical, orderly, and iterative process that can be done step by step as shown in Figure 2. Most of the requirements are flowed down to the receiver designer from the Systems Engineering Group or directly from the customer. It is assumed, however, that an on-going dialog between these disciplines (and other support groups) has taken place before the generation of the specification. Even so, error budget allocation, system interface definition, and specification review and negotiation must continue. This is also the point in the design stage that transparent enhancements or self-imposed requirements may be agreed to or implemented.

Transparent enhancements refer to additional functions, test aids, or operational modes that have no visible external effect on system operation but increase its value or capability with minimum impact. Self-imposed requirements would address criteria for design simplicity based on an in-house technology base, the focusing of internal IRAD efforts, and decisions to spend additional nonrecurring engineering (NRE) on a full-scale development (FSD) program to output a design that will be cost-effective in production.

Block Diagram Evolution

Receiver Architecture. Given a multioctave RF input spectrum and the requirement to output contiguous segments at a specified IF and bandwidth, a hetrodyning approach (frequency plan) must be derived to provide frequency translations while preventing or minimizing unwanted outputs (spurs) or radiated transmissions. Spurs include those internally generated (IG) with no RF input and those caused by the application of one or more RF signals. Examples of IG spurs are direct leakage of LO signals (or inherent spurs on LO line) to output ports, or internal mixing of multiple LO's (or their spurs) to generate signals within the receiver input or output passband. Spurs caused by the application of one or more RF signals include single- and multiple-tone intermodulation products due to the nonlinearities of mixers (and to a lesser degree amplifiers) and images which result from the fact that for each LO frequency there are two RF frequencies that will produce a given IF. One is the desired output and the other is the image frequency. The receiver must reject the image prior to mixing. When a receiver utilizes more than one conversion, the image problem is more complex since each conversion will generate an image frequency that must be considered.

Derivation of the conversion scheme for a receiver is an iterative process. Not only must the designer address spurious considerations, but he or she has to continually assess the realizability of the preselection and filtering requirements. In parallel, the designer must keep in mind the complexity imposed on the LO subsystem by the candidate design. This requires looping between the frequency plan and LO approach steps shown in Figure 2. Following the LO approach step, the output should be a first-level block diagram showing the conversion plan and the filters, preselectors, and LO's required to augment it.

Frequency Plan. Given the requirement to fold a 2 to 6 GHz and a 6 to 18 GHz input into 2 to 2.5 GHz IF bandwidth, a number of frequency plans were examined. For example, the 6 to 18 GHz band could have been downconverted to a 3 to 5 GHz first IF using four fixed LO's (selectable 11, 13, 15, 17 GHz with high-side/low-side conversion). The 2 to 6 GHz band is then upconverted using a fixed LO (selected by analysis from the 11, 13, 15, or 17 GHz used for the 6 to 18 GHz band). Another set of four fixed LO's would then be used to downconvert the 3 to 5 GHz in four discrete 500 MHz slots to 2 to 2.5 GHz.

This approach was examined for its apparent simplicity. It does not require the use of a synthesizer although there are additional hardware associated with the interim conversion to 3 to 5 GHz. However, it was realized early in the design phase that it was necessary to provide overlap in the 500 MHz segments to allow spectrum centering. This would require a comb generator on 250 MHz centers, followed by a 7-channel preselector. Alternately, a phase-locked voltage controlled oscillator (VCO) with digital and analog control circuitry could have been used.

At this point, with the complexity of the initial design growing, the use of a synthesizer becomes more attractive. It allows for the use of a single conversion from 6 to 18 GHz down to 2 to 2.5 GHz. Providing

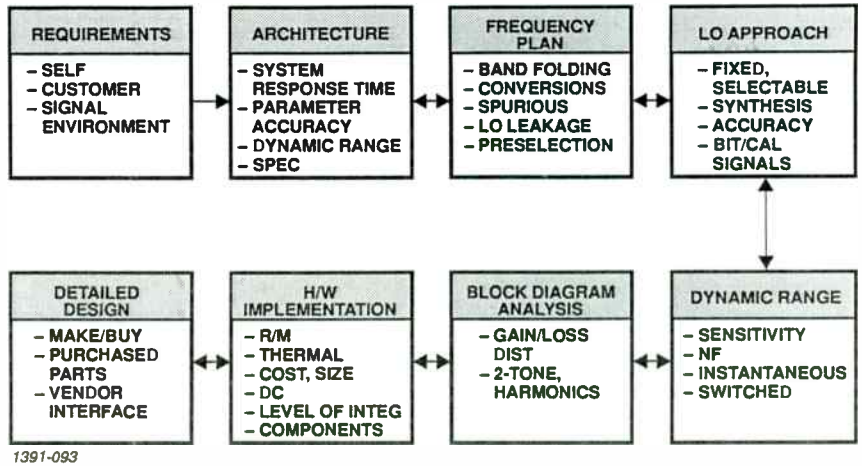

Figure 2. Receiver-Subsystem Design Flow

a 250 MHz stepping LO (synthesizer) will aid spurious rejection (no wideband interim IF) and add flexibility. As an added benefit, since 25 MHz IF CAL steps are required, it was decided to also provide 25 MHz steps at RF as well. With the availability of gallium arsenide (GaAs) monolithic microwave integrated circuit (MMIC) high-speed dividers, both the upper (250 MHz) and the lower (25 MHz) phase-locked loops require only minimum size. The smaller step size provides an order of magnitude improvement in the CAL and BIT capability of the system.

A subset of the frequency plan is the upconversion and preselection required to fold the 2 to 6 GHz band into the 6 to 18 GHz path. Only the 6 to 18 GHz band will be addressed, with the reader keeping in mind that similar analysis would be required for the 2 to 6 GHz band before implementation.

The next refinement is to determine the optimum architecture for frequency encoding and pulse parameter preprocessing. To minimize hardware requirements, the ideal design would initiate processing directly at baseband (2 to 2.5 GHz). With the present maturity of instantaneous frequency measurement (IFM) receivers, frequency encoding is most efficiently done at baseband. Given the requirement to encode pulse amplitude and DOA accurately, wide dynamic range logarithmic IF (LIF) amplifiers and constant phase limiters (CPL's) are required. LIF's are just becoming available over the 2 to 2.5 GHz frequency range and are not yet MIL qualified, while CPL's with a 500 MHz bandwidth and acceptable phase characteristics are not yet available. Based on this, an additional downconversion to 0.5 to 1.0 GHz where LIF's and CPL's are readily available is used.

The selected frequency plan resulting from all the above trade-offs is summarized in Figure 3. Note that as technologies mature, the transition to IF processing directly at baseband is simple and orderly. This is a good example of P^3I and addition by subtraction.

Mixer Spurious Responses. The major contributor to receiver spurious responses are mixers since they are nonlinear devices and generate undesirable outputs at all ports. In addition to leakage between ports, two types of IM products are generated: single tone and multiple tone. Single-tone products result from

nonlinear mixing of one RF input with the LO and have the following form (reference 1):

$$f = \pm mf_R \pm nf_L \quad (1)$$

where m = 1, 2, 3, . . . and n = 1, 2, 3, . . .

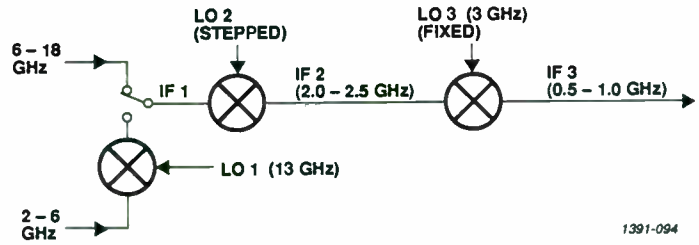

Figure 3. Selected Frequency Plan

Multiple-tone products are caused by two or more RF signals mixing with the LO and have the following form:

$$f = (\pm m_1 fr_1 \pm m_2 fr_2 \pm m_3 fr_3 \ldots) \pm nf_L \quad (2)$$

where $m_1, m_2, m_3 \ldots = 0, 1, 2, 3, \ldots$ and $n = 0, 1, 2, 3, \ldots$

When structuring a frequency plan, the products of interest are the single-tone IM's, image frequencies, and leakage. (Multiple-tone products will be addressed during the two-tone analysis done as a subset to the overall dynamic range modeling.) Charts are often used to predict single-tone spurious frequencies. There are different ways to produce a spur chart, each particularly suited for some special application. A chart generated by Brown (reference 2) is reproduced here as Figure 4 because of its simplicity.

The use of equations for spur analysis is useful but tedious; while spur charts are convenient for highlighting areas of concern. However, neither provide insight into the amplitudes of the spurious responses. Detailed spur analysis is best done with the aid of a computer program. A public domain program in common use is MEIXER (reference 3). It is a program that calculates the level of spurious responses from the 1 X 1 response of a mixer with an RF preselector before the mixer and an IF filter after the mixer. Use of this program allows inputting the filter and mixer characteristics as well as signal levels. The MEIXER program has been modified by AIL Systems Inc. (NEWMIX) to allow better modeling using catalog devices with less data entries. This modified version will be used for subsequent analysis.

A number of vendors publish charts that indicate "trends" in IM suppression as a function of input RF power and frequency. These predictions however, are based on operation in an ideal 50 Ω medium not normally encountered. Anzac, at one time, included IM charts in its catalog, but no longer does so. Its present position is that: "publicized spur charts are not even useful as a design guideline and should probably be totally disregarded in favor of actual measurements at system operating frequencies and power levels," (reference 4).

The NEWMIX program and others use the intercept point measured in dBm as a figure of merit for IM distortion, with a high intercept point desirable for minimum distortion. The concept applies to all nonlinear devices, with mixers and amplifiers being of the most concern. As with mixer spurious responses, IM distortion predictions are most accurate for small signal analysis and are subject to errors as compression is approached or when inputs and outputs are not terminated in 50 Ω (a condition typical of a filter skirt). Intercept point is discussed in detail in the Intercept Point as a Dynamic Range Consideration section.

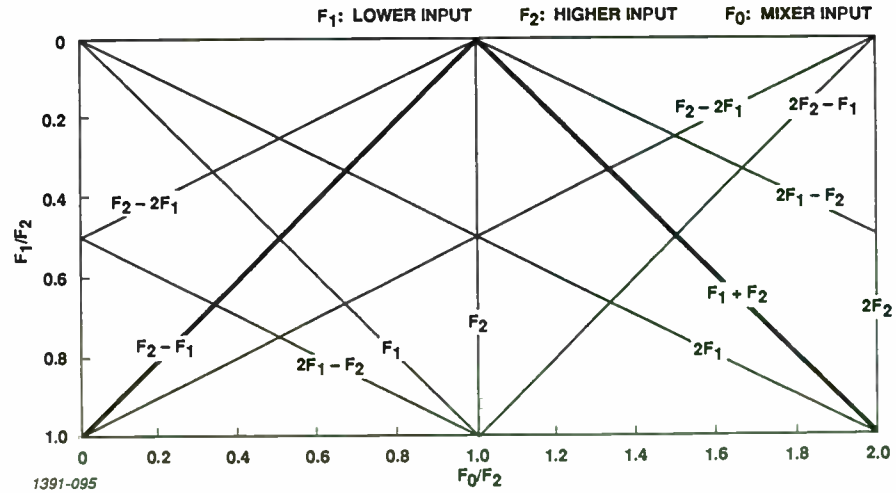

Figure 4. Normalized Spur Chart (Upconversion and Downconversion)

Graphical Spurious Analysis of the Selected Frequency Plan. Once the frequency plan has been selected, a rigorous M X N spur analysis must be done for verification and to determine the required filtering. A recommended first step is to generate application specific spur charts for each band. Figure 5 plots the LO frequencies that are required to cover each contiguous 2 GHz input slot in the 6 to 18 GHz range and provide a 500 MHz IF output centered at 2.25 GHz. The desired responses (1, -1), (-1, 1) are shown along with the resulting spurious responses up to the third order. From here it is determined that an LO range of 8.5 to 15.75 GHz with a crossover from the high side to the low side of the LO at an RF input of 13.5 GHz is optimum for spurious rejection and results in a LO tuning range less than an octave. Not shown in Figure 5, since resultant spurious products are typically greater than 55 dB below the desired output, is the (-2, 0) response which can produce unwanted M X N products for the LO > RF condition.

A subset of the frequency plan is the upconversion and preselection required to fold the 2 to 6 GHz band into the 6 to 18 GHz range. An optimum approach to minimize mixer spurious responses is to provide input preselection, followed by an upconversion using a fixed13 GHz LO. Matched filters are used prior to recombining (an alternate is to use separate mixers for each path which eliminates the inboard SP3T switches but increases the LO drive requirements). The selected subband is then inputted to the common baseband mixer for conversion to the 2 to 2.5 GHz IF. This approach is shown in Figure 6a. The subband breaks shown there have been optimized by trading the number and complexity of the filters vs. spurious performance.

A more straightforward method is chosen as shown in Figure 6b. Here, the output preselector has been replaced by a notch filter to minimize LO leakage. The output is then fed into the appropriate 2 GHz wide channel in the 6 to 18 GHz preselector. This is a less hardware-intensive approach (of particular concern in a 3-channel system) and has only a minor impact on spurious free dynamic range. Figure 7 summarizes the resultant spurious analysis. The (2, 1) response, shown graphically, illustrates the need for the selected band break (two filters) in the 2 to 4.75 GHz region.

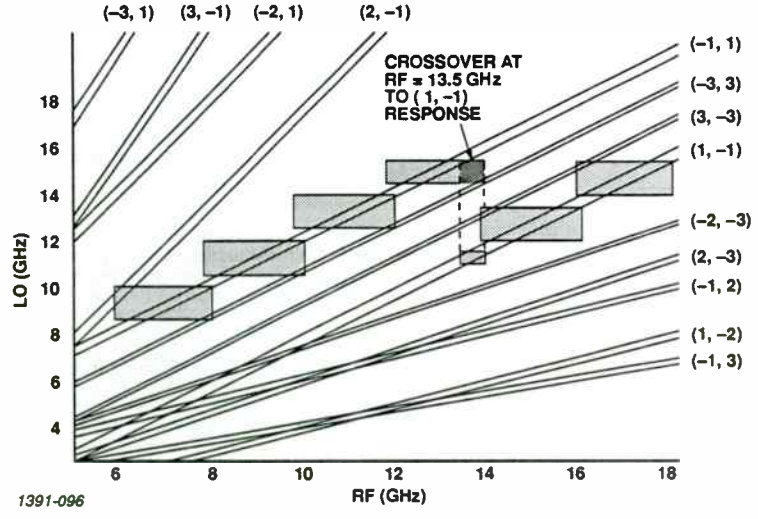

Figure 5. 6 – 18 GHz Band M X N Spur Chart

Computer-Aided Spurious Analysis. The next step in the analysis of the frequency plan is to utilize the NEWMIX spurious analysis computer program previously discussed. Use of this program requires the entering of data relative to RF and LO frequencies, mixer type and parameters, RF and RF filter bandwidths and selectivity, maximum M X N order to be tested, spur rejection level floor, signal levels at mixer input, and other pertinent characteristics. This analysis must be done for all nine subbands; however, only one will be shown here. Table 2 is the resultant NEWMIX printout for the 8 to 10 GHz subband. Note that except for the 3 X 3 response in the RF input region of 9.75 to 10.25 GHz, all spurious responses are predicted to be below 55 dB.

The results obtained by running NEWMIX must be looked at in the same light as vendors' M X N data. The program simply takes mixer intercept point and isolation (balance) specifications supplied by vendors and automates the calculations, while assuming that all mixer interfaces are matched and driven with the correct LO levels.

Keep in mind that M X N rejection involves trade-offs between noise figure, dynamic range, and hardware complexity. Decreasing the RF gain before the mixer will improve M X N performance but the degrade noise figure. More complex preselectors and higher dynamic range mixers (with attendant impact on the LO subsystem requirement) could also improve odd order spurious rejection. Once the M X N analysis is completed and the frequency plan is finalized, the block diagram is updated to add the required preselection and filtering. This is shown in Figure 8.

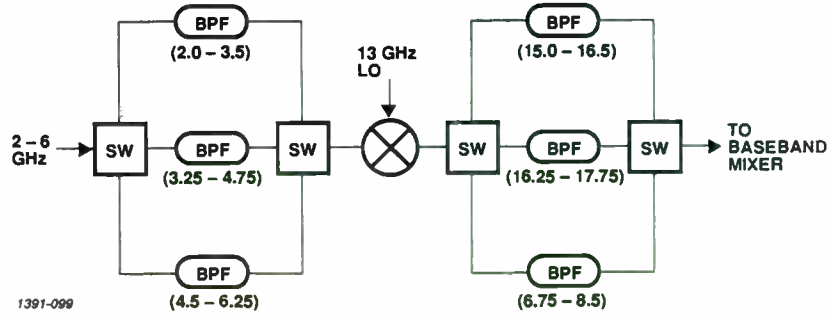

Figure 6a. "Optimum," Complex 2 – 6 GHz Band Folding

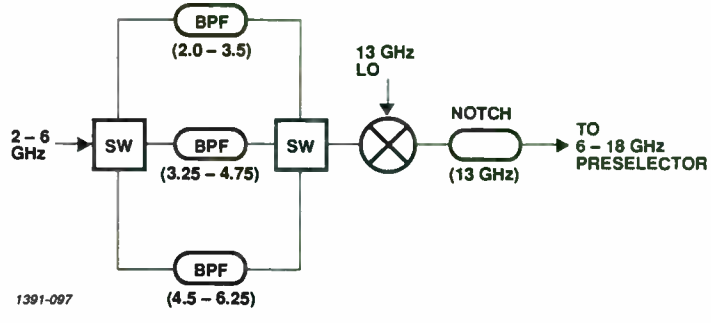

Figure 6b. Simplified 2 – 6 GHz Band Folding

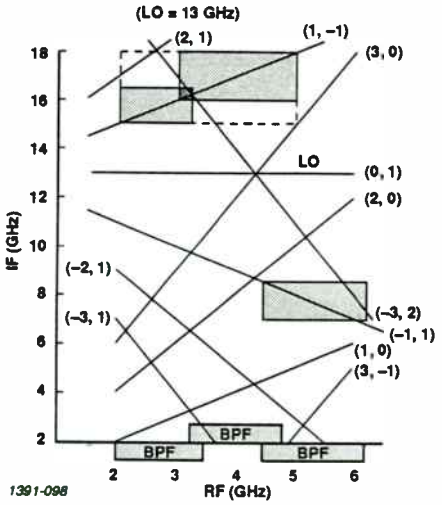

Figure 7. 2 – 6 GHz M X N Spur Chart

Dynamic Range Overview. For purposes of this discussion, the dynamic range is defined as follows: the amplitude difference between the smallest and largest signals that can be measured simultaneously by the receiver. Further, we are mainly concerned with the operational dynamic range: the power range of signals over which the receiver and processor can detect and encode all parameters to specified accuracy. The low end of the dynamic range (system threshold) is set by the noise floor of the receiver in conjunction with the detector signal-to-noise (S/N) ratio required to meet the probability of detection (POD), false alarm rate (FAR), and parameter measurement accuracy. The high end of the dynamic range is set by the maximum RF input signal before spurious responses exceed threshold. Operational dynamic range has two subsets: instantaneous and total. Instantaneous refers to the range of signals that can be processed for a fixed gain setting, while total is the full range of signal amplitudes that can be processed with the utilization of automatic gain control (AGC) and fine and coarse gain adjustment.

It is important to point out, however, that information can still be obtained from a receiving system outside of its "full spec" dynamic range. For example, if we consider "degraded" operational dynamic range, meaning that the measurement accuracy of key parameters is allowed to degrade, the useful dynamic range is extended slightly at each end.

If one addresses only the frequency measurement capability of the receiver, the dynamic range can be extended further. A receiver using an IFM or limiter/discriminator typically can measure accurate frequencies to lower S/N ratios than are required for pulse parameter encoding. By using amplitude limiters the large signal measurement capability is also extended. Another commonly used dynamic range definition is the RF-IF linear dynamic range, defined as the difference between the noise floor and the 1 dB compression point. This definition has some application as a figure of merit but is of little use in designing a receiver.

Figure 9 graphically illustrates the relationship between the various methods used to describe single signal dynamic range. In our case, it is emphasized that we are talking about operational spurious-free

Table 2. M X N Spurious Analysis – 8 to 10 GHz Subband

```
MIXER TEST FOR  60  dB REJECTION
INPUT RANGE :   6  TO  18
IF RANGE    :   2  TO  2.5
RF FILTER FROM  7.75  TO  10.25  WITH  10  SECTIONS
IF FILTER FROM  1.9375  TO  2.5625  WITH  10  SECTIONS
SIGNAL AT   :  -5  DBM
MIXER INTERCEPT AT  :   10  DBM WITH  20  DB BALANCE IMPROVEMENT
      AND EVEN ORDER INT. IMPROVEMENT OF  10  DB
MAX ORDER TESTED IS  3  *  3

THE LO IS =  10.5

+OR-     SPUR       SIGNAL      SIG      LO OSC      LO        ATTEN
         FREQ       FREQ        HAR      FREQ        HAR       LEVEL

LO PRESELECTOR LEAKAGE DUE TO THE  1  HARMONIC IS  43.78207
AT A FREQUENCY OF  10.5
-&-      2.5        9.25        2        10.5        2         55
-&-      2.25       9.375       2        10.5        2         55
-&-      2          9.5         2        10.5        2         55
-&+      2.25001    7.750004    3        10.5        2         60
-&-      2.250008   9.749997    3        10.5        3         50
-&-      2.00001    9.83333     3        10.5        3         50

THE LO IS =  10.75

+OR-     SPUR       SIGNAL      SIG      LO OSC      LO        ATTEN
         FREQ       FREQ        HAR      FREQ        HAR       LEVEL

LO PRESELECTOR LEAKAGE DUE TO THE  1  HARMONIC IS  57.12561
AT A FREQUENCY OF  10.75
-&-      2.5        9.5         2        10.75       2         55
-&-      2.25       9.625       2        10.75       2         55
-&-      2          9.75        2        10.75       2         55
-&+      2.000012   7.833337    3        10.75       2         60
-&+      2.250012   7.916671    3        10.75       2         60
-&-      2.250012   9.999996    3        10.75       3         50
-&-      2.000012   10.08333    3        10.75       3         50

THE LO IS =  11

+OR-     SPUR       SIGNAL      SIG      LO OSC      LO        ATTEN
         FREQ       FREQ        HAR      FREQ        HAR       LEVEL

-&-      2.5        9.75        2        11          2         55
-&-      2.25       9.875       2        11          2         55
-&-      2          10          2        11          2         55
-&+      2.000012   8.000004    3        11          2         60
-&+      2.250012   8.083337    3        11          2         60
-&-      2.250015   10.25       3        11          3         50
```

Table 2. M X N Spurious Analysis – 8 to 10 GHz Subband (Cont)

THE LO IS = 11.25

+OR-	SPUR FREQ	SIGNAL FREQ	SIG HAR	LO OSC FREQ	LO HAR	ATTEN LEVEL
-&-	2.5	10	2	11.25	2	55
-&-	2.25	10.125	2	11.25	2	55
-&-	2	10.25	2	11.25	2	55
-&+	2.00001	8.16667	3	11.25	2	60
-&+	2.250008	8.250003	3	11.25	2	60

THE LO IS = 11.5

+OR-	SPUR FREQ	SIGNAL FREQ	SIG HAR	LO OSC FREQ	LO HAR	ATTEN LEVEL
-&-	2.5	10.25	2	11.5	2	53
-&+	2.000008	8.333336	3	11.5	2	60
-&+	2.250008	8.416669	3	11.5	2	60

THE LO IS = 11.75

+OR-	SPUR FREQ	SIGNAL FREQ	SIG HAR	LO OSC FREQ	LO HAR	ATTEN LEVEL
-&+	2.000006	8.500002	3	11.75	2	60
-&+	2.250004	8.583335	3	11.75	2	60

THE LO IS = 12

+OR-	SPUR FREQ	SIGNAL FREQ	SIG HAR	LO OSC FREQ	LO HAR	ATTEN LEVEL
-&+	2.000004	8.666668	3	12	2	60
-&+	2.250004	8.750001	3	12	2	60

THE INPUT DATA IS LISTED BELOW:

```
1230 DATA 10.5,12.6
1240 DATA 6,18
1250 DATA 2,2.5,.25
1260 DATA 3,3
1270 DATA 9,2.5,60
1280 DATA 2.25,.625,60
1290 DATA 10,10
1300 DATA 3,8,20,.5
1310 DATA -5,60,60
1320 DATA -1,-1
```

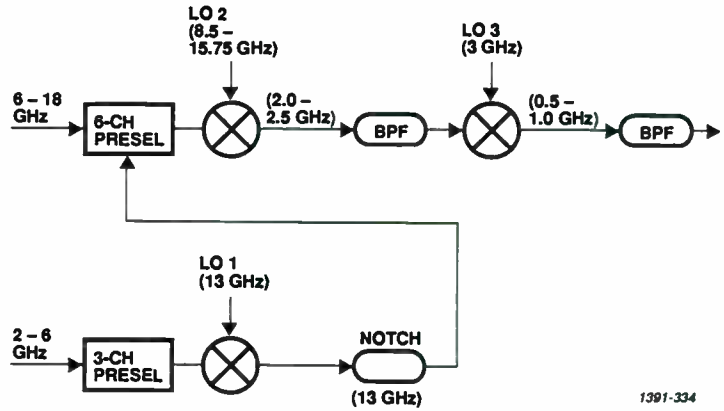

Figure 8. Preselectors and Filters Added

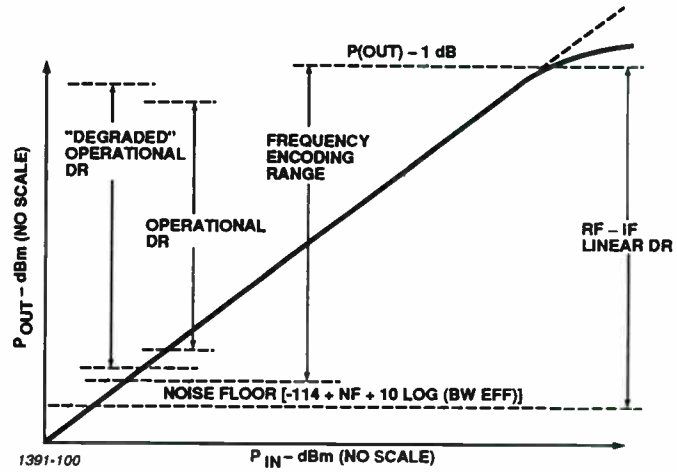

Figure 9. Single-Signal Dynamic Range

two-tone dynamic range. The distinction is specifically made between two-tone and second harmonic dynamic range. In a multioctave receiver, relatively high level in-band and out-of-band signals will generate in-band second harmonic and second order $f_1 + f_2$ and $f_1 - f_2$ responses. These can be handled by high level signal presence detectors in conjunction with back-end spur rejection logic.

Intercept Point as a Dynamic Range Consideration. The intercept point concept as a measure of the two-tone spurious free dynamic range of nonlinear devices such as amplifiers and mixers is the most commonly used method of defining two-tone dynamic range capabilities. When the input vs. output power of a device is plotted on a log-log scale, it will have a 1:1 slope in the linear range. If the second-order IM products are plotted on the same scale, they have a slope of 2:1 and third-order products have a slope of 3:1. The intercept point is defined as the intersection of a linear extension of the three slopes. Most devices will have the same second- and third-order intercept point. Balanced amplifiers, however, exhibit even order cancellation, resulting in a 15 to 20 dB higher second-order intercept point.

Figure 10 is a graphic presentation of the intercept point. Only the third-order response is shown since the resultant spurious products almost always fall within the passband of even a moderate bandwidth receiver. With two in-band input signals, the spectrum at the output will include the following components:

$$F_1 \pm 2F_2 \text{ and } F_2 \pm 2F_1 \quad (F_1, F_2 = \text{input signal frequencies})$$

As shown in the figure, the third-order spurious levels (in dBm) for a given input power (two equal signals) are readily obtained through the intersection of two lines (the third-order line and a line parallel to the y-axis) and represent the following relationship:

$$y = IM_3 = 3(P_1 + G) - 2PI_3 \quad \text{(reference 5)}$$

where IM_3 = third-order spurious level ($x = P_1$ in Figure 10)
P_1 = input power level
G = amplifier gain
PI_3 = amplifier third-order intercept point

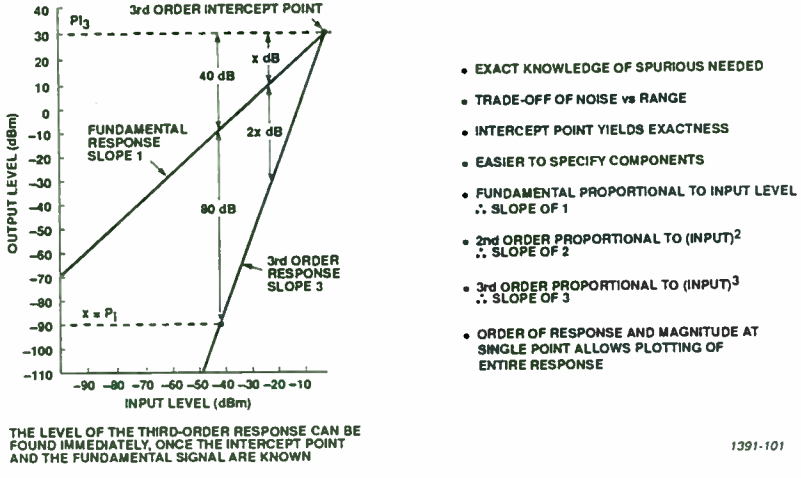

Figure 10. Intercept Point - Two-Tone Analysis (Two Equal Signals)

At this point, we will introduce a new term, K-factor. It is defined as the absolute power level (in dBm of the IM two-tone products generated when the power level of each fundamental is at 0 dBm. For amplifiers, the levels are at the output, while for nonlinear devices with loss (mixers, switches), the levels refer to the input.

The second-order K-factor (K_{11}) can be shown to be related to the second-order intercept point (IP_2) for M, N = 1 as follows:

$$K_{11} = -IP_2 \text{ (dBm)}$$

Similarly, the third-order K-factor (K_{21}) for (M = 2, N = 1) is related to the third-order intercept point (IP_3) as follows:

$$K_{21} + -2IP_3$$

Sometimes receivers are required to meet certain second- and third-order rejection levels for specific but unequal power levels. From this information, the designer must calculate the required intercept point of the components used in the design. This is done by normalizing the two unequal input signals to a set of equal signals that yield the same worst-case spurious condition. Figure 11 summarizes the formulas used to make this and other calculations and transformations for third-order intercept point and two-tone rejection.

Dynamic Range Analysis. Before doing the dynamic range analysis, the design must be updated to add amplifiers at the appropriate points. An RF preamplifier is needed for noise figure considerations at the front end of each band. In the 2 to 6 GHz band, an additional amplifier is needed after the upconversion to minimize second-stage noise figure (NF) contributions by compensating for losses to that point. Amplifiers are then added at the common 2 to 2.5 GHz IF and the final IF at 0.5 to 1 GHz.

The dynamic range analysis must mainly consider NF and two-tone spurious rejection. Because of the number of iterations involved, this is best done with the use of application specific software. An in-house program in common use is DCNFKF. From component data inputted by the operator, this program calculates the cumulative gain, NF, and third-order IM levels for a cascaded string of active and passive components. The output data not only predicts the overall performance, but also tabulates the cumulative NF and IM/signal ratio on a stage-by-stage basis. This enables the designer to adjust the gain-loss distribution and component requirements to perform "what if" scenarios to converge on the optimum design.

The DCNFKF program calculates the cumulative third-order spurious level by an in-phase voltage summation of the individual stage contributions rather than a power summation. This is a prudent worst-case assumption, particularly with multioctave bandwidths.

Before doing the detailed dynamic range analysis, we must "fill in the blanks" on the block diagram. Figure 12 is based on data arrived at after having done so. It shows one channel's worth of "on line" hardware, from the RF input to the final IF output. At the 6 to 18 GHz input, a SPDT switch is used to allow selection of signals from the antenna or injection of a BIT/CAL signal. Following the switch is the RF preamplifier, implemented with a bypass mode for dynamic range extension. The gain of the amplifier is selected based on dynamic range analysis and the pad value is adjusted for a nominal 40 dB gain step. This provides a total of 90 dB dynamic range (50 dB instantaneous), with a 10 dB overlap at the switching point.

The RF preamplifier feeds an isolator and the 6-channel preselector that provides the 2 GHz contiguous subbands. The preselector is followed by a matching pad, a mixer to downconvert to the 2 to 2.5 GHz first IF, another matching pad and the IF filter. Following the filter is an IF amplifier, which can be implemented as a variable gain unit to allow gain balance between channels. A hybrid is then used to split the signal and provide the required 2 to 2.5 GHz predetected sample and the IFM input.

Following the hybrid, a SPDT switch is used to allow inputting of a 2 to 2.5 GHz BIT/CAL signal, followed by the second conversion to 0.5 to 1 GHz. Next is the 500 MHz band-pass filter (centered at 2.25 GHz) needed to set the overall RF-IF bandwidth, followed by gain at the final IF. At this point, the signal is power split to provide signal samples to a phase detector module and a pulse parameter encoder.

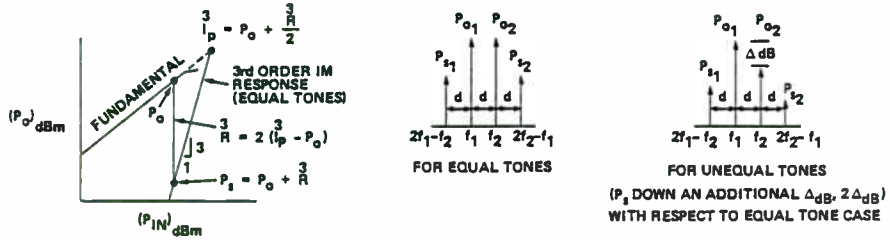

FORMULAS	DEFINITIONS
NOTE: ALL UNITS ARE IN dB OR dBm	
① $\frac{3}{P_{s_1}} = 2P_{o_1} + P_{o_2} - 2I_p^3$ (FOR UNEQUAL TONES)	3rd ORDER SPURIOUS OUTPUT LEVEL ($\frac{3}{P_s}$) IN dBm IS EQUAL TO TWICE THE FUNDAMENTAL OUTPUT POWER (P_o) PLUS THE OTHER FUNDAMENTAL MINUS TWICE THE INTERCEPT POINT
② $\frac{3}{P_{s_2}} = P_{o_1} + 2P_{o_2} - 2I_p^3$	
③ $\frac{3}{P_s} = 3P_o - 2I_p^3$ (FOR EQUAL TONES)	3rd ORDER SPURIOUS LEVELS ($\frac{3}{P_s}$) FOR EQUAL TONES IS SIMPLIFIED TO THREE TIMES THE POWER OUTPUT LEVEL OF EACH TONE (P_o) MINUS TWICE THE INTERCEPT POINT
④ $\frac{3}{P_s} = P_o - \frac{3}{R}$ (FOR EQUAL TONES)	3rd ORDER LEVEL IN TERMS OF 3rd ORDER REJECTION ($\frac{3}{R}$)
⑤ $\frac{3}{R} = 2(I_p^3 - P_o)$ (FOR EQUAL TONES)	3rd ORDER REJECTION ($\frac{3}{R}$) IS EQUAL TO TWICE THE DIFFERENCE BETWEEN THE 3rd ORDER INTERCEPT POINT (I_p^3) AND THE FUNDAMENTAL POWER (P_o)
⑥ $I_p^3 = \frac{1}{2}(3P_o - \frac{3}{P_s})$ (FOR EQUAL TONES)	3rd ORDER INTERCEPT POINT IS FOUND BY TAKING ONE-HALF THE QUANTITY [THREE TIMES POWER (P_o) MINUS THE 3rd ORDER SPUR LEVEL ($\frac{3}{P_s}$)]
⑦ $I_p^3 = P_o + \frac{\frac{3}{R}}{2}$ (FOR EQUAL TONES)	OR INTERCEPT POINT IS FOUND BY ADDING HALF THE 3rd ORDER REJECTION ($\frac{3}{R}$) TO THE OUTPUT POWER (P_o)
⑧ $\frac{3}{R'} = \frac{3}{R} + \Delta$ OR $\frac{3}{R} + 2\Delta$	3rd ORDER REJECTION UNEQUAL TONES ($\frac{3}{R'}$) IS GREATER THAN 3rd ORDER REJECTION FOR EQUAL TONES ($\frac{3}{R}$) BY AN AMOUNT EQUAL TO THE DIFFERENCE IN TONES (Δ) AND TWICE THE DIFFERENCE (2Δ)

91-102

Figure 11. Two-Tone Third-Order Spurious Relationships

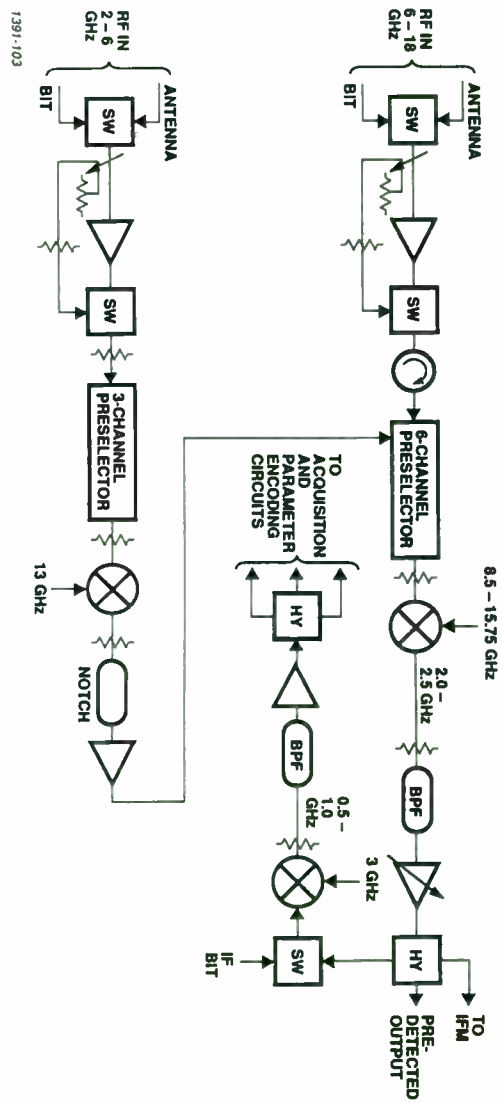

Figure 12. Single-Channel Receiver Block Diagram

The RF-IF gain required is determined by establishing the minimum signal needed by the LIF's used in the amplitude encoding circuitry and the CPL's preceding the phase detectors. Assuming that -50 dBm is needed, the RF-IF gain is calculated as follows:

$$\text{Gain (dB)} = P_{out} - P_{in}$$

where P_{out} = -50 dBm
P_{in} = -65 - ANT gain - ANT/RCVR losses
= -65 - 0 - 5 = -70 dBm
Gain (dB) = -50 - (-70) = 20

For the 2 to 6 GHz input band, the gain must be adjusted to provide the same input level to the 6-channel preselector as in the 6 to 18 GHz band, since the rest of the circuitry is common.

Dynamic Range Simulations. At this point, we are ready to establish the final gain-loss distribution of the receiver. This involves iterating the design using the DCNFKF program until the required results are obtained. Table 3 summarizes the results for the 6 to 18 GHz band. The final design was arrived at by iterating performance criteria for readily available components. A comparison of the simulated results and the specification is shown below. The -30 dBm input level used to perform the IM analysis is determined by considering the 40 dB two-tone dynamic range required above -70 dBm (-65 dBm sensitivity, less the 5 dB of ANT/RCVR losses previously assumed).

	NF (dB)		IM/SIG SUM (dB)		IM Level (dBm)	
Band	(A)	(B)	(A)	(B)	(A)	(B)
6 to 18	9.5	9.1	-40	-49.9	-70	-79.9

Note: (A) = spec and (B) = simulation result.

LO Group and BIT/CAL Implementation

The LO and BIT/CAL configuration was tracked as the receiver design evolved, and it is now possible to block out its design. Figure 13 summarizes the requirements. Starting from a 250 MHz stable reference, fixed LO's at 3 GHz and 13 GHz must be generated and a stepping synthesizer covering 8.5 to 15.75 GHz must be implemented. Additionally, RF and IF BIT/CAL signals must be provided. The 3 GHz is generated by using a comb generator and selecting the 12th harmonic. A tap is provided to select the 1 GHz comb, which is multiplied and filtered to provide the 13 GHz LO. A second 13 GHz output is provided for the BIT/CAL function which is discussed later in this section.

The 250 MHz reference also feeds the synthesizer. A detailed synthesizer design is not within the scope of this paper. However, a typical implementation would divide the 250 MHz reference down to a lower frequency suitable for phase detection. A VCO covering the 4.25 to 7.875 GHz range, followed by a doubler, could be used to generate the 8.5 to 15.75 GHz output that is required. A 2-channel switched preselector would then split the output into two bands to provide spurious rejection.

With the availability of GaAs prescalers up to 10 GHz, the divider chain required to divide down the VCO output for phase/frequency comparison is greatly simplified. The phase locked loop needed to generate the 25 MHz frequency steps is also relatively simple to implement, given the silicon and GaAs analog and digital MMIC technology available today. Such a design is easily compatible with the 1 msec tuning requirements and, for adjacent step tuning, which will be orders of magnitude faster. Referring back to Figure 13, the 250 MHz reference is also used to provide coherency for a 2 to 2.5 GHz VCO used to generate IF and RF frequency and amplitude modulated CAL/BIT signals. The amplitude modulation (AM) can be provided by a digitally programmable attenuator following the VCO. This, in conjunction with frequency tuning of the VCO, will provide fine grain amplitude and frequency calibration at RF and IF.

The 2 to 2.5 GHz IF CAL is upconverted by mixing with the 8.5 to 15.75 GHz synthesizer, to provide RF CAL/BIT for injection at the receiver front end. A 6 to 18 GHz preselector (4 CH: 3 GHz centers) is used to reduce spurious CAL signals and to reject power robbing image responses. The output of the preselector directly provides the CAL signals for the 6 to 18 GHz RF band; while mixing it with the fixed 13 GHz LO provides CAL for the 2 to 6 GHz band. The fast step-to-step tuning of the synthesizer provides CAL times that are consistent with a high POI system, since the CAL cycle can be a very small percentage of overall on-station time.

Table 3. Noise Figure - Two-Tone (6 to 18 GHz Band)

```
THE OUTPUT DATA IS LISTED BELOW:
--------------------------------

TWO TONE TEST
POWER LEVELS ARE
-30  DBM AND  -30  DBM

 COMPONENT      STAGE      CUM      STAGE      CUM      KFT        IM/SIG
                NF         NF       GAIN       GAIN                RATIO
DUMMY           0.0        0.000      0.0        0.0
DUMMY           0.0        0.000      0.0        0.0
SW              2.0        2.000     -2.0       -2.0
CPR1            0.3        2.300     -0.3       -2.3
PRE  AMP        6.0        8.300     31.0       28.7     -56.0      -58.6
SW              2.0        8.301     -2.0       26.7     -80.0      -86.6
ISOL            0.9        8.301     -0.9       25.8
PRE  SEL        8.0        8.310     -8.0       17.8     -80.0     -104.4
PAD             2.0        8.316     -2.0       15.8
MXR             8.0        8.404     -8.0        7.8     -36.0      -64.4
PAD             2.0        8.465     -2.0        5.8
BPF             2.0        8.559     -2.0        3.8
VGA             4.0        8.925     21.7       25.5     -56.0      -63.0
DIV             6.5        8.930     -6.5       19.0
SW              1.5        8.933     -1.5       17.5     -80.0     -105.0
MXR             6.5        8.967     -6.5       11.0     -40.0      -63.0
BPF             2.0        8.993     -2.0        9.0
AMP             3.5        9.077     14.5       23.5     -60.0      -73.0
DIV             3.5        9.080     -3.5       20.0
TERM            0.0        9.080      0.0       20.0

  IM/SIG  COHERENT SUM    -49.94  DB
  IM LEVEL                -79.94  DBM
  NOISE FIGURE             +9.08
  NUMBER OF ELEMENTS       20
```

Hardware Implementation

Actual hardware implementation will now be discussed. Table 4 summarizes some of the major factors that must be considered. They are mainly self-explanatory and the only one that will be discussed in detail is the integration philosophy.

In a multichannel system, there are two types of integration that can be considered: vertical and horizontal. Vertical (or parallel) integration means packaging the identical functions of each channel together in a single assembly. This concept is illustrated in Figure14a. Horizontal (or serial) integration refers to packaging dissimilar functions associated with a single channel together. This approach is shown in Figure 14b.

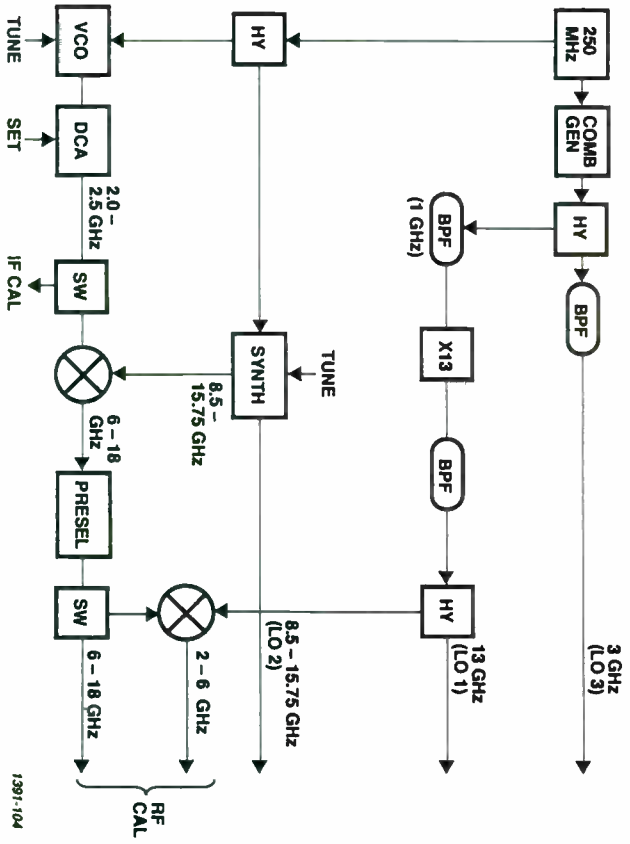

Figure 13. LO/CAL/BIT Generation

Table 4. Hardware Implementation Considerations

I.	**FACTORS**	
	a.	Cost/Size/Weight
	b.	Repairability/Testability/Reproducibility
	c.	Cost Driver Trade-offs
	d.	NRE Towards Low Production and Maintenance Costs
	e.	Acquisition Costs vs. LCC
	f.	FSD vs. Production Options
	g.	Mechanical and Thermal Considerations
II.	**INTEGRATION PHILOSOPHY**	
	a.	Vertical Less Mixing of Expertise; Peas in a Pod; Channel-to-Channel Tracking, Testing, and Field Replacement Easier
	b.	Horizontal Reduced Assembly Types (at SRA/SRU Level Only)
III.	**VERTICAL IS CHOICE**	
	a.	Increased NRE (?) at Subsystem Level
	b.	Less NRE at Component Level
	c.	More Recurring at Subsystem Level
	d.	Less Recurring at Component Level
Rationale for Vertical Integration Preference: Acquisition cost on a new program is about the same for horizontal and vertical integration, but the LCC for a vertically integrated implementation is less, leading to a reduced overall cost of ownership.		

The major advantage of vertical integration is that the resulting assemblies involve less mixing of expertise (amplifier experts will make only amplifiers) and the integral packaging of functions associated with all the channels enhance amplitude and phase tracking and ease testing (peas in a pod). Further, if an amplifier associated with one channel fails in the field, the amplifier assembly is replaced and channel-to-channel tracking is automatically maintained. Additionally, common circuitry (such as decoders, LO distribution hybrids and switch drivers) can support all channels.

Integrating horizontally by channel results in assemblies that contain a myriad of components requiring different expertise – a cost and performance detriment. Note also (as shown in Figure 14b) the LO hybrids must be remotely located, requiring additional space and phase-tracked interconnecting cables. Further, the replacement of an assembly associated with a single channel impacts channel matching.

Horizontal integration, however, can lead to a reduced number of assembly types at the SRU/SRA level (but not at subassembly level). For example, in a 3-channel system, a designer can build one SRU/SRA by part number and use it three times. Vertical integration, on the other hand, can lead to reduced NRE and more efficient packaging at the subassembly level — again due to the minimum mixing of expertise and the repetitive nature of the subasemblies. Further, the recurring costs at the subassembly level are less for the same reasons. The trend toward Standard Electronic Modules (SEM's) generally sets the number of functions in a module and favors the vertical integration approach.

Performance and reliability is enhanced with vertical integation, mainly because people are doing what they do best and thus will deliver a better product. Further, since there is less mixing of technologies, there is a minimum of entering and exiting different implementation mediums (stripline to microstrip to coaxial to discrete, etc.). Such transitions adversely impact reliability and performance. In an operational environment, vertical integration leads to a shorter Mean Time to Repair (MTTR) since the replacement of a subassembly is not likely to affect system alignment.

The above considerations should normally lead to a choice of vertical integration. The acquisition costs on a new program will be roughly the same for horizontal or vertical integration. However, the LCC (rule of thumb: 10 times the acquisition costs) will be less for the vertical integration approach.

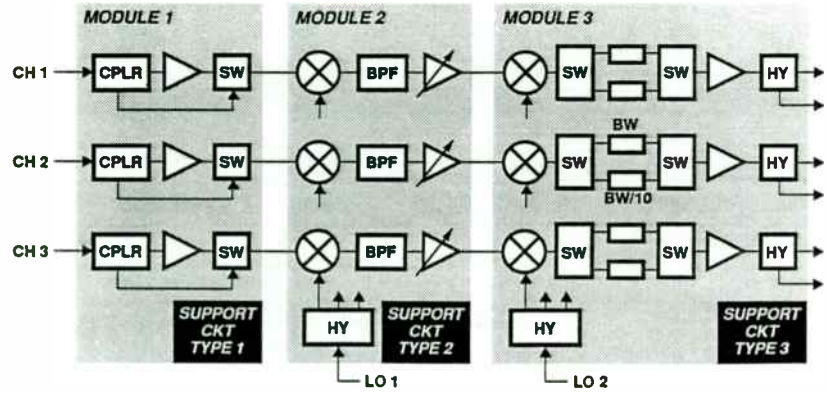

A. VERTICAL

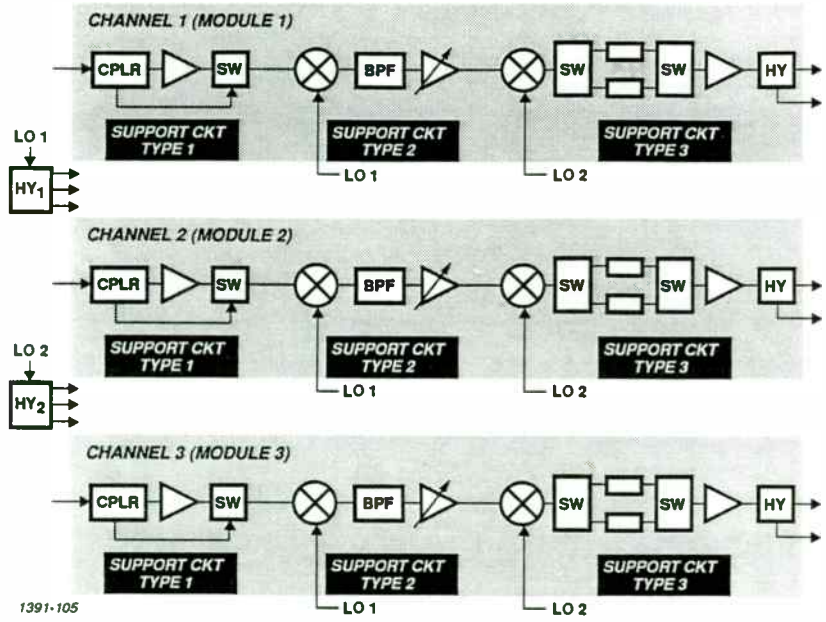

B. HORIZONTAL

Figure 14. Integration Approaches

SUMMARY

The intent of this paper is to present a logical step-by-step approach to the design of an RF/IF subsystem design with emphasis on the fact that it is an iterative process that converges on an optimum design. Each military program has unique factors that drive the final implementation, but the common thread is overall cost of ownership. The designer must look at approaches that lead to lower costs over the lifetime of a program.

Table 5 summarizes some of the factors to be considered when making the transition from initial design to military hardware. Two points are worthy of elaboration. The first is to adapt one's design to utilize the most cost-effective technology and maximize the use of standard components, even if it means slight performance compromises. For systems of the 1990's, both retrofit and forward fit, MMIC is the technology of choice and should be used wherever feasible. This is particularly true for forward fit applications where the receiver architecture can be designed around available (or projected soon to be available) MMIC chips. The library of catalog MMIC chips and multifunction modules is vast and is growing daily. Of particular interest for new designs are the MMIC single and multifunction chips that soon should be available as a result of the multiphase DARPA MIMIC Program. Custom components, whether MMIC or MIC, are higher risk, cost more, take longer to get, and in some cases, are larger and consume more power.

Table 5. Detailed Design Phase Considerations

I.	**MAKE/BUY DECISIONS**	
	a.	Standard Components vs. Custom
II.	**TECHNOLOGY**	
	a	Discrete – MIC – MMIC – Hybrid
	b.	Size – Cost – Performance – Risk – Schedule
	c.	Quantities – Production Follow-On
III.	**COMPONENTS**	
	a.	Amplifiers: NF, DR, Cost, and Size
	b.	Preselectors: Complexity and Overlap
	c.	Mixers: Most Vendor Specs are Typical and Assume Broadband 50 Ω World
	d.	Integration Level vs. Cost, Schedule, Risk, Performance, and Reliability.
IV.	**SPECIFICATIONS**	
	a.	Know What You Want – Do Not Overspec or Overtest
	b.	Listen to Supplier – Encourage Dialogue
	c.	Extra Decibels Could be a Killer
	d.	Keep Specs Simple and Clear, Be Specific and Minimize Documents
	e.	One Component Equals One Document (and Refer to Mil Spec A/R)
	f.	Use Supplier's Standard Screening and Processes – The Supplier Knows Them – It Costs More to Deviate – Up or Down

ACKNOWLEDGMENTS

The author wishes to thank Dr. B. Mangla, Mr. L. Oliva, and Mr. J. Taub for their thoughtful review of this paper, and Ms. L. Lundon for her patient assistance in preparing the material.

REFERENCES

1. Watkins-Johnson Company, RF and Microwave Designer's Handbook, 1988/1989.
2. Brown, T. T., "Mixer Harmonic Chart," Electronic Buyers Guide, June 1953.
3. Meixner, R. P., "BASIC Computer Algorithm Spots Spurious Responses," Microwaves, March 1977.
4. Anzac Division of Adams Russell Co., Inc., RF and Microwave Signal Processing Components, June 1989.
5. Tsui, J., Microwave Receivers with EW Applications, New York, NY: John Wiley & Sons, Inc., 1986.

RS232 COMMUNICATION FOR TURN-KEY TEST STATIONS

Warren F. Walls

Erbtec Engineering
2760 29th Street
Boulder, CO 80301
(303) 447 - 8750

ABSTRACT

Automated test stations used to monitor quality assurance have become mandatory in most production situations in order to insure accuracy and traceability while keeping the cost of operation down. Many pc based stations use a combination of GPIB and RS232 communication formats to control the test equipment and interface with the device under test. It is important that the hardware and software work together to catch communication errors and gracefully handle interruptions in the communication links. The different formats of RS232 communication hardware were investigated and a couple of different C libraries were generated in order to produce a reliable and robust test station.

INTRODUCTION

Erbtec Engineering has set a goal to be the preferred supplier of systems solutions that address the RF electronics requirements of quality conscious Original Equipment Manufacturers. In the process of trying to keep up with this goal it has become mandatory that test stations be designed to evaluate each module in larger products as well as have a controlled burn room system for initial and final burn-in cycles for these larger products. During the process of putting together different stations it became apparent that a reliable serial communication library needed to be generated. Test stations that communicate with many different devices under test for hours on end are very susceptible to locking up and possibly crashing a whole night's burn-in cycle. Therefore, this communication library needed to have functions that would never halt a program if the serial communication failed and they needed to report when, and sometimes how, a communication request failed. These software features as well as typical hardware arrangements are discussed below.

THE RS232 COMMUNICATION LINK

The RS-232 format, EIA232-D, was originally set up by the Electronic Industries Association in 1969. This standard specifies that RS-232D will operate up to 20 kbps and at a distance of less than 15m. A one, or high state, is reported when a signal of less than -3 volts, with respect to ground, is present on the data line. A signal of greater than +3 volts is interpreted as a zero or low state. With serial communications, data travels only on one line, one bit at a time. A particular system may send data on one line and receive it on another, but a complete piece of information is only dependent on the data coming from one line. There are three different modes in serial communications: Simplex, Half Duplex, and Full Duplex. The first mode, simplex, allows information to only travel in one direction. This would apply to a computer talking to a printer. The printer only receives data from the computer and it never sends data back to the computer. Half Duplex allows two computers to send information back and forth, but only one direction at a time. This is analogous to a CB radio because a person must let go of the transmit

button when they are done talking so that the other person may speak. The third mode, Full Duplex, allows for data to travel in both directions at the same time. Modern telephones operate in Full Duplex because they allow people to talk and listen simultaneously.

The RS-232 communication format was originally set up using a 25 pin connector. The allocation of these 25 pins is shown in Figure 1. The full twenty-five pin connector is capable of implementing both synchronous and asynchronous communication.

ASYNCHRONOUS COMMUNICATION

Asynchronous communication involves sending packets of information that are randomly spaced apart. Each packet contains both data bits and control bits. The group of data bits makes up one character. A common character set that is used to convert letters into a series of pulses is the ASCII code which was created by the American Standards Commission for Information Interchange. This seven bit code can be used to represent many different letters. The information bits are grouped between a start and stop bit which signify the beginning and end of each frame. The start bit, which is a signal low, is followed by seven data bits, a parity bit, and finally a stop bit. The stop bit can last a minimum of one to two bits before another start bit may be asserted. A parity bit is often added to the end of the seven bit character in order to help catch errors. Parity checking is either done in either even or odd mode. The number of high data bits are added together and then the parity bit is high or low depending upon whether an extra one is needed in order to make the total count of ones even or odd. Parity checking is one of the simplest ways to detect whether an error has occurred, but it is not able to correct the error. Other methods of error checking and error correcting are possible in digital communications, but RS-232 communication only invokes parity checking.

The RS-232 asynchronous communication channel is fairly effective because even if the receiver is 5% slower than the transmitter, the last bit is only off by 45% and the data will be received correctly. If a larger timing error is encountered, or noise jumps onto the channel, a framing error may result. Asynchronous communication is very cheap and easy to implement, but it results in an overhead of two to three bits per character.

Asynchronous communication is possible using only pins 1-8 and 20 of the original 25 pin connector. Because of this, a new 9 pin connector arrangement of RS-232 was created which consolidates the necessary signals into a smaller package. The mapping of the required pins from the 25 pin connector into the 9 pin connector is shown in Figure 1 along with the new names that were applied to the smaller connector's pins. In asynchronous communications there are only two lines that data travels across; the other five lines are used for control purposes.

The TxD line is used to transmit data from the computer to the receiver; and data is received by the computer on the RxD line. Two grounds are supplied: A common or signal ground and a protective or shielding ground which is often connected to the connector case ans is ultimately connected to earth ground. Good shielding is often a necessity. Especially in places where many wires will run next to one another, a shielded cable will help to reduce anamolies due to crosstalk and noise. When a computer is on and a serial port is active, the DTR or Data Terminal Ready line is active. When a

receiving unit gets the DTR signal it responds by activating DSR, Data Set Ready. In Half Duplex, the DCD, Data Carrier Detect, is activated only by the receiving unit. In other modes, the DCD is active the entire time the communication link is operating. When the computer wants to send data, it activates the RTS, Ready To Send, line and then looks at the CTS, Clear To Send, to see when the receiving unit is ready to receive the computer's data. These two lines were originally designed to switch a half duplex modem from transmit to receive.

There are two general categories of devices that use RS-232 communications: Data Terminal Equipment (DTE) and Data Circuit terminating Equipment (DCE). The differences between the two are in whether certain signal wires are treated as inputs or outpouts. For two devices to communicate, each device's inputs must be connected to the other device's outputs.[1] A comparison of the two devices is made in Table 1. Terminals and printers are DTE devices, while modems are DCE devices. In order to connect two DTE devices together, like two computers, one must use a device called a null modem. This device takes care of some of the handshaking lines and it switches the talk and listen lines on one end. The device illustrated in Figure 3 is required in order to use the Lattice C library of serial communication commands. The null modem shown in Figure 4 illustrates the connections necessary to use the DOS interrupt serial communication commands.

SYNCHRONOUS COMMUNICATION

Synchronous communication requires a clock line to be included in the collection of signal wires, or encoded into the data stream. This approach significantly reduces the control overhead and therefore speeds up the rate at which information travels across the link. The entire 25 pin connector is used in RS-232 synchronous communications. The synchronous control and timing lines are listed in Figure 2. Synchronous communications will not be discussed any further as it is not the popular choice for most serial communication involving personal computers.

DOS INTERRUPT SERIAL COMMUNICATION

Now that we have established the hardware configurations, it is time to discuss two different approaches to the software. One method of communicating with a serial port on a MSDOS based computer is through interrupt calls. The first thing that must take place before communication may begin is the initialization of the port. The following sample of code shows how the initialization is accomplished.

```
init_232(k)          /* The integer k corresponds to the Com port number */
int k;               /*   eg.  for COM1 set k=1.                         */
  {
  int flags;
  union REGS in,out;

  in.h.ah=0;
  in.h.al=0xE3;              /* This represents the initialization parameters */
  in.x.dx=k-1;               /* The dx sets the communications port           */
  flags=int86(0x14,&in,&out);
  }
```

This procedure sets up the baud rate, parity, stop bit, and location of the port (9600 baud, no parity, 1 stop, 8 bits). After the initialization is accomplished, characters may be sent and received through the port.

During communications, one needs to be able to check a port's status without

[1]DigiBoard Incorporated, 6751 Oxford Street, St. Louis Park, MN 55426.

committing to the port when nothing is there and thereby possibly locking up the program. The status procedure, shown below, returns an integer which contains 8 bits that represent the condition of the port.

```
stat_232(k)                          /* bit 7  timed-out                        */
int k;                               /* bit 6  transmission shift register empty */
  {                                  /* bit 5  transmission hold register empty  */
  int flags,b,c;                     /* bit 4  break detected                    */
  union REGS in,out;                 /* bit 3  framing error                     */
                                     /* bit 2  parity error                      */
  in.h.ah=3;                         /* bit 1  overrun error                     */
  in.x.dx=k-1;                       /* bit 0  data ready                        */
  flags=int86(0x14,&in,&out);
  b=out.h.ah;
  c=out.h.al;
  return(b);
  }
```

This returned value can then be logically ORed with test bits to determine which bits are on. The table next to the procedure shows the definition of each bit.

The basic interrupt call to receive a character is shown below.

```
in_232(k)            /* The integer k specifies the com port to use: */
int k;               /*   eg.  for COM1 set k=1.                     */
  {
  int flags,b,c;
  union REGS in,out;

  in.h.ah=2;
  in.x.dx=k-1;
  flags=int86(0x14,&in,&out);
  b=out.h.ah;
  c=out.h.al;
  return(c);
  }
```

This procedure sets the computer's registers and then returns the data after the interrupt call. The major failing of this procedure is that if the port doesn't exist or if there is a problem with the port, the program will hang forever, thus locking up the program and rendering the computer useless. This approach also doesn't check the data or wait to see if data is on its way. Approaches like this can cause a whole burn-in station to hang in the middle of the night. This procedure needs to be further enhanced in order to ensure that it will return regardless of the status of the serial port and warn the user if the data is possibly bad. The new version of this procedure is shown below. A clock call, which is not system or clock speed dependent, is used to time how long a channel is checked. The status of the port is also checked before the interrupt call is made so that it is certain that the program will not hang. Finally, the data is checked to see if it was received correctly. If the procedure is not successful, it returns a negative one to warn the calling procedure that an error has occurred.

```
in_232(k)            /* The integer k specifies the com port to use:  */
int k;               /*   eg.  for COM1 set k=1                       */
  {
  int flags,b,c;
  union REGS in,out;
  double t1;

  t1=clock();
  do
    {
    if ((stat_232(k)&0x01)==0x01);
      {
      in.h.ah=2;
      in.x.dx=k-1;
      flags=int86(0x14,&in,&out);
      b=out.h.ah;
      c=out.h.al;
      if((b&0x80)==0x80)
        return(-1);
      return(c);
      }
    }
  while ((clock()-t1)<0.10);
  return(-1);
  }
```

Similar considerations, to these just discussed when one is receiving data, must be mode when one wishes to send data out through the port. The following procedure will return regardless of the condition of the port.

```
out_232(c,k)            /* The integer k is the com port number.     */
char c;                 /*   The character c is the data to be sent. */
int k;
  {
  int flags,b;
  union REGS in,out;
  long t1;

  t1=clock();
  do
    {
    if ((stat_232(k)&0x20)==0x20);
      {
      in.h.ah=1;
      in.h.al=c;
      in.x.dx=k-1;
      flags=int86(0x14,&in,&out);
      b=out.h.ah;
      if((b&0x80)==0x80)
        return(-1);
      return(0);
      }
    }
  while ((clock()-t1)<0.10);
  return(-1);
  }
```

Notice that this procedure also checks the status of the port and uses a timer to check for some specified amount of time before giving up. Also, the port is check to see if the data was sent correctly. As before, if any thing fails, a negative one is returned, otherwise a zero is returned.

The MSDOS interrupt procedures are able to work with many different ports using different versions of the operating system on different machines. With a third party board, we were able to use these procedures in order to talk to COM1 through COM20.

LATTICE C SERIAL COMMUNICATION PROCEDURES

In order to make some of the software more general so that it may be used on machines using operating systems other than MSDOS, we investigated the Lattice C version 6.05 serial communication library. From these functions similar procedures to those discussed above were created. The differences in how to initialize a port are shown below.

```
init_232(k)
int k;
  {
  com_port = ComOpen("COM",k,9600L,8,NO_PARITY,1,4000,1,0);
  if (com_port==0)  return(-1);
  return(0);
  }
```

In this procedure the k once again specifies which COM port is to be used, but it only works with COM port 1 or COM port 2. This procedure sets the various parameters of the port like the init_232 procedure discussed earlier. If the initialization is successful, the address is assigned to com_port, if it is not successful, a negative one is returned.

The Lattice C library did not have a function similar to the stat_232 DOS interrupt call. Instead one can check for the carrier line and whether or not a port has been opened, as shown below.

```
ComCarrier(com_port);     returns:  1 carrier present
                                    0 no carrier detected

ComStatus(com_port);      returns: -1 if comport not open
                                   # of char. on input buffer
```

The C library already had some basic functions built in for sending and receiving data

from the serial ports. The simplest of these is ComGetc(). This procedure goes out to the port and returns a character. This simple call is not near adequate for the complexity of the equipment and programs involved in a test station. The procedure shown below has similar arguments as those in the first in_232 code shown above. Notice that a clock is again used to account for possible imperfections in the hardware timing.

```
in_232()
 {
 double t1;

 t1=clock();
 do
  {
  if (ComStatus(com_port)>0)
    return(ComGetc(com_port));
  }
 while ((clock()-t1)<0.10);
 return(-1);
 }
```

The final basic communication block that we need to cover is how to send out a character using Lattice C library functions. The one shown below simply checks to see if the communication port is legal before trying to send a character out. This is accomplished using the ComCarrier procedure which checks to make sure that the carrier line is on.

```
out_232(c)
unsigned char c;
 {
 if (ComCarrier(com_port)==0)
   return(-1);
 ComPutc(com_port,c);
 return(0);
 }
```

CLEARING OUT THE SERIAL PORT

The basic communication functions discussed above were designed so as to check to see if an error occurs or if no communication is possible. The next step is to have a procedure which systematically clears out the serial port. From time to time, hardware on either end may have a hick-up or someone might echo data onto the bus which gets in the way. In either case, this port needs cleared and readied for useful communication to continue. The following two procedures accomplish this task, the first using the DOS interrupt calls and the second using the Lattice C calls.

```
klean(k)
int k;
 {
 double t1;

 if((stat_232(k)&0x08)==0x08) return(-1);
 t1=clock();
 do
  {
  if((stat_232(k)&0x01)==0x01)
    {
    in_232(k);
    t1=clock();
    }
  }
 while((clock()-t1)<0.10);
 out_232('\r',k);
 t1=clock();
 do
  {
  if((stat_232(k)&0x01)==0x01)
    {
    in_232(k);
    t1=clock();
    }
  }
 while((clock()-t1)<0.10);
 return(0);
 }
```

The DOS interrupt version shown above checks to see if there is data to retrieve and retrieves it until time runs out. At that point a carriage return is sent and once again the port is checked for data which is then in turn pulled off until time runs out. The Lattice C version shown below follows a similar process, but it uses slightly different procedure names.

```
klean()
 {
 double t1;

 t1=clock();
 do
  {
  if (ComStatus(com_port)>0)
    {
    ComFlush(com_port);
    t1=clock();
    }
  }
 while((clock()-t1)<0.10);
 out_232('\r');
 t1=clock();
 do
  {
  if (ComStatus(com_port)>0)
    {
    ComFlush(com_port);
    t1=clock();
    }
  }
 while((clock()-t1)<0.10);
 }
```

HIGHER LEVEL COMMUNICATION CALLS

Now that the basic procedures have been created, the next level of procedures need to be addressed. These procedures may not necessarily appear in one's general serial communication library. These higher level communications need to handle the negative ones which are passed back by failures in the general communication procedures. This particular example procedure is called when one wishes to put a large amplifier into its off state. The first line of the procedure sends the off command out to the serial port. If this fails a negative one will be returned. The program then proceeds to clear out the serial port (klean) and again tries to send the off command. If this second try fails, the procedure returns a negative one otherwise it returns a zero.

```
amp_off()
 {
 if ((send out data to turn amp off)==-1)
   {
   klean();
   if ((send out data to turn amp off)==-1)  return(-1);
   }
 return(0);
 }
```

This approach can be modified slightly to suit one's particular tastes, but in general it will give a piece of equipment two tries to change modes before a higher level procedure is notified of the failure. Many other custom procedures can be written in similar fashion to enhance the robustness and integrity of the whole program.

One important tool to protect a program is the ability to control manual "control-c" or "control-break" commands. The following procedure can be used to catch these keys and close all ports and files before terminating or, if one chooses, they may merely negate the effect of the keys.

```
main()
  {
  onbreak(brk);
  .
  .
  .
  }

brk()
  {
  close ports;
  close files;

  return(1);
  }
```

You can put anything in the brk() routine that you want to have executed when control-c or control-break is pressed. If you return a 0 instead of a 1, the brk() routine will be executed and the main program will continue running; the DOS control-c routine will not be called.

CONCLUSION

When setting up a complicated test station or burn-in system one must first decide how many units must be communicated with during a test run. If more than two units are involved, the MSDOS interrupt library may be used, otherwise the Lattice C version is quite sufficient. The hardware issues must be addressed such as good cables and handshaking requirements. After this is completed, low level and high level procedures may be written following a style that makes sure that every procedure will always return and with some useful information to let the calling procedure understand how the communications are doing. The method of passing a negative one for failed calls works quite well when one is using higher level procedures to maintain a watch over a procedure's success.

ACKNOWLEDGMENTS

Paul Beaty and Heidi Walls were very instrumental in the process of assembling and testing different stations which tried and proved the effectiveness of this approach to serial communications.

REFERENCES

Advanced MSDOS. Microsoft Press. Redmond, WA. 1986.

Lattice C. Lattice, Inc. Lombard, IL. 1989.

DigiBoard. DigiBoard Inc. St. Louis Park, MN. 1990.

DTE	DCE	9pin	Label	25pin	Circuit	Description
case gnd	case gnd	case	gnd	1	AA	Protective ground
output	**input**	**3**	**TxD**	**2**	**BA**	**Transmitted data**
input	**output**	**4**	**RxD**	**3**	**BB**	**Received data**
output	**input**	**8**	**RTS**	**4**	**CA**	**Request to send**
input	**output**	**7**	**CTS**	**5**	**CB**	**Clear to send**
input	**output**	**9**	**DSR**	**6**	**CC**	**Data set ready**
sig. gnd	**sig. gnd**	**1**	**GND**	**7**	**AB**	**Signal ground (common return)**
input	**output**	**5**	**DCD**	**8**	**CF**	**(Data) Carrier detect**
				9		(Reserved for data set testing)
				10		(Reserved for data set testing)
				11		Unassigned
				12	SCF	Secondary received line signal detector
				13	SCB	Secondary clear to send
				14	SCA	Secondary transmitted data
				15	DB	Transmission signal element timing (DCE source)
				16	SBB	Secondary received data
				17	DD	Receiver signal element timing (DCE source)
				18		Unassigned
				19	SCA	Secondary request to send
output	**input**	**2**	**DTR**	**20**	**CD**	**Data terminal ready**
				21	CG	Signal quality detector
input	output	6	RI	22	CE	Ring indicator
				23	CH/CI	Data signal rate selector (DTE/DCE source)
				24	DA	Transmit signal element timing (DTE source)
				25		Unassigned

Figure 1 25pin versus 9pin RS-232 Connector

Circuit	Type	To:	Function
	Data Signals		
BA	Transmitted Data	DCE	Data generated by DTE
BB	Received Data	DTE	Data received by DTE
	Control Signals		
CA	Request to Send	DCE	DTE wishes to transmit
CB	Clear to Send	DTE	DCE is ready to transmit; response to request to send
CC	Data Set Ready	DTE	DCE is ready to operate
CD	Data Terminal Ready	DCE	DTE is ready to operate
CE	Ring Indicator	DTE	Indicates that DCE is receiving a ringing signal on the communication channel
CF	Carrier Detect	DTE	Indicates that DCE is receiving a carrier signal
CG	Signal Quality Detector	DTE	Asserted when there is reason to believe there is an error in the received data
CH	Data Signal Rate Selector	DCE	Asserted to select the higher of two possible data rates
CI	Data Signal Rate Selector	DTE	Asserted to select the higher of two possible data rates
	Timing Signals		
DA	Transmitter Signal Element Timing	DCE	Clocking signal, transitions to ON and OFF occur at center of each signal element
DB	Transmitter Signal Element Timming	DTE	Clocking signal, as above; both leads relate to signals on BA
DD	Receiver Signal Element Timing	DTE	Clocking signal, as above, for circuit BB
	Ground		
AA	Protective Ground	NA	Attached to machine frame and possibly extenal grounds
AB	Signal Ground	NA	Establishes common ground reference for all circuits

Figure 2 25pin RS-232 Function Description

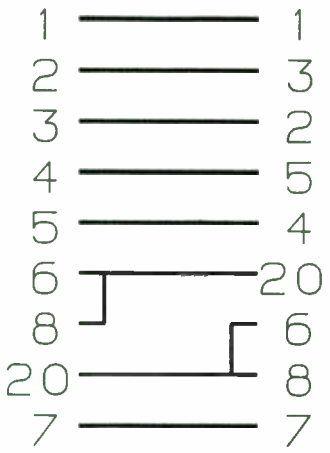

Figure 3 **Lattice C Null Modem**

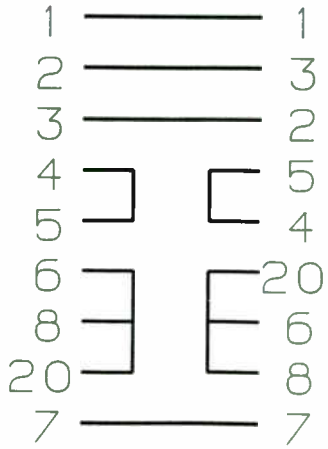

Figure 4 **Dos Interrupt Null Modem**

OPTIMIZE MIXER PERFORMANCE THROUGH SWEPT FREQUENCY & POWER CHARACTERIZATION

Joel Dunsmore and Barry Brown
Hewlett-Packard Co., Santa Rosa, CA

Agenda:

Mixer Basics
Mixer Characteristics
Non-Linear Effects
Mixer Test System and
Group Delay Measurements

PATSS1

Abstract:

The mixer is the key non-linear element in frequency converter systems, but recent advances in technology enable integration of filter and amplifiers with the mixer. These elements can dramatically affect the performance of the system. For example, RF input match of a mixer changes with the impedance presented at the IF. This is true even in high isolation mixers due to changing operating point. For this reason match and conversion loss must be measured under actual end use conditions. Mixers do not always behave in an expected manner. For instance, at very low LO drive levels, the "small signal" RF drive level can significantly affect the conversion loss in a non-linear fashion. Swept-power conversion loss measurements reveal this unexpected behavior.

This paper describes the basics of non-linear mixer behavior, using non-linear CAE modeling to illustrate the concepts. Measurement techniques are presented which allow viewing this behavior directly with a vector network analyzer, as well as techniques to compensate for RF and IF path losses to achieve accurate conversion loss measurements. A calibration method for measuring group delay through mixers is presented, also.

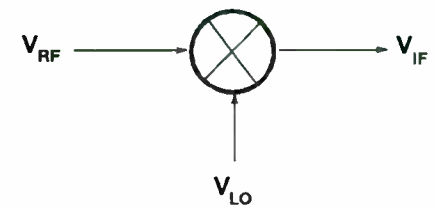

$$V_{LO} = \sin\omega_{LO}t \qquad V_{RF} = \sin\omega_{RF}t$$

$$V_{IF} = (\sin\omega_{LO}t) \cdot (\sin\omega_{RF})t$$

$$V_{IF} = 1/2 \cos(\omega_{LO} - \omega_{RF})t - 1/2 \cos(\omega_{LO} + \omega_{RF})t$$

PATSS2

A mixer is a non-linear device, which converts input signals at one frequency band into output signals at a different band. An ideal mixer can be represented as a multiplier whose IF output signal is the product of its two inputs, the RF and LO signals. If the inputs are sinewaves, the output is easily calculated:

$$V_{LO} = \sin\omega_{LO}t \qquad V_{RF} = \sin\omega_{RF}t$$

$$V_{IF} = (\sin\omega_{LO}t) \cdot (\sin\omega_{RF})t$$

$$V_{IF} = 1/2 \cos(\omega_{LO} - \omega_{RF})t - 1/2 \cos(\omega_{LO} + \omega_{RF})t$$

So the output contains signals at the sum and difference of the input frequencies, giving rise to frequency translation.

This introductory section will provide further understanding of the basic operation of mixers by examining two mixer designs: single-balanced and double-balanced mixers.

SINGLE-BALANCED MIXER

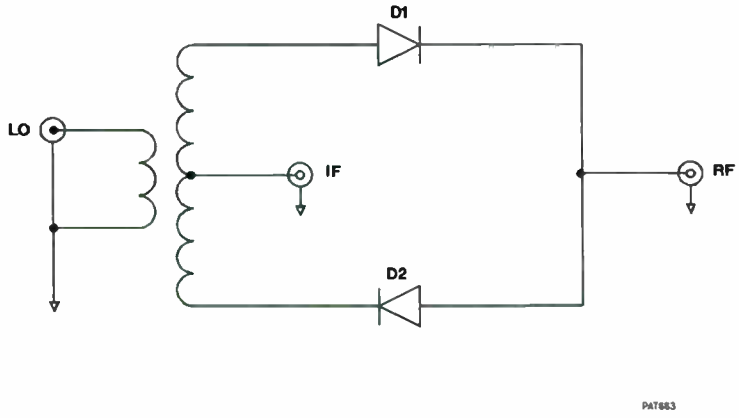

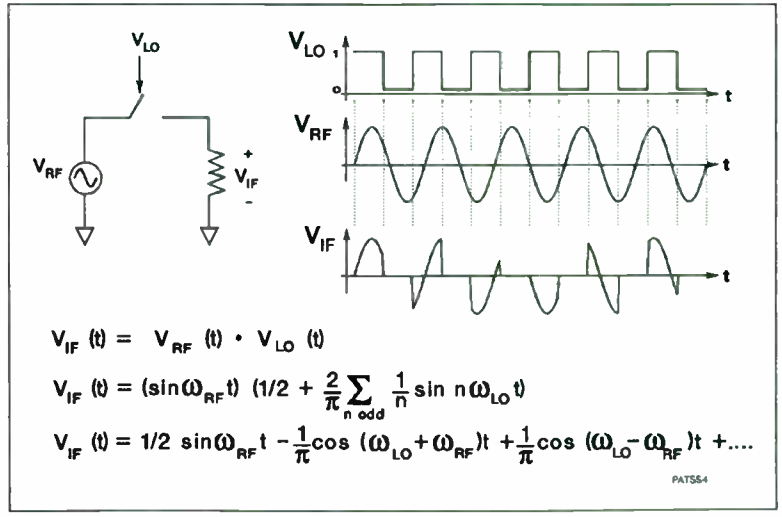

First, consider the single-balanced mixer, one configuration of which is shown above. A signal is applied to the LO port, causing an LO current to flow in the diodes which is large enough to switch them on and off. A smaller signal is applied to the RF port which causes an RF current to flow in the diodes. The diodes provide the mixing action to produce currents in the IF port at the sum and difference frequencies $f_{LO} + f_{RF}$ and $f_{LO} - f_{RF}$. If the balun and diodes are perfectly matched, then the LO signal will appear at neither the RF port nor the IF port; i.e., the LO to RF and LO to IF isolation will be perfect. However, this structure provides no isolation between RF and IF ports. This is usually accomplished by filtering in these ports.

The operation of the single-balanced mixer can be explained by representing the two diodes as an ideal switch between the RF and IF ports. When the LO signal is positive, the switch is closed; when the LO is negative, the switch is open. The IF voltage can be calculated by multiplying the RF voltage times an ideal squarewave which represents the switch closing and opening at the LO frequency:

$$V_{IF}(t) = V_{RF}(t) \cdot V_{LO}(t)$$

$$V_{IF}(t) = (\sin\omega_{RF}t)\ (1/2 + \frac{2}{\pi}\sum_{n\ odd}\frac{1}{n}\sin n\omega_{LO}t)$$

$$V_{IF}(t) = 1/2\ \sin\omega_{RF}t - \frac{1}{\pi}\cos(\omega_{LO}+\omega_{RF})t + \frac{1}{\pi}\cos(\omega_{LO}-\omega_{RF})t + ...$$

So the IF voltage contains signals at the RF frequency, and at the sum and difference of the RF and LO frequencies.

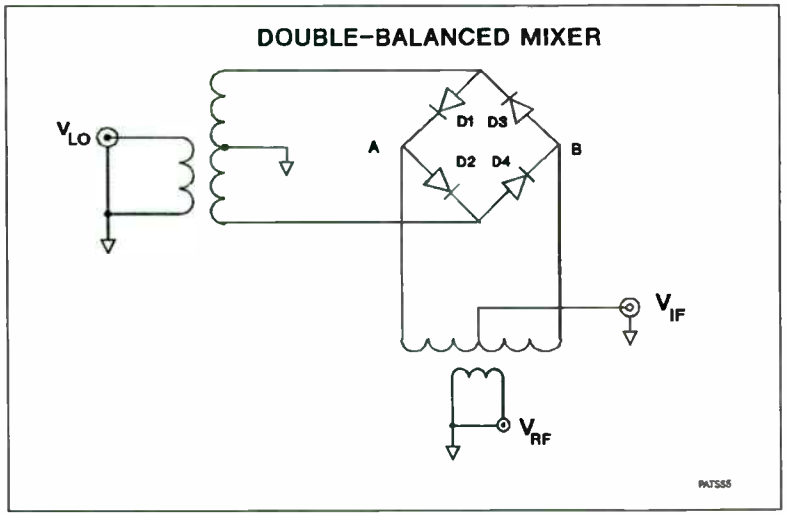

The double-balanced mixer, shown here, offers improved isolation over the single-balanced design. All three ports of the mixer are inherently isolated from each other by the symmetry of the design. During the positive half-cycle of the LO, diodes D1 and D2 are conducting, and point A is at ground potential, so $V_{IF} = V_{RF}$. During the negative half-cycle of the LO, D3 and D4 are on, point B is at ground, and $V_{IF} = -V_{RF}$.

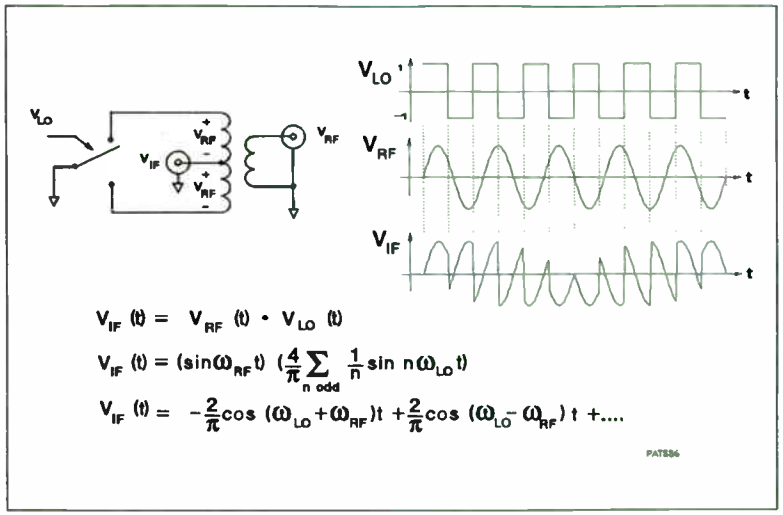

This operation can be explained by once again replacing the diodes by a switch controlled by the LO. When the LO voltage is positive, the switch is down, when it's negative, the switch is up. Multiplying the RF and LO waveforms gives the IF voltage:

$$V_{IF}(t) = (\sin\omega_{RF}t)\,(\frac{4}{\pi}\sum_{n\ odd}\frac{1}{n}\sin n\omega_{LO}t$$
$$V_{IF}(t) = -\frac{2}{\pi}\cos(\omega_{LO}+\omega_{RF})t + \frac{2}{\pi}\cos(\omega_{LO}-\omega_{RF})t + \ldots$$

Notice that, unlike the single-balanced mixer result, the IF signal has only the sum and difference mixing products with no RF signal leakage.

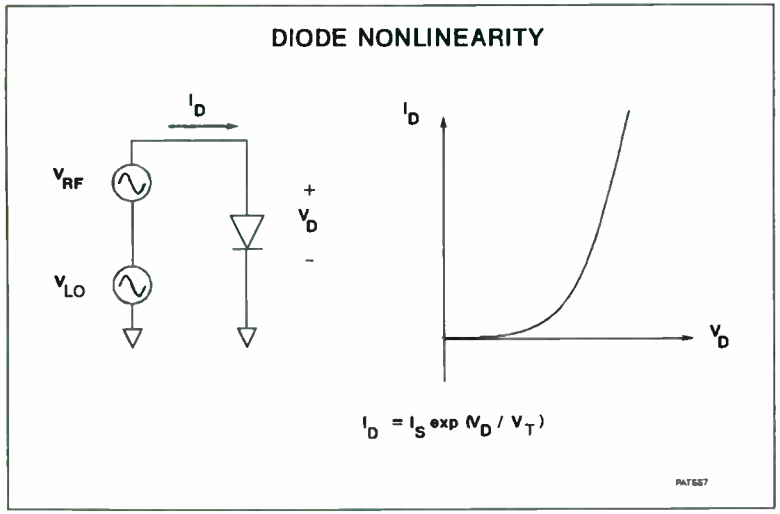

Of course, the diodes do not form a perfect switch as in the idealized mixers discussed so far. In fact, a diode has a very nonlinear transfer function which gives rise to higher order mixing products and distortion. Consider a single diode with an applied voltage equal to the sum of two sinewaves at the RF and LO frequencies.

$$I_D = I_S \exp((V_{RF} + V_{LO})/V_T) = I_S \exp((\sin W_{RF}t + \sin W_{LO}t)/V_T)$$

The exponential can be expanded in a power series,

$$e^x = 1 + X + 1/2\,X^2 + 1/6\,X^3 + \ldots.$$

which yields the following output frequencies:

First order:	$\sin W_{RF}t$, $\sin W_{LO}t$	(feedthrough)
Second order:	$\cos(W_{LO} + W_{RF})t$, $\cos(W_{LO} - W_{RF})t$,	(sum and difference)
	$\cos(2W_{RF}t)$, $\cos(2W_{LO}t)$	(second harmonics)
Third order:	$\sin(2W_{RF} - W_{LO})t$, $\sin(2W_{RF} + W_{LO})t$,	(2:1 and 1:2 spurs)
	$\sin(2W_{LO} - W_{RF})t$, $\sin(2W_{LO} + W_{RF})t$,	
	$\sin(3W_{RF}t)$, $\sin(3W_{LO}t)$	(third harmonics) etc.

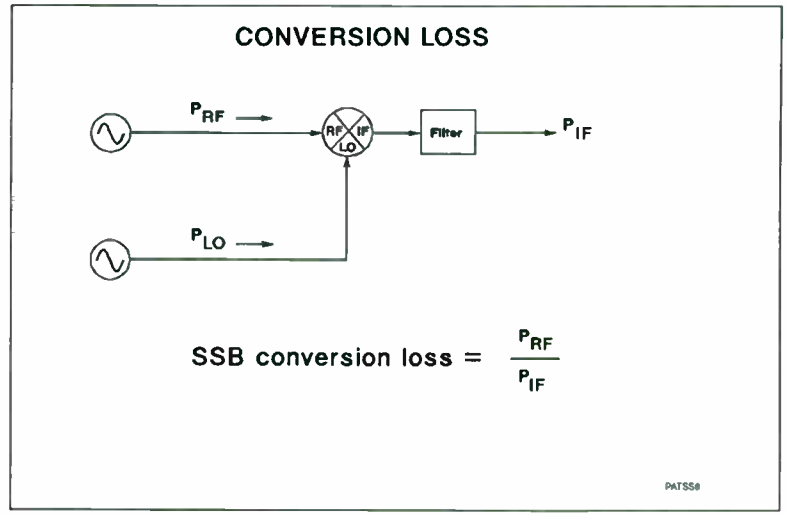

In this next section, the common characteristics and specifications of mixers will be explained.

One of the most important specifications of a mixer is its conversion loss, defined as the ratio of the RF input power to the output power of the desired IF signal, at either $W_{LO} + W_{RF}$ or $W_{LO} - W_{RF}$. Shown above is the definition of SSB conversion loss. In general, the value of the loss is a function of the frequencies and power levels of the RF and LO signals, so it should be measured and specified carefully.

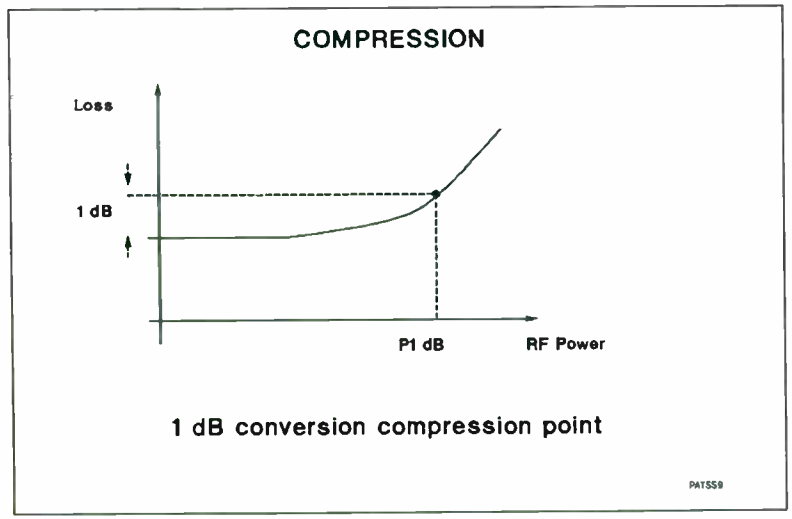

When the RF input power is increased, the IF output power will also increase, with a constant conversion loss, until the mixer enters compression. At this point, the IF power cannot increase as rapidly as the RF power, so the loss goes up. This is called conversion compression, and the 1 dB compression point is defined as the RF input power level (in dBm) at which the conversion loss has increased 1 dB over its small-signal value, as shown in the diagram. In a double-balanced mixer, this point will typically be 5 to 10 dB less than the LO power level. It is a strong function of LO power, and also varies with frequency.

A related, but different, mixer parameter is the 1 dB desensitization level. It expresses the change in the conversion loss for a small input signal caused by the presence of a second, larger interference signal at the input. It is the power level of the large interference signal which causes a 1 dB increase in the conversion loss of the small signal.

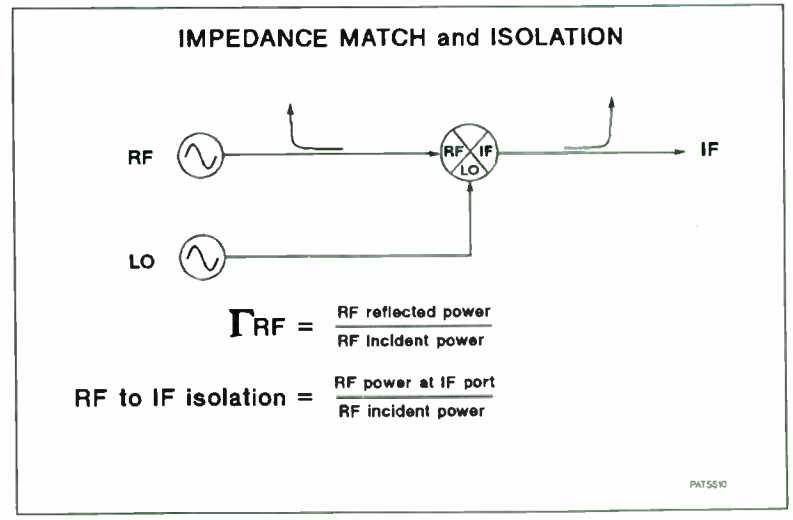

The impedance mismatch at all three ports of the mixer can be an important system consideration. The impedances of all three ports are strongly affected by the LO power, which alters the diode operating point. Impedance mismatch is commonly measured with a network analyzer.

There are six different isolation terms defined for a mixer; LO to RF, LO to IF, RF to IF, RF to LO, IF to RF, and IF to LO. The first three are the more commonly specified isolation parameters. They represent unwanted direct leakage of the signals.

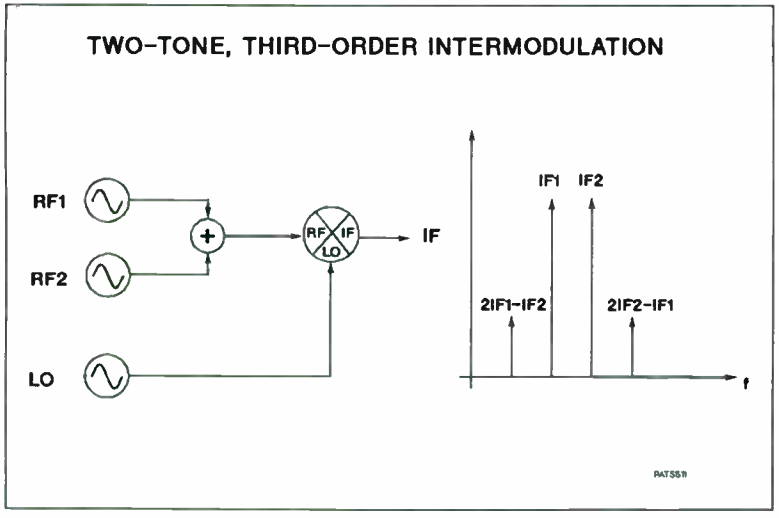

A very commonly specified measure of the signal distortion produced by a mixer is its two-tone intermodulation distortion. When the RF input consists of two different frequency signals, the nonlinearity of the mixer can produce undesirable products in the IF output. The most significant of these is usually the third-order products, shown above. A related figure-of-merit for the mixer is its third-order input intercept point, or TOI. This is the theoretical input level at which the intermodulation distortion signals would become as large as the desired IF output signal, calculated from the measured distortion as:

$$TOI = PIN + 1/2\ IMD_3$$

where TOI is third-order intercept point

and IMD_3 is the level (in dBc) of the third-order intermodulation signals at an input power level PIN (dBm).

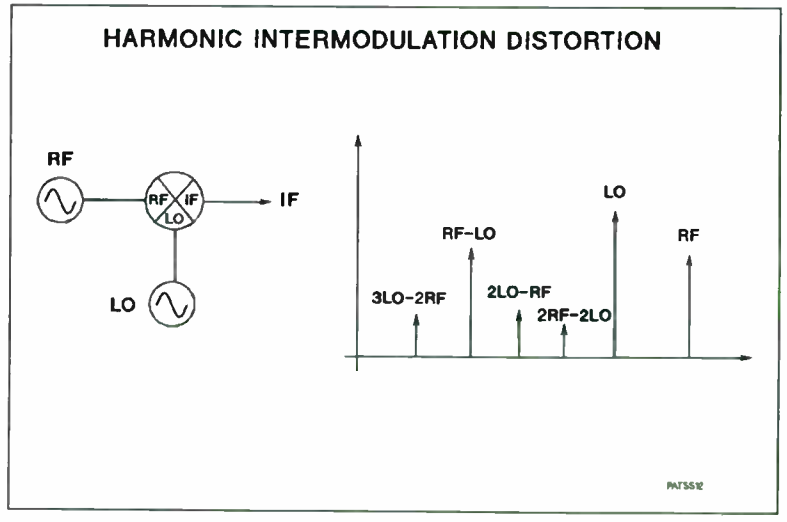

Harmonic intermodulation distortion in a mixer produces unwanted output signals at frequencies equal to the sum and difference of harmonics of the RF and LO, expressed as $mF_{LO} +/- nF_{RF}$. Performance of a mixer in this regard is often unspecified because the levels of these distortion products depend on frequencies, power levels, and terminating impedances. However, it may be an important parameter, particularly in broadband systems. As the RF input frequency is swept across a moderate range, it is very difficult to keep all of the distortion products out of the IF bandwidth. Some of the distortion products may sweep at different rates and even in the opposite direction to the input signal. In these applications, the distortion of the mixer must usually be characterized under its intended operating conditions.

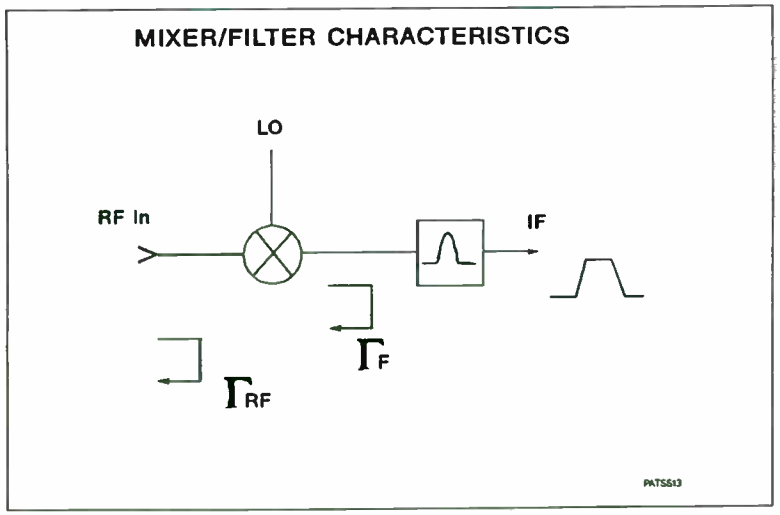

Mixers are often followed by IF filters tuned to select channels in the IF. The match, or impedance of the IF filter may affect the input match of the mixer in the RF frequency range. This can occur even in mixers with RF to IF isolation, as the IF impedance may change the operating point of the diodes in the mixer.

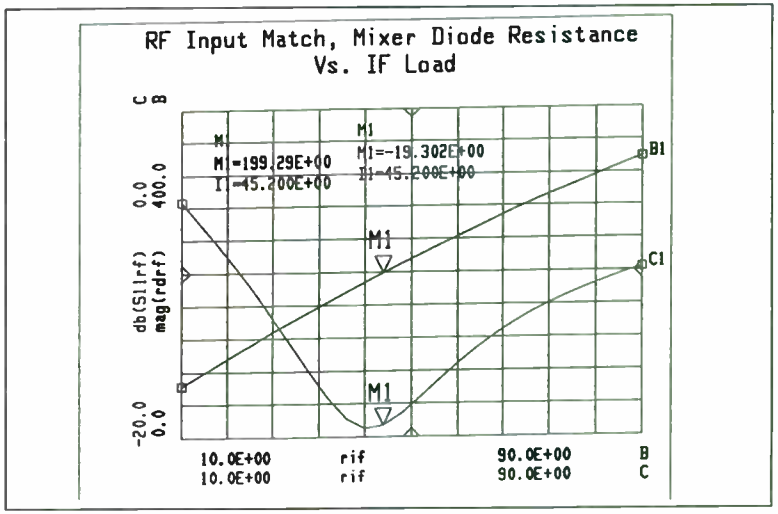

In this model, the RF match, and the diode operating point are displayed as a function of the load impedance of the IF port. Notice that even though there is considerable isolation between RF and IF ports, the IF impedance substantially changes the RF match.

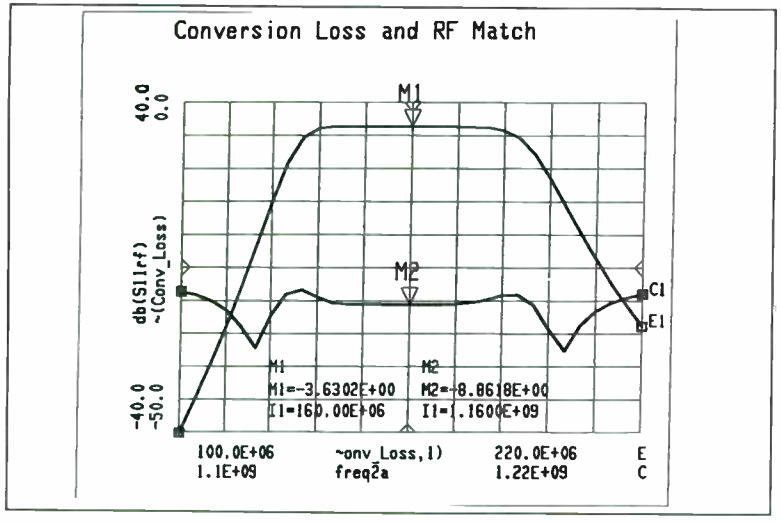

Here, the frequency of the RF and IF are swept to show the passband of the IF filter. Even though the passband is at the IF freq (130-190 MHz), the shape of the passband appears in the RF match at RF frequencies. Note that this is a non-linear affect. The change in match of the BPF is translated in frequency, up to the RF range. Thus, the isolation of IF to RF, at the RF range, does not predict the extent of dependence of the RF match on IF impedance.

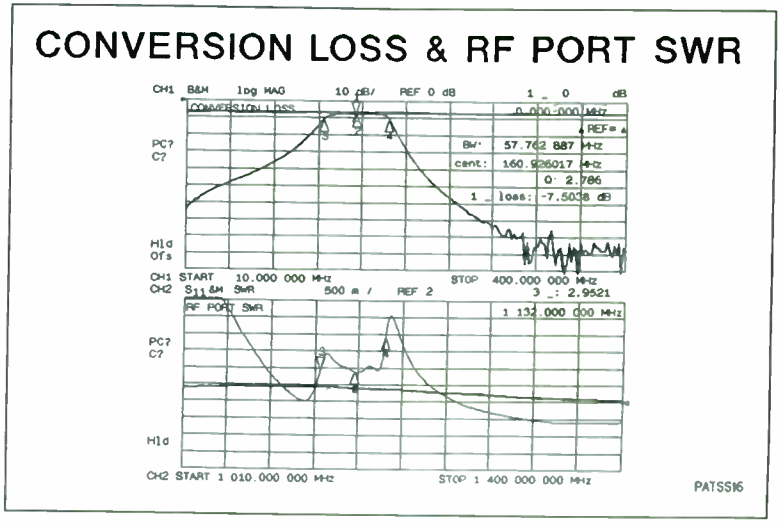

This is a real measurement of a mixer/filter combination. The upper trace shows conversion loss with and without the filter. The lower trace shows RF input match with and without the filter. Note that the match is measured over the RF range, yet we see a change in match which reflects the shape of the filter at the lower IF range. This measurement will allow the match effects of the filter on the RF to be monitored, while adjusting the passband response of the IF filter.

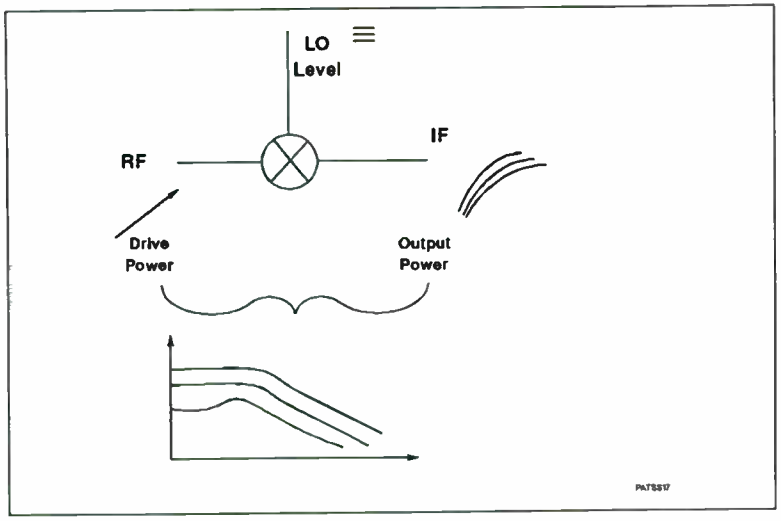

A common non-linear effect in mixers is the change in conversion loss as a function of RF input drive power, also called conversion loss compression. The input power at which the conversion loss has increased by 1 dB is a common figure of merit. This point, as well as the minimum conversion loss are a function of LO drive power. Interestingly, at small LO drive levels, the point of minimum conversion loss may not occur at the minimum RF drive, resulting in a conversion loss vs. RF drive function which first shows expansion, then quickly falls into compression.

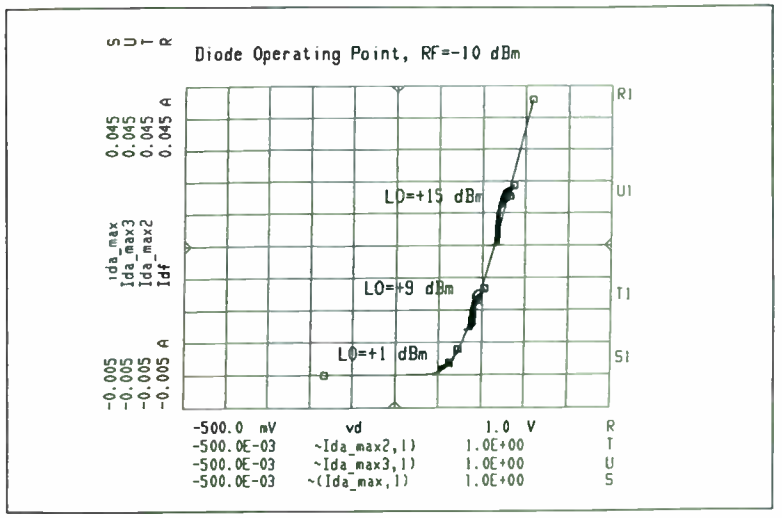

Here, the diode operating point is shown vs. LO drive power. Notice at higher LO drives, the slope of the curve increases, indicating smaller diode rf resistance. This plot was made by plotting instantaneous voltage and current across the diode over an RF & IF cycle.

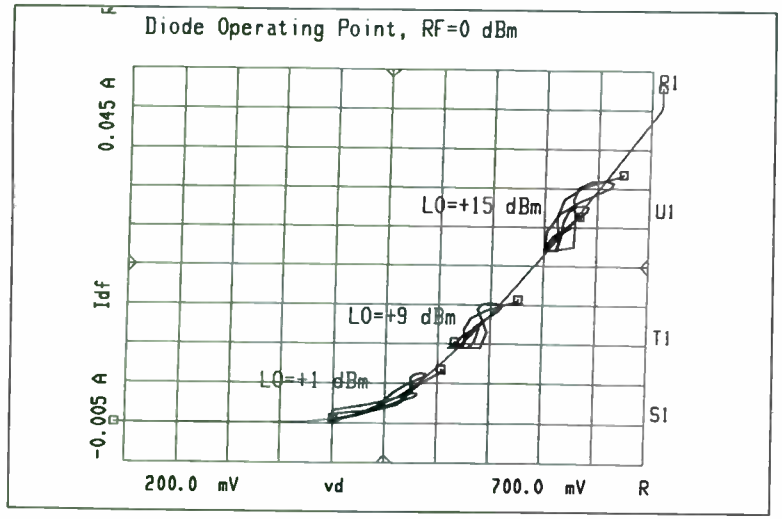

Here, the operating point vs. RF input drive is shown, notice for small LO drive, the larger RF signal pushes the operating point higher, thus reducing the diode rf resistance. The i-v trajectory does not exactly follow the DC curve due to reactive elements in the mixer model, namely, diode capacitance. The boxes on each trace, which represent the peak of the voltage across the diode, move on the curve due to changes in IF voltage.

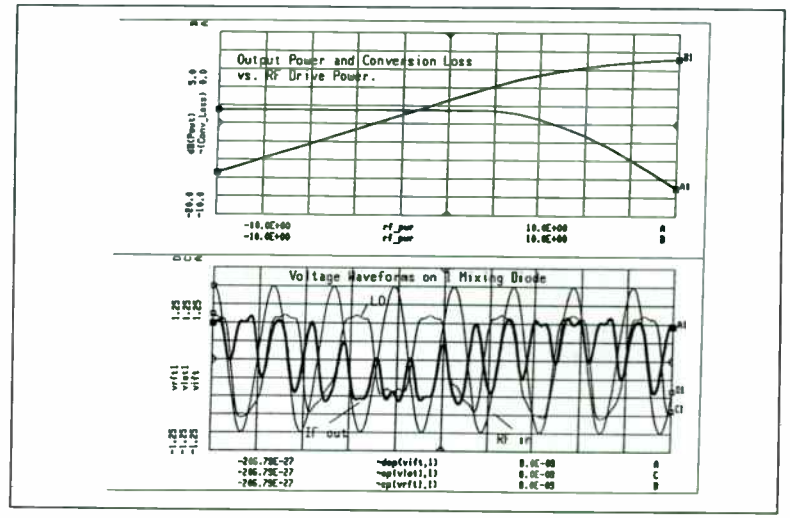

The upper trace shows the effect of increasing RF drive on conversion loss. The output power is also shown. The lower trace shows the input and output voltage waveforms. It is clear that the clipping of the RF by the mixing diodes limit the maximum IF output. This is the mechanism which causes compression in the mixer.

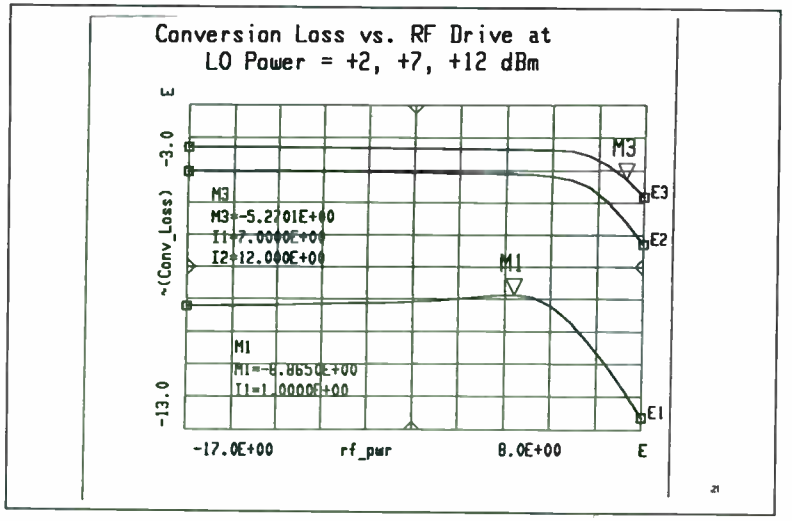

Here, the mixer compression is modeled at three levels of LO drive power. Notice at very low LO drive power, the conversion loss decreases with higher RF drive. This is a result of lower diode resistance with RF drive. At even higher RF drive, the diodes clip the RF and compression ensues.

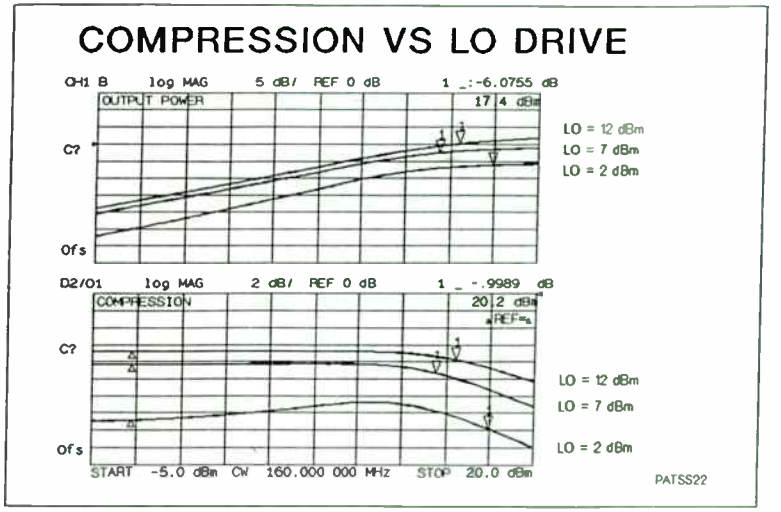

Here is a measurement of conversion loss and output power vs. RF input drive for three different LO drive powers. The mixer is specified for LO drive levels from +7 to +12 dBm. At +2 dBm, the conversion loss is reduced by 3 dB, and the expansion effect of RF drive on conversion loss is evident.

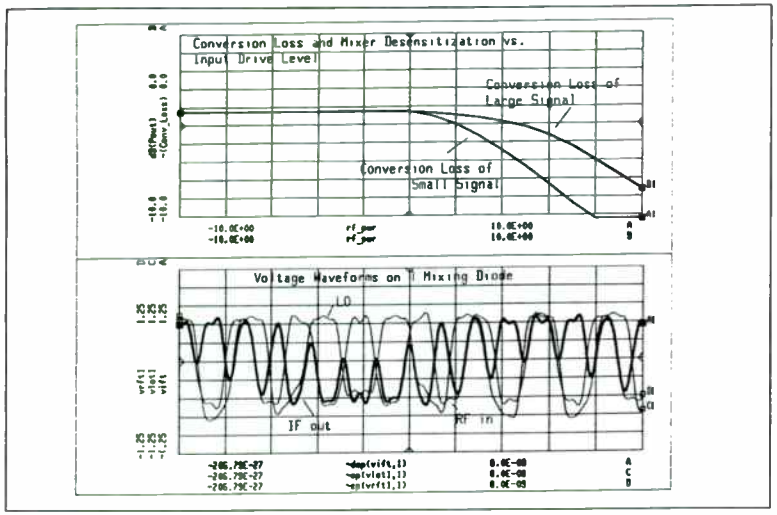

Mixer desensitization occurs when an adjacent channel signal which is much larger than the desired RF reduces the sensitivity of the mixer. Here the model of the mixer shows the curve of conversion loss vs. the undesired signal power. The lower plot shows the voltage waveforms for the mixer with and withiout the adjacent channel signal. The diode current waveform clearly shows how the undesired signal saturates the mixer diodes, causing clipping of the small signal.

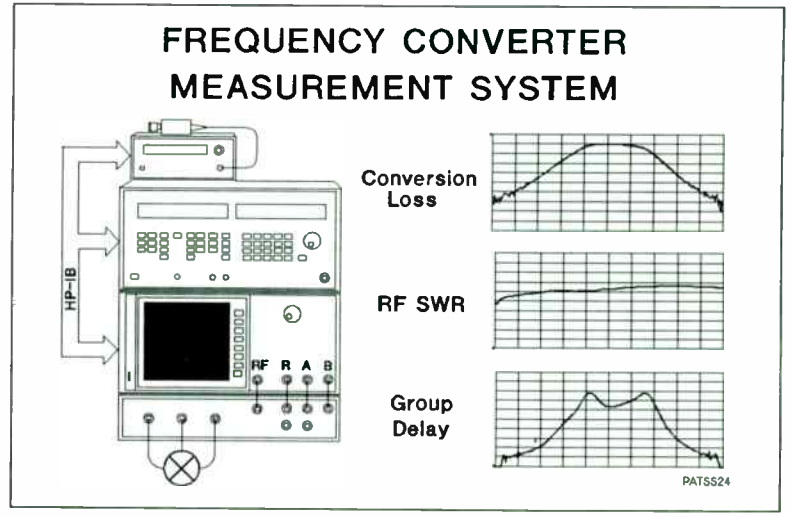

The HP 8753C network analyzer, with a specially designed three port test set, provides the ability to characterize conversion loss, compression, return loss (SWR) and griup delay with a single connection.

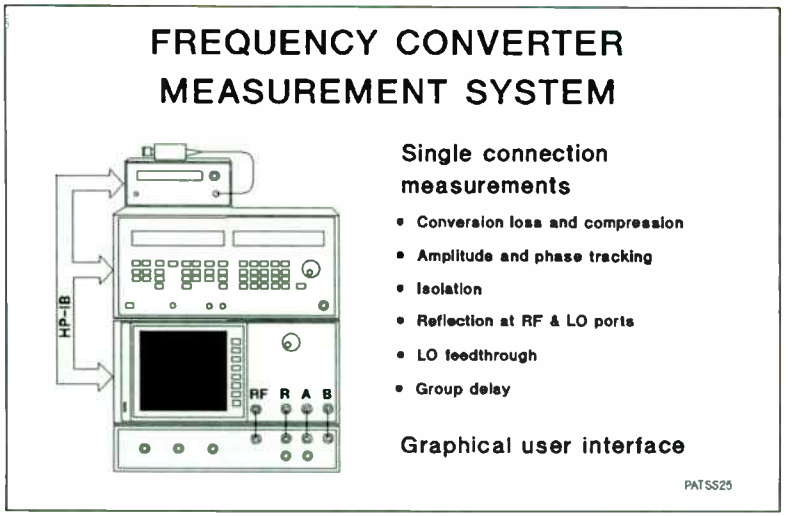

This test set provides for single connection testing of mixers and frequency converters. Simultaneous measurement of parameters including conversion loss, isolation, feedthrough, group delay and SWR can be made directly.

Next, each element of the test system will be explained in detail. This includes: the HP 85046A H20 Mixer Test Set, new enhancements for the HP 8753C RF Network Analyzer and the HP 8625A Synthesized RF Sweeper.

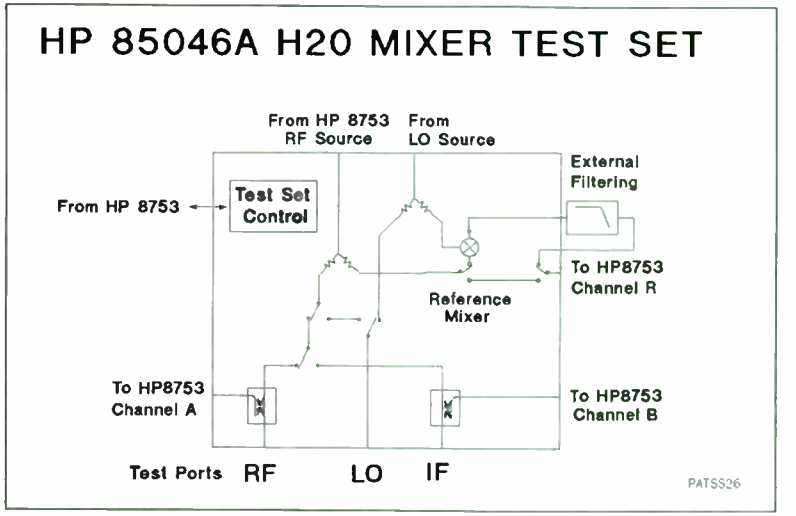

This simplified block diagram shows the switching capability and the R channel mixer necessary to simplify frequency converter measurements with the vector network analyzer. The internal mixer is used to provide an R channel signal necessary to phase lock the RF source, as will be explained later. Ports for custom filtering are provided so that easy selection of IF frequency ranges can be made. The filter is necessary to prevent measurement inaccuracies due to unwanted signals being sampled in the HP 8753C receiver. Control of the switches is accomplished through special soft key sequences on the network analyzer.

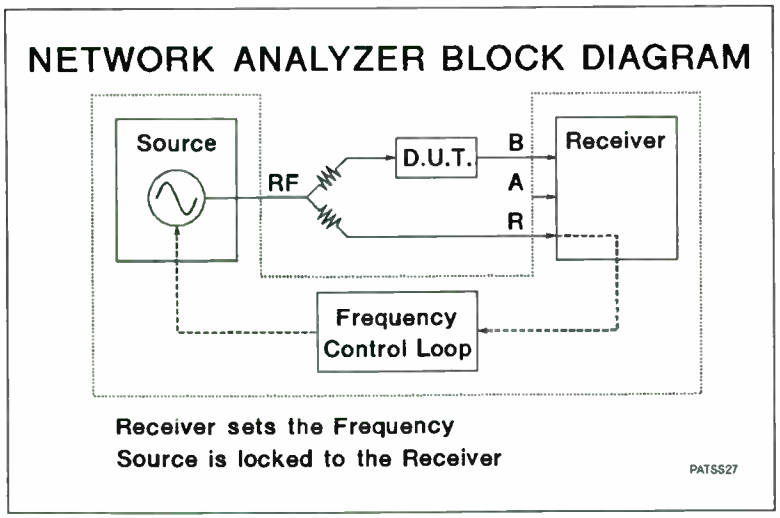

The HP 8753C network analyzer consists of a three-channel, tuned receiver, a 300 kHz to 3 GHz RF source, and frequency control loop circuitry. The receiver contains a swept, synthesized local oscillator which determines the frequency of the analyzer, and the source frequency is made to track the receiver by the frequency control loop. A sample of the R channel IF signal is fed back to the control loop, and there must be a connection between the RF source and the R channel to complete the loop. Without this connection, the source frequency is undetermined.

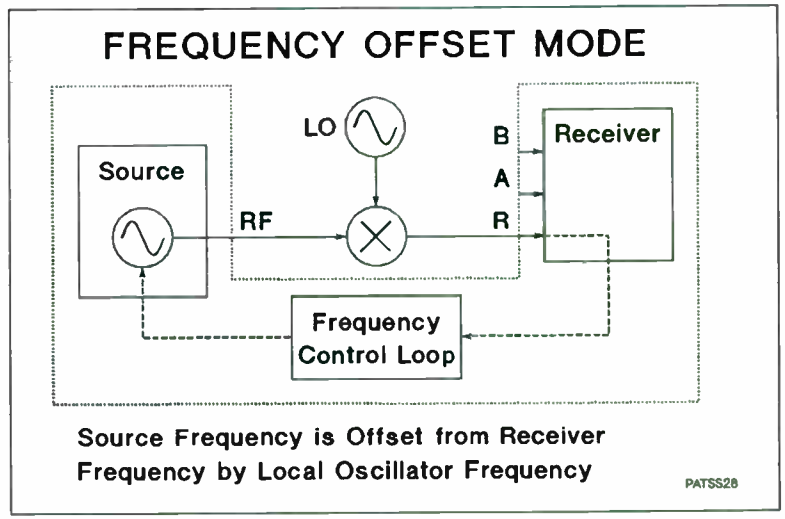

The HP 8753C has a special mode of operation, called frequency offset mode, which provides the ability to make swept measurements of frequency converters [1]. In this mode, a mixer is placed in the R channel connection to cause an offset between the source and receiver frequencies. The frequency control loop still makes the source track the receiver, but they will be offset by the local oscillator frequency.

A filter is generally required after the mixer to select the proper mixing product (i.e., LPF passing RF - LO frequencies for downconverters, HPF passing RF + LO frequencies for upconverters).

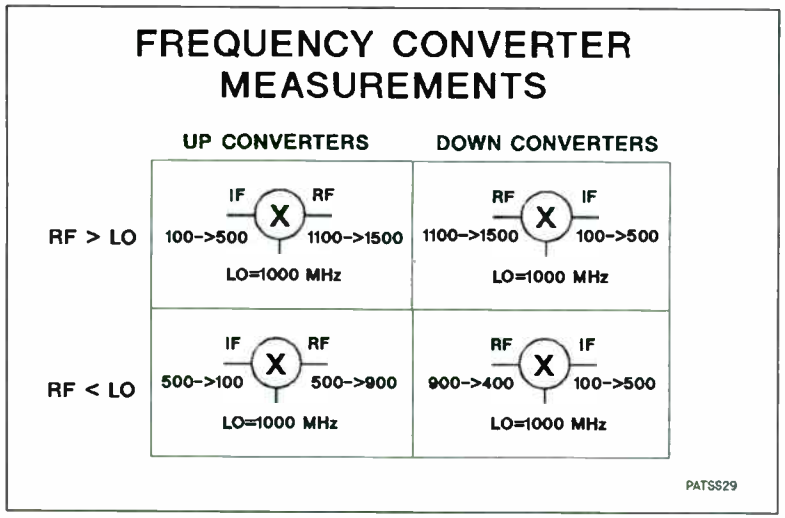

Frequency offset mode provides full capability for frequency converter measurements with swept RF and fixed LO frequencies. Both down-converters and up-converters, high-side LO and low-side LO converters can be measured.

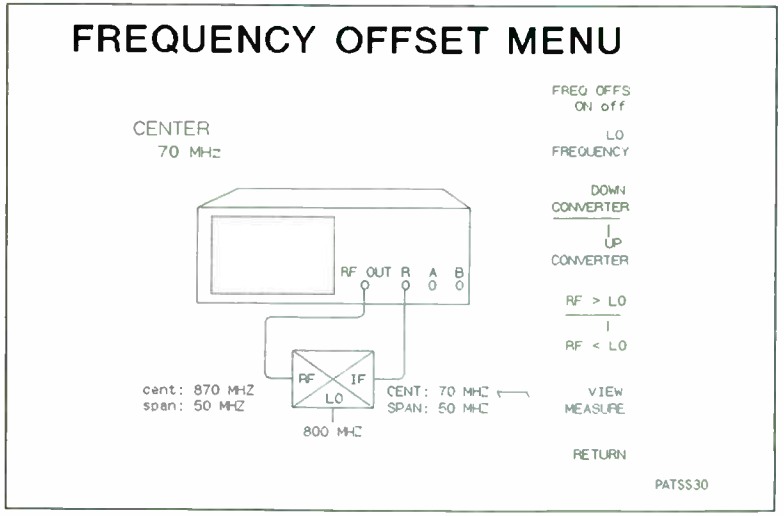

Selection of the device type (UPCONVERTER or DOWNCONVERTER), High or low-side LO injection (RF > LO or RF < LO), and the desired RF, LO and IF frequencies is done through the FREQUENCY OFFSET menu. Since these parameters are interdependent, the displayed RF, LO and IF frequencies are automatically updated when any single parameter is changed.

FIXED IF MEASUREMENTS

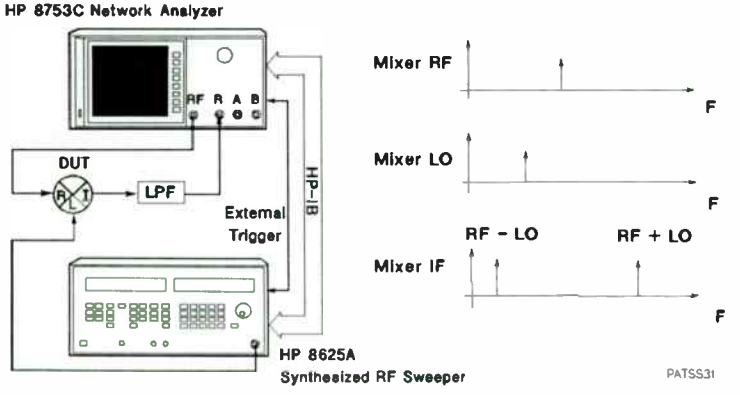

This slide shows the frequency domain of a fixed IF measurement being made. The offset between the RF and LO signal frequencies is constant at the selected IF frequency as the two-signal sources sweep. Thus the conversion loss display will be the conversion loss as a function of RF frequency.

SOURCES OF ERROR

TRANSMISSION MEASUREMENTS:

(Conversion Loss, Compression, Group Delay)

- **Frequency response of RF drive and receiver**
- **Mismatch - return loss of cables and devices**
- **Harmonics, linearity, spurious signals**

PATSS32

In most measurements, there may be several sources of error. For conversion loss, isolation, and power measurements, frequency response errors (sometimes called flatness, or rolloff), and mismatch errors (from non-ideal source and load impedances) typically cause the largest uncertainties in measurements.

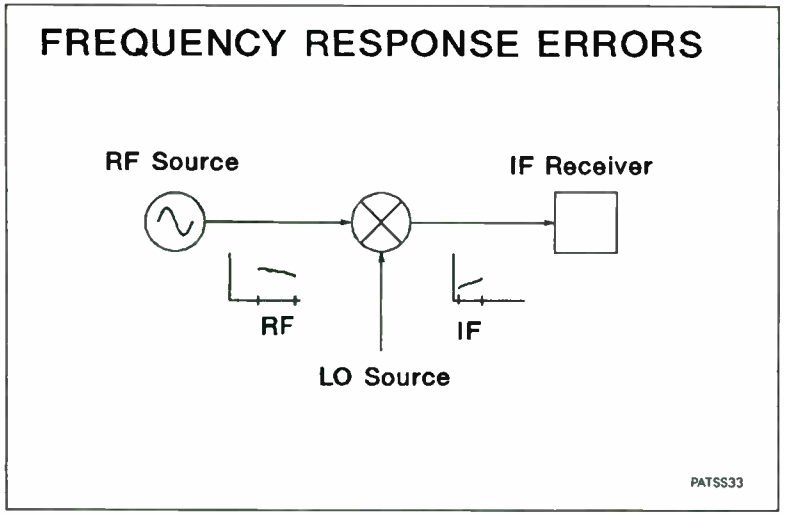

Frequency response errors have two parts: nominal offsets (caused by pads, couplers, etc.) and flatness (different responses at different frequencies). The offset is quite easy to account for, but correcting for flatness errors requires careful characterization over a frequency range. For frequency converters, it is especially important to consider the flatness effects since the RF (source) is at one frequency and the IF (receiver) is at another.

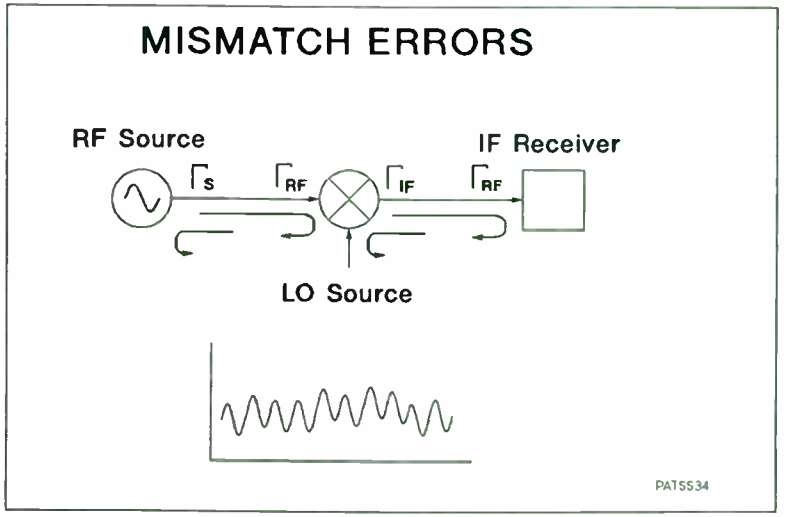

Mismatch errors, due to non-ideal source and load impedances, have a smaller but quite noticeable effect on measurements. This is most commonly seen as ripple on a trace, from a poor match at the end of a cable. For normal 2-port measurements, the effects of mismatch can be predicted if both the forward and reverse transmission and reflection parameters are measured. From this measurement, and an earlier measurement of the system, during the user calibration, a corrected response is calculated to remove the effects of mismatch. However, in frequency converter conversion loss measurements, mismatch cannot be corrected for because the input and output frequencies are not the same, and the forward and reverse parameters do not depend, in a linear fashion, upon the source or load impedances. For this reason, padding cables and fixtures near the device under test provides good match and reduces mismatch uncertainties. Fortunately, the wide dynamic range of the HP 8753C allows considerable padding without diminishing the quality of the measurement.

Harmonics, Linearity (sometimes called dynamic accuracy of log fidelity), and spurious signals can

contribute to measurement error. However, the tuned nature of the receiver eliminates unwanted signals, and the digital IF eliminates detector logging and other linearity errors.

In reflection measurements, such as RF or IF port match, system errors such as source match, frequency response, and directivity may add to uncertainties. Fortunately, these are linear measurements for which correction techniques are well known.

GROUP DELAY CONSIDERATIONS

- Calibration required to remove measurement system errors
- Standard cal techniques NOT possible for frequency translation measurements
- Cal standard is broadband double-balanced mixer

ANZAC	MDC-123	30-3000 MHz	0.5 nsec
MCL	ZFM-4	DC-1250 MHz	0.6 nsec

- Attenuators needed to reduce mismatch errors
- Typical accuracy better than +/- 0.5 nsec.

PATSS35

A vector network analyzer can be used to measure the group delay of most frequency converters, but calibrating the measurement is a problem. When measuring a linear device, such as a filter, a through connection is used as a calibration standard (delay = zero), but this will not work in a converter measurement, where the analyzer's source and receiver are at different frequencies. The solution is to use a very broadband mixer with very small group delay as the calibration standard. Two such mixers have been characterized for this purpose (3) and the accuracy of this technique is excellent.

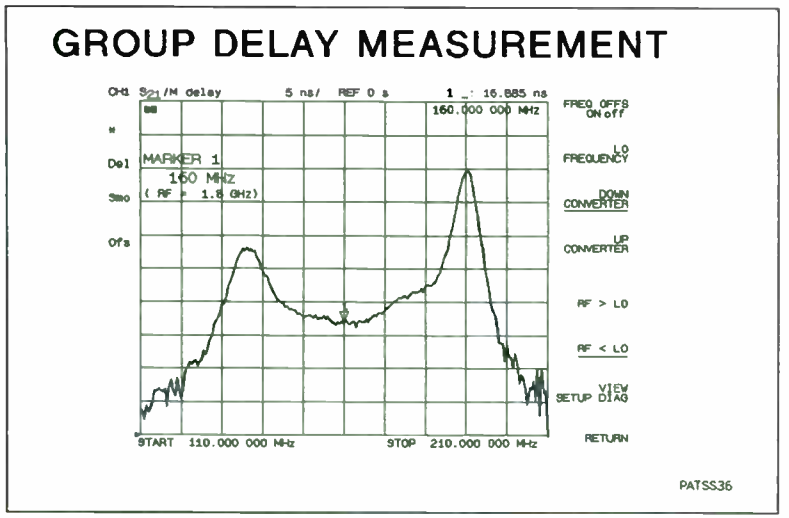

Here is the resulting data from an example group delay measurement. Most frequency converters can be measured in this manner, but note that if the DUT has a built-in LO, this LO signal must be available on an auxiliary output connector, or it must be phase-locked to a reference signal which is available. This is because an exactly identical LO signal must be applied to the test set and the DUT, or no group delay measurement is possible with this system (3).

REFERENCES:

1. Brown, Barry A., "New Measurement Techniques for Testing Both Linear and Nonlinear Devices with the HP 8753B RF Network Analyzer", Proceedings RF EXPO 89, pp. 227-237, February 1989.

2. Dunsmore, Joel. "Measuring Power with a Vector Network Analyzer", Microwaves & RF, pp. 78-87, January 1991.

3. Brown, Barry A., "Measurement of Frequency Converter Group Delay", Microwave Engineering Europe, pp. 41-46, July/August 1990.

4. Hewlett-Packard Product Note 8753-2A, "Mixer Measurements with the HP 8753 Network Analyzer", August 1990, HP publication number 5952-2771.

5. Hewlett-Packard Product Note 8753-3, "Applications of the Test Sequence Function", December 1988, HP part number 08753-90133.

Testing North American Dual-Mode Cellular,

Japan Digital Cellular Transceivers

DAVE HOOVER

Hewlett-Packard Company
Spokane Division
R&D Project Manager
R&D Lab Department
1620 Signal Drive
Spokane, WA 99220

ABSTRACT

Rapid growth in current cellular systems has caused saturation in many urban markets. This has spurred the development of new digital cellular standards to increase the spectrum efficiency of cellular radios. The system chosen for the North American and Japanese digital cellular system utilizes a modulation known as π/4 DQPSK. This paper will present a method for generating π/4 DQPSK modulated signals as well as a technique to verify the modulation accuracy. Finally, a test system designed for the NADC system will be described which performs all necessary analog tests, and for the digital mode performs transceiver tests including bit error rate sensitivity, and call processing protocol.

BIOGRAPHY

DAVE HOOVER: Dave Hoover is an R&D Project Manager for the Spokane Division of Hewlett-Packard. He received his BSEE degree in 1980 and his MSEE degree in 1981 from the University of Washington. He joined HP in 1981 and worked on the HP 8657B Signal Generator and developed the frequency doubler. Dave has also worked on the GSM European digital cellular system and developed the HP 11835 data buffer and contributed to the development of the HP 11847A software package. Dave is an inventor on a patent for a synthesis technique used in the HP 8645A Signal Generator, and on a patent pending for the HP 11846A generator's filter technique. Currently Dave is working on the HP 8953DT NADC Test System .

INTRODUCTION:

This paper covers the following: (1) A review of basic digital modulation techniques which will provide a better understanding of the NADC (North American Dual-Mode Digital Cellular and JDC (Japan Digital Cellular) systems. (2) A technique for generating π/4 DQPSK modulation will be described which is used by HP's two current signal generators. (3) A digital signal processing algorithm will be reviewed which can measure the accuracy of the π/4 DQPSK modulation. (4) A complete manufacturing test solution for NADC radios will be described utilizing Hewlett-Packard's π/4 DQPSK sources and analyzers.

Why Digital Modulation Techniques?

Digital modulation is replacing analog modulation systems for at least two main reasons. In North America, the FCC has only allocated a fixed frequency band for cellular transmission. In large cities, such as New York, Toronto, Chicago, it is very difficult to gain access to the cellular network. Digital techniques promise a significant increase in spectrum utilization. (See slide 3)

In addition, the frequency bands used for cellular transmission are prone to fading or multipath transmission. Digital techniques can improve transmission quality by error

correction techniques. In addition, in Europe another digital system (GSM) is being invented so radios will work across country boundaries in Europe.

I Q diagrams, or in-phase and quadrature-phase diagrams, are commonly used to describe phase modulation systems. By making a two dimensional coordinate system, it is possible to represent the amplitude of the RF signal by the length of a vector from the origin to the specified point in the coordinate system. The phase of the system can be represented by the angle from a particular reference point. This slide shows an I Q diagram for QPSK modulation, which can take on four potential phase states. In this diagram, each phase state has equal amplitude, and is separated from another point by 90°. The QPSK timing diagram shows what happens to the phase of the RF carrier for a given transmitted data pattern. (See slide 4)

DQPSK, or Differential Quadrature Phase Shift Keying, is very similar to QPSK. The main difference is that in DQPSK the data pattern transmitted is referenced to the previous phase state; no phase reference is required at the receiver to demodulate data. Since no phase reference is required, the receiver is easier to build. (See slide 5)

$\pi/4$ DQPSK is a slight modification to DQPSK. If the phase transitions for a given bit pattern are defined as shown in the table, the phase transitions for $\pi/4$ DQPSK are rotated 45° from their DQPSK equivalents. $\pi/4$ DQPSK is the modulation type that was chosen for both the North American and Japan digital cellular systems. (See slide 6)

The possible phase transitions for $\pi/4$ DQPSK are $\pm$ 45° and $\pm$ 135°. If the initial phase state was at the I axis, the possible phase states are shown in figure A, at time T1. Figure B shows the possible phase states that would occur at time T2. Notice that a total of eight phase states will be possible although only four are possible at any given time. In the next symbol period the other four phase states can be output. All eight potential phase states are shown in figure C. (See slide 7)

So far we have only considered unfiltered phase transitions from one phase state to the next. Without any filtering the effects of a band limited channel would cause some smearing of data pulses as they are transmitted. This makes data detection more difficult, and therefore filtering is applied to the transmitter, receiver, or both to eliminate the effect of intersymbol interference. In addition, unfiltered phase transitions would cause a large amount of spectral splatter. This would affect adjacent channels, and is unacceptable. (See slide 8)

The filtering chosen for the NADC and JDC systems is called a raised cosine Nyquist filter. One important characteristic of Nyquist filters is that the impulse response has nulls at all symbol times except the symbol at time 0. This implies that adjacent symbols will not affect the transmission of the symbol at time 0. If the data can be sampled precisely at time T, 2T etc, no intersymbol interference (ISI) will be present. The roll-off factor of the filter is noted as α. As the value of α increases, the required bandwidth to transmit a given symbol rate increases. It can be seen that the lobes of the impulse response are

much smaller for increasing alpha. For a larger value of α, more bandwidth is required, but less ISI will be present if there is some timing jitter on sampling the data. (See slides (9 & 10)

For optimum signal-to-noise a matched filter in the transmitter and receiver is required. To achieve this, the Nyquist filter response was modified to take the square root of the frequency response and put similar filters in the transmitter and receiver. The impulse response of a Nyquist and root Nyquist filter with α=0.35 is shown in the figure. Notice that the nulls of the root nyquist impulse response no longer has nulls at symbol decision points. This implies that the transmitted data will have some ISI. The ISI should be eliminated by applying the root nyquist filter in the receiver. (See slide 11)

The NADC and JDC systems use time division multiple access (TDMA) techniques. Multiple users are assigned to the same frequency channel and are assigned timeslots in which to transmit.

These systems have six timeslots per frame implying that up to six users can use a given frequency channel simultaneously. (See slide 12)

NADC and JDC are the two man $\pi/4$ DQPSK system, but the two systems differ in a number of areas. The NADC and JDC systems. The NADC system uses the current analog cellular allocated band, while the JDC system has two basic bands. The channel spacing is slightly different between the two systems which leads to a different data rate and filter roll-off factor for the two systems. The NADC system is slated for turn on approximately one year before the JDC system. (See slide 13)

The NADC frame structure is 40msec long, and each timeslot is 6.67msec long. Timeslot 1 is repeated immediately after timeslot 6 and repeats continuously in this manner. (See slide 14)

The base-to-mobile and mobile-to-base formats for NADC are slightly different. The location of the sync word is different in the two formats. The first three symbols in the mobile-to-base format are a guard time to allow the previous transmitter power to ramp down. The base-to-mobile slot does not incorporate this feature since the base station is CW. (See slide 15)

The JDC slot format is quite different from the NADC slot format. Location of sync word, length of the sync word, and most other characteristics are different. The total number of bits in a JDC slot are less than in the NADC; however, the slot length in time is identical since the bit rate is slower for the JDC system. (Slide 16)

Examples of One Implementation for Generation πDQPSK:

A source for generating π/4 DQPSK is the HP 11846A and HP 11846A Opt 001 combined with a vector signal generator such as the HP 8780A. (See slide 18)

The HP 8780A has a wide RF range, spanning from 10 MHz to 3 GHz. This covers the NADC and JDC bands plus has significant RF range for future higher frequency systems.

The HP 11846A has two selectable voltage output ranges: a low range designed to be used with the HP 8780A; and a higher voltage range that can be used with an externally supplied I Q modulator.

With the HP 8780A, the I Q offset can be adjusted to very low levels, (on the order of -50 dBc) or increasingly worse levels. This can be useful in testing receiver tolerance to I Q offset imbalance.

The HP 8780A and HP 11846A combination has excellent vector error specifications on the order of only 1%. This is much better than current system transmitter specifications. (See slide 19)

The HP 11846A generate a square root raised cosine filtered I-Q output using an FIR (finite impulse response) type of digital filter. The HP 11846A implementation uses a ROM-based FIR filter, which allows a fairly simple hardware design. The incoming data bits are input to the serial-to-parallel converter which separates the first and second bit of each symbol into separate data paths. The symbol data is then differentially encoded and enters a shift register. The length of the shift register is determined by the FIR filter length. In the case of the HP 11846A, the FIR filter length is eight, making the output of the shift registers eight-bit parallel data. Outputs from both shift register banks are applied to the ROM address lines, giving 16 address bits. The ROMs performs a convolution of the input data with the filter's impulse response to produce the I-Q output data.

The HP 11846A updates the I-Q updates at a rate 16 times the NADMCS symbol rate. This allows the HP 11846A to generate a smooth I-Q trajectory between symbol decision points, which is necessary to control unwanted spectral energy. For 16 sub-intervals per symbol, four address bits are required to be presented to the ROM address line. Adding the 16 address bits mentioned above, this implies a total ROM address space of 20 bits, or 1M bytes of address space. For 16-bit-output ROMs, this implies 16M bytes of storage for both the I and Q ROMs was impractical, so a different approach to a ROM-based filter was implemented.

The filter block shown on slide 20 shows the filter block diagram used in the HP 11846A. The key difference is that the I and Q ROMs have been replaced by cosine and sine ROMs. The I and Q outputs are not generated by an additional and subtraction of the sine and cosine ROM data. The key to being able to use this type of approach was

recognizing that π/4 DQPSK can be generated from DQPSK by a 45-degree rotation every symbol. By using a coordinate transformation technique, the I and Q outputs are broken down into their cosine and sine components. The results is that the address bits required for any of the ROMs in this implementation are:

Number of Bits	Description
8	Bits from shift register, either the first or second bit per symbol.
3	Bit counter. This counts the 45-degree rotation module 8.
4	Sub-interval counter.

The number of address bits to any given ROM is therefore 15. In this implementation, four ROMs (two ROMs for the I channel and two ROMs for the Q channel) are required, compared to the two ROMs in the conventional filter implementation. The overall results is a reduction by a factor of 16 (2^{20} bits of address space for the conventional approach versus 2^{16} bit (2^{15} x 2) of address space for the HP approach) in the memory required to implement the FIR filter. This reduction of memory not only saves cost, but significant printed circuit board area. In addition, since all of the filter information is stored in ROM, as new communication systems come on line, potentially with different filter characteristics, only a ROM change is required to meet the needs of these systems. (See slide 20)

The HP 8657D Dual-Mode Signal Generator is a conventional analog signal generator from 100 kHz to 1.04 GHz, and a π/4 DQPSK digital modulation signal generator in the NADC and JDC frequency bands. (Slide 21)

The performance on the HP 8657D is basically the same as the HP 8657A Signal Generator. The digital modulation capabilities are band oriented to the JDC and NADC bands. The error vector magnitude specifications are more than adequate to test the NADC and JDC radios. (See slide 22)

So far, we have described two RF sources for π/4 DQPSK modulation. In order to test digital radios the correct data and sync patterns must be output. This requires a flexible data generator to be able to drive the data inputs on the HP 11846A and HP 8657D. Hewlett-Packard offers the HP 11835A Opt 002 Data Buffer as the data source of choice for testing cellular radios. (See slide 23)

The HP 11835A Opt 002 reference board provides NADC and JDC bit and symbol clock outputs that can be locked to a convenient external reference. In addition, the synthesis technology used in the HP 11835A allows offsetting of the bit and symbol clock frequencies for use in testing to the NADC system specification.

The HP 11835A is connected to a HP series 300 computer via a parallel data cable. The computer is used to generate the desired data pattern, and then the data is downloaded to the HP 11835A. The data is synchronized to the desired clock rate, and then is output in a serial data stream. Flexible state machine control allows control suitable to a TDMA communication system. (See slide 24)

An example of two types of sources for testing π/4 DQPSK systems are the HP 11846A and HP 11846A Opt 001 with the HP 8780 which provides very wide frequency coverage, and excellent modulation accuracy. The HP 8657D provides NADC and JDC band π/4 DQPSK coverage at a price suitable to manufacturing test systems. (See slide 25)

Measuring Modulation Accuracy of π DQPSK Transmitters:

An example of measurement solutions is the HP 11847A/B which are software-based signal processing algorithms. The signal under test is downconverted to a suitable IF frequency that can be digitized by a high performance digitizer. Once the signal has been digitized, a patented algorithm is applied to measure the accuracy of the signal under test. (See slide 27)

The signal processing approach used in the HP 11847A/B allows for excellent measurement accuracy -approximately 0.25%. Amplitude droop, IQ offset, magnitude, phase and vector error are measured. In addition, full analysis graphs of Eye diagrams, Constellation diagrams, FFT's of IF frequencies, and graphs of magnitude, phase, frequency, and vector error are all provided. (See slide 28)

Overall signal processing is shown on a block diagram on slide 29. The signal under test in down-converted to a suitable IF frequency. This is digitized and sent to the computer for analysis. The first step is to demodulate the incoming signal and determine the data symbols that were transmitted. Since the transmitter filtering characteristics are known an ideal reference signal can be constructed. The best fit between the ideal reference signal and received data is then obtained and the measurement results are then output. (See slide 29)

The signal processing system flow diagram is shown on slide 29A. The input to the flow diagram is a discrete-time IF signal derived from the transmitter signal under test. The transmitter signal is down-converted and digitized to produce the discrete-time signal fed through the IF bandpass filter. The purpose of the IF bandpass filter is to eliminate harmonics of the IF signal that may be produced when the transmitter signal is down-converted, and to reduce quantization noise created by the digitization process. A significant reduction in quantization noise is realized by initially sampling the IF signal at a high rate (~41.15 times the symbol rate specified for U.S. digital cellular radios). The sampling rate then is reduced by a factor of four from the input to the output of the IF bandpass filter.

The clock delay, which is the time interval from the first sample from the IF bandpass filter to the leading edge of the first full symbol interval following this first sample, is estimated in the clock-delay estimator. In the clock-delay estimate, the modulated IF signal from the output of the IF bandpass filter is squared to produce a signal component at a frequency equal to the symbol clock rate. This squared IF signal is then fed through an FIR bandpass filter that is tuned to the symbol rate. The phase of the signal at the output of this filter provides a very accurate estimate of the symbol clock delay.

After the clock delay, τ, has been estimated, the IF signal is resampled by a Nyquist interpolation filter. The purpose of resampling is to provide an integral number of samples per symbol interval and to provide samples precisely at the detection decision points. To minimize the amount of arithmetic necessary following the resampler, and to minimize signal processing errors that contribute to the measurement inaccuracy, a rate of five samples per symbol was chosen for the resampler.

The output of the resampler provides the basic discrete-time IF signal used by the remainder of the signal processor. The uncertainty of the symbol clock phase has been removed so that these samples occur at a rate of five samples per symbol with every fifth sample accurately located at a detection decision point in time.

Following the resampler, the signal processing functions are performed in three passes. To understand the need for multiple passes, consider the signal originating at the transmitter. This signal passes through a square root raised cosine filter in the transmitter and, for a matched receiver, it passes through another square root raised cosine filter in the receiver. The cascading of the two square root raised cosine filter produces the Nyquist frequency response necessary to avoid intersymbol interference. To perform square root raised cosine filtering, the receiver must know the precise frequency of the transmitter. In the signal processor described here, the data is detected and the parameters of the transmitter signal are estimated in the first pass during which noncoherent processing of the IF signal at the output of the resampler is performed. The initial estimates obtained in the first pass are used in the second pass to perform coherent baseband processing.

In the second pass, the IF signal is coherently down-converted to in-phase and quadrature baseband signals which are passed through square root raised cosine filters. The square root raised cosine filtered signals are used again to detect data and obtain refined estimates of the signal parameters. The detected data from the two passes is compared for consistency. A difference implies bit detection errors. The detected bits are used to generate an ideal reference signal, and the refined estimates of signal parameters are used to correct the I-Q origin offset, carrier frequency and phase, and amplitude scale and droop factors of the signal under test. The compensated signal under test and the reference signals are compared to obtain measurements of rms magnitude and phase errors and rms error vector magnitude.

During pass 2 only one sampled value per symbol at the decision points is used. This provides measurements of carrier frequency error and error vector magnitude in a minimum amount of time. Detailed plots of various signals as a function of time over the duration of a burst are calculated in the third pass using up to 20 points per symbol. In addition, Fourier transforms of various signals can be computed in the third pass. (See slide 29A)

HP 11847A Measurement Results

```
Captured peak signal level at digitizer input was approximately -4.94 dBm
Clock delay =.066 symbol intervals from first time sample

DEMODULATED DATA IS:
--------------------------------------------------------------------

1          11         21         31         41         51

0000000000 0000000001 0001111011 1101100110 0000000000 0000000000

61         71         81         91         101        111

0000000010 1011001100 1010001110 1010100100 0101100111 0010110100

121        131        141        151        161        171

1110101000 0101011110 1000000110 1000100001 1100100001 1111000011

181        191        201        211        221        231

0100011100 1000010100 0000101101 0101000110 0011101111 1100111000

241        251        261        271        281        291

1010111000 0100111011 0011100000 0001010000 1010010100 0010111011

301        311        321

0111011110 1100

Burst Amplitude Droop = -.0001 dB per Symbol
Carrier Frequency Error = -4.794 Hz
I/Q Origin Offset (carrier feedthrough) = -39.76 dB

TEST RESULTS
------------------------------------------------------------
Magnitude error = .792 percent RMS at decision points
Phase error = .444 degrees RMS at decision points
Error Vector magnitude = 1.108 percent RMS at decision points
```

This sample output is the first measurement screen from the HP 11847 software. The demodulated data is shown as well as whether the proper sync word was located. The key measurements are also shown such as error vector magnitude.

I-Eye Pattern

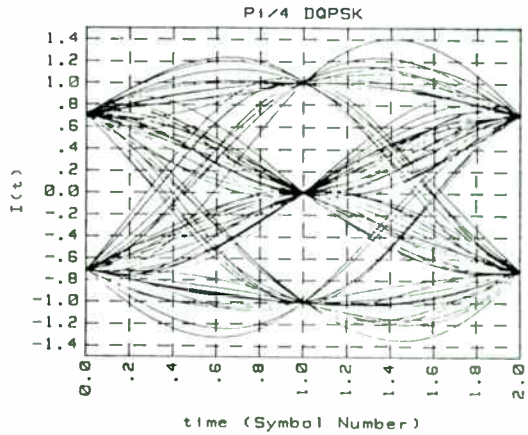

This graph shows an Eye diagram for the I data, traces overlapped. This measurement was for approximately 1% vector error. Notice again the tight convergence of the data.

I-Q Pattern

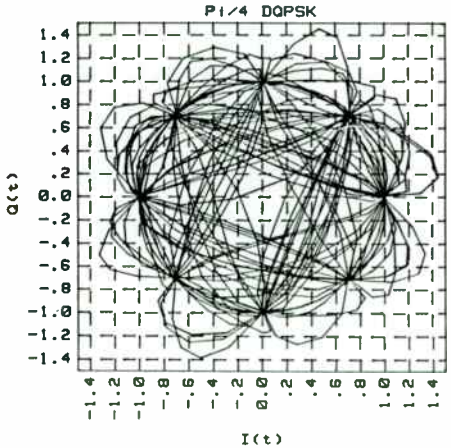

This graphs shows an I Q graph for a error vector magnitude of approximately 1%. This data was plotted with five samples per symbol. Notice the tight constellation points.

Error Vector Magnitude

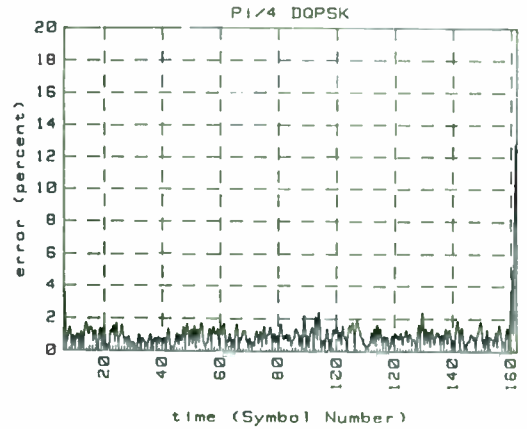

This graph shows the error vector magnitude plotted over an entire timeslot. The red lines show the measurement at the symbol decision points. This measurement was again for approximately 1% vector error.

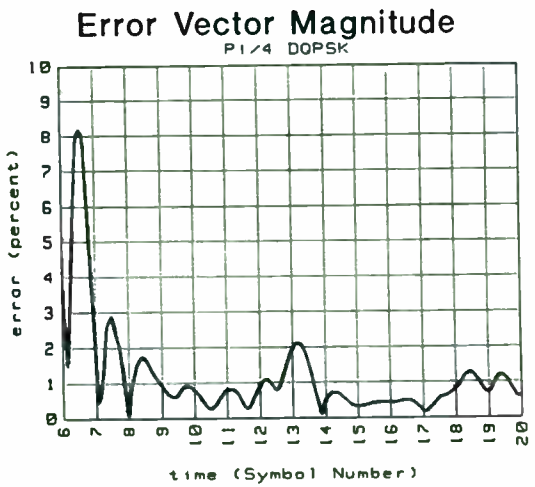

This graph shows the zoom capability of the software. This graph is part of the previously displayed graph. Only the data marked with the red vertical lines is used in the overall error vector magnitude result.

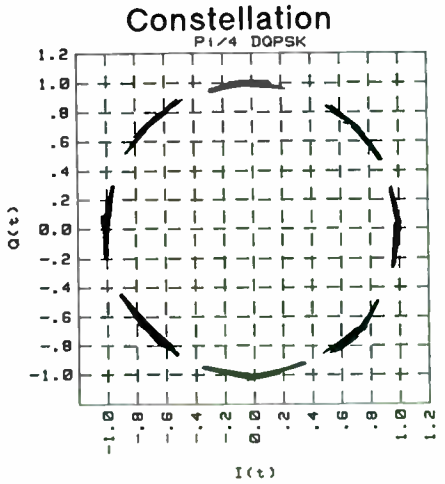

This graph is for a vector error of approximately 15%. All of the error is due to phase error and almost none in amplitude. It can be seen how that with increasing error the probability of detection error increases.

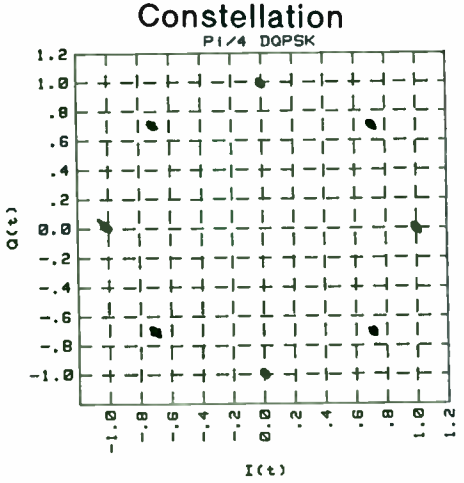

This graph shows the constellation diagram for a slot of approximately 1% error vector magnitude. This allows an easy way to see the effect of increasing vector error.

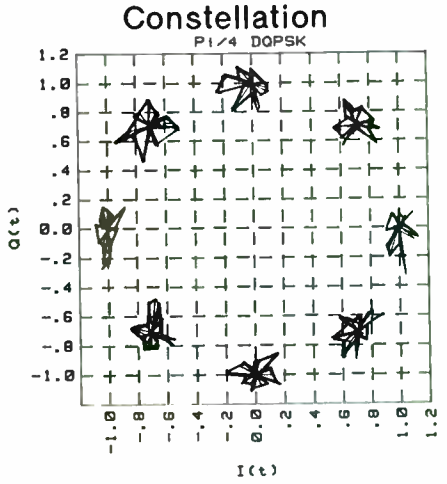

This graph is for a slot vector error of approximately 15% with almost equal contributions from amplitude and phase.

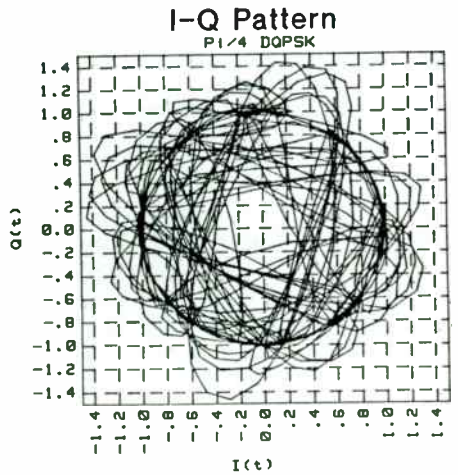

This graph is an I Q diagram for the 15% vector error case with all of the error coming from phase distortion.

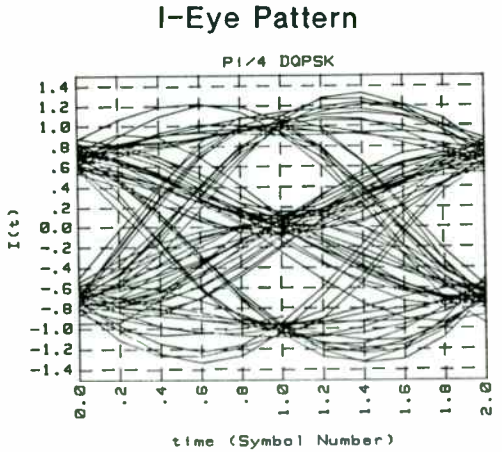

This is a Eye diagram for the 15% vector error case. Notice the fuzzy detection decision points compared with the earlier Eye diagram.

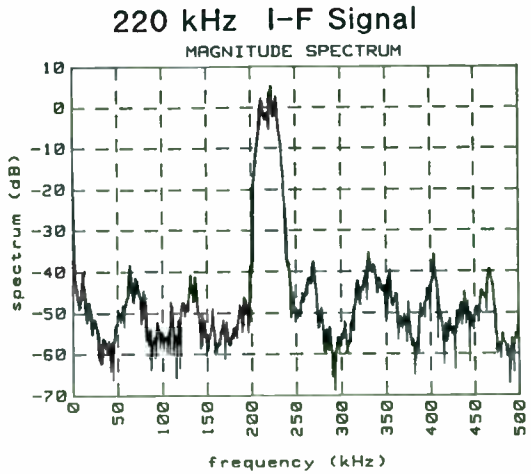

This graph shows the FFT of the incoming sampled IF signal. The HP 11847A uses an IF of 220 kHz.

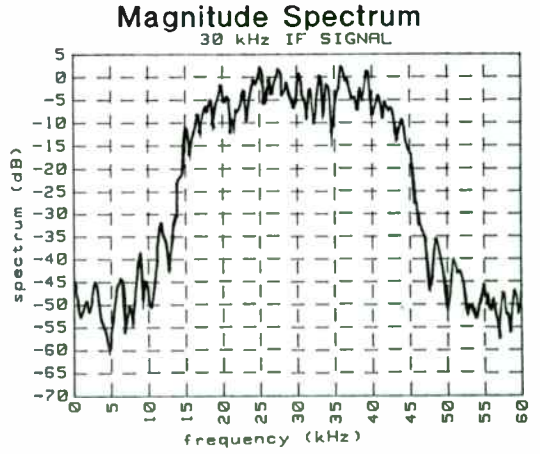

The HP 11847 software mixes the incoming IF signal down to 30 kHz. The magnitude spectrum at this point is shown. The NADC system uses a 30 kHz channel, so it is interesting to look at the spectrum at 15 kHz, and 45 kHz, the adjacent channel boundaries. Notice that the signal is only about 15 db down at the channel boundaries.

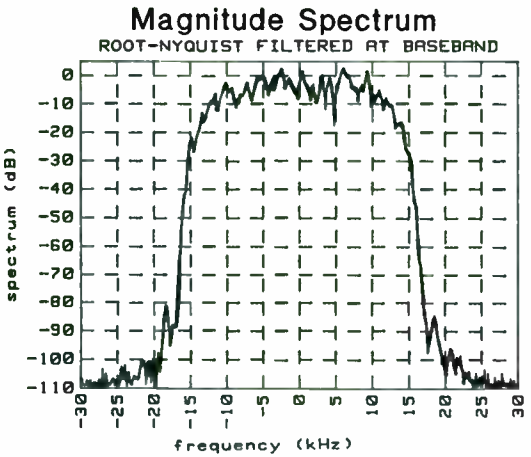

This slide shows the 30 kHz signal with the receiver filtering added. The filtering is now a full Nyquist response. Notice the improved sideband levels.

Hewlett-Packard provides a signal processing approach to measuring π/4 DQPSK modulation. This patented technique results in excellent measurement accuracy with fast measurement results. All key measurements for the NADC and JDC system are made by the HP 11847A/B software package.

An Example of a Test System for NADC System:

An example of a test system for NADC system is the HP 8953DT system which is made up of the Hewlett-Packard analog cellular test system, plus a DOS-based computer and DSP analysis software. DSP techniques allow for real time demodulation of the NADC and JDC modulation. This allows making BER sensitivity measurements and word error rate measurements for the NADC system.

Protocol tests can be performed by sufficient software to allow for the necessary commands to be sent to the radio. This results in a test system suitable for manufacturing test of digital cellular radios. (Slide 45)

The HP 8953DT system performs a complete set of analog tests for the analog mode of the NADC radios. The digital tests that are performed can be grouped into two categories: (1) sensitivity type measurements (2) protocol type tests. (See slide 46)

H-P currently has several products designed to assist in the testing of JDC radios.

These include:

- HP 11846A Opt 001
- HP 8780A Signal Generator
- HP 8657D Signal Generator
- HP 11847B Analysis Software
- HP 11759A RF Channel Simulator (Fader)

In addition, the HP 11835 Opt 002 Data Buffer provides a flexible data source so that the proper slot data can be sent to the radio under test.

Hewlett-Packard is currently investigating the possibility of developing a JDC test system. We should be able to give additional information in late 1991. (See slide 47)

This paper has summarized Hewlett-Packard's testing strategy for NADC and JDC radios. We reviewed some essential digital modulation basics, and then looked at how to generate π/4 DQPSK modulation. Next, we looked at signal processing algorithm suited to make extremely accurate measurements of π/4 DQPSK modulation. Finally, the HP 8953DT test system was described which implements a total manufacturing test solution for North American Dual-Mode Cellular radios. Hewlett-Packard is currently investigating developing a test system for JDC radios and we should have some additional information in late 1991.

Testing North American Dual-Mode Cellular and Japan Digital Cellular Radios

Course Overview

- Review of Digital Modulation
- Generating $\pi/4$ DQPSK Modulation
- Measuring $\pi/4$ DQPSK with DSP Techniques
- Test System for NADC Radios

Section I

Why Digital Modulation Techniques?

- Increased capacity in fixed spectrum
- Improved performance in severe fading environments

Review of Digital Modulation
IQ Diagrams for QPSK & DQPSK Modulation

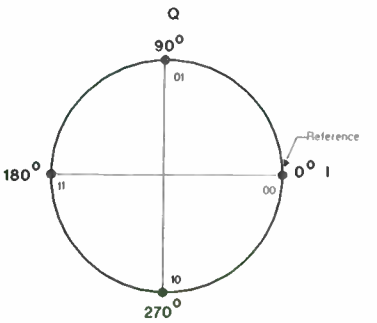

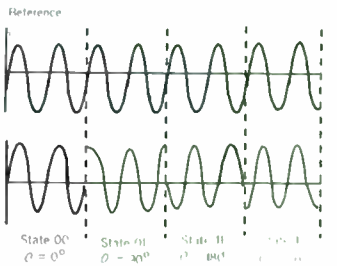

DQPSK Characteristics

- Four potential phase states
- Data symbols defined relative to the previous phase state
- No absolute phase reference required for DQPSK

Symbol	DQPSK Phase Transition
00	0^o
01	90^o
10	-90^o
11	180^o

Unfilter Phase Transitions for π/4 DQPSK

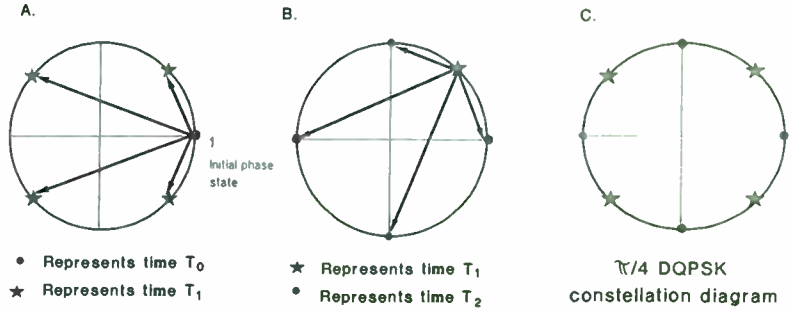

Possible phase transitions:
+/-45 °
+/-135°

Comparison between DQPSK and π/4 DQPSK Modulation Formats

Symbol	DQPSK Phase Transition	π/4 DQPSK Phase Transition
00	0^o	45^o
01	90^o	135^o
10	-90^o	-45^o
11	180^o	-135^o

Intersymbol Interference

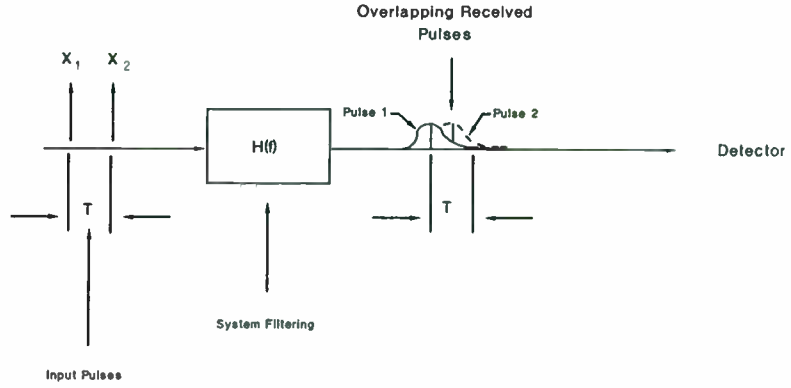

Filtering to Reduce Intersymbol Interference

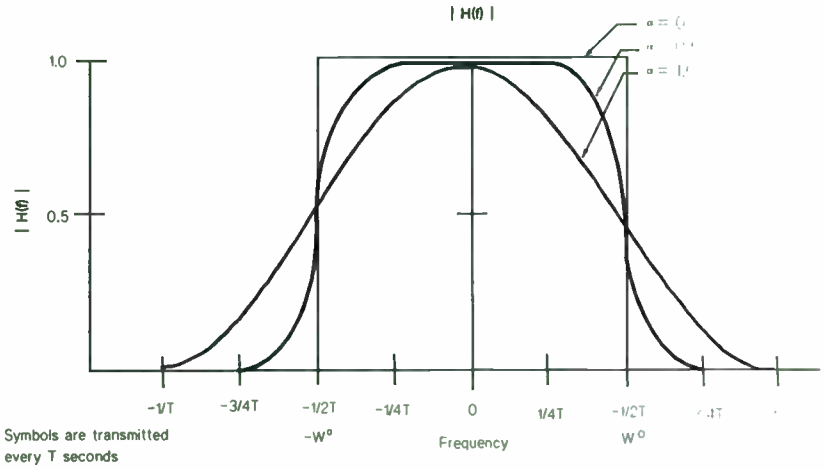

Filter Frequency Transfer Function

Filtering to Reduce Intersymbol Interference

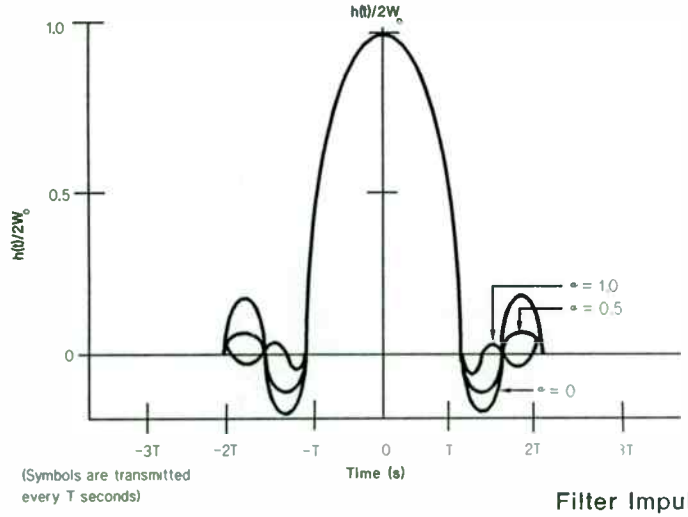

Filter Impulse Response

Comparison of Nyquist and Root Nyquist Impulse Response

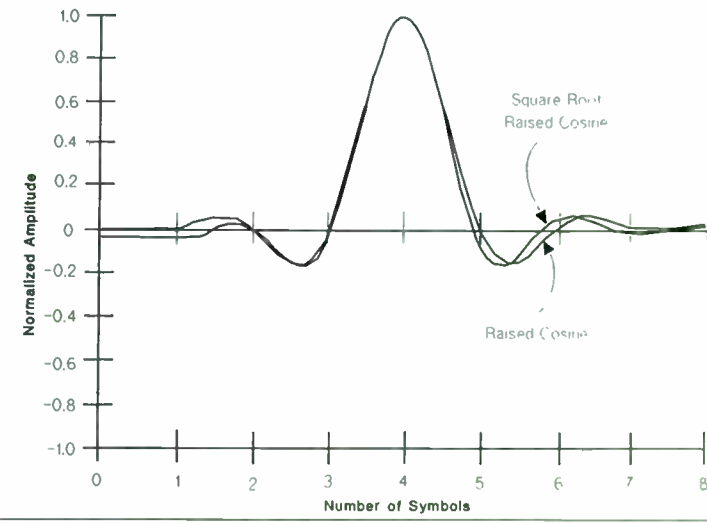

NADC/JDC Frame Structure

- Both systems use Time Division Multiple Access (TDMA)
- Frames are the basic unit of time
  - One frame is 40 msec, divided into 6 slots
  - One user can be assigned to each time slot

PI/4 DQPSK - SYSTEM COMPARISON

NADC vs. JDC	NADC	JDC
Frequency Range	824 - 849 MHz up 869 - 894 MHz dn	810 - 826 MHz dn 940 - 956 MHz up 1429 - 1441 MHz dn 1447 - 1489 MHz up 1453 - 1465 MHz dn 1501 - 1513 MHz up
Slots/Frame	6	6
Users/Channel	3 - 6	3 - 6
Mod. Data Rate	48.6 kbits	42.0 kbits
Channel Spacing	30 kHz	25 kHz
No. of Channels	831 freq. channels w/3 users/channel	1600 freq. channels w/3 users/channel
Modulation	Pi/4 DQPSK	Pi/4 DQPSK
Speech CODEC	VSELP 8 kbits/s	VSELP 8 kbits/s
Filter Factor	0.35 Root Nyquist	0.50 Root Nyquist
Tested w/fading	yes	No, equalizer is optional
Introduction	1991-1992	1992-1993

NADC - SLOT FORMAT - 6.667 msec timeframe

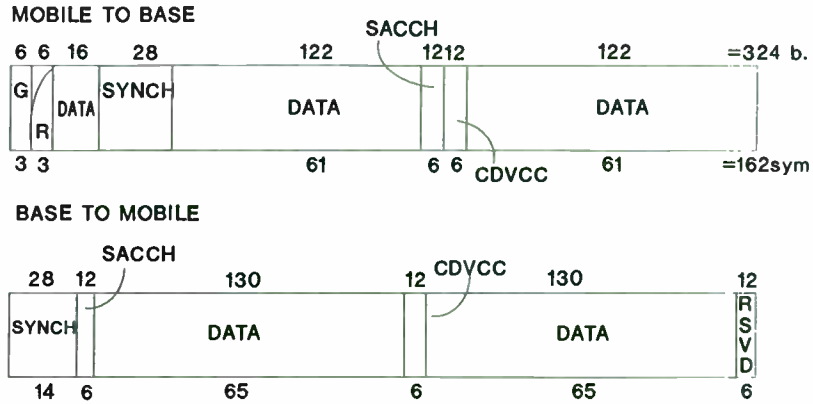

NADC Frame Structure

Traffic Channel

1 frame = 40 msec = 1944 bits (972 symbols) [25 frames/sec]

1944 bits/frame x 25 f/sec = 48.6 kbit/sec
972 symbols/frame/6 slots/f = 162 symbols/timeslot
6.67 msec
20.576 usec/bit, 41.152 usec/symbol

JAPANESE DIGITAL CELLULAR

Information Physical Channel

UPLINK SIGNALING FORMAT Timeslot = 280 bits

R	P	TCH (FACCH)	SW	CC	SF	SACCH	TCH (FACCH)	G
4	2	112	20	8	1	15	112	6

DOWNLINK Bit Total = 280 bits

R	P	TCH (FACCH)	SW	CC	SF	SACCH	TCH (FACCH)
4	2	112	20	8	1	21	112

G = Guard Bit
R = Ramp Time
P = Preamble
SW = Synch Word
TCH = Info. Transfer Channel (Data Bits, or FACCH)
CC = Color Code
SACCH = Slow Associated Control Channel
RCH = House keeping bit
SF = Steal flag

Section II

Hewlett-Packard Sources for Generating π/4 DQPSK

HP 11846A π/4 DQPSK IQ Generator with HP 8780A Vector Signal Generator

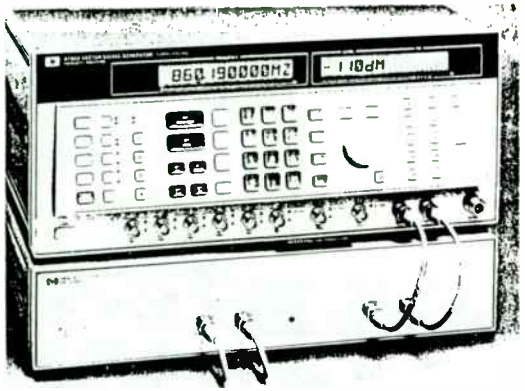

Specifications of HP 11846A with HP 8780A

- 10 MHz – 3 GHz frequency coverage
- .35V and 5V peak outputs
- Nullable IQ offset
- Vector error of typically 1% vs NADC system spec of 12.5%

Block Diagram of HP 11846A

Conventional

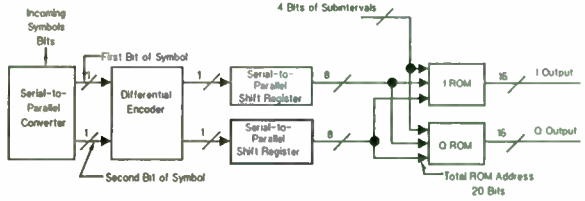

Improved Implementation

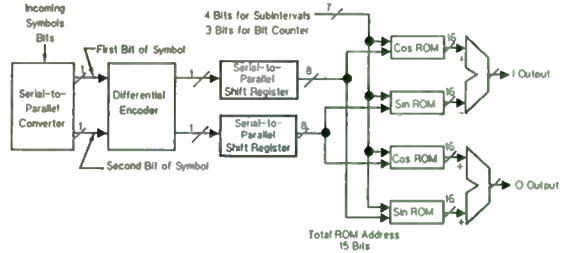

HP 8657D π/4 DQPSK Signal Generator

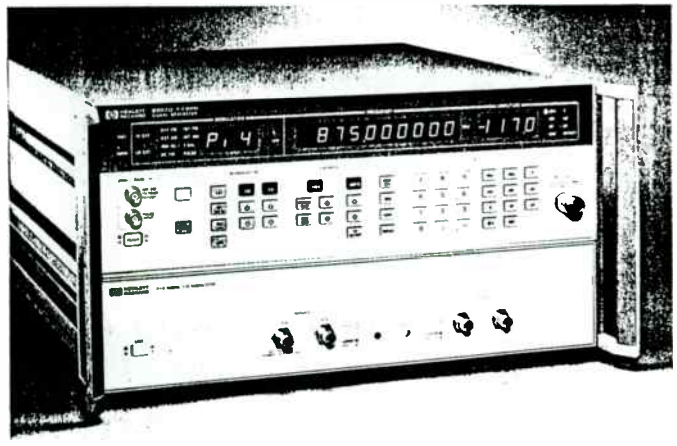

Digital Data Sources for TDMA Communication Systems

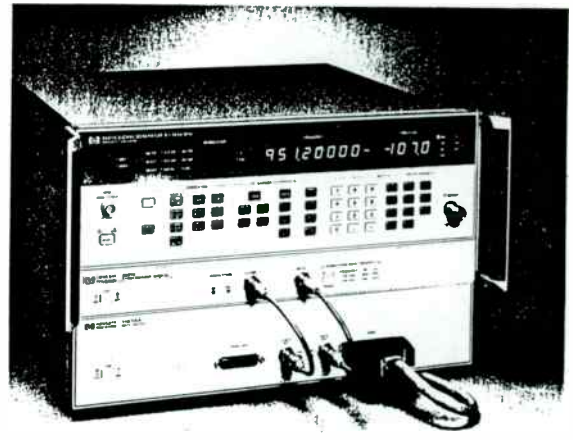

Specifications of the HP 8657D

- Analog specifications the same as HP 8657A
- Digital specifications:
  - π/4 DQPSK modulation
  - Filter roll-off factors of .35 and .5
  - Frequency range: 10 MHz - 129.9 MHz
    810 MHz - 965 MHz
    1420 MHz - 1540 MHz
  - Data rate (symbol clock) 20-25 kHz
  - Error vector magnitude <4% 10 MHz - 129.9 MHz
    and 1420 - 1540 MHz
    <3.5% 810 MHz - 965 MHz

Key Specifications of the HP 11835A Opt 002

- Provides NADC/JDC bit clock and symbol clock outputs locked to external reference
- Allows offsetting of bit and symbol clock for NADC testing spec
- Data streams are generated in software by a computer (HP Series 300)
- Allows continuous, non-repeating data bit streams
- Clock and data outputs will drive HP 11846A, HP 8657D, and HP 8657A/B Opt 022 (European cellular)
- Flexible state machine control allows configuration for TDMA systems
- Parallel data outputs can be used to drive DAC's and frequency agile signal generators

Summary

- Hewlett-Packard provides RF sources for both the NADC and JDC standards

	HP 11846A and HP 8780	HP 8657D
Frequency Coverage:	10 MHz - 3 GHz	100 kHz - 1030 MHz analog mode NADC and JDC bands for digital
Filter Factors:	.35 for HP 11846A .5 for HP 11846A Opt 1	.35 and .5
Symbol Rates:	20 - 25 kHz	20 - 25 kHz
Error Vecter:	Mag 1%	3% - 4%
Price:	$65,000 U.S.	$22,500 U.S.

Section III

Measuring Modulation Accuracy of π/4 DQPSK Transmitters

HP 11847A/B π/4 DQPSK Modulation Measurement Software Package

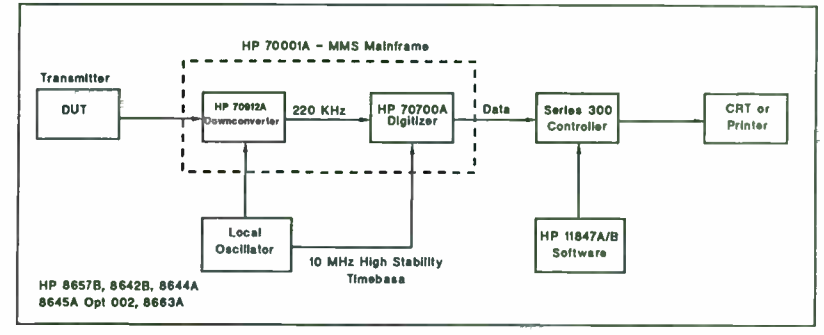

Key Features of HP 11847A/B

- Excellent measurement accuracy, ~0.25%
- Shows demodulated data
- Measures amplitude droop, IQ offset, magnitude, phase and vector error
- Displays FFT's
- Displays eye diagrams and constellation diagrams
- Measures single burst, ten burst average and baseband IQ signals

HP 11847A/B Overall Signal Processing Block Diagram

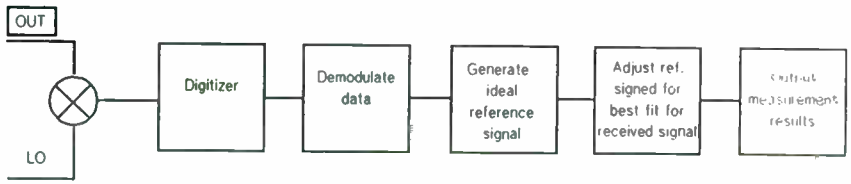

HEWLETT PACKARD

HP 11847A/B Signal Processing Block Diagram

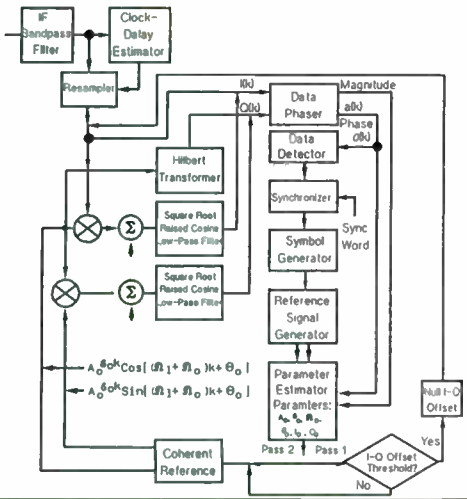

HEWLETT PACKARD

Summary

- Hewlett-Packard provides measurements of π/4 DQPSK for NADC and JDC formats
- Excellent measurement accuracy
- Full analysis graphs
- Fast measurement speed

HEWLETT PACKARD

Section IV

HP 8953DT Test System for NADC

HEWLETT PACKARD

8953DT – NADC MOBILE TEST SYSTEM

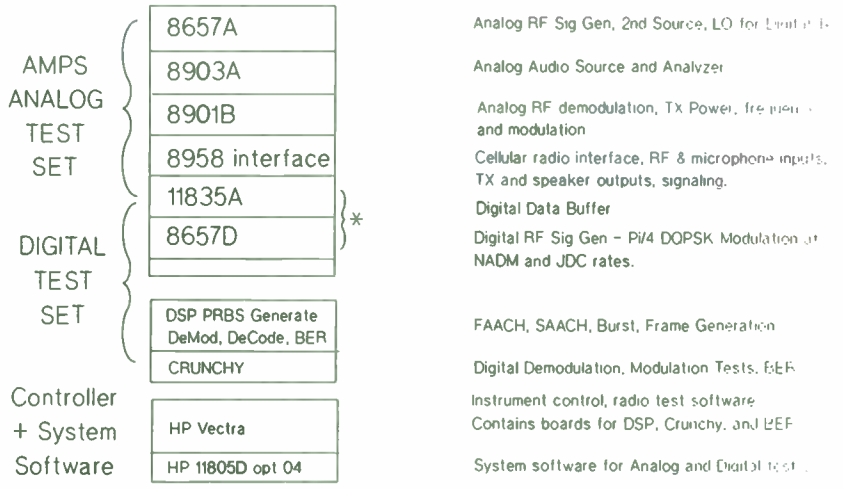

* 8953DT opt 001 adds additional 8657D/11

Tests Done by HP 8953DT
Dual-Mode Cellular Radio Test System

1. Provides full set of analog tests
2. Provides digital tests
   - Receiver
     - Usable sensitivty (bit error rate on uncoded data)
     - RSSI (received signal strength indicator)
     - Co-channel performance
     - Adjacent/alternate channel desensitization
   - Transmitter
     - RF power output
     - Modulation accuracy (HP 11847-type measurement)
   - Call Processing
     - Origination – Mobile initiated call set-up
     - Paging – Network initated call set-up
     - DTMF – Dual-tone multi-frequency
     - Handover – D -> D, D -> A, A -> D
     - Order digital to change power

JDC Testing Strategy

Currently Available Products

- HP 11846A Opt 001 π/4 DQPSK IQ Generator
- HP 11847B Modulation Measurement Software
- HP 8657D Dual-Mode Signal Generator
  - Supports .5 ⍺ π/4 DQPSK in JDC frequency bands
- HP 11835A Opt 002 Data Buffer
  - Provides a programmable data source to be used with HP signal generators such as HP 11846A Opt 001, and HP 8657D
- HP 11795A RF Channel Simulator (Fader)

Future Products

- Currently investigating a manufacturing test solution for JDC

Summary

- Reviewed digital modulation basics
- Described HP 11846, HP 8780, HP 8657D π/4 DQPSK sources
- Described a modulation verification system, HP 11847A and HP 11847B
- Described a complete test system for NADC radios
- Investigating a manufacturing test solutions for JDC

POWER TRIODE TUBE CURVE TRACER

Lee A. Erb and Warren F. Walls

Erbtec Engineering
2760 29th Street
Boulder, CO 80301
(303) 447 - 8750

ABSTRACT

Even in this modern day of monster silicon devices, power triodes are still an economical choice for high power RF applications. The need to be able to check production units, investigate returns, and screen tubes for engineering designs has prompted the design of a general purpose tube tester. The power triode curve tracer has been designed to characterize a large variety of air cooled tubes in a computerized fixture. Standard curve tracer functions as well as the ability to measure tube specific characteristics have been designed into a safe and easy to use station which could produce informative graphs and tables.

INTRODUCTION

The power triode is still a very economical device to use in the design of high power RF amplifiers, but the individual cost of returned tubes with unexplained performance can get atrocious. It is this very problem, along with the desire to have a general station capable of testing new tubes for future designs, that motivated the design of a power triode tube tester. The main objective was to find modern day, and somewhat inexpensive, parts to produce a safe and effective computer controlled test fixture. The first round of design involved surveying the various Mil spec test processes and typical manufacturer test schemes to come up with a composite circuit. The final test fixture, along with a computer, will reside entirely in a seven foot rack.

VACUUM TUBE HISTORY

The history of the electron tube and eventually the transistor has primarily evolved around man's desire to communicate over long distances. Early work like that of Guglielmo Marconi used a large spark gap to transmit morse code. Marconi transmitted a message across the English Channel and from Cornwall, England to Saint John's Newfoundland in March 1899 and on 12 December 1901, respectively. These achievements prompted a general public desire to continue the development of devices which would be useful in wireless communication. Although Thomas Edison proposed the theory behind the

diode in 1883, it was not until 1905 when Sir J. Ambrose Fleming developed the first diode, initially called the Fleming Valve, which was useful in detecting high frequency radio waves. Soon after Fleming, Lee De Forest added a third electrode to the Fleming Valve to produce the audion or triode. The third electrode was a zigzag wire placed between the anode and cathode of the diode. The development of the triode was a giant step forward in electronics and communications because one could now easily amplify signals.

The new triode device prompted many people to build home radios in order to communicate with each other. Hiram Percy Maxim organized the American Radio Relay League in 1914 in an effort to coordinate the activities of amateur radio operators. This new organization, which soon grew to a considerable size, was called into service when the United States declared war in 1917. For the first time, the US Government realized the advantage of having control over communications and was not willing to give it up. Congress placed a ban on amateur radio operations that lasted until 1 October 1919. During this time, many amateur radio operators and the general public lost interest.

After the ban was lifted, a new surge of interest arose in radio broadcasts. The war had stimulated technical development to the extent that vacuum tubes were now being used for both receiving and transmitting. A new invention in 1918, the superheterodyne receiver, by Edwin Armstrong marked a significant improvement in radio sets. The first regular commercial radio broadcasts began in 1920 when NBC formed the first permanent national radio network. During the 1930s the military, pilots, and police started to use radio sets in their everyday activities. All of this led to the "golden years" of radio which ran from 1925 until 1950 at which time television took over with its new large variety in programming. Franklin D. Roosevelt became the first president to appear on television.

Back during World War I, power triodes worked well, but as the interest rose in their uses, so did the airwave traffic. It became necessary for tubes to operate at higher frequencies. At this time, interelectrode capacitance in the triode limited its high frequency use. This capacitive effect, which caused tubes to produce an oscillating frequency instead of amplifying the desired signal, could be reduced significantly by adding a screen grid between the control grid and the plate. Walter Schottky, a German physicist, invented this new device called the tetrode during World War I. This is the forerunner to the practical four-electrode tube developed in 1924 by Albert W. Hull, an American engineer.

This new electron tube, the tetrode, was the simplest of a new class of tubes called multi-electrode tubes. Unfortunately, the tetrode was not quite a perfect solution. It has some nonlinearity characteristics during low-voltage operation as a result of a phenomenon called secondary emission: electrons arriving at the plate from the cathode cause other electrons to be emitted from the plate and collected by the screen grid. In 1926, Benjamin D. H. Tellgen, a Dutch engineer, proposed to add yet another grid called a suppressor grid. This grid is usually connected to the cathode and serves to suppress this problem of electrons collecting on the screen grid. The end result is the pentode, or five-electrode tube.

The whole electronics world was turned upside down in 1947 when three men working for Bell Laboratories (John Bardeen, Walter Brattain, and William Shockley) created the first transistor. This device had three electrodes, two of which made electrical contact to the component with tiny wires pressed against the surface of a small semiconductor crystal to form a closely spaced pair of rectifying regions in which current could flow in only one desired direction. These new point-contact transistors were very fragile and poorly characterizable until 1952 when Shockley invented an improved version which used a pair of pn junctions similar to the pn junction of a semiconductor junction diode. Shockley also designed the field effect transistor. And finally, the late 1950s saw the invention of the silicon integrated circuit by two men working for Fairchild Semiconductor Company: Robert Noyce and Gordon Moore.

While tubes were still the only amplifying device available and before transistors were able to handle a lot of power, they were used in radio receivers and transmitters, logic circuits, power control devices, electronic instruments, and many other applications. A selection of some modern power triodes are shown in Figure 1.

In many high power RF applications, tubes are still a practical solution. Modern transistors and other semi-conductors have been created to handle quite a bit of voltage and current, but not more than a few hundred watts in RF amplifier applications. Because of the die size and therefore small thermal time constants, a 5mS pulse looks like CW to a FET whereas the same pulse doesn't heat a tube beyond a level that can't be controlled. A popular RF transistor is capable of handling about 20 amps, 60 volts peak and operate at about 100 MHz maximum. Nearly 150 of these $85 devices would have to be purchased and combined in order to create an amplifier that would match a $2,700 power triode which can put out 20 kW using a 5mS RF pulse. Many more heat sinks and cooling fans are necessary to keep all of the transistors cool, than

what are needed to keep one power triode cool. The power triode is also able to work at much higher voltages and therefore lower currents than the transistors; making impedance matching relatively simple.

MODERN TUBES TYPICALLY USED IN VHF RF POWER AMPLIFIERS

In the past few years, solid state technology has pushed up the threshold power level for which vacuum tubes are the more practical technology to use to produce large amounts of RF power. Even though, modern tube designs have made their use easier and more efficient. The typical tube used today above 250 Watts has an external anode structure allowing for direct heat removal. Forced air is the most popular heat removal method until power levels climb above about 15 kW where water cooling is more practical in most cases.

Modern tubes typically utilize ceramic for insulators and vacuum containment envelopes. The older glass envelopes allowed the user to observe the internal structure and its glowing elements during use. (Electrical abuse to the tubes could be detected at times by the color of the glow of elements within the tube.) The ceramic insulators trade off this unique feature for a much more rugged material which is less susceptible to damage.

Thoriated tungsten is usually used as the electron emitting material in large vacuum tubes. The power required by these "filaments" is quite high in relationship to that required by the "heaters" used in the indirectly heated oxide cathodes. Modern tube designs have allowed the use of larger oxide cathode emitters. The small cathode and grid geometries in oxide cathode tubes allow higher gain with lower grid current. In depth tube facts and applications can be found in the book Care and Feeding of Power Grid Tubes published by VARIAN EIMAC, 301 Industrial Way, San Carlos, CA 94070.

TETRODES

The tetrode power vacuum tube contains four active elements usually in a coaxial configuration. These start at the innermost element with an electron source made with a thoriated tungsten filament or an indirectly heated oxide cathode. The second element is the control grid which is used to control the flow of electrons from the cathode. Third is the screen grid which electrically isolates the control grid from the anode structure. The outer element, the anode or plate, is used to collect the electrons that are emitted from the cathode. The tetrode is usually operated in a grounded cathode configuration and exhibits high gain and

good linearity. Drawbacks to the tetrode are the need for a screen grid power supply with the proper interlocks with other element power supplies and the need to "neutralize" the circuit it operates in. Neutralization compensates for the internal tube element capacities and lead inductances that influence the control grid operation. An improperly neutralized amplifier stage will likely turn into a power oscillator or exhibit tuning and gain problems.

TRIODES

The triode power vacuum tube contains only three active elements. For VHF frequencies and below, the coaxial element configuration is used. Upper UHF frequencies dictate a planar element configuration which minimizes the lead length connecting the elements to the outside circuitry. The triode contains the same cathode, control grid, and anode elements as the tetrode but has no screen grid. The triode is usually operated in the grounded grid configuration in amplifier circuits which results in stable operation and the use of a minimum number of power supplies. In the grounded grid configuration, the cathode input circuit is at a low real impedance and the cathode drive currents appear directly in the tube output current. Drawbacks to the triode are lower power gain than the tetrode and slightly poorer linearity, but circuit simplicity outweighs those issues. The grounded grid triode has been selected as the tube of choice for a number of products at Erbtec Engineering.

A typical grounded grid amplifier circuit block diagram can be found in Figure 2. This example uses a Varian Eimac 3CX15,000B7 triode operating in class AB service as described in the tube data sheet.[1] Copies of select data sheet pages can be found in Figure 3. Figure 4 is a copy of the "Grounded Grid Constant Current Characteristics" curve set found in the data sheet. The illustrated plate circuit load line should closely meet the data sheet example application. The independent operating point values

are:

Plate voltage supply	6.0 KV
Plate idle current	0.6 Amps
Resonant load impedance	1000 Ohms

From these values and the curves, other parameters can be determined.[2]

---

[1]Varian tube information has been used to show typical performance characteristics. No vendor indorsement is intended.

[2]It must be noted that graphical data and first order approximations were used to derive these values therefore variations from actual performance may exist.

Peak plate current	9.6 Amps
Peak plate voltage swing	4.8 KV
Idle current cathode bias	+33 Volts
Peak cathode voltage swing	118 Volts
Cathode input impedance	24.6 Ohms
Tube gain	16.1 dB

The 3CX15,000B7 tube is a ceramic-metal tube where the internal mechanical parts cannot be seen. Figure 5 is a picture of the internal structure found in this tube. Precision alignment must be maintained between the striped cathode and the grid bar assembly to insure low grid current and desired electron control. It must be noted that this tube is intended to be mounted by bolting its grid flange directly to the amplifier chassis thus providing low grid lead inductance and the best isolation possible between its input and output circuitry.

WHY TEST and WHAT TO TEST FOR?

Very few electronic components are tested by the user these days. Solid state devices rarely fail but if they do, they usually fail in a mode that it is easy to recognize. Vacuum tubes however have a "wear out mechanism" that allows it to soft fail over a period of time during which it "sort-of works". Transistors and ICs usually have specified minimum, typical, and maximum operating parameters such as gain, threshold voltage, and speed as a result of imposed JEDEC and military standards. These devices are production tested at the factory in order to guarantee their ranges. RF power grid vacuum tubes very rarely come with other than "typical" specifications leaving the designer guessing at circuit tolerances and the QA department at a loss for test limits to apply to incoming and warranty return inspections.

A tube manufacturer rarely measures a complete family of curves for each of their production line tube. Building large vacuum tubes involves many manual steps; resulting in variations among devices. The size and variety of vacuum tube devices do not lend themselves to automated testing. Manufacturers limit their production acceptance tests to a few representative operating points reflecting tube applications for which they believe the typical user is interested in. Unless the user is operating the tube beyond these regions, or he is interested in precise linearity, the spot tests should properly characterize the production tubes. Unfortunately little is known about what the factory tests are or what limits they apply. The only way to get this information is to ask the manufacturer. If you

find that the ranges of parameter values allowed are excessive for your applications, it may be worth asking for special testing for your application. Note that additional charges are often incurred for these services.

A case in point, Figure 6 shows a plot on the 3CX15,000B7 characteristic curves where a "current division" manufacturing acceptance test is conducted and shows the allowable range of values. Independent variables are 1200 V plate voltage and 12 A plate current. Limits are set on the dependent variables of grid-cathode voltage range of 85 to 140 Volts and maximum grid current of 800 mA. Although these may be reasonable limits for the data sheet application amplifier, grid current problems can arise for certain parts of the plate voltage swing range when used in high power pulsed operation. It is imperative that the design engineer have this test limit range data available to do a valid circuit design.

The tube manufacturer will perform the same acceptance tests on tubes returned for warranty. The tube's performance and heater-on hours will determine the warranty reimbursement, if any. In the case of an original equipment manufacturer supplying replacement tubes, he must be able to perform similar tests on the tubes returned to him. An RF power amplifier and the system it is in are complex devices. As a result, vacuum tubes are often falsely blamed for many other system performance problems.

Special high power pulsed operation of vacuum tubes may require different testing thresholds. The two parameters that allow for high power pulsed operation are high peak cathode currents and the ability for the anode structure to dissipate the average heat collected. Plate load lines will utilize the upper left part of the tubes characteristic curves. Plate dissipations during a pulse may be many times the steady state capability of the tube, but the short pulse duty cycles and long thermal time constants allow acceptable anode temperatures. Special testing is not needed for the tube anode dissipation. The cathode, however, produces a cloud of available electrons for conduction within the tube. High cathode currents deplete this electron cloud with time. A worn out cathode will not rebuild this electron cloud as fast or maintain as high a CW electron flow as needed. Therefore, pulsed high current cathode emission testing is needed.

Special RF testing of tubes may be necessary if the application circuitry performance is sensitive to variations in some tube parameters. These effects could be important in both CW and pulsed operation.

Interelectrode capacities could effect tuning. Thermal effects may mechanically change the internal tube structure to the extent that it impacts circuit operation. Grid currents become excessive or change polarity with variations in RF plate voltage swing or load line. Plate to grid or cathode arcing may occur for large plate voltage swings. Any of these circuit sensitivities may require that special tests be performed to insure proper operation in one's circuit.

DESIGN OF A TUBE TEST FIXTURE

Through the process of trying to determine what characteristics are important to measure and further, how they should be measured, we have developed some basic goals for our multi-purpose tube tester. The first of these goals is automatic operation. In order to insure consistency in the process and be able to efficiently manage the data and circuit configurations we decided that the tube tester needs to be computer controlled and be contained in a single relay rack. The actual chamber where the tube resides needs to be easy to service and able to protect the user from both high voltages and high temperatures. Such a chamber should minimize user time wasted by sequential measurements on different tubes, and reduce the health threat to individual operators. The engineering department needs the tube tester to analyze new tubes for future amplifier designs and also as a diagnostic tool to measure characteristics of tube failures and other tube related problems. The quality assurance department needs the tester to screen returned and defective tube for warranty procedures. All of the tube data should be stored in such a way that long term archival back up is possible with a computer network system. In the long run this will help to maintain traceability and performance of the tubes. The tube tester also needs to have safety mechanisms for the individual tubes under test since they will be stressed in different ways and may be susceptible to high voltage arcs. Defective tubes may exhibit failure mechanisms which induce high stress on the tube measurement equipment and the tube under test. High internal currents due to shorts, arcing, and gassy conditions must not destroy the test fixture or the tube under test. The following sections discuss the different military standards tests and some of the features and benefits of each one. These were studied in a first attempt to understand which tests should be included in the composite tube tester schematic.

HEATER CURRENT TEST

The heater or filament current test is designed to test the condition of this

structure in the tube. A measurement of the heater current provides an indication of the thermal power available to the cathode to produce electrons. The circuit block diagram shown in Figure 7 illustrates the general arrangement necessary to run a sufficient heater test. The current through the heater, I_f, is measured for particular values of the filament voltage, E_f. This test can be conducted with either DC or AC applied to the heater of an indirectly heated cathode tube. The current drawn by a filament is typically several to tens of amps. The supply must be current limited to a safe value because the resistance of the heater will be extremely low until it warms up. After a steady state has been achieved, data can be taken. The independent variable and dependent variable in this test are the heater voltage, E_f, and the heater current, I_f, respectively. This test is covered by Mil spec: Mil-E-1E Method 1301.

CATHODE EMISSION TEST: PULSED

The Mil spec, Mil-E-1E method 1231A illustrates the first of two tests which characterize cathode emission. The cathode is responsible for supplying an abundant source of electrons, which is critical for good tube operation. In this particular test, the plate and grid are tied together. A large voltage is then pulsed from the plate to the cathode. The amount of voltage, e_{td}, required to draw a predetermined amount of current, i_s, signifies the performance of the cathode. The block diagram shown in Figure 8 illustrates the general circuit configuration. This test needs to be conducted using a short pulse instead of a DC signal because the current densities obtained are high enough that they can damage the tube if left on too long.

CATHODE EMISSION TEST: ΔI_k

The ΔI_k test is another useful method for investigating cathode emission. This test is specified under MIL spec MIL-E-1E Method 2212 and its circuit block diagram is shown in Figure 9. Although this test can be conducted either by holding the cathode voltage or the plate current constant during the test, the MIL spec only calls out the usage of a constant cathode voltage. With the constant cathode voltage method, the cathode voltage is set to result in a specific plate current. It is then pulsed on for a specific time during which one measures the plate current droop with time as the electron cloud is depleted. If the plate current were kept constant, the cathode voltage would increase with time as it tries to maintain the electron cloud. Either way, this test characterizes the cathode's ability to emit electrons.

CHARACTERISTIC CURVE TEST: CURRENT DIVISION

The circuit block diagram for the current division test, which is discussed in MIL spec MIL-E-1E Method 1372A, is shown in Figure 9. This test is usually done close to saturation in the area of peak anode voltage swing at full amplifier output where excessive grid currents can become troublesome. The plate voltage and plate current are the independent variables in this test. The grid-cathode voltage is pulsed so as to draw the desired amount of anode current. The interesting data is the grid-cathode voltage that was required to accomplish the desired anode current and the resulting grid current. Out of range grid to cathode voltage or a high grid current indicates a tube geometry problem.

CHARACTERISTIC CURVE TEST: TOTAL GRID CURRENT

The total grid current is discussed in MIL spec MIL-E-1E Method 1266A. The plate voltage is set to its specified level, and then the grid-cathode voltage is increased until the plate current reaches a specified level. The grid is still negative with respect to the cathode at this time so that regular cathode electrons are not attracted to the grid. The current through the grid measures the gas current in the tube. This current is created by electrons that are flowing from the cathode to the plate and colliding with gas molecules in the tube. This ionizes the molecules, and the positive ions flow to the control grid which is the most negative element inside the tube. This flow of positive ions is measured by I_c as shown by the circuit block diagram in Figure 10.

CHARACTERISTIC CURVE TEST: GRID VOLTAGE

The Grid Voltage Test, which is useful in determining the tube geometry (cathode-grid spacing), is discussed in MIL spec MIL-E-1E Method 1261. The circuit block diagram shown in Figure 11 illustrates an appropriate configuration. This test collects the data from which the characteristic curve set is derived. The plate voltage is set and the cathode-grid voltage is adjusted until the desired amount of plate current is seen. At this point, the cathode-grid voltage, E_c, is recorded as well as the grid current for a specific plate current. This test may be repeated for different values plate voltage and current in order to determine a full data set for curve generation. Specific data is usually taken to determine the class AB idle current operation point as well as the cutoff bias point of the tube.

SYSTEM CONFIGURATION

To date we have been surveying the manufacturer's specifications and military specifications in order to determine our overall test system configuration. Over the entire lifetime of some of our amplifier products we have collected and archived many amplifier and tube parameters. A particular characteristic such as idle current bias voltage can quickly be gathered up from the data files and graphed or printed in a table with respect to amplifier or tube serial number. This vast amount of data will be very useful in compiling Statistical Process Control data. This data will also help qualify the tube tester once it is completed. We will be able to scan new batches of tubes for certain parameters and quickly compare them to the long history of data stored on disk.

A block diagram of the proposed composite circuit is shown in Figure 12. Notice that several different power supplies will be available, each with some sort of automatic computer control. Different circuit configurations are possible because of the large switches that will change the connections and provide pulses when necessary. The current through each branch and the voltage between the tube terminals will be monitored by the computer. We have presently acquired many of the necessary components and plan to have test results in the future.

Figure 1 Modern Power Triodes

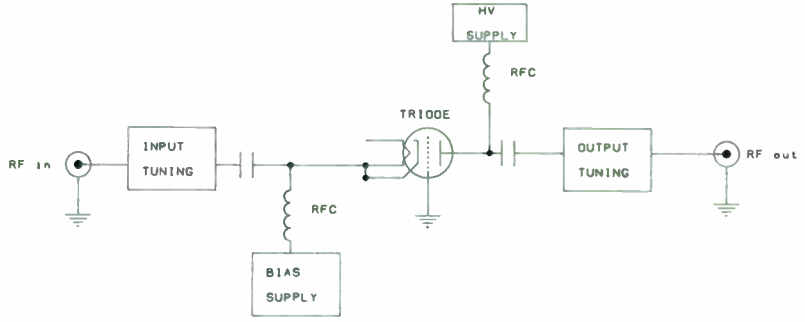

Figure 2 Grounded Grid Triode Amplifier

TECHNICAL DATA

3CX15,000B7
HIGH-MU POWER TRIODE

The EIMAC 3CX15,000B7 is a ceramic/metal high-mu power triode designed especially for use as a cathode-driven Class AB rf power amplifier. It is forced-air cooled, with an anode dissipation rating of 15 kilowatts.

The 3CX15,000B7 uses a beam-forming cathode and control grid geometry to produce high gain and outstanding intermodulation performance in linear amplifier service. These attributes make the tube well suited for SSB communications equipment.

The tube does not require a socket. It is designed to be bolted directly to the chassis by the grid flange. Cathode and heater connections are also made by bolting directly to the amplifier circuitry. This reduces equipment cost and complexity.

GENERAL CHARACTERISTICS[1]

ELECTRICAL

Cathode: Oxide-coated Unipotential		
Heater Voltage	15.0 ± 0.75	V
Heater Current (approx.), at 15.0 Volts	15.0	A
Minimum Cathode Warmup Time, at 15.0 Volts[2]	6	Min
Amplification Factor (average)	200	
Maximum Frequency For Full Ratings	110	MHz

RADIO FREQUENCY POWER AMPLIFIER
CATHODE DRIVEN - Class AB Service
ABSOLUTE MAXIMUM RATINGS:

DC PLATE VOLTAGE	6500	VOLTS
DC PLATE CURRENT	3.75	AMPERES
PLATE DISSIPATION	15.0	KILOWATTS
GRID DISSIPATION	25	WATTS
DC GRID CURRENT	±0.1	AMPERES
INSTANTANEOUS GRID-TO-CATHODE VOLTAGE	560	VOLTS

*Will vary from tube to tube
#Delivered to the load

TYPICAL PERFORMANCE, TO 30 MHz (measured data)

Plate Voltage	6.0	kVdc
Zero Sig. Plate Current	0.6	Adc
Max. Sig. Plate Current	2.6	Adc
Cathode Bias*	+35	Vdc
Grid Current*	30	mAdc
Driving Power*	300	W
Useful Power Output#	10.2	kW
Power Gain*	15.3	dB
Cathode Input Impedance	24	Ohms
Resonant Load Impedance	1000	Ohms

MECHANICAL

Overall Dimensions:	
Length	8.6 in; 218.5 mm
Diameter	7.5 in; 90.5 mm
Cooling	Forced Air
Net Weight (approximate)	13 lb; 5.9 kg
Operating Position	Vertical, Base Up or Down
Recommended Air-System Chimney	EIMAC SK-316
Base	Designed for Direct Chassis Mounting
Maximum Operating Temperature, Ceramic/Metal Seals & Anode Core	250°C
Available Anode Connector Clip	EIMAC ACC-3

VA5110 (March 1989, supersedes October 1988) 2184 Printed in U.S.A.

Figure 3 3CX15,000B7 DATA SHEET

varian
power grid & x-ray tube products
301 Industrial Way / San Carlos, CA 94070 / U.S.A. / (415) 592-1221

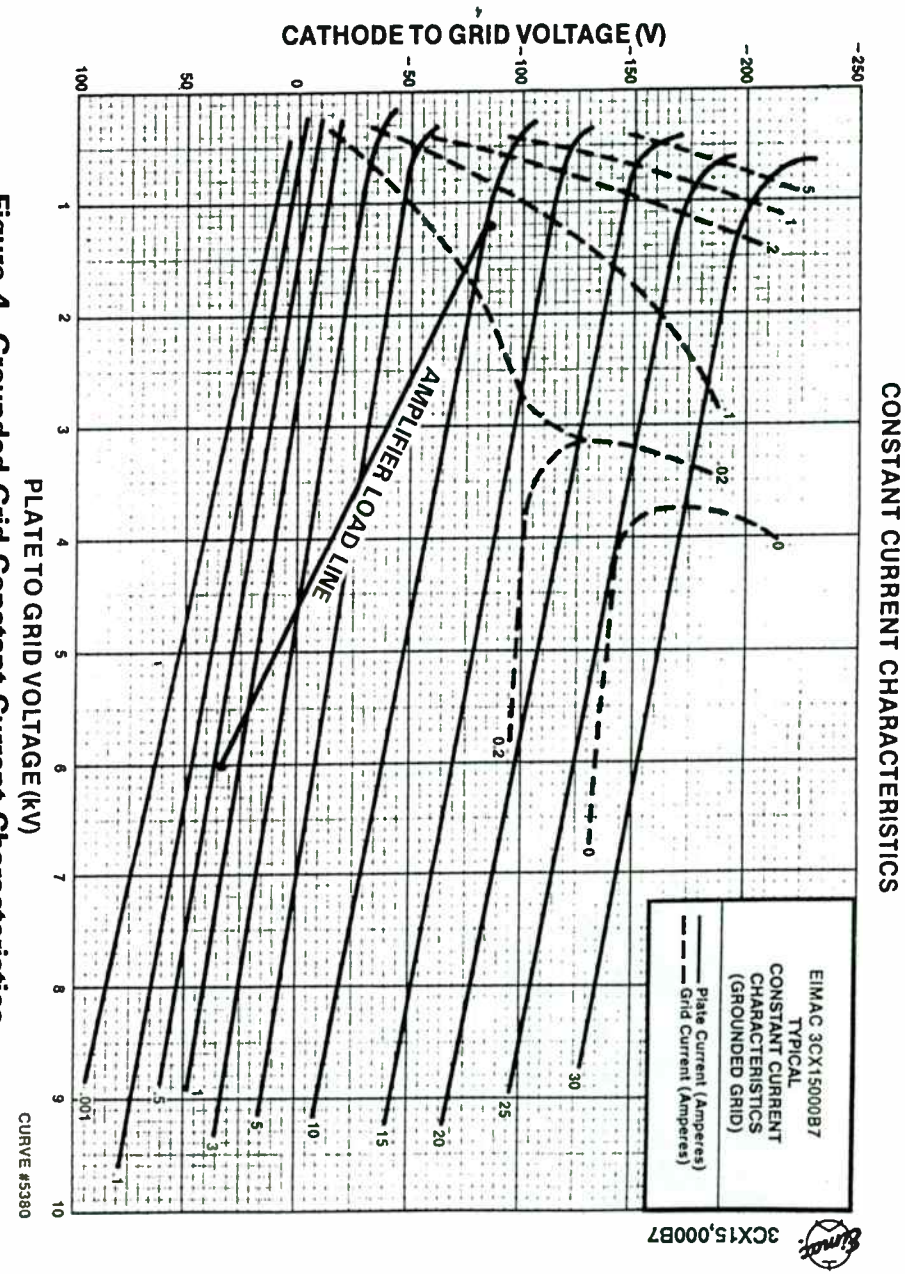

Figure 4 Grounded Grid Constant Current Characteristics

GROUNDED GRID
CONSTANT CURRENT CHARACTERISTICS

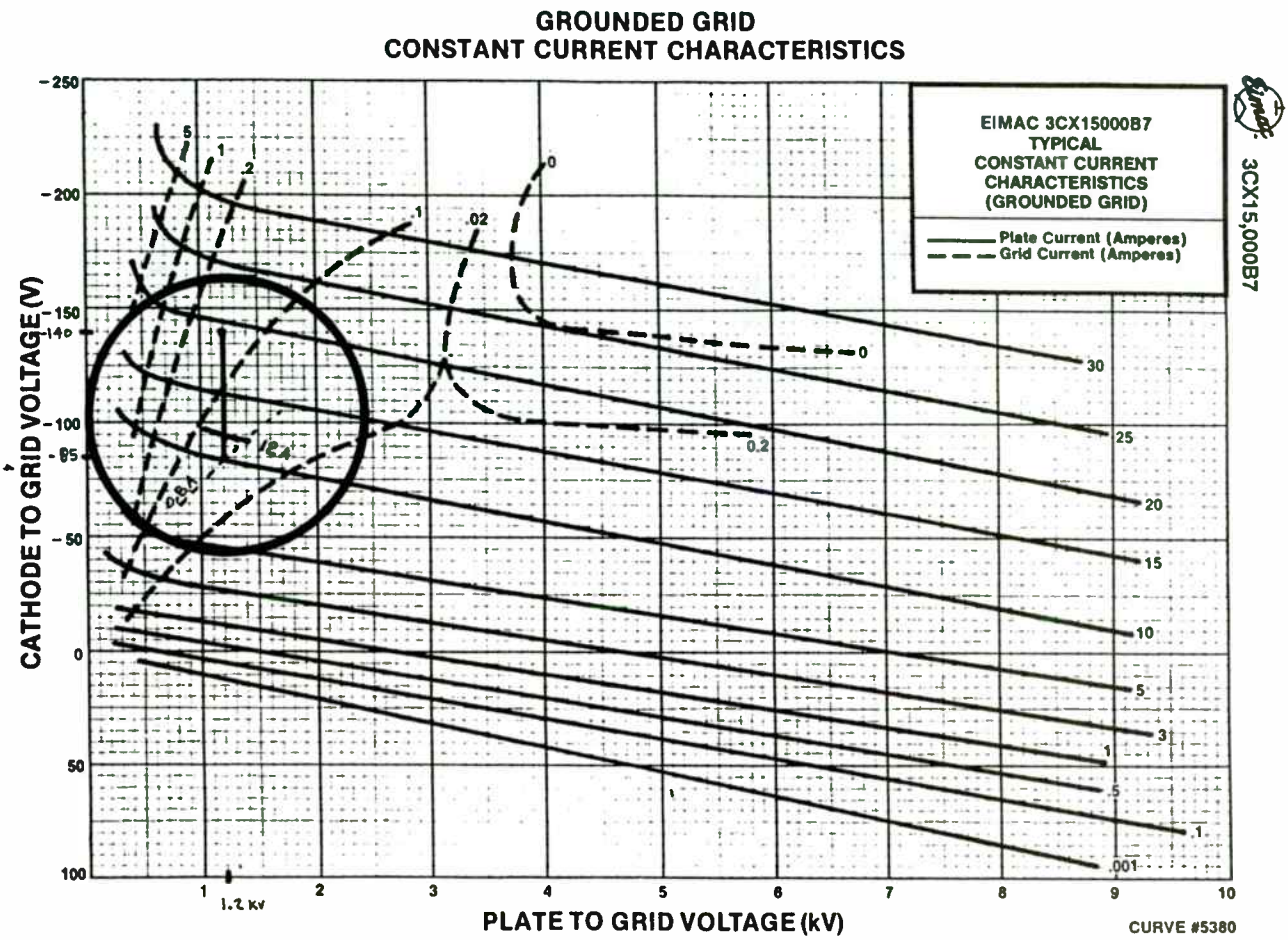

Figure 6 **3CX15,000B7 "Current Division" Test**

Figure 5 **Internal View of a Power Triode**

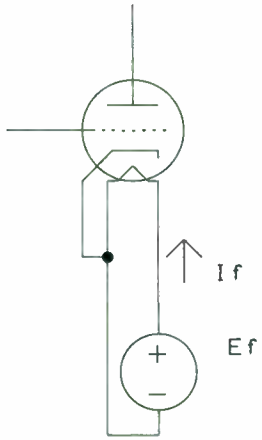

Figure 7 **Heater or Filament Current Test**

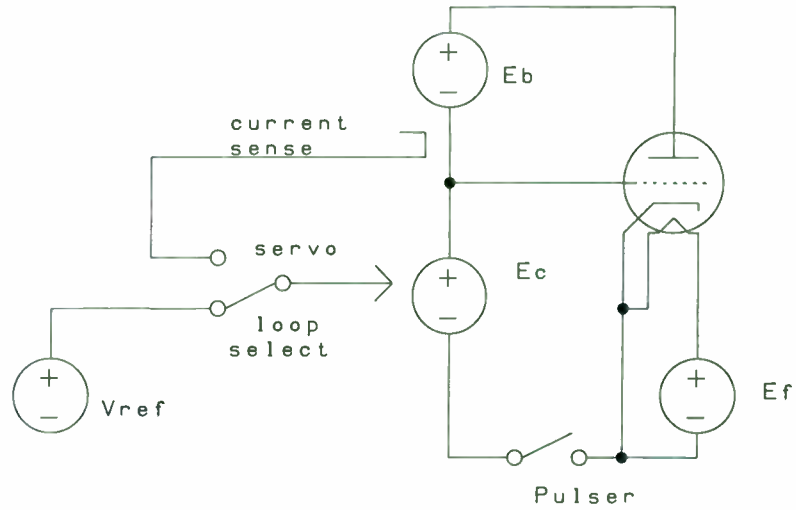

Figure 9 **Current Division and ΔI_k Test**

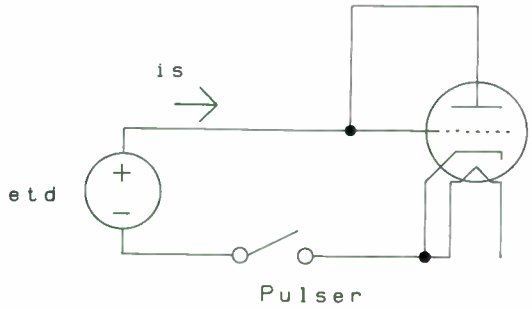

Figure 8 **Cathode Emission Test**

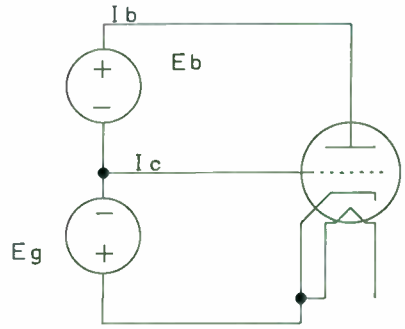

Figure 10 **Grid Current Test**

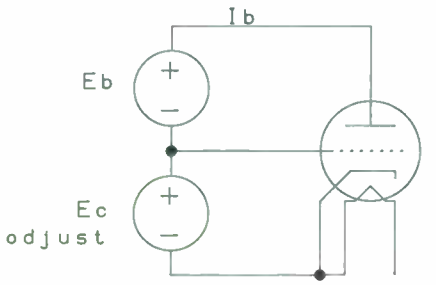

Figure 11 **Characteristic Curve Test: Grid Voltage**

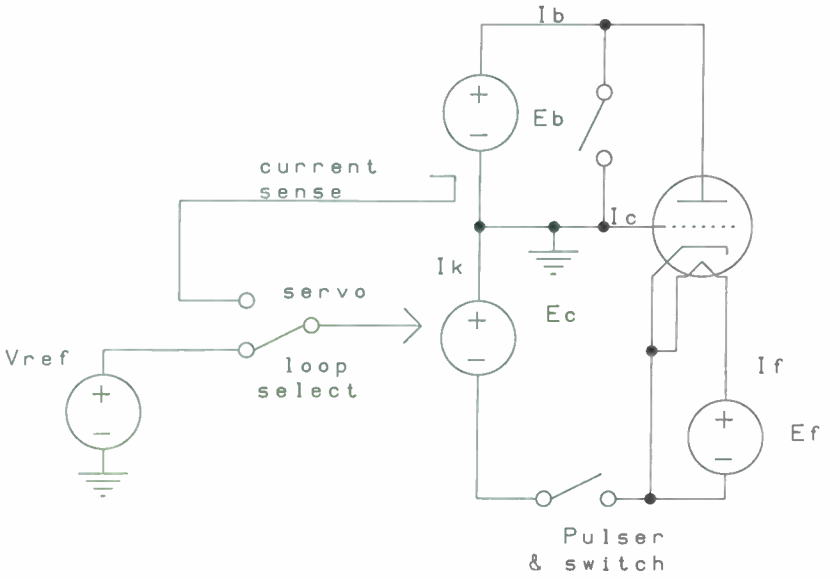

Figure 12 **Composite Tube Tester Block Diagram**

FILTERS WITH IMPROVED DELAY CHARACTERISTICS

William B. Lurie, Consultant
Boynton Beach, Florida

In the earlier days of filter usage, attention was concentrated on amplitude characteristics, without much thought regarding phase or delay. With more sophistication in the applications, however, it became evident that in many cases system performance could be controlled or improved by a consideration of phase or delay. A variety of methods of predicting or controlling these parameters will be described here.

First, let us review some of the basic definitions. A signal, in passing through any frequency-sensitive device (which will henceforth be called a filter), must suffer some changes in amplitude and phase. Conservation of energy dictates that the amplitude must be reduced, perhaps differently at different frequencies, which leads to typical plots of amplitude and delay versus frequency such as Figure 1 for a low-pass filter.

If $\Phi(\omega)$ is the phase at radian frequency ω, then the envelope delay is defined as its derivative

$$\tau = -\frac{d\phi}{d\omega}$$

Any filter, as a black box, can be described by its transfer function, which is a mathematical description of the filter, conveniently expressed in the form of a ratio of two polynomials with p as the frequency variable. The numerator polynomial is shown as a number of factors, in the form

$$(p-z_1)(p-z_2)(p-z_3) \text{ ----- etc.}$$

and the roots z1, z2, etc. are called the ZEROS of the transfer function. Obviously, at each of these frequencies, the value of the transfer function must become zero, and the filter output is zero.

Similarly, the denominator polynomial is factored

$$(p-p_1)(p-p_2)(p-p_3) \text{ ----- etc.}$$

and the roots p1, p2, etc. are called the POLES of the transfer function. For a stable, passive device, there are certain restrictions on the pole and zero locations. Looking at a typical low-pass filter (Figure 2), the poles and zeros are marked as X's and O's, and certain inferences can be drawn:

POLES may appear on the negative real axis.
POLES not on that axis must be in complex conjugate pairs.
POLES may not appear anywhere in the right half-plane, or on the $j\omega$ axis.
ZEROS may appear anywhere in the plane, but unless they are on the real axis, they must be in complex conjugate pairs.

For those who may not be familiar with the term, a minimum-phase system (as far as this discussion is concerned) is one with all of its zeros in the left half plane or on the $j\omega$ axis. In all cases, the number of zeros at real frequencies including zero, may equal but not exceed, the number of poles. Any excess of poles over zeros corresponds to that number of zeros at infinity.

Returning now to the study of filters, their amplitude and delay, consider a set of low-pass filters, all with 1 Hz as their 3 db frequency, all consisting of 5 poles and no zeros. In Figures 3 and 4 are seen the amplitude and delay for several conventional minimum-phase types. Curves A are for the maximally-flat-amplitude ('Butterworth') case, and curves B are for an equal-ripple-amplitude ('Chebychev') case with .5 db of ripple. Curves C are for the 'Bessel' type of filter, whose delay is maximally-flat, decreasing monotonically. Curves D are for a special class, a compromise between A and C.

Several facts are quite evident. When the amplitude is flat, the delay rises as the cutoff is approached (A). When the amplitude is bounded within limits but is not monotonic, out closer to the cutoff (B), the delay rises even more, and has ripples corresponsing to the amplitude ripples. When the delay is maximally flat, the amplitude rolls off in a more gradual fashion toward the 3 db point, and indeed thereafter as well. Curve D, as might be expected, follows the Bessel roll-off in the passband, falling off more quickly as the amplitude corner is turned.

It is obvious from the curves of Figure 4 that the delay is not constant across the passband, and this can lead to distortion of various kinds as a signal containing more than one frequency component is transmitted through such a filter. What is being shown here is a low-pass filter, for simplicity. Analogous behavior for other classes of filter can be expected.

Design classes A, B, and C are rigorous, controlled mathematical designs, while class D is a compromise generated by approximation or optimization methods. There are many additional classes which will not be discussed here. Classes A through D are all minimum-phase networks, and have been tabulated in the literature.

The question naturally arises: what does one do if one needs a passband with less delay variation, and can not tolerate the gentle, rounded passband shapes of classes C and D? In all minimum-phase filters, rounded shape and constancy of delay are inextricably related by physical law, which leads to either of two solutions: use some sort of delay-corrector, or try some non-minimum phase design approach.

The use of amplitude-equalizers is quite feasible, but these unfortunately have their own effect on delay, usually in the direction of additional delay near the cut-off. There are, however, two types of delay equalizers which have no effect on amplitude, and it is quite feasible to add as many 'sections' of equalization as are required to the delay curve (within practical limits). There is no contradiction of the physical laws, since each delay-equalizer is itself a non-minimum phase network: its own transfer function has zeros in the right half-plane, mirror images of its left half-plane poles.

An alternative is to use a non-minimum phase design for the filter right from the start; in other words, place zeros in the right half-plane either on the positive real axis, or as complex conjugate pairs with positive real part. Two methods of doing this will now be described, the first dating to a patent issued to H. W. Bode sixty years ago [1], explained in very clear terms in Guillemin's excellent text [2]. The second is much more recent [3] and lends itself to exact synthesis by modern methods. As the foundations for both have been adequately covered, they will be described here only in enough detail so that the ideas may be understood.

Bode's method is essentially an image-parameter method (the only available back in 1931). Consider the two branches of a symmetrical lattice, such as Figure 5. The transfer phase will show an exact multiple of 180° whenever a branch impedance pole (X) of either branch is opposite an impedance zero (O) of the other branch. If these strings of poles and zeros are long enough, the phase will not only go through 180° at regular intervals, but will also tend to be uniform in between, making its derivative, the delay, constant. Bode showed, by rigorous (and exquisite) mathematical means, how the poles and zeros of the branches can be located to make the delay constant over more and more of the passband, closer and closer to the cut-off. The method is valid and gives exact designs, but suffers from a serious practical defect. The exact lattice designs yield very complex lattice structures which can not be made into equivalent ladders. Even when partially expanded, because of the symmetry involved, they are comparatively uneconomical in number of components.

Rhodes' method is more modern, in that it starts by generating a polynomial possessing equally-spaced phase points, and deriving therefrom a transfer function which can be synthesized. In Reference [7] can be found a number of graphs and an excellent description of the properties of these transfer functions.

It is interesting to note that the zeros, within each degree, may be found in various locations. Sometimes they are on the real axis, in pairs, right and left of the $j\omega$ axis. Sometimes they are on the $j\omega$ axis (in conjugate pairs of course), thus creating infinite-rejection points at real frequencies, and sometimes they appear as quads of zeros, in all four quadrants, symmetrically about both the real and imaginary axes. From these tabulations, the networks can be synthesized, and an example below will show one such network.

A study of these curves will show that this entire class of filters (those derived from Rhodes' polynomials) has common properties. The amplitude is flatter over more of the passband than Butterworth filters, and the delay is as well. The delay stops being constant at about .75 of the 3 db point, takes a distinct rise, peaking just before the 3db point, and then falling off. The amounts of these rises depend, of course, on the degree and the parameter ϵ.

One example has been worked out to show here, comparing a 'Rhodes' filter with one designed as a conventional low-pass, with one delay-equalizer added. Table I lists the transfer function poles and zeros; Figures 6 and 7 plot the amplitude and delay, for both. The schematic diagrams, with element values, are in Figures 8 and 9.

The Rhodes filter has delay over 75% of the passband slightly flatter than the other, but then the delay rises substantially, before falling off after the cut-off. The conventional filter has delay much more constant over a larger part of the full passband. The Rhodes filter, being non-minimum phase, is able to turn the corner more sharply than the conventional one. After turning the corner, the Rhodes filter falls off somewhat faster, but the 74 db to 3 db shape factor is about the same, as are all flybacks. Perhaps one of these designs is superior to the other, but in order to say so, one would first have to establish the criteria for making such a judgement, and these may be different in different systems applications.

The Rhodes filter transfer functions, in themselves, are an interesting set, mathematically. No matter where they appear, the zeros are always so located as to have no effect on phase or delay, which are therefore completely determined by the pole locations. The amplitude resulting from the poles, without any zeros, is nothing like flat, rolling off much too fast. The zeros are so placed as to flatten off the amplitude curve (perhaps with some ripple), and, as was mentioned, may be on the positive and negative real axis (in pairs), or on the jw axis (in pairs), or in quads, one in each quadrant, or in various combinations of these.

This same idea, of creating a desired delay curve with the poles, and modifying the resulting amplitude with zeros, can be used with other than Rhodes-generated polynomials. For example, Feistel [4] created a tabulation based on Bessel pole locations (maximally-flat delay), and all zeros so located, on the jw axis, that the stopband has equal returns. In this case, with no zeros in the right half-plane, they are minimum-phase networks, and as a consequence the rounded-nose constraint is still operative.

This leads to an interesting design approach, for creating a filter with amplitude and delay curves approximating desired shapes. The desired delay curve is tabulated, and an optimization routine is used to loacte a set of poles to approximate that curve to any acceptable accuracy. The amplitude will not be acceptable at this stage. Now the optimizing routine is used again, to locate a set of zeros which, in addition to the poles, yields an amplitude response meeting its requirements to whatever accuracy is obtainable. In this process, the zero locations are allowed to roam through the complex plane, but constrained to such combinations which, as described, have no effect on overall delay response. Finally, the network is synthesized from the complete set of poles and zeros.

The schematics of Figures 8 and 9 are quite similar, and it may be a source of some concern, as to how the non-minimum phase portion, containing a negative inductor, is realized physically. This is done using mutual inductance, as described in the literature [5, 6]. Actually, in fortuitous cases where an achievable value of coupling coefficient in a tapped inductor is called for, the Tee of inductors shown in the figures can be realized by a single tapped winding on one core, which may yield some economies of size and parts count in production.

The author wishes to express gratitude to Dick Abrahams of Radio Systems, Inc., Ft. Lauderdale, FL, for his kind assistance in preparing figures for this presentation.

REFERENCES

[1] U. S. Patent No. 1,828,454, Oct. 20, 1931
[2] E. A. Guillemin, COMMUNICATION NETWORKS, Vol. 2, pp. 412-422
[3] J. D. Rhodes, IEEE MTT Vol. 18, June 1970, pp. 290-301
[4] K. H. Feistel and R. Unbehauen, FREQUENZ, Bd. 19/1965 Nr. 8, pp. 265-282
[5] H. Matthes, NTZ No. 4/1965, pp. 177-185
[6] W. B. Lurie, Paper at RF EXPO/East, Nov. 14, 1990
[7] P. A. Herzig and T. R. Swanson, 'A Polylithic Crystal Filter Employing a Rhodes Transfer Function', Proc. 32nd Annual Symposium on Frequency Control (1978), pp. 233-243

RHODES FILTER	CONVENTIONAL FILTER, EQUALI
POLES	POLES
-.503538+j.147211	-1.046798
-.45929 +j.406403	-.820022+j.623387
-.395276+j.699066	-.297934+j.959421
-.165402+j.960377	-.651709+j.397583
ZEROS	ZEROS
0 +j 3.6949	0 +j3.57496
-.73373+j .383261	0 +j5.78443
+.73373+j .383261	+.651709+j.397583

TABLE I

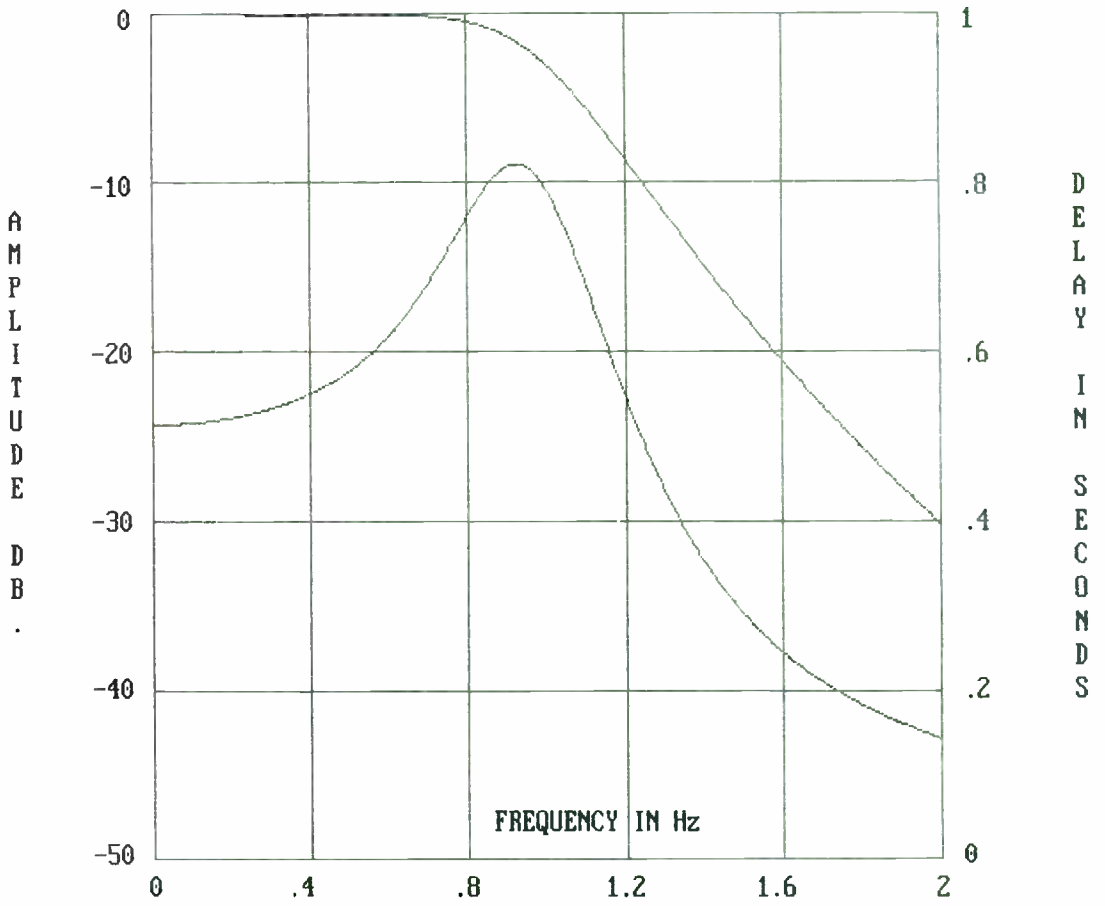

FIGURE 1 -- LOWPASS FILTER AMPLITUDE AND DELAY

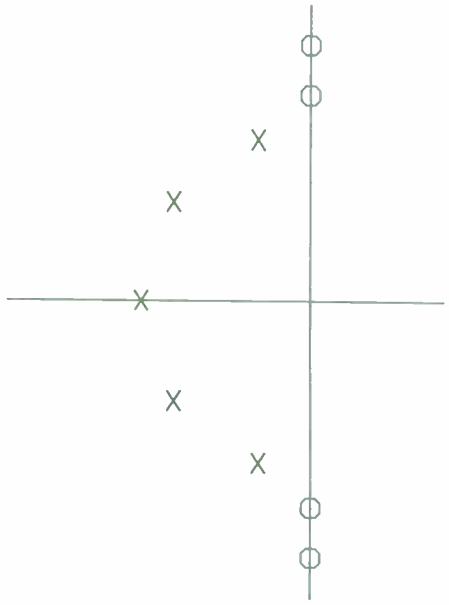

FIGURE 2

TYPICAL TRANSFER FUNCTION
FOR LOW PASS FILTER

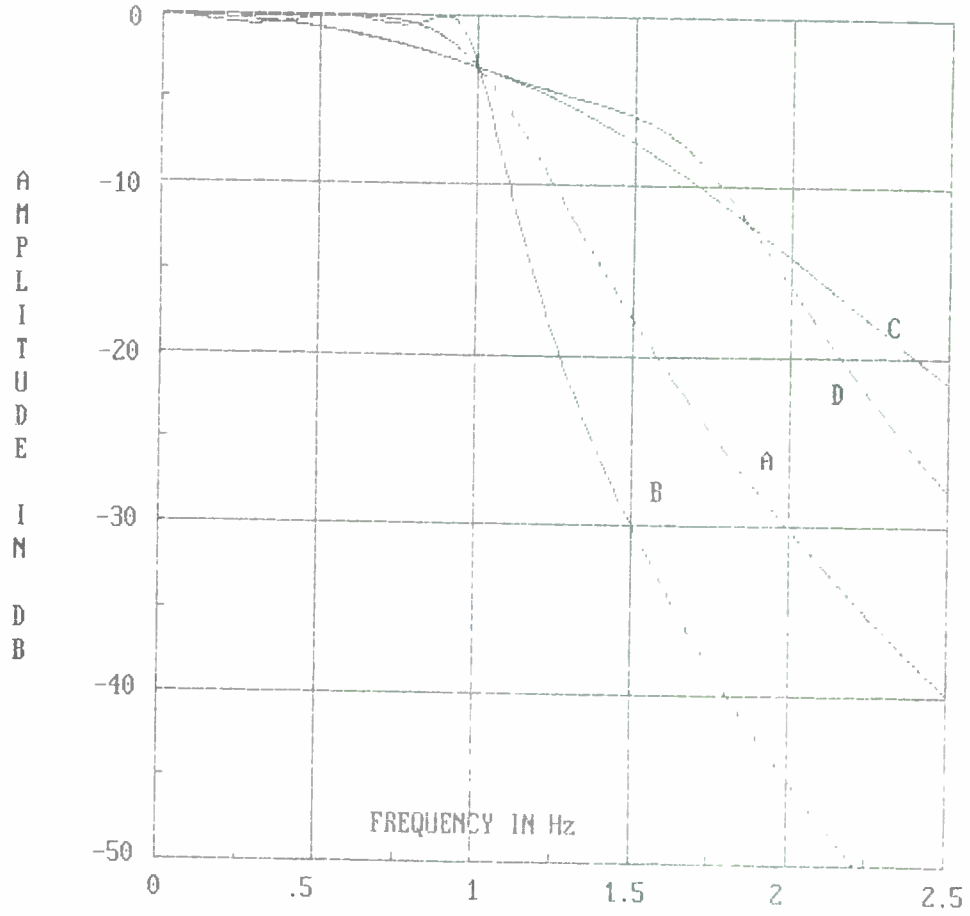

FIGURE 3 -- AMPLITUDE, 4 LOWPASS FILTERS

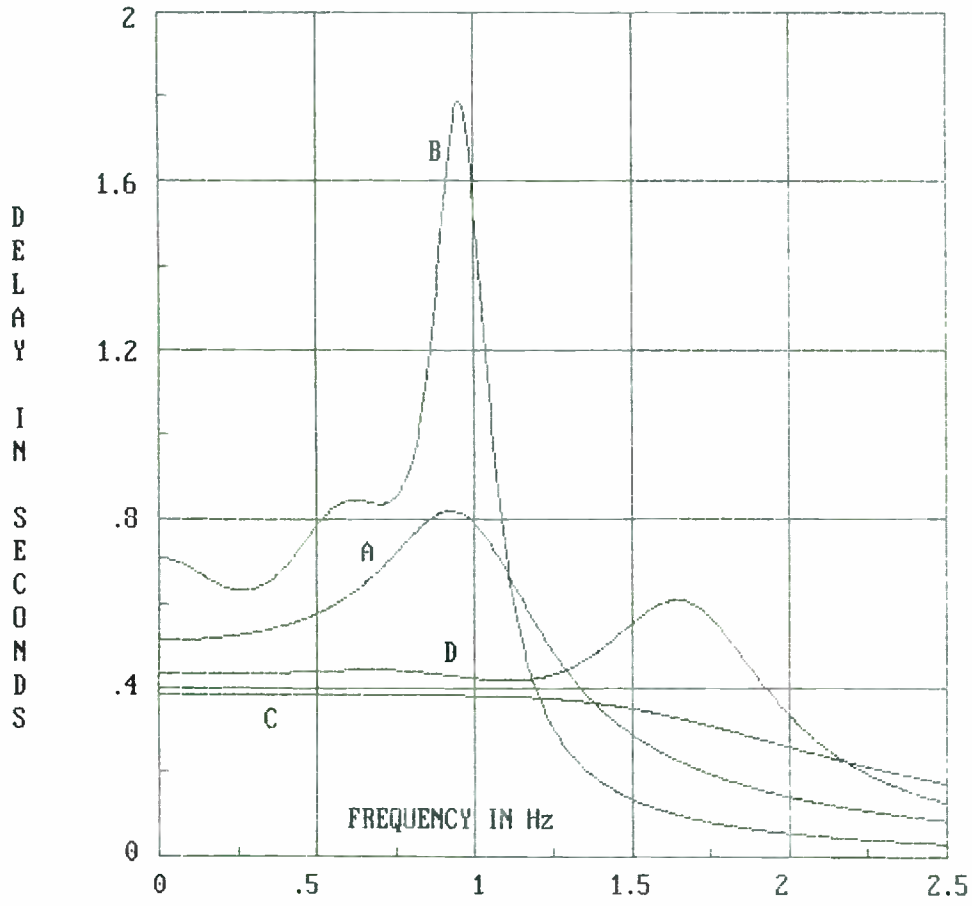

FIGURE 4 -- DELAY, 4 LOWPASS FILTERS

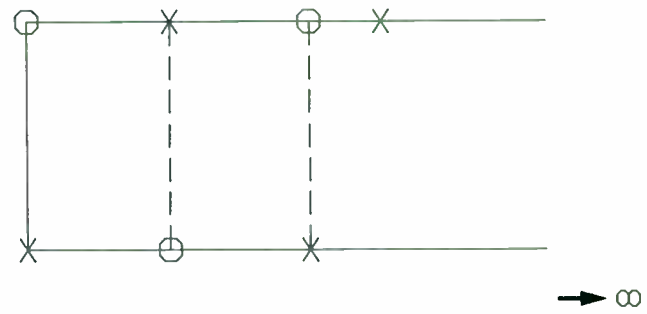

FIGURE 5

BRANCH IMPEDANCES OF SYMMETRICAL LATTICE

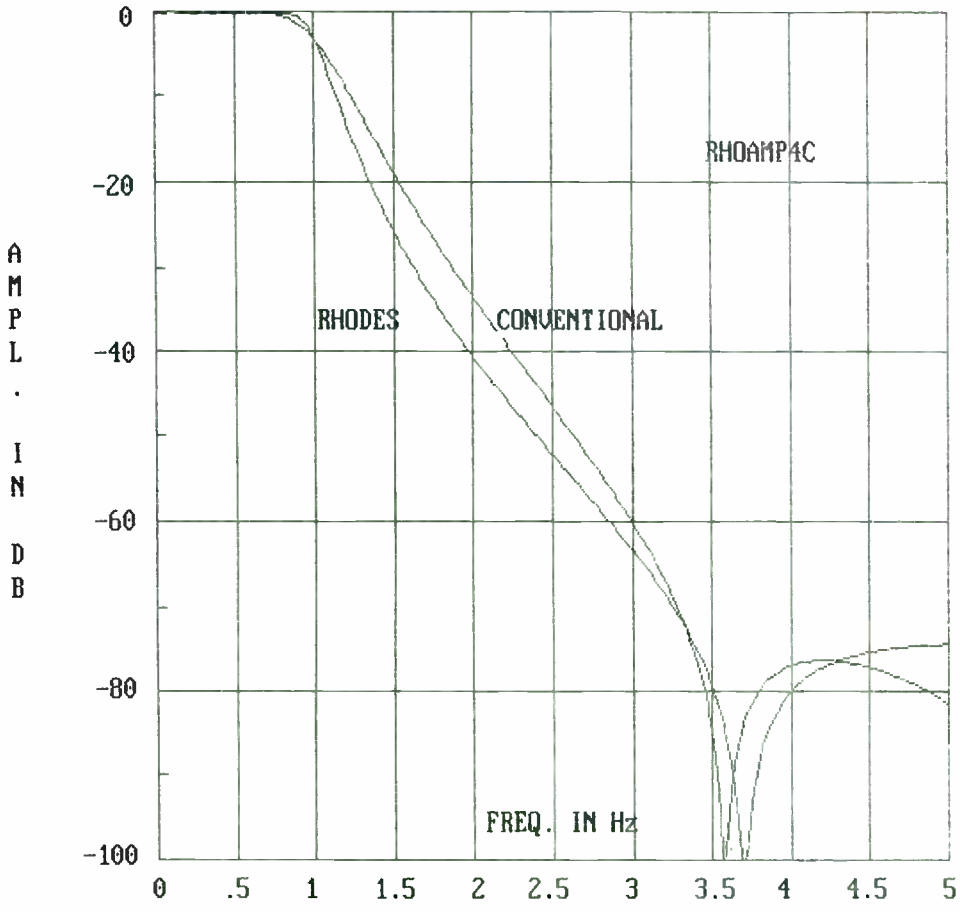

FIGURE 6 -- DELAY-EQUALIZED vs RHODES M=4

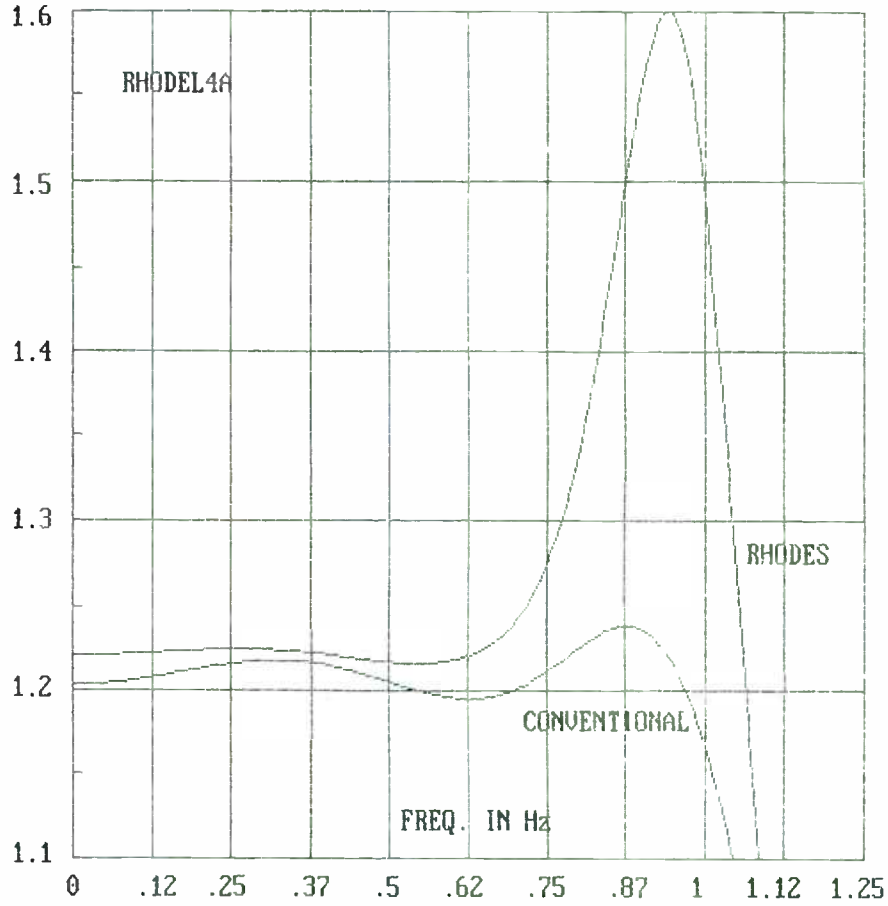

FIGURE 7 -- DELAY-EQUALIZED vs RHODES M=4

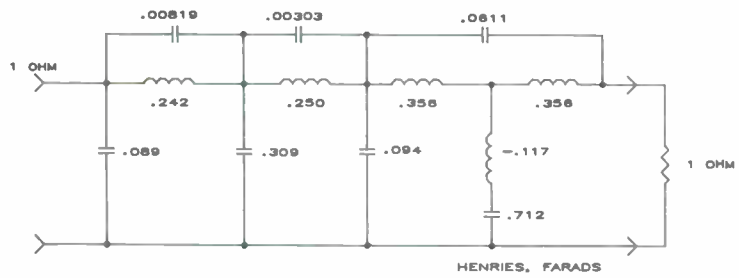

FIGURE 8

CONVENTIONAL FILTER, EQUALIZED, PER FIG. 6 AND 7

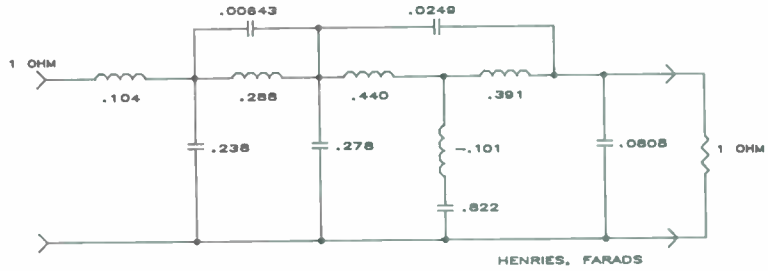

FIGURE 9

RHODES FILTER PER FIGS. 6 AND 7

DESIGN OF FILTERS WITH UNSYMMETRICAL STOPBANDS

William B. Lurie, Consultant
Boynton Beach, Florida

One of the oldest methods of designing bandpass filters consisted of cascading successive sections, each providing attenuation where needed in either the upper or lower stopband, whether symmetrical or not [1]. The various sections were matched to each other in the passband on an image-impedance basis, resulting in more or less flat passbands. More recently, the availability of catalogs of low-pass prototype filters [2], coupled with the techniques of various low-pass to band-pass transformations [3], led to the routine creation of bandpass filters, geometrically symmetrical with respect to frequency. The most modern technique, and the most versatile, is to use a pole-placer program to create a transfer function to meet the exact passband and stopband requirements, symmetrical or otherwise, and then directly synthesize the network from that transfer function. This last method, however, requires the ultimate in sophisticated software, which, although available, is perhaps beyond the reach of many filter designers. The present paper presents a technique, not the ultimate in versatility, perhaps, but as a compromise quite often giving acceptable results.

Traditionally, passbands are specified in terms of flatness or amount of ripple tolerable, usually over a bandwidth mentioning some specific maximum loss. Another paper in this same session describes a method for achieving abritrarily shaped passbands and stopbands, and extends further by letting the designer have some control over envelope delay as well.

As illustrations, several examples will be given based on the same lowpass prototype (C-04-05-23-B in the Saal catalog [2]). The first is a narrow-band crystal filter, centered at 200 kHz, with a design bandwidth of 200 Hz. By using various straightforward design techniques based on Humpherys [4], the symmetrical design of Figure 1 is derived, with amplitude response shown in Figure 2. Note that, on a geometric scale, the stopbands are symmetrically placed, and even on an arithmetic scale, with a bandwidth as low as 0.1%, it would still be quite symmetrical.

Suppose, however, that a single-sideband filter were required, with the upper -40 db point no higher than 200.16 kHz, with the lower stopband allowed to flare out considerably. In the design process, a bilinear transformation could be used. This is a mapping process which, in essence, keeps the edges of the passband fixed, distorting the frequency axis throughout the entire stopband, thereby relocating the frequencies of infinite loss [5]. The results, shown in Figures 3 and 4, indicate that topologically, the schematic has not changed, but the element values and response curve are quite different. It is not the purpose of this paper to instruct in detail, or to present formulas or programs, but rather to illustrate what can be achieved by following the methods described [4, 5].

It is interesting to note that the bilinear transformation process distorts the frequency axis while keeping the filter response constant in terms of the old frequency variable. Conversely, relative to a new linear frequency axis, the transfer function is changed or distorted, all the while holding the edges of the passband fixed. The mathematical relationship is rather simple:

$$\omega = \frac{1-(\Delta\omega)\times v}{v-(\Delta\omega)}$$

where the old frequency ω corresponds to a new frequency v, and $\Delta\omega$ is the finite frequency to which two former zeros at infinity are transported.

In the example just given, the locations of frequencies of infinite attenuation of the symmetrical filter were at +300 Hz and -300 Hz from center, and at infinity, while in the transformed filter they are at 116 KHz, 210.5 KHz, 216 KHz and 238 KHz. The effect of the transformation was to move the peak on the low side down to zero frequency, the peak that was at infinity in toward the passband on the high side, to a new location $\Delta\omega$, andto move the high-side peak in closer to the pass-band, obviously causing the filter's upper transition band to become much narrower. The passband ripple locations change also, but their magnitude does not.

As a second example, consider the same low-pass prototype frequency of 10.7 MHz. The design can be accomplished with ease, using the Holt and Gray transformation [6], and the schematic and response of Figures 5 and 6 result. Again, suppose the requirements exist for a lower-sideband filter, to reach -40 db by 10704.65 KHz on the high side. Again, the bilinear transformation is invoked in the design process, and now the results of Figures 7 and 8 are obtained, plotted for crystal Q's of 80000.

It may seem that the two examples given are quite similar and indeed they are, in performance. The configuration, however, are quite different. In the first example, the entire transfer function is created in one section, using four crystals, while in the second example, two sections of two crystals each are seen. The difference may be subtle, and involved with manufacturing technology, not particularly pertinent in this paper.

In all sideband filters, it is not uncommon to find that more corner rounding appears at the sharper transition from passband to stopband, due to the lower effective Q in the poles near the sharper cutoff. In wideband cases, this is not as pronounced because the effective Q is considerably higher. For those who might not be as familiar with the term, effective Q is defined as the actual resonator Q multiplied by the fractional bandwidth (the actual bandwidth divided by the center frequency). It is not uncommon also to find, in sideband cases, a rather wide range of motional parameters to be required among the various resonators, and effect which can be seen in the above examples. This effect is present no matter what design technique is used, but methods are available to accomodate rather wide ranges of values.

The same method can be applied to L-C filters, for example with the 'minimum-coil' lowpass-to-bandpass transformation [3], with quite similar results, although the mathematical techniques are somewhat different. Consider a sixth order elliptic lowpass filter (C-06-20-32-B), to reach and maintain 75 db stopbands with a shape factor of 1.94:1. A bandpass filter has been designed using the same transformation, in which the infinte-rejection points are located three above and one below the passband. Obviously, in a symmetrical type of transformation, two would have been above and two below. Note in Figures 9 and 10 that these are 44 KHz below, and 10.5 KHz, 16 KHz, and 38 kHz above the passband. As with the crystal filters above, the highly unsymmetrical nature of the transformation can lead to sometimes awkward element values, but proper care in the synthesis process, along with a number of Norton transformations performed on the synthesized network, can alleviate this. In the schematic of Figure 9, the range of inductance values is only about 3.5 to 1, although the ratio of terminating resistance is somewhat larger.

The author expresses gratitude to Dick Abrahams of Radio Systems, Inc., Ft. Lauderdale, FL, for his kind assistance in preparing figures for this presentation.

REFERENCES

[1] Zobel, O., BSTJ Jan. 1923, 'Theory and Design of Uniform and Composite Electric Wave Filters'

[2] Saal, R., Tables (Der Entwurf von Filtern mit Hilfe des Kataloges normierter Tiefpasse), Telefunken GMBH, 1965

[3] Saal & Ulbrich, IRE Transactions on Circuit Theory, CT-5, Dec. 1958, pp. 284-317

[4] Humpherys, D. S., 'The Analysis, Design, and Synthesis of Electrical Filters', Prentice Hall, Inc., 1970

[5] Humpherys, pp. 347,586

[6] Holt, A. G. J., and Gray, R. L., IEEE Trans. Circuit Theory, Vol. CT-15, Dec. 1968 pp. 492-494, 'Bandpass Crystal Filters by Transformation of a Low-Pass Prototype'.

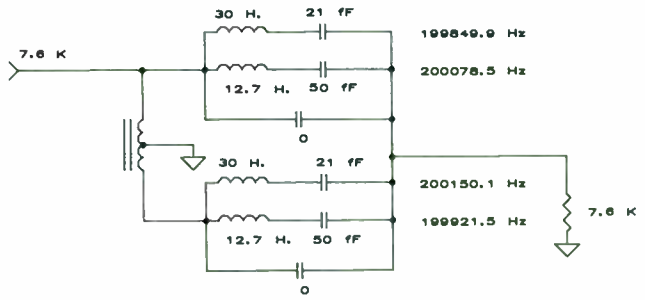

(CRYSTAL FREQUENCIES AS SHOWN ABOVE)

FIGURE 1

SYMMETRICAL 200 KHz BANDPASS

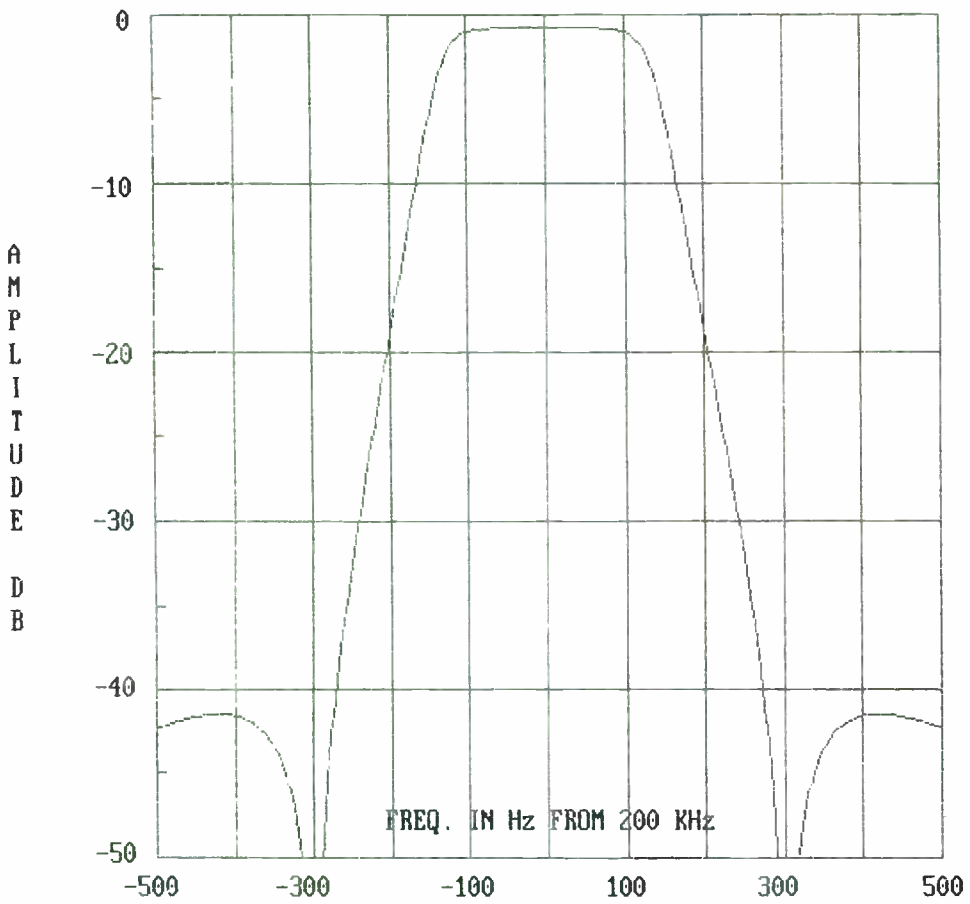

FIGURE 2 -- SYMMETRICAL 200 KHz BANDPASS

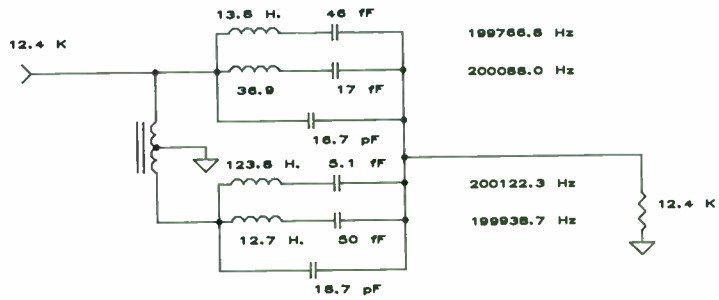

(CRYSTAL FREQUENCIES AS SHOWN ABOVE)

FIGURE 3

LOWER SIDEBAND, 200 KHz BANDPASS

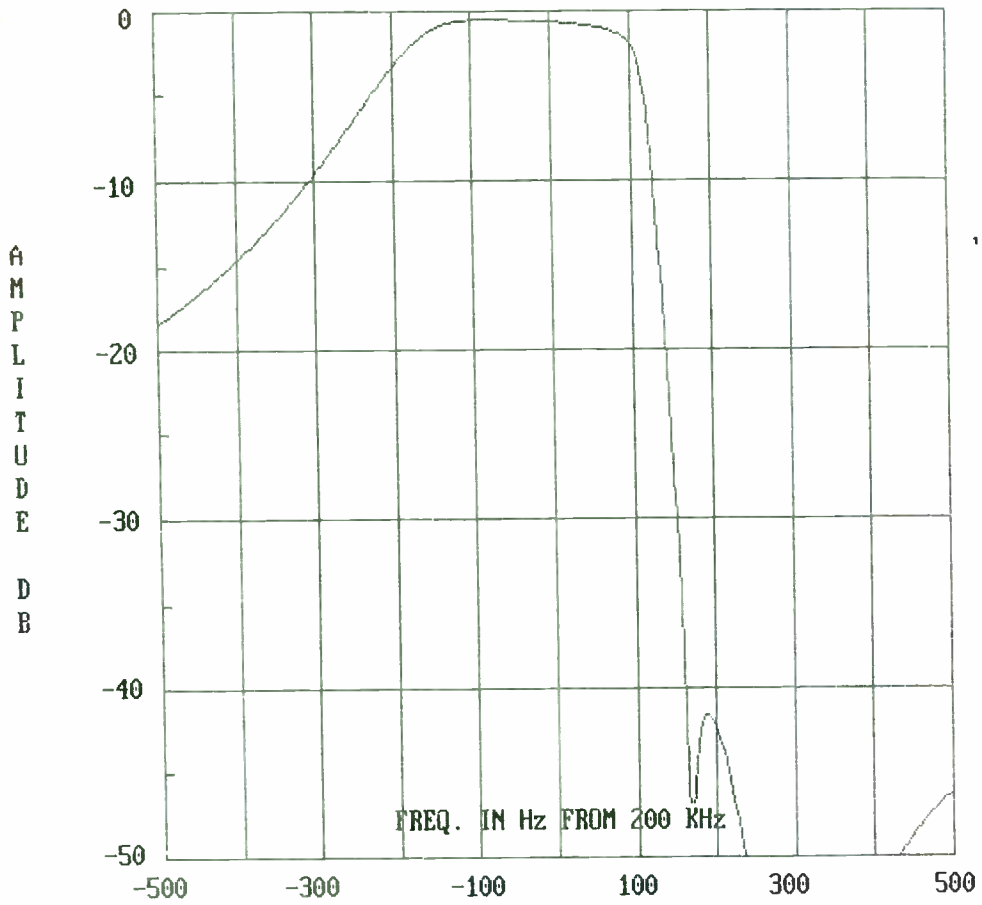

FIGURE 4 -- LOWER SIDEBAND, 200 KHz BANDPASS

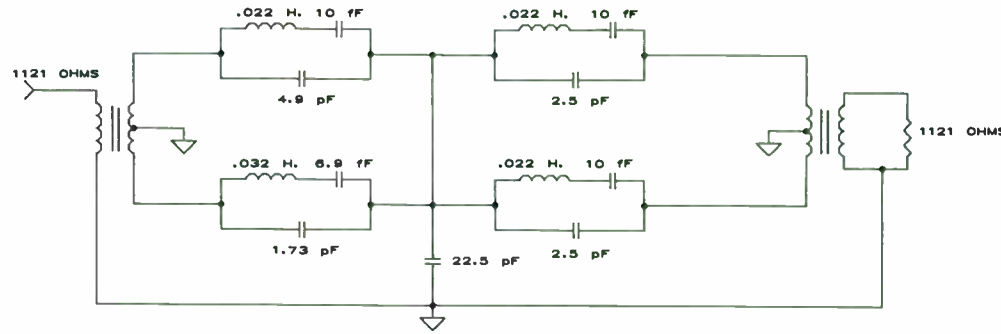

FIGURE 5

SYMMETRICAL 10.7 MHz BANDPASS

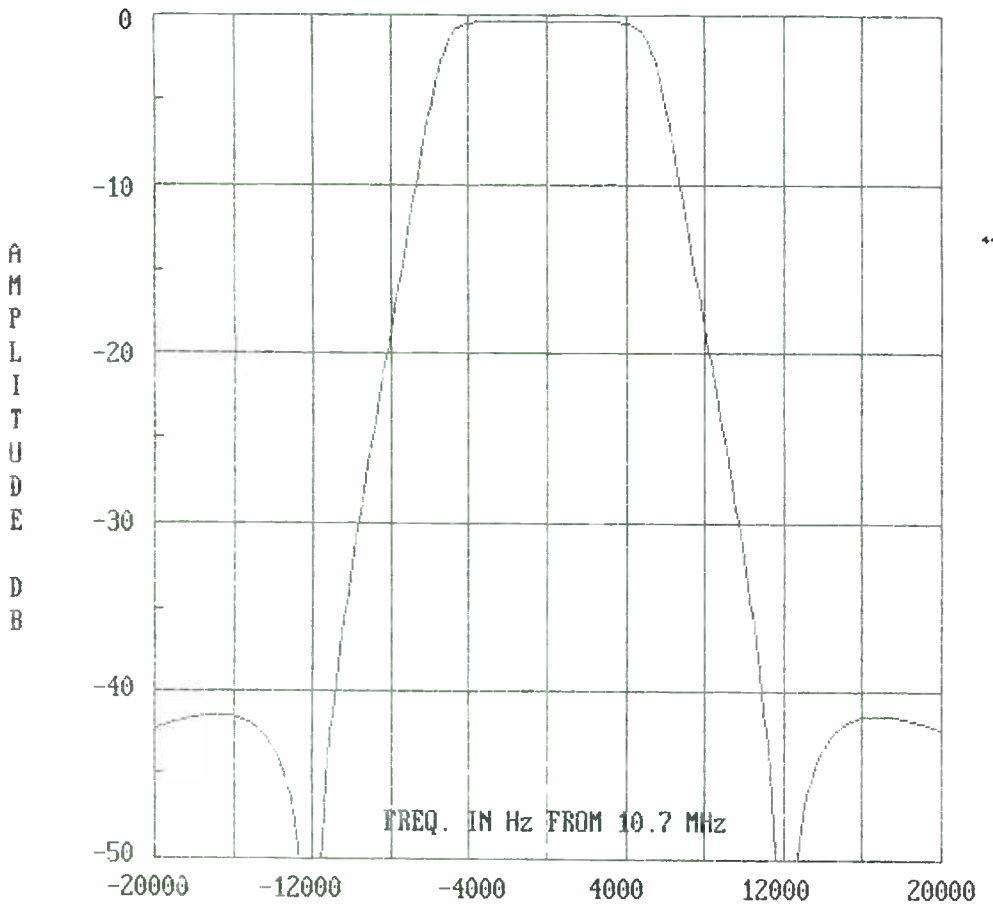

FIGURE 6 -- SYMMETRICAL 10.7 MHz BANDPASS

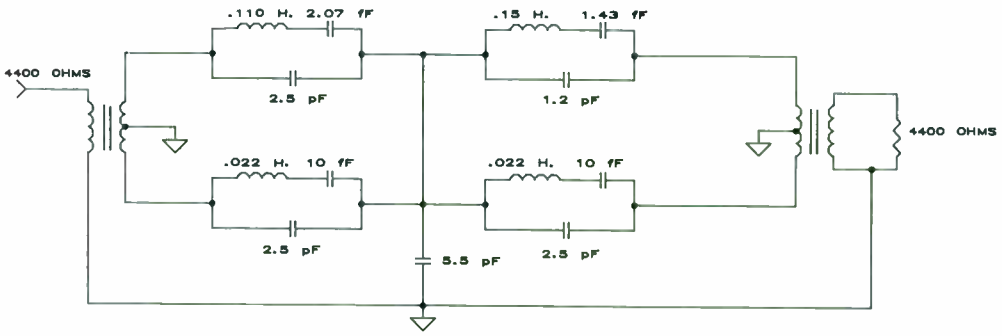

FIGURE 7

LOWER SIDEBAND 10.7 MHz BANDPASS

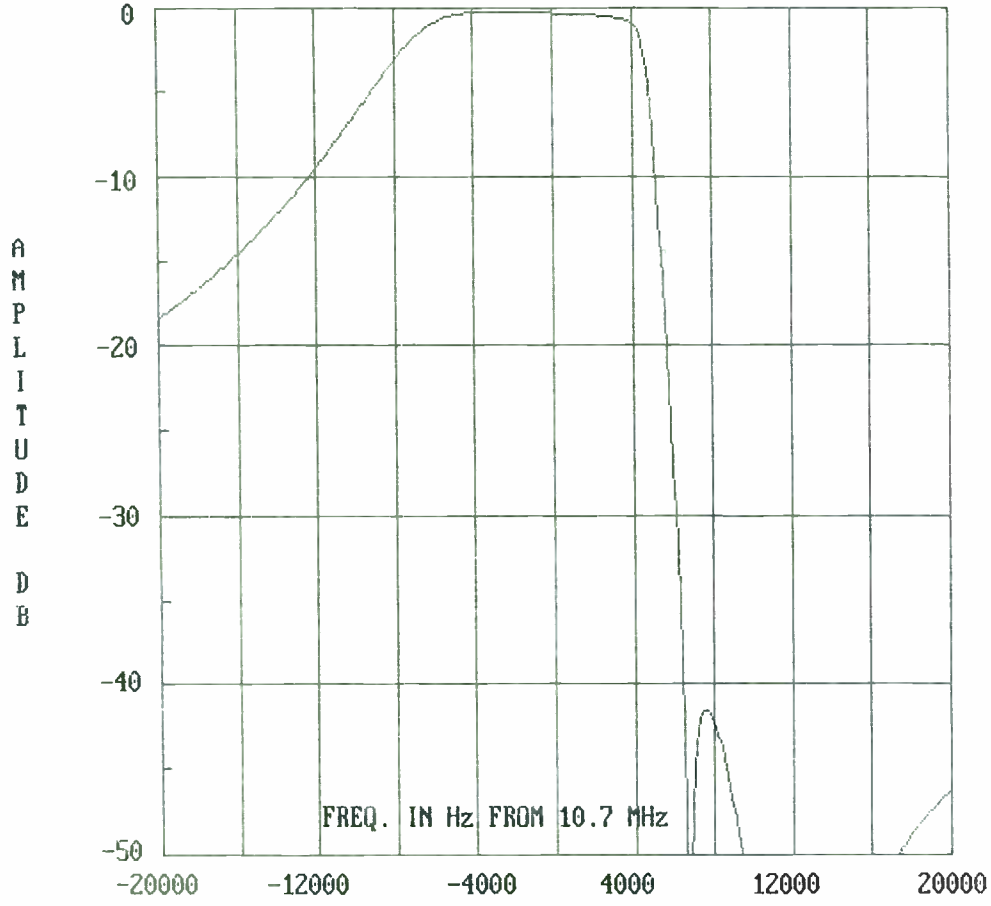

FIGURE 8 -- 10.7 MHz LOWER SIDEBAND FILTER

05-SEP-91 09:15

1	....R....	200.000000 ohm	
2	L	1.055825 mH	
3	....C....	551.831720 pF	
4	C	246.312722 pF	
5	....C....	415.164370 pF	
6	L C	959.544916 uH	RES.FREQUENCY
		465.228929 pF	238.206781 kHz
7	....C....	498.460656 pF	
8	C	195.554695 pF	
9	....C....	4.829238 pF	
10	L C	964.571968 uH	RES.FREQUENCY
		592.378991 pF	210.548906 kHz
11	...L.C...	896.992534 uH	RES. FREQUENCY
		2.095383 nF	116.089781 kHz
13	....C....	1.350829 nF	
14	C	201.102738 pF	
15	....C....	60.351406 pF	
16	L C	760.318803 uH	RES.FREQUENCY
		713.684110 pF	216.057453 kHz
17	....C....	2.461453 nF	
19	....L....	301.221406 uH	
21	....R....	2.000000 kohm	

COMMAND:
> !
>

FIGURE 9 -- L-C FILTER, BILINEAR TRANSFORMED

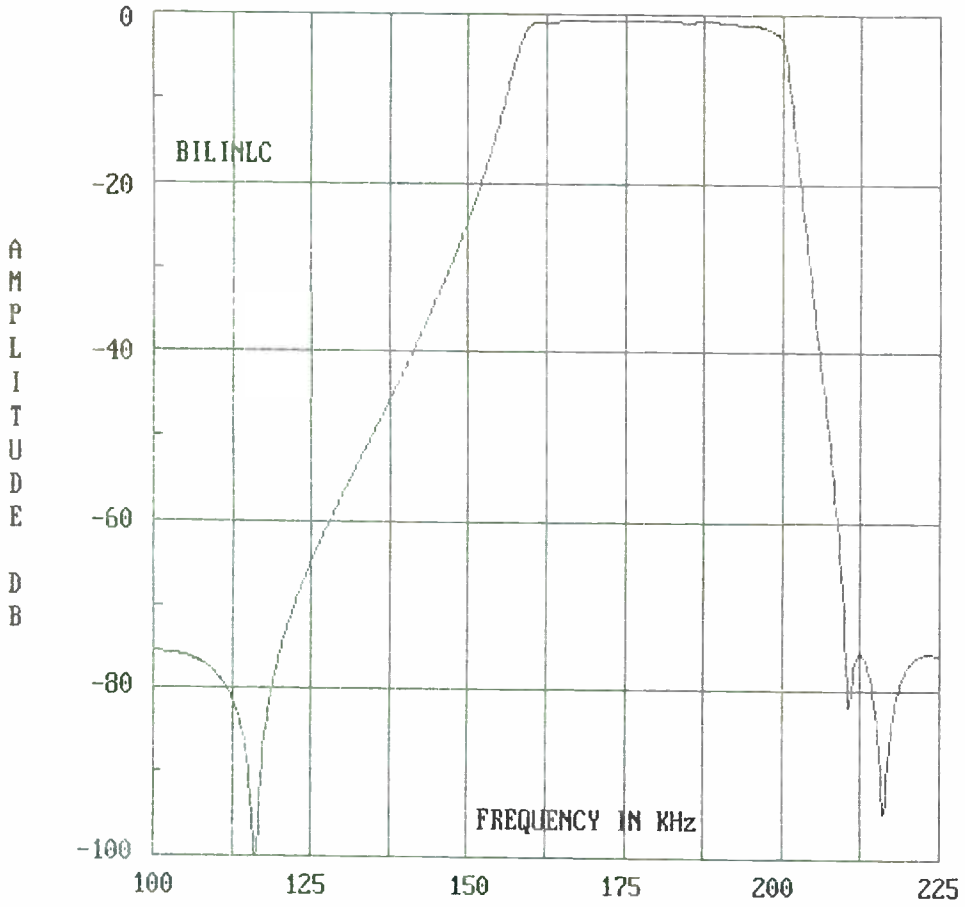

FIGURE 10 -- L-C FILTER -- LOWER SIDEBAND

APPROXIMATION OF FILTERS WITH SHAPED PASSBANDS

GEORGE SZENTIRMAI

DGS Associates, Inc.,
1353 Sarita Way
Santa Clara, CA 95051

ABSTRACT

An optimization procedure is described developed specifically for the approximation of filter transfer functions to provide arbitrary passband loss (and possibly delay) shapes. This permits the design of analog (passive LC or active RC), digital or microwave filters with other than flat passband loss performance.

The method is implemented in a powerful, interactive computer program running on personal computers.

1. INTRODUCTION

All known filter approximation procedures yield transfer functions that have flat passband behavior, either maximally-flat, or equal-ripple type. Quite often we need a filter that has a specified shape, usually to compensate for some other piece of equipment that introduces a distortion in the passband. This could be, for example, a piece of lossy cable, or a sample-and-hold circuit.

There are several other optimization methods, some are available as computer programs, which can handle problems of this type, but all methods known to us operate on the circuit element values. This presents problems, the first one is finding a circuit with element values to start the optimization with. The other is the convergence problem. Optimization procedures are notorious for ill-conditioning and filter circuits are known to have a performance, that is quite insensitive to component values in the passband, aggravating the problem.

Our first decision was therefore to operate on the transfer function, expressed specifically in terms of its poles and zeros. This makes it possible to track the realizability of the function during the optimization, and at the same time avoids the problem of finding a circuit first. The sensitivity problem is also alleviated in this formulation. The only disadvantage is the need for a synthesis step that can take a given transfer function and find a circuit implementation of it. Since our S/FILSYN program is generally available, this last step can be easily implemented.

Using the transfer function also makes it possible to extend the method to work with both IIR digital as well as microwave filters by a simple modification of the evaluation algorithm.

2. ERROR FUNCTION

The next step is to formulate an error function specifically applicable to filters. We selected the standard, weighted and squared error sum, with minor variations.

In the passband, the error is the actual deviation of computed loss from desired loss. If delay is also specified, the same sort of delay error is also computed, but we need an additional delay weight to make the delay error comparable to that of the loss.

In the stopband, the error is proportional to the actual transfer function magnitude, multiplied by the required stopband loss and the specified weight. One difference is that if the computed loss is greater than the required one, the error is assumed to be zero.

While this formulation is simple to compute, it does not readily lead to the popular equal-ripple approximation, although a little experimentation with the weights can get us quite close. Furthermore, the overall error is a non-continuous function of the variables, which are the (complex) poles and zeros of the transfer function. A consequence of this is that optimization algorithms that need analytical gradients, cannot be used.

3. OPTIMIZATION STRATEGIES

Out of the many available strategies, we have selected three that have served us well in the past and seem to perform creditably here as well. These three methods can be used in any order, any number of times in a simple, interactive manner and the progress of the optimization can be observed.

The first is the standard Nelder-Mead simplex method that is very effective as a starting point. While it is slow, it is guaranteed to work and is also very fast.

This is followed by two, more powerful methods, one is Powell's method, the other is a gradient method that calculates the derivative information approximately itself. These two strategies should be alternated once the iteration is started by the simplex method.

4. DATA INPUT AND OUTPUT

Both the requirements and the initial transfer function data are read in from simple ASCII files that have free formats. The requirements are in simple table formats, containing either three or five columns. These are frequency, loss, loss weight and possibly delay and delay weight columns. No requirements can be indicated simply by a zero weight column entry. Blank lines and comments following the "!" comment symbol, can be used freely to make the file more readable.

The initial pole-zero data file contains the zeros first, in a real-imaginary pair per line format, followed by the poles in the same form. Only one of a complex conjugate pair need be entered and these initial data can usually be obtained from a filter program providing a flat passband, but meeting all stopband requirements.

5. EXAMPLE

As our example, we selected a lowpass filter with a passband shape to compensate the (sin x)/x rolloff produced by a sample-hold circuit from zero to 1.8kHz and a 40 dB stopband loss from 2.2 kHz.

The requirements are stored in the file called EXAMPLE.REQ, the first few lines of which are shown below:

```
This is the title line. 2/7/91

FREQ       LOSS     LW     DLAY     DW
  kHz        dB              msec

 0.1      -0.007    1.     2.       1.
 0.2      -0.029    1.     2.       1.
 0.3      -0.065    1.     2.       1.
 0.4      -0.116    1.     2.       1.
 0.5      -0.182    1.     2.       1.
 0.6      -0.264    1.     2.       1.
 0.7      -0.361    1.     2.       1.
 0.8      -0.474    1.     2.       1.
 0.9      -0.603    1.     2.       1.
 1.0      -0.750    1.     2.       1.
 1.05     -0.830    1.     2.       1.
 1.10     -0.914    1.     2.       1.
 1.15     -1.003    1.     2.       1.
 1.20     -1.097    1.     2.       1.
 1.25     -1.197    1.     2.       1.
 1.30     -1.301    1.     2.       1.
 1.35     -1.410    1.     2.       1.
 1.40     -1.525    1.     2.       1.
 1.45     -1.645    1.     2.       1.
 1.50     -1.772    2.     2.       1.
 1.55     -1.904    2.     2.       2.
 1.60     -2.043    5.     2.       2.
 1.65     -2.188    5.     2.       2.
 1.70     -2.341    5.     2.       2.
 1.75     -2.500    5.     2.       2.
 1.80     -2.668    5.     2.       2.

 2.2      40.0     10.    1.       0.0
 2.3      40.0     10.    1.       0.0
 2.4      40.0     10.    1.       0.0
 2.5      40.0     10.    1.       0.0
 2.6      40.0      5.    1.       0.0
 .
 .
```

The table contains delay requirements in order to show their form as well, but for the sake of brevity we shall ignore them.

The initial design is the transfer function of an elliptic low-pass filter with 2 kHz passband edge frequency and .2 dB passband loss ripple, yielding about 42 dB loss from 2.2 kHz and above.

When we call the program, the following conversational data entry takes place:

```
      **** OPTIMIZING PREPROCESSOR ****

Copyright (C) 1991 DGS Associates, Inc.
          All Rights Reserved.

          Version 1.0   3/1/91

FIRST WE NEED THE TABULATED REQUIREMENTS
ENTER FILE NAME
> example
ENTER NORMALIZATION FREQUENCY (UPPER EDGE OF PASSBAND)
> 2kHz
ENTER OVERALL DELAY WEIGHT
> 0
```

The zero weight entered here makes the program effectively ignore the delay requirements completely. Otherwise this weight helps in balancing the loss and delay requirements.

```
FILTER KIND - LUMPED: 0, DIGITAL: 1 OR MICROWAVE: 2
> 0
APPROXIMATING FUNCTION DATA IS NEXT
ENTER DEGREE (SHOULD BE NO MORE THAN 12)
> 7
ENTER MULTIPLICITY OF ZERO AT ZERO
> 0
ENTER NUMBER OF IMAGINARY-AXIS ZEROS
```

```
> 3
ENTER NUMBER OF COMPLEX ZEROS
> 0
WE SHALL READ (NORMALIZED) INITIALIZATION DATA FROM A FILE NEXT
ENTER FILE NAME
> test7
```

We needed to tell the program about the starting approximation. Complex zeros are in fact, quadruplets of zeros and are used mainly if delay requirements also play a role. The actual data was in the TEST7.DAT file.

```
ANY OF THESE TO REMAIN FIXED? (Y/N)
> y
ENTER THE SERIAL NUMBERS OF THE  3 ZEROS YOU WISH TO REMAIN FIXED
ENTER "A" IF YOU WISH ALL TO REMAIN FIXED
> a
ENTER THE SERIAL NUMBERS OF THE  4 POLES YOU WISH TO REMAIN FIXED
>
```

Any of the zeros and/or poles could be kept fixed. A good practice is to keep all the imaginary axis zeros fixed, especially if the original design already met the stopband requirements.

Next we get a summary of the design, followed by an initial evaluation of the function. Note that asterisks indicate those parameters which are going to vary during the optimization.

```
This is the title line. 2/7/91                          16-JUL-91 09:03
   NUMBER OF POINTS SPECIFIED  =   48
   STARTING POINT              =  100.00000  Hz
   END POINT                   =   10.00000 kHz
   LOSS AND DELAY REQUIREMENTS
   # OF LOSS POINTS SPECIFIED  =   48
   # OF DELAY POINTS SPECIFIED =   26
   OVERALL DELAY WEIGHT        =    0.000000E+00
LUMPED FUNCTION IS SPECIFIED

APPROXIMATING FUNCTION:

*** ZEROS ***
  0.0000000D+00     1.3960145D+04
  0.0000000D+00     1.5512946D+04
  0.0000000D+00     2.3559077D+04

*** POLES ***
  6.3590848D+03 *   0.0000000D+00
  4.0599311D+03 *   8.4782425D+03 *
  1.4488977D+03 *   1.1826487D+04 *
  3.2072560D+02 *   1.2712486D+04 *

NUMBER OF VARIABLE PARAMETERS =  7

**** RESULTS OF THE ANALYSIS ****

   FREQUENCY          LOSS VALUES              DELAY VALUES
     IN HZ          ACTUAL    DEVIATION      ACTUAL      DEVIATION

 1.000000E+02     -1.205517   -1.198517   2.731306E-04   -1.726869E-03
 2.000000E+02     -1.174179   -1.145179   2.721680E-04   -1.727832E-03
 3.000000E+02     -1.129631   -1.064631   2.712588E-04   -1.728741E-03
 4.000000E+02     -1.081760    -.965760   2.713084E-04   -1.728692E-03
 5.000000E+02     -1.041572    -.859572   2.733658E-04   -1.726634E-03
 6.000000E+02     -1.019100    -.755100   2.784973E-04   -1.721503E-03
 7.000000E+02     -1.021324    -.660324   2.876740E-04   -1.712326E-03
 8.000000E+02     -1.050106    -.576106   3.016452E-04   -1.698355E-03
 9.000000E+02     -1.100338    -.497338   3.207477E-04   -1.679252E-03
 1.000000E+03     -1.158710    -.408710   3.446437E-04   -1.655356E-03
 1.050000E+03     -1.184677    -.354677   3.580432E-04   -1.641957E-03
 1.100000E+03     -1.204555    -.290555   3.721219E-04   -1.627878E-03
 1.150000E+03     -1.215462    -.212462   3.866358E-04   -1.613364E-03
 1.200000E+03     -1.215031    -.118031   4.013793E-04   -1.598621E-03
 1.250000E+03     -1.201927    -.004927   4.162652E-04   -1.583735E-03
 1.300000E+03     -1.176365     .124635   4.314292E-04   -1.568571E-03
 1.350000E+03     -1.140579     .269421   4.473496E-04   -1.552650E-03
 1.400000E+03     -1.099106     .425894   4.649755E-04   -1.535025E-03
 1.450000E+03     -1.058773     .586227   4.858538E-04   -1.514146E-03
 1.500000E+03     -1.028229     .743771   5.122555E-04   -1.487745E-03
 1.550000E+03     -1.016800     .887200   5.472875E-04   -1.452713E-03
 1.600000E+03     -1.032268    1.010732   5.949317E-04   -1.405068E-03
 1.650000E+03     -1.077091    1.110909   6.598018E-04   -1.340198E-03
 1.700000E+03     -1.142536    1.198464   7.461365E-04   -1.253864E-03
 1.750000E+03     -1.202026    1.297974   8.554297E-04   -1.144570E-03
 1.800000E+03     -1.211338    1.456662   9.838756E-04   -1.016125E-03
 2.200000E+03     41.200878     .000000   6.062770E-04    0.000000E+00
 2.300000E+03     41.204037     .000000   3.771280E-04    0.000000E+00
 2.400000E+03     47.603512     .000000   2.713049E-04    0.000000E+00
 2.500000E+03     55.670315     .000000   2.099962E-04    0.000000E+00
 .
 .
SUM OF ERROR SQUARES = 4.836155D+01
```

The shape is just what we would expect from an elliptic design. Stopband requirements are all met, the passband is flat, hence there is a shaped error.

Next we pick the first (simplex) method:

```
NO MORE ITERATION: 0 OR METHOD 1, 2 OR 3
> 1
METHOD NO. 1
ITERATION =  10  ERROR =   6.172057D+00
ITERATION =  20  ERROR =   2.723922D+00
```

```
ITERATION = 180  ERROR =   6.422698D-02
ITERATION = 190  ERROR =   6.379857D-02
ITERATION = 200  ERROR =   6.311827D-02
SIMPLEX -- NO CONVERGENCE IN 200 ITERATIONS
*** SIMPLEX *** IS FINISHED

APPROXIMATING FUNCTION:

*** ZEROS ***
  0.0000000D+00    1.3960145D+04
  0.0000000D+00    1.5512946D+04
  0.0000000D+00    2.3559077D+04

*** POLES ***
  6.6394973D+03 *  0.0000000D+00
  4.1727868D+03 *  8.4321571D+03 *
  1.8703567D+03 *  1.1182980D+04 *
  5.2221704D+02 *  1.1845223D+04 *
```

The method prints one line every tenth iterations and usually runs through the 200 iterations permitted. It does not converge, but the error function is reduced by nearly three orders of magnitude. Next we try Powell's method (# 2):

```
NO MORE ITERATION: 0 OR METHOD 1, 2 OR 3
> 2
METHOD NO. 2
ITERATION =  1  ERROR =   6.27097782D-02
ITERATION =  2  ERROR =   6.20576368D-02
ITERATION =  3  ERROR =   6.19004707D-02
ITERATION =  4  ERROR =   6.18820405D-02
ITERATION =  5  ERROR =   6.18820405D-02
ITERATION =  6  ERROR =   6.18767720D-02
ITERATION =  7  ERROR =   6.18767720D-02
ITERATION =  8  ERROR =   6.14290796D-02
CONVERGENCE NOT POSSIBLE DUE TO INACCURACY IN VALUES
*** OPTIM *** IS FINISHED

APPROXIMATING FUNCTION:

*** ZEROS ***
  0.0000000D+00    1.3960145D+04
  0.0000000D+00    1.5512946D+04
  0.0000000D+00    2.3559077D+04

*** POLES ***
  6.6585393D+03 *  0.0000000D+00
  4.1932002D+03 *  8.4286626D+03 *
  1.8698954D+03 *  1.1182980D+04 *
  5.2193400D+02 *  1.1845223D+04 *
NO MORE ITERATION: 0 OR METHOD 1, 2 OR 3
>
```

Somewhat better, but not much. Trying methods 2 and 3 a few more times we obtain an overall 2 to 1 further improvement and stop:

```
 .
 .
NO MORE ITERATION: 0 OR METHOD 1, 2 OR 3
> 0

**** RESULTS OF THE ANALYSIS ****

   FREQUENCY          LOSS VALUES              DELAY VALUES
     IN HZ          ACTUAL    DEVIATION      ACTUAL      DEVIATION

  1.000000E+02     -.063799    -.056799   2.755627E-04  -1.724437E-03
  2.000000E+02     -.065718    -.036718   2.762090E-04  -1.723791E-03
  3.000000E+02     -.074106    -.009106   2.777925E-04  -1.722208E-03
  4.000000E+02     -.095690     .020310   2.809984E-04  -1.719002E-03
  5.000000E+02     -.137976     .044024   2.866595E-04  -1.713341E-03
  6.000000E+02     -.207663     .056337   2.956622E-04  -1.704338E-03
  7.000000E+02     -.308993     .052007   3.088414E-04  -1.691159E-03
  8.000000E+02     -.442095     .031905   3.268500E-04  -1.673150E-03
  9.000000E+02     -.601805     .001195   3.499992E-04  -1.650001E-03
  1.000000E+03     -.777643    -.027643   3.781426E-04  -1.621858E-03
  1.050000E+03     -.867457    -.037457   3.939442E-04  -1.606056E-03
  1.100000E+03     -.956457    -.042457   4.108409E-04  -1.589159E-03
  1.150000E+03    -1.043669    -.040669   4.288776E-04  -1.571123E-03
  1.200000E+03    -1.128985    -.031985   4.482557E-04  -1.551744E-03
  1.250000E+03    -1.213484    -.016484   4.694282E-04  -1.530572E-03
  1.300000E+03    -1.299658     .001342   4.932067E-04  -1.506793E-03
  1.350000E+03    -1.391352     .018648   5.208689E-04  -1.479131E-03
  1.400000E+03    -1.493368     .031632   5.542438E-04  -1.445756E-03
  1.450000E+03    -1.610407     .034593   5.957352E-04  -1.404265E-03
  1.500000E+03    -1.745337     .026663   6.482088E-04  -1.351791E-03
  1.550000E+03    -1.896685     .007315   7.146313E-04  -1.285369E-03
  1.600000E+03    -2.056276    -.013277   7.974455E-04  -1.202555E-03
  1.650000E+03    -2.209761    -.021761   8.983865E-04  -1.101614E-03
  1.700000E+03    -2.346102    -.005102   1.021933E-03  -9.780675E-04
  1.750000E+03    -2.481264     .018736   1.191321E-03  -8.086787E-04
  1.800000E+03    -2.673250    -.005250   1.496080E-03  -5.039201E-04
  2.200000E+03     50.507189    .000000   4.142641E-04   0.000000E+00
  2.300000E+03     48.877527    .000000   3.041328E-04   0.000000E+00
  2.400000E+03     54.270189    .000000   2.379542E-04   0.000000E+00
  2.500000E+03     61.648714    .000000   1.938398E-04   0.000000E+00
  2.600000E+03     50.459917    .000000   1.624106E-04   0.000000E+00
 .
 .
SUM OF ERROR SQUARES = 3.017217D-02

APPROXIMATING FUNCTION:

*** ZEROS ***
  0.0000000D+00    1.3960145D+04
  0.0000000D+00    1.5512946D+04
  0.0000000D+00    2.3559077D+04
```

```
*** POLES ***
  7.0326176D+03 *  0.0000000D+00
  4.2790298D+03 *  8.2124372D+03 *
  1.7226037D+03 *  1.1111420D+04 *
  4.4100840D+02 *  1.1959438D+04 *
MORE ITERATION: I, WRITE RESULTS TO FILE: F, MODIFY DELAY WEIGHT: M OR
QUIT: Q
> f
ENTER FILE NAME
> testout
*** DONE ***
WISH TO MODIFY DELAY WEIGHT? (Y/N)
> n
*** OPT PREPROCESSOR ENDED ***
```

The final evaluation shows a very good results, with a 0.06 dB error ripple and 7 crossovers, which indicates that we are at or very near the global optimum.

Finally, the transfer function was synthesized and the resulting passive LC implementation is shown below.

```
Optimized filter                                        16-JUL-91 09:08

   1   ....R....      500.000000  ohm
       .       .
   3   ....C....      216.598382 nF
       .       .
       .    ....
   4   .    L  C       85.623027 mH      RES.FREQUENCY
       .    ....       21.042283 nF        3.749544 kHz
       .       .
   5   ....C....      109.308412 nF
       .       .
       .    ....
   6   .    L  C      185.128894 mH      RES.FREQUENCY
       .    ....       22.445909 nF        2.468962 kHz
       .       .
   7   ....C....       44.541339 nF
       .       .
       .    ....
   8   .    L  C      103.569734 mH      RES.FREQUENCY
       .    ....       49.543570 nF        2.221826 kHz
       .       .
   9   ....C....        4.717056 nF
       .       .
  11   ....R....        2.694467 kohm
       .       .
```

This circuit was analyzed in the frequency domain and the results together with the passband details, are shown on the next page.

6. SUMMARY

A rugged optimization scheme has been developed for the design of analog, digital and microwave filters with arbitrary passband loss and possibly delay shapes. The method works with the transfer function poles and zeros, any of which can be kept fixed. This procedure avoids the problem of selecting a starting circuit together with the associated convergence problems. In exchange, we subsequently need to find the ciruit that implements the transfer function found.

Experience with the computer program implementing the procedure has been very satisfying.

7. REFERENCES

[1] D. M. Himmelblau: Applied Nonlinear Programming. McGraw Hill Book Co., NY 1972 Chapter 4

[2] M. D. J. Powell: An Efficient Method for Finding the Minimum of a Function of Several Variables Without Calculating Derivatives. Computer Journal, Vol. 7 1965 pp. 303-307

[3] D. Kahaner, C. Moler, S. Nash: Numerical Methods and Software. Prentice Hall, NJ 1989 Chapter 9.

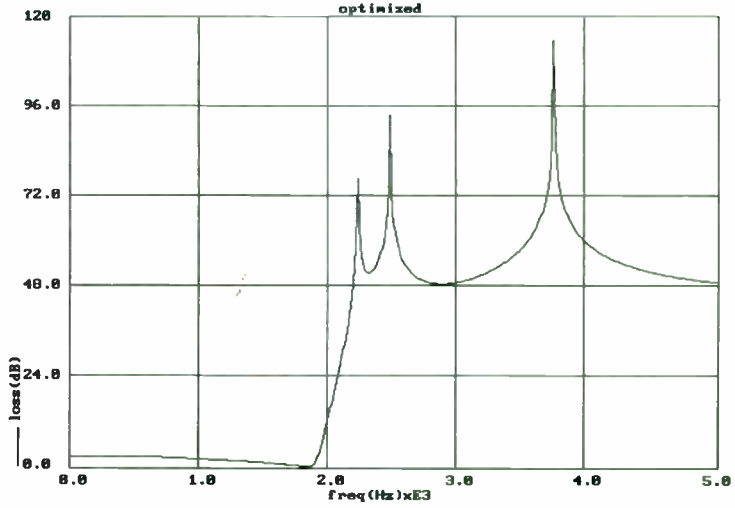

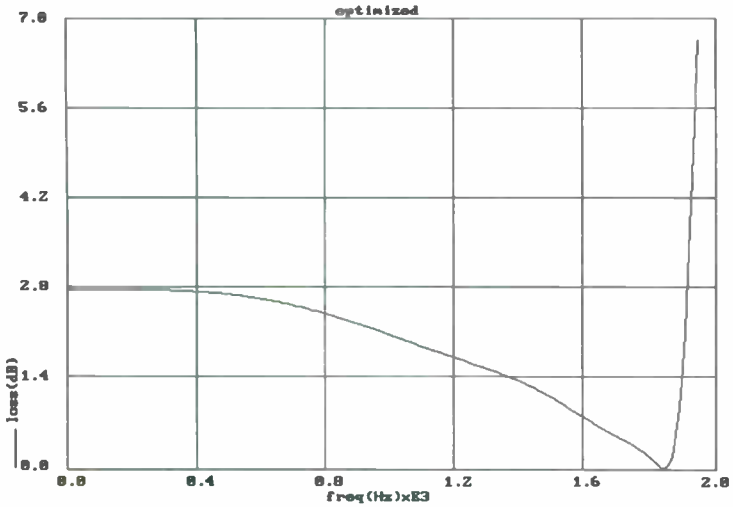

The MCXO, Characteristics and Applications

Brian E. Rose

Q-Tech Corporation
10150 W. Jefferson Blvd.
Culver City, Ca. 90232

Abstract

The MCXO is a new type of precision oscillator using dual-mode temperature sensing and digital frequency correction. It has many more options for interfacing with the user's system than conventional oscillators. Although it uses digital frequency correction, the output is phase-continuous.

1.0 Introduction

The MCXO (Microcomputer Compensated Crystal Oscillator) is a precision oscillator characterized by; 1. Dual mode crystal temperature sensing 2. Microcomputer error calculation and, 3. Digital frequency correction. In this paper the principles of operation of the MCXO will be briefly reviewed, the applications to frequency and time control discussed, and a description of it's output characteristics in the time and frequency domain developed.

2.0 Principles of Operation

The MCXO system is driven by two oscillators operating on a single SC-cut crystal. One oscillator excites the third overtone C-mode, while the second excites the fundamental C-mode. Since both modes have essentially identical temperature characteristics except for their first-order terms, the difference in frequency between the overtone mode divided by three and the fundamental mode is a nearly linear function of temperature. If the crystal 3rd overtone frequency is 10 MHz, then the difference frequency, Fb, is about 50 to 200 KHz, depending on the crystal design, and Fb has a slope on the order of -70 ppm per degree C. Using the crystal to measure it's own temperature avoids the thermometry problem which has limited the accuracy of conventional TCXOs for 30 years. Overall MCXO error is less than +/- 30 parts-per-billion over the temperature range of -55 to +85 degrees Celsius.

Figure 1 shows a block diagram of the type of MCXO which uses a Direct Digital Synthesizer, (DDS), and phase-locked-loop, (PLL), for frequency error correction. (1),(2)

(1) Benjaminson, A. and Stallings, S. "A Microcomputer-Compensated Crystal Oscillator Using A Dual-Mode Resonator", Proceedings of the 43rd Annual Symposium on Frequency Control, 1989.

(2) U.S. Patent No. 4,872,765 entitled "Dual Mode Quartz Thermometric Sensing Device", issued to Stanley S. Schodowski, U.S. Army LABCOM ETDL.

The 10 MHz crystal in the example is finished to be slightly below 10 MHz throughout the temperature range. The frequency correction, Df = 10MHz - Fo, generated in the DDS, is added to Fo in the 10 MHz PLL clean-up loop. The microcomputer takes the value of Fb from a counter (N1), and computes a number N2 which is the frequency control input to the DDS. N2 and N1 are related by polynomial equations which have been fit to calibration data in a least squares error sense. Because of an extremely low power budget, (75 milliwatts maximum for the entire MCXO), the DDS uses the overflow bit stream from it's adder as Df, without the sine look-up and D/A conversion stages usually associated with the DDS.

Aging correction of the MCXO can be accomplished in the field by application of a calibration signal which then automatically corrects the constant terms of the polynomial equations. It should be noted that even in those cases where the application does not allow aging correction, the MCXO provides a significant improvement in long term aging compared to conventional TCXOs. The improvement comes from the fact that the crystal in the MCXO is a third overtone SC-cut type, which has excellent long-term aging characteristics. In a conventional TCXO, a 10 MHz fundamental crystal must be used because the crystal has to be "pulled" for frequency correction. Overtone modes, and especially SC-cut overtones are very "stiff" (small motional capacity), and cannot be "pulled" the 20 or 30 parts-per-million (ppm) required for conventional temperature correction. That is why SC-cut overtone crystals are normally used only in ovenized oscillators.

3.0 Hysteresis and Residuals

Hysteresis

With a error on the order of +/- 3 x 10E-8, the MCXO falls between a conventional TCXO and an ovenized oscillator with respect to frequency vs. temperature accuracy. What are the limitations to the accuracy that can be achieved using the MCXO principle? Two characteristics of a typical frequency-temperature run can be observed in Figure 3. One is that as the temperature is cycled, the frequency in certain temperature ranges does not repeat, i.e. the curve is "open" in places. The second is that instead of smooth, flat curves, there are peaks or bumps. The first effect is due to hysteresis in the crystal, the second to limitations in fitting curves to the calibration data. The peaks and bumps are called residuals.

Hysteresis has been observed in crystals since the early days of compensated oscillators. Because of the great difficulty of measuring crystal temperature accurately with an external sensor, more hysteresis was often attributed to crystals than was warranted. Using the crystal to measure

it's own temperature eliminates that error and exposes the true hysteresis.

It is not clear why some crystals exhibit more hysteresis than others. Possible contributors include the quartz itself, process variations, plating techniques, and the crystal mount. At this time hysteresis appears to be the most fundamental limitation to accuracy, since residuals, discussed next, can be improved as software and hardware are improved.

Residuals

Limitations in digital memory, and the time required to take data, mandate that calibration data be taken at only a limited number of points. (Taking data at every 5 degrees Centigrade, for example, requires many hours per run). Consequently, there is a requirement to extrapolate between data points by fitting some mathematical model to the data. The frequency-temperature curves of AT and SC-cut crystals are essentially cubic. However, when attempting to curve-fit to accuracies required by the MCXO, more than a simple cubic equation is needed. Various interpolation methods have been explored. The present method divides the temperature range into three sections and fits a 6th order polynomial to each section, calculating the coefficients by the method of least squares.

The MCXO EEPROM memory must then store the 21 coefficients to be used in calculating the correction frequency for any temperature. Compared to an earlier method using a single 7th order polynomial, the three 6th's reduces residuals by factors of two to five, depending on the crystal.

4.0 Applications to Frequency and Time Control

The outputs of the MCXO described here are 10 MHz and 1 PPS signals. The 1 PPS signal is part of a time-keeping function which includes the ability to produce time-of-day (TOD) serial data and the ability to synchronize the 1 PPS output to an incoming 1 PPS signal and to set the time-of-day. This kind of time-keeping is possible because the microcomputer and ASIC give the unit a flexibility and computing power not normally associated with a small, very low power oscillator. In fact, the MCXO can be interfaced with a user system in a variety of ways. Figure 4 illustrates three of these options. In Figure 4.1, the microcomputer functions associated with the MCXO are absorbed by the central processing unit of the host system. This might be done to take advantage of existing processing power in the user's system, to save power, or to add more complex timekeeping modes. The MCXO then just consists of the calibrated dual mode oscillator supplied to the user with a calibration curve. In certain applications the entire frequency correction algorithm can be deleted because only

knowledge of the frequency is required, not constant frequency. Figure 4.2 illustrates a more conventional application of an oscillator, where the user supplies DC power and the oscillator provides a frequency, and they don't have much else to say to each other. However, even in this application, the MCXO is different because of the previously mentioned optional TOD and calibration interfaces. Figure 4.3 illustrates the other extreme, in which the computational power of the MCXO is used to perform additional timekeeping functions. These could include aging prediction and correction, slewing to synchronization, or other operations on the unit output.

5.0 DESCRIPTION OF THE MCXO's OUTPUT

Referring to the block diagram in figure 1, the 10 MHz output of the MCXO is generated by locking the difference between the VCXO output (at 10 MHz) and the overtone output of the dual-mode oscillator to the synthesizer output. The output frequency becomes Fout = Fo + Fd. The output spectrum will depend on the spectrum of all three sources, modified by the filtering effect of the PLL. To the first order the PLL will act as a low pass filter to the sum of the single-sided phase-noise spectra of Fo and Fd. For sideband offset frequencies larger than the PLL bandwidth, the output spectrum will be that of the VCXO itself. A unity-gain frequency of 10 Hz for the PLL was selected as a compromise between sideband reduction and a low PLL noise floor. The spurious frequencies from the DDS, and the PLL reference frequency, are filtered by the narrow PLL bandwidth.

6.0 Time Domain

An important characteristic of the MCXO's internal operation is that the synthesizer is often changing frequency as the ambient temperature changes and new corrections are computed. The effect on the output of these frequency steps will be examined in this section.

If the phase of the signal into a PLL is abruptly stepped, the phase error in the output will appear as is shown in figure 5. If the frequency of the input to the PLL is stepped, there are two possible cases. The phase and frequency may step, or the phase may be continuous while the frequency is stepped. This latter case holds true for the MCXO, since phase continuity is a characteristic of an appropriately designed DDS. Consequently, the output of the MCXO does not exhibit phase or frequency "jumps".Figure 6 shows an experimental method for observing the phase of the MCXO output. The unit under test drives one port of a double balanced diode mixer. The other mixer input is driven by a 10 MHz frequency standard. The filtered, amplified, output of the mixer can be examined on an oscilloscope. Figure 7 shows an oscilloscope trace resulting from such an experiment. As

the MCXO makes corrections, the slope of the phase trace changes ($\omega = d\theta / dT$) . But the curve is smooth and continuous, with no evidence of discontinuities.

Although this is an interesting way to observe the MCXO output at room temperature, it does not address the question of phase error under extreme conditions. To calculate the maximum phase error, one must find the maximum frequency step into the PLL. The MCXO thermal time constant, from case to crystal, is 16 minutes, measured on a prototype unit. Assuming an ambient temperature step of 100 degrees centigrade, the maximum slope of temperature vs. time is;

(1) $dT / dt = 100^{\circ} \times 1 / (\text{time constant})$

$= 100^{\circ} / 16 \times 60 = 0.104$ degrees/sec.

The MCXO makes corrections approximately once every 1/3 second, so delta T max. = 0.104 x 1/3 = .035 degrees. At a starting temperature where the crystal frequency-temperature curve is steepest ($\simeq$ 1 ppm / degree C.), the maximum frequency change is .035 ppm, or .35 Hz. Referring to figure 8, the maximum phase error with that input will be:

$d\theta = 0.44 \times \text{delta } f / f \text{ loop}$

$= 0.44 \times .35 / 10 = 0.154$ radians, or about 10 degrees.

Clearly, the loop will remain well behaved under these worst-case assumptions, and the output phase will exhibit no discontinuities.

7.0 Conclusion

The MCXO provides a combination of accuracy, low aging, and low power heretofore unavailable in precision oscillators. It's ability to provide time-of-day and synchronization, in addition to other timekeeping functions, provides the user with considerable flexibility in it's applications. Although using digital frequency correction, the use of a synchronous DDS and clean-up PLL makes the correction process smooth and phase-continuous.

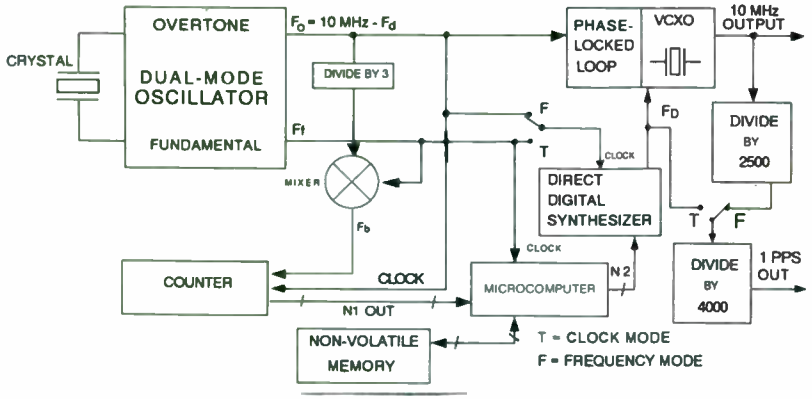

Figure 1

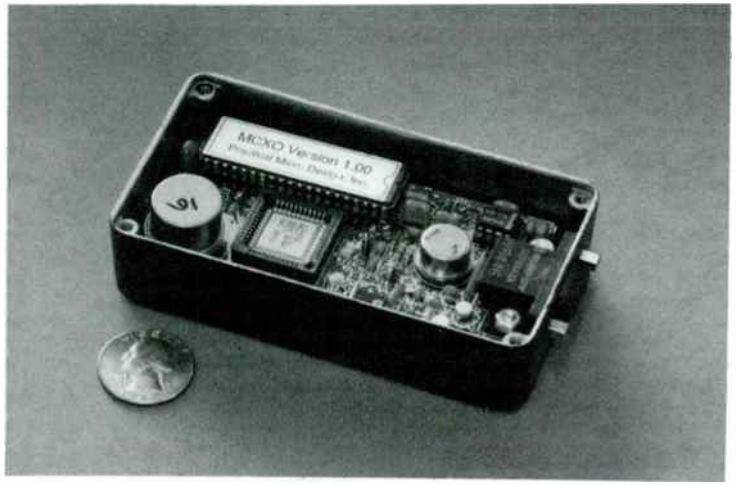

Figure 2

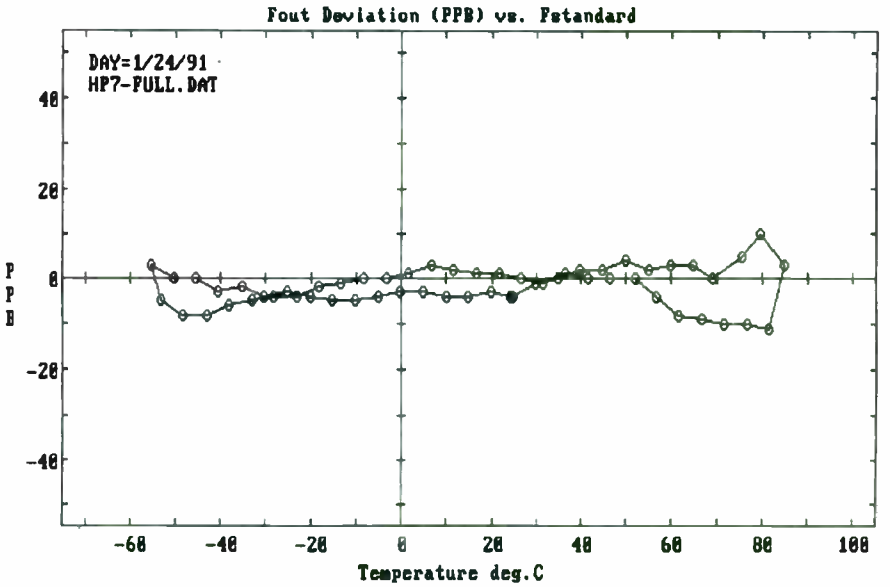

Figure 3

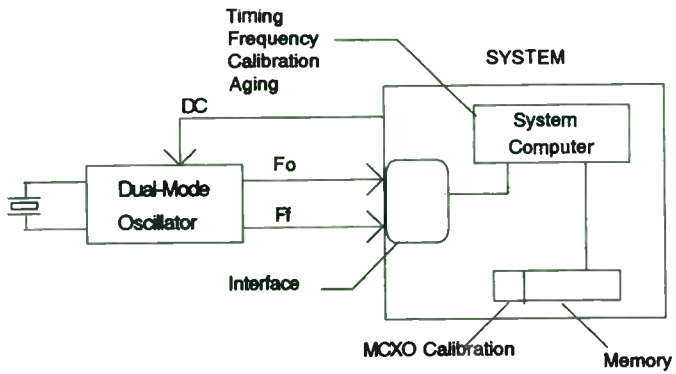

Figure 4.1

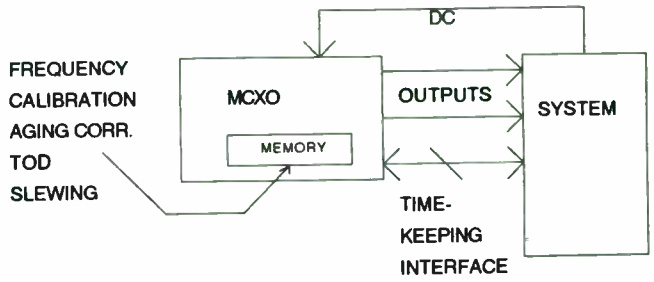

Figure 4.3

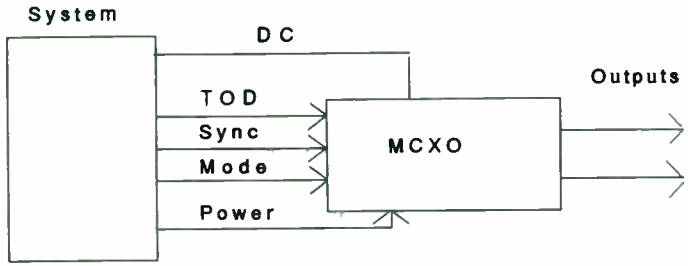

Figure 4.2

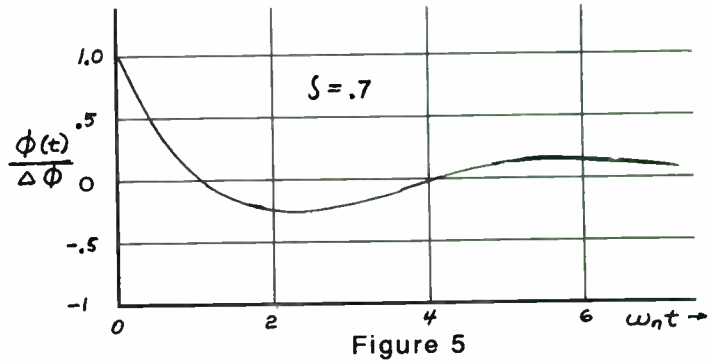

Figure 5

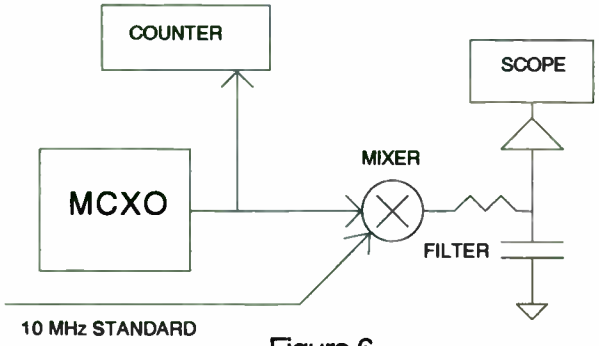

Figure 6

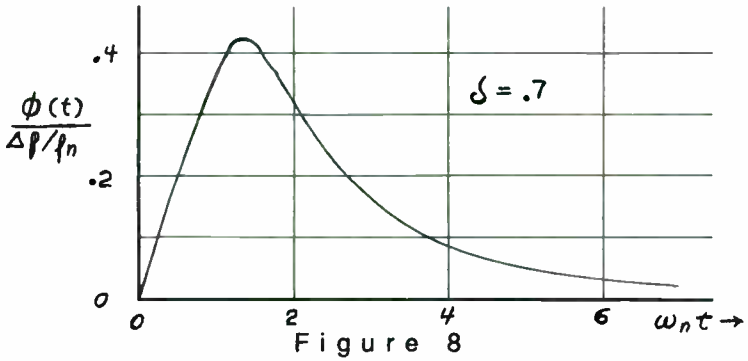

Figure 8

Counter, T = 10 S., ppB

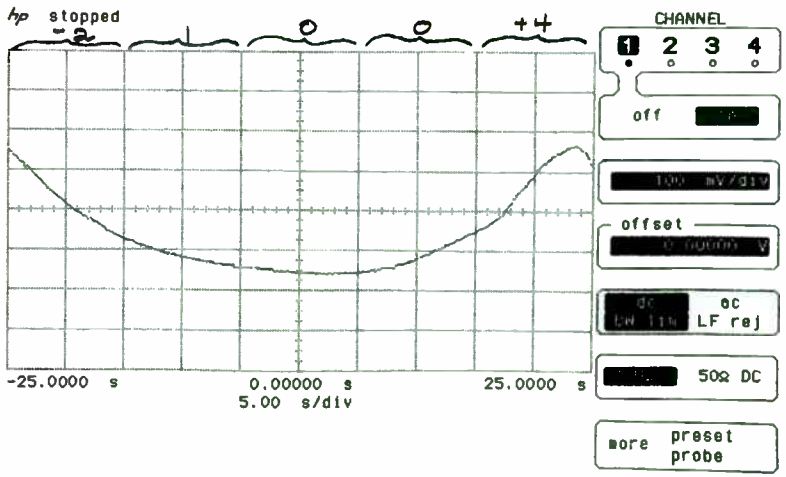

Figure 7

Microwave Oscillator Design
Demonstrated at 300 MHz Using SAW Filter/Resonators

by

Robert J. Weber
Department of Electrical Engineering and Computer Engineering
and
Microelectronics Research Center
Iowa State University
Ames, Iowa 50011

Abstract

The press of modern technology has required that the design of electronic circuits proceed in a timely but sure fashion. This is especially important in the design of MMICs (monolithic microwave integrated circuits). This paper summarizes a procedure that will help expedite the design of a microwave oscillator. The procedure is demonstrated using a SAW filter both as a two port device and a one port device. The SAW filter is used as a one port device in order to demonstrate the design of an oscillator having a high external Q and using a one port resonator.

Introduction

The procedures to be discussed in this paper are applications of the result of articles published previously but are described here using high Q resonators derived from SAW devices. The design is based upon a 2 Watt, 900 MHz stud mounted device. This paper will discuss 1) the active device characterization, 2) the termination impedances for a shunt oscillator, 3) some noise and stability considerations, and 4) a use of the SAW filter in a loop oscillator.

Device Characterization

The SAW filter is a nominally 300 MHz device used in this paper both in a one port and in a two port configuration. The power dissipated in the device has not been calculated. Therefore, the reader should consider the amount of power dissipated in the device before committing the device to use in a power oscillator. The active device chosen for the oscillator has a gain bandwidth product well above the operating frequency to minimize the power passed to or through the SAW device.

The device chosen for this oscillator demonstration was a Motorola MRF890. This is a 2 Watt, 900 MHz part. This part will allow an oscillator design for a least 2 Watts of output power at 300 MHz.

Figure 1 shows the calculation for the load on a part to produce optimum Class A power conversion efficiency from the DC power supply to output power. For this part, used at 21 volts for Vce and 155 mA for Icc, and using a nominal 3 pF for the output capacity, the optimum load is 82.154 + j 55.76 at 300 MHz. This represents a load of 120 ohms in parallel with an inductance of 176.8 ohms reactance to parallel resonate the output capacity of the part.

The S parameters for the device were measured using a fixture like that shown in Figure 2. The part was measured at full bias in the Class A mode using an HP8753C network analyzer. Extra attenuation was used on the output to prevent the device from over driving the network analyzer. The scattering parameters were measured from lov frequencies to high frequencies to allow the calculation of negative resistance output impedances over the possible frequency range for the completed oscillator. This will be described in more detail in the section on oscillator design.

The measured scattering parameters follow in EEsof Touchstone format.

```
! MOTOROLA MRF890
! VCE=19V IC=150mA
# GHZ S MA R 50
! SCATTERING PARAMETERS:
```

0.04	.633	-166	24.0	146.2	.00638	61	.655	5.49
0.1	.737	-175	14.52	118.6	.00988	56	.538	-18.9
0.2	.752	178	8.04	98.5	.0138	62.3	.464	-32.0
0.3	.757	173.5	5.40	88.2	.0190	67.1	.463	-39.6
0.4	.760	169.4	4.19	78.1	.0243	69.2	.440	-49.3
0.5	.760	165.5	3.40	69.4	.0298	71.4	.447	-56.6
0.6	.753	161.9	2.85	61.1	.0355	70.9	.460	-63.6
0.7	.743	156.8	2.45	53.7	.0422	72.4	.470	-69.4
0.8	.730	152.5	2.15	46.6	.0490	71.9	.483	-75.5
0.9	.717	148.5	1.90	39.8	.0562	71.0	.498	-81.2
1.	.707	144.1	1.70	33.6	.0638	70.5	.506	-86.5
2.	.746	90.5	.803	-19.5	.164	43.8	.566	-147.6

The test fixture had an active bias circuit on it to control the bias of the MRF890 device. The inductor used for bias insertion to the fixture was parallel resonant at 300 MHz. This is the same inductor that should be used in the oscillator circuit when it is built.

The S parameters of the SAW filter were measured as well in the same fixture. Those S parameters follow here.

```
! RFMONOLITHICS SAW RESONATOR S PARAMETERS - 303.5 MHz
# GHZ S MA R 50
```

0.298000	0.986	-14.262	7.4E-03	-102.464	7.4E-03	-102.464	0.986	-14.262
0.301000	0.986	-14.285	0.010	-103.387	0.010	-103.387	0.986	-14.285
0.301400	0.986	-14.288	0.010	-103.510	0.010	-103.510	0.986	-14.288
0.301800	0.986	-14.291	0.011	-103.634	0.011	-103.634	0.986	-14.291
0.302200	0.986	-14.294	0.011	-103.757	0.011	-103.757	0.986	-14.294
0.302600	0.986	-14.297	0.011	-103.880	0.011	-103.880	0.986	-14.297
0.303000	0.986	-14.300	0.012	-104.003	0.012	-104.003	0.986	-14.300
0.303305	0.984	-15.050	0.022	-108.153	0.022	-108.153	0.984	-15.050
0.303325	0.984	-15.250	0.025	-108.753	0.025	-108.753	0.984	-15.250
0.303345	0.983	-15.450	0.028	-109.353	0.028	-109.353	0.983	-15.450
0.303365	0.982	-15.650	0.032	-109.953	0.032	-109.953	0.982	-15.650
0.303385	0.982	-15.850	0.035	-110.553	0.035	-110.553	0.982	-15.850
0.303405	0.980	-16.139	0.040	-111.799	0.040	-111.799	0.980	-16.139
0.303415	0.979	-16.420	0.045	-113.401	0.045	-113.401	0.979	-16.420
0.303425	0.978	-16.699	0.050	-114.998	0.050	-114.998	0.978	-16.699
0.303435	0.974	-16.980	0.056	-117.002	0.056	-117.002	0.974	-16.980
0.303445	0.970	-17.260	0.063	-119.001	0.063	-119.001	0.970	-17.260
0.303455	0.965	-17.750	0.072	-122.003	0.072	-122.003	0.965	-17.750
0.303465	0.954	-18.548	0.088	-126.995	0.088	-126.995	0.954	-18.548
0.303475	0.931	-19.500	0.113	-135.504	0.113	-135.504	0.931	-19.500
0.303485	0.884	-19.899	0.148	-151.253	0.148	-151.253	0.884	-19.899
0.303495	0.814	-17.999	0.187	-176.003	0.187	-176.003	0.814	-17.999
0.303505	0.819	-10.600	0.180	148.998	0.180	148.998	0.819	-10.600
0.303515	0.884	-8.675	0.138	126.527	0.138	126.527	0.884	-8.675
0.303525	0.930	-9.125	0.101	111.998	0.101	111.998	0.930	-9.125
0.303535	0.953	-9.949	0.077	104.007	0.077	104.007	0.953	-9.949
0.303545	0.964	-10.700	0.060	99.248	0.060	99.248	0.964	-10.700
0.303555	0.970	-11.379	0.050	96.801	0.050	96.801	0.970	-11.379
0.303565	0.976	-11.939	0.042	95.399	0.042	95.399	0.976	-11.939
0.303575	0.981	-12.498	0.035	94.002	0.035	94.002	0.981	-12.498
0.303585	0.981	-12.700	0.030	94.397	0.030	94.397	0.981	-12.700
0.303595	0.981	-12.900	0.025	94.797	0.025	94.797	0.981	-12.900
0.303610	0.979	-13.250	0.020	101.488	0.020	101.488	0.979	-13.250
0.303630	0.972	-13.250	0.022	119.997	0.022	119.997	0.972	-13.250
0.303650	0.980	-13.175	0.025	100.011	0.025	100.011	0.980	-13.175
0.303670	0.984	-13.300	0.020	88.501	0.020	88.501	0.984	-13.300
0.303690	0.985	-13.375	0.017	85.248	0.017	85.248	0.985	-13.375
0.303900	0.985	-13.900	5.0E-03	80.997	5.0E-03	80.997	0.985	-13.900
0.304300	0.985	-14.005	3.7E-03	80.486	3.7E-03	80.486	0.985	-14.005

Notice that the S parameters were taken at very small frequencies steps in the range of the resonant frequency and at coarser frequency steps outside the resonant frequency range. Well away from resonance, the device appears to be very close to 1.3 pF at each terminal. This value was used in the stability analysis of the oscillator away from resonance. These values were obtained in the test fixture used and may not represent the device in other test fixtures. It is important to measure the device in the configuration it will be used in.

Oscillator Design

Now that the device and filter S parameters are known, it is necessary to determine the optimum impedances to put on the device. It has been shown that the optimum common terminal impedance for the oscillator shown in Figure 3 is (1):

```
NUM(Gin) = Gopt(2*S12*S21*S31 -   S12*S31*S31
               + S11*S32*S31 - 2*S11*S22*S31)
 + Gopt*Gct(2*S12*S31*S23*S31 - 2*S12*S21*S33*S31
          - 2*S13*S31*S31*S22 + 2*S11*S22*S33*S31
               - S12*S31*S31 - 2*S11*S23*S31*S32
               + S11*S32*S31 + 2*S13*S31*S21*S32)
          + Gct(  S12*S31*S31 -   S11*S32*S31
              + 2*S13*S31*S31 - 2*S11*S33*S31)
   + (2*S11*S31 + S12*S31*S31 -   S11*S32*S31)

     DEN(Gin) = Gopt(S31*S32 - 2*S22*S31)
   + Gopt*Gct(2*S22*S31*S33 - 2*S23*S32*S31 + S31*S32)
               - Gct(S32*S31 + 2*S31*S33)
                    + (2*S31 - S32*S31)

               Gin = NUM(Gin)/DEN(Gin)
```

where Sij are the three port S parameters of the device, and where Gin is the input reflection coefficient for an oscillator with the terminal impedances between the output and the common terminal of the device being the optimum impedance for power transfer, Gct is the reflection coefficient for the impedance on the common terminal, and Gopt is the reflection coefficient of the impedance which gives optimum power conversion out of an amplifying device. This equation can be solved as has been presented previously and giving values for Gin and Gct. With these values, Gout of the device can be calculated using standard calculation procedures. It has also been shown that this equation can be solved using circles in the complex plane to describe the loci for Gin and Gct (2,3). The three port S parameters of the device are either measured or derived from the two port parameters. The calculations in the paper were from derived three port S parameters.

The results of that calculation are given by the following computer output listing.

Program Data Output is:

```
ENTER Z0
      50.000000
ENTER      2     FOR 2 PORT DATA
ENTER      3     FOR 3 PORT DATA
           2
ENTER      S     FOR S PARAMETERS
ENTER      Z     FOR Z PARAMETERS
ENTER      Y     FOR Y PARAMETERS
S
ENTER THE S PARAMETERS IN  VOLT-MAGNITUDE
                           PHASE-DEGREES
ENTER S11,S12,S21,S22
      .7570          173.5
    1.9000E-02       67.10
     5.400           88.20
     .4630          -39.60
```

```
ENTER THE OPTIMUM IMPEDANCE
      82.154000       55.760000
ENTER DATA FOR GAMMA SOURCE
ENTER THE TYPE OF INPUT YOU WISH
ENTER  QE  FOR EXTERNAL Q
ENTER  QU  FOR UNLOADED Q
ENTER  QL  FOR LOADED Q
ENTER  MA  FOR MAGNITUDE OF GAMMA
ENTER  CR  FOR CENTER AND RADIUS OF CIRCLE
MA
ENTER RADIUS OF REFLECTION COEFFICIENT
   7.800000E-01
ENTER THE DATA FOR GAMMA COMMON TERMINAL
ENTER THE TYPE OF INPUT YOU WISH
ENTER  QE  FOR EXTERNAL Q
ENTER  QU  FOR UNLOADED Q
ENTER  QL  FOR LOADED Q
ENTER  MA  FOR MAGNITUDE OF GAMMA
ENTER  CR  FOR CENTER AND RADIUS OF CIRCLE
MA
ENTER RADIUS OF REFLECTION COEFFICIENT
   9.500000E-01
RADIUS FOR 1          1.282051
RADIUS FOR 2      9.500000E-01
CENTER FOR 1,1       (0.000000E+00,0.000000E+00)
CENTER FOR 1,2       (0.000000E+00,0.000000E+00)
CENTER FOR 2,1       (0.000000E+00,0.000000E+00)
CENTER FOR 2,2       (0.000000E+00,0.000000E+00)
MAG3 =     9.500000E-01 OR     9.500000E-01
SOLUTION ONE
REFLECTION COEFFICIENTS IN MAG AND ANGLE-DEG
  INPUT REFLECTION COEFFICIENT IS     1.282051       -178.2359
2PORT LOAD REFLECT COEFFICIENT IS     .4487481        37.15366
GROUND INVERSE REF COEFFICIENT IS     1.052632        169.2688
 SOURCE REFLECTION COEFFICIENT IS     .7800002        178.2359
3PORT LOAD REFLECT COEFFICIENT IS     .4650027        39.00406
 GROUND REFLECTION COEFFICIENT IS     .9500000       -169.2688
IMPEDANCES IN REAL AND IMAGINARY FORM
                INPUT IMPEDANCE IS    -6.181211       -.7580125
       TWO PORT LOAD IMPEDANCE IS     82.15400        55.76000
GAMMA INVERSE GROUND IMPEDANCE IS    -1.293354        4.693004
              SOURCE IMPEDANCE IS     6.181211        .7580124
     OSCILLATOR LOAD IMPEDANCE IS     79.40652        59.30091
              GROUND IMPEDANCE IS     1.293354       -4.693004
ENTER CARRIAGE RETURN TO CONTINUE
SOLUTION TWO
REFLECTION COEFFICIENTS IN MAG AND ANGLE-DEG
  INPUT REFLECTION COEFFICIENT IS     1.282051       -1.149943
2PORT LOAD REFLECT COEFFICIENT IS     .4487481        37.15366
GROUND INVERSE REF COEFFICIENT IS     1.052632        32.82293
 SOURCE REFLECTION COEFFICIENT IS     .7800000        1.149943
3PORT LOAD REFLECT COEFFICIENT IS     .9765146        28.91561
 GROUND REFLECTION COEFFICIENT IS     .9500000       -32.82293
```

Notice that two solutions are given. In general one or both may not be realizable, however, for this device with these operating conditions, both solutions are realizable. Solution one was chosen since it requires less resistance in the common terminal. Since the collector and the base current flows through the emitter, the minimum resistance in that terminal was chosen. The magnitude of the reflection coefficient was chosen to be 0.95 to allow the use of a high but finite Q in the feedback impedance in the common terminal. A good technique would be to calculate the parameters using infinite Q in the common terminal feedback first and see approximately where the impedance lies and then establish the reflection coefficient magnitude or to use the Q option for Gct. The magnitude of the impedance on the input was derived from the locus of the S parameters of the SAW resonator.

The results of the above calculations were input into EEsof's Touchstone program for calculation. The final Touchstone file is given:

```
DIM
  FREQ GHZ
  RES OH
  IND NH
  CAP PF
  LNG MIL
  TIME PS
  COND /OH
  ANG DEG
VAR
CKT
 IND 1 0 L=0
 GROUND ON THE INPUT OF THE TWO PORT RESONATOR
 RES 1 0 R=1000000
 S2PC 1 3 0 SAW2PNEW.S2P
 TWO PORT RESONATOR S PARAMETER FILE
!
! REPLACE ABOVE WITH A 1.3 pF CAPACITOR FOR STABILITY CHECK
!  CAP 3 0 C=1.3
!
  IND 3 0 L=211.5
! INDUCTOR TO MAKE INPUT OF RESONATOR REAL AT f0
!
```

```
! TLIN 3 4 Z=400 E=80 F=.3035
! TRANSMISSION LINE TO VARY PHASE BETWEEN DEVICE AND RESONATOR
!
!
  CAP  3 0 C=.8622
  IND 3 40 L=137.92
  CAP 40 0 C=.8622
  IND 40 4 L=137.92
! TWO SECTION PHASE SHIFTER TO ROTATE LIKE 80 DEGREE TRAN. LINE
!
  CAP 4 0 C=1.3
!
  CAP 4 0 C=8.9905567
  IND 4 9 L=26.899963
  CAP 9 0 C=19.91439
! MATCH FROM INPUT OF TRANSISTOR
!
  CAP 9 31 C=10.48
  IND 9 31 L=26.24
  RES 31 0 R=75
! TANK TO DAMP OUT 600 MHZ AREA
!
  TLIN  9 10 Z=50 E=8.8413559 F=1
! ABOVE IS .2 INCH IN Er=2.45 MICROSTRIP
  S2PA 10 11 12 MOT890.S2P
  CAP 12 13 C=113.044
! EMITTER FEEDBACK CAPACITOR
  RES 13 0 R=1.2933
! EMITTER FEEDBACK CAPACITOR SERIES RESISTOR
  TLIN 11 15 Z=50 E=8.8413559 F=1
! ABOVE IS .2 INCH IN Er=2.45 MICROSTRIP
  IND 15 0 L=31.65144
  CAP 15 16 C=8.96736
! SHUNT L SERIES C OUTPUT MATCH
! RES 16 0 R=50
! OSCILLATOR LOAD COMMENTED OUT TO LOOK AT OUTPUT
  S2PB 16 17 0 INVERT.S2P
! ABOVE IS AN NEGATIVE IMPEDANCE INVERTER APPROXIMATION
! IT LETS TOUCHSTONE PLOT NEGATIVE IMPEDANCES ON THE SMITH CHART
  DEF1P 17  A
FREQ
!SWEEP .04 2  0.04   !  used for broadband stability check
SWEEP  .3034 .3036 .00002 ! used for inband impedance check
OUT
  A  S11
  A RE[Z1]  GR1
  A IM[Z1]
GRID
   RANGE .04 2 .04
   GR1  -100 25 25
   GR2  -180 180 20
```

Several features are shown in the listing. A two section lumped constant phase shifter is given. The calculation was done with a TLine line phase shifter shown in the listing. The required phase shift for optimum output impedance was chosen as 80 degrees. Figures 5, 6, and 7 shows the output impedance for three different values of phase shift. What is plotted in the figures is the negative of the output impedance. Since a negative impedance converter does not have a finite S matrix, the S matrix of the negative impedance inverter is approximated in Touchstone by the following S parameter matrix which appears to work with minimum roundoff error.

```
! INVERTER
# GHZ S MA R 50
! SCATTERING PARAMETERS:
!  1.E4 SEEMS TO WORK BETTER THAN 1.E5 FOR THESE IMPEDANCE RANGES
```

Converting this matrix to an ABCD matrix (which has a finite negative impedance converter matrix), we get A=1.00005, B=0.0025, C=0.000001, and D=-0.99995. Using these values, it can be shown that:

$$Zin = \frac{1.00005 + (0.0025/Zload)}{-0.000001*Zload - (0.99995/Zload)} = Zload$$

for moderate ranges of Zload around fifty ohms in magnitude.

A typical set of output runs would look like.

FREQ-GHZ	RE[Z1] A	IM[Z1] A	RE[-Z1] A	IM[-Z1] A
0.303400	25.338	30.644	-25.329	-30.633
0.303420	19.854	30.649	-19.854	-30.650
0.303440	13.860	31.274	-13.852	-31.253
0.303460	4.926	30.040	-4.925	-30.031
0.303480	-14.134	25.152	14.142	-25.174
0.303500	-51.210	-0.358	51.300	0.358
0.303520	-44.764	-126.260	44.638	126.198
0.303540	98.783	-91.158	-98.770	91.145
0.303560	100.924	-18.820	-100.903	18.822
0.303580	78.349	6.487	-78.328	-6.483
0.303600	72.326	15.078	-72.313	-15.074

The output plot of the oscillator using the negative impedance inverter to plot -Zout is shown in Figure 5 for no phase shift and in Figure 6 for 80 degrees of phase shift and in Figure 7 for a lumped constant phase shifter.

Stability Calculation

In the Touchstone file above, the stability network to prevent oscillation at a frequency not controlled by the SAW is added to damp oscillations at 600 MHz. The output impedance plots for the oscillator with and without the suppression network are shown in Figures 8 and 9.

Loop Oscillator

The loop oscillator design equations are given in Figure 10, A brief description of a loop oscillator design follows.

```
! date:  July 31, 1991
! Loop Oscillator
DIM
  FREQ GHZ
  RES OH
  IND NH
  CAP PF
  LNG MIL
  TIME PS
  COND /OH
  ANG DEG

VAR

CKT
!
! CAP 9 0 C=9.33
!  ABOVE MINUS 1.3 PF FOR SAW
  CAP 9 0 C=8.03
  IND 1 9 L=26.899963
  CAP 1 0 C=19.91439
! MATCH FROM INPUT OF TRANSISTOR
!
  TLIN  1 20 Z=50 E=8.8413559 F=1
! ABOVE IS .2 INCH IN Er=2.45 MICROSTRIP
  S2PA 20 21 0 MOT890.S2P
  TLIN 21 2 Z=50 E=8.8413559 F=1
! RES 2 0 R=115
  IND 2 0 L=83
!  LOOP CLOSURE
  CAP 2 5 C=.75
  TLIN 3 5 Z=285 E=245.5 F=.3035
  s2pB 3 9 0 SAW2PNEW.S2P
  IND 3 0 L=214.8
  RES 3 0 R=425

  IND 2 7 L=31.5
  CAP 2 0 C=5.198
!MATCH TO 50 OHMS FROM 115 OHMS
!PHASE SHIFT TO GET REACTANCE ACROSS REAL LINE
  TLIN 7 8 Z=50 E=40 F=.3035
  S2PC 8 10 0 INVERT.S2P

!  DEF2P  4 2    RESON
   DEF1P 10 RESON

OUT
   RESON S11
!  RESON DB[S22] GR2
!  RESON DB[S11] GR2
!  RESON DB[S21] GR1
!  RESON ANG[S21] GR3
!  RESON ANG[S11] GR3
!  RESON RE[Z2]
!  RESON IM[Z2]
   RESON RE[Z1]
   RESON IM[Z1]
FREQ
   SWEEP .30345 .30355 .00001
!  SWEEP .2999 .29991 .00001

GRID
   RANGE  .3033 .3038 .0001
   GR1  -30 0 5
   GR2  0 -10 2
   GR3 -180 180 20
```

The output calculation follows listed as negative Zout.

FREQ-GHZ	RE[-Z1] RESON	IM[-Z1] RESON		RE[-Z1] RESON	IM[-Z1] RESON
0.303450	-9.559	14.565	0.303510	40.934	-26.159
0.303460	-6.004	18.571	0.303520	24.077	-35.836
0.303470	0.258	24.568	0.303530	12.292	-35.470
0.303480	13.462	29.429	0.303540	4.919	-32.887
0.303490	34.848	24.129	0.303550	0.201	-30.286
0.303500	50.937	-0.563	0.303550	0.181	-30.259

Conclusion

A design sequence has been presented which shows a technique using a high Q resonator for the design of microwave oscillators. Although the frequency was 300 MHz, the same type of design would be done for a MIMIC at higher microwave frequencies including up into the millimeter wavelength range.

Acknowledgments

The author would like to acknowledge the provision of parts from Motorola and from RF Monolithics as well as the provision of Touchstone software from EEsof.

Bibliography

1. R. J. Weber, "Oscillator Design Using S-Parameters and a Predetermined Source or Load", 45th Annual Symposium on Frequency Control, May 1991.

2. R. J. Weber, "A Microwave Oscillator S-Parameter Design Technique and Computer Algorithm," 34th Midwest Symposium on Circuits and Systems, May 1991.

3. R. J. Weber, "Oscillator Design Techniques Using Calculated and Measured S-Parameters," Tutorial presented at the 45th Annual Symposium on Frequency Control, May 1991.

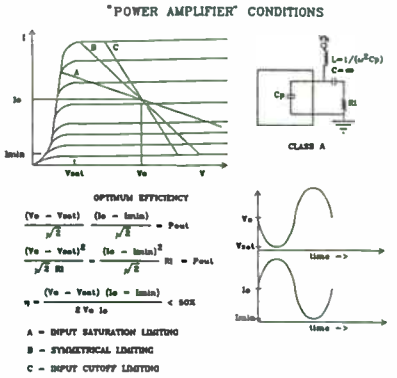

FIGURE 1: LOAD LINE CONSIDERATIONS

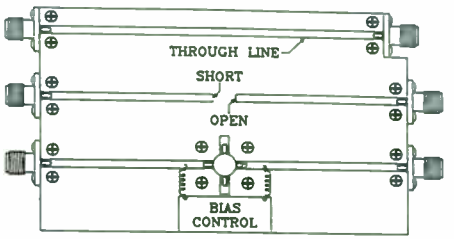

Figure 2: Test Fixture Drawing

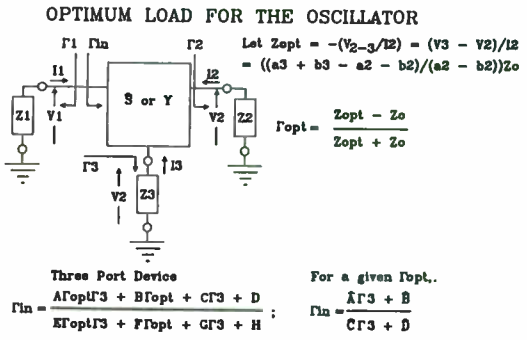

Figure 3: Three Port Oscillator Configuration

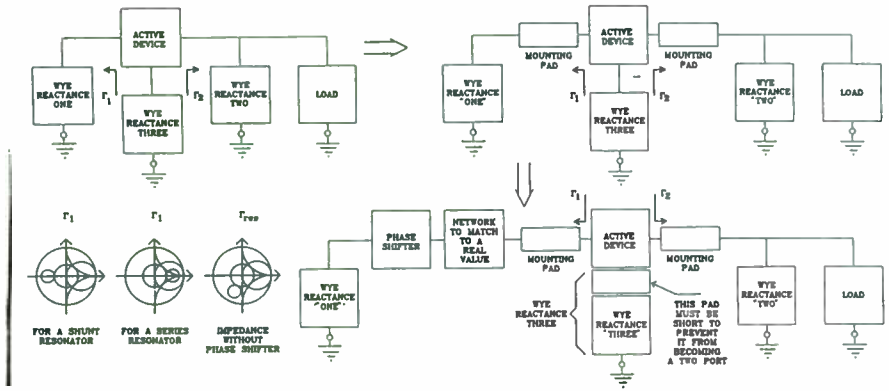

Figure 4: DESIGN SEQUENCE FOR A "TWO PORT - THREE PORT" OSCILLATOR

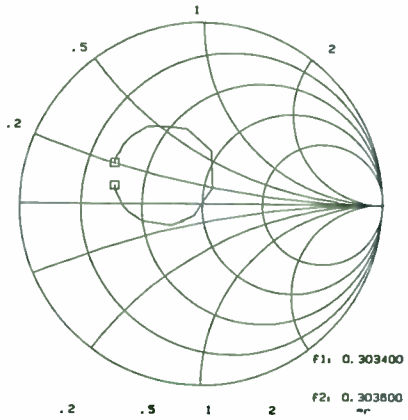

Figure 5: Plot of -Zout for no Phase Shifter

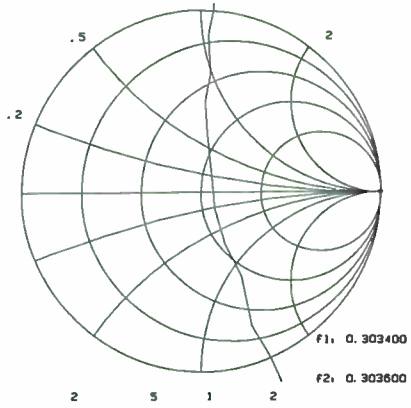

Figure 6: Plot of -Zout for 80 deg Phase Shifter

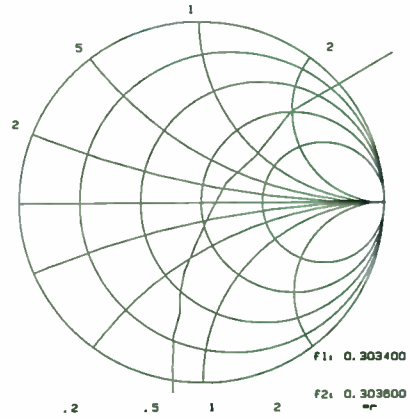

Figure 7: Plot of -Zout for Lumped Constant Phase Shifter

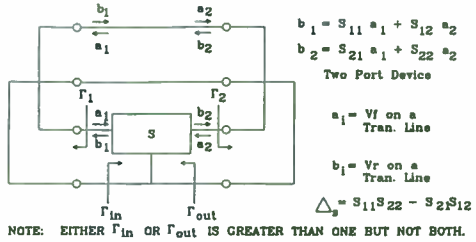

NOTE: EITHER Γ_{in} OR Γ_{out} IS GREATER THAN ONE BUT NOT BOTH.

CONDITION FOR OSCILLATION IS

$$1 - S_{21} - S_{12} - \Delta_s = 0$$

IF S_{11} & S_{22} ARE = 0

THEN

$$1 + S_{21}S_{12} - S_{21} - S_{12} = 0$$

LOOP OSCILLATOR CONDITONS - LOAD IS IN "S"

Figure 10: Loop Oscillator Design Equations

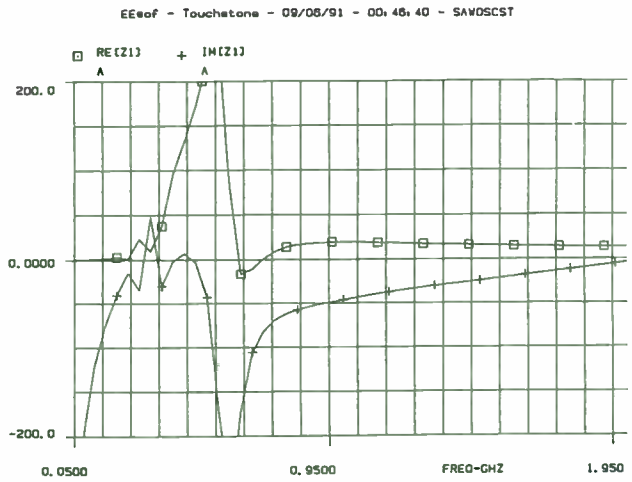

Figure 8: Output Impedance With no Suppression Network (Not valid at SAW resonance frequency)

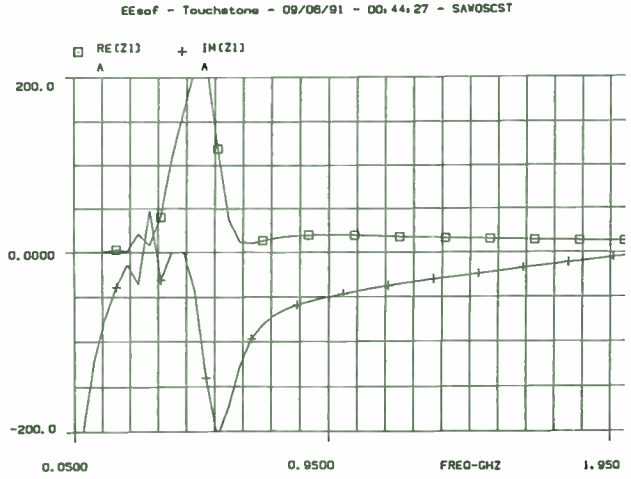

Figure 9: Output Impedance With the Suppression Network (Not valid at SAW resonance frequency)

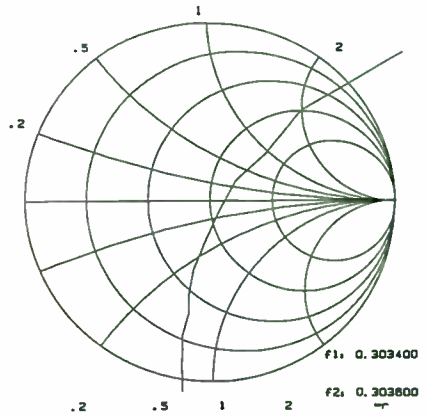

Figure 7: Plot of -Zout for Lumped Constant Phase Shifter

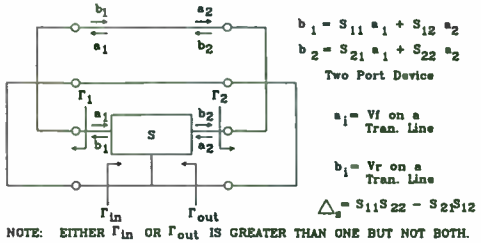

$b_1 = S_{11} a_1 + S_{12} a_2$

$b_2 = S_{21} a_1 + S_{22} a_2$

Two Port Device

a_i = Vf on a Tran. Line

b_i = Vr on a Tran. Line

$\Delta_s = S_{11}S_{22} - S_{21}S_{12}$

NOTE: EITHER Γ_{in} OR Γ_{out} IS GREATER THAN ONE BUT NOT BOTH.

CONDITION FOR OSCILLATION IS

$$1 - S_{21} - S_{12} - \Delta_s = 0$$

IF S_{11} & S_{22} ARE = 0

THEN

$$1 + S_{21}S_{12} - S_{21} - S_{12} = 0$$

LOOP OSCILLATOR CONDITONS - LOAD IS IN "S"

Figure 10: Loop Oscillator Design Equations

FINAL DRAFT, 9/6/91

DEVELOPMENTS AND DIRECTIONS IN 200 MHZ VERY HIGH POWER RF AT LAMPF

Richard Cliff, Edgar D. Bush, Russell A. DeHaven,
Harlan Ward Harris and Mark Parsons

Los Alamos National Laboratory (LANL)
Los Alamos Meson Physics Facility (LAMPF)
MP-8, MS H826, Los Alamos, New Mexico 87545

ABSTRACT

The Los Alamos Meson Physics Facility (LAMPF), is a linear particle accelerator a half-mile long. It produces an 800 million electron-volt hydrogen-ion beam at an average current of more than one milliamp.

The first RF section of the accelerator consists of four Alvarez drift-tube structures. Each of these structures is excited by an amplifier module at a frequency of 201.25 MHz. These amplifiers operate at a duty of 13 percent or more and at peak pulsed power levels of about 2.5 million watts.

The second RF accelerator section consists of forty-four side-coupled-cavity structures. Each of these is excited by an amplifier module at a frequency of 805 MHz. These amplifiers operate at a duty of up to 12 percent and at peak pulsed power levels of about 1.2 million watts.

The relatively high average beam current in the accelerator places a heavy demand upon components in the RF systems. The 201-MHz modules have always required a large share of maintenance efforts. In recent years, the four 201.25 MHz modules have been responsible for more than twice as much accelerator down-time as have the forty-four 805 MHz modules. This paper reviews recent, ongoing, and planned improvements in the 201-MHz systems.

The Burle Industries 7835 super power triode is used in the final power amplifiers of each of the 201-MHz modules. This tube has been modified for operation at LAMPF by the addition of Penning ion vacuum "pumps." This has enabled more effective tube conditioning and restarting. A calorimetry system of high accuracy is in development to monitor tube plate-power dissipation. Conversion of the driver amplifier for the 7835 from "plate-pulse modulated" to "drive-modulated" operation is planned. Development of a data acquisition and diagnosis system is in progress. Conversion to solid-state RF components where possible, modification of the Alvarez structure coaxial RF windows, replacement of the 7835 filament power supplies, and additional modifications to the 7835 tube are also under consideration.

1. ACCELERATOR CONSTRUCTION

The construction of LAMPF was proposed in 1962 and begun in 1968. In 1970 the first phase of construction was completed with the production of a proton beam at 5 million electron volts. A year later 100 million electron volts was achieved and the design energy of 800 million electron volts was attained the following year.

The facility was formally commissioned as the Clinton P. Anderson Meson Physics facility in 1972 in memory of the late Senator from New Mexico. An average beam current of one-half milliamp was achieved in 1978 and a current of one milliamp became routine after 1983.

The LAMPF accelerator was built in four principal sections: a very-low-energy electrostatic accelerator section (called the injector area), a low-energy RF accelerator section, a medium-energy RF accelerator section, and an experimental area. See Figure 1.1.

There are actually three electrostatic accelerators in the injector area. They are of the "Cockcroft-Walton" type and each contains its own hydrogen-ion source. These three accelerators all inject hydrogen-ion beams at 750 thousand electron volts into the low-energy RF accelerator. They may be operated simultaneously and their beams interleaved into the low-energy RF accelerator together.

The low-energy RF accelerator section operates at 201.25 MHz. It boosts the beam to 100 million electron volts for acceptance into the medium-energy RF accelerator section. See Figure 1.2. The low-energy accelerator consists of four resonant structures known as "Alvarez tanks." See Figure 1.3.

The medium-energy RF accelerator section operates at 805 MHz and boosts the beam to as much as 800 million electron volts for collision with targets in the experimental area. The forty-four accelerator segments of this section are of the "side-coupled-cavity" type. This structure was developed at Los Alamos for LAMPF and is now widely applied in similar applications.

2. ACCELERATOR OPERATION

LAMPF is unique in its high average particle flux, which reduces the time required to accomplish research objectives. Production

of this high flux beam has placed an increasing demand upon the RF systems. During the initial years of operation, RF duties were in the six to eight percent range. After 1978, duty was increased about three-quarters of a percent each year in an effort to produce significantly higher beam flux.

201-MHz duty reached about thirteen percent during the 1984 run, then was decreased to about 11.5 percent from 1985 until the beginning of 1989 to reduce power costs. Concern about 7835 tubes caused a reduction of 201-MHz RF duty to about ten percent for the 1989 run, but the 201-MHz duty was increased to about eleven percent in 1990 and back to about twelve percent for 1991.

All of the systems of the complex were originally sized for operation at a maximum beam duty of twelve percent. This corresponds to a maximum design 201-MHz RF duty of about 14.4 percent. By performance standards for such facilities, this is extreme. In comparison, radar and accelerator facilities capable of comparable power levels generally operate in the range of one-tenth percent to two percent RF duty.

It is also notable that operation has been pushed so close to the original design limits. All of the LAMPF systems were sized with relatively narrow duty margins. The 201-MHz systems, particularly, have in recent years encountered problems related to the combined requirement for high peak RF power levels and high duty.

The performance of 7835 tubes in operation at LAMPF declined after about 1982. This decline appears to correlate with a combination of factors: an order of magnitude reduction in annual tube production levels due to the retirement of military systems; discontinuance of tube RF testing at the factory as a cost-reduction measure instituted by customers; and increased RF duty at LAMPF. Low-duty users of the tube have seen relatively minor changes in 7835 performance during the same period.

The effects of LAMPF high-duty operation have begun to be felt on other parts of the 201-MHz systems. Advancing system age is a factor as well. Recently problems have been encountered in maintaining the 7835 filament power supplies and the RF driver amplifiers. Efforts are underway to replenish low stocks of spare parts through custom manufacturing and to replace components and subsystems which have become difficult to buy or support.

The 201-MHz systems have always required about as much RF system maintenance time as all of the 805-MHz systems taken together. See Figure 2. However, the accumulating effects of 201-MHz problems in recent years is clear. Even though there are forty-four 805-MHz modules and only four 201-MHz modules at LAMPF, the 201-MHz systems have come to be responsible for more than twice the amount of accelerator down-time during operating periods.

3. 201-MHZ RF SYSTEMS

The 201.25-MHz RF systems are designated as RF modules one through four. See Figure 3.1. Modules two through four are identical and module one is very similar to them. Each RF module feeds a corresponding Alvarez accelerator tank. Module one is required to produce RF power at only about 400,000 watts peak. Modules two, three and four are each required to produce about 2.6 million watts peak.

The control requirements on the modules are stringent. During each RF pulse, the module output amplitude is to be automatically maintained within +/- one percent of the amplitude required. At the same time, the output phase is to be held constant to within +/- one degree of that required. It is anticipated that these requirements may have to be tightened still more in the future.

The accelerator must be a coherent structure so a single RF source signal is used to drive all of the RF modules. The source oscillator used is stable to one part in one hundred billion. Its signal is frequency multiplied to provide drive for the RF modules at 201.25 and 805 MHz.

The phase of the distributed source signal is adjusted at each module and then fed to a solid-state interface amplifier (IFA). See Figure 3.2. The signal from the IFA drives the intermediate power amplifier (IPA) which drives the final power amplifier (PA) of each module. The output power of each PA is adjusted for amplitude control.

The intermediate power amplifiers were originally designed and built by RCA. Each IPA contains a chain of three vacuum tubes: two Burle 7651 tetrodes and a Burle 4616 tetrode. See Figure 3.3. The first 7651 accepts pulsed RF input from the IFA at a level of about 25 watts. This stage is a common-cathode amplifier with pulsed bias and produces output RF at about 300 watts.

The second 7651 is a common-cathode stage with constant bias and boosts the RF signal to about 5,000 watts. The 4616 is a common-cathode, constant bias stage operated in class B with pulsed plate and screen supplies. It is used to produce pulsed RF at about 150,000 watts, though it can put out much more. All three stages of the IPA have resonant input and output tuners constructed in coaxial "cavity" form.

The input of the 4616 is coupled with a "paddle-type" variable capacitor to a water-cooled coaxial "de-Qing" load. Variation of coupling of drive to this load permits amplitude control of the 4616 output over a wide range. In this application, this assists in adjusting to PA input drive requirements. The two 7651 tubes are air-cooled and the 4616 tube is water-cooled. The 4616 DC plate supply is series switched by a pulse modulator employing an Eimac 4CW100,000 tetrode.

The final power amplifiers were originally designed and manufactured by Continental Electronics. See Figure 3.4. Each PA contains a single Burle 7835 triode as a common-grid amplifier with a cathode resistor to provide RF self-biasing. The amplifier is enclosed in a pressure tank containing dry air at about 40 PSI to assist in holding off high voltage.

Input and output impedance matching is accomplished by coaxial sliding-stub tuners. Blocking of the DC plate voltage is realized by quarter-wave sections of large-diameter, dielectric-filled coaxial line which nest around the tube and parts of the input and output tuners.

Chilled air is circulated through the PA to cool amplifier parts and to assist in cooling the 7835. The center conductor of the input tuner of the amplifier is water-cooled where it contacts the tube cathode. The 7835 also requires plate, grid and cathode/filament cooling water.

The 7835 DC supply is series switched by a pulse modulator employing two Eimac 4CW250,000 tetrodes. Amplitude control of the PA output is accomplished by plate modulation, that is, variation of the modulator voltage drop. The RF output of the amplifier is a nine-inch coaxial line which quickly tapers in an adapter section to a fourteen-inch line.

The 7835 triode is constructed in a double-ended coaxial configuration. See Figure 3.5. The large physical size of the tube, about 14 inches in diameter by about 17 inches tall, makes this configuration advantageous for operation at frequencies up to 400 MHz. It allows the active input and output regions of the tube to be centered on the standing voltage maxima of the input and output tuners.

Inside the tube, 96 thoriated tungsten filaments are arranged in a ring about the central tube core. Grid wires are wound on supports between each of the filaments. The plate ring is outside of the filament and grid assembly. The tube can operate class-B common-grid under a DC plate supply of up to 40,000 volts and can produce output RF at up to 7.5 million watts peak at low duty.

Peak plate current can be up to 300 amps. The tube filaments require about 6800 amps at about 3.6 volts during operation. At such high current, there is a drop of over a volt in the conductors between the filaments and their supplies. Plate cooling-water flow required is in the range of 100 to 160 gallons per minute, depending upon tube plate-power dissipation.

Because of its large size, if the 7835 is not operated under sufficient RF drive, oscillation at a frequency of about 1.2 GHz can occur within the tube itself. This requires that the tube be operated under a pulsed plate supply and in a drive saturated condition in any application.

4. RECENT 7835 TUBE MODIFICATIONS

In the last few years, several aspects of the 201-MHz systems have attracted interest as possible areas for improvement. Improvement of the mean time before failure (MTBF) of the 7835 tube at LAMPF is the principal area in which work has been done to date. This has been a difficult problem for several reasons. First, no other user of the tube has experienced problems comparable to those encountered at LAMPF so no external assistance is available.

Second, resources which could be devoted to work on this problem have been limited. To date, very little formal failure analysis of problems has been possible. The principal LAMPF problem is continuing failure of tube ceramic plate insulators during operation. About two tubes per year have been lost this way since 1988.

Third, a total of only three of these tubes are operated at full power at LAMPF for only a portion of each year. The effects of changes in operating procedures and tube modifications take a long time to evaluate. Modifications must also wait on proposal evaluation, purchasing, and manufacturing lead time.

Several initial moves were made about three years ago, but the first successful action was taken at the insistence of J. Doss of MP-8 at LAMPF. After some discussion, it was decided to have a small Penning ion vacuum gauge installed on all tubes ordered for delivery to LAMPF. It was intended that these devices should serve as diagnostic vacuum gauges on the tubes.

The Penning gauge operates by ionizing gas molecules in a fairly hard vacuum. The gas ions are caused to strike a metal target and are then frequently trapped by sputtering in the target or against the gauge enclosure walls. The resulting ion current is proportional to vacuum quality and is measured to provide a reading of that quality. That is, the device operates as a vacuum gauge.

A bonus provided by this type of gauge, however, is the trapping of many of the gauge ions. As a result, the device also functions as a vacuum pump and is now generally referred to as an ion vacuum pump rather than a gauge. Beginning in 1990, a miniature "ion pump" of the Varian "Vacion" type, a "vacion" pump in everyday usage, was installed on all 7835 tubes manufactured for LAMPF. See Figure 4.1.

Because the device was so small, it was expected that it would not provide any improvement in tube vacuum. However, as the modified tubes were delivered and put into operation, surprises were provided by the new diagnostic information made available. Peculiarities were found in the filament turn-on gas burst. See Figure 4.2. This burst is a transient period of poor tube vacuum which occurs when the tube filaments are turned on.

In the 7835s at LAMPF, the amplitude of this filament warm-up gas burst increases for the first few hundred tube operating hours. It seems to peak out after a few hundred additional hours of operation. Then it does not decrease appreciably for thousands of additional operating hours.

It is reasonable to believe that the burst itself results from gas adsorbed to metal surfaces inside the tube. The gas is boiled off as the filaments heat up. A gas burst also occurs when RF is applied to the tube, which presumably heats additional internal tube surfaces. See Figure 4.3. But it is puzzling that much more gas evolves as tube aging proceeds.

When the tubes are first started, the bursts are relatively small and brief. It is more puzzling that the behavior persists for thousands of operating hours. After a start-up burst, the tube vacuum gradually improves to a level on the order of 10^{-5} torr, once the tube is over a few hundred hours old. But, even at several thousand hours of tube operation, the burst will occur whenever the tube is restarted.

Most puzzling, the burst makes its appearance unchanged even if a tube is operated under excellent vacuum for a period of days or weeks, then turned off only for seconds and restarted. As diagnostic data are accumulated, this pattern should become more explicable. It is fair to suspect that this operation is essentially normal under high duty requirement.

As additional operating experience and vacion current data became available, more remarkable results emerged. It was found that, in the general hurry to get back into service under normal operating conditions, it had previously been common practice at LAMPF to unknowingly operate these tubes in an excessively gassy condition.

Most surprising, it became apparent that the tubes would produce full power with little or no arcing at vacuum levels on the order of 10^{-4} torr. This capacity of the tube must be considered astounding. The effect on tube lifetime of this mode operation is difficult to quantify but could not be positive.

A new pattern for operation of these tubes was developed. The vacion "gauges" began to be used to pump the tubes down to operating vacuum more rapidly after turning the filaments back on. It was found that the new tube vacion "gauge" was an effective vacuum pump after all. See Figure 4.4.

This new pattern avoided operation of the tube at excessively poor vacuum. But it was probably shortening the useful life of the vacion gauge/pump by operating it in the poor vacuum condition instead. This kind of operation can cause a vacion pump to overheat and short out or at least to outgas. This abuse of the pumps was questionable but considered necessary under production conditions.

In response to concern about shortened vacion service life, although no vacion failures had been experienced, it was decided to have two of the vacion pumps installed on each tube instead of just one. This would enable extended "abusive" vacion pump operation, increase pumping speed and could be done for a nominal additional cost.

This modification of the 7835 tube has a unique appearance. However, several of these tubes have now been delivered and operated successfully. It is to be noted that no other user of the tube has decided to buy one of this type. At the same time, a search was initiated by R. DeHaven of MP-8 at LAMPF for a vacion pump which had a greater pumping capacity than the Varian type.

The volume available for installation of vacion pumps on the tube is severely limited. Also, it was determined that the diameter of the connecting tube could not be increased for improved gas conduction. A higher capacity pump would have a longer useful life on the tube, though it could not increase pumping speed. A pump no larger than the original but having a higher capacity was required.

An ion pump incorporating new technology recently developed by Perkin Elmer was found by W. Boedeker of MP-8. See Figure 4.5. These pumps include dual metal sputtering targets for better effectiveness on a variety of gases and incorporate more compact samarium-cobalt magnets.

The first two tubes manufactured with two Perkin Elmer pumps have been delivered, but neither has yet been operated. It should prove possible to operate the dual pumps simultaneously to

shorten the time needed for tube conditioning. Alternating operation of the pumps should greatly reduce pump overheating in poor vacuum conditions.

5. 7835 TUBE CALORIMETRY

Development of a calorimetry system with which to monitor average power dissipation in the 7835 tube was begun recently. It is hoped that this system will be a useful tool in attempting to achieve higher RF duty and power in routine operation in the future. Also, the ability to continuously monitor tube performance with good accuracy will enhance understanding and control of normal system operation. It should eventually provide useful tube-failure information as well.

Tentative plans call for the 7835 plate cooling-water flow and temperature change to be monitored in each PA. See Figure 5.1. Initial tests have indicated that it may be necessary to monitor other cooling water supplies as well. A high-accuracy temperature difference thermometer using platinum resistive temperature detectors (RTDs) has been developed by A. Browman of MP-DO and L. Hasenack of MP-8 at LAMPF. See Figures 5.2 and 5.3.

This difference thermometer uses precision operational amplifiers to boost the difference in voltage drops across a pair of RTDs supplied by matched constant-current sources. Component values are selected so that a thermometer output of one volt DC corresponds to a RTD temperature difference of one degree Celsius.

The difference thermometer must be calibrated for the pair of RTDs used. Calibration is performed in stirred water baths monitored by precision mercury thermometers and has correlated to within 0.05 C. This calibration method has not yet been checked by a NIST traceable lab.

The 7835 plate-cooling-water temperature change under normal operating conditions in the LAMPF systems is about six degrees. The indications are that this difference thermometer design is accurate in these systems to within one percent. Using the thermometer alone, it is possible to see the approximately 30,000 watts of beam loading very well against the roughly 2.5 million watts of plate dissipation.

Installation and testing of flowmeters in the water systems, test of computer monitoring of flow and of temperature difference, and calculation of average dissipation are in progress under the direction of M. Parsons of MP-8 at LAMPF. The advertised accuracy of the flow meters is +/- one-half percent of the full-scale reading.

It is likely that some surprises and adjustments still lie ahead in development of a system with satisfactory accuracy. However, results to date promise that it will be possible to closely monitor and continuously record relatively small changes in RF system performance and clear up many puzzling details of system behavior. It is planned to push ahead on this project as rapidly as possible.

6. CURRENT DIRECTIONS

At present, discussion of and planning for a number of modifications to the 201-MHz systems is in progress. Improvement of the 7835 MTBF will continue to receive as much attention as possible. The potential cost savings are considerable. Further adjustments in tube operating procedures may evolve.

It is also hoped that it will be possible to pursue a detailed analysis of the LAMPF ceramic failure mechanism. 7835 ceramic failures have always been a problem at LAMPF though the situation has become much more serious recently. See Figure 6.1. It seems significant that no other user of the tube has experienced difficulty in this area.

A plan to further modify the 7835 tube is under consideration at this time. This proposal was developed by E. Robertson, on loan from the US Air Force to the Materials Science and Technology Division at LANL, and J. Eshleman of Burle Industries. See Figure 6.2. The tube plate and grid seals to the two outer ceramic insulators are made by means of single steel retaining rings on the outer surfaces of the four insulator edges.

It is proposed to modify the construction of the tube so that each seal will be made by means of a pair of rings, one on the inner ceramic surface and one on the outer. Definition of the proposal for this effort is in progress and it may be undertaken soon.

It appears that high-duty operation is primarily responsible for the LAMPF ceramic failure problem. The failure mechanism is suspected to be an excessively uneven heating of the ceramic material. Three possible sources of this heating have been suggested. First, localized light carbon deposits appear to be associated with the point of failure in at least two cases. It is possible that some resistive mechanism is heating the ceramic material in such areas.

The second possibility is that RF heating of some metal parts of the tube becomes excessive at high duty, and localized ceramic heating results. The third possibility, suggested by E. Meyer of the Accelerator Technology Division at LANL, is that the ceramic material might be experiencing x-ray induced electron avalanche. It has been established that some x-rays are incident on the

insulators during operation of the tube. It is even possible that two or all three of these suspected heat sources is involved.

Another possible cause for the LAMPF 7835 ceramic failures is water from cooling system leaks contacting the tube during operation. There is excellent evidence that this has occurred on two occasions. Opinion is divided on whether this mechanism can be blamed for the full ceramic failure history. Another sore point has resulted from marking a number of tubes with temperature indicating paint in an effort to catch a record of ceramic heating. Several marked tubes have failed with a complete absence of high ceramic temperature indications.

All of the suspected mechanisms will be difficult, time-consuming, and expensive to test thoroughly. An initial analysis plan has been developed by E. Robertson. It is suggested that a state-of-the-art computer model of the insulator and seal structure be developed. The model would then be tested by strain gauge measurements during actual assembly of the seals at the factory. Iteration of the model would be performed if needed until its predictions could be used with confidence.

The model would then be used to find areas in the insulators where the material strength margins were narrow. These areas should correlate with the areas in which actual failures have occurred. Heat-transfer modelling could then be used to discover the locations and amounts of heating which would have to occur in order to exceed strength margins in the failure areas. It is hoped that it will be possible to begin work developing and testing the model this fall.

Another improvement which is needed in the 201-MHz systems is of serious concern but must be entirely deferred at this time. Each Alvarez accelerator tank is excited by means of a coupling loop driven by the corresponding RF PA output coaxial line. See Figure 6.3. Each coupling loop assembly includes a coaxial RF dielectric window to support the tank vacuum.

The original design for these assemblies planned dome-shaped windows which would extend into the tanks. This would have kept each loop on the air side of the vacuum barrier and precluded possible multipactoring problems. When difficulties were encountered, a compromise design was adopted which placed the vacuum barrier back toward the amplifier and left the loop in vacuum. Fortunately, no multipactoring appeared after this was done.

The original RF windows were to have been ceramic but the compromise windows were finally fabricated from Rexolite. It has turned out that the windows for each of the four tanks must be replaced at least once per year. The annual cost for this maintenance has attracted notice.

Furthermore, it appears that this problem is much more serious at high duty and high power. This situation must be corrected if operation at higher duty and power in the future is to be achieved. Development of a satisfactory window from a material such as high-purity alumina or possibly silicon nitride is needed.

It has been apparent for some time that much improvement is needed in the speed and accuracy with which 201-RF system problems can be diagnosed. Also, a complete and continuous record of the behavior of each RF module is needed. Work has been begun by M. Parsons to collect performance parameters for each RF module with an A/D data acquisition system. Initially, the data will be processed by the LAMPF central control computer (CCC).

Eventually, it is expected that the 201-MHz systems will be monitored primarily by a stand-alone computer such as a micro-vax. It should be possible, after accumulating some operating experience with the completed system, to develop algorithms which will rapidly diagnose RF-module problems which have been previously been difficult to identify. It should also be possible to employ off-the-shelf software to handle large quantities of data easily for more effective maintenance scheduling and analysis of failure trends.

The IPAs are another area requiring attention. They should be more reliable and easier to maintain if the plate pulsed supplies for the 4616 tubes are eliminated. The requirement for the present pulse modulators appears to arise principally from the fact that IPA and PA share a single DC high-voltage supply.

An effort to replace the IPA modulators with separate DC supply is planned. The results of initial tests by V. LoDestro of the LINAC Division at Brookhaven National Laboratory and of tests at LAMPF have been positive. It should also be beneficial to convert the first two stages of the IPA to solid-state amplifiers. V. LoDestro has also tested this concept with positive results at Brookhaven.

The higher duty requirement at LAMPF complicates this project. However, an effort to accomplish such a modification is under consideration. Also, the 7835-tube filament power supplies have now reached an age at which they demand an excessive amount of maintenance time. It is hoped that funding will be available to replace these units over the next few years.

ACKNOWLEDGMENTS

The authors wish to acknowledge the kind assistance of J. D. Doss, MP-8, and O. van Dyck, MP-DO, both of LAMPF, in preparing

this paper. Special thanks go to C. Friedrichs of the Los Alamos Accelerator Technology Division, AT-5, and A. Browman, MP-DO, LAMPF.

BIBLIOGRAPHY

Humpheries, Stanley; **Principles of Charged Particle Accelerators**; Wiley-Interscience; 1986

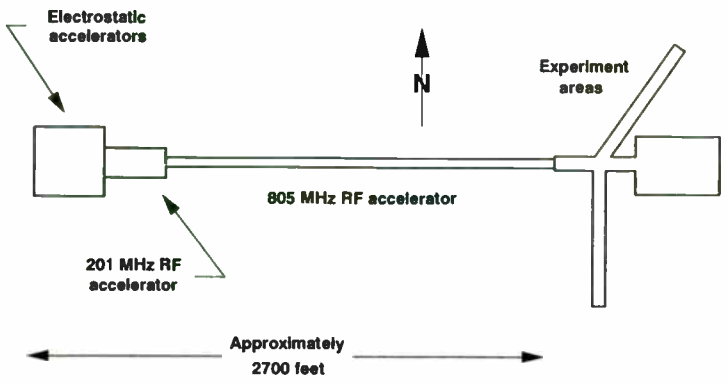

Figure 1.1 LAMPF accelerator facility

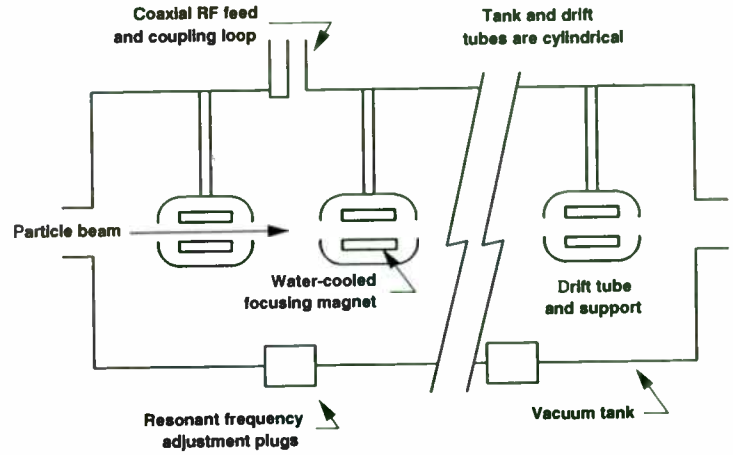

Figure 1.3 Alvarez tank accelerator structure

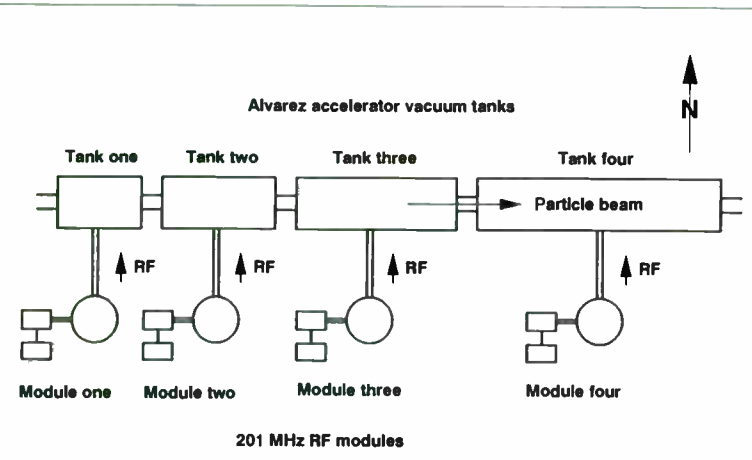

Figure 1.2 201 MHz accelerator section

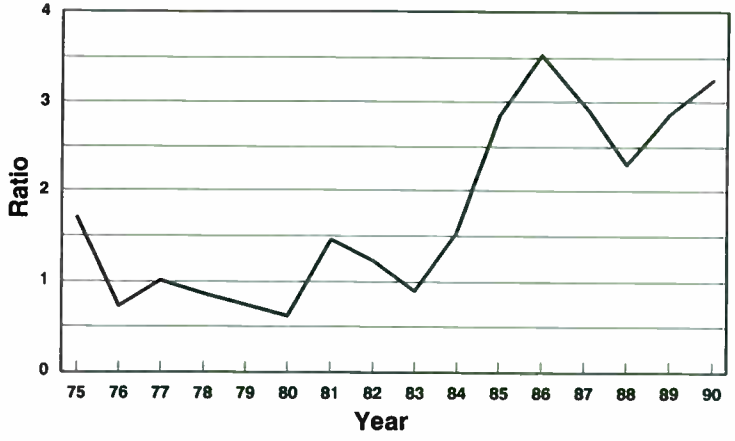

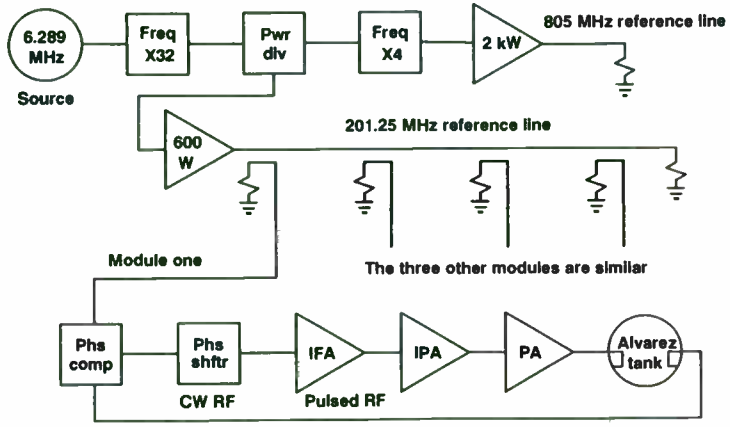

Figure 3.1 201 MHz RF system
After R. DeHaven

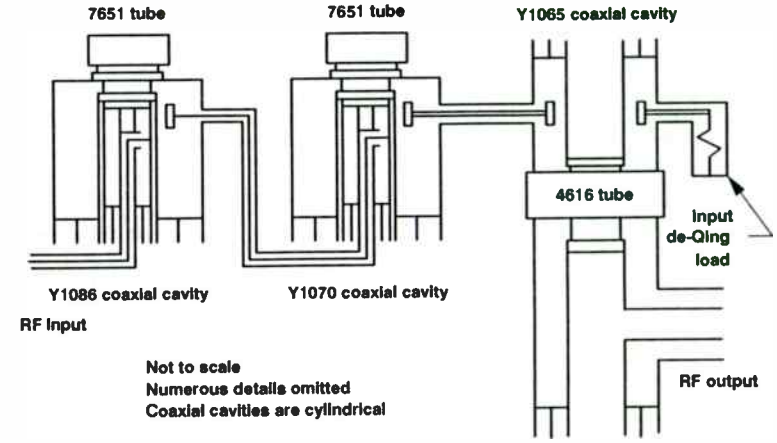

Figure 3.3 201 MHz intermediate power amplifier
RCA Y-1068C 200 MHz amplifier

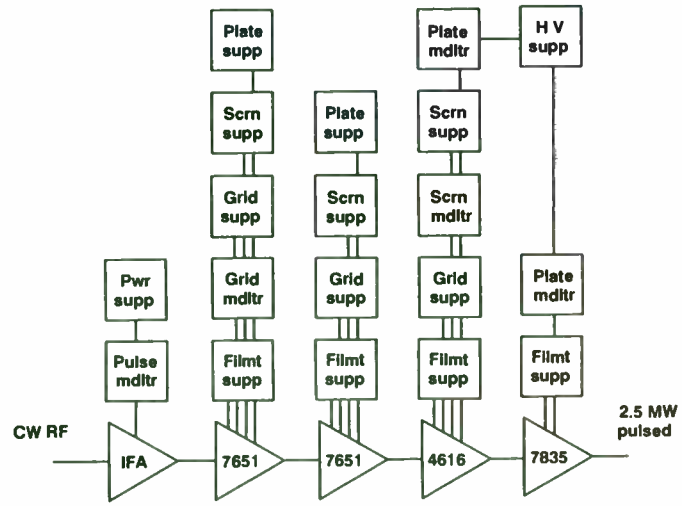

Figure 3.2 201 MHz amplifier chain

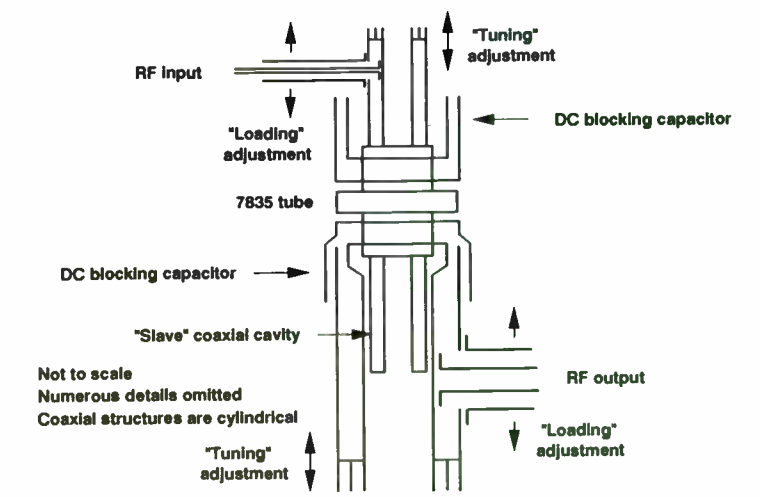

Figure 3.4 201 MHz final power amplifier
Continental 200 MHz amplifier

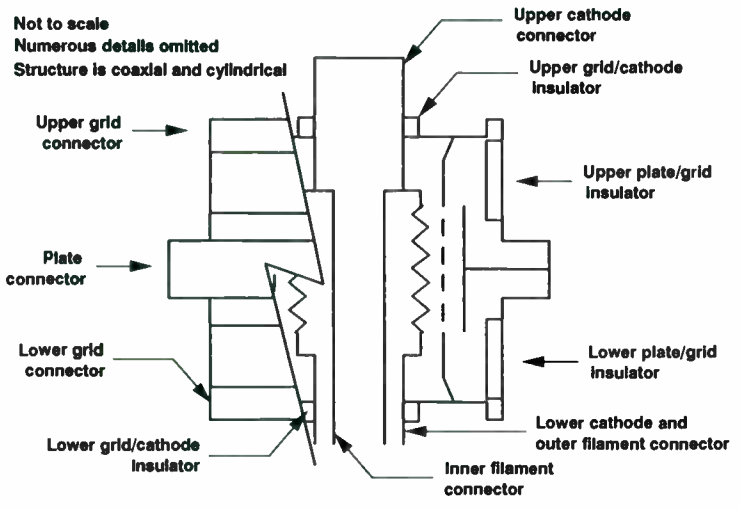

Figure 3.5 Burle 7835 triode

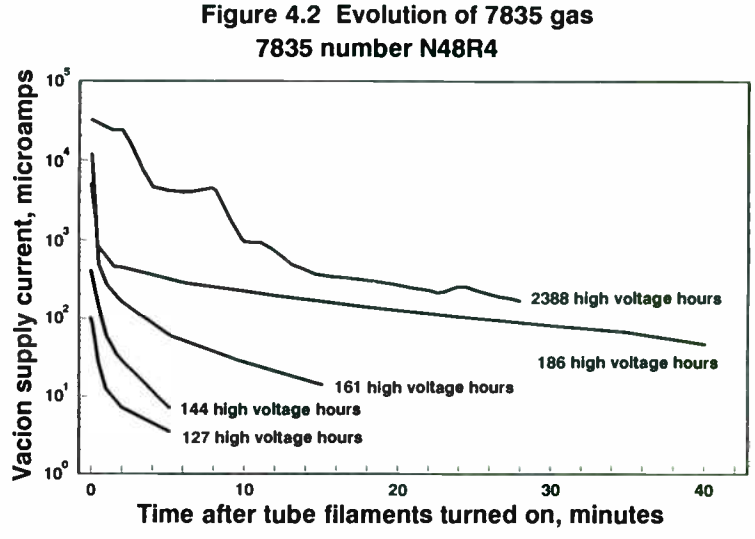

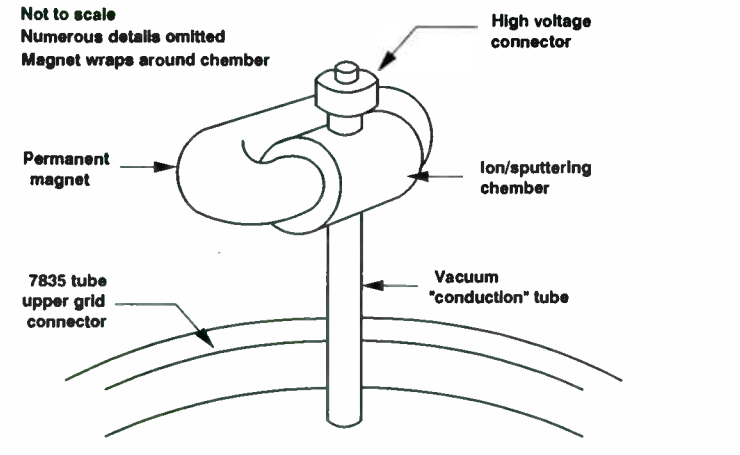

Figure 4.1 Varian-type miniature Penning ion pump

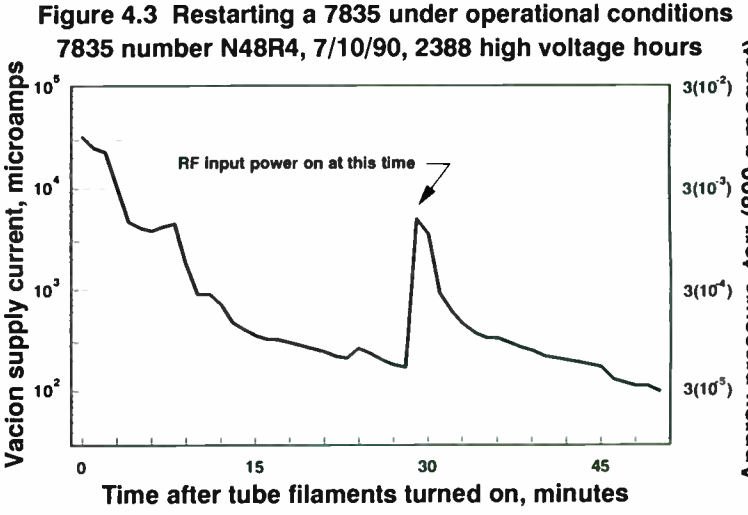

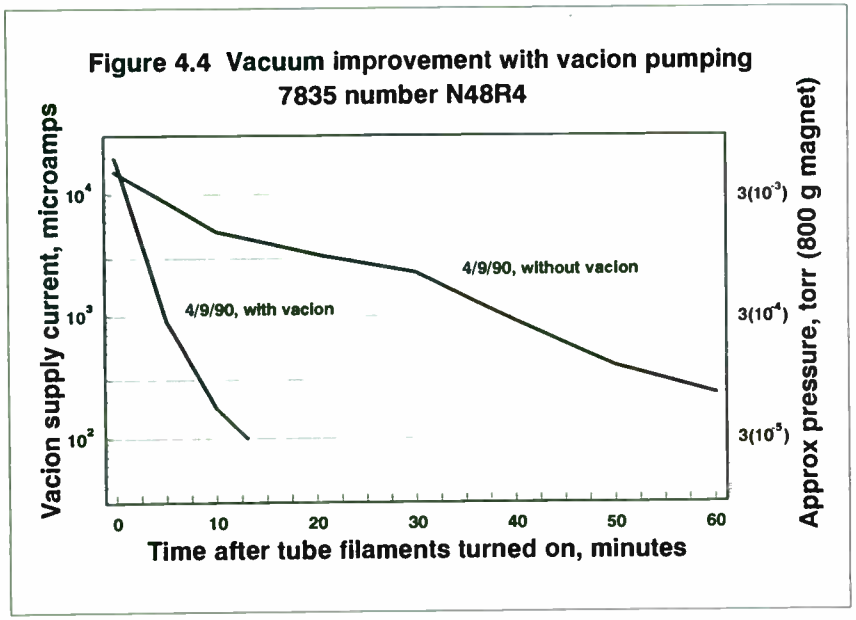

Figure 4.4 Vacuum improvement with vacion pumping 7835 number N48R4

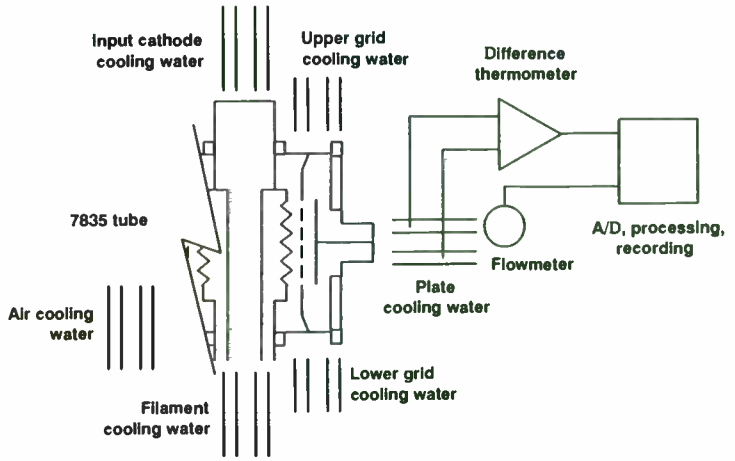

Figure 5.1 Tentative 7835 plate calorimetry system

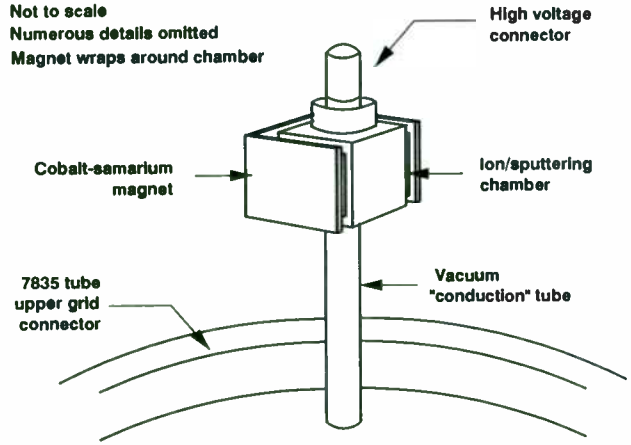

Figure 4.5 Perkin Elmer miniature ion pump

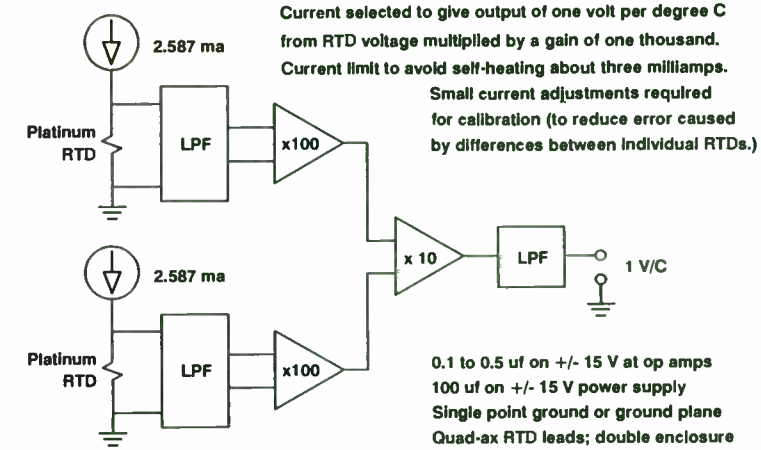

Figure 5.2 Temperature difference thermometer

After A. Browman

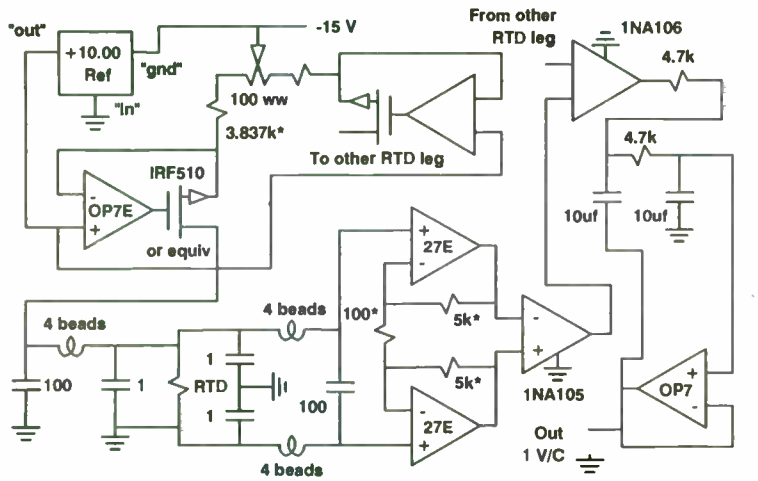

Figure 5.3 Temperature difference thermometer schematic

After A. Browman

* resistors 0.01 %; 100 uf tan; 1 nf RF.

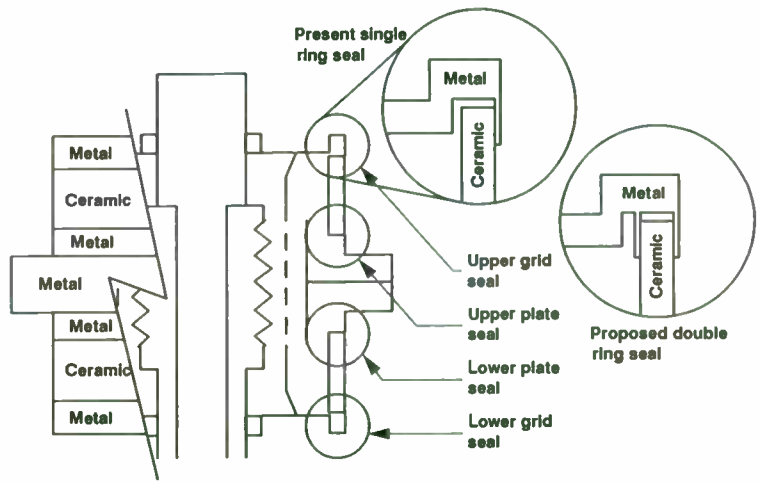

Figure 6.2 Present and proposed 7835 insulator seals

Figure 6.1 Ceramic plate insulator failures at LAMPF 7835 electron tubes by manufacturing date

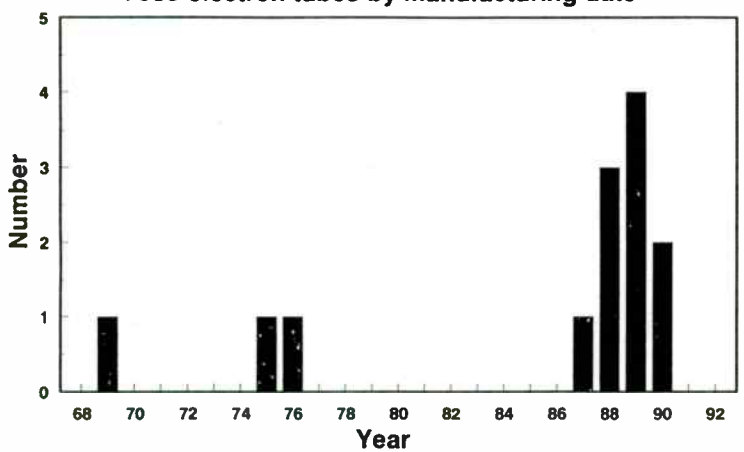

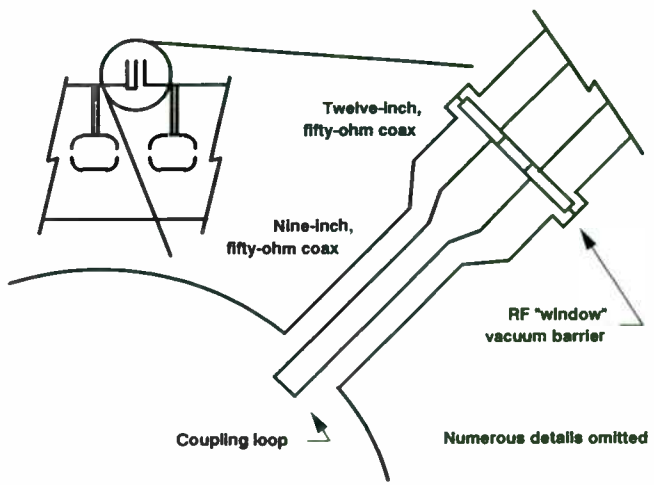

Figure 6.3 Alvarez tank feed loop and vacuum window

Low Frequency Circulator/Isolator Uses No Ferrite or Magnet

By Charles Wenzel
Wenzel Associates, Inc.

This is the Grand Prize winner in the Design category of the 1991 RF Design Awards Contest. For his achievement, the author was awarded an HP 8591A portable spectrum analyzer from Hewlett Packard.

The ferrite circulator/isolator is an amazing and important tool for the microwave engineer. Unfortunately, for frequencies below several hundred megahertz, the size of the magnets and ferrite becomes unworkable and the cost skyrockets. With the advent of remarkably fast op-amps, it has become practical to construct a low power equivalent to the circulator that works all the way down to DC and exhibits superb reverse isolation and impedance characteristics to frequencies above 100 MHz.

Suitable for small signal applications, the active circulator is excellent for matching and tuning antennas, amplifiers, and oscillators. Figure 1 shows a schematic of the circuit. Figure 2 is a photo of the prototype of the device. The isolated 50 ohm resistance presented at each port makes experiments with non-linear or reactive devices such as detectors, mixers, frequency multipliers, and filters straightforward since both the signal source and the analyzer are isolated from the device under test. Engineers working with lower RF frequencies will find the active circulator to be a welcome addition to the test bench.

The purpose of the circulator is to absorb all energy entering a port and to pass that energy on to the next port. High reverse isolation ensures that the energy flows in one direction around the circulator and that the impedance of one port is not affected by the other ports. The microwave circulator uses the non-linear properties of ferrite immersed in a magnetic field whereas this circuit uses high speed operational amplifiers.

For the circulator to work properly, each port must exhibit the characteristics of a Thevenin equivalent consisting of a 50 ohm resistor and a voltage source with a voltage twice as large as the voltage arriving at the previous port. Note that this voltage source ignores signals leaving the previous port as well as any signals on any other ports. The factor of two makes up for the drop across the Thevenin resistance when a 50 ohm load is connected.

First, the 50 ohm resistance results from the two, 100 ohm resistors leading to virtual grounds — that is points that are held at a fixed voltage regardless of the current.

The Thevenin voltage source is a little less obvious since the two 100 ohm resistors are connected to two different voltages that average to the desired factor of two. Each op-amp amplifies its input signal by 3.236 which is applied to one of the resistors. A voltage divider drops this voltage down to 0.764 which is applied to the positive input of the next op-amp. Since the other resistor is connected to the feedback node of this op-amp, it sees the same 0.764 size signal. The average of 3.236 and 0.764 gives the desired factor of two. Figure 3 shows the forward gain versus frequency for different supply voltages

The differential gain is set so that signals leaving a port terminated with 50 ohms will generate no output at the following port. A load impedance other than 50 ohms generates a "reflection" which is passed on to the next port. The op-amps provide inherent reverse isolation as shown in Figure 5 and the power handling capability is shown in Figure 4.

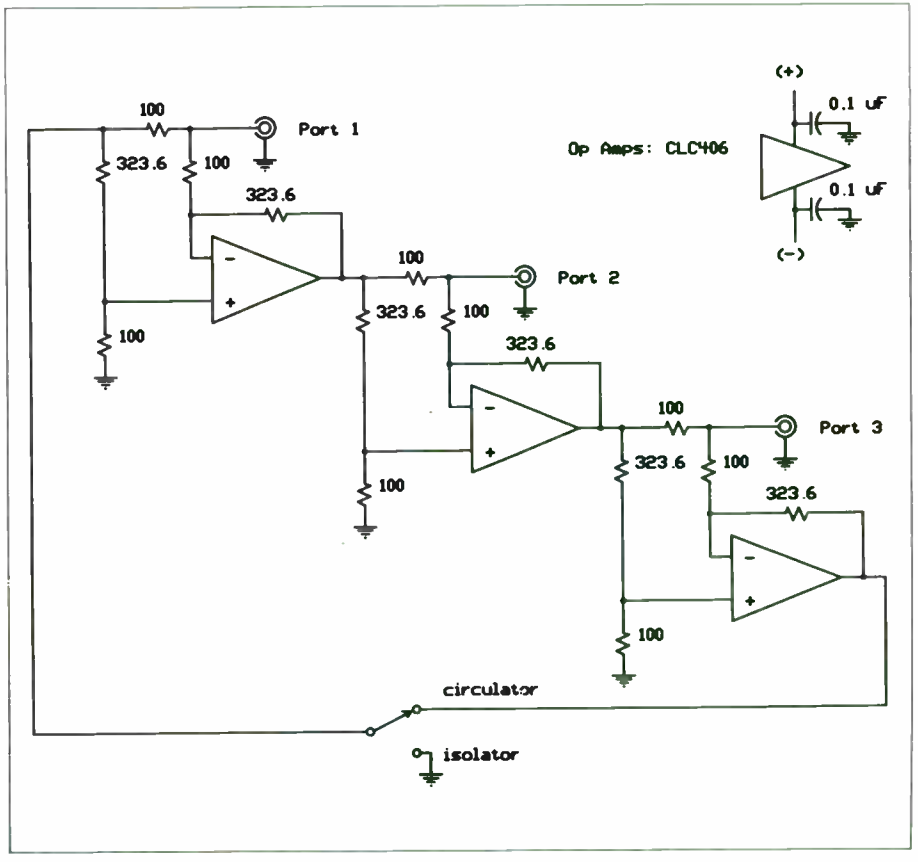

Figure 1. Schematic of low frequency circulator/isolator.

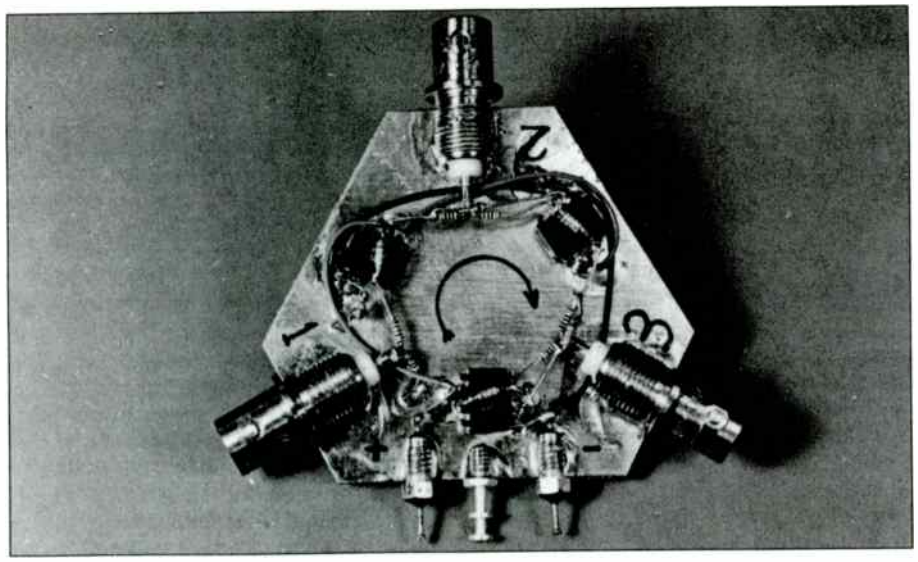

Figure 2. Constructed low frequency circulator/isolator.

The purist will note that a polarity reversal occurs from one port to the next due to the inverting op-amp configuration. More ports may be easily added to the circulator by repeating the obvious pattern.

Since the circulator works down to DC, its behavior can be observed with a multimeter. The port resistance can be measured with an ohm-meter and during the measurement the ohm-meter's test voltage appears at the next port (inverted). If -1 VDC is applied to port 1 then 1 VDC will appear across 50 ohms at port 2 and 0 VDC will appear at port 3 (as -1 VDC due to the op-amp inversion). Now if port 2 is shorted then the 1 VDC will "reflect in phase" and will destructively add to give 0 VDC at port 2 (an unusual way to describe why a short gives 0 VDC). This inverted volt circulates to port 3 where 1 VDC appears across the load!

Component Selection

The CLC406 op-amp selected for this design is not the fastest or highest power device that Comlinear Corporation manufactures, but instead represents the economy end of the spectrum with a price below $10. As Figures one through three show, this inexpensive amp delivers impressive performance at 5 VDC, even better performance near the absolute maximum rating at 6.8 VDC, and amazing performance well above its specified limit at 12 VDC! Operating above maximum ratings is not recommended. A better choice would be to select a faster, more powerful op-amp (or use sockets).

Stable, low inductance precision resistors are required for optimum results. The 323.6 ohm resistance can be achieved by paralleling a 330 ohm with a 16.8 kohm. The resistor values shown may be scaled to build a circulator with a different characteristic impedance. For example, a 75 ohm circulator would use resistors 1.5 times larger in all positions. It is interesting to note that a circulator could be built with a different characteristic impedance at each port.

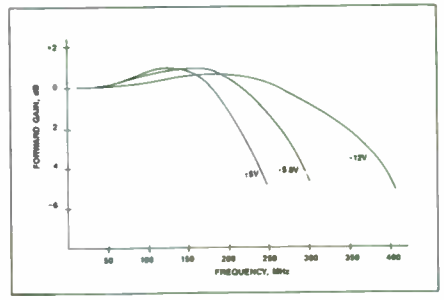

Figure 3. Forward gain versus frequency for different supply voltages.

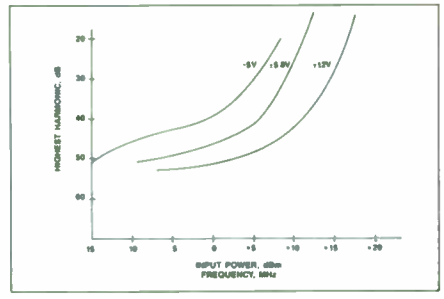

Figure 4. Distortion versus input power for different supply voltages.

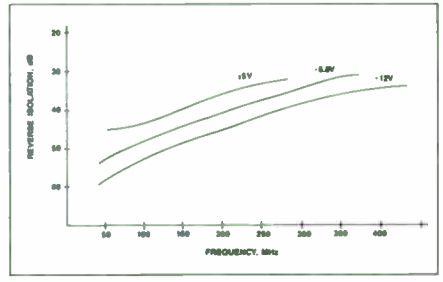

Figure 5. Reverse isolation versus frequency for different supply voltages.

Bypass capacitors must be connected to both power supply pins of each op-amp to the ground plane. The prototype uses 0.1 uF ceramic chip capacitors soldered directly from the IC to the ground plane.

Applications

The circulator is a natural choice for the matching and tuning of low level amplifiers. With the signal source connected to port 1, the amplifier's input or output to port 2, and a signal analyzer to port 3, the amplifier is turned for maximum return loss by adjusting for minimum signal at port 3. A high return loss is synonymous with a good VSWR since a well matched amplifier will "return," as a reflection, very little of the input signal. Figure 6 shows a typical application of the circulator/isolator.

Low level signal sources may also be adjusted for 50 ohm output impedance in a similar way. Simply adjust the frequency of the test signal until it is close to the carrier then tune the source for minimum reflection. Again, the re-

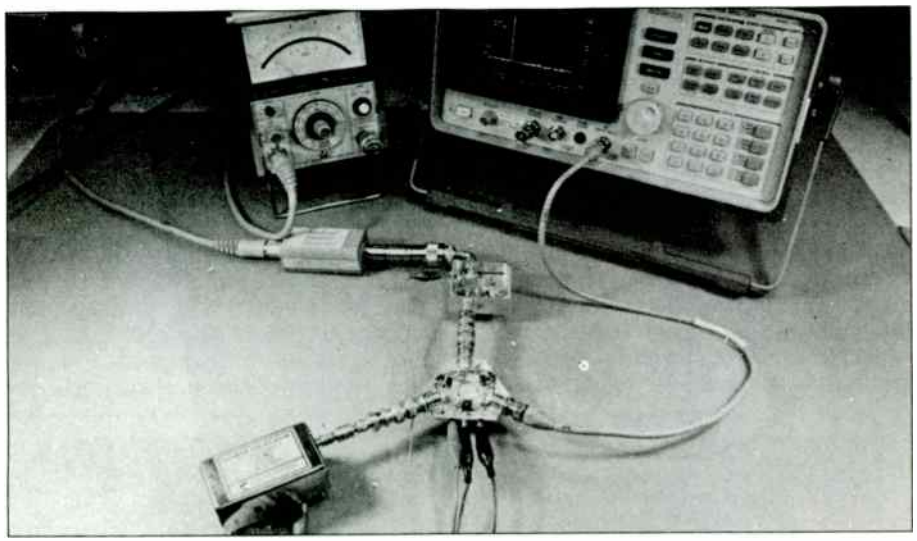

Figure 6. Typical application: adjusting the input impedance of a frequency multiplier.

flected signal appears at the next port. If the source's amplitude is too high for the circulator's op-amps to handle, just add an accurate attenuator. The circulator's accuracy is sufficiently high to "see" the return loss of a source through a small pad. Remember, the test signal passes through the pad twice and is attenuated each time so the return loss will seem better than it actually is by twice the attenuator value. In fact, a pad terminated with an open or short will exhibit a return loss exactly twice the pad's attenuation factor since the return loss of an open or short is zero.

Antennas may be tuned in a similar manner without using large signals that might cause interference with others. A low power generator is connected to port 1, the antenna to port 2, and some form of power or signal level indicator to port 3. The signal level at port 3 is proportional to the transmission loss and should be minimized by tuning the antenna matching network.

A time domain reflectometer is easily realized by applying a fast square wave or pulse to port 1 and connecting the device or cable under test to port 2. Breaks in the cable or other high impedance anomalies will reflect pulses with the same polarity as the input whereas shorts or lower impedances will reflect inverted pulses. Remember the inversion from one port to the next. A clean test signal is necessary for good results.

Conclusion

The active circulator brings many of the features of its big brother, the microwave ferrite circulator, down to the lower RF frequencies. Although the active version obviously lacks the power handling capabilities of typical circulators, the small signal applications abound. ***RF***

About the Author

Charles Wenzel is President of Wenzel Associates, a manufacturer of speciality crystal oscillator products for high purity, high stability applications. Founded in 1978, his company has developed high performance oscillators for instrumentation, communications, and military systems. Wenzel Associates has 36 employees, and boasts the world's lowest noise crystal oscillator, as measured by the National Institute of Standards and Technology (NIST).

His winning design was the result of considerable experimentation and design using discrete transistors, all of which failed to work. Recently-developed high-speed operational amplifiers allowed Charles to realize the goals of high isolation, stability, and controlled input and output impedances. He reports that a number of typical low-frequency op amp circuits were tried at RF using these devices, with good success.

Charles, a native of Austin, has a BSEE from the University of Texas. His hobbies include experimenting with new circuits and relaxing while playing his guitar. He can be reached at Wenzel Associates, Inc., 14050 Summit Drive, Austin, TX 78728; telephone (512) 244-7741.

Theoretical Basis for a Comprehensive Passive Filter Synthesis Program

MICHAEL G. ELLIS

U.S. Army Corps. of Engineers

3909 Halls Ferry Rd.

Vicksburg, MS 39180

Introduction

This program is a collection of subprograms, with a common menu and a transparent file structure, for the design of passive filters. This article is intended to assist the user in understanding the source code by providing a flowchart (Figure 1) of the program and explaining the basic underlying equations for each module. It is not meant to be a tutorial and assumes knowledge of filter synthesis. A companion manual, with problem examples, for the RF filter design program can be obtained from RF Design Software Service in RF Design magazine (RFD-0791) and includes the source and compiled code.

All modules were compiled with Quickbasic 3.0. Any module that is modified must be recompiled with Quickbasic 3.0 in order to interact with the other existing modules. Later versions of Quickbasic can be used to compile the modules only if all modules are recompiled with the same version of Quickbasic.

Summary of Functions

I. Module RF (Configure Monitor)

The program RF test the monitor for EGA, CGA, or monochrome CGA graphics modes prior to program execution. RF then produces a file called MONITOR that contains a single number. The number 1, 2, or 4 indicates monochrome, CGA, or EGA modes respectively. The highest available mode is always used. (Later on, modules that produce graphic output will first read the file MONITOR in order to scale the graph properly.) "RF" then chains to the main menu RFDESIGN.

II. Module RFDESIGN (Determine Pole-Zero Locations)

Module RFDESIGN is the main menu, and also the brains of the program. Poles and zeroes for Butterworth, Tchebyscheff (Chebyschev), and elliptic lowpass filters are generated in RFDESIGN. Also transforms for lowpass-to-highpass, lowpass-to-bandpass, and lowpass-to-bandstop are done in this module on a pole-zero basis only. An alternate menu function is available in order to exercise the special function modules to be described later (Figure 1). RFDESIGN produces the file TFILE which passes data to either PAS2, CELLIP, or SELLIP for Butterworth/Tchebyscheff, even order elliptic lowpass, and odd order elliptic lowpass filters.

All filters designed by RFDESIGN are started as lowpass prototypes with cutoff frequency, w_c, given by

$$w_c = 2 \pi f_c, \quad \text{with } w_c = 1.$$

Prototype Lowpass Butterworth Filters

The pole locations of a Butterworth filter can be obtained from

REAL PART	IMAGINARY PART
$\cos[(i-1)\pi/N]$	$\sin[(i-1)\pi/N]$ for N odd and i = 1,2,...,2N
$\cos[(i-0.5)\pi/N]$	$\sin[(i-0.5)\pi/N]$ for N even and i = 1,2,...,2N

where N is the order of the filter.

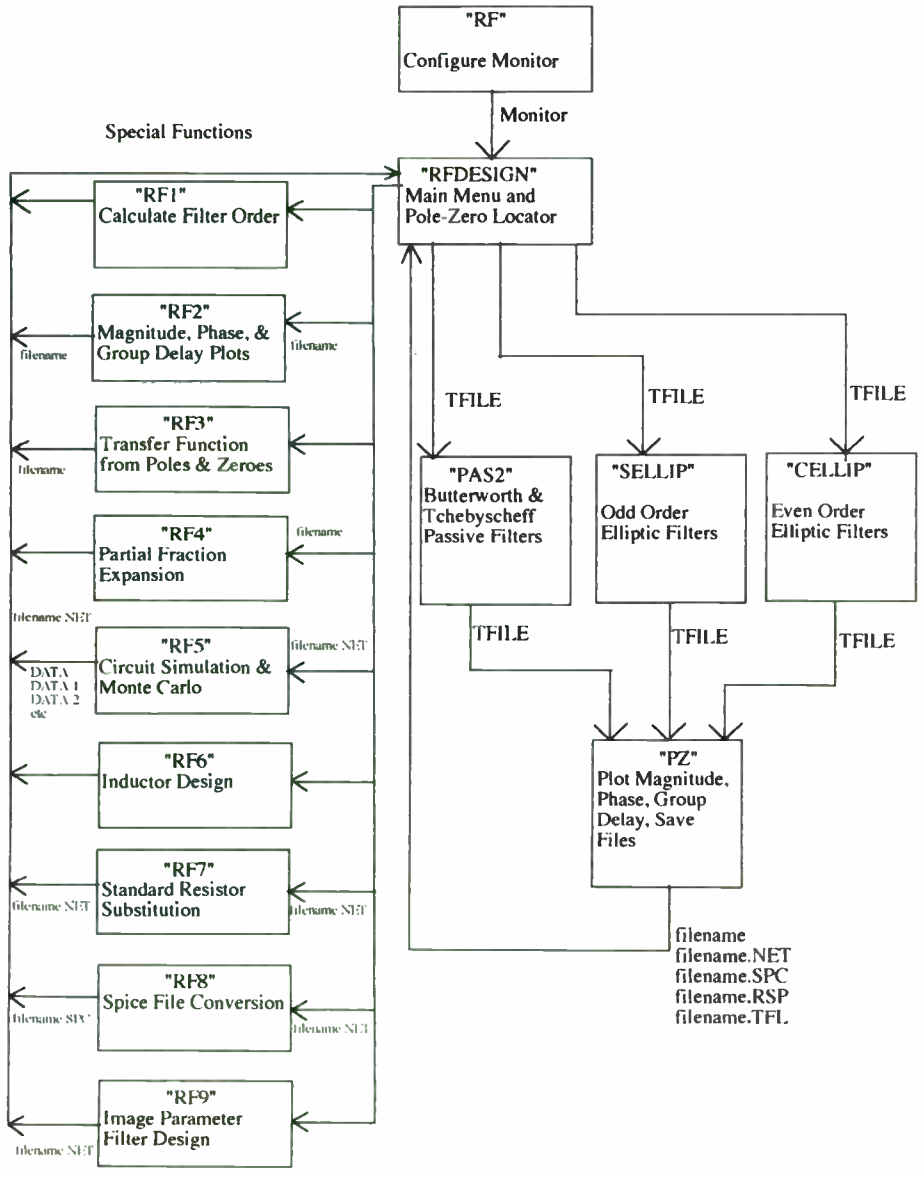

Figure 1. Flowchart

Subroutine 2210 in RFDESIGN selects only those points that have negative real components to be the poles of the Butterworth lowpass filter of order N = FILORD and stores them in array "ROOT" where

ROOT(K,1) = the real part of the Kth pole

and

ROOT(K,2) = the imaginary part of the Kth pole, for K = 1,2,....,N.

These are the left hand poles of the unit circle. All attenuation characteristics for the Butterworth lowpass filter can be computed directly from the equation

$$G(s)G(-s) = \frac{1}{1 + w^{2N}} = [Mag]^2 \qquad \text{for } 0 \le w < \infty$$

where w radians/sec = $2\pi f$ in Hertz and s = jw.

For Butterworth filters, the required filter order for an attenuation of K db at w_c is given by the basic Butterworth equation

$$\frac{1}{1 + w^{2N}} = 10^{(-K/10)} \qquad \text{where K db} = 10 \log [Mag]^2 \cdot$$

For example, if N = 5, the gain at w = 2 radian/second is

$$\frac{1}{1 + w^{(2*5)}} = 0.0009756 = [Mag]^2 = -30.1 \text{ db.}$$

This result will be important later for lowpass to bandpass transformations.

Prototype Lowpass Tchebyscheff Filters

If a Tchebyscheff filter is required, the poles of the Butterworth filter are first computed and then transformed into Tchebyscheff poles. The user selects the passband ripple in db, which must be converted to a voltage quantity. The equation

$$G(s)G(-s) = \frac{1}{1 + e^2[T_n(w)]^2} = [Mag]^2$$

defines a Tchebyscheff lowpass filter of order N where $T_n(w)$ can be specified as

$$T_n(w) = \cos [n \arccos(w)] \quad \text{for } 0 \le w \le 1$$

$$T_n(w) = \cosh[n \operatorname{arccosh}(w)] \quad \text{for } w > 1$$

or with the recursive formula

$$T_{n+1}(w) = 2wT_n(w) - T_{n-1}(w)$$

and

$$T_0(w) = 1$$
$$T_1(w) = w$$
$$T_2(w) = 2w^2 - 1$$
$$T_3(w) = 4w^3 - 3w$$
$$T_4(w) = 8w^4 - 8w^2 - 1, \text{ and so on.}$$

Solving the equation for e,

$$\varepsilon = \sqrt{10^{(0.1*\text{ripple in db})} - 1}$$

where the "ripple in db" is the passband ripple in db and is specified by the user.

$$\text{Alpha} = \frac{1}{\varepsilon} + \sqrt{1 + \frac{1}{\varepsilon^2}}$$

The equations that transform the Butterworth poles to Tchebyscheff poles are given by

$$A = 0.5 * (\text{Alpha})^{1/n} - 0.5 * (\text{Alpha})^{-1/n}$$

$$B = 0.5 * (\text{Alpha})^{1/n} + 0.5 * (\text{Alpha})^{-1/n}$$

Lines 2520 to 2560 transform the poles to Tchebyscheff poles using the constants A and B, and generate a numerator constant, GAIN, such that the dc gain of the Tchebyscheff lowpass prototype is unity. In essence, the real part of each Butterworth pole is multiplied by A, and the imaginary part of each Butterworth pole is multiplied by B. These equation are coded below, with GAIN initialized to 1.

```
2520  FOR I = 1 TO N
2530  ROOT(I,1)=A*ROOT(I,1)
2540  ROOT(I,2)=B*ROOT(I,2)
2550  GAIN = GAIN*SQR(ROOT(I,1)^2+ROOT(I,2)^2)
2560  NEXT I
```

For a Tchebyscheff lowpass with 3db passband ripple, e can be calculated to be 0.9976284 and the attenuation at any frequency, w, beyond 1 radian/second can be calculated from

$$10 \log \frac{1}{1 + \varepsilon^2 |\cosh(n \operatorname{arccosh}(w))|}$$

By definition,

$$\operatorname{arccosh}(w) = \ln \left[w + \sqrt{w^2 - 1} \right]$$

and

$$\cosh(w) = 0.5 * e^w + 0.5 * e^{-w}$$

where e = 2.7182818.

Prototype Lowpass Elliptic Filters

Elliptic filters are defined by the equation

$$G(s)G(-s) = \frac{1}{1 + e^2[R_n(w)]^2} = [Mag]^2$$

where

$$R_n(w) = B_1 w \prod_{i=1}^{(n-1)/2} \frac{w_{oi}^2 - w^2}{w_{zi}^2 - w^2} \quad \text{for n odd,}$$

and

$$R_n(w) = B_2 \prod_{i=1}^{n/2} \frac{w_{oi}^2 - w^2}{w_{zi}^2 - w^2} \quad \text{for n even,}$$

with $w_{zi} = \frac{w_1}{w_{oi}}$

where w_1 = the first frequency > 1 radian/second where the filter meets the prescribed stopband loss. For example, $R_n(w)$ for a 5th degree elliptic filter is

$$R_5(w) = \frac{B_1 w (w_{o1}^2 - w^2)(w_{o2}^2 - w^2)}{(w_{z1}^2 - w^2)(w_{z2}^2 - w^2)}$$

The function, $R_n(w)$, is called the Tchebyscheff rational function, or sometimes the Zolotarev function. If the zeroes, w_1/w_i, are picked so that the passband is equiripple, then the stopband will automatically be equiripple. Several different numerical techniques can solve for the poles and zeroes of the Tchebyscheff rational function, including

(a) the Tchebyscheff method can be applied to the rational function followed by an iterative method known as the second Remes algorithm (2), or

(b) the Simplex method of linear programming can be used to solve a Vandermonde set of linear simultaneous equations (3), or

(c) the Jacobian elliptical integral can be numerically evaluated for the poles and zeroes (16).

Method (c) is most commonly used. This procedure was researched by Cauer in 1931 and uses the elliptical function, sn(u), to solve for the poles and zeroes. It is summarized as follows.

Defining $L^2 = \frac{10^{0.1*AMIN} - 1}{10^{0.1*AMAX} - 1}$

where AMIN is the minimum attenuation in the stopband and AMAX is the maximum attenuation in the passband. The required filter order, N, can be computed by

$$N = \frac{K(1/w_1)\, K'(1/L)}{K'(1/w_1)\, K(1/L)}$$

where K(k) is defined as $\int_0^{\pi/2} (1 - k^2 \sin^2 x)^{-1/2}\, dx$

and K'(k) is defined as $\int_0^{\pi/2} (1-(1-k^2)\sin^2 x)^{-1/2}\,dx$

is the complete elliptic integral. Typically, a closed Newton-Cotes integration formula based on the trapezoidal rule will require the interval of integration to be subdivided into more than 1000 sub-intervals for accurate results. Once N is determined, U can be calculated as

$$U = \frac{(2\ I - 1)*K(1/w_1)}{N} \qquad \text{for N even and I = 1,2,....,N/2}$$

and

$$U = \frac{(2\ I\ )*K(1/w_1)}{N} \qquad \text{for N odd and I = 1,2,..,(N-1)/2.}$$

Now Ø must be determined using the equation

$$U = \int_0^{Ø} (1-(1/w_1)^2\sin^2 x)^{-1/2}\,dx$$

Then sn(U) = sin(Ø) = w_{oi} and $w_{zi} = w_1/w_{oi}$.

The equations, given by (16), are summarized below.

$$R_n(w) = B_1\, w \prod_{i=1}^{(n-1)/2} \frac{w_{oi}^2 - sn^2(U)}{w_{zi}^2 - w_1^2 sn^2(U)} \quad \text{for n odd,}$$

and

$$R_n(w) = B_2 \prod_{i=1}^{n/2} \frac{w_{oi}^2 - sn^2(U)}{w_{zi}^2 - w_1^2 sn^2(U)} \quad \text{for n even,}$$

with U defined previously.

The constant B is easily found once the poles and zeroes are known since $R_n(w) = 1$ at $w = 1$. The voltage transfer function, G(s), is determined by rationalizing as in the following example for N even.

$$G(s)G(-s) = \frac{|(w_{z1}^2 - w^2)(w_{z2}^2 - w^2).....|^2}{|(w_{z1}^2 - w^2)(w_{z2}^2 - w^2).....|^2 + e^2|B_1(w_{o1}^2 - w^2)(w_{o2}^2 - w^2).....|^2}$$

since $s = jw$, substituting $w = s/j$ for each w ($w^2 = -s^2$) and combining the denominator terms yields

$$G(s)G(-s) = \frac{P'(s)}{Q'(s)} \qquad \text{where P'(s) and Q'(s) are polynomials in s.}$$

The function G(s) is simply $\frac{P(s)}{Q(s)}$

where P(s) is formed from the left half zeroes of P'(s)and Q(s) is formed from the left half zeroes of Q'(s)and the constant, e, is determined exactly as in the Tchebyscheff case. Lines 6500 to 8660 of module RFDESIGN contain the source code for generating the elliptic poles and zeroes as described in this section.

Bandpass Transformations

In module RFDESIGN, only the poles and zeroes, and not the element values, are transformed. For passive filters, the modules PAS2 (for Butterworth/Tchebyscheff), CELLIP (for even order elliptic filters), and SELLIP (for odd order elliptic filters) transform the lowpass filter on a component-by-component basis before the final filter is displayed.

Each filter is a polynomial in the variable s (s = jw) and each transformation is based on replacing the variable s with another variable from the Table below. The substitution of s by s/1000 will convert a normalized lowpass filter such that the cutoff frequency will be 1000 radians/second and is the equivalent of frequency scaling. A list of common transforms is given below.

Table 1 - Bandpass Transformations

$s \longrightarrow$	$\frac{s}{w_u}$	1 rad/sec lowpass to w_u rad/sec lowpass
$s \longrightarrow$	$\frac{w_u}{s}$	1 rad/sec lowpass to w_u rad/sec highpass
$s \longrightarrow$	$\frac{s^2 + (w_u * w_l)}{s * (w_u - w_l)}$	1 rad/sec lowpass to bandpass
$s \longrightarrow$	$\frac{s * (w_u - w_l)}{s^2 + (w_u + w_l)}$	1 rad/sec lowpass to bandstop

where

w_l = lower frequency cutoff, and

w_u = upper frequency cutoff.

These transformations may be applied to either the poles and zeroes of the transfer function (as in RFDESIGN), or to the individual components after the design of a lowpass prototype (as in PAS2, CELLIP, and SELLIP).

For the lowpass to bandstop transformation, a normalized lowpass is designed such that 1 rad/sec is the boundary of the stopband, rather than the edge of the passband. This is done so that when the lowpass is transformed into a bandstop, the frequency response between the upper frequency bandstop, w_u, and the lower frequency bandstop, w_l, is guaranteed to meet the specified bandstop attenuation.

For example, consider a Butterworth bandstop filter with a desired attenuation of 40 db between 100Hz and 200Hz, designed from a 2nd order Butterworth lowpass.The frequency at which the lowpass first obtains an attenuation of 40 db can be found from

$$\frac{1}{1 + w^{2(2)}} = \frac{1}{10^{(40/10)}} = [Mag]^2 = 0.0001$$

Solving for w, $w = 9.9974991$. At frequencies greater than 9.9974991 radians/sec, the response will be attenuated by more that 40 db.. The transfer function, G(s), is found from

$$G(s)G(-s) = \frac{1}{1 + w^4}$$ Substituting w = s/j yields,

$$G(s)G(-s) = \frac{1}{1 + s^4} = \frac{1}{1 + 1.414s + s^2} \quad \frac{1}{1 - 1.414s + s^2}$$

Selecting the half that has roots with negative real parts,

$$G(s) = \frac{1}{1 + 1.414s + s^2}$$

This is the normalized transfer function with 3db cutoff at 1 rad/sec. Applying the lowpass to lowpass transformation with w_u = 1 / 9.9974991 yields

$$G(s) = \frac{1}{1 + 1.414(9.9974991)\, s + (9.9974991)^2\, s^2}$$

which is now attenuated by 40db at w = 1 rad/sec. Now applying the lowpass to bandstop transformation with

w_l = 628.318 radians/sec (100Hz), and

w_u = 1,256.636 radians/sec (200Hz),

$$G(s) = \frac{1}{1 + 9.9971(1.414)\frac{s(628.3)}{s^2 + 2(628.3)^2} + (9.9971)^2\frac{s(628.3)}{s^2 + 2(628.3)^2}\,\frac{s(628.3)}{s^2 + 2(628.3)^2}}$$

which simplifies to

$$G(s) = \frac{\left[\frac{s}{628.318}\right]^4 + 4\left[\frac{s}{628.318}\right]^2 + 4}{\left[\frac{s}{628.318}\right]^4 + 14.14\left[\frac{s}{628.318}\right]^3 + 103.99\left[\frac{s}{628.318}\right]^2 + \frac{28.28\, s}{628.318} + 4}$$

The program always provides the normalized transfer function with the denormalization factor, 628.318, in this case, stored in the transfer file, TFILE. The transformation can also be applied directly to the individual elements of a passive lowpass network. Applying a bandpass transformation to a series inductance maps the impedance

Ls into $\frac{L\, s(w_u - w_l)}{s^2 + (w_u * w_l)}$ which converts the inductor, of inductance L, into a parallel inductor-capacitor combination with the values show in figure 2.

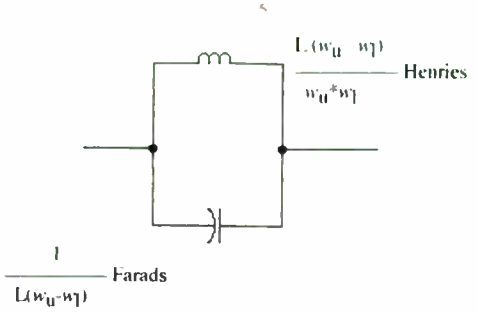

Figure 2. Transformed Inductor

File Transfer Format

After a given design is completed, the module RFDESIGN will produce the file TFILE that will contain the poles, zeroes, and all other information about the design. The user may desire to write custom routines to interface with this file. The following example of the file TFILE is given for a Butterworth bandstop filter with 20db attenuation at 1000Hz and 2000Hz, designed from a lowpass prototype with filter order = 1.

TFILE is used to transfer data from the main module, RFDESIGN, to the modules PAS2, CELLIP,SELLIP, and PZ.

Table 2

```
0                    '0=printer unavailable, 1=printer available
1                    '0=active, 1=passive, 2=digital, 3=switched
                      capacitor
2                    '0=lowpass, 1=bandpass, 2=bandstop,
                      3=highpass
0                    '0=Butterworth, 1=Tchebyscheff I,
                      2=Tchebyscheff II/elliptical, 3=elliptical
2                    'FILORD, filter order =2
2                    'NZ, number of zeroes
0                    'normalized real part of zero #1
1.414213562373095    'normalized imaginary part of zero #1
0                    'normalized real part of zero #2
-1.414213562373095   'normalized imaginary part of zero #2
-0.2052411784483716  'normalized real part of pole #1
0                    'normalized imaginary part of pole #1
-9.744633192617828   'normalized real part of pole #2
0                    'normalized imaginary part of pole #2
2                    'Fh/FL  (see below)
6283.185308          'DENORM, Denormalization factor, multiply
                      poles and zeroes by this to denormalize
1000                 'FL, low frequency cutoff in Hertz
2000                 'Fh, high frequency cutoff in Hertz
1                    'WL (always 1 for bandpass or bandstop)
0                    'SFREQ, sampling frequency for digital and
                      switched capacitor filters
0                    'TD, 1/SFREQ (for digital and switched
                      capacitor filters)
0                    'WLD, warped low frequency cutoff for digital
                      and switched capacitor filters
0                    'FCUTOFF, cutoff frequency for lowpass or
                      highpass, 0 otherwise
0                    'WHD, warped high frequency cutoff for digital
                      and switched capacitor filters
1                    'GAIN, gain factor, usually 1
9.9498743710662      'PZSCALE, normalized frequency in radians/sec
                      at which lowpass prototype first
                      meets the desired bandstop attenuation
0                    'AX, bandpass ripple for elliptic filters
0                    'AN, stopband attenuation for elliptic filters
0                    'SLR, source and load resistance for elliptic
                      passive filters
0                    'DUAL, 0 = standard passive circuit, 1=dual
```

III Module PAS2 (Butterworth and Tchebyscheff Filters)

PAS2 generates the schematic from the data given in TFILE. The pole-zero locations in TFILE are not used to determine the element values. A set of equations published in the March 5th issue of EDN (1974) can be used to determine element values which are stored in the variable PAS(I) for I = 1 to N, where N is the filter order.

III.

Butterworth Case

$$PAS(I) = 2 \sin [(2*I-1)*1.570795/N] \quad \text{for } I = 1, 2, \ldots\ldots, N$$

Tchebyscheff Case

For I = 1 to N

$$X_1 = 10^{(ripple/10)} - 1$$

$$X_2 = \sqrt{X_1}$$

$$\beta = (1/N) \ln [1/X_2 + \sqrt{(1/X_2)^2 + 1}]$$

$$\phi = (2*I - 1) *1.570795/N$$

$$A_k = \sin(\phi)$$

$$\sinh = 0.5*e^{\beta} - 0.5*e^{-\beta}$$

$$B_k = \sinh^2 + \sin^2(I*\pi/N)$$

If I = 1 then $PAS(I) = 2*A_k/\sinh$

If I > 1 then $PAS(I) = 4*A_k*A_{km1}/(PAS(I-1)*B_{km1})$

$$A_{km1} = A_k$$

$$B_{km1} = B_k$$

Next I

The equations from EDN will not allow unequal termination resistances for Butterworth and Tchebyscheff filters. The following set of equations from Porter (17) allow for unequal termination resistances.

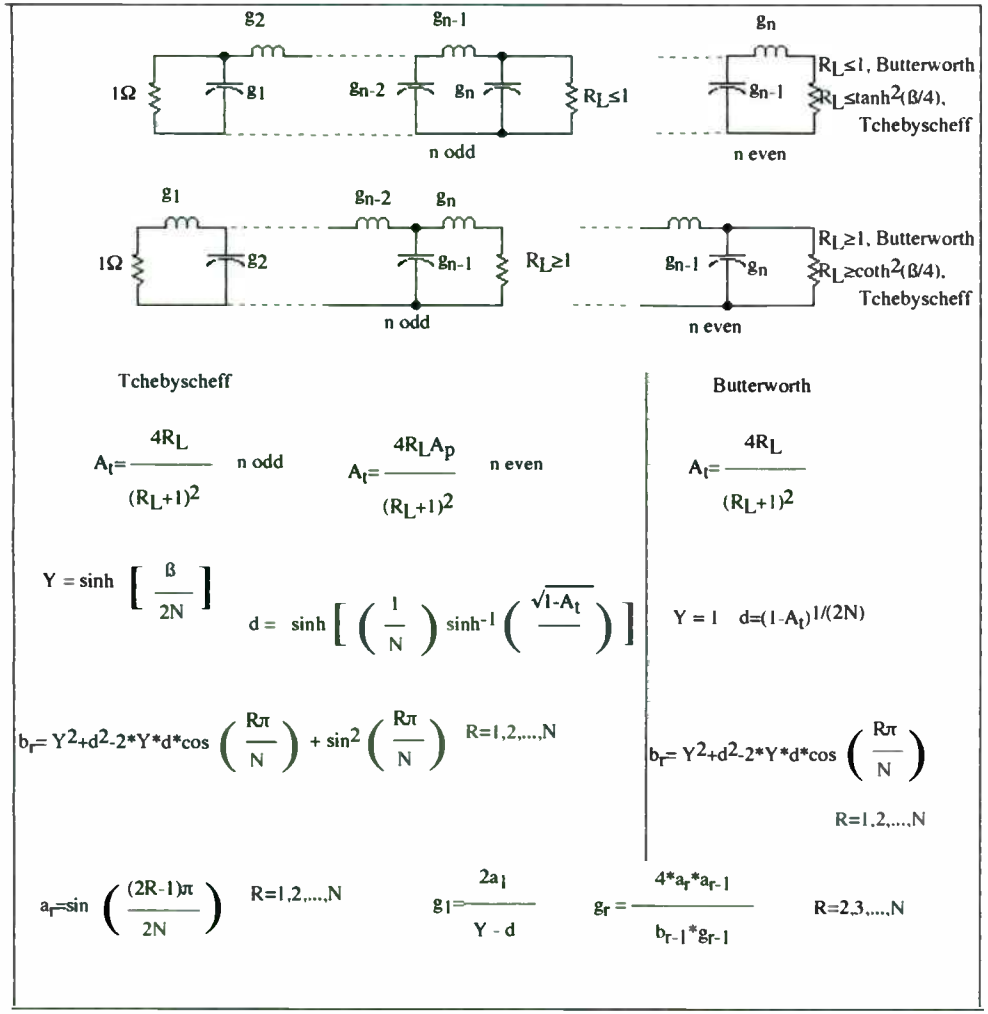

Figure 3. Doubly terminated filters.

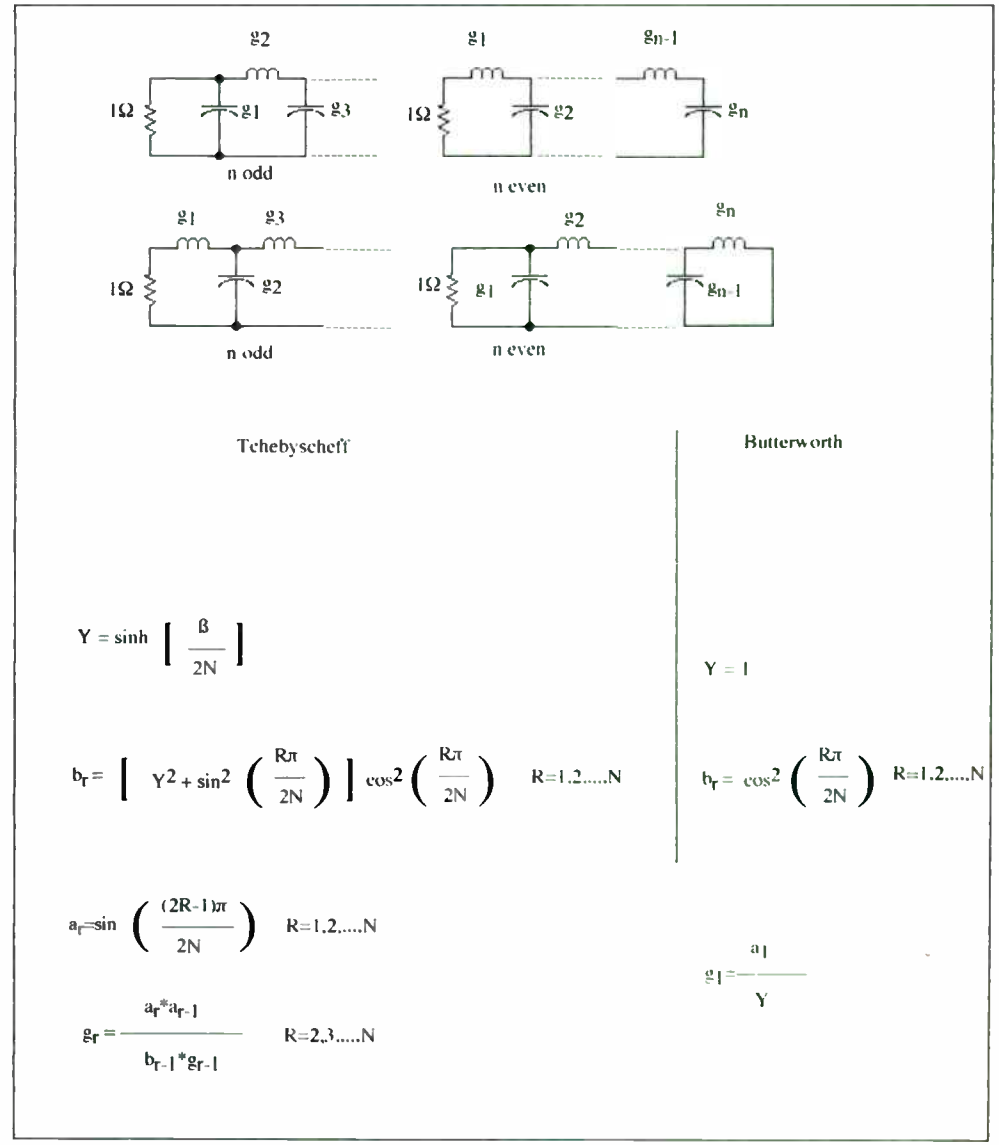

Figure 4. Singly terminated filters.

Figure 3 contains the formulas for doubly terminated Butterworth/Tchebyscheff filters while Figure 4 contains the equations for singly terminated filters. The equations listed below are the Tchebyscheff filter parameters definitions to be used in the formulas in Figures 3 and 4.

Table 3. Filter Parameter Definitions.

n: number of poles or filter elements

A_m: passband ripple in db

$$A_p = 10^{(A_m/10)}$$

$$\varepsilon = \sqrt{A_p - 1}$$

$$\beta = 2 * \sinh^{-1}\left(\frac{1}{\varepsilon}\right)$$

$$Y = \sinh\left(\frac{\beta}{2N}\right)$$

Evenly terminated lowpass Tchebyscheff filters of even order are not possible to implement in a passive configuration, so the program alters the end termination to achieve the closest possible match. Magnitude scaling, frequency scaling, and bandpass transformations are done in module PAS2, after the initial lowpass prototype is generated from the equations in Figures 3 and 4.

Impedance Scaling

All filters are designed with 1 ohm terminating resistors. The network is impedance scaled by a factor R so that the resulting filter is terminated in a resistance of R ohms. The scaling processs involves dividing all capacitors by the value R and multiplying all inductors and resistors by the same constant R.

Frequency Scaling

Scaling from a cutoff frequency of 1 radian/sec to a higher cutoff frequency of w_c radians/sec involves dividing all inductors by w_c and dividing all capacitors by w_c. Any resistors in the network will be unaffected by the scaling process since resistors are not frequency dependent devices.

IV Module SELLIP (Odd Order Elliptic Lowpass Schematics)

SELLIP produces filters from odd order lowpass prototypes using the permutation method to calculate trap section elements (14). The lowpass prototype is impedance scaled, frequency scaled, and any necessary passband transformations are applied to each element before the network schematic is displayed. Elements values are determined by using formulas for both the input impedance of the passive network, Z_{in}, and the derivative of the input impedance, Z'_{in}.

Using the previous definition for elliptic filters,

$$\left[\frac{V_o(s)}{V_{in}(s)}\right]^2 = G(s)G(-s) = \frac{1}{1+\varepsilon^2[R_n(w)]^2}$$

Let $K(s)K(-s) = e^2[R_n(w)]^2$, then $G(s)G(-s) = \dfrac{1}{1+K(s)K(-s)}$, or

$H(s)H(-s) = 1 + K(s)K(-s)$, using $H(s) = 1/G(s)$. Both $H(s)$ and $K(s)$ are rational functions with numerator and denominators identified as

$$H(s) = \frac{E(s)}{P(s)} \quad \text{and} \quad K(s) = \frac{F(s)}{P(s)} .$$

Therefore $E(s)E(-s) = P(s)P(-s) + F(s)F(-s)$.

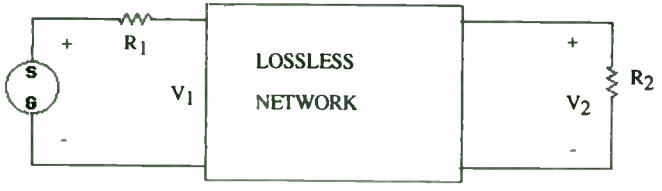

Figure 5. General Lossless Network

For the circuit in Figure 5, the ABCD matrix is

$$\begin{bmatrix} A & B \\ C & D \end{bmatrix} = \frac{1}{\sqrt{R_1R_2}} \begin{bmatrix} (He+Ke)R_1 & (Ho+Ko)R_1R_2 \\ (H_o-K_o) & (H_e-K_e)R_2 \end{bmatrix}$$

where the e subscript denotes an even polynomial, and o an odd polynomial, such that

$$H_e = \frac{E_e(s)}{P(s)} \quad \text{and} \quad H_o = \frac{E_o(s)}{P(s)} ,$$

$$K_e = \frac{F_e(s)}{P(s)} \quad \text{and} \quad K_o = \frac{F_o(s)}{P(s)} .$$

The input impedance is $\dfrac{A}{C} = \dfrac{(H_e+K_e)R_1}{(H_o-K_o)}$

Alternatively, the ABCD matrix can also be written as

$$\begin{bmatrix} A & B \\ C & D \end{bmatrix} = \frac{1}{\sqrt{R_1R_2}} \begin{bmatrix} (Ho+Ko)R_1 & (He+Ke)R_1R_2 \\ (H_e-K_e) & (H_o-K_o)R_2 \end{bmatrix}$$

which gives rise to the dual network.

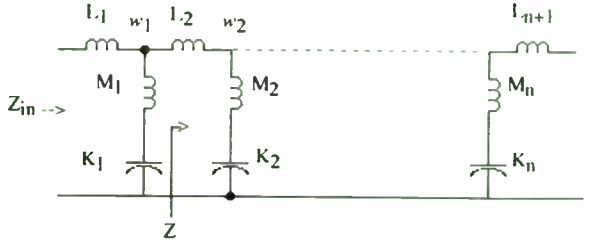

Figure 6. Elliptic lowpass midseries filter topology.

The analysis of the input impedance will use the midseries topology of Figure 6. Suppose the (M_1,K_1) branch is resonant at $s_1 = w_1$. Then the input impedance in the neighborhood of that frequency is

$$Z_{in}(s) = s L_1 + M_1 \left[s - \frac{s_1^2}{s} \right]$$

The impedance Z, seen to the right of (M_1, K_1) in Figure 6 is not zero in practical cases. Differentiating the previous equation with respect to s yields

$$Z'_{in}(s) = L_1 + M_1 \left[1 - \frac{s_1^2}{s^2} \right]$$

From a Taylor series approximation valid in the neighborhood of trap frequency s_1, Z_{in} must be

$$Z_{in} = L_1 s_1 + (L_1 + 2M_1)(s - s_1) + \ldots\ldots +.$$

Now it is possible to identify element values of the first three elements in Figure 6 that cause the notch at w_1. Setting s equal to s_1 yields

$$L_1 = \frac{Z_{in}(s_1)}{s_1}.$$

Setting s equal to s_1 in the derivative yields

$$M_1 = \frac{Z'_{in}(s_1) - L_1}{2}.$$

Since M_1 and K_1 are resonant at w_1,

$$K_1 = \frac{1}{M_1 w_1^2}.$$

The significance of these results comes from the independent knowledge of $Z_{in}(s)$ and $Z'_{in}(s)$ by knowing the impedance function in pole/zero form, especially at the notch frequencies.

Amstutz (14) produced a method of permutating each trap into the input position and applying a recursive formula that yields all of the element values. This method is not susceptible to the round-off errors that would occur by simply continuing down the ladder toward the load end. The permutation method of calculating trap elements is explained in detail in Cuthbert (10). Lin and Tokad (18) describe the minor tests to be added to the permutation algorithm so that all element values are positive.

V Module CELLIP (Even Order Elliptic Lowpass Schematics)

CELLIP produces type C elliptic filters from even order lowpass prototypes using the permutation method to calculate trap section elements. However, evenly terminated even order elliptic lowpass filters are theoritically impossible to realize unless the order of the numerator is reduced by a factor of two. A sixth order elliptic filter would be realized as a type C elliptic filter with 4 zeroes and 6 poles. Module CELLIP recomputes all poles and zeroes and re-writes TFILE before implementing the filter schematic.

VI Module PZ (Graphical Analysis Program and File Saver)

This program calculates magnitude, phase, and group delay using only the poles and zeroes of the filter transfer function, G(s). If $p_i + j\, p_{i1}$ is a pole of G(s), and $z_i + j\, z_{i1}$ is a zero of G(s), then

$$G(s) = \prod_{i=1}^{n} \frac{s-(z_i + j\,z_{i1})}{s-(p_i + j\,p_{i1})}$$

$$\text{the magnitude of } G(s) = |G(s)| = \prod_{i=1}^{n} \sqrt{\frac{(w-z_{i1})^2 + z_i^2}{(w-p_{i1})^2 + p_i^2}}$$

$$\text{the phase of } G(s) = \angle G(s) = \sum_{i=1}^{n} -\arctan\frac{w-p_{i1}}{p_i} + \arctan\frac{w-z_{i1}}{z_i} \quad \text{, and}$$

the group delay of G(s) is defined as the negative of the derivative of the phase of (Gs) with respect to w, therefore

$$\text{Group Delay} = \sum_{i=1}^{n} \frac{1}{1+\left[\frac{w-p_{i1}}{p_i}\right]^2}\frac{1}{p_i} - \frac{1}{1+\left[\frac{w-z_{i1}}{z_i}\right]^2}\frac{1}{z_i}$$

Module PZ will produce several save files, including

"filename" which is used by modules RF2 and RF4 for extended magnitude, phase, group delay response and for impulse and step response, respectively,

"filename.NET" which is used by module RF5 for circuit simulations and Monte Carlo analysis,

"filename.SPC" which is a spice compatible input file developed around PSPICE for PC's,

"filename.RSP" which contains the magnitude, phase, and group delay response as an ascii file, and

"filename.TFL" which saves the TFILE for a particular problem.

VII Module RF1 (Calculate Filter Order)

RF1 calculates the required filter order N from specifications of passband ripple, stopband ripple, passband edge frequency, and stopband edge frequency. If the filter specifications are given in terms of a bandpass, bandstop, or highpass characteristic, then the passband transformations discussed previously are used to map these characteristics to lowpass specifications so that the existing formulas, given in this article, can be used directly to calculate the required filter order. Usually for a bandpass filter or a bandstop filter, the order of the filter is determined by either the bandpass-to-bandstop transition, or the bandstop-to-bandpass transition, but not both..

VIII Module RF2 (Magnitude, Phase, and Group Delay)

Module RF2 basically supports the same analysis as PZ, but allows more flexibility in specifying frequency range and input coefficients. There are three ways to enter data into the program. The transfer function can be read from a file, or the coefficients of the numerator and denominator of G(s) can be typed in directly from a keyboard, or the coefficients of the quadratic functions of G(s) can by typed in from a keyboard. In the latter case, a cascade utility is available to allow cascading of the responses for the separate quadratic sections.

IX Module RF3 (Transfer Function from Pole-Zero Locations)

This utility builds a Lagrange polynomial from the roots of the polynomial and is used in conjunction with the filter design program to construct a transfer function from its poles and zeroes.The algorithm works as follows.

Case I: Consider the polynomial (x - r1)(x - r2). The polynomial coefficients are x^2 - (r1 + r2+) x + (r1*r2).

Case II: For the polynomial (x - r1)(x - r2)(x - r3), the direct form of the polynomial can be written as

x^3 - (r1 + r2 + r3)*x^2 + (r1*r2 + r1*r3 + r2*r3)x

- (r1*r2*r3).

Case III: For the polynomial (x - r1)(x - r2)(x - r3)(x - r4), the direct form of the polynomial is

x^4 - (r1 + r2 + r3 + r4)x^3 + (r1*r2 + r1*r3 + r1*r4

+ r2*r3 + r2*r4 + r3*r4)x^2

-(r1*r2*r3 + r1*r2*r4 + r1*r3*r4 + r2*r3*r4)x

+ r1*r2*r3*r4..

The pattern is evident and is easily programmed

X Module RF4 (Partial Fraction Expansion & Inverse Laplace)

Finding the impulse response of a transfer function G(s) involves three steps.

(1) Obtain the partial fraction expansion of G(s).

(2) Obtain the analytical expression for the impulse response from a lookup table.

(3) Evaluate the analytical expression and plot the voltage response versus time.

If the step response of the transfer function is desired (instead of the impulse response) then the procedure is identical except G(s)/s is used in place of G(s) for step (1).

The partial fraction expansion is obtained by using Gaussian elimination to solve a set of linear simultaneous equations for the coefficients of the residues. This method results in a Vandermonde matrix which is generally not numerically stable for filters of order greater than 10. Verification routines have been added in this module to verify the intermediate results.

Cuthbert (10) provides a method of partial fraction expansion that avoids the numerical instabilities due to solving the Vandermonde matrix. A recent publication by Westreich (19) extends this technique to the general case where the numerator and denominator can have arbitrary order. However, for any of these methods, the roots of the denominator must first be known. If the input data is taken from a stored file, then the module RF4 will have direct access to the poles of the transfer function. Once the partial fraction expansion is determined, the impulse, or step, response can be evaluated directly from a lookup table of Laplace transforms in the computer program. This table is constructed to handle both simple and multiple poles.

Table 4

F(s)	f(t)
1	unit impulse at t = 0
1/s	1, (unit step at t = 0)
$1/(s+a)$	e^{-at}
$w_o/(s^2 + w_o^2)$	$\sin(w_o t)$
$s/(s^2 + w_o^2)$	$\cos(w_o t)$
$w_o/[(s+a)^2 + w_o^2]$	$e^{-at} \sin(w_o t)$
$(s+a)/[(s+a)^2 + w_o^2]$	$e^{-at} \cos(w_o t)$
$1/s^2$	t
$1/(s+a)^2$	$t\, e^{-at}$
$1/[(s+a)^2+w_o^2]^2$	$e^{-at}[\sin(w_o t)-(w_o t)\cos(w_o t)]/(2w_o^3)$
$s\, F(s)$	$d[f(t)]/dt$

XI Module RF5 (General Circuit Simulation & Monte Carlo Analysis)

A simple circuit simulation routine is provided for users who do not have access to a version of Spice. RF5 will handle circuits with up to 25 nodes and will do either an exact simulation or a Monte Carlo simulation using a random variable with a uniform distribution over the specified tolerance. This module has been written to allow optimization of passive circuits manually. The main program, RFDESIGN, will not allow elliptic filters with unequal terminations. RF5 lets the user change the source, or load, termination and modify the L-C components values accordingly so that an approximate elliptic response is preserved.

The procedure is

(1) select the stored design as the input data file,

(2) run an exact analysis of the original circuit,

(3) change the source, or load, termination resistor to the desired value,

(4) select option (10) in the program menu that says "Repeat with changes and show error",

(5) modify the inductor and capacitor values to minimize the mean square error term and repeat (4).

The mean square error given in the program is a measure of the deviation of the shape of the original response to the shape of the modified circuit response regardless of the difference in insertion loss between the two circuits. This manual iteration procedure will quickly converge to a point where no further improvement in the response can be obtained.

XII Module RF6 (Air Core Inductor Design)

RF6 predicts the number of turns of wire to achieve a certain inductance for an air coil, using an approximation that is valid for a single layer of turns. Given

L = the desired inductance in Henries,

A = the diameter of the coil in inches, and

B = the length of the coil in inches,

the number of turns is computed by the formula,

$$N = \frac{1}{A}\sqrt{L*1E6*(9A+10B)}$$

XIII Module RF7 (Standard Resistor Substitution)

Module RF7 reads filename.NET and replaces any resistors with the nearest 10%, 5%, or 1% values. The new file can be used for Monte Carlo simulations or Spice simulations. Lines 460-490 give the 10% resistor values, 590-660 give the 5% values, and 750-930 contain the 1% resistor values. These lines may be edited to delete or add values.

XIV Module RF8 (Spice File Conversion)

RF8 converts files to Spice compatible files. The output file must be edited to add the frequency range of analysis before using Spice.

XV Module RF9 (Image Parameter Filters)

Image parameter filters were popular during the 1940's because they give a sharper response than Tchebyscheff and require very simple calculations to get the inductor and capacitor values. The derivation of the procedure given below can be found in (13).

Let f_c = the cutoff frequency of the lowpass prototype in Hertz,

$w_c = 2\pi f_c$,

R = termination resistance (equal at both ends)

m = 0.6

$$\text{compute } L = \frac{2R}{w_c}$$

$$\text{compute } C = \frac{2}{R * w_c}$$

The filter becomes

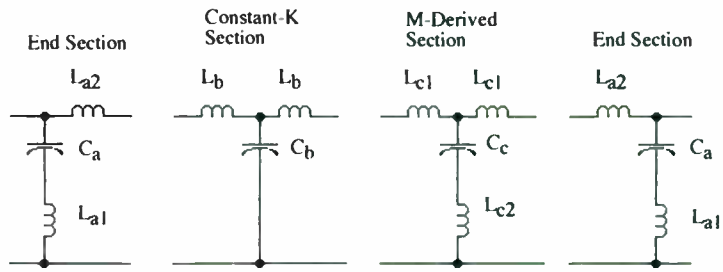

$L_a = m*L/2$ $\quad L_b = L/2$ $\quad L_{c1} = x*L/2$ $\quad L_{a2} = m*L/2$

$C_a = m*C/2$ $\quad C_b = C$ $\quad C_c = x*C$ $\quad C_a = m*C/2$

$$L_{a1} = \frac{(1-m^2)*L}{2*m} \qquad L_{c2} = \frac{(1-x^2)*}{4*x} \qquad L_{a1} = \frac{(1-m)*L}{2*m}$$

where $x = \sqrt{(1 - [\, w_c/w_\infty \,]^2)}$

The user specifies the frequency, w_∞, in the stopband for each M-derived section. Also the number of constant-K sections, the number of M-derived sections, and a w_∞, for each M-derived section must be specified. The sections are then cascaded by the program to create the entire filter. Bandpass transformations are done as required.

Summary

A new program is in development that will also realize active, digital, and switched capacitor filters. In the past several months, enhancements have been made to allow operation in conjunction with a digital signal processor (DSP). The filter coefficients can be automatically downloaded to the DSP to realize Infinite Impulse Response (IIR) filters, and finite impulse response filters (FIR) including window designs and the Parks-McClellan algorithm.

Active filters are being researched that will allow stable circuits with Q's up to 5000. Custom switched capacitors filters, based on the bilinear Z transform are now supported.

References

1. A First Course in Numerical Analysis, Ralston, A, and Rabinowitz, P., 1978, McGraw-Hill
2. Numerical Analysis, Burden, Richard and Faires, J. Douglas, PWS-Kent Publishing Company
3. Linear Programming and Extensions, Wu, Nesa and Coppins, Richard, McGraw-Hill
4. Handbook of Filter Synthesis, Zverev, Anatol I., Wiley-Interscience, 1967
5. Active Inductorless Filters, Mitra, Sanjit K., IEEE Press 1971
6. Passive and Active Network Analysis & Synthesis, Budak, Aram, Haughton Mifflin, 1974
7. Electronic Filter Design Handbook, Williams, Arthur B., McGraw-Hill, 1981
8. Theory and Application of Digital Signal Processing, Rabiner, Gold, Prentice-Hall, 1975
9. Switched Capacitor Circuits, Allen, Sanchez-Sinencio, Van Nostrand Reinhold Company, 1984
10. Circuit Design Using Personal Computers, Cuthbert, John Wiley and Sons, 1983
11. Programs for Digital Signal Processing, Digital Signal Processing Committee, IEEE Press, 1979
12. Operational Amplifiers, Design and Applications, Tobey, Graeme, Huelsman, Burr-Brown, 1971
13. Microwave Engineering, Pozar, David M., Addison-Wesley, 1990
14. Elliptic Approximation and Elliptic Filter Design on Small Computers, Amstutz, P., 1978, IEEE Trans. Circuits syst., December, pp1001-1011
15. An $O(N^2)$ Algorithm for Partial Fraction Expansion, Chin, F. Y., and Steiglitz, K., 1977, IEEE Trans. Circuits Syst., January, pp. 42-45
16 Approximation Methods for Electronic Filter Design, Daniels, Richard W., McGraw-Hill
17. Chebyshev Filters with Arbitrary Source and Load Resistance, Porter, Jack, RF Design Magazine, pp 63-68.
18. On the Element Values of Mid-series and Mid-shunt lowpass LC Ladder Networks, IEEE Trans. Circuit Theory, Lin, C. C., and Tokad, Y., December, 1968, pp. 349-353.
19. Partial Fraction Expansion Without Derivative Evaluation, Westreich, David, IEEE Trans. Circuits and Syst. June 1991, pp 658-670

DESIGN OF LOW NOISE RF AND MICROWAVE AMPLIFIERS

Richard C. Webb
Webb Laboratories
139 E. Capitol Drive Suite 4
Hartland, Wisconsin 53029
TEL (414) 367-6823 FAX (414) 367-6824

ABSTRACT

A comprehensive tutorial begins with discussion of system noise contributions and then dedicates itself to noise characteristics of RF and microwave small-signal amplifiers. Design examples unify the interdependence of amplifier gain, port VSWR, stability and noise performance of open loop as well as feedback arrangements. Single-ended and balanced configurations are compared. Finally, the theory and practice of noise measurement are discussed.

A comprehensive hand-out will be provided at time of presentation, or may be obtained at no cost by contacting the presenter.

OUTLINE

Introduction
- System Noise Contributions
  - Antenna Noise
    - Background Contribution
    - Ohmic (Antenna) Contribution
  - Feedline Noise
  - Intrinsic Receiver Noise
    - Noise Temperature
- *Example*

The Generic Small Signal RF Amplifier Block
- The Travelling Wave Approach
  - Scattering Parameters
  - Gain
  - Input & Output Impedances
  - Stability
  - Noise Factor and Noise Figure
  - Noise in Cascaded Stages

The Active Device
- Scattering Parameters
- Minimum Achievable Noise Figure
- Optimum Noise Source Impedance
- Noise Resistance
- Optimum Load Impedance
- Measurement of Device Parameters

The Single-Stage Single-Ended Amplifier
- Stability Considerations
  - Maximum Available Gain
    - Simultaneous Conjugate Match
  - Maximum Stable Gain
  - Gain Degradation with Port Mismatch
- Optimum Noise Performance
  - Optimum Source Impedance
  - Optimum Load Impedance
  - Gain and Input VSWR Degradation
    - Apparent Minimum Noise Paradox
  - Noise Degradation with Port Mismatch
- *Example*

The Single Device Amplifier With Feedback
- Lossy Feedback
  - *Example*
- Lossless Feedback
  - Transformer-Coupled Feedback

The Balanced Amplifier
- Noise Performance
- Advantages
  - Input Match
  - Stability
  - Dynamic Range
- Disadvantages
  - Complexity
  - Difficulty of Tuning
- *Example*

Design Method Summary

Noise Measurements
- General Technique
- Cooled Source Termination Method
  - *Example*
- Noise Diode Method
  - *Example*

DESIGN OF LOW NOISE

RF & MICROWAVE AMPLIFIERS

Richard C. Webb
Webb Laboratories
Hartland, Wisconsin

NOISE FACTOR

$$F = \frac{S_i / N_i}{S_o / N_o}$$

MAIN OUTLINE

Introduction
The Generic Small Signal Amplifier Block
Device Characterization
The Single Device Amplifier
The Single Device Amplifier With Feedback
The Two-Stage Amplifier
The Balanced Amplifier
Design Method Summary
Noise Measurements

NOISE FIGURE

$$NF = 10 \, LOG_{10} (F)$$

THE LINEAR AMPLIFIER

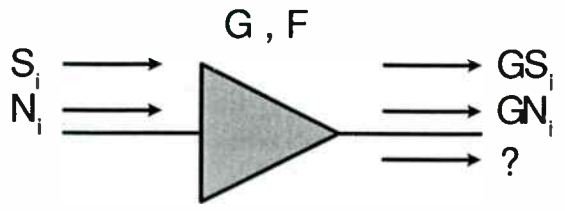

NOISE FACTOR

$N_o = G [N_i + (F - 1) (290) K]$

If $N_i = (290) K$

then

$N_o = G F (290) K$

and

$$\frac{S_o}{N_o} = \frac{G S_i}{G F (290) K}$$

NOISE FACTOR

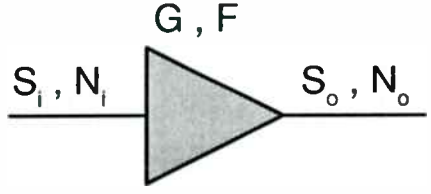

$S_o = G S_i$

$N_o = G N_i + G (F-1) (290) K$

$N_o = G N_i + G K T_n$

$T_n = 290 (F-1) =$ Noise Temperature - °K

$K = 1.38 \times 10^{-23}$ joule / °K (Boltzmann)

IEEE DEFINITION OF NOISE FACTOR

$$F = \left. \frac{S_i / N_i}{S_o / N_o} \right|_{T_s = 290\,^{\circ}K}$$

ANTENNA & RECEIVER NOISE

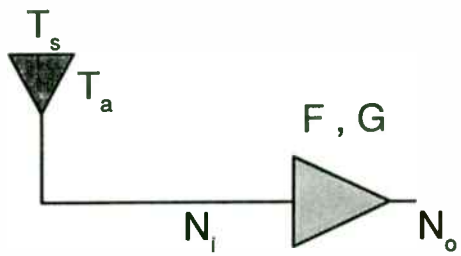

$N_i = K [\eta T_s + (1 - \eta) T_a]$

$N_o = G K [\eta T_s + (1 - \eta) T_a + 290 (F - 1)]$

η = ohmic antenna efficiency

WHY CARE ABOUT NOISE FIGURE?

Example:

$T_s = 10\ ^oK$ $T_a = 300\ ^oK$ $\eta = 96\%$

NF (dB)	N_i (dBm/Hz)	Δ (dB)
0	-183.33	0
0.1	-182.54	0.79
0.2	-181.86	1.47
0.5	-180.21	3.12
1.0	-178.21	5.09

EQUIVALENT IDEAL AMPLIFIER

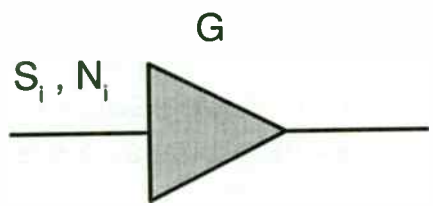

$N_i = K [\eta T_s + (1 - \eta) T_a + 290 (F-1)]$

CASCADED STAGES

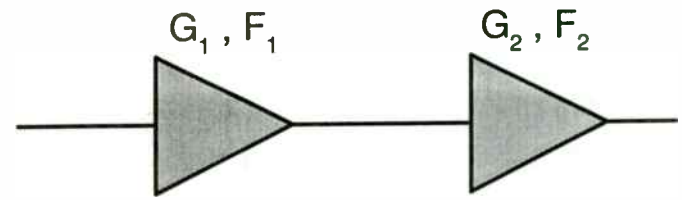

$G_c = G_1 G_2$

$F_c = F_1 + \frac{F_2 - 1}{G_1}$

THE TRAVELLING WAVE APPROACH

Based on S-Parameters
Convenient
Relates Easily to Gain, Port VSWR
Relates Easily to Stability
Relates Easily to Noise Performance

TRANSMISSION & REFLECTION

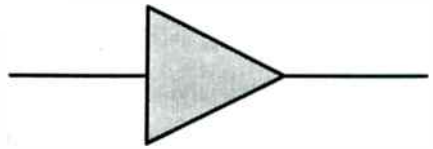

Assume 50Ω S-Parameters in a 50Ω System

S_{11} = Input Reflection Coefficient
S_{22} = Output Reflection Coefficient
S_{21} = Forward Voltage Gain
S_{12} = Reverse Voltage Gain (Isolation)

SCATTERING PARAMETERS

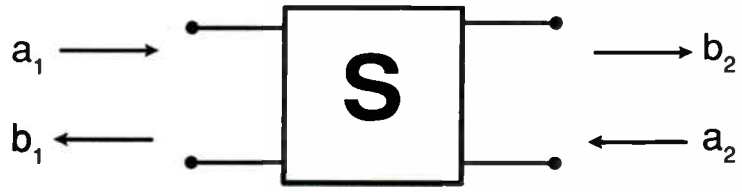

$$\begin{bmatrix} b_1 \\ b_2 \end{bmatrix} = \begin{bmatrix} S_{11} & S_{12} \\ S_{21} & S_{22} \end{bmatrix} \begin{bmatrix} a_1 \\ a_2 \end{bmatrix}$$

STABILITY RELATIONSHIPS

$$K = \frac{1 + |\Delta|^2 - |S_{11}|^2 - |S_{22}|^2}{2\,|S_{21}\,S_{12}|}$$

$$\Delta = S_{11}S_{22} - S_{21}S_{12}$$

STABILITY RELATIONSHIPS, ETC.

$$B_1 = 1 + |S_{11}|^2 - |S_{22}|^2 - |\Delta|^2$$

$$B_2 = 1 + |S_{22}|^2 - |S_{11}|^2 - |\Delta|^2$$

$$C_1 = S_{11} - \Delta S_{22}^*$$

$$C_2 = S_{22} - \Delta S_{11}^*$$

$$\Gamma_{ms} = C_1^* \frac{B_1 \pm [B_1^2 - 4|C_1|^2]^{1/2}}{2|C_1|^2}$$

$$\Gamma_{ml} = C_2^* \frac{B_2 \pm [B_2^2 - 4|C_2|^2]^{1/2}}{2|C_2|^2}$$

For $\Gamma_{ms,l}$ use + if $B_{1,2} > 0$ and - if $B_{1,2} < 0$

DEVICE CHARACTERIZATION

1. Measure S-Parameters
2. Measure Noise Data:

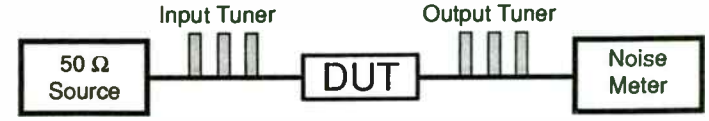

3. Adjust Tuners for Minimum Noise Figure
4. Read F_{opt}
5. Measure Γ_{opt} at Input Tuner Output

REQUIRED DEVICE INFORMATION

S-Parameters

F_{min} - Minimum Achieveable Noise Figure

Γ_{opt} - Optimum Source Reflection Coefficient

R_n - Equivalent Noise Resistence

or

F_o - Insertion Noise Figure

DEVICE CHARACTERIZATION CONTINUED

6. Remove Tuners
7. Reconnect DUT in Noise Measurement Apparatus
8. Read F_o
9. Calculate R_n

EXAMPLE - DEVICE CHARACTERISTICS

S11	S21	S12	S22
$.61 \angle 152°$	$1.89 \angle 55°$	$.099 \angle 79°$	$.47 \angle -30°$

F_{opt} - dB	Γ_{opt}	R_n - Ω
1.2	$.10 \angle 15°$	8.5

K = 1.120
G_{max} = 10.7 dB

EXAMPLE - MATCHED AMPLIFIER

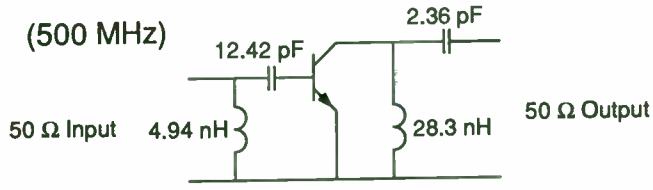

$|S_{21}| = G_{max}$, $|S_{11}| = |S_{22}| = 0$

Noise Figure = 4.9 dB (F_{opt} = 1.2 dB)

EXAMPLE - CONJUGATE MATCH

Source: $\Gamma_{ms} = .846 \angle -154$ = 4.40 - j11.46 Ω

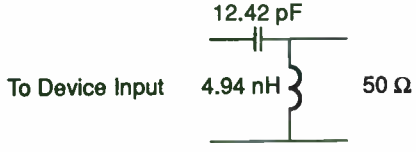

Load: $\Gamma_{ml} = .795 \angle 27$ = 85.6 + j67.5 Ω

EXAMPLE - NOISE MATCH

At 500 MHz : Noise Source = 60.6 + j3.17 Ω

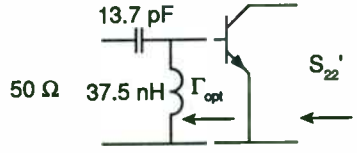

1. Synthesize Optimum Noise Source
2. Connect Active Device
3. Measure Device Output - S_{22}'
4. Synthesize $S_{22}'^*$
5. Attach $S_{22}'^*$ to Device Output

EXAMPLE - NOISE MATCH

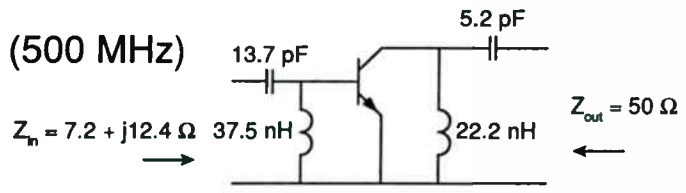

Input VSWR = 7.34 : 1
Output VSWR = 1 : 1
Gain = 5.98 dB
G_{max} - Gain = 4.72 dB
Noise Figure = F_{opt} = 1.2 dB

FIXING THE INPUT VSWR

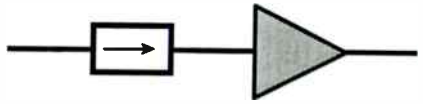

1. Input VSWR = 1 : 1
2. NF Degrades by Isolator (Circulator) Loss
3. Stability Generally Improved

THE BALANCED AMPLIFIER

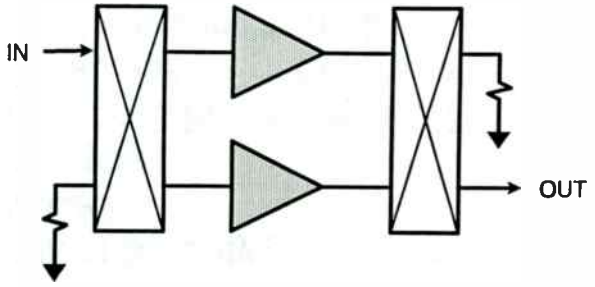

1. Input VSWR = 1 : 1
2. NF Degrades by Hybrid Loss Only
3. Comp. Point Improves by ~3 dB.

DESIGN METHOD SUMMARY

1. Make Tentative Device Selection
2. Make Preliminary S-Parameter and Noise Data Determination
3. Investigate Stability In-Band and Out-of-Band
4. Do Preliminary Design. Verify Reasonable Operation via Suitable CAE Tool.

DESIGN METHOD SUMMARY CONTINUED

5. Design Bias Arrangement Based on Topology of Preliminary Matching Networks.
6. Look at Stability and RF Performance via CAE
7. Prototype
8. Measure S-Parameter and Noise Characteristics of Complete Amplifier
9. Calculate Stability Traits

NOISE MEASUREMENT IN GENERAL

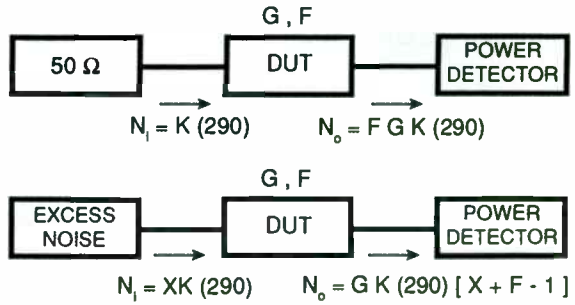

MICROWAVE ELECTRONIC WARFARE SYSTEM ENHANCEMENTS USING MMIC TECHNOLOGY

John D. Summerville
AIL Systems Inc.
Melville, New York 11746

ABSTRACT

The military market of the 1990's is driven by the need to provide small, reliable, and cost-effective solutions to both retrofit and forward fit designs of electronic warfare (EW) systems. The multiyear Defense Advanced Research Projects Agency's Microwave/Millimeter-Wave Monolithic Integrated Circuits (DARPA MIMIC) Program illustrates that the Department of Defense (DoD) recognizes that GaAs MMIC (gallium-arsenide monolithic microwave integrated circuitry) is the technology that will allow the radio frequency (RF) and intermediate frequency (IF) subsystem portions of EW systems to meet these objectives.

This paper will discuss MMIC insertion methodology that combines Defense Advanced Research Projects Agency (DARPA) MIMIC Program and commercially available GaAs chips with in-house MMIC designs to form key elements of a design library. This methodology will allow the design team to take maximum advantage of existing and anticipated near-term GaAs MMIC and related technologies. It will be demonstrated that intelligent application of MMIC and MMIC compatible approaches to EW designs will minimize nonrecurring engineering (NRE) and time-to-market, and will provide an early return on heavy industry and government investments in GaAs MMIC. The term "MMIC compatible" describes devices, components, and functions that are not monolithic but have attibutes such as small size, compatible thermal dissipation, number of inputs and outputs, etc., that allow them to be integrated into MMIC based modules. The methodology will be presented in the context of both new designs and upgrades to existing ones.

INTRODUCTION

The current military philosophy on EW systems was recently summarized by a key systems engineering director on the avionics portion of the F-22 Program: "We stopped providing the best of everything, which automatically elevated the cost and risk involved... Engineers had to justify design dollars rather than dBs" (reference 1).

Current thinking, as illustrated by statements like the one above, and the euphoria of the last few years surrounding GaAs MMIC, has energized the minds of EW design teams to the question: "Does MMIC belong in our system?" The answer is emphatically, Yes! The utility of any emerging technology is measured by how quickly and innovatively it can be transformed into a product. The benefits that MMIC technology can bring to military EW systems are summarized qualitatively in Table 1. These benefits will be illustrated by examples of typical receiver and exciter functions which are discussed in the context of MIC, first-cut MMIC/MIC, and time-phased MMIC designs.

With MMIC moving toward practical applications, designers must realize that it is a powerful technology, but not utopia to all RF/IF designs. There will be times when a mix of MMIC, MIC, and discrete technology is the optimum solution. Examples of such cases will be applied to receivers and exciters to allow for efficient MMIC/MIC trade-offs early in the design phase.

During the electrical design phase, issues related to cost-effective producibility must be considered. They will be discussed in conjunction with suggested trade-offs to lead to an optimum final product.

TECHNICAL DISCUSSION

MMIC Insertion Methodology

To take maximum advantage of MMIC technology, a design team needs a step-by-step procedure for an orderly, time-phased insertion of MMIC/MMIC compatible subassemblies into military EW systems. Figure 1 summarizes a MMIC insertion methodology geared toward providing the design team with ready access to a circuit library based on repetitive EW functions.

Table 2 summarizes a number of design library building blocks that are based on the use of existing, broadband chips. It is more efficient to design with available MMIC chips than to "reinvent the wheel." Force feeding existing chips into system architecture allows EW suppliers to concentrate on value added engineering. Custom MMIC should be used only when a suitable function is not available or quantities warrant an investment in a custom design. There may also be cases where a strategic company advantage can be gained by using custom devices.

As shown in Figure 1, GaAs MMIC chips are available from the DARPA MIMIC Program, commercial suppliers, and in-house designs. Using these chips, the design library forms the basis for generic, MMIC/MIC modules for military application (MMIC chips and MIC support circuitry combined to form multifunction RF/IF assemblies). Prior to the application of the implementation methodology, these sources will be reviewed.

DARPA. DARPA MIMIC chips are generally more complex, have better performance specifications, and are more application specific than commercial chips, allowing integrated modules to be built with fewer active components to realize smaller size and reduced costs. DARPA chips should soon be economically available to subsystem designers.

Merchant Vendors. The number of MMIC chips available commercially number in the hundreds. In addition to amplifiers and switches that are relatively common, examples of readily available chips from representative vendors include downconverters from Avantek, Pacific Monolithics, TI and TRW; digital and analog attenuators from MA/COM, TRW, and others; and a wide variety of chips from Alpha, including MMIC's for MMW applications.

In-house Designs. Some EW systems' houses have a resident MMIC capability to provide additional flexibility in designing custom chips for strategic benefit. AIL Systems Inc. has a unique approach to in-house designs where several MMIC and QMMIC (quasi-MMIC) chips have been developed for EW applications. (QMMIC is a design procedure where all circuit functions except the active devices are implemented monolithically.) This allows the designer to realize most of the benefits of MMIC, with enhanced performance, reduced NRE costs, and quicker turnaround time. QMMIC designs can later be updated to a fully monolithic implementation.

Selected Trade-offs

The technology used to implement individual functions into MMIC intensive modules will have a major impact on performance, size, and producibility. Since mixers and filters are two of the more repetitive EW functions that require trade-offs early in the design phase, they are discussed below.

Mixers and Converters. A lot of work has been done using MMIC mixers as upconverters and downconverters. This includes the use of planar diodes for millimeter-wave applications and field-effect transistors (FET's) for singly and doubly balanced RF and microwave circuits. However, the number of MMIC mixers that are readily available from commercial sources is limited, with Pacific Monolithics having what is probably the most extensive line of catalog MMIC converters. In mid-1990, TI/DARPA announced complementary MMIC upconverters and downconverters, each covering 6 - 18 GHz with an IF range of 0.1 - 8 GHz, but as of June 1991, they were not yet available commercially. TI is now in the "preproduction sample" phase of a 6 - 18 GHz MMIC mixer (with a user specified IF BW) that can be used as either an upconverter or a downconverter.

M/A-COM has recently announced two GaAs mixers. One is a double balanced device covering 6 - 14 GHz, the second is an image rejection unit covering 8 - 16 GHz, both with a 0.1 - 1.5 GHz IF range. They are expected to be available in production quantities in late 1991 or early 1992. The image rejection mixer requires the addition of an external IF quadrature hybrid.

Considering the present limitations of MMIC mixers and converters, their applicability must be examined on a case-by-case basis since conventional MIC mixers may offer better dynamic range and bandwidth performance. MMIC converters with on-chip RF, IF, and local oscillator (LO) amplifiers offer tremendous size and cost advantage but as with MMIC mixers, must be used judicially. Additionally, many applications require preselectors immediately prior to and after heterodyning, which means the user needs access to the RF and IF ports of the mixer.

Filters. Typically, over 50 percent of the volume of current EW subsystems is made up of filters. However, a lot of work is yet to be done to address noise and dynamic range considerations before active monolithic filters are practical as signal processing components in EW systems. In the near term, the RF designer must look at filters that are small enough to be printed and integrated into modules or printed (or dropped in) on the parent board. High-

K ceramic materials lend themselves to small printed filters in the lower microwave frequencies, and should be considered as an alternate to lumped-element designs.

For RF and the lower microwave frequencies below 1 GHz, miniature lumped-element devices are usually still the best choice. Up to about 6 GHz such filters can be designed using surface-mount technology compatible with microstrip. For low frequency filters, miniature chip components can be also be used unpackaged within a module, or directly on a parent board.

With the choice of optimum filter topology a crucial issue during the productionizing of a program, MMIC compatible filter implementation is discussed in depth later under "Technology Choice Examples Relating to Productionizing."

Next Higher Assembly Implementation. Once the design library building blocks are identified and the appropriate MMIC/MIC modules are designed, they must be combined into complete RF/IF assemblies (SRU's or SRA's) as shown in Figure 1. The modules can be either outfitted with connectors or installed into a microstrip parent board. Maintainability and testability can be enhanced at the SRU/SRA level with switches, and printed built-in-test (BIT) couplers.

MMIC/MIC Integrated Modules

Three examples of integrated MMIC/MMIC compatible modules that have been or are being built at AIL are discussed in detail below. Each of them was designed using the MMIC insertion methodology described. Chips from DARPA and commercial sources were used along with MIC support circuitry and in-house designs of printed filters. All designs were done using CAD/CAE tools, allowing cost-effective, timely design updates by electronic modification of electrical and mechanical parameters.

N-Channel Preselector Assembly. Figure 2 is a block diagram of a two-channel preselector, variations of which are used in many EW systems. The input RF path includes a signal sampler with a detector and associated video circuitry to provide high-level signal presence capability. The prototype unit used MMIC switches with MIC drivers, and edge-coupled microstrip filters on alumina substrates. Figure 3 is a photograph of the prototype. It measures 1.6 in. X 0.9 in., with the width driven by the MIC switch drivers. Prior to production, MMIC switches can be used with on-chip drivers to reduce the size and cost. Where performance requirements allow, interdigital microstrip filters will replace the edge-coupled designs to further reduce size and production costs.

RF Downconverter. Downconverters are one of the most commonly encountered functions in EW systems. AIL has recognized this and made the inclusion of a versatile MMIC based downconverter module in our design library a high priority. Figure 4 illustrates the MMIC based design for a generic wide-band

downconverter. It accepts an input over the EW frequency range of 2 - 18 GHz, and with appropriate LO's and application specific filters, all or a selected portion of the input spectrum can be downconverted to IF. The downconverter can be implemented using the TI/DARPA chips discussed earlier. These chips also include on-chip switches and TTL drivers to provide a bypass mode for frequencies below 6 GHz. The filters use standard carriers with application specific substrates.

Digitally Controlled Amplifier/Attenuator Assembly (DCA). The ability to dynamically adjust the end-to-end gain of an RF/IF chain of components in an EW system is key to operational versatility. Multichannel electronic support measures (ESM) systems need a convenient way to normalize channel-to-channel gain, which can vary as a function of frequency, temperature, and component parameter windows. Exciters have similar needs for rapid, real-time amplitude control. AIL has addressed these needs with the DCA module shown in Figure 5. The key MMIC device is the 6-bit digitally controlled chip developed by TRW/DARPA. It covers a frequency range of dc to 2 GHz with a dynamic range from +31 to -31 dB and includes on-chip decoding. Data on the DCA chip is shown in Figure 6. A cost-effective application for the DCA is in exciter systems that employ digital RF memories (DRFM's), where the DCA module would be used both at the DRFM input to rapidly adjust the input level and at the DRFM output to provide dynamic level setting prior to upconversion.

MMIC Forward Fit Examples

MMIC Upconverter for Exciter Applications. AIL has also addressed the fact that exciter upgrades in the 1990's will include band extensions to counter new frequency threats. Figure 7 shows a block diagram of an upconverter built for this application. A narrow input frequency range is used to generate a broadband output that includes the input range and the upper and lower sidebands. The design was implemented with three modules as indicated by the dotted lines in Figure 7.

Figures 8 and 9, respectively, are photographs of the input and output modules. The input module uses a commercial MMIC amplifier and switch with MIC driver (to be replaced by recently available switches with on-chip drivers). The active divider was developed by ITT/DARPA. The output module uses a dual-gate MMIC amplifier (implemented with the DARPA/Teledyne 2 - 18 GHz chip mentioned earlier) to provide automatic gain control, and the high-power output stage is a fixed gain block from TI. The preselector module is identical to the unit previously discussed.

Dual-band, Two-Channel Receiver. Figure 10 illustrates AIL's design for an ultra-lightweight, highly reliable, dual-band, two-channel receiver. The use of existing DARPA and commercial MMIC chips from the design library enabled the receiver to simultaneously meet all its design parameters, where high performance and reliability requirements were coupled with the need for low production costs, low dc power, small size and weight, and ease of maintainability.

TRW's model A-H06 MMIC log IF amplifier (LIF) developed on the DARPA Program was key to the successful design and implementation of the receiver. It is available as a chip or in a 0.27 in. square surface-mount device. It operates from 0.3 to 2 GHz, has greater than 55 dB of dynamic range, and provides both a video output for amplitude information and a limited IF output which is used for encoding the relative phase between the channels. Figure 11 is data taken on a packaged LIF.

The downconversion is provided by a commerical MMIC chip (Pacific Monolithics) and includes RF, LO, and IF on-chip amplifiers. The LO function is implemented by two small, MMIC dielectric resonator oscillators (DRO's) from Pacific Monolithics in a 0.5 in. square surface-mount flatpack. The inherent repeatability of MMIC processes enhanced the channel-to-channel tracking required. The LO distribution is done via a four-port, printed hybrid. This approach is MMIC compatible and less costly when compared to a switch, and minimizes the dc power and attendant thermal impact.

MMIC Retrofit Example

The above examples of MMIC implementation were forward fit. The next case represents a retrofit where the degree of freedom is limited since system architecture is fixed and the designer's task is to reduce the volume and cost and/or improve performance, reliability, and maintainability.

RF Converter Productionizing Example. Figure 12 is a strawman example of a complete wide-band converter shop replaceable assembly (SRA). A conventional mid to late 1980's implementation could require up to 20 standalone MIC and discrete assemblies and associated RF cables and provide limited fault isolation due to size constraints. If a 1990's retrofit were required to reduce the size and cost of the converter, it could be integrated into seven MMIC/MIC modules (shown shaded in Figure 13). With careful gain and loss distribution, the RF downconverter library building block shown in Figure 4 is used for downconverters A, B, and D by simply selecting the required filters. For performance considerations, the mixer used in the amplifier/upconverter module is a MIC drop-in device. The simplified block of the (DCA) shown in the output network is identical to the building block discussed earlier. An equivalent MIC DCA could have required either three separate assemblies (an input amplifier, a programmable attenuator, and an output amplifier) or a custom MIC assembly with attendant cost and development time.

A major contributor to the high cost of maintaining a fielded system over its operating life is the time it takes to locate a failed subassembly. The small size of MMIC components allows a greater emphasis on fault isolation. This is illustrated by the four signal samplers shown in Figure 12 which can easily be implemented using MMIC technology.

Design Library Utility Assessment

Table 2 presented an initial MMIC library consisting of 16 candidate building blocks that should be available to the subsystem designer. Table 3 verifies the usefulness of the library elements (1 through I6 in each table) by summarizing their broad application in the design of the integrated modules and the SRA-like assemblies discussed. Furthermore, it shows that it is practical to have entire functional modules (preselector, downconverter, and DCA) resident in the library.

The Flip-side of MMIC

Although versatile, MMIC must be applied intelligently. The designer must determine if MMIC is the technology that best fits his or her needs. As an example, for proof of concept hardware on a large platform, size may not be a consideration and MMIC may not be the best choice. Furthermore, MIC still offers performance improvements in certain cases. MMIC amplifiers generally have higher noise figures than their hybrid equivalents because of higher losses associated with monolithic inductors and capacitors. Lower noise figures are achievable with discrete low noise [field-effect transistors (FET's) and high-energy mobility transistors (HEMT's)] devices and MIC matching techniques. The use of active devices in place of those that are traditionally passive (couplers, power dividers, combiners, and isolators) must be evaluated on a case-by-case basis. For routine signal splitting and combining functions, the active splitters offer multioctave frequency operation, and size and cost advantages. However, a common application for a passive directional coupler is at the front end of a receiver for signal sampling or BIT injection. Here, insertion loss and dynamic range are paramount and an active MMIC signal splitter could not be used. In other cases, dc power and thermal considerations may outweigh the other advantages of MMIC.

Table 4 compares typical, readily achievable MMIC and MIC performance parameters for selected receiver and exciter EW functions in the 2 - 18 GHz frequency range. The table is intended as a guide to the designer when specific performance requirements override the size, cost, and reliability benefits of MMIC. As time goes on GaAs MMIC technology will improve, bringing full monolithic implementation of complex EW functions closer to reality.

Although RF and microwave switches are common EW functions, they are not included in Table 4 because the many configurations and trade-offs required for a specific application make straightforward comparisons difficult. The same tradeoffs (insertion loss vs isolation, speed vs dc power, size, and cost, etc.) that apply to MIC also apply to MMIC switches. MMIC switches (with and without on-chip drivers) are available up to SP4T and virtually any switching matrix function can be achieved in MMIC with appropriate cascading. In general, a monolithic implementation will be smaller and less costly than a MIC pin diode equivalent but will have less RF power handling capability. GaAs MMIC switches are inherently fast (2 - 5 nsec) but as with MIC, achieving this speed in a practical application is a function of system delays, control pulse rise times, and the driver and decoding circuits.

MMIC Producibility Issues

Producibility is the ability to cost effectively manufacture reliable products in a timely manner. Major factors affecting producibility include ease of manufacturing, testability, and maintainability. The design team must choose the appropriate mix of technology, components, materials and processes that together meet the producibility criteria. Every effort must be made to implement a design that minimizes the investment in materials and touch labor prior to test. Troubleshooting and rework is costly, time-consuming, and impacts reliability. Ideally, initial investment would be reduced to the point where a module is scrapped if failures with nonobvious causes are detected at initial test. This is not as drastic as it seems. GaAs reliability is improving, economical on-wafer RF probing is becoming a reality, and 4 in. wafers with 78 percent more chip area are replacing the conventional 3 in. ones. All of this will result in dramatically lower chip costs and reduce the odds of installing defective chips. These facts, when linked with reduced packaging costs and automated manufacturing, will minimize the module pretest investment.

As a means of illustrating the production benefits that can be realized by a well thought out design approach, a number of technology and implementation issues that must be addressed early in the subsystem design are discussed in detail below.

Packaging. Packaging is a major consideration when integrating MMIC and MMIC compatible devices into modules. Current estimates show that less than $100 worth of components, when integrated, screened and tested as a military module can cost well over $1000. A large part of this added cost is in the packaging. Unfortunately, most standard MMIC packages are not of a convenient form factor to be used for multichip MMIC functions with the required support circuitry. This is particularly true when the module contains filters and/or mixers. However, in certain cases, catalog packages can be used. Figure 13 shows a 2 - 18 GHz multifunction MMIC module built at AIL, housed in an ultra-small commercial hermetic package that contains six 50-ohm feedthroughs.

Alcoa Electronic Packaging, Inc. (Alcoa) has recently announced two sizes of multilayer cofired ceramic microwave packages for multichip modules to 18 GHz. They are presently available in two sizes, with one RF input and one RF output each, and up to 20 dc connections. Figure 14 shows the Alcoa packages.

Because of the limitations on RF interfaces on most commercial packages, an 18 GHz package has recently been designed by AIL and is a candidate for use as a standard. It features 16 feedthroughs distributed on four sides and measures 0.68 in. X 0.40 in. X 0.085 in. For maximum flexibility, all feedthroughs are 50-ohm microstrip.

For applications below 5 GHz, housings are readily available. Many hold two or more chips, each in its own cavity and are available with interconnecting pins, or with feedthroughs from one cavity to the next. In some packages, cavities are side by side, others have cavities on two different levels, one above the other.

In the near future, affordable packaging should be less of an issue. As part of the DARPA Phase 3 Program, Raytheon and TI are using an injection molding process, forcing copper and tungsten into a cast, rather than using conventional machining techniques. It is expected that this process can cut microwave module housing costs by 4:1 in large (10,000) quantities (reference 2). Similar work in metal matrix technology is also being done commercially by the LECD L. P. Division of the Lanxide Corporation as well as others.

Filters. Filters have a major impact of the size and cost of MMIC based modules and the need for microwave filters small enough to be integrated into modules cannot be overemphasized. Candidate technologies include printed edge- coupled and interdigital filters. Also warranting consideration for certain applications at the SRA level are filters built into coaxial cables.

Edge-coupled microstrip filters represent a mature technology with widespread application in EW systems. However, they tend to be large and not congruous with MMIC. Interdigital microstrip filters, although more complex to design, offer a small, compact form factor extremely compatible to integration with MMIC. Table 5 summarizes some of the major characteristics of edge-coupled and interdigital microstrip filters. Despite the disadvantages of slightly higher loss, bandwidth (BW) limitations, and more complicated design and CAE analysis steps, interdigital microstrip filters should be the first choice for use in MMIC modules. Typically, the design phase of an interdigital microstrip filter will be longer and more costly (may require more than one iteration) than that of an edge-coupled equivalent. Despite this, the resulting small size and compatibility with MMIC makes them a prudent investment.

A seven section band-pass filter centered at 10.5 GHz (BW = 500 MHz) in edge-coupled microstrip will be about 1-in. long when printed on material with a dielectric of 10.2. If done interdigitally on the same material, it will be about 0.13 in. X 0.25 in. Figure 15 illustrates the size and form factor differences between edge-coupled and interdigital microstrip filters on alumina.

DRO's. New materials (generally based on the titanates) have been developed that are ideal for MMIC based DRO's because of their small size. Until recently, the advantages offered by using MMIC devices in the active circuitry of DRO's was negated by the resonator size. This is no longer true (recall the drop-in DRO's in the dual-band, two-channel receiver discussed previously).

Thermal and Input/Output (I/O) Considerations. The level of MMIC integration and size reduction will often be limited by thermal aspects and the number of I/O connections. This is particularly true from the thermal point of view where package geometry may indicate an ability to achieve a higher level of integration than heat removal capacity will allow. Here, the design team earns its keep by making meaningful thermal trade-offs at the system design levels, where decisions should be made regarding the choice of active (which dissipate power and have dynamic range limitations) or passive signal splitters, isolators, and gain equalizers. As heat removal and packaging technologies mature, the percentage of active MMIC content and the level of integration in the RF/IF portions of EW systems will increase but probably

never approach what may appear feasible based on size alone. A notable exception is the area of smart munitions and expendable decoys where long-term operational reliability and life cycle costs (LCC's) are not issues and thermal requirements can be eased.

Other MMIC Producibility Issues

Once MMIC is accepted as the requisite technology for future EW applications, a major commitment must be made above and beyond design engineering. Capital investments are required in CAO/CAE engineering workstations and automatic test equipment (ATE) such as microwave chip probe stations with associated optical aids, and microstrip test fixtures for module level test and evaluation. They should be integrated into MMIC/MIC test stations with peripherals that include computer controlled ATE with network analyzers, spectrum analyzers, and multiple output programmable power supplies. This investment in equipment must be accompanied by a similar commitment to engineering and test personnel training.

Since the major benefits of MMIC are realized in cost-effective production, manufacturing facilities must also be upgraded and personnel trained. Included here are automated manufacturing approaches and a test philosophy that recognizes the improving reliability and yield of MMIC. Testing at the chip level should be limited to lot sampling, with 100 percent acceptance testing reserved for the integrated module level.

Beyond these investments, concurrent engineering and colocated work areas where design and manufacturing engineering work hand-in-hand from project inception through a successful pilot run are necessary. This ensures a design that is electrically acceptable and can be economically produced in a production environment. Toward this goal, there is an emerging philosophy that suggests that prototypes not be built by special groups like model shops. They normally are staffed with highly skilled personnel who can not only fabricate and assemble parts with sketchy information but can also make do with marginal manufacturing processes (reference 3). Building prototypes in specialized facilities fails to recognize the realities of a production environment.

SUMMARY

The importance of cost in the military EW market of the 1990s cannot be overemphasized. Subsystem designers must be innovative in their approach to new designs and retrofits. As MMIC continues to mature, the cost savings can be great. This is especially true when one considers acquisition and LCC. With the promise of higher reliability, on-chip BIT, and low impact (due to small size) redundancy, the maintenance costs of a fielded MMIC intensive system will be much less than the presently accepted LCC of ten times the initial cost. Electrical specification adherence is achieved more readily with MMIC due to a higher level of integration, leading to fewer RF interfaces, and resultant interaction effects. Repeatability is greatly improved due to inherent MMIC process controls, and tuning and alignment requirements

are reduced. The methodology presented should help designers make meaningful judgments for current and future requirements to ensure the best mix of technologies.

Although this paper concentrates on MMIC as applied to microwave receiver and exciters, the methodology and processes discussed apply equally to all EW systems. Two excellent examples of other areas where MMIC can make a major impact are in phased-array and millimeter-wave (MMW) applications. The small size and economies of scale associated with MMIC make multiple element active aperture phased arrays practical. Further, the advent of MMW MMIC components (particularly amplifiers and downconverters) make the addition of MMW capabilities more economical.

In conclusion, to be successful in the 1990's RF designers must apply MMIC technology in a sensible manner. This means a good electrical design that can be produced efficiently. This is best accomplished by involving all disciplines in the design from the earliest stages to make in-depth trade-offs prior to finalizing the design. The extra decibels of the 1980's may not be worth the dollars of the 1990's.

ACKNOWLEDGMENTS

The author wishes to thank Messrs. J. Rella, G. Tangredi, and J. Taub for their support in accomplishing the work described; Mr. J. Sheinwald for his major technical contributions in the design and testing of MMIC chips and modules; Dr. B. Mangla for his thoughtful review and suggestions in organizing the material presented; and Ms. L. Lundon for her patience through my many rewrites.

REFERENCES

1. Herskovitz, S., "Evaluations Over, On With the Real Thing!" Journal of Electronic Defense, Vol. 14, No. 7, July 1991.

2. Adams, C., "MMIC: Cutting Costs In Design, Fab & Test," Military & Aerospace Electronics, Vol. 2, No. 4, April 1991.

3. Denig, C. "Using Microwave CAD Programs to Analyze Microstrip Interdigital Filters," Microwave Journal, Vol. 32, No. 3, March 1989.

4. Grayzel, A. "A Useful Identity for the Analysis of a Class of Coupled Transmission Line Structures," I.E.E.E. Trans Microwave Theory Tech, Vol. MTT-22, Oct. 1974, pp. 904-906.

5. Shina, S., Concurrent Engineering and DFM for Electronic Products. New York, NY: Van Nostrand Reinhold, 1991, Chapter 1.

Table 1. Summary of MMIC Benefits

Parameter	Benefits
Electrical performance	Specification compliance achieved due to higher level of integration and fewer RF interfaces and attendant interactions. Repeatability is enhanced due to inherent MMIC process control and reduction in tuning and alignment. Gain/phase matching typically two to three times better with MMIC.
Cost	Acquisition costs reduced by a factor of 4:1. LCC will yield even more significant savings. LCC's are estimated at 10 times the acquisition costs in some quarters for current, non-MMIC systems. Here, improved reliability, greater potential redundancy, and more sophisticated self-test come into play.
Size (volume)	Analysis of major EW systems showed an estimated 10:1 reduction in volume when MMIC was introduced even though filters, isolators, and support circuitry were unchanged. Estimates were as high as 20:1 when an entire component could be realized in MMIC form. In a complete subassembly, where power supplies, filters, and other components which cannot be reduced by MMIC are included in the volume, reductions can be about 6:1. Similar results are predicted for weight and cable reductions.
Reliability	MTBF's of MMIC versions of EW subsystems are appreciably better, based on a failure rate analysis assuming screened parts.

Table 2. Design Library Building Blocks

Description	Key Parameters	Technologies/Notes
1. 2 - 18 GHz Preamplifier (with AGC)	G = 20 dB, P(out) = 20 dBm, NF = 4 to 7 dB	DARPA MIMIC chip is basis for design
2. dc 2 GHz 6-BIT DCA	62 dB range, TTL compatible	DARPA chip is design base
3. 6 - 18 GHz MMIC Compatible Filters	Small size	Microstrip on alumina (K = 10)
4. 2 - 6 GHz MMIC Compatible Filters	Small size BPF's, LPF's	Microstrip on high K (18-22) ceramic
5. Broadband Up and Down Converters	RF, LO = 8 - 18 GHz TTL RF bypass mode	Based on DARPA and commercial MMIC and MIC mixers
6. Active Signal Splitter	2 - 18 GHz, 1 - 8 GHz, 0.01 - 3 GHz	DARPA MIMIC/commercial
7. High-Speed Switches (with, w/o drivers)	To 18 GHz, SPST, SPMT	Monolithic PIN and GaAs based commercial chips
8. Passive Signal Samplers	Small size	Microstrip
9. Temperature Compensation Module	Small size, AGC control of MMIC FET's	MIC on alumina
10. 0.5 - 6 GHz Amplifier Family	A. Low NF, high gain B. Medium power	Commercially available MMIC
11. Switch Drivers	A. High Speed PIN B. High speed GaAs	MMIC on substrate and silicon MMIC chip
12. 6 - 18 GHz Amplifier Family	Low noise and general purpose	DARPA and commercial devices
13. 0.3 to 10 GHz General Purpose Amp	6 dB NF, P(out) = 10 dBm	Commercial, DARPA MMIC
14. 0.1 to 15 GHz Variable Attenuator	>20 dB variation, high dynamic range	GaAs MMIC
15. 0.3 - 2 GHz LIF	>55 dB range, limited IF output	DARPA/TRW chip and 0.27 $in.^2$ SMD
16. Subminiature DRO's	9 - 14 GHz in 0.5 $in.^2$ SMD	Commercial source

Table 3. MMIC Designs Related To Library Building Blocks

Design Example	Library Elements Utilized	
Integrated Modules		
N-Channel Preselector	3, 4:	MMIC Compatible Filters
	7, 11:	MMIC Switches, Drivers
Downconverter	1, 12:	MMIC Amplifier Family
	3, 4:	MMIC Compatible Filters
	5:	Broadband Downconverter
	6:	Active Signal Splitter
DCA Assembly	2:	6-BIT Digital Ampl/Atten
	7:	High Speed Switch/with Driver
	10:	0.5 - 6 GHz Ampl Family
SRA/SRU Level		
MMIC/MIC Upconverter for Exciters (Note 1)	1, 10, 12:	MMIC Amplifier Family
	3, 4:	2 - 6 GHz MIC Compatible Filters
	5:	Broadband MIC Converter
	6:	Active Signal Splitter
	7, 11:	MMIC Switches, Drivers
Dual-Band 2-Channel Receiver	5:	MMIC Downconverter
	15:	0.2 - 2 GHz LIF
	16:	Subminiature DRO (SMD)
RF Converter Productizing Example (Note 2)	3, 4:	MMIC Compatible Filters
	5:	Broadband MIC Converter
	6, 8:	Active, Passive Signal Samplers
	7:	MMIC Switches
	10:	0.5 - 6 GHz Ampl Family
	13:	0.3 - 10 GHz Ampl Family

Notes:

1. In addition to the library elements indicated, the MMIC/MIC Upconverter uses the N-Channel preselector integrated module discussed previously as an end item.

2. In addition to the library elements indicated, the RF converter productionizing example uses the downconverter integrated module described previously as an end item in three of the four conversion functions.

Table 4. Selected MMIC and MIC Performance Comparisons (1)

FUNCTION	TYPICAL PERFORMANCE	
	MMIC	MIC
Wideband Amplifiers (2)		
Noise figure: <2 GHz	4 dB	1.5-3 dB
2-8 GHz	5 dB	2-4 dB
6-18 GHz	6-10 dB	5-8 dB
2-18 GHz	7-10 dB	5.5-9 dB
Input VSWR (3)	2.5:1	2.0:1
Output VSWR (3)	2.75:1	2.5:1
P(out) (3), (4)	10-20 dBm	15-25 dBm
In-Phase Power Dividers		
Gain	2 dB	-3.5 dB
Frequency Range (5)	0.03-3 GHz, 1-8 GHz, 5 - 17 GHz	octave (large, multisection units have wider BW's)
Noise Figure	5-10 dB	3.5 dB
dc Power	0.8-1.4 W	NA (passive)
Phase Tracking	+/- 2 deg	+/- 5 deg
Amplitude Tracking	+/-0.25 dB	+/- 0.5 dB
Isolation Between Outputs	20-25 dB	15-20 dB
P(out)	10-15 dBm	NA (passive)
Mixers		
Conversion Loss (6)	7-12 dB	5-10 dB
RF, LO port BW's	to 12 GHz	to 26 GHz
IF BW	to 3.5 GHz	to 10 GHz
MXN Spurious (7)	20-30 dBc	40-50 dBc
Two-tone Products (7)	20-30 dBc	40-50 dBc

Table 4. Selected MMIC and MIC Performance Comparisons (Cont)

Notes:

1. The performance parameters given are a cross section of typical values from vendor data sheets and are not intended to represent the best performance available for either MMIC or MIC.

2. Wide-band amplifiers can be optimized for noise figure, usually at the expense of output power. For this reason, the lowest noise figures shown in the table are not necessarily available in the same device as those with high output power (Narrow-band amplifiers can achieve appreciably better performance.) A single MMIC amplifier that goes the furthest in combining the best of all worlds is the 2 - 18 GHz DARPA/Teledyne JV-1050 chip. It features 20 dB gain (at 100 °C, P(out)>20 dBm, and AGC range of 20 dB, P-P gain rippler (2-17 GHz) of 2 dB, and a noise figure of 4 dB at 2 GHz and 7 dB at 18 GHz (both at 25 °C). It is scheduled to be commercially available as Teledyne part number TMM-8901 in mid-1991.

3. Performance can be improved with balanced configurations at the expense of dc power, cost, and size.

4. P(out) for amplifiers represent 1-dB compression point of catalog devices for receiver and exciter driver applications and does not include amplifiers for high-power requirements.

5. Frequency range entries are operating BW's of MMIC power dividers readily available. The 5 - 17 GHz unit is the ITT/Alpha 279-11 developed on the DARPA MIMIC program. AIL has found it (based on a small number of samples) to be usable over a 2 - 18 GHz range with only slightly degraded performance.

6. Conversion loss for MMIC mixers is for devices without on-chip gain.

7. Typical performance for RF inputs at -10 dBm, LO drive of +13 dBm, and well-matched mixer ports.

Table 5. Edge-Coupled and Interdigital Microstrip Filters Compared

Parameter	Edge Coupled	Interdigital
Design	Straightforward	More complex
CAE Analysis	Straightforward	Must ignore coupling between nonadjacent lines when modeling. Errors small with higher dielectric substrate (Note 1)
Size	Relatively large	Small/compact
MMIC compatibility	Poor	Excellent
Second harmonic re-entry	Yes	No (Note 2)
Loss	Low	Higher (Note 3)

Notes:

1. Widely used microwave CAD programs (Touchtone-trademark of EEsof Inc. and Super-Compact trademark of Compact Software Inc.) are generally restricted to the analysis of singly coupled transmission line sections. Modeling multiple-coupled interdigital lines with these programs must be done by making certain assumptions (reference 4). Work by Grayzel (reference 5) has pointed out that multiple-coupled line structures can be modeled as parallel sections of singly coupled lines if coupling between adjacent lines is ignored. This results in some errors in the model - more pronounced at lower substrate dielectric constants.

2. Microstrip interdigital filters normally do not re-enter until the third harmonic.

3. Normally not a problem unless the filter is used in the front end of receiving systems prior to RF gain.

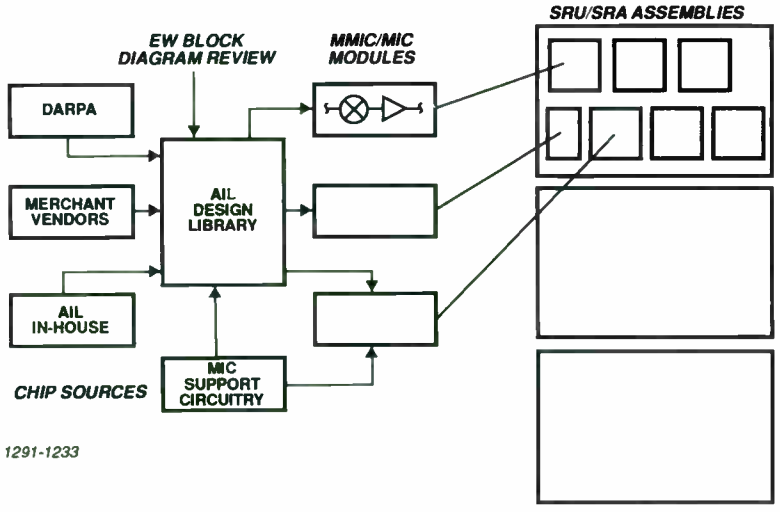

Figure 1. MMIC Insertion Methodology Flow Chart

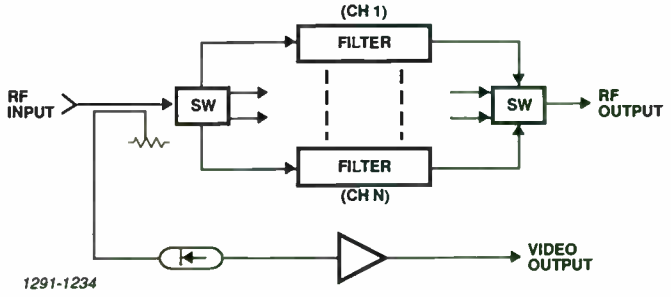

Figure 2. Switched Preselector Block Diagram

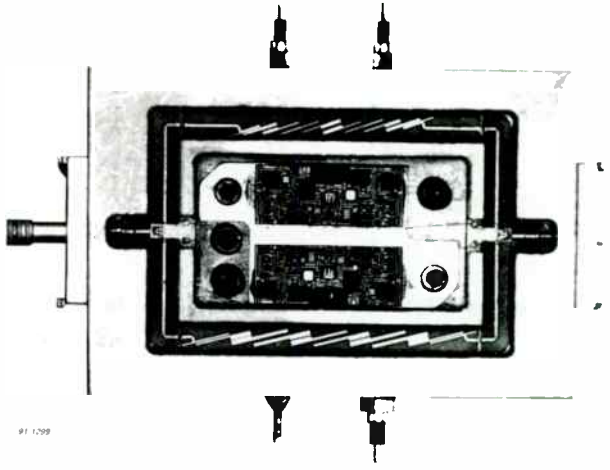

Figure 3. Prototype Preselector

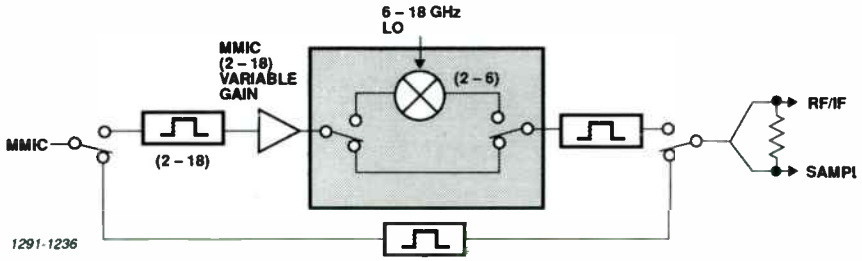

Figure 4. MMIC RF Downconverter

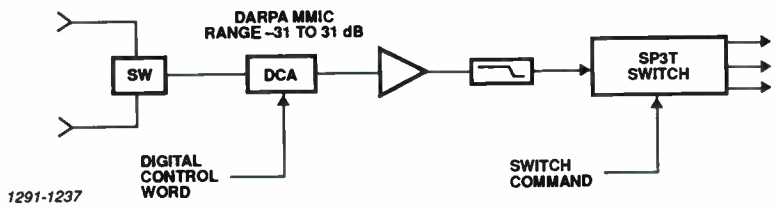

Figure 5. MMIC DCA Block Diagram

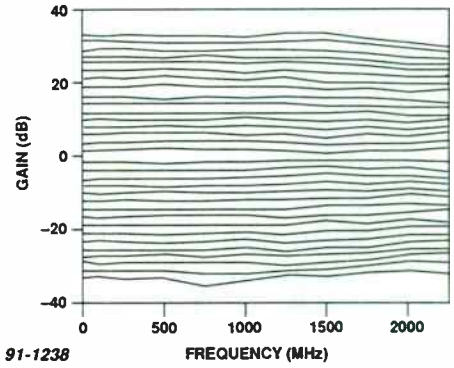

Figure 6. DCA Chip Data (Courtesy of TRW)

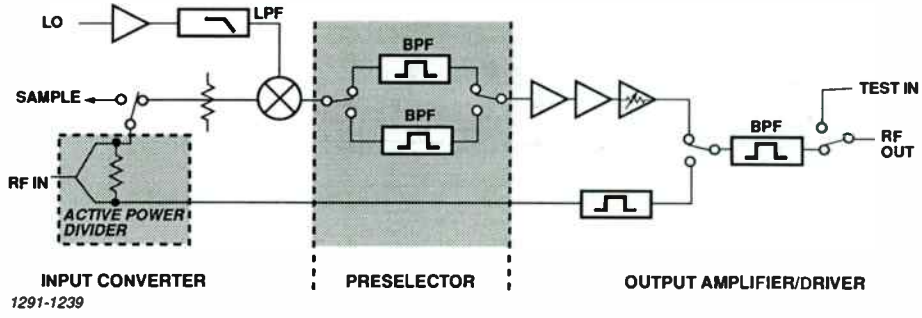

Figure 7. MMIC/MIC Exciter Upconverter

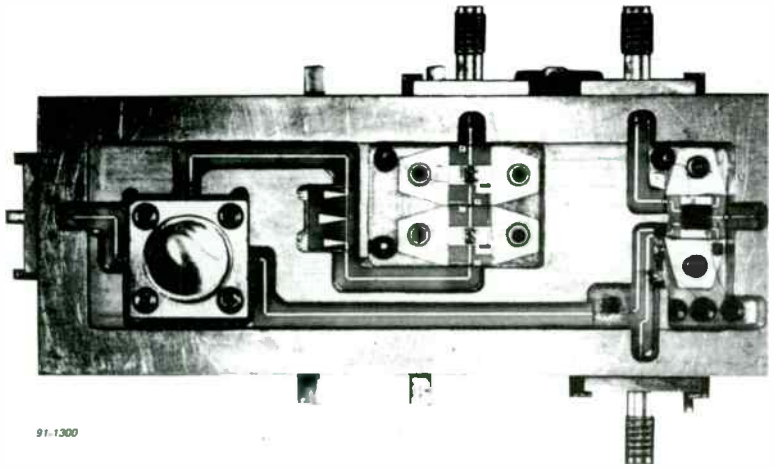

Figure 8. Upconverter Module

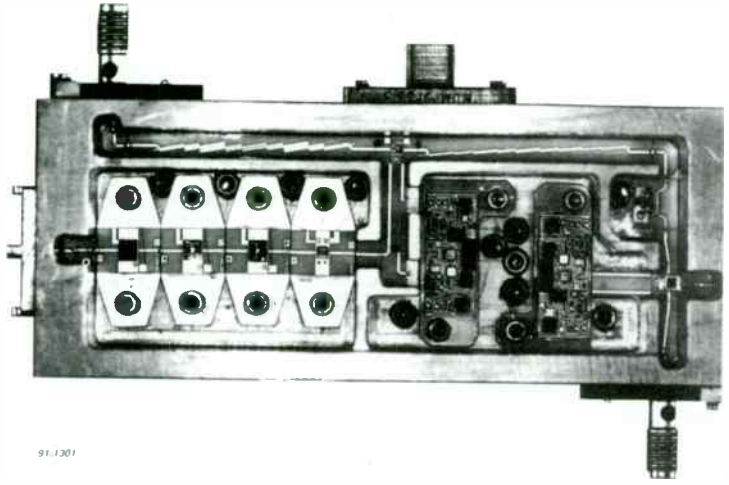

Figure 9. Output Amplifier/Driver

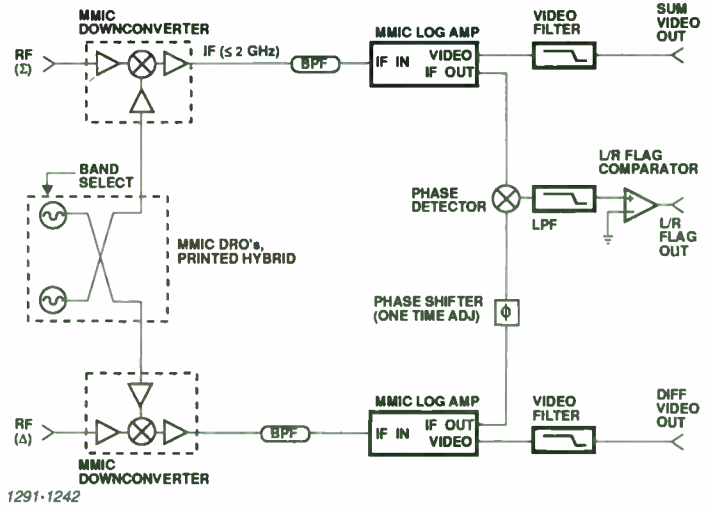

Figure 10. Dual Band, Two-Channel MMIC Receiver

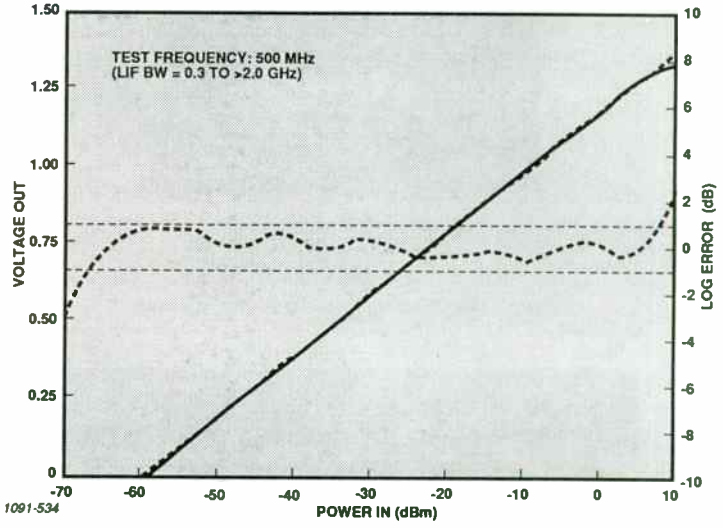

Figure 11. MMIC Log IF Data

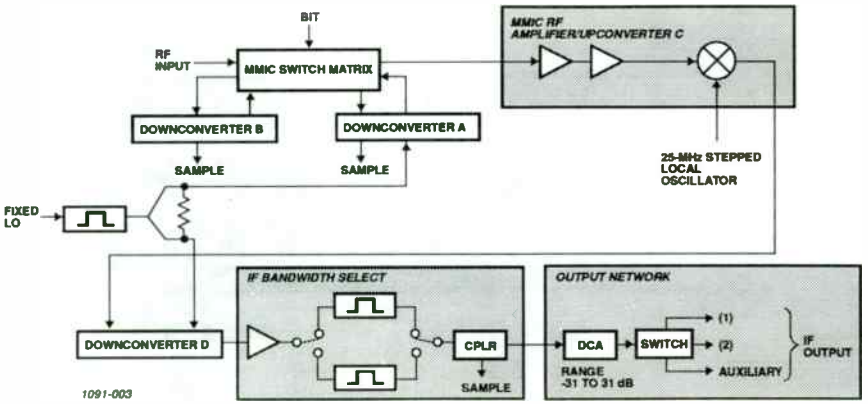

Figure 12. Strawman MMIC/MIC Integrated Wide-Band Converter

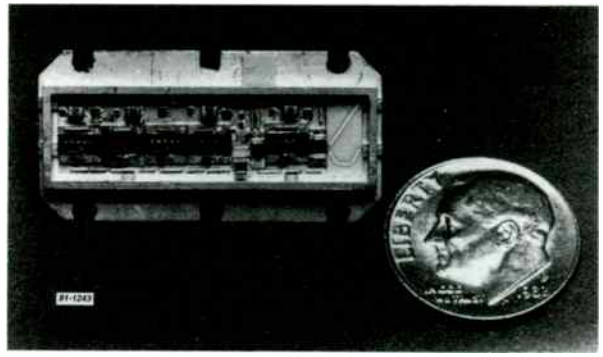

Figure 13. AIL Multifunction MMIC Module

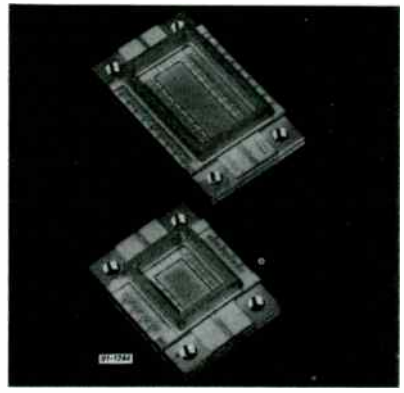

Figure 14. Multichip Packages (Courtesy of Alcoa)

1291-1245

A. Edge-Coupled Design

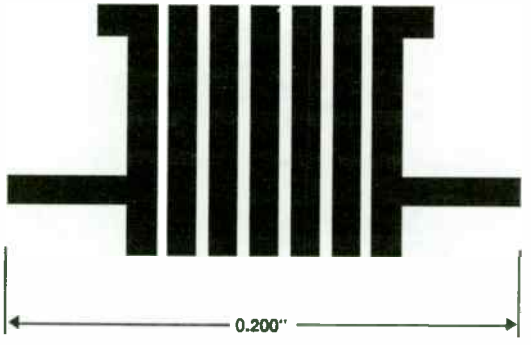

1291-1246

B. Interdigital Design

Figure 15. Microstrip Filter Topology (Seven Section BPF, F = 10.5 GHz)

EFFECTIVE MMIC TESTING STRATEGIES FOR ENGINEERS

by

Jesse D. Sheinwald

AIL Systems Inc.

Melville, New York 11747

ABSTRACT

Monolithic Microwave Integrated Circuitry (MMIC) is an important technology that is being implemented into an increasing number of new designs. An understanding of the various testing methods used for MMIC is imperative for the successful, cost-effective utilization of this cutting-edge technology.

The two principal categories of MMIC testing are chip level and substrate (carrier) level. This paper describes under what conditions chip level testing may be used and when substrate level must be used. The operational requirements of the different types of test stations used will be explained along with their accuracy, repeatability, and ease of use. Considerations of probe and test station care and safety will be made. A description of the various calibration techniques used on probe stations and their relative merits will be included. In addition, a discussion on the future of MMIC testing and how MMIC test techniques can be expanded into the testing of conventional microwave hybrid circuits will be presented.

INTRODUCTION

Even though MMIC technology has been around for a number of years, it has not reached the level of maturity that engineers have come to expect from its analog and digital counterparts. A circuit designer cannot, yet, examine a data sheet, take a MMIC chip from a waffle pack, install it in a circuit, and have it always work as expected. Experience has shown that to successfully implement MMIC's in real designs requires that the user have some actual test data, taken in his own environment, for the chips in question. This becomes especially important early in the design cycle. Performance verification of the MMIC's used in a design can help avoid operational problems later. Additionally, verification of chip specifications can make overall designs better by making the designer aware of lot-to-lot variations of chip parameters, as well as give an awareness to idiosyncrasies of chip operation.

Until microwave and RF engineers can leaf through MMIC catalogs with the same sense of security as their analog and digital counterparts, a MMIC testing program must be a part of all MMIC related jobs. To be successful implementing a state-of-the-art technology like MMIC, the engineer's best tool is a thorough knowledge and understanding of the parts being used.

Testing Categories

The testing of MMIC's falls into two broad categories: chip level and substrate (carrier) level.

Chip level means testing the MMIC chip straight out of the box with no other circuit elements involved. As will be discussed later, a chip must be designed to be probed for testing at this level.

Substrate or carrier level testing means that the chip is tested on an actual or facsimile circuit substrate. Some chips cannot be probed and must be tested this way. Other chips must have additional external circuit elements to operate and also must be tested this way. A MMIC that can be probed at the chip level may also be tested at the substrate level. However, the converse is not true.

Chip Level Testing

There are three major reasons to test MMIC's at the chip level. The primary reason is specification verification. Unlike conventional discrete microwave circuitry (in which there is often wide latitude of adjustment for the designer to achieve his goals), much of the final performance of a final assembly using MMIC's is heavily dependent on the performance characteristics of a few components that cannot be "tweaked" or changed in any way. Owing to lot variations, revision changes and component aging, it is imperative that the designer guarantee to himself that the MMIC's that are being designed into a circuit or system can indeed deliver what is wanted.

The secondary reason for chip level testing of MMIC's is for operational understanding of the chips being used. This becomes especially more important as the functional density of MMIC's increases. Depending on individual chip design, things like bias schemes, gain and switch control can be unclear and nonintuitive. Being able to experiment with and test out different bias and control modes of a MMIC before a final design is attempted can help avoid problems later on. Again, because a MMIC represents a fixed structure that cannot be changed it is important to note that the operation of the MMIC be fully understood early in the design cycle. For example, one problem that an engineer often faces when designing with MMIC is undesired low frequency oscillation. Regardless of their actual function, most MMIC's represent a complex, high-gain circuit in a very small area. Therefore, attention must be paid to assure that it is operating properly and that it is not oscillating at some undesired point. This can be done before a design is fully commenced when the MMIC is tested at the chip level.

The final reason for chip level testing is that it enables the engineer to test and experiment with MMIC's at the fundamental physical level of device. This gives the circuit design engineer insight and appreciation of the level of technology that MMIC's represent that are unobtainable when dealt with at the discrete circuit or system level.

The MMIC Probe Station (Reference 1)

Figure 1 shows what is properly called a wafer probe station. Unless the engineer works for a foundry, or has a close working relationship with a foundry, he will never have the need to test undiced MMIC wafers. End users usually see only diced chips, which are tested on this same apparatus.

At first glance, a probe station looks like a complex, intimidating device. However, it is really quite simple, and most of its bulk and complexity is only to provide a stable platform on which to place the chip and to support the probes. With the probe station, expensive, precision probes are used to make stable and precise electrical and mechanical contact on a small chip of semiconductor that may be much less than a hundredth of a square inch in size and no more than 5-mil thick. The "business end" of the probe station is in the center where the stage and probe heads are. This is the true working area of the station. Note that this station can handle up to four MMIC probes at a time.

MMIC Probes

Figure 2 shows the details of a typical MMIC probe. The purpose of a probe is to provide an electrically smooth, low reflection transition from a coaxial (in millimeter waves waveguide) world into the planar world of the MMIC. The MMIC probe can be thought of as a coax-to-coplanar waveguide transition. Much of its size is taken up by the mass of its housing so that it may be easily handled, stably mounted, and have enough space for a coaxial connector. In addition, there is a large amount of polyiron composite mode suppression material on the bottom of the probe to keep moding and reflections to a minimum.

When selecting a probe for an application, there are two key parameters that must be fulfilled:

1. Pitch

2. Footprint

Pitch simply means the spacing between the contacts of the probe. It is usually listed in microns (1 micron = 0.0394 mil), and must match the spacing of the test site on the chip.

Footprint refers to the configuration of the contacts of the probe. For example, the probe in Figure 2 has a ground and a signal contact next to each other. This is referred to as a ground-signal (GS) probe. However, if the places listed as RF in and RF out are examined on the MMIC chip in Figure 3, a ground contact, signal contact, and another ground contact will be evident. For proper testing, this chip would require a ground-signal-ground probe, or GSG. Contact configurations are always listed from a top-down perspective, looking down on the coaxial connector side.

RULE: For correct testing, the pitch and footprint of the probe must match the pitch and footprint of the contact on the MMIC.

Calibrating MMIC Probes

Just as in any other network measurement, the quality of the measurements made are dependent on the quality of the calibration that is loaded into the instrument. Figure 4 shows the different standard configurations that are required to make what is known as a SOLT (short-open-load-thru) calibration. To make a SOLT calibration requires that a good calibration substrate mounted on the stage of the probe station is made and that the proper software is loaded into your network analyzer. The SOLT calibration is analogous to the standard coaxial calibration that most people are familiar with in the non-MMIC world. Other MMIC probe calibration techniques that are in use, or are coming into practice are TRL (thru-reflect-line) (reference 2), LRM (line-reflect-match) (reference 3) and LRL (line-reflect-line) (reference 4). When properly done, the SOLT calibration is useful for most MMIC's. The other techniques, however, do have their applications and their advocates. It is best to keep in mind that calibration techniques are an ongoing area of development, in which new methods are still being devised and the old are still being refined.

Probe Station Configuration

Figure 5 shows a complete MMIC probe station with a Hewlett-Packard 8510B network analyzer. For best results, a set of dedicated, phase-matched, semirigid, coaxial cables should be used with the station. Figure 6 shows a detail of the stage of the probe station with a MMIC chip being tested. The two MMIC probes are clearly visible with their distinctive coplanar waveguide triangular tips and coaxial cables coming out of the top sides. The other two straight probes are needle probes that are used to deliver bias and control voltages into the chip under test.

Key Points About MMIC Chip Probing

The testing of MMIC chips by directly probing them is a useful and powerful technique for evaluating the performance of individual chips. The first few times that chips are tested will be informative, showing how easy and accurate testing can be accomplished. With proper care, and a good calibration, good results will always be obtained. There are a few points to keep in mind about MMIC testing that are worth remembering:

1. Take care of the probes; they are the only interface with the surface of the MMIC. They are not to be snagged on clothing and they are to be cleaned only with isopropyl alcohol and no other solvent. They are to be handled only by the body and stored either on the probe station itself, or the pedestal in their shipping container. They are amazingly tough for what they are, and although the manufacturer claims they can withstand a 20-mil deflection, testing that claim should be avoided. Although prices are dropping, probes are still very expensive. Although they are quite robust, when mishandled, they can be destroyed in an instant.

2. The testing of a MMIC chip is usually nondestructive to the chip. However, a lack of operator care can inadvertently destroy the chip under test. Also keep in mind that if the same chip is tested too many times, the metalization of the footprint could wear off to the point of uselessness.

When Chip Probing Techniques are not Appropriate

As powerful a technique that manual chip probing is for testing, there are situations where it is not the best or expedient choice. These situations are:

1. In circuit probing

2. Highly repetitive probing

A common response when someone first sees chip probing performed is, "We can test hybrid circuits the same way!" Unfortunately, a direct transition cannot be made although methods and equipment are coming into the marketplace that will enable similar tests to be done. First, MMIC probes are almost all 50-ohm characteristic impedance. Most non-RF circuits are much higher in impedance than that. A 50-ohm probe would seriously load down and alter the performance of that circuit.

Second, the angle of the MMIC probe contact is about 11 degrees with respect to horizontal--a very gradual slope for a densely packed hybrid. Also, the coplanar waveguide structure of most MMIC probes is incompatible with hybrid packaging. Probe manufacturers appreciate these problems and, wishing to increase their customer base, they are coming out with products to address them. Within the last year physically narrow, steep-angled, high-impedance probes designed for in-circuit hybrid testing have reached the market.

Manual probing is fine when a few MMIC's at the chip level are being tested. However, if an entire undiced wafer is to be tested, it would become a difficult, tedious task to probe manually. Fortunately, for such a job there are motorized, computer-controlled stages available that can be programmed for multiple-site testing. Again, unless there is a very close working relationship with a foundry, such a device should not be required.

Carrier Level Testing

As powerful and useful that chip level testing is, it does have two major limitations. First, not all chips are designed to be probed. Most early MMIC chips that were designed before chip probing equipment came into common use do not have test footprints at their inputs and outputs. Remember, without a footprint, a probe cannot make contact. Second, some MMIC's require some external components to operate successfully. The amplifier is the primary building block of the MMIC world. This is true for devices that are not ostensibly amplifiers. When analyzing how much gain there is available on a typical MMIC, the engineer can have the equivalent of one hundred or more dB gain per inch. This can lead to some potentially "RF hot" situations. To tame this condition, bias and control lines are often heavily bypassed to keep the MMIC chip from breaking into unwanted oscillations. It is very difficult to introduce enough dc and control line bypass capacitance on a chip level testing

station to be meaningful. With carrier level testing you can rectify both of these problems. In addition, carrier level testing has these other advantages:

1. More "real world"

2. Has no test fixture expenses

3. There are no connector interfaces

By real world we mean that all of the external components that a MMIC may require for proper operation can be included in the testable assembly. A typical testable carrier assembly is shown in Figure 7. Note the jumpers that select the bias point of the chip and the capacitor that bypasses the bias. These additions would be impossible to introduce at the chip level.

Traditional test fixturing and the precision machining and assembly that they require are expensive in terms of both money and time. If there is a project that requires many different test fixtures, then a good part of both budgets can be easily burned up. A commercial test fixture designed for carrier level testing is a one-time capital expense that can be used repeatedly for any number of different carriers. It can potentially pay for itself on one medium-sized job.

One major drawback to traditional test fixturing is that, due to reflections at the connector interfaces, the engineer never really knows what he has. Carrier level test fixtures are designed for minimum reflections at their probe interfaces. In addition, as long as the recommended TRL calibration technique is used, these reflections are accounted for in the calibration stored in your network analyzer.

Carrier Level Test Fixture (Reference 5)

A sophisticated carrier level test fixture is shown in Figure 8. This device, because of its high degree of adjustability, is well-suited for the development or engineering laboratory. For the production environment, there are simpler, more cost-effective units available. See Figure 9 for details on the adjustments and the placement of the substrate under test.

This fixture provides a high degree of adjustability in both the X and Y planes. The Z plane adjustment is what clamps the substrate under test in the fixture and assures good electrical contact by the coaxial launchers. The backstop adjustment provides a reference position so that once the fixture is adjusted for a particular substrate, the engineer can perform multiple tests on the same substrate and always find the proper test position without the readjustment of the unit. Each model of carrier level test fixture comes with its own customized calibration kit. Direct current and control signals are introduced into the circuit under test via needle probes similar to what is used during chip level testing.

A carrier level test fixture is also a highly precise instrument. For good performance, and accurate, repeatable results, care must be taken so that the launchers (probes) are not damaged. This is most easily done by never exceeding

the physical limits of your fixture and never attempting to set the launchers up without visually watching their placement.

Limitations of Carrier Level Testing

1. Reverse side of substrate must be metalized

2. Minimum size, 0.120 X 0.120; Maximum size, 4 X 4 (inches)

3. Thickness 0.005 - 0.150 (inches)

Note: 2 and 3 for model MTF-26

Therefore, carrier level test fixtures are not limited to the testing of MMIC hybrid carriers. They are also useful for the testing of any passive microstrip circuit that can be mounted into them and have RF successfully launched into them. We have successfully tested many microstrip filters in this manner.

SUMMARY

At the present time, and in the near future, the ability to test MMIC's will be an important part of their successful implementation in actual circuits. For the designer, testing should become an active part of the design process, for unlike digital or standard analog circuits, RF devices can often exhibit idiosyncrasies that do not show up on data sheets. As the digital and analog world speed up, they too will have to be tested utilizing these same concepts.

ACKNOWLEDGMENTS

The author would like to thank Messrs. J. Rella, G. Tangredi, and J. Summerville for their support in this program.

REFERENCES

1. Model 42 Microwave Probe Station Instruction Manual, Cascade Microtech, Beaverton, OR, 1987.

2. Engen, G. and Hoer, C., "Thru-Reflect-Line: An Improved Technique for Calibrating the Dual Six-Port Automatic Network Analyzer," I.E.E.E. Trans. Microwave Theory and Technique, Vol. MTT-27, December 1979, pp. 987-93.

3. Davidson, A., Strid, E., and Jones, K., "Achieving Greater On-Wafer S-Parameter Accuracy with the LRM Calibration Technique," 34th Automatic RF Techniques Group Conference Proceedings, November 1989.

4. D. Williams, R. Marks and K. Phillips, "Translate LRL and LRM Calibrations," Microwaves and RF, February 1991, pp. 78-84.

5. Model MTF-26 Microstrip Test Fixture Instruction Manual, Cascade Microtech, Beaverton, OR, 1989.

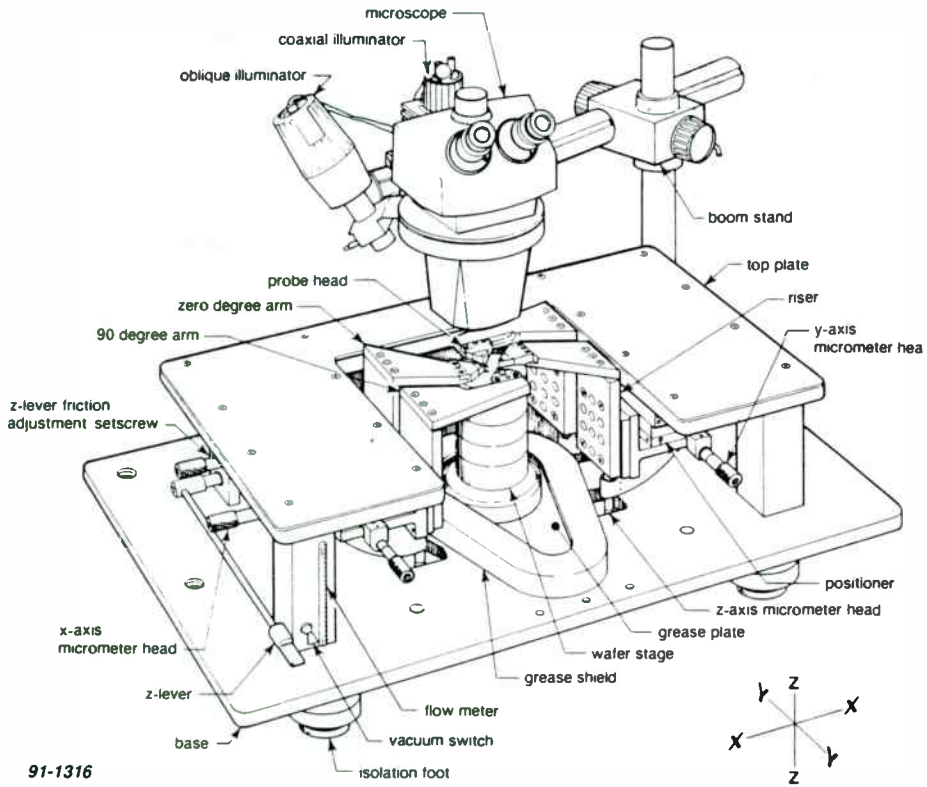

Figure 1. Wafer Probe Station

MICROWAVE PROBE HEAD

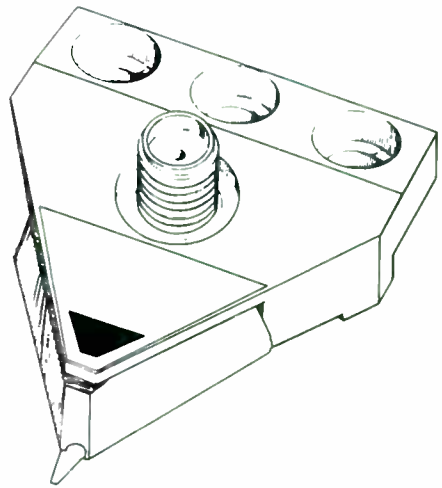

WPH-001-XXX PROBE CONTACT SEQUENCE

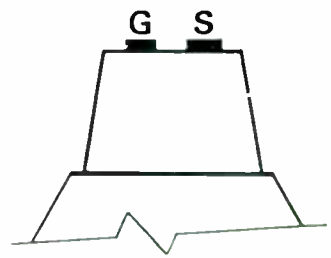

Figure 2. MMIC Probe

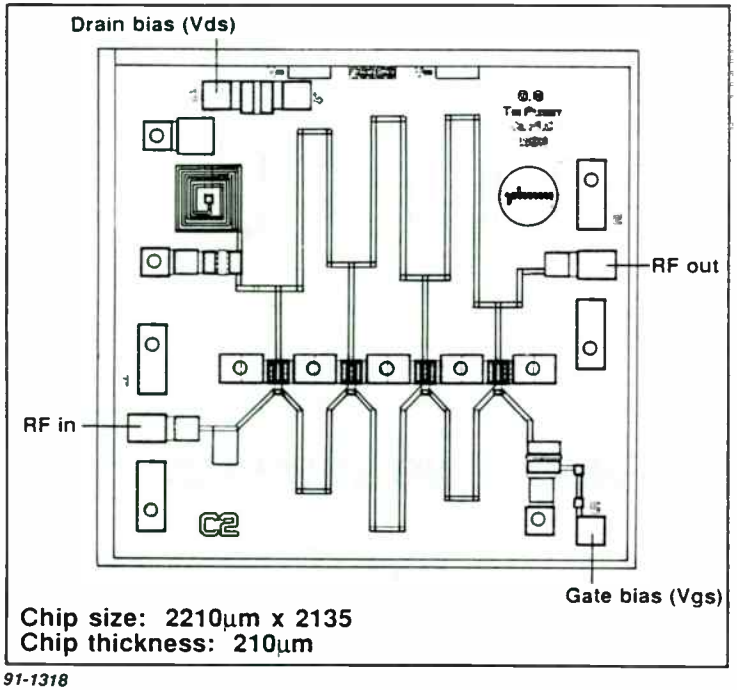

Figure 3. Typical MMIC Amplifier Chip

ELECTRICAL OPERATION

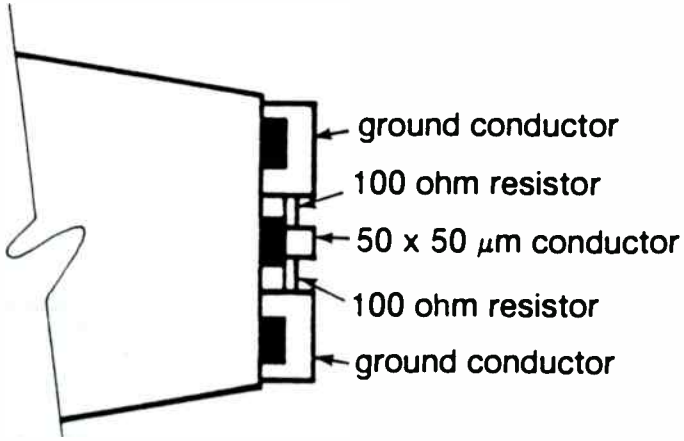

GSG PROBE ON 50 OHM LOAD

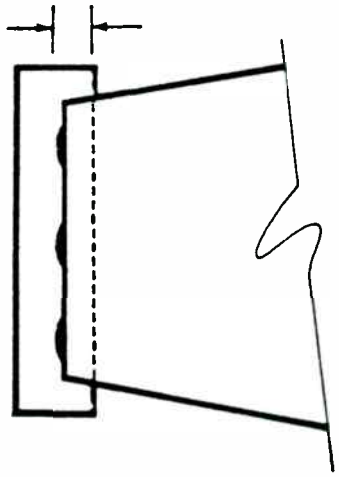

CENTER CONTACTS ON SHORT-CIRCUIT WIDTH

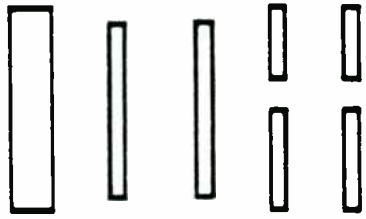

SHORT

GSG SHORT-CIRCUIT STANDARDS

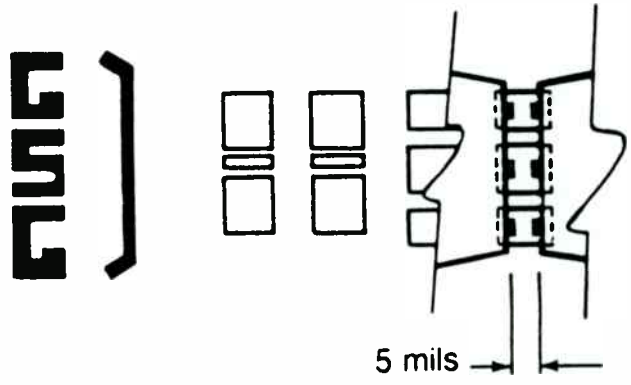

GSG PROBES ON A THROUGH-CONNECTION STANDARD

91-1319

Figure 4. SOLT Calibration

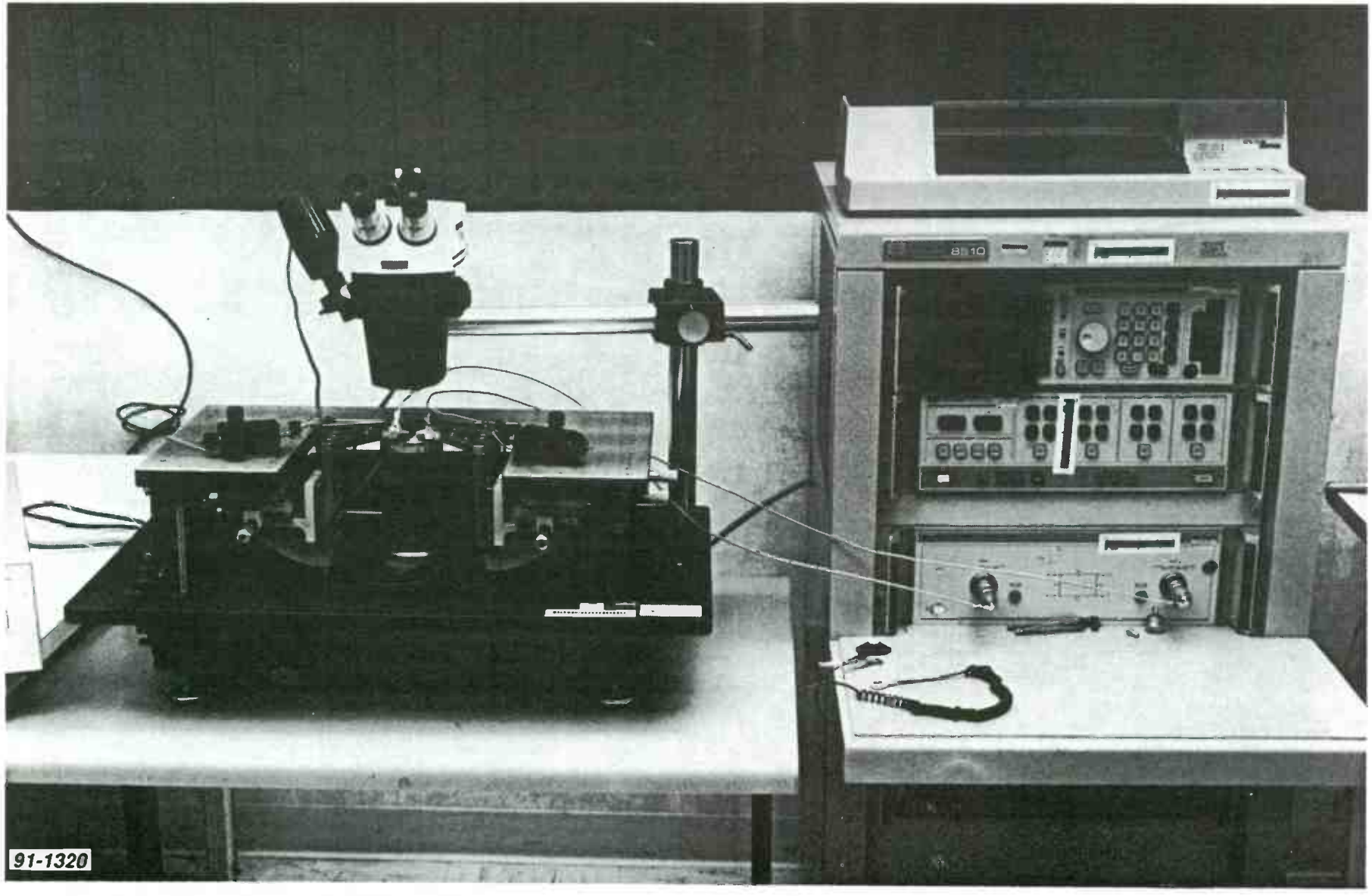

Figure 5. MMIC Probe Station with Network Analyzer

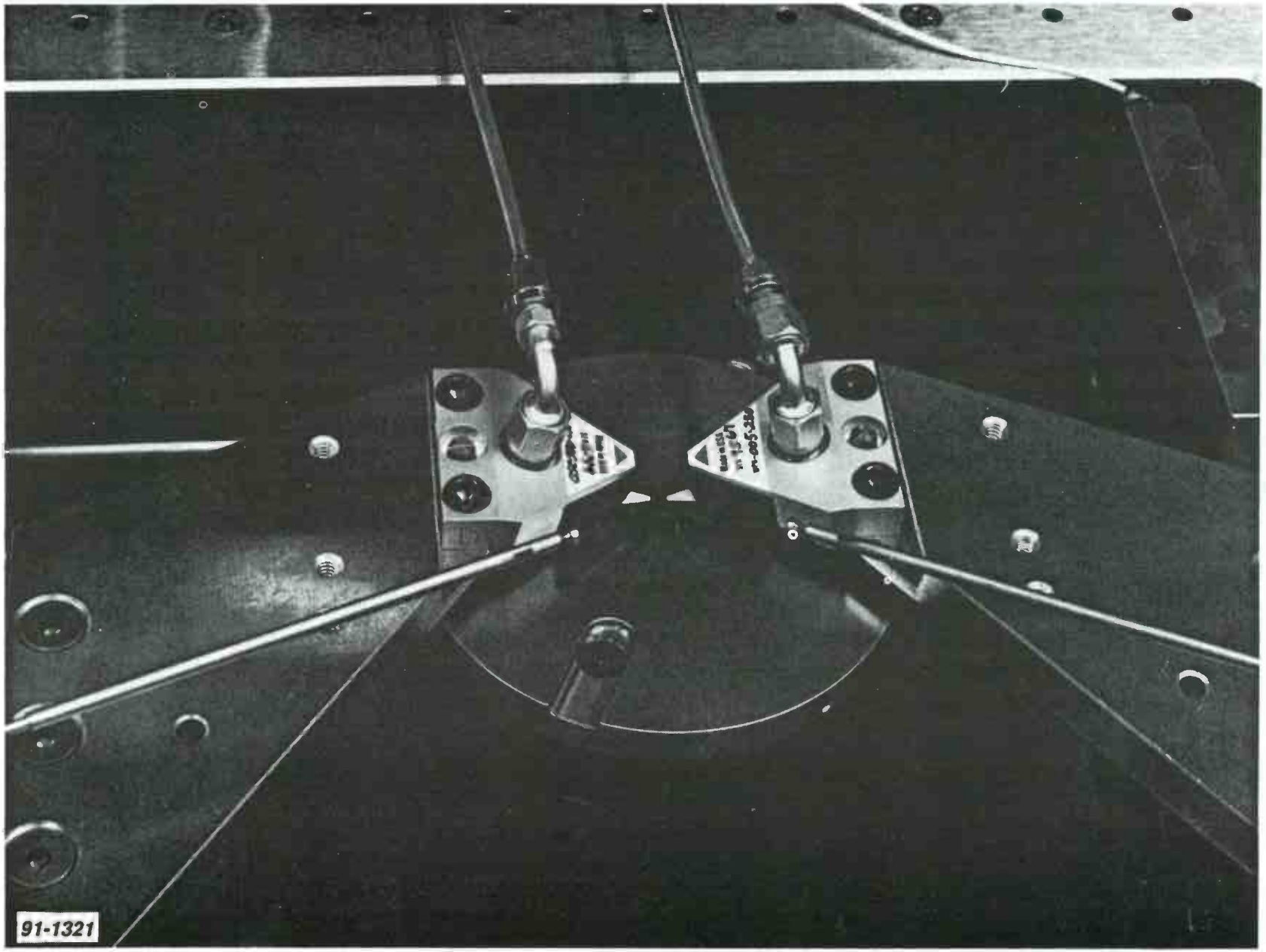

Figure 6. Probe Station Stage Detail

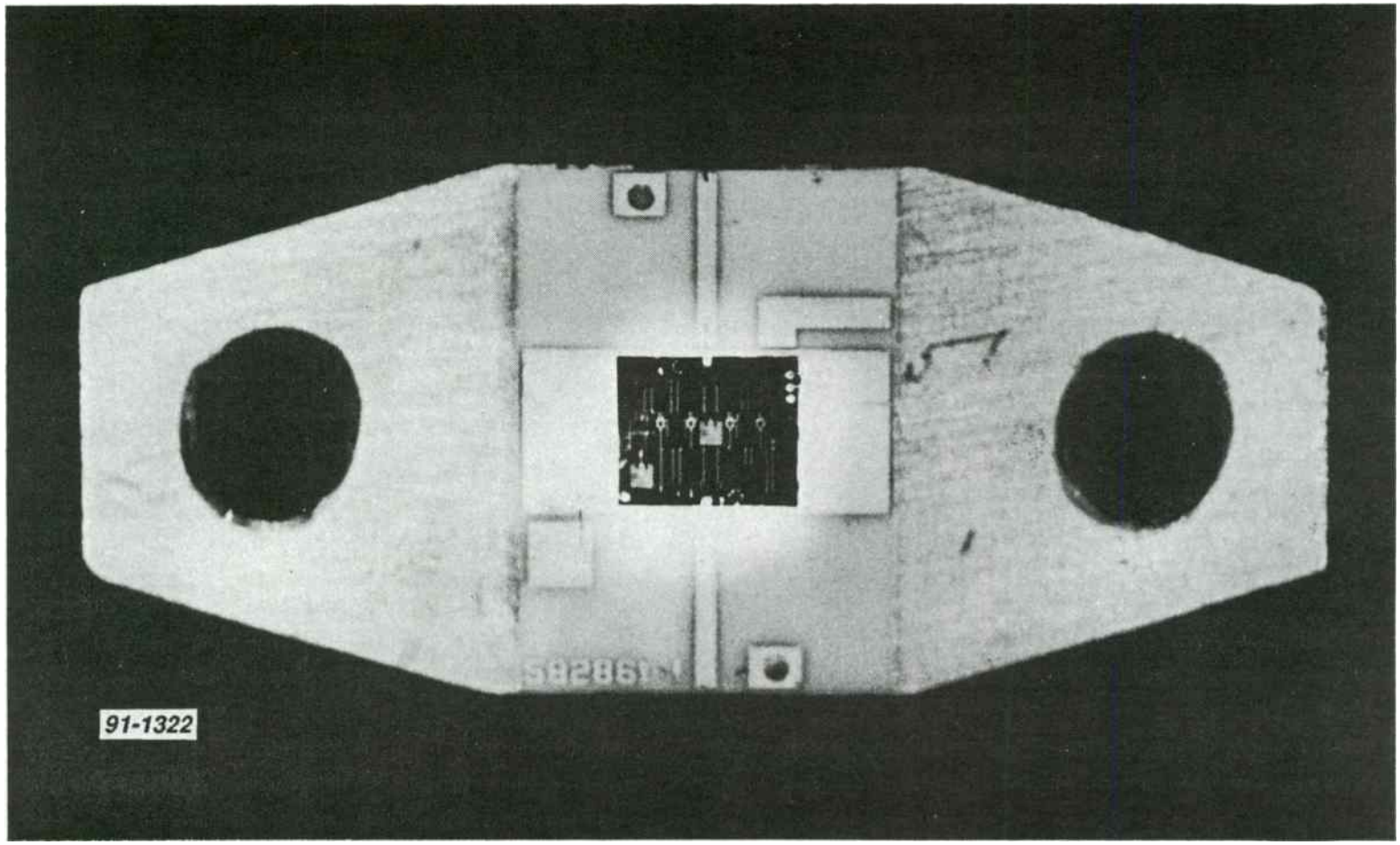

Figure 7. Testable Carrier Assembly

MODEL MTF26 FEATURES

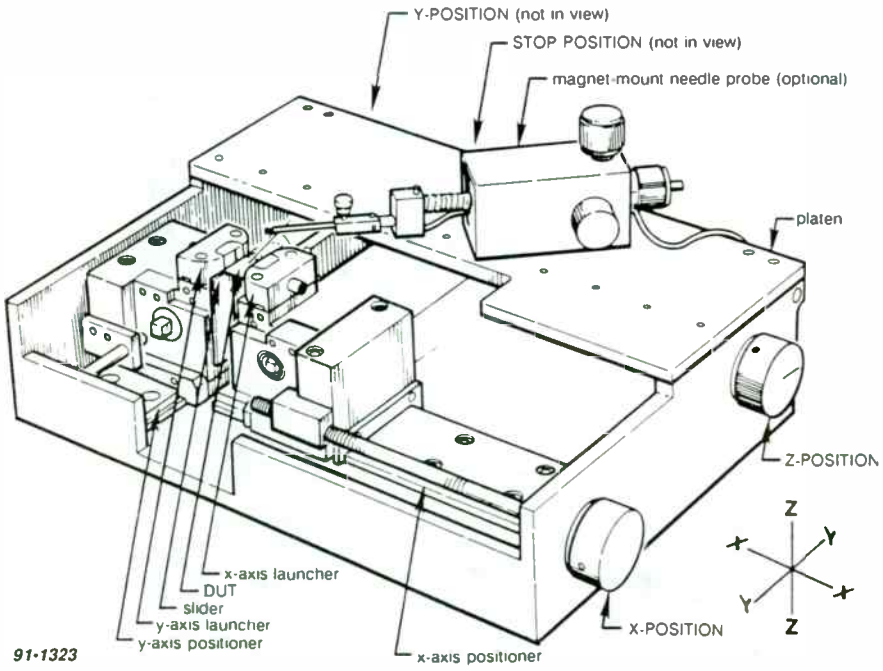

Figure 8. Carrier Level Test Fixture

CONTROL LOCATIONS

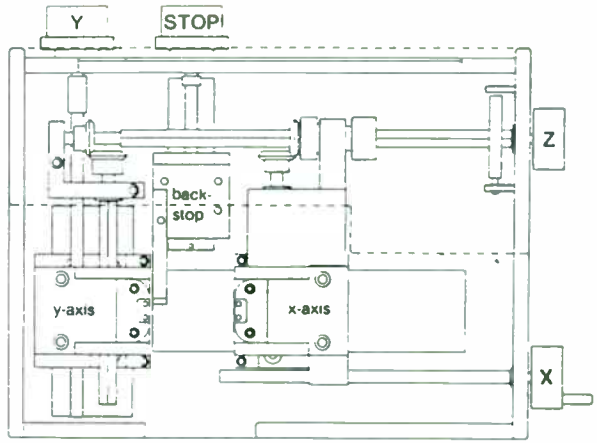

Z-POSITION CONTROL

Figure 9. Details of Test Fixture

SILICON MMIC AMPLIFIER HITS THE 20/20 GAIN/POWER(dBm) MARK AT UHF

R. GREEN and D. OSIKA

SGS–Thomson Microelectronics
211 Commerce Drive
Montgomeryville PA 18936

Abstract

The RF industry, especially the mobile radio/cellular market, has been requesting Microwave Monolithic Integrated Circuits (MMIC) of increasing complexity and power. One such requirement is for a linear, high gain (> 20dB), and substantial output power (> +20 dBm) device for use in RF power amplifiers at 900 MHz. Using silicon MMIC technology, hybridized versions of a two stage cascaded broadband amplifier using 50 Ω gain blocks are evaluated and compared with their simulated performance. The hybrid amplifier has been constructed in a conventional 4 lead ceramic package. Finally the design and process technology for producing a true single MMIC to provide these performance levels is discussed and the results from its fabrication reported on.

1.0 INTRODUCTION

The RF community has consistently requested increased performance levels from solid state devices and microwave monolithic integrated circuits (MMIC). This increased performance trend has been accelerated by the current market and future predictions for expanded personal communications. Additionally, the overall selling price for these systems is a critical component in the success and continuation of the communication market. Product cost must include the material, labor, capital and corporate expenses necessary for producing it. Design and realization of a component in a cellular radio/personal communication system must take into account all these cost considerations and its performance contrasted to other available technologies. The performance/cost ratio of electronics is an extremely useful way to normalize and compare competing techniques and technologies.

The increasing requirements of users with applications from HF to Microwaves will produce advances similar to those seen in cellular radio but at a rate which is proportional to its market size and growth potential. The users in these frequencies will continue to benefit from the technologies which occur due to cellular/personal communications and which have applications in their band of interest.

These considerations have indicated that the need for a 50 Ω silicon MMIC which can produce a power level (+20 dBm) capable of directly driving a power amplifier stage. Additionally, this MMIC should be capable of being driven by a device with a noise figure sufficiently low enough to meet the system's needs. The driver device

may only be capable of producing an output power of about 1 mW or 0 dBm due to this noise constraint. The goal of this 20 dB gain/+20 dBm power device is planned to operate from a DC supply voltage of 9.0 volts and a cost goal which can be competitive with the other technologies capable of providing this block function.

2.0 SILICON MMIC TECHNOLOGY

In the past several years silicon MMIC technology has produced steadily increasing levels of performance and complexity. Commercially available silicon MMICs perform a variety of block functions necessary for signal processing and amplification. A wide range of amplifier specifications have been demonstrated for low noise, power and gain. To allow comparison between different designs, the Power–Gain Product vs Frequency has been plotted and is shown in Figure·1. The silicon MMICs which produce the highest Power–Gain Product have incorporated collector isolation techniques. Active devices on these circuits have the collectors biased individually and use RF feedback paths to increase performance and stability. This graph also reports the SGS–Thomson Microelectronics hybrid amplifier (HAMP0572) performance which was achieved. A fully monolithic version of this hybrid has been designed and is being fabricated to achieve similar RF characteristics.

3.0 HYBRID AMPLIFIER (HAMP) DESIGN

The hybrid approach to a 20 dB gain/+20 dBm power amplifier for the cellular market was chosen to prove the concept of monolithic implementation, as well as to quickly introduce this low cost (<$15) amplifier to the market place.

To create the hybrid amplifier we selected from our standard product line the two most suitable silicon MMIC design along with MOS capacitors which are used for DC blocking and RF feedback. These die are placed in a low cost, studded screen metallized BeO package (referred to as X072) which will provide a suitable heat sink to dissipate power. This package has four leads (see Figure 2) input, output, ground and a second D.C. power connection.

The reason for this second power lead is that at higher powers even the input amplifier draws a significant amount of current, requiring a low valve dropping resistor to maintain a suitable operating voltage. Of course, this resistor also provides a substantial amount of negative RF feedback, thus severely dropping the gain of the output stage. This approach is definitely counter productive.

One attempt at providing RF isolation between the two stages is to use a good RF ferrite with a minimum value of 1 KΩ (if such a component exists at these frequencies). However even if this approach was technically possible it would substantially increase the hybrid's complexity, size and cost. Therefore, the only practical alternative at this time was to provide a separate power lead. Remaining leads of this package provide the input, ground and output with bias.

The die are eutectically mounted with two interstage bonds and two double stitched ground connections which provides a minimum of inductance. A stabilized epoxy is then used to encapsulate the entire top side of the package. With this simple structure we can manufacture these amplifiers in volume and at a low cost. For applications requiring small size and large volume production there is a stud less package with an isolated metallized bottom available which can be soldered to a heatsink.

As seen in Table 1 an AMP 5 has a 1 dB power compression point of +23 dBm which was an obvious choice for use as the output device. However, the driver was not quite as evident.

Amplifier	Gain @1GHZ (dB)	P 1dB (dBm)	Id (mA)
AMP 19	15.0	14	45
AMP 11	11.5	17	60
AMP 5	8.5	23	165

TABLE 1

To achieve the goal of an overall gain of 20 dB, it appears that either combination of AMP 19–AMP 5 or AMP 11–AMP 5 will achieve this easily. The problem is that the XO72 package is substantially larger, for heat dissipation requirements, than the standard MMIC packages, and thus requires longer bond wires. The longer bond wires have a negative effect on gain when they connect the ground pads of the

Darlington MMIC's to the package ground; i.e., more negative feedback. The longer bond wires plus the extra length in the screened ground lead reduces the overall gain for an AMP 11–AMP 5 combination. A simulation where we include a simple model of the bond wires and the parasitic package capacitance is shown in Figure 3.

The AMP 11–AMP 5 looked very good in terms of power handling capabilities; (i.e., A +17 dBm part driving a +23 dBm device) but it fell short on gain. The AMP 19–AMP 5 had the opposite problem, sufficient gain, including the package parasitics, but short on power. To see the problem with the power, we investigated the relationship between the 3rd order intercept point and the −1 dB power compression point of a Class A amplifier.

That is

$$P_I \cong P_{1dB} + 10.6 \text{ dBm} \qquad 1\text{–}1$$

One way to find the cascaded 1 dB compression point is to find the cascaded intercept point and subtract about 10.6 dB to find the compression point. A worst case assumption is made that the distortion products will add in phase yielding the 3rd order cascaded intercept point for two stages from (Ref 1 & 2)

$$I_p^{(3)} = -10 \log \left[\frac{1}{i_1 g_2} + \frac{1}{i_2} \right] \qquad 1\text{–}2$$

Where $i = 10^{[I(dBm)/10]}$ to convert from dBm to linear.

$g_2 = 10^{G_2/10}$

And G_2 = gain of output stage dB.

i_1 is the output intercept point of the first stage.

i_2 is the output intercept point of the second stage.

NOTE: Variables with capital letters have units in dB and dBm.

Variables with small letters have linear units; i.e., watts.

Another way to use this equation is to take the output intercept of the driver stage (io) and input intercept (i_i) of output stage to find the interstage intercept (I_{INT})

$$I_{INT} = -10 \log \left[\frac{1}{i_O} + \frac{1}{i_i} \right]$$

The interstage intercept point can be added to the ideal gain of the output stage to obtain the output intercept point $I_p^{(3)}$

$$I_p^{(3)} = I_{INT} + G2$$

However, what we really want is the cascaded compression point. As there is only a fixed offset between the 3rd order intercept point and 1 dB power compression point, we can use the same interstage approach for the 1 dB point as well.

Therefore, the effective interstage compression point is

$$P_{1dB\ INT} = -10 \log \left[\frac{1}{p_i} + \frac{1}{p_o} \right]$$

Where

$P_i = P_2 - G_2$ in dBm

P_i is the input 1dB compression point of the output stage (mw)

G_2 is the gain (in dB) of the output stage

P_2 is the 1dB compression point of the output stage

p_o is the linear output compression point of the first stage

p_i is the linear input compression point of the second stage

Then the combined 2 stage compression points is

$$P_{1dB} = P_{1dB\ INT} + G_2$$

For example amplifier stages capable of producing power levels of +14 and +23 dBm and gain of 14 dB and 8.5 dB respectfully.

Input compression point of the output stage can be shown to be

$+23\ dBm - 8.5\ dB = +14.5\ dBm$

$p_1 = 10^{14/10} = 28.18$

$p_1 = 10^{14/10} = 25.12$

The interstage compression point is

$$P_{1dB\ INT} = -10 \log \left[\frac{1}{25.12} + \frac{1}{28.18} \right] = +11.23\ dBm$$

Therefore the overall 1 dB power compression point of the two cascaded amplifiers is

$$P_{1dB} = +11.23 + 8.5 = +19.7\ dBm$$

So the AMP 19–AMP 5 combination has sufficient gain but is marginal on power. There is a solution to this problem. The output power of the first stage may be increased by raising the bias point of the device to allow a larger dynamic current swing. This is true only if increasing the device current does not significantly lower the Ft or raise the junction temperature of the device to an unacceptable level. As the AMP 19 was originally designed for use in an alumina package, now in a BeO package like the X072 there will be a much lower thermal resistance. Thus the die can basically handle a higher collector current. As can be seen in Figure 4 increasing the current from 45–60 mA increases the Ft; therefore, the 1 dB power compression point also increases to achieve the power margin we need.

From Figure 5, it can be seen that the AMP 19–AMP 5 combination is more suited for the 20 dB gain/+20 dBm power requirement than the AMP 11–AMP 5 combination. Additional, the overall amplifier noise figure is lower for the AMP 19–AMP 5. Intermodulation test definitions need to be clarified at this point. According to the military standard (Ref 2,) (1131 A–2204B), the distortion products are referenced to one of the two tones of the test signal. For commercial E1A standard, the amplitudes of the distortion products is referenced to the peak envelope power, which is 6 dB higher than the power of either of the two tones. An amplifier that meets the military IMD spec of –30 dB is equivalent to an E1A IMD spec of –36 dB. In terms of IMD, we specify our MMIC according to the more conservative military standard, so for those of you following the commercial E1A standard, the spec will improve by 6 dB.

For the monolithic approach we choose to go with the AMP 11 – AMP 5 combination to ensure meeting the output power criterion. The output stage of the AMP 11 has been increased to achieve increased power capability. The bias resistor

across the base emitter junction of the output device was changed t.. bias the Darlington pair to the same current at approximately 9 volts while keeping the emitter resistor as low as possible for maximum gain. The pitch of the emitter fingers of the AMP 5 has been decreased, which results in a reduction in the base area. This reduces the collector base capacitance, which in turn increases Ft and therefore gain.

For the AMP 5 section, the bias point has to be shifted to work off of an internal 9 volts instead of 12.5 Volts. The AMP 11 – AMP 5 combination is still potentially low on gain; therefore, the emitter resistor of the AMP 5 is further reduced to increase the gain of this stage.

As these designs require a specific operating current, a dropping resistor is used to approximate a constant current source with a voltage supply. This means that this monolithic version is ideally suited to be operated from a 12 volt external supply.

6.0 PROCESS DESCRIPTION

The fabrication of silicon MMICS has evolved into a cost effective solution for many RF and IF applications. A variety of circuit elements can be fabricated concurrently with the active device structures. The design of silicon MMIC circuits with complex topography can increase system manufacturability, performance, and reliability. A fully ion implanted device fabrication sequence is used to produce devices with an Ft in excess of 10 GHZ. This device profile is incorporated into a fine line interdigitated transistor structure.

Process capabilities have allowed this design to use 1.0 micron metal fingers and

spaces which produce a device with a 4.0 micron emitter to emitter pitch. The fine line emitter and base openings are sub half micron (0.4 μm) which produce low emitter base junction capacitance and allow an increased frequency of operation. Utilization of these structures produces a high packing density which can be expressed as the emitter periphery to base area which is equal to 0.43 μm^{-1} (11 mil^{-1}) Achievement of a high ratio means an associated low collector base junction capacitance for the required emitter periphery.

The resistors of the circuit are fabricated using ion implanted LPCVD polysilicon which allows precise control of their values. Additionally, the fabrication of resistors with different resisitivity properties is easily achieved with the use of selective implantation. Film thickness and doping levels can be varied to achieve a desired current density through the resistor which is not possible with the use of thin film metals. High current density in metal films has a direct effect on device reliability and lifetime.

A refractory/gold metallization is used to achieve a highly reliable monolithic circuit. This proprietary metal system has been life tested under accelerated conditions to show a projected MTF of above 10^6 hours at a T_j of 150°C. All contacts to the silicon areas of the device utilize this system to provide comparable reliability.

Collector isolation is achieved using a trenched epitaxial structure with air bridge interconnects. A cross section of this is shown in Figure 6. The substrate of the chip is eutectically mounted to the ground plane and collector contacts for the individual *n*–type epitaxial regions are brought to the surface. Additionally a parallel technique which uses undoped polysilicon to refill the trench is being

investigated. The reduced dielectric constant of this material will be contrasted against the advantages of planar processing which it provides.

7.0 DEVICE LAYOUT

The layout of a full monolithic two stage Darlington was accomplished with various electrical and thermal considerations. Minimization of the thermal effects due to the power dissipated in the output device was achieved with splitting the device into two halves. Additionally, to provide current sharing to both devices which compromise the output section resistive finger ballasting was used on the emitters. Increased current demand by an area is passed through the associated resistive section providing an increasing voltage drop causing debiasing of the region.

A die size of 500 μm x 600.0 μm was chosen to allow it to be assembled in a 200 mil round BeO hermetic solder sealed package. A package of this nature will allow the device to be screened to the various quality assurance levels required for electronic amplifier applications.

8.0 2 STAGE MONOLITHIC AMPLIFIER PERFORMANCE

Fabrication of the amplifier is continuing and the first run is currently at air bridge metallization. The voltage vs current characteristics of a single device is shown in Figure 9. These initial measurements have provided valuable information about improving doping levels and optimizing substrate starting material. Collector base breakdowns of 25 volts have been achieved which should be sufficient for 9 volt device operation.

9.0 CONCLUSION

Increasing complexity and performance requirements for the next generation communication systems is influencing the design approaches taken by component manufacturers. The incorporation of similar and multi functional blocks of a system into a single monolithic component is increasing. This paper has present a 20 dB gain/+20 dBm Pout part which can be used to replace a multi–stage amplifier chain. A goal of low cost, <$15, was an additional requirement which is necessary to allow success for this product.

A second development stage to produce a fully integrate silicon MMIC has been initiated. The preliminary measurements were encouraging and indicate that it may be introduced to the marketplace, hopefully at an increased cost savings over the hybrid version, in the near future.

References

1 Stephen Maas,
Non–Linear Microwave Circuits, Artech House 1988 pp 171–172

2 Ricky E Hawkins PE
"Combining gain, noise figure and intercept points for cascaded circuit elements"
RF design March 1990 pp 77 – 81

3 Helge Granberg
"Measuring the intermodulation distortion of the linear amplifiers"
Motorola application note EB38

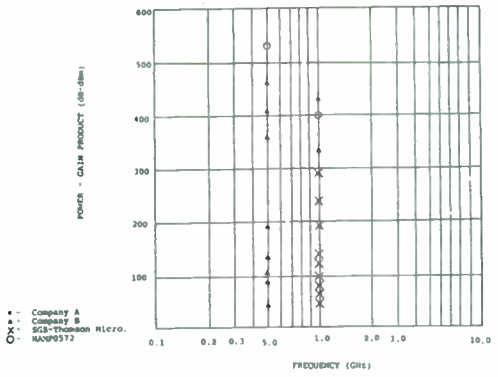

Figure 1 Silicon MMIC Power-Gain Performance Levels

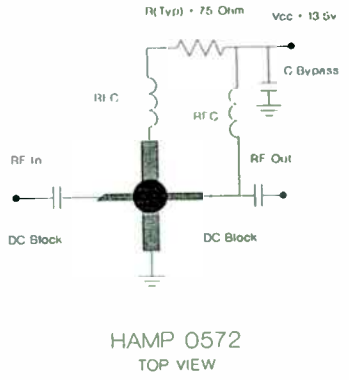

Figure 2 Hamp0572 Bias Configuration

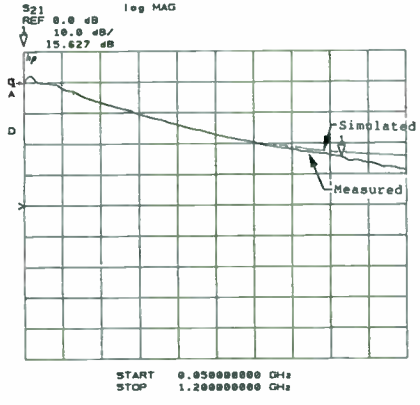

Figure 3 AMP11
AMP5 Simulated vs Measured S21

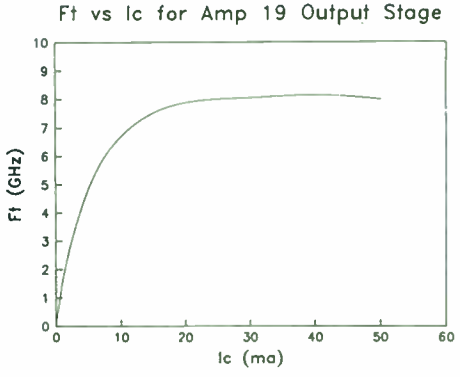

Figure 4 Ft vs IC for AMP19 Output Transistor

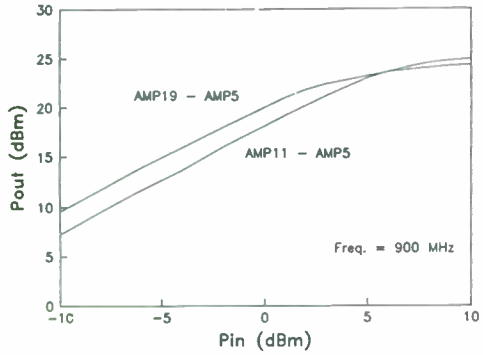

Figure 5 Pin vs Pout Characterists of the Hybrid Amplifiers AMP11 - AMP5 and AMP19 - AMP5

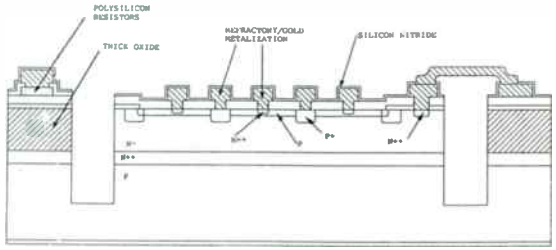

Figure 6: Cross Section of Isolated Collector Structure

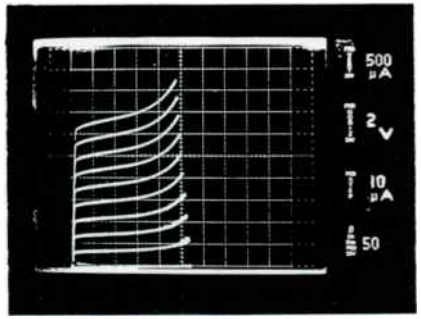

Figure 7: Monolithic Amplifier Device I-V Characteristics

THE DISTRIBUTION OF GAIN AND SELECTIVITY IN RECEIVERS

IR. WILLEM J. VOGEL

Modern Applied Technology Engineering

MATE Electronics

P.O. Box 2139
5600 CC Eindhoven
The Netherlands
Tel. 01131 40 430696

ABSTRACT

In this paper, the optimum distribution of gain and selectivity in receiver circuits is investigated. After a description of the problem, the noise and the mechanism of selectivity and intermodulation in receivers are studied. It is found that there is a trade-off between the linearity of the active circuits in a receiver and the selectivity of the passive circuits between the stages of the receiver. For obtaining a unique measure for the quality of the receiver, it is not sufficient to specify only the third-order intercept point of the receiver for two incoming frequencies. It is better to specify the output third-order intercept point of each stage of the receiver and the used distribution of gain and selectivity. This paper is terminated with some practical design rules for receiver circuits.

THE DISTRIBUTION OF GAIN AND SELECTIVITY IN RECEIVERS

IR. WILLEM J. VOGEL

1. INTRODUCTION.

In the system study on the applicability of receivers the question arises why a receiver circuit with a wideband input circuit in practice does not function as good as a circuit with a narrow bandpass filter as a selective input circuit. In this paper, it is shown that for optimum receiver circuit design, it is important to choose the right gain distribution when the characteristics of the filters between the active stages of the receiver are known.

The target of this paper is to find some practical design rules for obtaining receiver circuits with the lowest possible noise and intermodulation characteristics over a wide range of input signal levels.

It is shown that in the frontend of the receiver the power gain must be as low as possible to achieve a good intermodulation free dynamic range (IMFDR), but not too low because then the receiver circuit becomes insensitive due to a high noise figure. In receiver design, it is important to know which number of undesired signals can pass through each stage of the receiver circuit and to know the noise and the intermodulation (IM) characteristics of each stage. The use of optimum gain distribution can realise significant improvements of the specifications of practical receivers.

2. THE GAIN DISTRIBUTION PROBLEM.

In receiver design, the positioning of selectivity and gain in the system is very important. Furthermore, it is necessary to determine the optimum specifications of each amplifier and each mixer section with respect to the noise figure and the third-order intercept point (IP3) of the complete receiver. For receivers using filters of more than one half octave bandwidth, also the second-order intercept point (IP2) is an important figure of merit of the design.
In general, the filters in the receiver sections will have different selectivity. The gain distribution problem can now be described as the problem of determining where and how much gain must be placed in the receiver to achieve optimum performance. It can also be described as the problem of finding the optimum circuit with respect to the application of distributed or concentrated selectivity in the receiver.

In figure 1, the block diagram of a single conversion superheterodyne receiver is depicted. This receiver contains a preselection filter, an RF preamplifier, a mixer and oscillator to convert the desired signal to the intermediate frequency (IF), IF filters and amplifiers and a detector with an automatic gain control (AGC) circuit. In some receivers of this type, additional preselection filters are used between the RF preamplifier and the mixer circuit.
In the next section of this paper, fundamental properties of receivers like this type are studied which are found to be very important for designing receivers with optimum performance.

3. FUNDAMENTAL PROPERTIES OF RECEIVERS.

A very important figure in receiver design is the lowest detectable signal level, which is determined by the bandwidth, the noise figure of the receiver, the type of modulation of the incoming signal and the quality of the detector at low-level input signals. Another important figure is the level of incoming signals at which IM products exceed the lowest detectable level. The difference between these levels is the so-called intermodulation free dynamic range (IMFDR). Usually, the IMFDR of a receiver is specified with two signal sources at a certain distance in the frequency spectrum. However, this is not a unique measure for the quality of the receiver, because two different receivers with exactly the same IMFDR can be of completely different performance due to the use of different filters and gain distribution. Furthermore, the type of IM is important in receiver design. In most practical cases only the second-order and third-order IM are important.

3.1. NOISE.

In fig. 2, a noisy resistor and its Thévenin equivalent is depicted. The noise e.m.f. / $(Hz)^{\frac{1}{2}}$ of a resistor is dependant of the value of the resistor and its temperature. The available noise power is independant of the resistor value. A noisy amplifier will degrade the signal to noise ratio (SNR) at the output with respect to the SNR at the input.

The noise factor of the amplifier is usually defined as the SNR at the input divided by the SNR at the output when the temperature of the source resistor is equal to the room temperature (300°K). In fig. 3, a cascaded circuit of noisy amplifiers is depicted. The noise factor of a series of circuits connected in cascade was shown by Friis (1944) to be

$$f = f_1 + \frac{(f_2 - 1)}{g_1} + \frac{(f_3 - 1)}{g_1 g_2} + \ldots + \frac{(f_m - 1)}{g_1 g_2 \ldots g_m} \qquad (1)$$

where f_1 and g_1 are the noise factor and available power gain of the first stage, f_2 and g_2 are those of the second stage and so on. When g_1, g_2, g_3 and so on are large enough, the noise factor of the cascaded circuit approximates the noise factor of the first stage, which is equal to f_1. Too much gain in the first stages of a receiver where the ultimate selectivity is not yet realised will reduce the IMFDR of the receiver too much and is therefore not recommended.

3.2. SELECTIVITY AND INTERMODULATION.

Let us investigate now the mechanism of selectivity in the receiver. For simplicity, it is first assumed that the spectrum of the signals supplied to the receiver is a uniformly crowded spectrum of AM broadcast signals as depicted in figure 4. In practice, this is not true and some received signals are of a much higher level than some other signals. However, when nothing is known about the incoming frequency spectrum, the uniformly crowded spectrum is one of the best possible approximations to use for receiver calculations. The usual receiver concept is that the selectivity of the filters increases as they are placed nearer to the receiver output circuit. It is assumed now that this concept is used and that the selectivity characteristics of the filters are as depicted in figures 5, 6 and 7.

Furthermore, it is assumed that the bandwidth of the preselection filter is small enough to guarantee that the second-order IM products of the RF preamplifier and mixer combination are outside the passband of the input filter and that the second-order IM products are not converted to the IF passband by the mixer circuit. In that case, in the frontend only the third-order IM and crossmodulation (XM) are important. In the IF part of the receiver, it is possible that the bandwidth of the filters is more than one half octave, in which case second-order IM in the IF part of the receiver becomes also an important figure for receiver performance. Especially, this is the case when receiver has a "zero IF" as used in direct conversion receivers. Second-order IM in direct conversion receivers is often known as the AM-breakthrough effect in the detector part of the receiver.

Remark that the AGC of the receiver only reacts on the signals which can pass through the filter with the smallest bandwidth. In this example this is the second IF filter. The most difficult task for a receiver is to receive very weak signals at the desired center frequency where very strong neighbour signals are present in the frequency spectrum, because the AGC is not active and the power of the undesired signals in front of the second IF stage is maximal. This situation can be created by removing the desired frequency part of the test spectrum of fig. 4 and leaving all other signals intact. This situation is depicted in figure 8. At the output of the receiver the noise and IM can be measured. Now, requirements can be found on power handling capacity of the active parts of the receiver when the level of the input signals at which all the IM products are below the noise level of the receiver and the selectivity of the filters used in the receiver are specified.

It is not evident that the first IF filter must always be a small bandwidth type, because such a filter has in general a high insertion loss and more power gain is needed in the frontend with its disadvantage of a lower IMFDR. A first IF filter with a larger bandwidth usually has a lower insertion loss and less power gain in the frontend of the receiver is required. However, the power gain of the first IF stage must be kept sufficiently low to realise a good IMFDR for signals which can pass through the first IF filter but which are blocked by the second IF filter.

This system set-up results in more power gain to be positioned after the last IF filter. To prevent wideband noise, some additional lowpass filtering after the detector stage can be necessary. As can be seen now, in the measurement set-up of fig. 12, for each component of the signal spectrum of fig. 8, one of the following three conditions is fulfilled:

1. The signal component is rejected by the preselection filter and is not present at a high level in the receiver.

2. The signal component can pass through the preselection filter, but is rejected by the first IF filter.

3. The signal component can pass through the preselection filter and the first IF filter, but is rejected by the second IF filter.

For simplicity, it is assumed that the filter characteristics are rectangular. In practice, this is not true and some corrections on the calculated results are necessary. Signals fulfilling condition 1 do not contribute much to the IM of the receiver. For signals fulfilling condition 2, only the performance of the RF preamplifier and mixer combination is important. To obtain a good figure of merit for these signals, we have to know the IP3 at the input of the receiver frontend including the preselection filter.

The input IP3 can be found as follows: When two signal sources of equal amplitude at frequencies f_1 and f_2 are connected to the receiver, third-order IM products can be found at frequencies $2f_1 - f_2$ and $2f_2 - f_1$. When the distance between the level of the desired signals and the level of these IM products is x dB, the input IP3 is $\frac{1}{2}$ x dB above the level of the desired signals. The output IP3 of the frontend (preselection filter + preamp + mixer circuit) is the input IP3 times the gain of the frontend. When the IP3 and the noise level of the frontend are known, it is possible to calculate the level of two dominant signals of equal amplitude where IM products are equal to the noise level. With this information, it is easy to calculate the IMFDR of the frontend now.

When a large number (n) of uncorrelated signals of equal power pass through the preselection filter, the power of the third-order IM products in each channel in the center of the frequency spectrum is approximately $(3/2)\cdot(n-1)^2$ times the power of the third-order IM products which are produced by any two signals (worst-case condition). The input level for obtaining the same power of third-order IM products produced by n equal level signals in comparison with that produced by two equal level signals must therefore be decreased by:

$$o_3 = 0.88 + 10 \log (n - 1) \quad dB \qquad (2)$$

For video (CATV) systems with many signals with the same frequencies for the synchronization pulses, all signals are partly correlated and the correction formula (2) for the input level is not valid. For these systems, another correction is often used as a rule of thumb:

$$o_3 \text{ (video)} = 7.5 \log (n - 1) \quad dB \qquad (3)$$

For signals fulfilling condition 3, not only the input IP3 of the frontend is important, but also the input IP3 of the first IF amplifier in comparison with the output IP3 of the frontend divided by the insertion loss of the first IF filter. For wideband IF circuits, also the IP2 of the circuits is important for determining the performance of the receiver. Again, we have to know the number of signals that can pass through the first IF filter. This number is smaller than the number of signals that can pass through the preselection filter due to the smaller bandwidth of the first IF filter.

Frequency conversion of signals does not influence the relative position of in-band third-order IM products at $2f_1 - f_2$ and $2f_2 - f_1$, where f_1 and f_2 are the frequencies of any two components of the input signal of the receiver. In the worst case, third-order IM of the cascaded amplifier stages add in phase and the following cascaded stage equation for the IP3 of the receiver frontend including the first IF amplifier can be derived:

$$\frac{1}{IP} = \frac{1}{ip_1\, g_2 g_3} + \frac{1}{ip_2\, g_3} + \frac{1}{ip_3} \qquad (4)$$

where IP is the output IP3 of the frontend, first IF filter and first IF amplifier in cascade, ip_1 is the output IP3 of the frontend, ip_2 is the output IP3 of the first IF filter and ip_3 is the output IP3 of the first IF amplifier (fig. 13). Note that when the IF filter is a fully linear passive circuit, ip_2 is infinite and the second term of (4) is zero. The terms in (4) are ratios, not dB or dBm.

The input IP3 of the receiver can be found by reducing the output IP3 by the total gain of the receiver. With IP_i as the input IP3 of the cascaded circuit, (4) can be rewritten as:

$$\frac{1}{IP_i} = \frac{g_1}{ip_1} + \frac{g_1 g_2}{ip_2} + \frac{g_1 g_2 g_3}{ip_3} \qquad (5)$$

As can be seen now, the input IP3 of the cascaded circuit is lower than or equal to the input IP3 of the first amplifier in the circuit. Also, the output IP3 of the cascaded circuit is lower than or equal to the output IP3 of the last amplifier in the circuit.

From (4) and (5) the very important conclusion can be drawn that too much gain in the part of the receiver where the ultimate selectivity has not yet been realised will seriously degrade the input IP3 of the receiver. Therefore, in the optimum receiver, the gain in the front-end must be just sufficient for realising a good sensitivity, but too much gain (as often used in old-fashioned tube receivers) will seriously degrade the performance.

Furthermore, the desired signal to noise ratio and the output level of the signal before the detector as a function of the input signal level by means of the AGC characteristics of each stage in the receiver must be specified. Normally, at low-level input signals, the AGC is only active in the IF part of the receiver. When the signal to noise ratio exceeds a certain value, the AGC becomes active in the RF part of the receiver. In that case, the input IP3 of the receiver can be changed. Requirements can now be specified for the linearity of the amplifier stages as a function of the AGC voltage or AGC current.

The gain of the circuit used in the last IF stage where the ultimate selectivity is realised can in practice be very large. This can result in a wideband noise spectrum after the detector circuit. Therefore, additional lowpass filtering after the detector and/or bandpass filtering before the detector can be needed.

4. PRACTICAL RULES FOR RECEIVER DESIGN.

From the preceding sections of this paper, it can be concluded that it is possible to give some practical rules which will lead to a good receiver design with the available components. Using the uniformly crowded signal spectrum as test input signal, the following practical design rules are recommended:

1. Specify the required sensitivity of the receiver by the noise figure and the bandwidth of the receiver. This noise figure will always be higher than the noise figure of the available preamplifier. It is of good design practice not to require a noise figure of the complete receiver which is too close to the noise figure of the preamplifier because this will lead to excessive high gain requirements for the preamplifier following formula (1) and a low input IP3 following (5) which will lead to a low IMFDR. Especially, a low noise figure is not very meaningful in an environment with high interference and noise at the input of the receiver.

2. Specify the desired maximum power gain of the receiver. This can be calculated when is known at which signal to noise ratio the signal power at the input of the detector must be equal to the maximum power at this position. This is also the point at which the AGC of the receiver will begin to reduce the total receiver gain.

3. Specify the filters to be used in the receiver. Important specifications are the bandwidth and the insertion loss of these filters. When these specifications are known, it is possible now to calculate the required maximum power gain product of all the active parts of the receiver.

4. Now the question arises how the maximum power gain product must be distributed in the complete receiver. Therefore, it is needed to optimize the gain of the frontend for realizing the required noise figure and a good IMFDR. Also, a calculation can be made for the actual IMFDR for n input signals compared with that for two signals. The number n can easily be calculated by dividing the input bandwidth of the receiver by the final bandwidth. The advantage of a good preselection filter, even in receivers of high dynamic range, can be seen very clearly now. Following (2), it is very advantageous to keep n as low as possible.

5. Calculate the required gain of the first IF stages for not too much degrading the input IP3 of the receiver for in-band but out-of-channel (condition 3) signals. Due to the lower bandwidth of the first IF filter, the number of simultaneously present signals in the first IF amplifier (m) is lower than the earlier calculated number of signals (n) in the frontend of the receiver. Therefore, some degrading of the input IP3 following (5) for condition 3 signals is allowed without degrading the performance of the receiver.

6. Investigate the degradation of the receiver performance due to second-order intermodulation. Especially, second-order IM has to be investigated in wideband IF and LF circuits, as used in some types of direct conversion receivers.

7. Now, it is possible to calculate the required maximum gain of the receiver stages after the selective filters. Investigate the necessity of additional filtering at the detector stage for suppressing of wideband noise. Because the gain after the selective filters can be very large and because this gain can be very non-linear, the minimum required stopband attenuation to prevent IM from out-of-channel signals in the last IF amplifier has to be investigated now.

8. Specify the desired signal to noise ratio and the output level of the signal before the detector as a function of the input signal level by means of the AGC characteristics of each stage in the receiver. It is recommended to investigate the distribution of receiver gain and selectivity for each value of the AGC voltage (or current) now, especially when the receiver is realised as an integrated circuit design with low flexibility. Sometimes, the use of filters with other insertion loss and selectivity characteristics can improve receiver performance considerably.

5. CONCLUSION.

1. For each type of receiver, it is possible to find an optimum for the distribution of gain and selectivity in the circuit.

2. There is a trade-off between the intermodulation-freedom (linearity) of the active stages of a receiver and the selectivity of the passive circuits between the stages of the receiver.

3. For optimum design strategy for a receiver, it is necessary to calculate the number of undesired signals that can pass through each active stage of the receiver.

4. When nothing is known about the incoming frequency spectrum, one of the best possible approximations is the uniformly crowded spectrum with the exception of the channel at which the receiver is tuned.

5. For obtaining a good overview of receiver performance, it is recommended to specify the output IP3 of each stage of the receiver separately together with the used filters and the used gain distribution.

6. For receivers with AGC, additional requirements are found for the linearity, the gain distribution and the signal to noise ratio at the detector stage.

6. LITERATURE.

1. IMD and intercept points of cascaded stages, W. Richardson, W3IMG; article published in Ham Radio, november 1984, p. 28 - 34.

2. Dynamic range - fact or fiction ? , P. Hawker, G3VA, RSGB (IBA), article published by the Institution of Electronic and Radio Engineers (IERE), publication no. 68, 1986.

3. The IMFDR of bipolar switching mixers, H.C. Nauta and E.H. Nordholt, IERE publication no. 68, 1986.

4. Graphical selection of mixer frequencies, G.T. Anderson, W2HVN, Ham Radio, june 1985, p. 41 - 43.

5. Quiet! preamp at work, H.P. Shuch, N6TX, Ham Radio, november 1984, p. 14 - 20.

6. High dynamic range receivers, J. Reisert, W1JR, Ham Radio, november 1984, p. 97 - 105.

7. Broadband amplifiers in receiver design, J. Reisert, W1JR, Ham Radio, november 1986, p. 91 - 97.

8. Satellite broadcast reception: the FM approaoh to signal distribution in individual and community antenna systems, J.G. Chaplin a.o. , E.B.U. Review - Teohnical no. 202, december 1983.

9. Electronic Distribution System Engineering Data, N.V. Philips' Gloeilampenfabrieken, Eindhoven, The Netherlands, Dept. ELA/EDS, HBG3, G.M. Kuyk, 2nd printing, september 1977.

10. Kabelfernseh-Hausanlagen, K.H. Flitsch, Funkschau no. 19 - 1982, (W. Germany), p. 55 - 57.

11. Transmission systems for communications, Bell Telephone Laboratories - Revised Fourth Edition, december 1971.

12. Recommended methods of measurements on audio equipment - UAN-LL059, N.V. Philips' Gloeilampen-fabrieken, Eindhoven, The Netherlands, Dept. DSD, product division audio and video, february 1978.

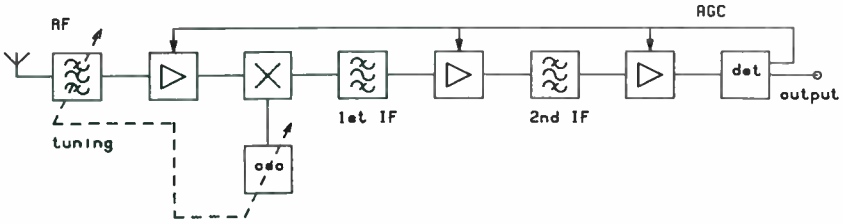

Fig.1. Block diagram of a superheterodyne receiver.

Fig.3. Cascaded circuit of noisy amplifiers.

$f = f1 + (f2 - 1)/g1 + (f3 - 1)/g1g2$

f = noise factor of the complete circuit

f1,f2,f3 are the noise factors and g1,g2,g3 are the power gains of the first,second and third amplifier stage respectively.

Fig.2. a. Noisy resistor.
b. Noise-free resistor and noise voltage source.

$\bar{E}^2 = 4kTR\Delta f$ $\quad k = 1.38 \times 10^{-23}$ J/°K

$P = kTB$ $\quad T$ = temperature in °K

B = bandwidth in Hz

Δf = difference between upper and lower frequency of noise spectrum

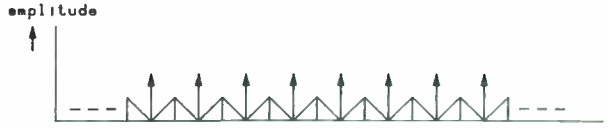

Fig.4. Uniformly crowded frequency spectrum of AM signals.

Fig.5. Passband of preselection filter.

Fig.6. Passband of first IF filter

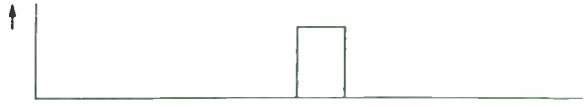

Fig.7. Passband of second IF filter.

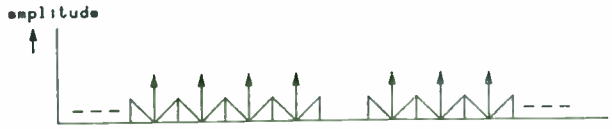

Fig.8. Signal spectrum for testing receiver performance.

Fig.9. Passband of preselection filter

Fig.10. Passband of first IF filter.

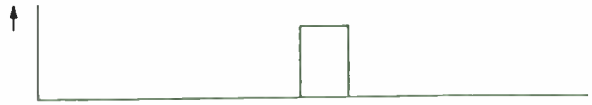

Fig.11. Passband of second IF filter.

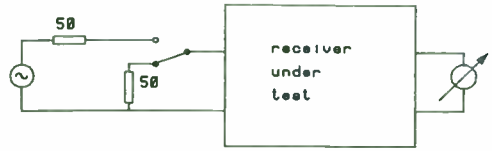

Fig.12. Set-up for testing receiver performance.

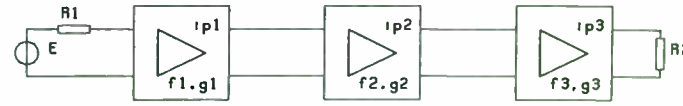

Fig.13. Cascaded circuit of amplifiers with third-order non-linearities.

$$1/IP = 1/ip1g2g3 + 1/ip2g3 + 1/ip3$$

$$1/IP_I = g1/ip1 + g1g2/ip2 + g1g2g3/ip3$$

IP = output third-order intercept point of the cascaded circuit
IP_I = input third-order intercept point of the cascaded circuit

ip1, ip2, ip3 are the output intercept points of the first, second and third amplifier stage respectively

Tunable Notch Filter for Interference Rejection

Eric D. Adler and Edward A. Viveiros

Harry Diamond Laboratories

Signal Processing Systems Branch

2800 Powder Mill Rd.

Adelphi, MD 20783

Abstract

Wideband receiving systems are constantly plagued by the effects of overpowering narrowband interferers. These interfering signals can be self-induced spurious responses or co-located transmitter signals. The presence of these interferers greatly limits a wideband receiver's ability to detect and characterize lower level signals of interest. A fixed notch filter with additional frequency tuning hardware can be used effectively to suppress these interfering signals. This "tunable" notch filter (TNF) architecture must cover a wide passband while attaining a narrow rejection bandwidth to minimize distortion of the system's frequency response. It also must be capable of tuning in fine frequency steps to effectively place the interfering signal at the center of the notch. In addition, this filter section should be cascadable to provide interference suppression of multiple signals simultaneously.

This paper discusses the development of a cascadable, TNF section for a 30-MHz wideband intercept receiver, including the TNF concept, formulation of system requirements, notch filter development, frequency tuner requirements, and effects of cascading sections. Computer simulations are used to predict the performance of the notch section and assist in the design process. The notch section performance is assessed via measured data from a prototype section. These measured data are also compared with simulated data to assess the accuracy of the simulations.

Introduction

In today's electronic warfare (EW) environment, overpowering narrowband interferers can greatly limit a wideband receiver's ability to detect and characterize low-level signals. This problem can be alleviated by reducing the power of the interfering signals via notch filtering. A tunable notch filter would provide flexibility to the system to adapt to the dynamic signal environments often encountered. This pre-filtering of undesired signals can effectively extend the dynamic range of wideband systems.

Interfering signals can be self-induced spurious responses or co-located transmitter signals. These undesirable signals have various modulation types, transmission bandwidths, center frequencies, and power levels. A cascadable, TNF section would provide the preprocessing required for wideband intercept receivers to operate effectively in dense signal environments.

This paper looks objectively at the requirements for a TNF section in a VHF, 30 MHz bandwidth intercept receiver. The criteria evaluated include system requirements, notch

filter development, frequency synthesis, and cascaded sections.

Tunable Notch Filter Concept

The TNF concept uses a fixed frequency notch filter in a dual mixing scheme (see fig. 1) to effectively tune the center frequency of the notch filter. The first mixer converts the interfering signal of interest to the notch filter center frequency to achieve the desired signal attenuation. The notch filter effectively reduces the power of the interfering signal by its rejection attenuation. The second mixer restores the frequency band to its original form at the input of the first mixer. This common intermediate frequency (IF) architecture allows multiple notch filter sections to be cascaded to eliminate multiple interfering signals. The local oscillator (LO) provides signals to both mixers for frequency conversion and must provide fine resolution to tune the interferer into the notch filter's narrow rejection bandwidth. Additional filters and amplifiers are incorporated to set the gain and third-order intercept point as well as control the spurious responses of each cacadable section.

System Requirements

The performance specifications of the TNF section are driven by both the operational parameters of the system and the signal characteristics of the environment in which it is operating. The notch filter bandwidth and power handling capability of the TNF section are determined by the signal environment, while TNF section dynamic range, operating frequency, bandwidth, tuning range and resolution will be derived from the system operating parameters.

It is important to characterize which in-band signals are potential interfers before considering the appropriate notch filter specifications for this application. In the VHF band, interfering signals include commercial FM stations and narrowband FM signals. A commercial FM station has a modulating frequency of 15 kHz and a modulation index of 5, which yields a deviation of ± 75 kHz or an operating bandwidth of 150 kHz. A narrowband FM (NBFM) signal has a modulating frequency of 3 kHz and a modulation index of 1, which yields a deviation of ± 3 kHz or an operating bandwidth of 6 kHz. In either case, an ideal notch filter with an appropriate 3-dB bandwidth (150 kHz for the commercial FM signal and 6 kHz for NBFM interferer) can effectively reduce the level of the unwanted signals.

The implementation of a TNF bank for wideband single frequency excision requires selecting a common IF frequency so that tuning produces minimal spurious products. One LO is required to drive both the mixer before and after the notch filter. The opportunity remains rather great for spurious products because of the dual mixing in the single TNF section. The non-linear characteristic of a mixer produces a larger number of spurious products at the output. It is essential to choose a common IF which will not contain any of the higher power spurious responses within the system passband. A common IF of 730 MHz was chosen for this particular application to be compatible with an existing in-house system.

In order to take advantage of the high rejection bandwidth of a notch filter in a wideband system, other system requirements need to be examined. These requirements include dynamic range of surrounding RF components, synthesizer resolution, and tuning bandwidth.

Notch Filters

Notch filtering is by no means a new topic for this application. In fact, filter manufacturers are very active in notch filter development efforts for various systems. A fixed notch filter must have the same passband as the system in order to avoid complex band splitting and reconstructing. It also must be capable of rejecting the interferer without distorting the

rest of the system passband. This means the notch filter should have a narrow rejection bandwidth (equivalent to the transmission bandwidth of an unwanted signal), large notch depth, sharp shape factor, and minimal ripple in the passband. A TNF section must have a passband twice that of the system passband with the notch in the center in order to tune either end of the spectrum to the notch center frequency. This allows the filter to be placed anywhere in the system passband without the need for complex frequency inversion schemes.

It is apparent that more than one filter is needed for rejecting interferers in this band due to the different signal characteristics. These filters are difficult to produce, especially with a ±30 MHz passband included in the specifications. In evaluating the different filter topologies, surface acoustic wave (SAW) based notch filters approach specifications for commercial FM signals, while crystal notch filters could be used for narrowband FM rejection.

A notch filter developed by RF Monolithic (RFM) uses SAW resonators as terminations to a quad hybrid circuit. The ports are tuned so that all energy is absorbed in the notch band. When both ports are identically matched the remaining power is transmitted through the isolation port. The wide passband requirements of the TNF are essentially needed in the hybrid. Cascading two filters offers a wide 3-dB bandwidth of 450 kHz, and a 30-dB rejection bandwidth of 100 kHz. The 3-dB bandwidth is measured relative to the filter insertion loss of 6 dB. This filter is very well suited for rejecting commercial FM signals as well as interferers with wider bandwidths (see fig. 2).

Most crystal filters today use single and monolithic dual resonators for high-frequency applications over traditional overtone devices. In the past, fundamental resonators were limited in frequency (45 to 70 MHz) and wideband applications were nonrealizable, using third-overtone resonators. The fundamental resonator's frequency varies inversely to the wafer thickness, thus a more fragile structure at higher frequencies. Third-overtone resonators have high impedance which results in a high insertion loss and less rejection attenuation. Methods to compensate these devices result in an undesirable spurious response in the stopband.

Piezo Technology uses a relatively new method for obtaining high-frequency fundamental resonators. They use chemically-milled, ring-supported monolithic dual resonators in their filter designs. These fundamental resonators offer low impedances and increased bandwidth. The notch filter that Piezo Technology has designed is that of a 4-pole bandpass filter for wide passband requirements imbedded with a 4-pole rejection filter for shape factor and rejection depth of the notch. Their filter has a 3-dB notch rejection bandwidth of 85 kHz and an ultimate rejection of greater than 80 dB at the notch center frequency of 150 MHz (see fig. 3) relative to the 1-dB insertion loss of the filter.

The following sections will concentrate on the application of the Piezo Technology filter which could be used to reject NBFM signals. The design philosophy is easily adapted to implement the RFM filter for wider bandwidth signals or any other filter and system configuration.

Frequency Synthesis

The final phase of the design involved selection of a suitable tunable LO for tuning the notch to the desired frequency. An approach in which the notch filter, associated RF hardware, and frequency synthesis can be configured in a modular system, such as a digital phase lock loop, would best suit this application. The phase lock loop is small and has low power consumption compared to other methods for frequency synthesis. It offers good spurious output performance and coherent operation is easily obtained with a single reference oscillator driving multiple sections.

The performance requirements for a phase lock loop for this application is to tune in small frequency steps over a wide bandwidth. The Piezo Technology crystal notch filter has a 60-dB bandwidth of about 20 kHz for rejecting the NBFM signal. This would require a synthesizer step size of about 5 kHz to effectively eliminate the 6-kHz bandwidth of the NBFM signal. This fine step size requires a narrow loop bandwidth on the order of 100 Hz. Tradeoffs between loop bandwidth and phase noise or loop settling time is always a factor in a single loop design. The PLL synthesizer output should also have reasonably low phase noise in order not to degrade the phase noise of the input signal. In order to achieve this, a low phase noise reference oscillator and low noise operational amplifiers should be used in the PLL design. Finally, tuning range for this application is 30 MHz with the center frequency determined by the common IF. A D/A converter could be implemented within the loop to coarse tune the voltage controlled oscillator and increase the overall tuning speed of the synthesizer.

Simulated and Measured Data

The notch filter and tuning method are the most critical for a design of this nature. The best performance will not be achieved if the surrounding RF hardware cannot meet predetermined specifications. An attribute highly desirable for this design is high spurious free operating range, which means maintaining the self-induced spurs at some acceptable level, and a high third-order intercept level for each section of the TNF. The third-order intercept point is a figure of merit for determining the largest usable signal. The TNF noise figure is normally not a factor since the sections are inserted after the receiver, which means the dominant noise figure is that of the receiver. Each section must also have unity gain and no net frequency translation so that the sections can be cascaded. EEsof's Omnisys microwave system simulator was used in conjunction with the measured S-parameters of the notch filter in order to accurately model the performance of the TNF section.

Various TNF reponses are included, demonstrating the optimization of the supporting RF components using the simulated data and then comparing them to the measured data. The first plots are those of the output spectrum of TNF section showing the two-tone third-order spurs. The relative level of these spurs could be used to determine the third-order intercept point of the TNF section (see fig. 4 and 5). The next set of plots show two tones of equal amplitude passing through the TNF section. One tone is placed at the notch center (rejected) while the other is 100 kHz away (passed)(see fig. 6 and 7). The rejection of a narrowband FM signal (6-kHz bandwidth) is shown in figures 8 and 9.

Multiple interferers can be rejected simultaneously by cascading several TNF sections. Figure 10 shows a simulation of three cascaded sections notching out three different parts of the 30-MHz band. This result is obtained with minimum distortion to the rest of the passband.

Conclusion

Tuning fixed notch filters exhibiting narrow rejection bandwidths and wide passbands has shown to be an effective manner for eliminating existing narrowband interferers in the VHF band. Effective interference suppression can be achieved by matching the notch filter rejection bandwidth with the interfering signal bandwidth. The Piezo Technology crystal notch filter is well suited for attenuating NBFM and other narrowband spurious signals, while a SAW-based notch filter by RF Monolithic can be used for commercial FM and wider interferers.

Tuning these filters over a 30-MHz passband requires a synthesizer source that can cover

the passband in small steps. A digital PLL is capable of these tuning requirements. Supporting hardware including mixers, amplifiers, and splitters are also important for specifying and meeting critical spurious free dynamic range requirements. All components are available in pc-mount form to design a modular TNF section which includes the notch filter, single-loop PLL synthesizer, and RF components. Cascading several TNF sections provides for multiple interferer suppression.

References

[1] C. Hartman, J. Andle, and M. King, "Saw Notch Filters." IEEE Ultrasonic Symposium (1987), pp 131-138.

[2] M. D. Howard and R. C. Smythe, "Quartz Crystal Filters: a review of current issues." RF Expo East Proceedings (1990), pp 501-514.

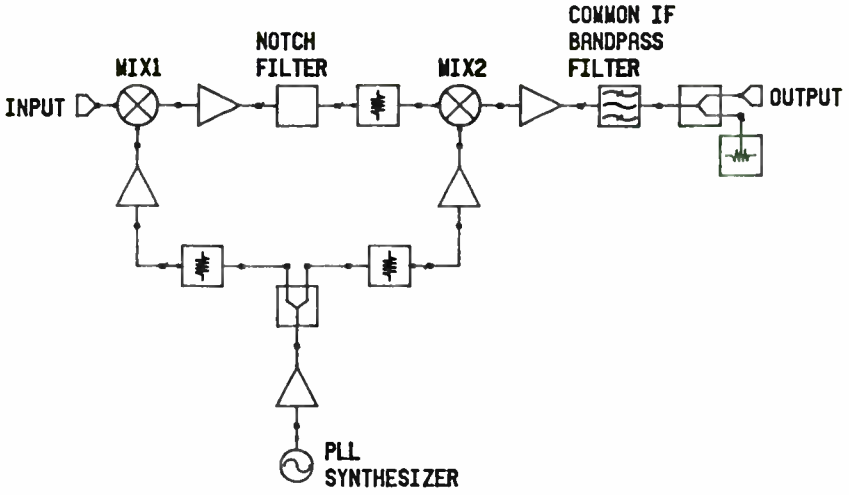

Figure 1: Schematic of TNF section.

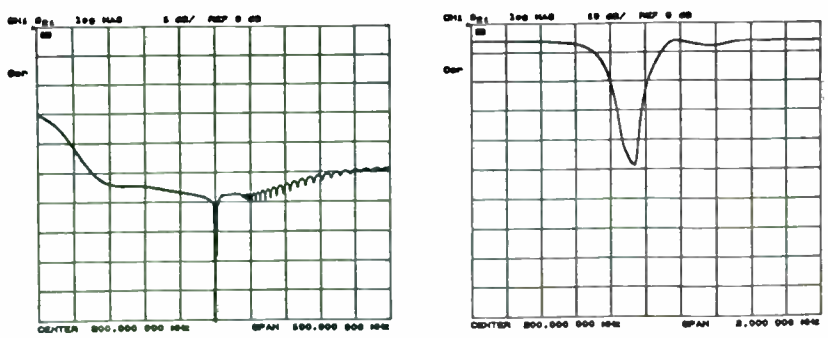

Figure 2: RFM notch filter measured response.

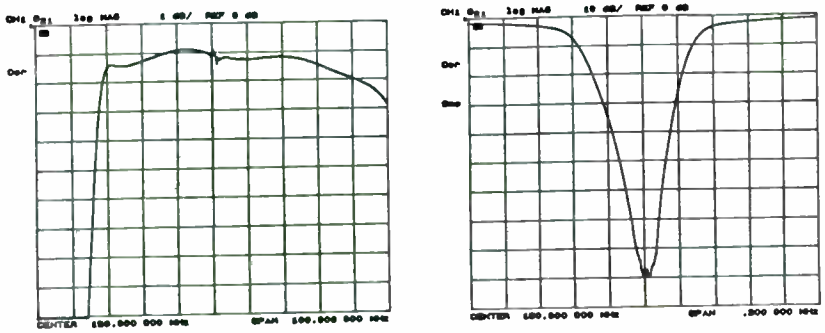

Figure 3: Piezo Technology notch filter measured response.

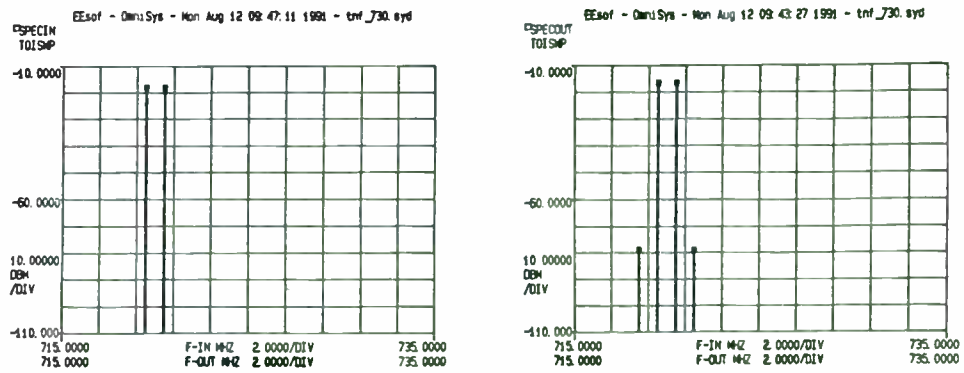

Figure 4: Simulation of two-tone, third-order spurs.

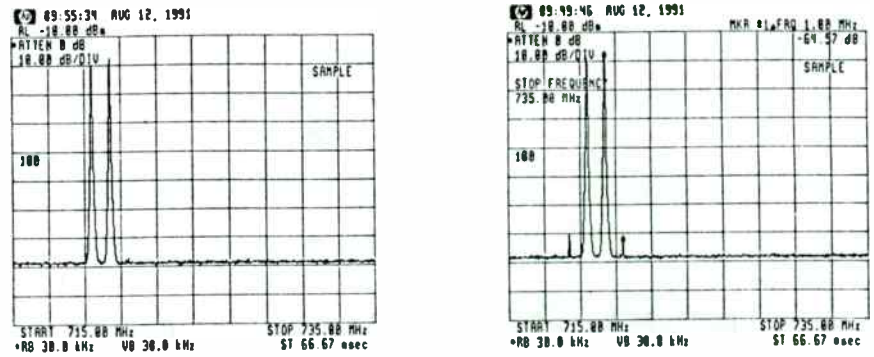

Figure 5: Measurment of two-tone, third-order spurs.

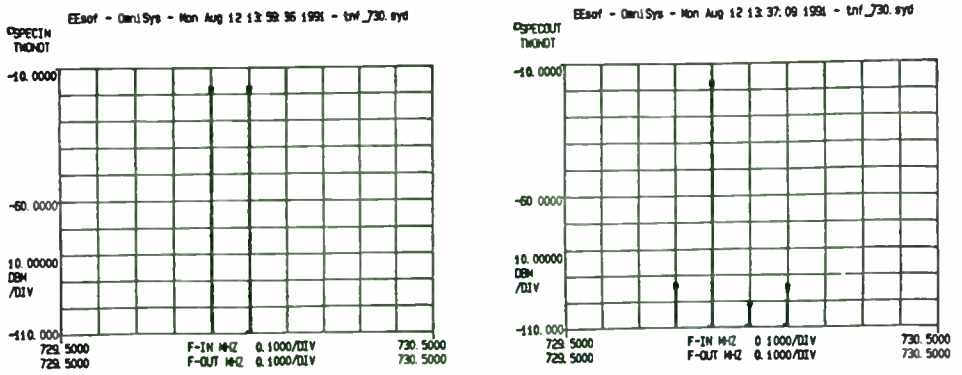

Figure 6: Simulation of rejection of single tone with two-tone input.

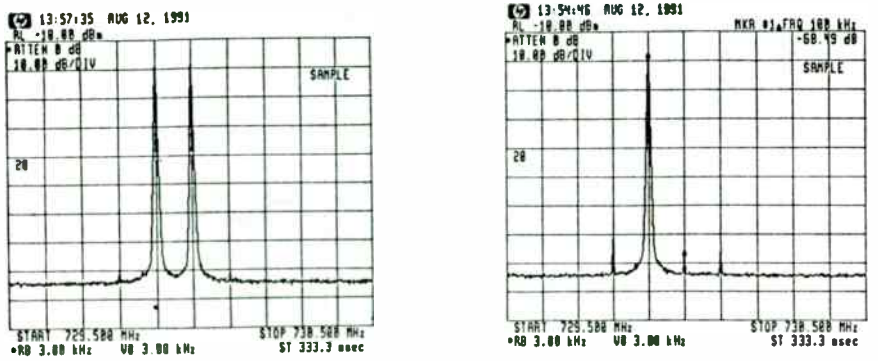

Figure 7: Measurement of rejection of single tone with two-tone input.

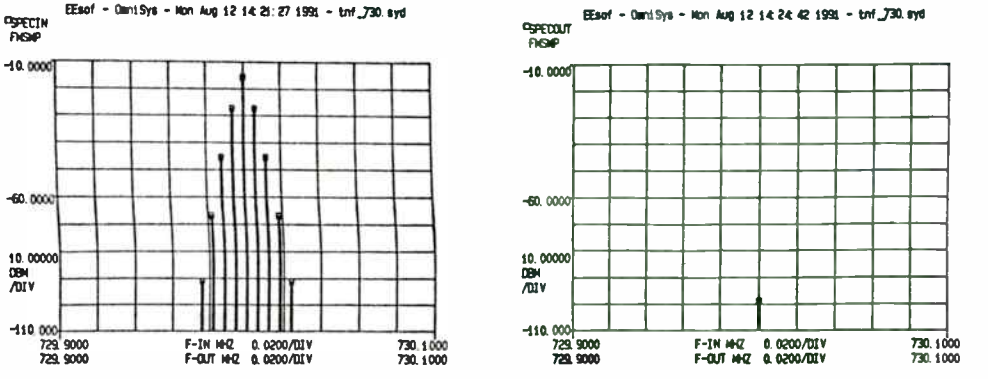

Figure 8: Simulation of narrow-band FM signal rejection.

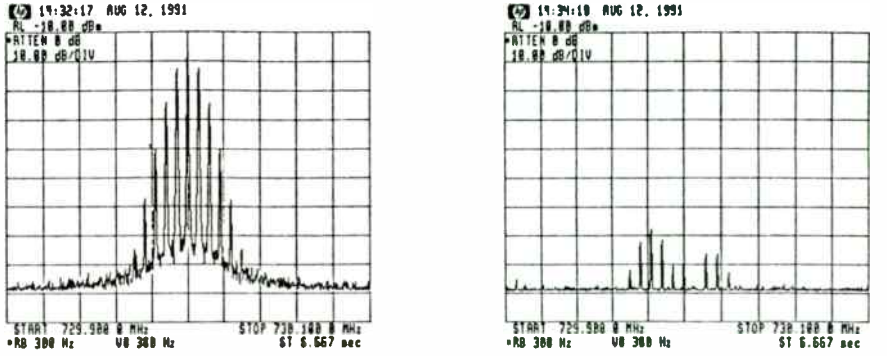

Figure 9: Measured data of narrow-band FM signal rejection.

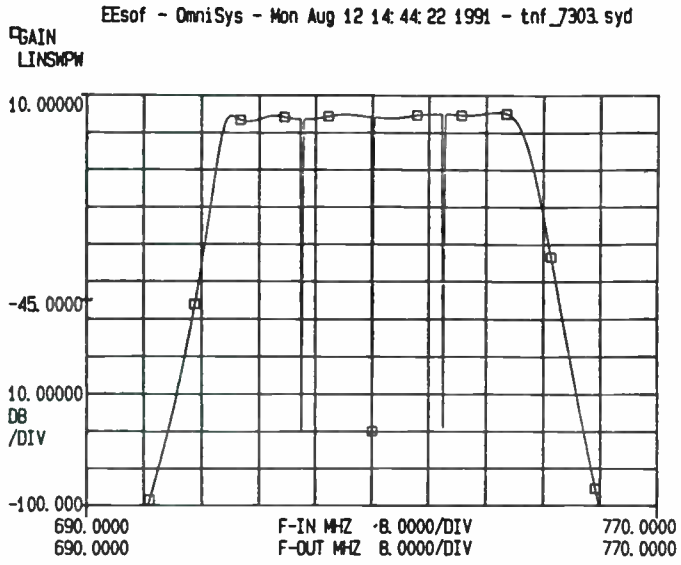

Figure 10: Simulated response of three cascaded TNF sections

SPURIOUS ANALYSIS OF SUPERHETRODYNE RECEIVERS AND FREQUENCY SYNTHESIZERS

SHERMAN VINCENT, SHAMIM AHMED

Raytheon Company
Electromagnetic Systems Division
6380 Hollister Avenue
Goleta, California 93117

ABSTRACT

Determining the optimum system architecture to achieve the required spurious rejection levels in superhetrodyne receivers and synthesizers is a time consuming task requiring the detailed analysis of several design iterations. This paper will identify how spurious signals are created and how to predict the level and frequency of these signals. A novel computer program developed to speed the analysis will be presented. The program allows the user to model a typical receiver with an input preselector, RF amplifier, mixer, and output IF filter. The program output is a tabulation of spurious frequencies, their order, and level.

OUTLINE

SURVEY OF COMPONENT TECHNOLOGIES FOR 900, 2400, AND 5700 MHz UNLICENSED SPREAD SPECTRUM TRANSCEIVERS

by

Al Ward
Avantek Field Applications Engineer
101 W. Renner Rd.
Richardson, Texas 75081

Abstract

This paper will present a survey of device technologies presently available on the market today for use in unlicensed spread spectrum transceivers at 900 MHz, 2400 MHz, and 5700 MHz. The paper begins with a look at the system level specification and then discusses the individual component specifications. Component specifications for the TR Switch/LNA/Frequency Conversion/IF Amplifier stages in the receiver section plus the Modulator/Frequency Conversion/Power Amplification stages of the transmitter are analyzed with respect to available device technolgies. Both GaAs and Silicon technologies in both discrete and MMIC form are considered. A comparison between technology, frequency, and performance is presented along with some cost considerations. Design techniques are presented along with actual working circuits.

The FCC has authorized the use of spread spectrum in three bands designated for ISM (Industrial, Scientific, Medical) use. Spread Spectrum is a technology that allows several users the ability to use the same frequency with minimal interference between users. Each signal is spread out over a much larger frequency band and transmitted. Only a receiver with the proper spreading code can properly de-spread the broadband signal and make it now appear identical to the transmitted signal. It is very difficult for any other type of receiver tuned to any frequency in the spread bandwidth to detect the existence of the spread signal. It appears to be broadband noise with no real intelligence added.

The three frequency bands authorized are 902 to 928 MHz, 2400 to 2483 MHz, and 5725 to 5850 MHz. The maximum power output as authorized by FCC regulations Part 15 for unlicensed spread spectrum is +30 dBm effective radiated power. With an omnidirectional antenna of 0 dBi gain, the transmitted power can be +30 dBm (1 watt). If the antenna gain is raised to 3 dBi, then the maximum transmitted power can be no greater than +27 dBm (1/2 watt). The actual transmitter power required for a particular application depends on the receiver noise figure, the attenuation characteristics of the path and the desired signal to noise ratio. Typical transmit powers will be in the +20 to +30 dBm range.

RECEIVER ARCHITECTURE

Two basic receiver types that convert RF energy to baseband signals will be discussed. The most basic receiver is the direct conversion concept where detection is done at the RF frequency. This dictates that all low noise amplification and preselection filtering in front of the detector be done at the RF frequency. Figure 1 shows a typical direct conversion transceiver. At 900 MHz, this is a possible approach but at the higher frequencies, it becomes more difficult to build adequate filtering at the RF frequency for most applications. An alternative is the superheterodyne type of receiver as shown in Figure 2 where the RF signal is downconverted to an IF signal generally in the 70 to 500 MHz frequency range. It is considerably easier to narrow up the signal at the IF frequency as opposed to the RF frequency. With modern day surface acoustical wave (SAW) devices, filters with a 3 dB bandwidth of less than 0.1 % at frequencies up to 1 GHz are possible.[1] The following sections will discuss the major RF and IF components in a typical transceiver.

LOW NOISE AMPLIFIERS (LNAs)

900 MHz

Todays silicon bipolar technology can produce devices with noise figures as low as 1 dB at 900 MHz increasing to 2.5 dB at 2.4 GHz. One such device is the Avantek AT-41411 discrete bipolar device available in a low cost surface mountable plastic SOT-143 package. This particular device boasts a 4 micron emitter to emitter pitch with an f_t of 7 GHz. This device provides minimum noise figure with a generator source impedance of 50 ohms, thereby requiring no input match for lowest noise figure. All that is required is to match the output of the device for gain and stability and add the appropriate bias decoupling networks. The device can be reactively matched or standard resistor feedback can be used to obtain broadband stability and still retain fairly good noise figure and moderate gain. A suitable circuit is shown in Figure 3. This circuit employs a simple feedback network that provides gain flatness and stability with minimal degradation in noise figure. Gain measures 17 dB at 900 MHz. At 900 MHz, the addition of the feedback network will increase the amplifier noise figure from 1.5 dB to 1.75 dB. Depending on front-end filter and T/R switch losses, the noise figure of the AT-41411 may be adequate for use in the front-end.

An alternative to the discrete silicon bipolar approach is the use of silicon MMIC technology. The silicon MMIC has certainly revolutionized the design of modern day communication systems. The Avantek MODAMP^{tm} series of silicon MMICs provides noise figures as low as 3.2 dB at 900 MHz and a gain of 17 dB with no additonal matching required. One such device is the Avantek MSA-0611 in a low cost SOT-143 package. The MODAMP^{tm} series of MMICs is manufactured using a 10 GHz ft, 25 GHz fmax silicon bipolar process which utilizes nitride self-alignment, ion implantation and gold metalization to achieve excellent performance, high uniformity and high reliability. The MODAMP^{tm} is a Darlington connected transistor pair using a combination of shunt and series resistive feedback to establish the desired gain-bandwidth performance.

Using the MMIC is a simple matter of supplying a bias decoupling network on the output side of the device and a simple dc blocking capacitor on the input side. A simple circuit is shown in Figure 4. The devices can be biased with a simple series resistor or a current source using a PNP device.

The main limitation of the MODAMP^{tm} process is that both device collectors are electrically connected together. This makes it more difficult, as an example, to bias up the first device for lower noise and simultaneously obtaining a high gain bandwidth product. A new MMIC process, called ISOSAT^{tm}, that overcomes this shortcoming has been developed by Avantek. The process uses state of the art submicrometer electron beam lithography and an isolated collector technology that yields noise figures as low as 2.3 dB at 900 MHz and 28 dB gain. One such device is the Avantek INA-02186 which is provided in a low cost surface mountable .085 inch diameter plastic package. As with the standard MODAMP^{tm}, only simple bias decoupling networks are required to use the device. No additional matching structures are required.

For the ultimate in low noise performance, the GaAsFET device is still the best performer. Today's GaAsFET technology has produced "off the shelf" devices with less than 0.5 dB noise figure at 900 MHz and 2400 MHz. One such device is the Avantek ATF-10136, a 500 micron device, which is available in a low cost

metal-ceramic "micro-x" package offering a 0.5 dB noise figure with an associated gain of greater than 20 dB gain at 900 MHz.

Using a GaAsFET at frequencies below 2 GHz generally does require extra engineering precautions in order for the LNA to provide stable gain. By using a combination of source inductance and resistive loading it is possible to use GaAsFET devices at these frequencies successfully.[2] Using good engineering practice it is best to expect no more than about 17 dB gain from a single device in this frequency range. More gain is possible at the expense of stability.

In order to reduce cost, several component manufacturers supply GaAsFET chips in low cost plastic packaging. One such device is the ATF-13284 250 micron low noise FET in the low cost .085 inch diameter plastic package. Its rated noise figure is about 0.1 dB higher than the ATF-10136 due mainly to package losses.

Generally the larger devices, (i.e. 500 micron and larger) are easier to use at the lower frequencies because they have lower gain and are easier to stabilize. A review of the device S Parameters reveals that the impedances associated with the larger devices are lower than the smaller devices, therefore making it easier to obtain a lower loss impedance match.

2400 MHz

The AT-41411 discrete silicon bipolar device discussed in the previous section will also provide a 2.5 dB noise figure at 2400 MHz. A suitable circuit is shown in Figure 5. Simple reactive matching provides a 2 dB noise figure and 9 - 10 dB gain with good stability. Alternative approaches include the use of low cost silicon MMICs. The INA-03184 is another member of the ISOSAT^{tm} based MMICs discussed earlier, providing a 3 dB noise figure and 23 dB gain at 2400 MHz.

The lowest noise approach is still the GaAsFET. The ATF-10136 500 micron low noise GaAsFET will provide a 0.5 dB LNA noise figure at 2400 MHz. For lower cost, the ATF-13284 in plastic will provide very nearly the same noise figure performance with slightly more gain. A suitable circuit is shown in Figure 6. The circuit shown in Figure 7 is etched on low loss 0.031 inch thickness teflon based material with a dielectric constant of 2.2. The circuits are discussed in more detail in an application note.[3] The LNA requires no tuning during production other than setting the bias point which can be easily accomplished by the use of active biasing. The LNA circuit dimensions can also be scaled to allow the use of the inexpensive epoxy-glass type of dielectric materials.

Recent advances in Pseudo-Morphic High Electron Mobility Transistor (PHEMT) technology have yielded devices with measured noise figures as low as 0.25 dB at 2 GHz. One such device is the Avantek ATF-35076. Preliminary results show that the ATF-35076 can achieve an LNA noise figure that is about 0.1 to 0.2 dB lower than the ATF-10136 at 2.3 GHz. Although the device is capable of very low noise figures, the limiting factor may very well be the ability to match to the very high input impedances offered by the HEMT type devices at low frequencies.

Retaining the low noise figure of the LNA at the system level may necessitate the use of a two stage GaAsFET LNA followed by a gain block with a slightly higher noise figure. The GaAsFET amplifiers discussed in this paper are easily cascaded for increased gain.

5700 MHz

The only reasonable approach to an LNA at 5700 MHz is through the use of FETs. A two stage LNA using the ATF-10136 series of devices will produce a 1 dB noise figure with an associated gain of 18 to 20 dB.[4] A schematic of an LNA is shown in Figure 8. The circuit is etched on Duroid^{tm} material with a dielectric thickness of .031 inches and a dielectric constant of 2.2. All matching networks are etched microstripline circuitry requiring no tuning during production. The etched circuit is shown in Figure 9. The use of active biasing will also insure the proper biasing point regardless of device to device variations with different production lots.

Achieving a noise figure of less than 1 dB is possible with the ATF-13136 series of devices. The ATF-13136 is a 250 micron device capable of a 0.8 dB noise figure and an associated gain of 13 dB per stage. A less expensive approach would be to use plastic FETs in the LNA. A two stage ATF-13284 (250 micron) series LNA will produce a 1.2 dB noise figure and gains as high as 24 dB.

MIXER TECHNOLOGY

Various options are available to the circuit designer. A typical communications receiver might use a passive double balanced mixer. A passive double balanced mixer offers good port to port isolation but requires atleast +7 dBm local oscillator power and yields conversion loss which the LNA must overcome.

Recent advances in silicon bipolar technology have made it possible to manufacture monolothic bipolar active balanced mixers for frequencies as high as 5 GHz. One such mixer is the Avantek IAM series of Gilbert Cell type active double balance mixers using the ISOSAT^{tm} process. The devices provide conversion gain up to 5 GHz and are usable with IFs as high as 2 GHz. Other advantages include insensitivity to load mismatch and good port to port isolation. In addition, local oscillator requirements are reduced over that required for a passive diode mixer. Typical LO drive requirements are between -5 dBm and 0 dBm. The only disadvantage is the inherent higher noise figure of the Gilbert cell structure, i.e. 15 dB. Since RF gain is just about as inexpensive as IF gain, this should not present a major problem for systems that do not require high dynamic range.

An example of a Gilbert Cell mixer is the Avantek IAM-81008 mixer housed in an inexpensive .180 inch square plastic package providing about 8.5 dB conversion gain at both 900 MHz and 2400 MHz. A typical circuit layout is shown in Figure 10. Providing an LNA with about 25 dB gain in front of the IAM-81008 will keep the receiver noise figure below 1 dB at both 900 and 2400 MHz. This can be accomplished with a two stage ATF-13284/ATF-13484 cascade. Even at 5700 MHz, the IAM-81008 still provides unity conversion gain which is still about 6 dB better than a passive balanced mixer. With a two stage ATF-13284/ATF-13484 LNA, the receiver noise figure drops to about 2 dB.

An alternative approach to the MMIC mixer is an active mixer using a discrete transistor. Numerous articles in the literature document the use of GaAsFET devices being used as single ended mixers.[5,6] These mixers are generally engineering intensive but once a design is optimized in the lab, it can usually be duplicated in the manufacturing area. Using the ATF-13484 as an active mixer at 2400 MHz yielded an SSB noise figure of 5 to 6 dB with several dB of conversion gain. 4 to 5 dB noise figures are

possible with the ATF-10136 device at a slight increase in cost. A simple circuit is shown in Figure 11. The RF is injected into the gate while the LO is injected into the drain. This has been shown to yield lower noise figures as compared to a gate LO pumped active mixer. The IF is extracted out the drain through the bias decoupling network. For some applications, only 1 RF stage may be required if a FET is also used as a mixer due to its inherent lower noise figure.

OSCILLATORS

The primary local oscillator is usually a free running oscillator phase locked to a low frequency standard such as a temperature stabilized 10 MHz crystal oscillator circuit. The VCO can take on the form of a simple reflection type circuit or a parallel feedback type of oscillator circuit. In general, the parallel feedback oscillator will provide several dB of improvement in phase noise performance as compared to a simple reflection type oscillator circuit. Dielectric resonators are a good choice for the frequency determining element for the 2400 and 5700 MHz lineups. However, their size is probably prohibitive at 900 MHz. A good alternative would be the use of a surface acoustical wave (SAW) resonator. For best phase noise performance, the silicon bipolar transistor is the preferred choice. The AT-41411 low cost transistor in the SOT-143 package will work well at L and S band frequencies. The extra package inductance of the SOT-143 device will make it marginal at 5 GHz. The same die in a lower inductance plastic package such as the AT-41486 will work well at 5 GHz.

IF AMPLIFIERS

Generally the requirements for the IF amplifier are not as critical as the LNA. Noise figure is generally not as important. Typically noise figures in the 3 to 5 dB and sometimes higher will not have an adverse effect on overall system noise figure if adequate gain is obtained from the LNA and if the mixer noise figure is not excessive. Generally, the IF amplifier is used to increase the power level from the preceding stages to the point that it effectively drives the demodulator to the proper level. It may therefore be more critical that the IF amplifier be capable of greater power output than the preceding stages to keep the later stages from compressing and generating undesired mixing products that may fall into the detection passband.

The moderate noise figure and power output requirements for the IF amplifier make the silicon MMIC a very inexpensive solution. The MMIC approach would also not be as engineering intensive as a discrete device approach. A good solution for IFs in the VHF frequency range is the MSA-1105. With less than a 4 dB noise figure , moderate gain (12 dB) and good power output capability (+17.5 dBm @ 1 dB gain compression), the MSA-1105 will meet most requirements for a high dynamic range IF amplifier. The device is housed in an inexpensive surface mountable .145 inch diameter plastic package. The device is designed to be driven from a current source supplying 60 mA. Device voltage is approximately 5.5 volts.

FILTERS

In a typical superheterodyne type of receiver, filters are normally required to shape the desired passband frequency and to reject undesired mixing products that are generated as a result

of performing frequency conversion in either the transmitter or the receiver. Generally bandpass filters are used in front of the LNA for out-of-band rejection and in front of the first mixer to provide image rejection. The loss of the first bandpass filter is the most critical as its loss adds directly to the receiver noise figure. A 0.5 dB loss filter will increase a receiver noise figure from 0.5 dB to 1.0 dB. The losses associated with the image reject filter are not as critical as its loss merely adds to the mixer noise figure. Since there is usually enough gain in the LNA, the overall effect of the loss is minimal on receiver noise figure.

One of the easiest types of bandpass filter to design and construct is the halfwave parallel coupled filter. At 900 MHz, the filter can be etched on inexpensive FR-4 or G-10 material and provide acceptable loss and reasonable out of band rejection. In order to alleviate tuning at the production level, it is best to design in some additional bandwidth to allow for some movement of the filter center frequency due to dielectric material variations from production run to production run. Choose a filter ripple level that won't add excessive passband amplitude ripple to the receiver. The basic design information is available in the literature.[7]

IQ DEMODULATORS/MODULATORS

A pair of IAM-81008 active mixers function as a QPSK demodulator with the RF ports fed in phase and the LO ports driven in quadrature. On the transmit side, the IAM-81008 will produce the BPSK waveform when driven by a psuedo-noise generator at the IF port and the appropriate clock frequency at the LO port.

TRANSMITTER

The low level stages of the transmitter can utilize the same technology devices as in the receiver stages. The output of the mixer is generally in the -10 dBm to 0 dBm level and this must be amplified linearly to the +20 to +30 dBm range. The following sections will consider the options appropriate for the desired frequency range.

900 MHz

Discrete silicon transistors in plastic packages is the least expensive way to generate moderate power at 900 MHz. The Avantek AT-41411 in the inexpensive SOT-143 package will boost the power level from the low level of a passive or Gilbert Cell mixer to the +10 dBm level. The Avantek AT-42086 silicon bipolar transistor is capable of generating 100 mW with a stable gain of 15 dB. This device uses similar process technology to the AT-41411 with the exception that the AT-42086 has 20 emitter fingers instead of 14 and is therfore capable of greater power output. A 2 stage amplifier consisting of an AT-41486 driving an AT-42086 is shown in Figure 12. A power input level of -10 dBm produces an output power of +20 dBm. The AT-41486 is biased at Vce = 8 volts at a collector current of 25 mA. The AT-42086 is biased at Vce = 8 volts and a collector current of 35 mA. The circuit was etched on .062 inch thickness FR-4.

Paralleling two AT-42086s with the use of Wilkinson combiners will provide a power level of 200 mW. The 86 type package is used at the higher power levels due to its superior thermal capability as compared to the SOT-143 package. Several companies are also manufacturing 1 watt output plastic devices.

The primary concern is how efficiently can the heat be extracted from the device since the actual power dissippated in this type of device can be as high as 2 to 3 watts. Avantek offers the AT-64020 in the .200 inch diameter BeO package providing over a half watt at frequencies as high as 4 Ghz.

Cascading a series of MMICs is also a possible approach. The Avantek MSA-1104 MMIC will provide 50 mW output with about 11 dB gain. For higher power output, the MSA-0505 will provide 65 mW. Both devices can be paralleled for an additional 3 to 6 dB increase in power. For higher power the MSA-0520 will put out 200 mW and the MSA-1023 device will supply 500 mW. Both devices are in the more expensive BeO packaging for the purpose of extracting heat.

2400 MHz.

At 2400 MHz, the AT-42086 will still provide 100 mW as it did at 900 MHz but with reduced gain. Paralleling 2 or 4 of these devices will provide 200 to 400 mW. At higher power levels, the AT-64020 discrete device will provide 500 mW at 8 to 10 dB gain with simple matching networks. At higher power levels the power GaAsFET is an alternative. The Avantek ATF-44101 will provide +32 dBm of power at 2400 MHz. A typical device lineup is shown in Figure 13.

Packaged GaAsMMICs are an alternative to generating broadband gain and power in the microwave region. The MGA-64135 is a two stage GaAsMMIC that provides 14 dB gain and a power output of +12.5 dBm at 2400 MHz making it ideal for a no-tune driver stage.

5700 MHz

Above 4 GHz, the only solution for microwave power is to use the GaAsFET. General purpose FETs, such as the ATF-26884 in plastic packaging, offer about +18 dBm of output power at 5700 MHz with greater than 10 dB of gain. The ATF-26884 is a 250 micron device. The MGA-64135 GaAs MMIC is also an alternative to achieving medium drive power (+12 dBm) at 5700 MHz. Higher power can be obtained by driving an ATF-21170 (750 micron) to +22 dBm and then driving an ATF-45101 (2500 micron) to +28 dBm. The disadvantage of the larger devices is the need to have a more efficient package for removing heat which tends to drive the cost up. A typical device lineup is shown in Figure 13.

SWITCHES

The function of transfering the antenna from the receiver to the transmitter can be accomplished easily with either PIN diodes or GaAsFET switches. PIN diodes have been used for years as a reliable and simple means of transfering power. Diodes have the advantage of being low loss but do require bias decoupling networks to use them effectively. They are typically used in both series and shunt configurations to keep the loss to a minimum while still retaining enough isolation so as not to burnout the receiver frontend device. PIN diodes are capable of handling very high power.

An alternative is the use of low cost GaAsFET switches. Losses are slightly higher but isolation is comparable to PIN diode switches. GaAsFET switches have the advantage of not requiring a large amount of dc current to switch between ports. One such device is the Avantek MGS-70008 available in the S-08 plastic package for low cost. The MGS-70008 typically has only

0.8 dB loss at 900 MHz increasing to 1.3 dB at 2400 MHz. Even at 5700 MHz the loss only increases to about 2 dB. Isolation is typically 40 dB at 900 MHz and 30 dB at 2400 MHz. Output power at 1 dB gain compression measures +26 dBm at 2400 MHz.

DIELECTRIC MATERIAL

The circuits presented in this paper have been designed for use in a microstripline environment. The bottom of the printed circuit board being the groundplane with the microwave circuitry etched on the top layer. The inexpensive FR-4/G-10 epoxy based materials will work well at 900 MHz and possibly 2400 MHz. The teflon based materials are suggested for the 2400 and 5700 MHz frequency ranges due to their lower loss. The lesser expensive epoxy based materials can be used effectively especially at 900 MHz and 2400 MHz if care is given in the design to the effect of the dielectric thickness and variation in dielectric constant. Suggestions are to include enough tolerance in the bandwidth of the bandpass filters so that changes in the dielectric do not reduce the desired bandwidth. Design amplifier stages with low Q elements so that the dielectric's effect on the circuit performance will be minimal.

CONCLUSION

This paper has given an overview of the device technologies presently available on the market today for use in spread spectrum transceivers. Both silicon and GaAs solutions have been presented for all transceiver functions. In some cases the MMIC approach is the most cost effective and less engineering intensive approach. In other cases such as the LNA or power amplifier, the discrete approach yields the best performance. Effort is being made to integrate the receiver and transmitter functions on a single MMIC. Numerous technical issues are being investigated such as heat considerations, packaging, good grounding, incorporation of filters to restrict bandwidth and obtaining low noise performance on an MMIC without the losses associated with resistive matching.

REFERENCES

1. A. Coon, "Capabilities and Applications of SAW Coupled-Resonator Filters", Proceedings of RF Expo West, Feb 5-7, 1991, pp 537-550.

2. A. Ward, "Low-Noise VHF and L-Band GaAs FET Amplifiers", RF Design, Feb, 1989, pp 38-48.

3. "S-Band Low Noise Amplifiers using the ATF-10136 and ATF-13284", Avantek Application Note AN-G004.

4. A. Ward, "Simple Low-Noise Microwave Preamplifiers", QST, May 1989, pp 31-36.

5. S. Maas, "Analysis and Design of GaAs MESFET Mixers", 1984 IEEE MTT-S Digest, pp 432-433.

6. P. Bura and R. Dikshit, FET Mixers for Communication Satellite Transponders", 1976 IEEE MTT-S Digest, pp 352-354

7. G.L. Matthaei, L. Young, and E.M.T. Jones, Microwave Filters Impedance Matching and Coupling Structures, McGraw-Hill, 1984

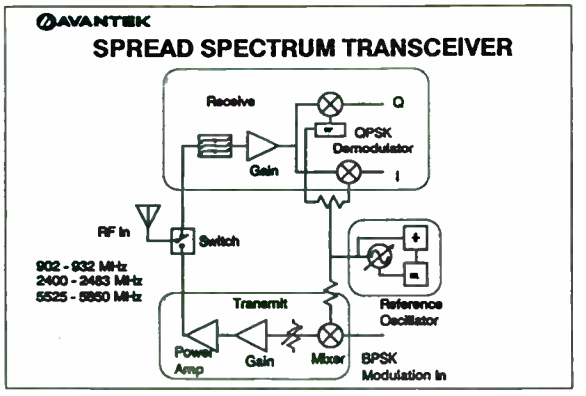

Figure 1. Direct Conversion Transceiver

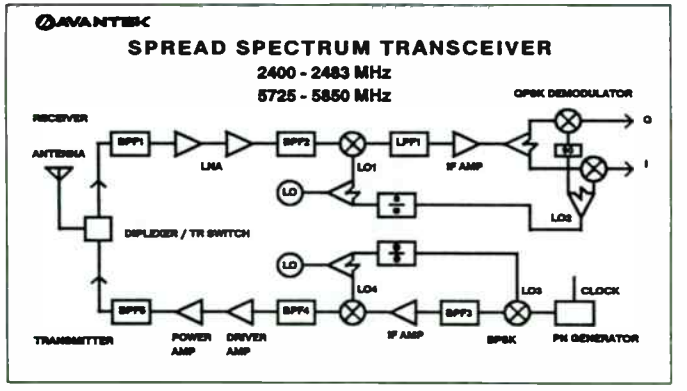

Figure 2. Superheterodyne Transceiver

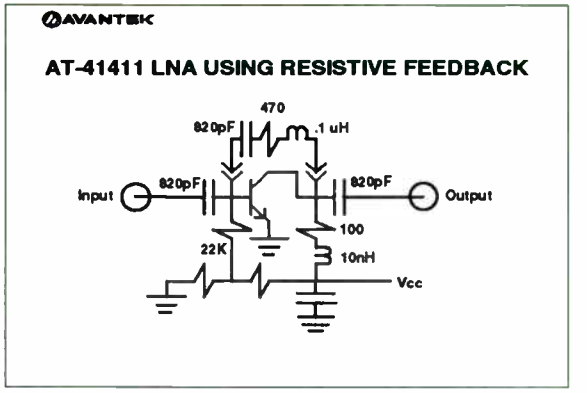

Figure 3.

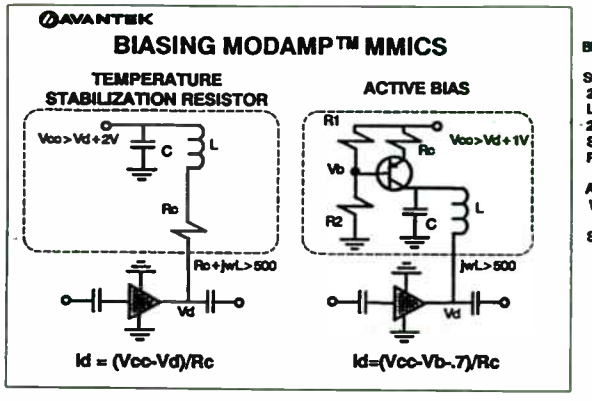

Figure 4.

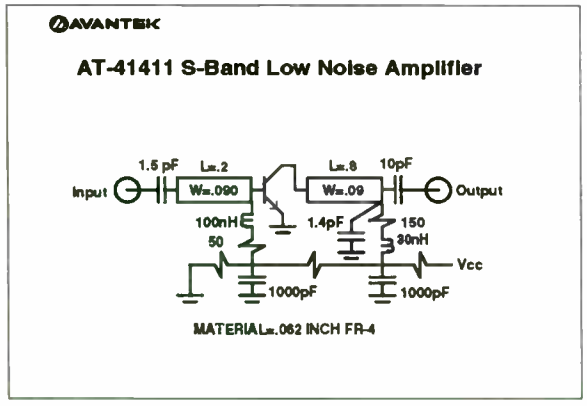

Figure 5.

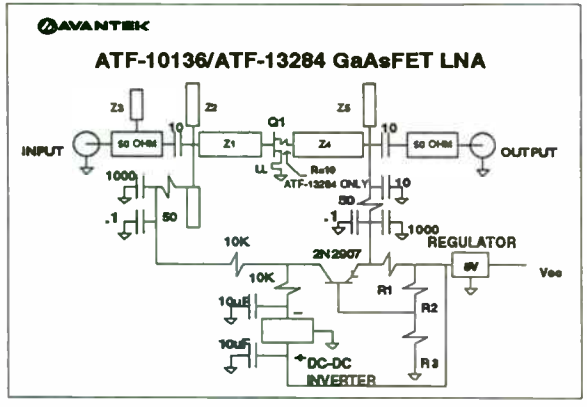

Figure 6.

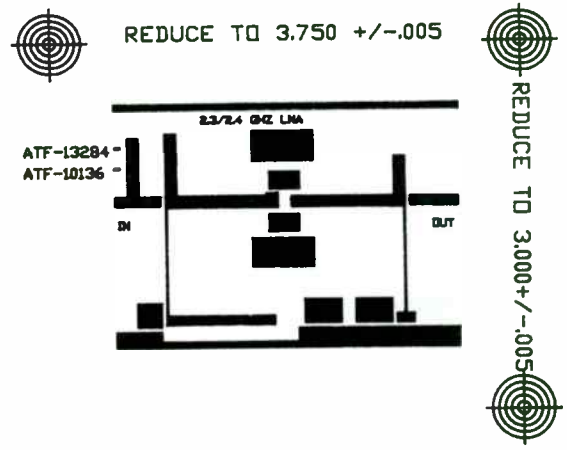

Figure 7. Artwork for S-Band GaAsFET LNA

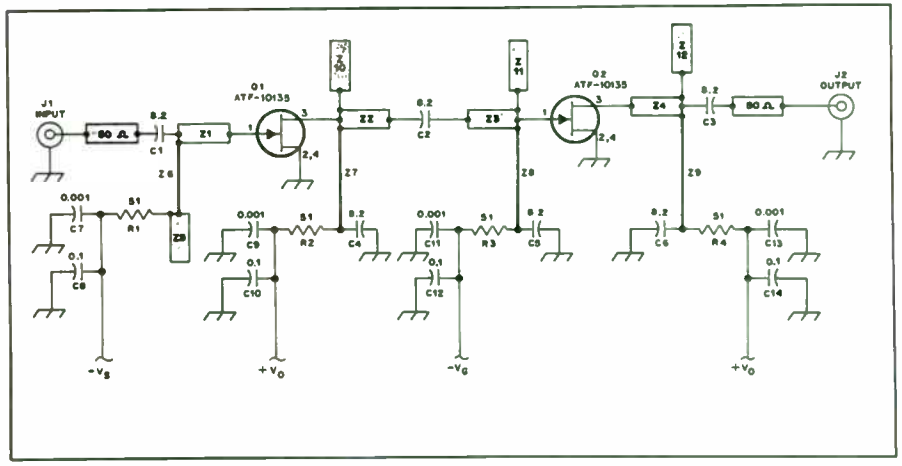

Figure 8. ATF-10136/ATF-10236 5800 MHz LNA

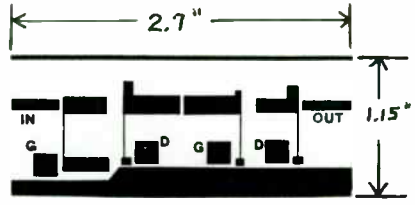

Figure 9. Artwork for 5800 MHz GaAsFET LNA

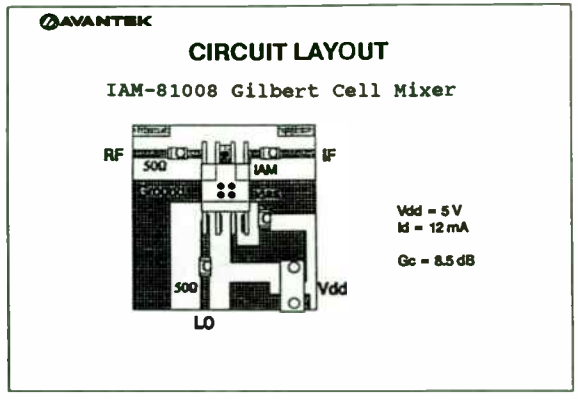

Figure 10.

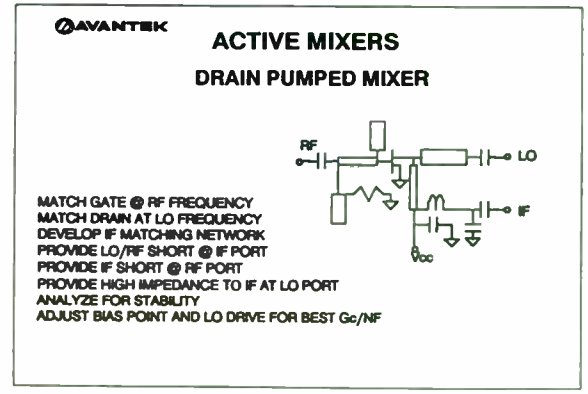

Figure 11. GaAsFET Active Mixer

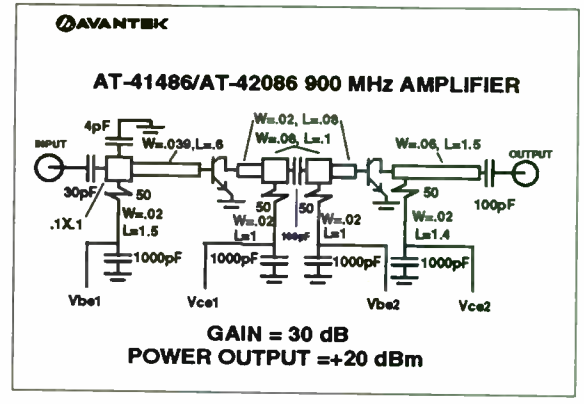

Figure 12.

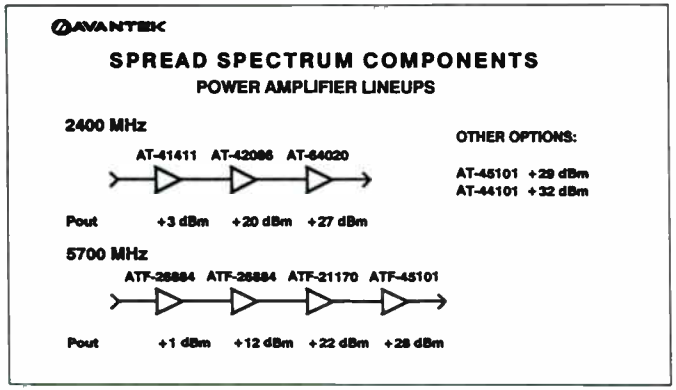

Figure 13.

INTEGRATED R.F. INTERFACES FOR RURAL CENTRAL OFFICES

M. V. Pitke
Tata Institute of Fundamental Research
Homi Bhabha Road, Bombay 400005, India

Abstract:

Emerging wireless information technology can provide several cost effective solutions to the problem of rural communication. An important cost factor in a switch is the line interface. A fully integrated radio interface eliminates several expensive components resulting in higher reliability and lower cost. Examples discussed include single channel extension, multichannel trunks and analog and digital multiple access radio. A modular design permits incorporation of advanced components as they become economically attractive.

Introduction:

Rural communication has been receiving increasing attention in several countries of the world. There are two broad scenarios: one relating to the needs of the industrialized countries and the other relating to the developing countries. Many problems are common to both situations. Considerable effort has been devoted in developing cost effective products for transmission as well as switching. Several low cost rural switches with good central office capabilities and VHF/UHF transmission systems are commercially available. However the overall cost structure is still not very satisfactory and one is forced to examine further possibilities of cost reduction. Benefitting from developments in other applications is also possible. Cordless, cellular and spread spectrum are some examples. However in all networks there is one common cost parameter. In switching systems, the cost of line circuits predominates, amounting to 60-65% of the overall cost. A significant fraction of this can be reduced by having closer integration of transmission with the switch. In this paper we shall discuss some of the issues involved.

. The Rural Network:

Rural networks are generally characterized by:

. Remote locations
. Lower density
. Older switches
. Poor transmission media

In order to provide cost effective service comparable to that in the urban areas, several innovative solutions are required. These will be based on digital signal processing and VLSI. There are two main components to be considered: Transmission and Switching. Switching has received considerable attention over the past decade. With the advent of large scale integrated circuits very low cost digital central offices with capacity of 100 lines or lower have been developed to provide high quality analog and digital communication facilities. Newer versions can support ISDN facilities also. Use of CMOS technology reduces considerably the power drain as also the air-conditioning requirement. Unattended operation and remote maintenance and monitoring have become a standard feature.

Fig. 1 shows the block schematic of a small switch. All subscriber lines terminate on the line card which performs the analog and digital conversion of the voice signals. These signals are stored in a buffer memory which acts like a switch and makes appropriate connections and disconnections under instructions from the microprocessor. Signalling information e.g. on-hook, off-hook conditions, digits dialled, etc. are first processed by a hardwired processor called signalling processor and the processed information is forwarded to the microprocessor. This method of handling signalling relieves the main processor of several repetitive real time consuming operations. The processor is left to deal with more intelligent operations.

Fault tolerance is achieved by duplication of critical hardware. In the scheme presented, the two microprocessor communicate with each other via an HDLC interface. Switches based on this approach are now in regular production and over half million lines have been produced.

Several solutions are available for handling the transmission problem. Three categories of interfaces cover all the needs. These are:

a) Single Channel Extension
b) Multichannel Trunk Interface (Analog and Digital)
c) Shared Channel System based on Frequency Division Multiplex (FDMA) or Time Division Multiple Access (TDMA)

Fig. 2 shows the structure of a typical subscriber line interface. Broadly speaking, components on the left of the dotted line like relays, coils and transformers

required for 2/4 wire conversion, ringing and protection, account for a major fraction of the total cost. Also, these are not easily amenable to LSI conversion. In the conventional approach, the radio interface equipment performs several functions just to make it compatible with the line circuit that has been specifically designed to interface long land lines. There will be a (redundant) 2/4 wire conversion just to match the 2 wire interface. All this will be eliminated if a "radio interface card" is provided which accepts 4 wire input directly from the VHF/UHF transceiver section. Fig. 3.

Trunk interface is similar to line interface (in fact they are interchangeable, which permits reconfiguration of the system for a particular situation or application) and similar considerations apply. However radio trunks could be multichannel analog (fdm) types or digital (tdm) types to provide upto 24/30 channel capacity. Use of digital signal processing techniques provides an extremely cost effective interface (Fig. 4).

The calling rate being low, the grade of service can be easily handled by having a few lines shared by a large number of subscribers. A multiple access system achieves this. Fig. 5 shows the organization. In the lower range where only a few channels are used, the frequency division multiplex is cost effective. Typically a small system will permit sharing of 2 channels by 16 or more subscribers. The interface hardware would be similar to the trunk interface system but will need additional control circuitry and software for managing subscriber service. Larger systems are best implemented using the time division multiplex technique. This has the added advantage of providing direct digital interface. Organization of a system is shown in Fig. 6.

Future Directions:

Very significant developments are taking place in the field of wireless information technology. A wide range of products are already in the field. These include the simple cordless telephony, the CT-2/telepoint, analog and digital cellular and the wireless LANS. There are also very important developments in components and the digital signal processors. As these technologies get into mass manufacture (chips) and thus widely used, their ever reducing cost makes them gradually attractive for incorporation into rural communication systems. The next decade will see an emergence of new, inexpensive products in this field.

Network Management:

The complete rural communication network can be optimized operated and maintained by a computerized network management system. This will further result in economy. However in order to be able to implement such a network, the switching centres are required to provide the necessary traffic and other information in a processed form along with the facility for remote control. Addition of "intelligence" (i.e. a microprocessor) is required to achieve this. This is also important if the system has to get integrated into the intelligent networks of the future.

Cost Projections:

Evaluation of various technology/design options indicate the following cost estimates for the various systems:

. Single channel extension per subscriber	:	$ 1000
. Trunk radio interface (Total 30 ch.)	:	$ 3000
. Multiple Access Radio 2/16, FDMA Analog per subscriber	:	$ 800
. Multiple Access Radio Digital 8/64 TDMA, per subscriber	:	$ 600

Concluding Remarks:

Radio technology provides a cost effective solution for rural networking. In order to benefit fully from the evolving advanced signal processing technologies and concepts, an integrated approach involving a total solution is required. This takes into account the transmission, switching, terminals and their integration into an optimum network that can be operated and maintained at low cost. The emerging wireless information technology will provide newer cost effective solutions that would permit, in addition to voice, an end to end digital connectivity. Hence the design has to be highly modular so that new technologies can be adopted and incorporated in a smooth manner.

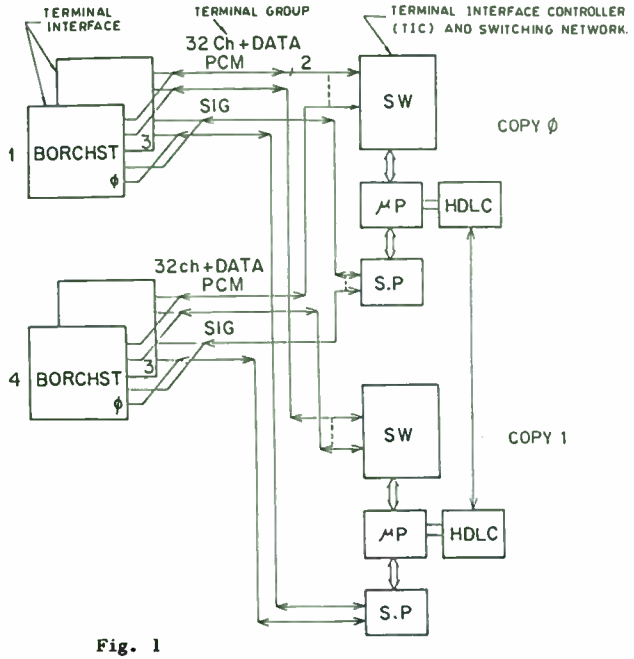

Fig. 1

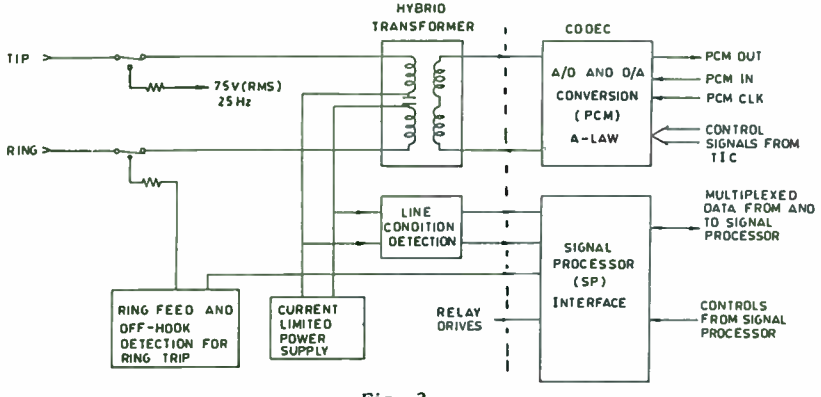

Fig. 2

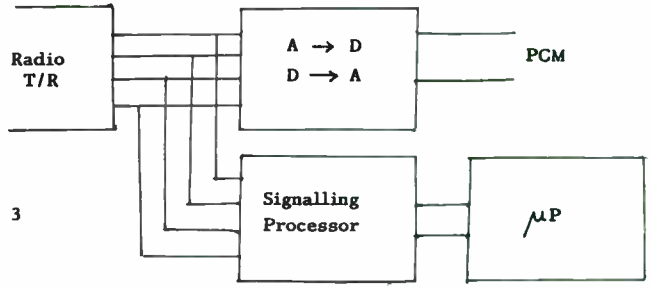

Fig. 3

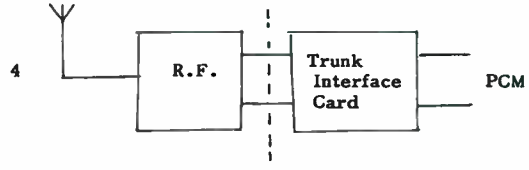

Fig. 4

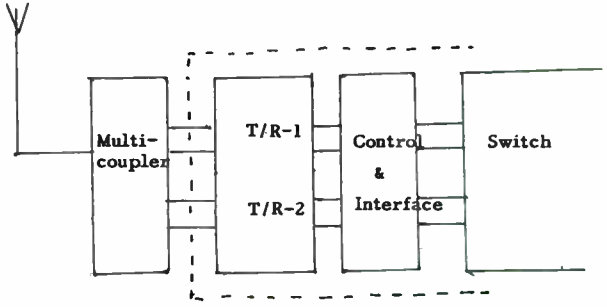

Fig. 5

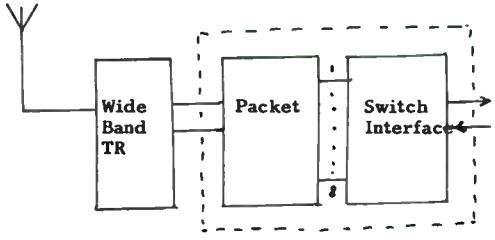

Fig. 6

PHASE MULTIPLEXED CORRELATION IN MULTIPLE ACCESS SPREAD SPECTRUM SYSTEMS

By

Glen G. Koller & Madjid A. Belkerdid

University Of Central Florida
Electrical Engineering Department
Orlando, Florida 32816

Abstract

The relatively new concept of Phase Multiplexed Correlation (PMC) is applied to the Code Division Multiple Access (CDMA) Direct Sequence Spread Spectrum (DSSS) environment to determine coarse acquisition advantages. Prior to the discussion of the PMC, the Conventional Sliding Correlator (CSC) design is reviewed to establish performance guidelines. Both systems are modeled in software where simulated results are compared to predicted calculations.

Introduction

The CSC is a coarse acquisition technique commonly used in DSSS systems. Its concept is based on an integration process that is used to exploit properties of pseudo-noise (PN) sequences. The CSC's simple design leads to an easy implementation but is rather inefficient in that it performs a serial search of the uncertainty region which usually requires a considerable amount of time. Its ability to lock onto a signal gradually deteriorates as transmitters (users) of equal power (as seen by the transmitter) are added and dramatically degrades when high powered interfering transmitters appear. Recall that the "near-far" problem is the situation where multiple transmitters are geographically located at different distances from the receiver. Even when each is transmitting at the same level (equal power), the one closest to the receiver is dominant. Attempts that are made to despread the signal of the furthest transmitter results in an overwhelming power disturbance from the closest transmitter. The disturbance appears as a high cross-correlation of the undesired codes to the local PN sequence.

It is shown, in an upcoming section, that the CSC can be modified to form the PMC. This new design proves to be advantageous in that the number of cells to be searched to acquire synchronization is reduced to only a fraction of what is required by the CSC. However, the price paid for the improvement is an increase in both channel noise and co-user interference. Fortunately, through flexibility of design, a compromise is possible that allows for some acceleration in acquisition in exchange for moderate performance concessions. Of course, application dictates the optimal mix. As in the case of the CSC, the PMC is tested in the CDMA arena using the Signal Processing Worksystem (SPW) by Commdisco. [1]

Conventional Sliding Correlator

Figure 1 contains a model of the CSC. A DSSS transmitter and an Additive White Gaussian Noise (AWGN) channel are included to generate realistic input signals to the correlator. For simplicity, the model is baseband which eliminates the need for a carrier. The transmitter consists of a binary random number generator to create the message signal and a PN sequence generator which is used as the spreader. The AWGN channel has controllable mean and variance. At the receiver, the signal is despread by a PN generator that is identical to the transmitting generator except for a possible phase shift, which can be as small as a fraction of a chip. An integration operation is performed on the signal over the interval $[0,T_d]$ to determine the level of correlation. The magnitude at the end of each interval is computed and sent to the comparator for threshold evaluation. A small value at the input of the comparator triggers a pulse from the pulse train which slides the local PN generator. A large value indicates a synchronized condition so no sliding occurs. As an example, the waveforms of figure 2 are generated with the following assumptions: the order of the PN generators is n=6; the chip rate is 63 times faster than the data rate (processing gain = 63); each chip contains 2 samples; the noise in the channel has zero mean and a variance of 0.5; the local generator slips by one-half chip increments; integration is performed per bit with assumed

bit and chip alignments; one chip is lost in each interval due to reset; and the threshold of the comparator is set at 95. Signal 2a is the sequence generated by the transmitting PN generator and 2b is the output of the local generator. The receiver code is intentional delayed (misaligned) by one sample (one-half chip) to force the local code generator to slide the entire length of the uncertainty region. Note that the system is incapable of backward motion. Signal 2c is the despreader output. It is a combination of pseudo random waveforms until synchronization occurs, in which it then turns into a sequence that resembles the original data stream. Signal 2d is the original message and can be used to validate 2c. Signal 2e is the control logic that sends the command to the PN generator causing it to slide. Missing teeth in this comb-like signal indicate that either the system is in synch or false alarms have occurred. The area between adjacent peaks corresponds to an interval of integration. Signal 2f is the output of the integrator. Its values are relatively small until the system reaches synchronization. The output of the integrator for the synchronized case is:

$$Y_{(synch)} = Ab_i(2p-1) + \sum_{j=0}^{2p-2} n(jt_s)a_j \qquad (1)$$

The equation is similar to the one developed in [2]. For the non-synchronized case, the first term is altered:

$$Y_{(no-synch)} = Ab_i \sum_{j=0}^{2p-2} a_j a_{(j+l)} + \sum_{j=0}^{2p-2} n(jt_s)a_{(j+l)} \qquad (2)$$

where A is the signal amplitude, b_i is the i^{th} data bit at the sampler (positive or negative), (2p-1) is the number of valid samples per interval, l is the phase lag of the cross-correlated codes, $n(jt_s)$ is the sampled noise, and a_j is the local PN code. To avoid false synchronization, equation 2 should be small compared to equation 1.

The mean time to acquire a signal is derived in [3] as:

$$\overline{T}_{acq} = \left[M\left(\lambda+\frac{1}{2}\right)T_c + \frac{(\lambda T_c P_F)}{(1-P_F)^2}\right] + \left(\frac{(1-P_D)}{P_D}\right)\left[2M\left(\lambda+\frac{1}{2}\right)T_c + \frac{(\lambda T_c P_F)}{(1-P_F)^2}\right] \qquad (3)$$

where λ is the area of integration, T_c is the period of one chip, P_D is the probability of detection, P_F is the probability of false alarms, and M is the additional chips examined for an incorrect decision. Equations for P_F and P_D are found in [4].

CSC in CDMA

Figure 3 contains an arrangement of multiple transmitters with data sources and spreading mechanisms comprised of individual, maximum length PN sequence generators of different code lengths. That is, no two transmitters are alike and the orders of the polynomials range from n=6 to n=34, where $N=2^n-1$ is the length of each sequence. Table 1 lists specifications of the transmitters used throughout this paper. In all upcoming examples, user #1 is assumed to possess the desired message. Therefore, the local code is designed to match the spreading code of transmitter #1, except for a possible phase shift. To account for near-far conditions, on-line multipliers are mounted at each transmitting branch. The new equations describing the output of the integrator are similar to those given in [2] and are shown below:

$$Y^k_{(synch)} = A^k b^k_i(p-1) + \sum_{j=0}^{p-2} n(jt_s)a^k_j + \sum_{r=1;r\neq k}^{M} A^r b^r_{(i-1)} \sum_{j=0}^{p-c-1} a^k_j a^r_j + \sum_{r=1;r\neq k}^{M} A^r b^r_i \sum_{j=p-c}^{p-2} a^k_j a^r_j \qquad (4)$$

$$Y^k_{(no-synch)} = \sum_{j=0}^{p-2} n(jt_s)a^k_{(j+l)} + \sum_{r=1}^{M} A^r b^r_{(i-1)} \sum_{j=0}^{p-c-1} a^k_{(j+l)} a^r_j + \sum_{r=1}^{M} A^r b^r_i \sum_{j=p-c}^{p-2} a^k_{(j+l)} a^r_j \qquad (5)$$

The equations reflect whole chip slippage at the receiver and one lost chip due to integrator reset. The superscript k represents the 'desired' user while r depicts the r^{th} interfering transmitter. The variable c is the point where neighboring bits meet.

As an example, a multiple access system using the first 4 transmitters of table 1 is modeled. System settings include: no channel noise; an integration period of 1023 chips; whole chip slippage; chip/bit/integrator alignment (with transmitter #1); and a threshold value of 675. Figure 4b is the despreader output for the case where the transmissions are at equal power levels. For this condition, the receiver accurately obtains synchronization and maintains it. Transmitter #3 is then boosted

(via the on-line multiplier) to simulate a 'near' transmitter, while the other three remain at unity as the 'far' transmitters. Amplification of #3 is increased, incrementally, until the system breaks down. Signals 4d and 4e show that with a power factor of 6, the system obtains synch but eventually loses it when the magnitude of the integrator's output drops to 610 (the threshold was set to 675). Viewing transmitter #3 as six identical users with unity power, system capacity is roughly 9 users.

The nonlinear characteristic of the near-far problem is best explained mathematically. Close inspection of the last two terms of equations (4) and (5) indicate a partial cancelling in the correlation process if the code sequences are dissimilar. This cancelling reduces the destructive tendencies of the interfering users. If the codes are identical, however, no cancelling occurs and the negative impact is maximized. The next section determines the number of users allowed onto the system for the ideal case of equal power. In doing so, it demonstrates (by elimination) the damaging effects of the near-far problem.

CSC in CDMA (Equal Power Levels)

Using the assumptions of the previous example (except here all transmitters have equal power), several simulations are performed. The first model has only two transmitters but an additional one is added for each subsequent simulation. As more transmitters are added, the system weakens until it can no longer operate effectively. It isn't until the 28th transmitter is added that the integrator output drops below threshold (see figure 5). System capacity is now approximately 3 times larger than it was in the previous example. It's amazing that 19 more users are permitted if the near-far problem is removed. Unfortunately, this ideal case is not very realistic. Despreader outputs for various equal powered transmitter combinations are given in figure 6. As predicted, the waveforms resemble noise filled sequences that worsen as the number of transmitters are increased. Zooming in on signal 6b, we find an M-ary type format with values ±4, ±2, and 0, (see figure 7). This is the result of summing 4 PN sequences. As the number of transmitters increase, so do the number of M-ary values.

Variations of the CSC

For certain applications, the CSC may be too slow. One method of improvement is to use a parallel bank of correlators with locally generated code spaced apart by an amount equal to the slippage of the local PN generator. This eliminates the uncertainty region which reduces the mean time to acquire synch. Acquisition time is then equal to the amount of time required by the integration process. Such a system is hardware intensive and is usually replaced by a hybrid of the CSC and parallel bank. Other CSC variations can be found in reference [4].

Phase Multiplexed Correlator

Another method of rapid acquisition is proposed in [5]. The new design is a modified CSC whose PN generator is replaced by a phase multiplexed generator (PMG). Compare the model of figure 8 to that of figure 1. The PMG produces L equally spaced, phase shifted replicas of the original maximum length PN sequence. These sequences are added together and used to despread the incoming signal. Internal redundancy of the PMG reduces the uncertainty region by a factor of L, assuming that the P_D equals one. The equation for calculating the number of phase shifts can be determined with the equation:

$$S = (N+1)/L \qquad ; \qquad L < (N+1) \tag{6}$$

One of the codes contains at least one less chip than the rest of the sequences in order to preserve the relation $N=2^n-1$. Of course, S cannot be increased without bound since the extra codes produce unwanted noise. Equations for the integrator output in a single transmitter system are given as:

$$Y^k_{(synch)} = A^k b_i^k (p-1) + \sum_{j=0}^{p-2} \sum_{W=1}^{L} n(jt_s) a_j^W + A^k b_i^k \sum_{j=0}^{p-2} \sum_{W=1,W\neq k}^{L} a_j^k a_j^W \tag{7}$$

$$Y^k_{(no-synch)} = \sum_{j=0}^{p-2} \sum_{W=1}^{L} n(jt_s) a^W_{(j+l)} + A^k b_i^k \sum_{j=0}^{p-2} \sum_{W=1}^{L} a_j^k a^W_{(j+l)} \tag{8}$$

As examples, a single transmitter system is modeled with 8, 32, 64, and 128 phase generators. Assumptions made include: no channel noise; whole chip slippage; and a comparator threshold

level of 930. Surprisingly, the receiver acquires synchronization and maintains it in all four cases. Figures 9 and 10 contain despreader and integrator outputs. The seemingly unbounded characteristic of the system is explained by the last term of equation (7). It is finite and much less (in magnitude) than the first term. As a matter of fact, it can be shown that the last term is equal to the negated number of phases if A^k and b_i^k are equal to one. If noise is included, its effects are minimized when statistical constraints are applied. To verify the validity of the PMG outputs, (i.e. to prove that each PMG is designed correctly), cross-correlations of the transmitter and receiver codes are determined and appear in figure 11.

PMC in CDMA

Unfortunately, as more transmitters are added, system performance declines. This is seen in the following equations:

$$Y^k_{(synch)} = A^k b_i^k (p-1) + \sum_{j=0}^{p-2} \sum_{W=1}^{L} n(jt_s) a_j^W + \sum_{j=0}^{p-c-1} \sum_{r=1;r\neq k}^{M} A^r b^r_{(i-1)} \sum_{W=1}^{L} a_j^W a_j^r + \sum_{j=p-c}^{p-2} \sum_{r=1;r\neq k}^{M} A^r b_i^r \sum_{W=1}^{L} a_j^W a_j^r + \sum_{j=0}^{p-2} A^k b_i^k \sum_{W=1;W\neq k}^{L} a_j^W a_j^k \quad (9)$$

$$Y^k_{(no-synch)} = \sum_{j=0}^{p-2} \sum_{W=1}^{L} n(jt_s) a^W_{(j+1)} + \sum_{j=0}^{p-c-1} \sum_{r=1}^{M} A^r b^r_{(i-1)} \sum_{W=1}^{L} a^W_{(j+1)} a_j^r + \sum_{j=p-c}^{p-2} \sum_{r=1}^{M} A^r b_i^r \sum_{W=1}^{L} a^W_{(j+1)} a_j^r \quad (10)$$

The extra code phases at the receiver are correlated with the incoming signals (noise and users) which changes the outcome of the integration process. More phases results in a larger disturbance. To illustrate this, a second transmitter is added to the previous example. While synchronization still occurs, it is quickly lost (see figure 12b). Reducing the number of phases while increasing the number of users lead to a better mix. Figure 12c is the integrator output for 8 phases and 7 transmitters. The signal looks good, however, one more user causes a break down (see figure 12d). For completeness, a final experiment is performed to study the near-far problem. An 8 phase, 4 transmitter system is modeled with the on-line multiplier of transmitter #3 incrementally increased from 2 to 4 in subsequent computer runs. With a multiplication factor of 2, the output was satisfactory. It stayed in sync for 23 integration periods. When increased to 3, the system maintained sync for 10 integration periods, and for a factor of 4, it only lasted for 2 periods. Figure 13 provides sample integrator outputs for the described cases. As expected, performance dropped due to a lack of cancelling terms in the correlated codes.

Synthesis of the PMG

In designing a PMG, a maximum length PN polynomial is selected. Phase shifted replicas are designed using a delay synthesis technique. There are many methods for creating delayed versions of a PN sequence. One method uses a parallel bank of PN generators with different initial values. Another uses strings of delay elements that are attached to the generator. An even better method (less hardware) uses polynomial theory and mod two arithmetic to multiply the PN polynomial by the prescribed shift, and then factors it into a polynomial of degree n or less.[5] This is done for each phase shift.

An example will help to clarify the latter approach. Suppose that an 8 phase PMG is desired from the following tenth order polynomial:

$$g(x) = 1 + X^2 + X^3 + X^6 + X^8 + X^9$$

The distance between neighboring sequences is calculated as (N+1)/L = 1024/8 = 128. However, one of the codes has a spacing of 127 in order to keep N=1023. Polynomials for phase shifted replicas are determined by individually multiplying g(x) by X^{128}, X^{256}, X^{384}, X^{512}, X^{640}, X^{768}, and X^{896} and factoring until the orders of the replicated polynomials are less than or equal to 10:

$g_1(x) = g(x) = 1 + X^2 + X^3 + X^6 + X^8 + X^9$

$g_2(x) = g(x)\, X^{128} = X^2 + X^4 + X^9$

$g_3(x) = g(x)\, X^{256} = X^7 + X^8$

$g_4(x) = g(x)\, X^{384} = X^2 + X^3 + X^5 + X^{10}$

$g_5(x) = g(x)\, X^{512} = X^4 + X^6$

$g_6(x) = g(x)\,X^{640} = X^3 + X^5 + X^9$

$g_7(x) = g(x)\,X^{768} = X^1 + X^2 + X^3 + X^4$

$g_8(x) = g(x)\,X^{896} = X^1 + X^7 + X^8 + X^9 + X^{10}$

These polynomials are realized in figure 14. To verify that the sequences are indeed shifted by the prescribed amounts, the cross-correlation of signal g(x) with the output of the phase multiplexed generator is shown in figure 15. Note that the correlation peaks occur for lags of 0, 128, 256, 384, 512, 640, 768, and 896, as expected. Applying these 8 sequences to the system of figure 8 results in a despreader output waveform similar to the one shown in figure 6c.

Summary

Determining the performance of a PMC operating in a CDMA environment is no easy task, particularly when the near-far problem is considered. Equations (9) and (10) are indicative of the complexities involved. These equations could be further enhanced by incorporating the following features: individual carrier frequencies for all users; random alignments between chips, bits, and the integration process; and differing chip sizes among the spreaders. Inclusion of these items would make the results more realistic, but, would not change performance trends. For simplicity, they were omitted. To graphically illustrate system tendencies for various scenarios, many examples were given. For instance, figures 9-11 show that a virtually unbounded number of phases is allowed at the PMG if only one transmitter is used. Once additional users appear, however, signal degradation prevails, see figure 12b. Near-far considerations drop the efficiency even further, as shown in figure 13. Of course, the PMC is not the only technique plagued by the effects of CDMA. The CSC also suffers from it. Figure 5 shows that under the given conditions, 28 users are allowed and figure 4 proves that a nonlinear decline to 9 users (equivalent to 9) occurs when one of the transmitters is boosted to 6 times the amplitude of the others. While the CSC is shown to perform better than the PMC, it must be pointed out that the PMC concedes to sacrificing accuracy for speed. The PMC is a relatively new design that is still under development. Further improvements should make it a viable technique for rapid acquisition.

As a final comment, this paper confirms that SPW is well suited for spread spectrum simulation.

References

[1] Commdisco Systems, Inc., Signal Processing Worksystem, Software Documentation, Product Number SPW1080, Version 2.7, August 1990.

[2] R. Skaug and J. F. Hjelmstad, SPREAD SPECTRUM IN COMMUNICATION. London, UK: Peter Peregrinus Ltd., 1985.

[3] R. L. Pickholtz, D. L. Schilling, and L. B. Milstein, "Theory of Spread-Spectrum Communications - A Tutorial", IEEE Trans. Comm., vol COM-30, May 1982.

[4] R. C. Dixon, SPREAD SPECTRUM SYSTEMS. New York: Wiley-Interscience, 1984.

[5] G. S. Rawlins, "A RAPID ACQUISITION TECHNIQUE FOR DIRECT SEQUENCE SPREAD SPECTRUM SYSTEMS BY A PN PHASE MULTIPLEXED CORRELATOR." Master's Thesis, University of Central Florida, Orlando, Florida, 1987.

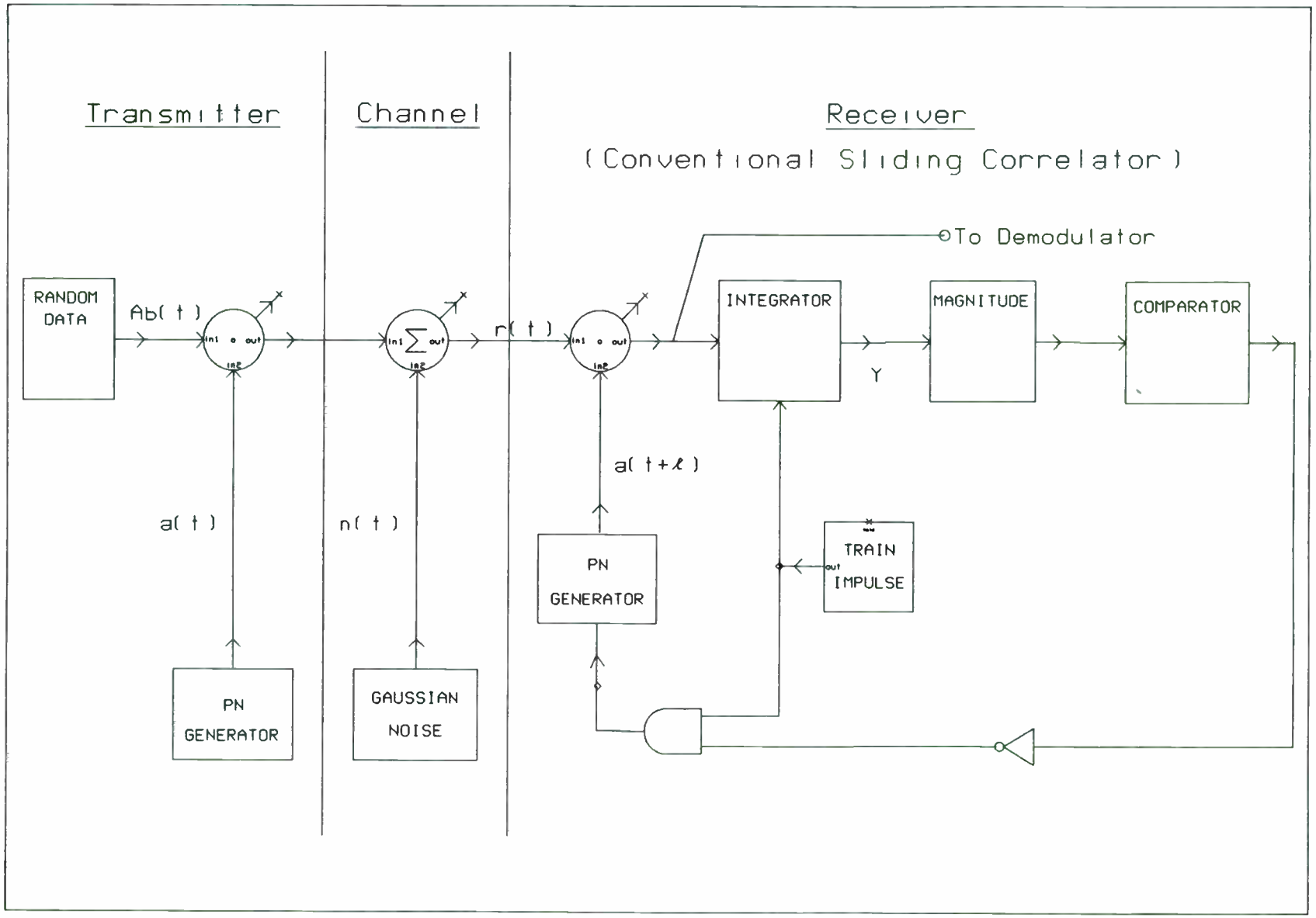

(Figure: 1)

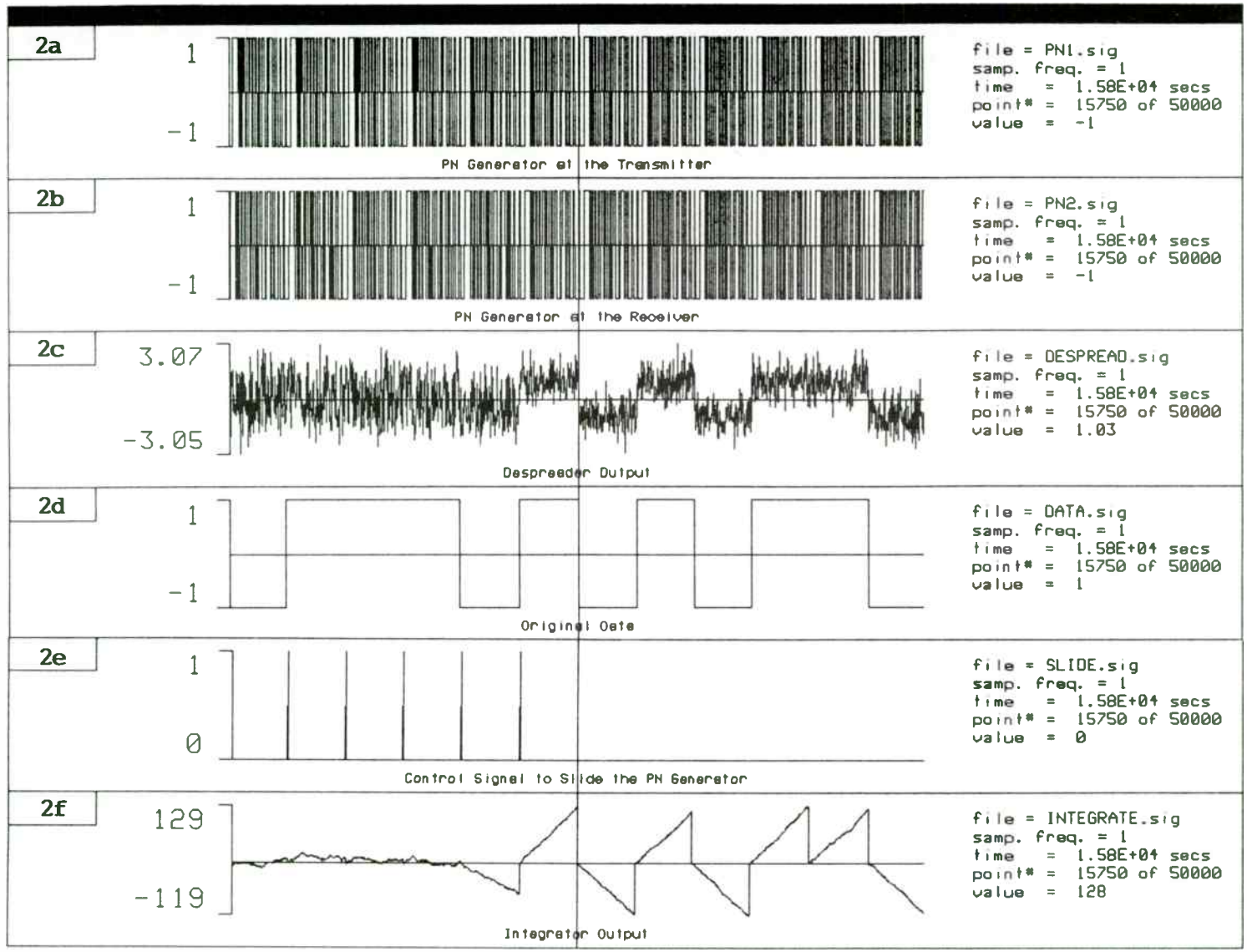

(Figure: 2)

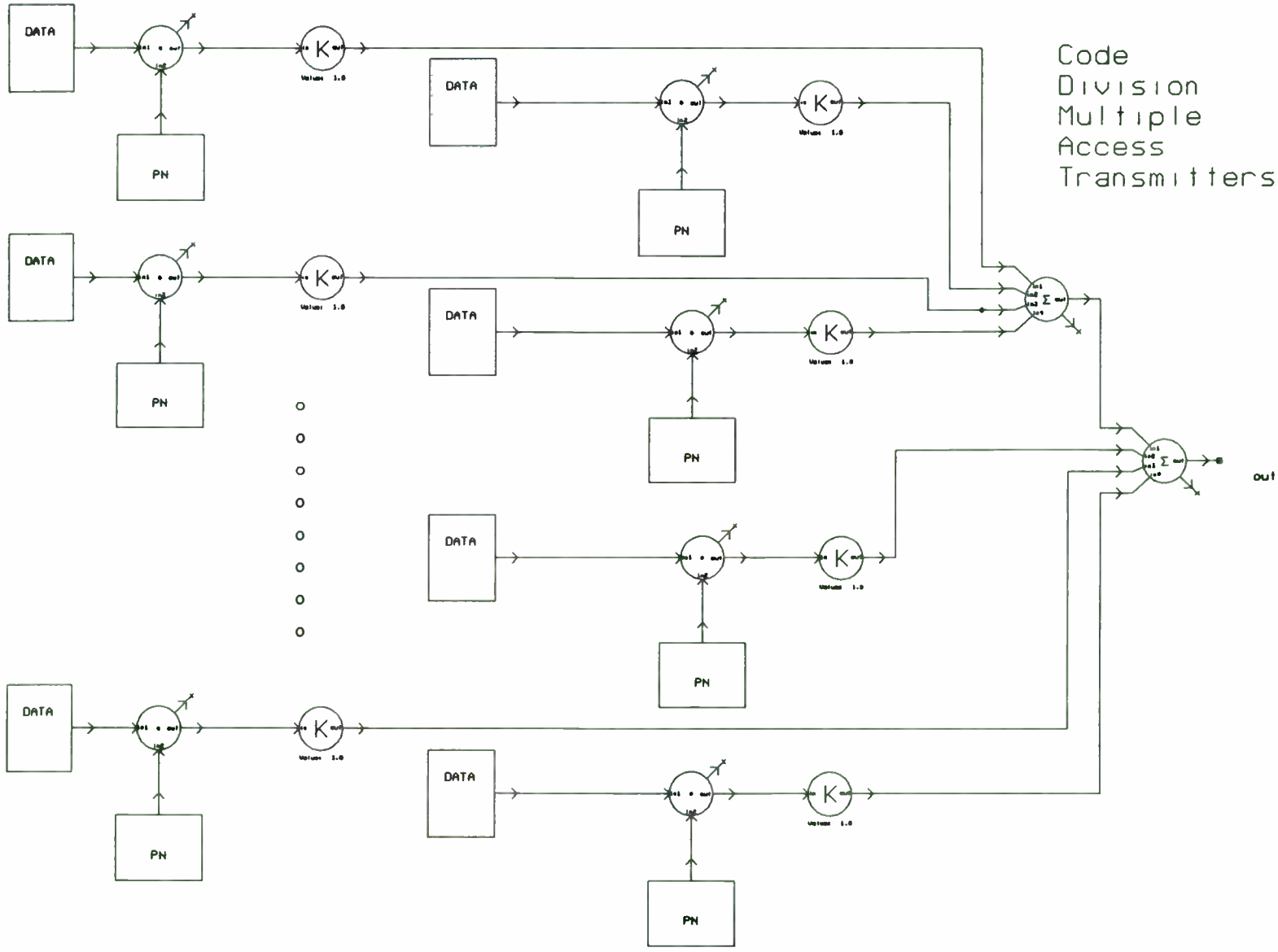

(Figure: 3)

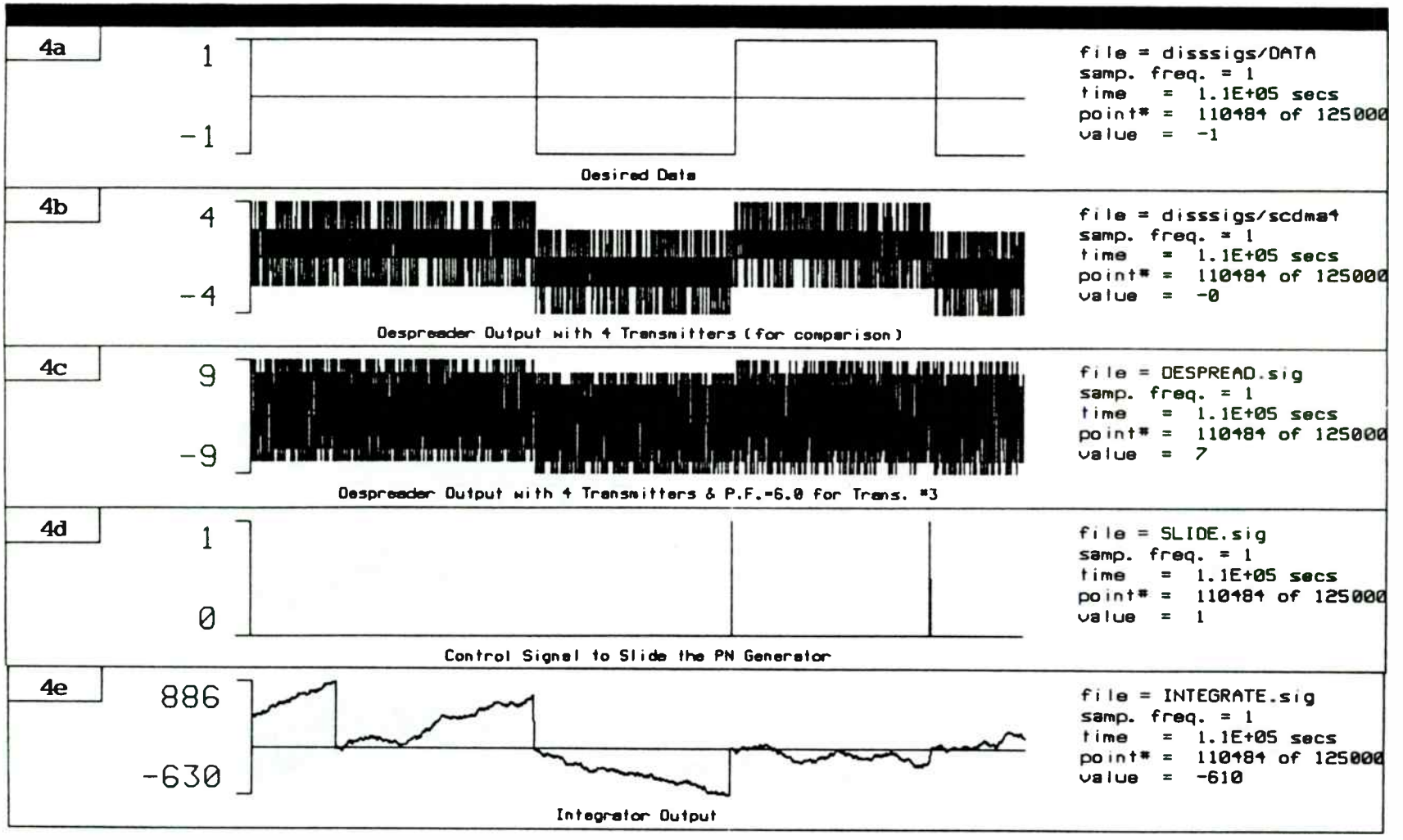

(Figure: 4)

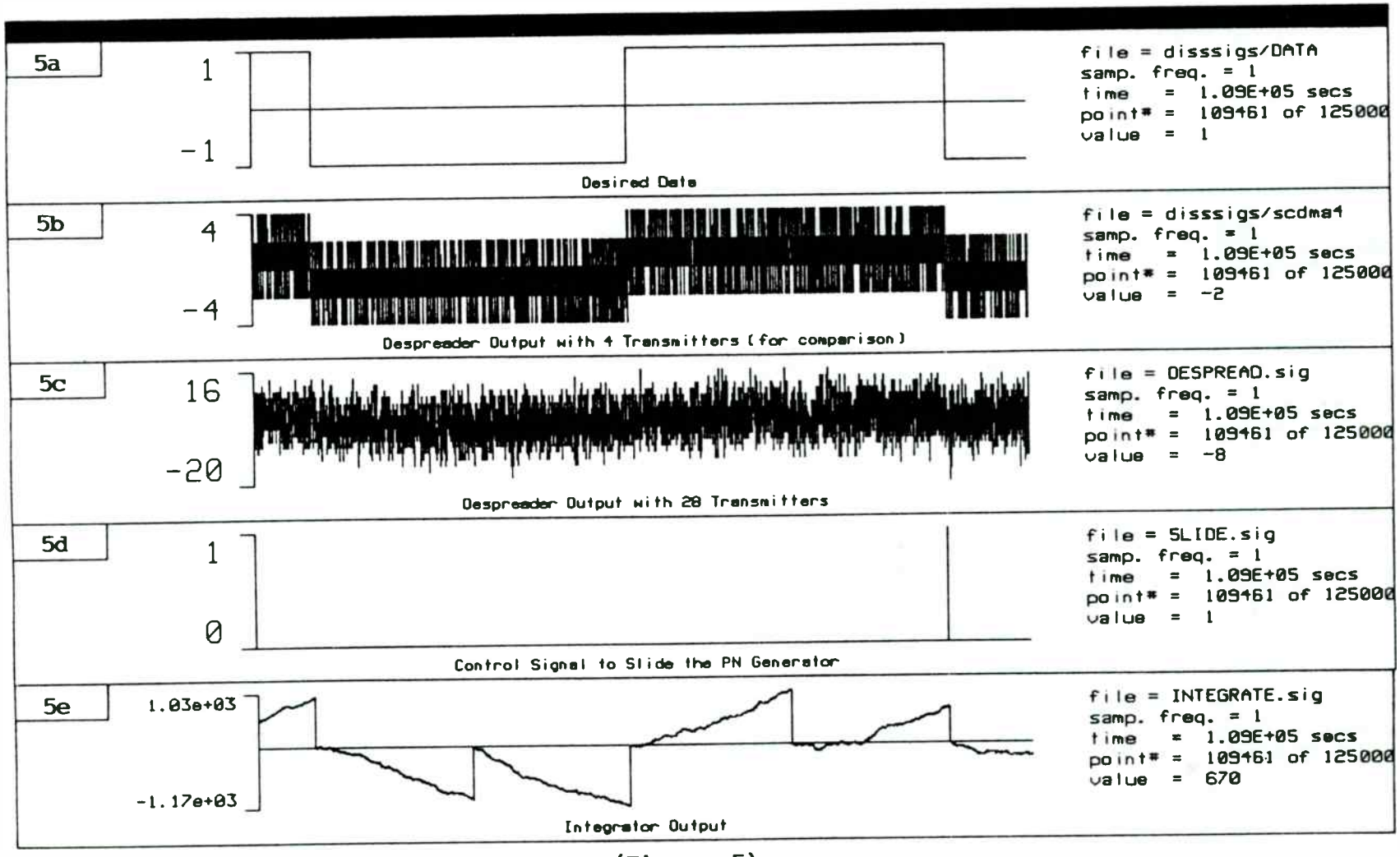

(Figure: 5)

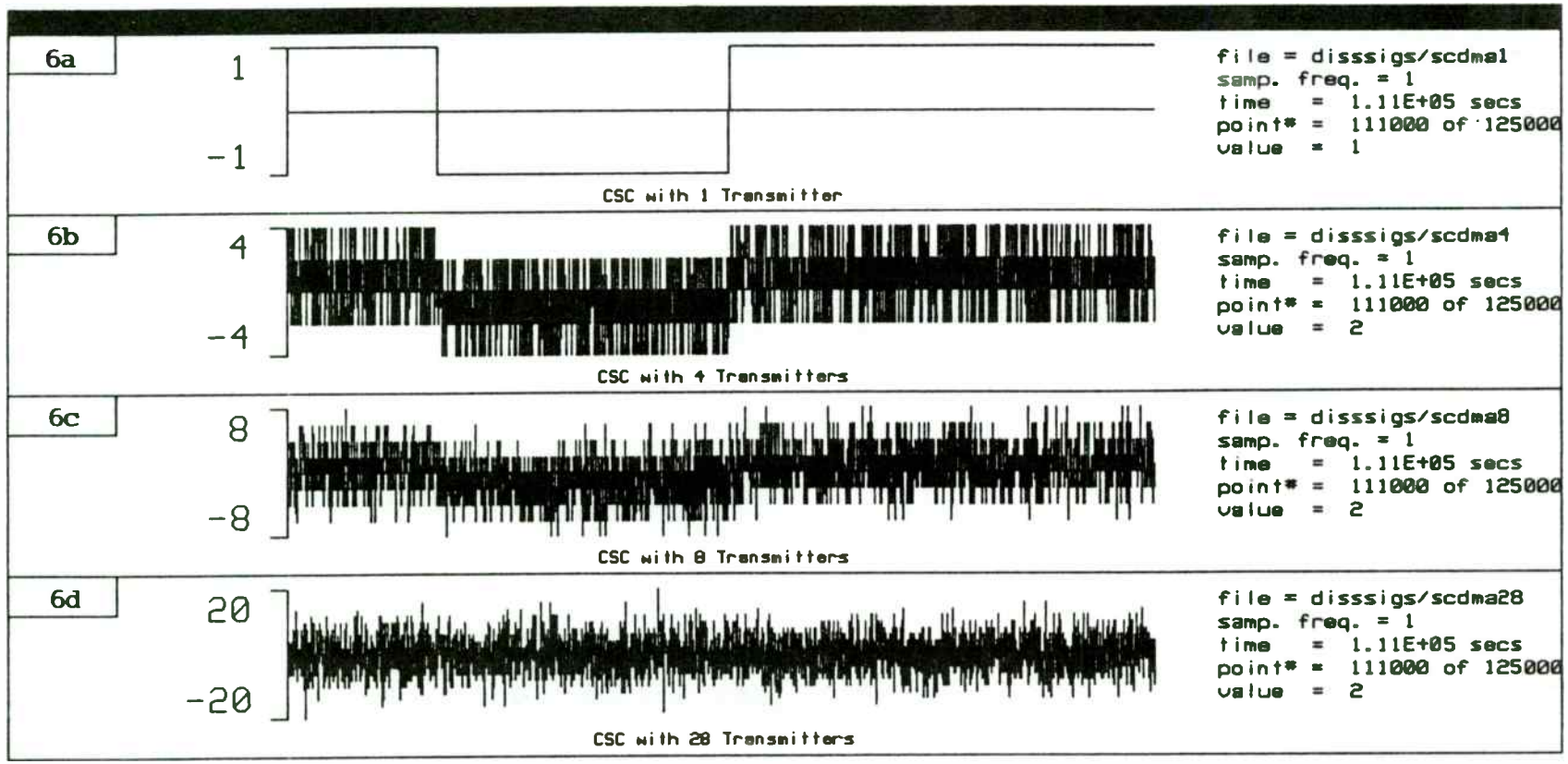

(Figure: 6)

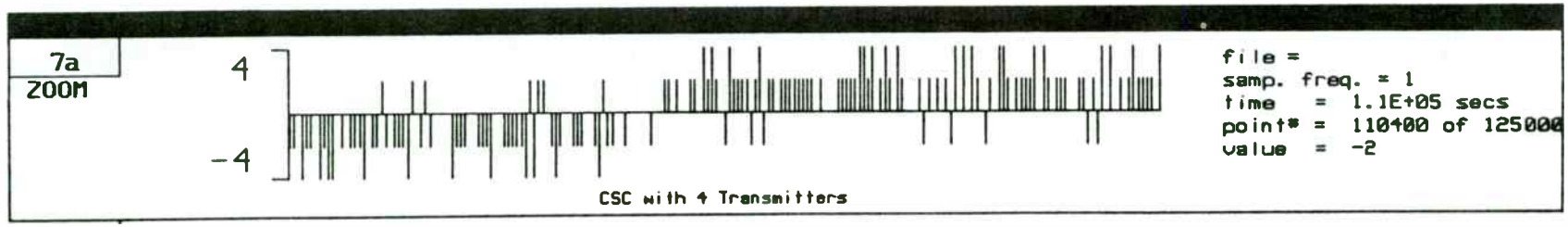

(Figure: 7)

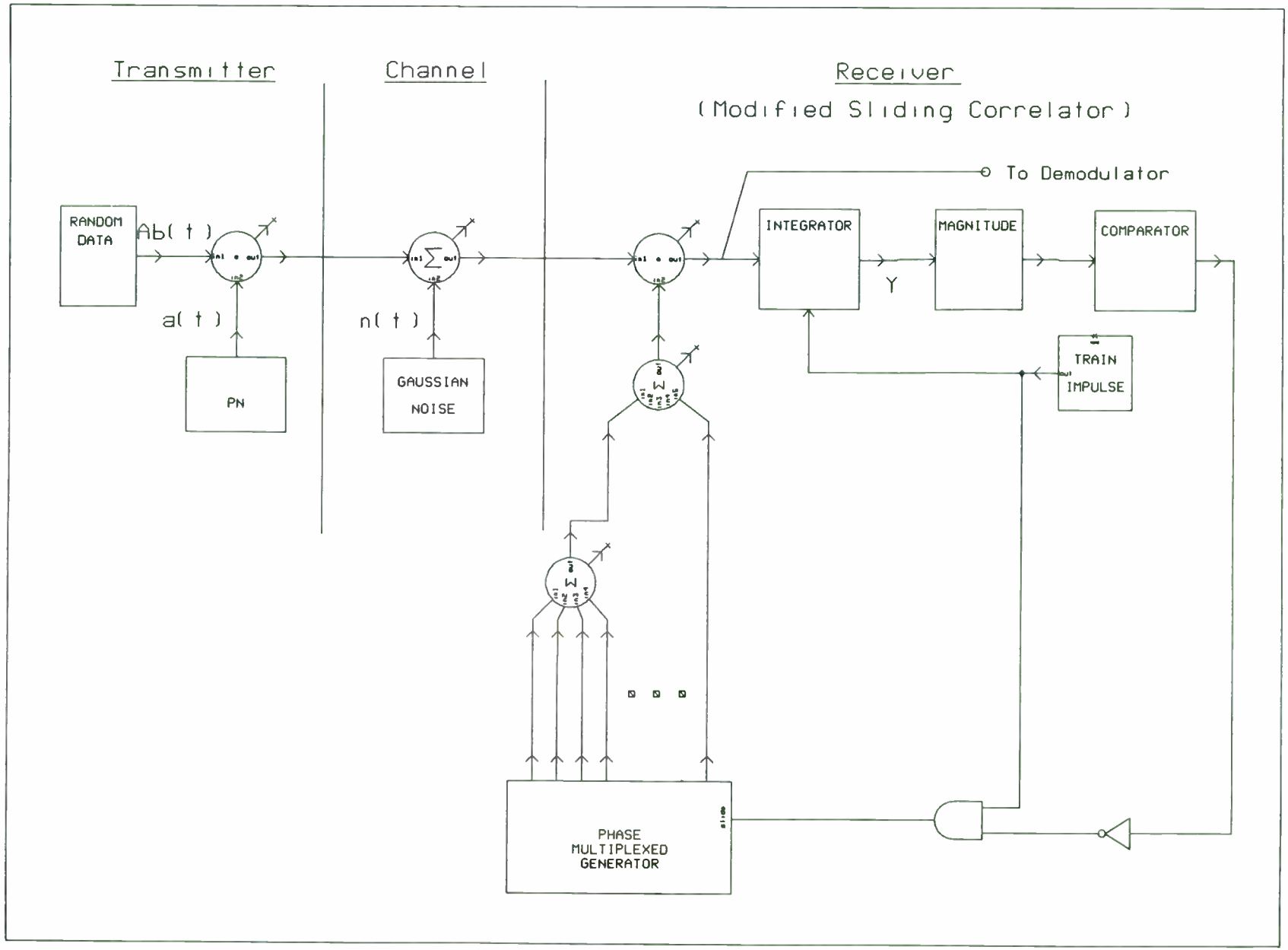

(Figure: 8)

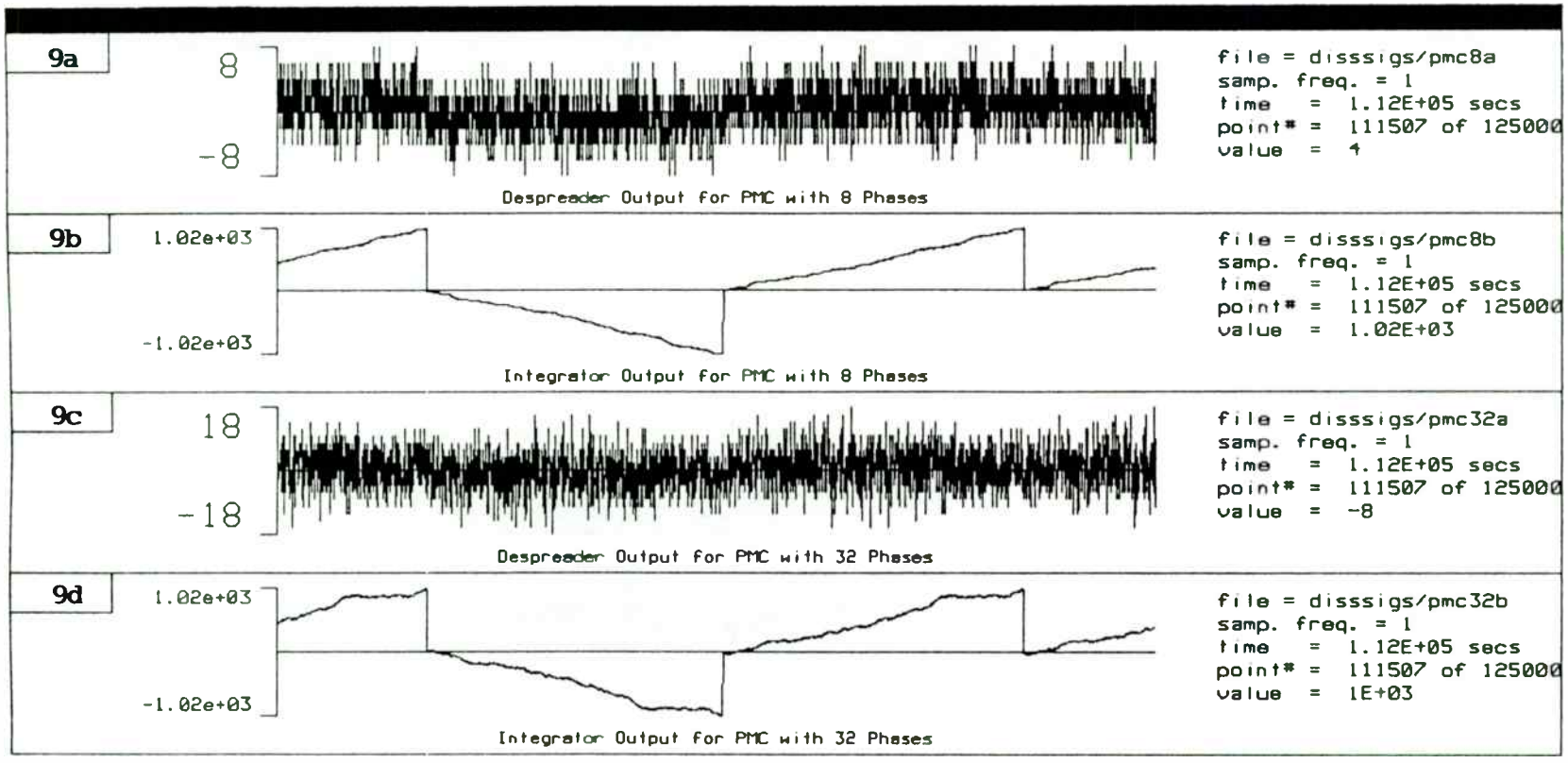

(Figure: 9)

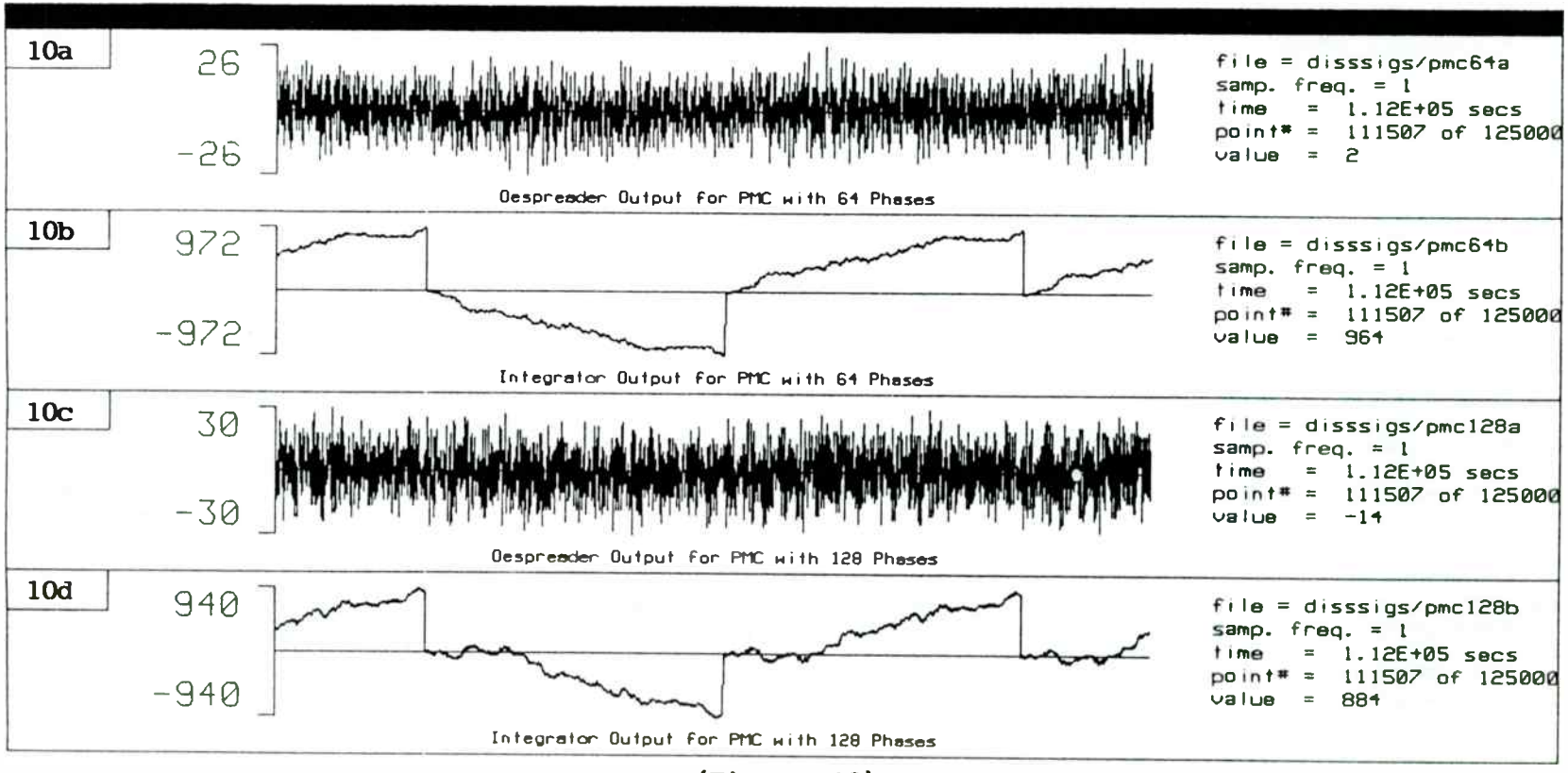

(Figure: 10)

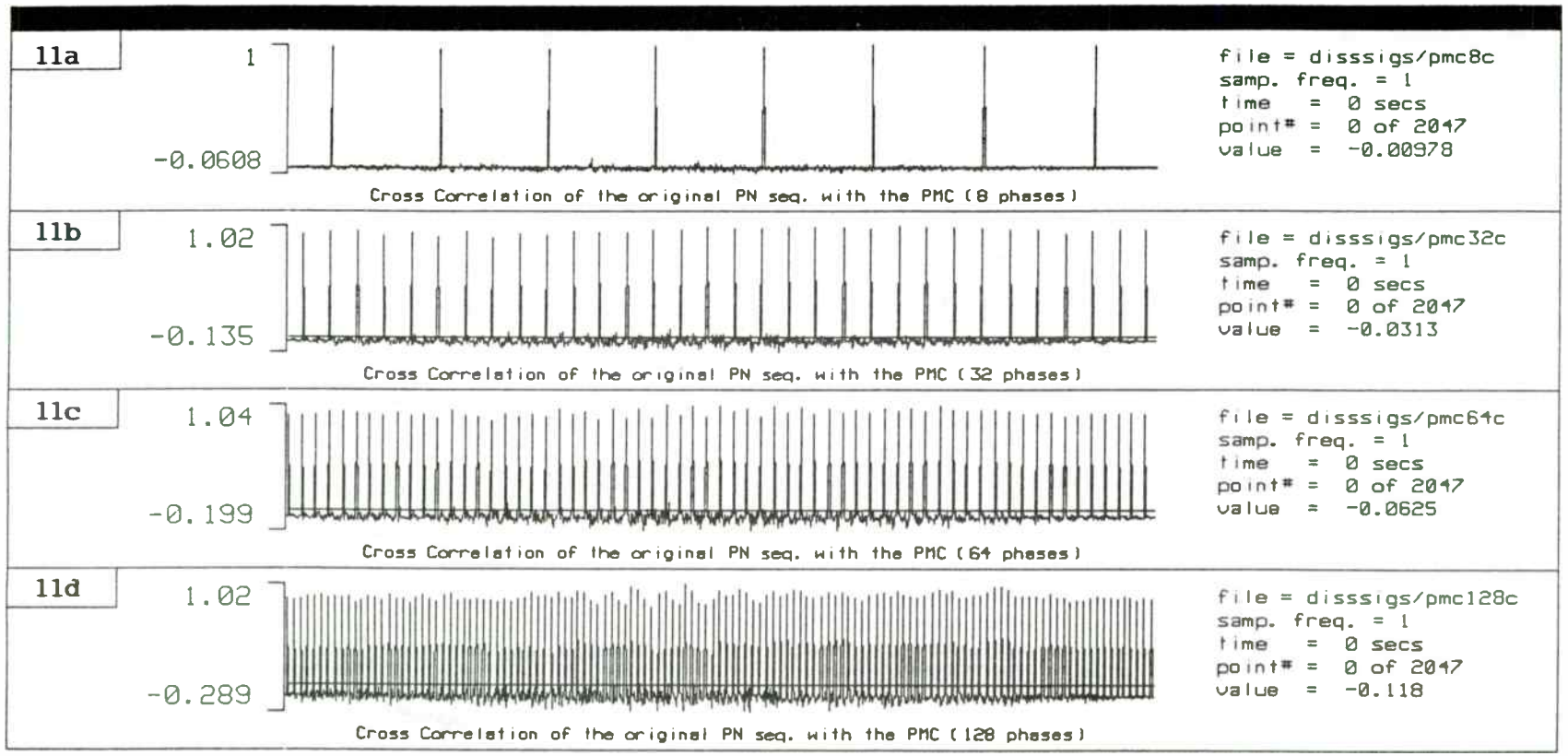

(Figure: 11)

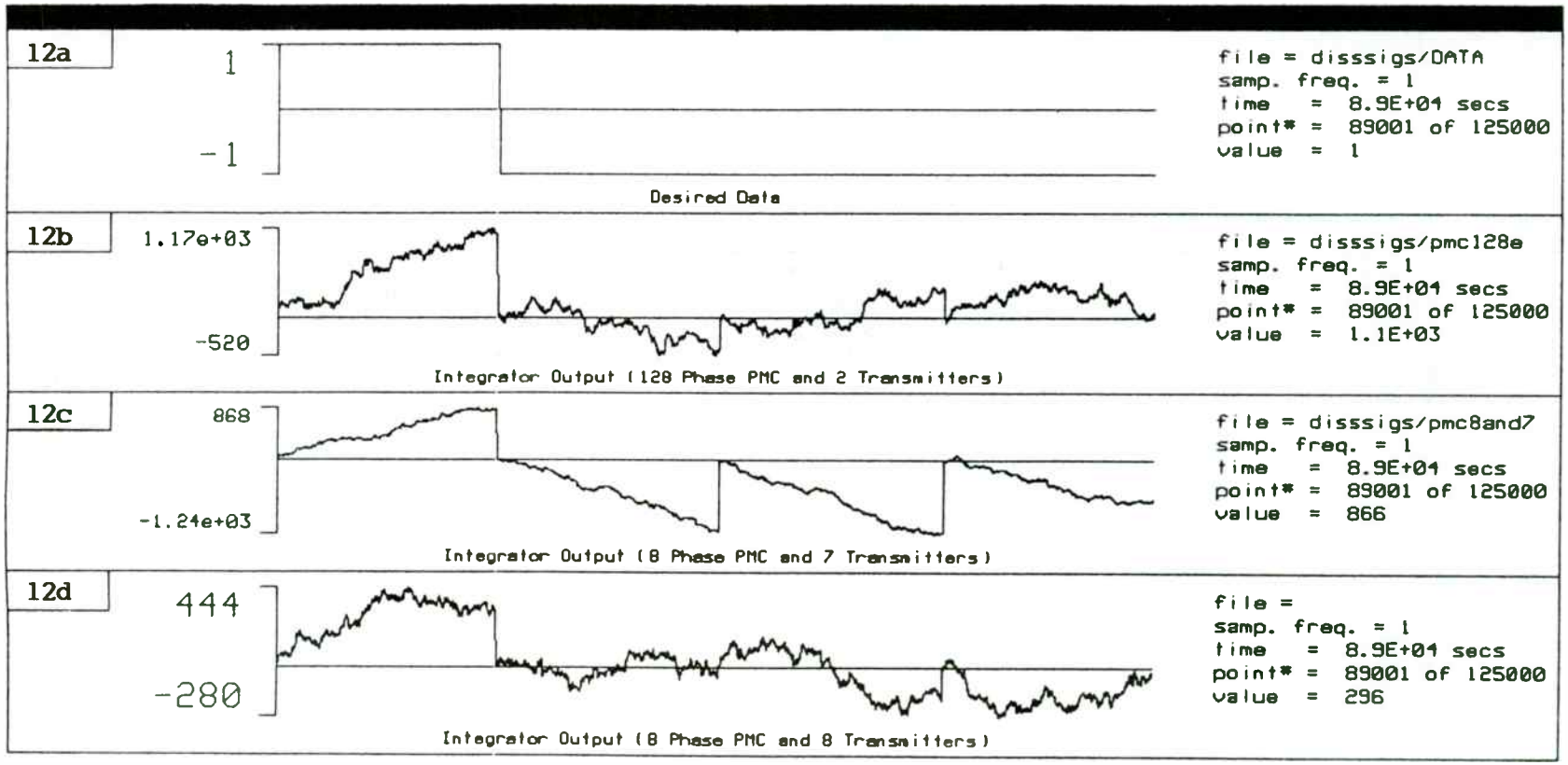

(Figure: 12)

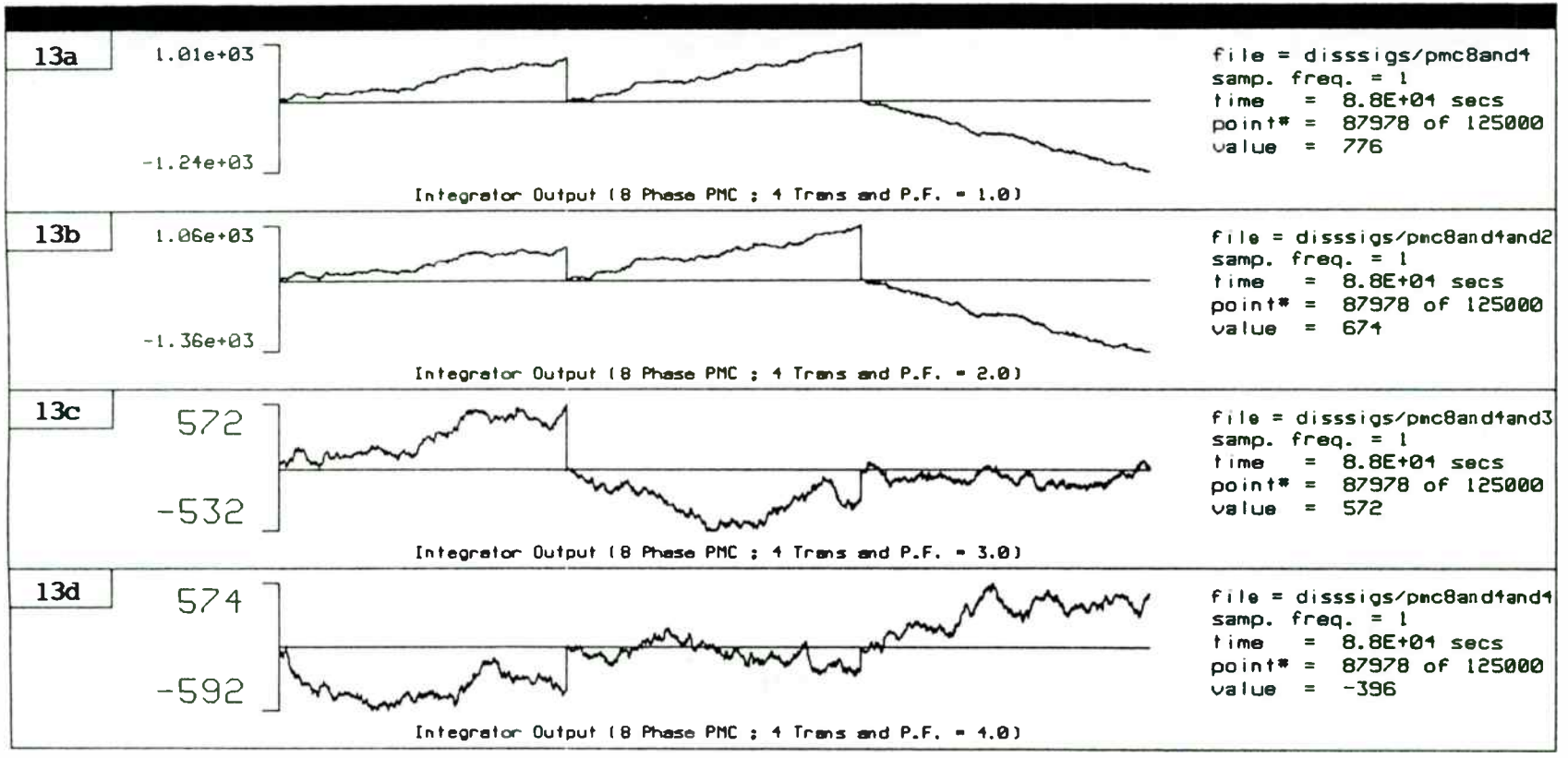

(Figure: 13)

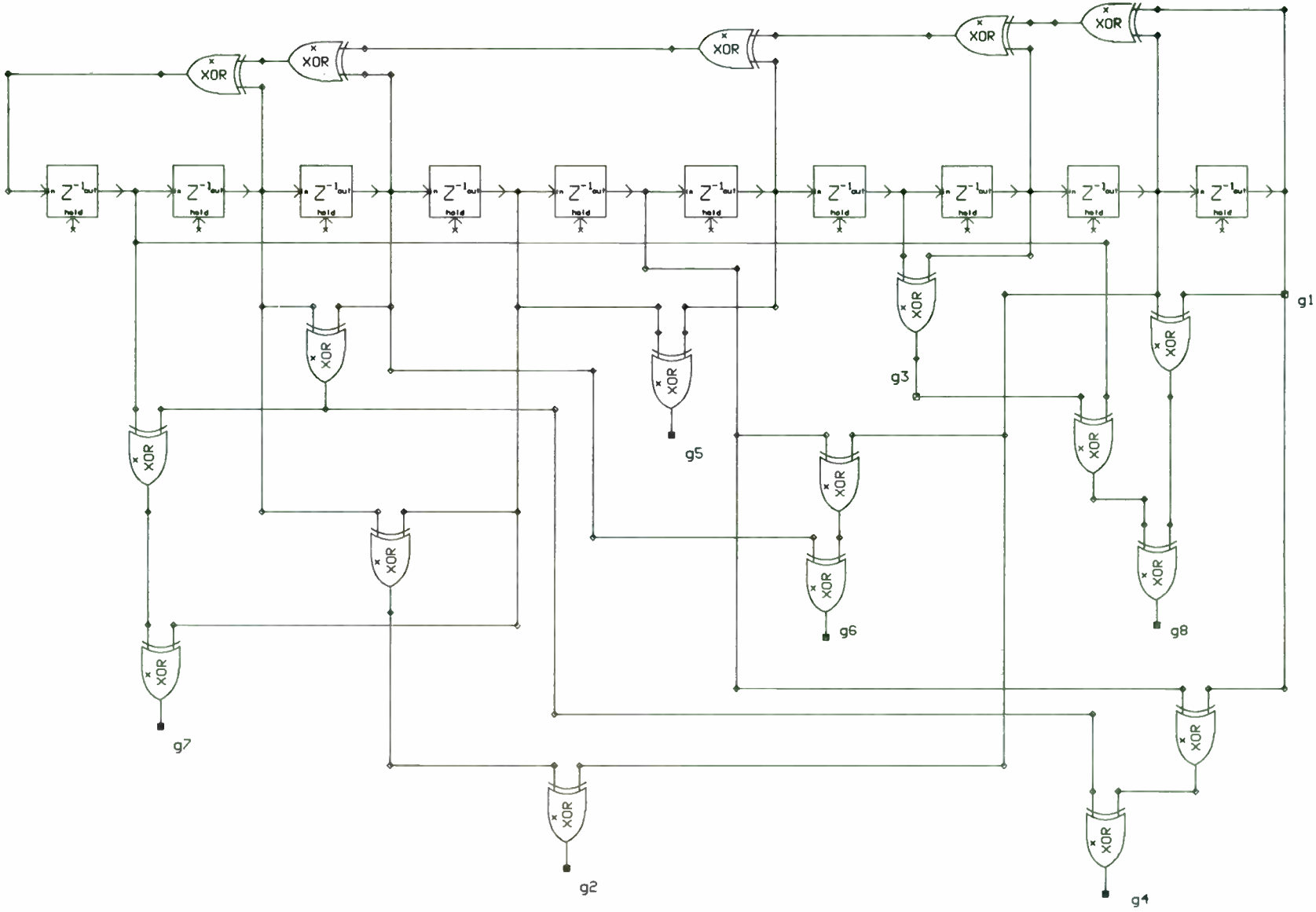

(Figure: 14)

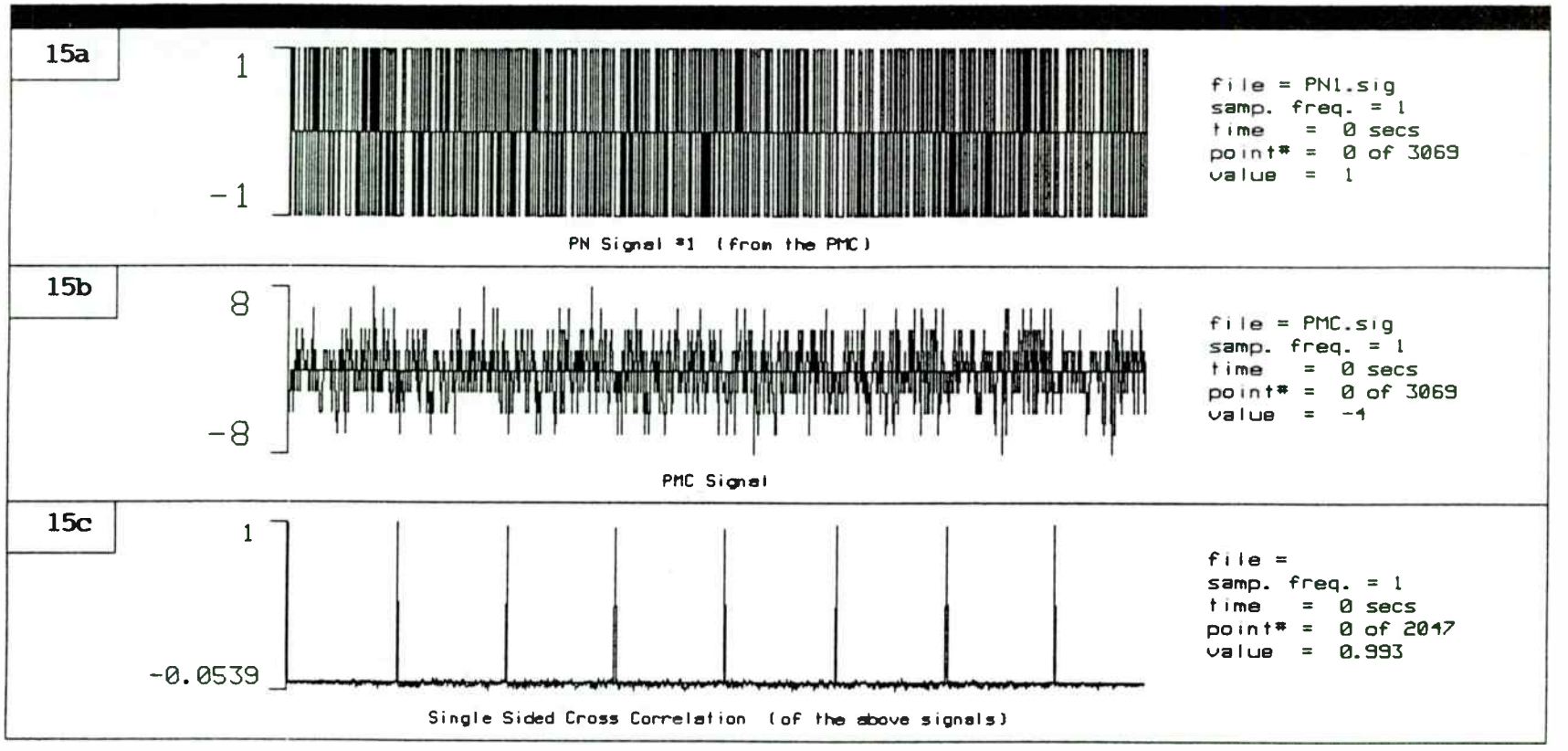

(Figure: 15)

TABLE 1: CSC in CDMA (transmitters)

Transmitters	Data PN Order	Data Sampling Frequency	Spreader PN Order	Spreader Sampling Frequency	Processing Gain
1	21	1023	10	1	1023
2	22	1023	9	1	1023
3	23	1023	11	1	1023
4	6	1023	12	1	1023
5	8	1023	27	1	1023
6	15	1023	15	1	1023
7	19	1023	13	2	511.5
8	12	1023	34	16	63.94
9	11	512	20	1	512
10	7	1023	26	4	255.8
11	16	1023	18	1	1023
12	31	2047	8	1	2047
13	33	1023	16	1	1023
14	14	255	23	2	127.5
15	20	1023	29	1	1023
16	25	1023	31	1	1023
17	18	511	25	1	511
18	17	1023	6	1	1023
19	24	1023	30	1	1023
20	30	511	14	2	255.5
21	13	1023	19	2	511.5
22	32	2047	21	1	2047
23	27	1023	7	1	1023
24	34	1023	22	1	1023
25	28	1023	17	2	511.5
26	9	511	33	1	511
27	29	1023	24	1	1023
28	10	511	32	2	255.5

MOBILE PACKET-SWITCHED DATA NETWORKS

John A. Kilpatrick
Manager, Data Systems Technology

RAM Mobile Data, Inc.
10 Woodbridge Center Drive
Woodbridge, New Jersey 07095

ABSTRACT

The age of mobile data is upon us, and all indications point to a worldwide growth comparable to the rapid growth of cellular telephony. This paper provides an overview of one of the options available to users, the Mobitex network, and gives some details of its over-the-air protocol. The Ericsson Mobitex packet switched mobile data system is now in operation in Scandinavia and Canada. RAM Mobile Data, Inc. is operating a growing national public Mobitex network in the U.S. and the U.K., and in other countries not yet announced. The system architecture is "open" which allows any company to enter the mobile data business by providing mobile and portable radio/modem/terminal equipment, and application software, to users of the Mobitex networks.

Introduction

As the radio spectrum becomes more and more congested, and the demand for mobile communications continues to grow, there is an urgent need to make efficient use of the airwaves. Packet-switched mobile data is one technology that can answer the users' demands, and yet is comparatively efficient in its use of spectrum.

As compared to voice, a general rule of thumb in engineering cellular telephone systems is that 25 customers can be served, with reasonable blocking probability, by each installed 30 kHz channel pair. In RAM's mobile data network, 300 to 1000 users can be supported per installed 12.5 kHz channel pair. The Mobitex system can transmit user packets at rates up to 560 characters per second, or sustain a user data rate up to 150 characters per second including all overheads such as channel access, error correction, and administrative overhead.

Packet switching can also provide significant efficiency improvements with respect to a data-over-cellular approach. For many applications involving short messages, the call setup time of a circuit switched call can be large in comparison to the message length significantly reducing the channel efficiency and increasing the delay.

Mobile data provide other important benefits over voice in many applications:

> In many cases, a dedicated mobile data system can provide messages service at lower cost per transaction than can a voice system, or even a voice system with overlaid data capability. This is because of the voice system's circuit switching technology which has minimum charges based on one minute or so of connection time. Thus sending even a short, one second message will incur this minimum charge. In a dedicated packet data system such as RAM's, there is no circuit setup time involved in the transmission making it feasible to charge strictly on the length of the message. There are some cases, of course, where it can be cheaper to send data by cellular. In a long file transfer where the data transmission time is large compared to the setup time, it can be cheaper to send data by cellular. But where messages are relatively short, it will always be cheaper to transmit data via a packet switched data system.
>
> A data system can provide a printed record of every transaction. Generally a voice system does not provide an historic record.
>
> Data is more private than voice. Data messages can be easily encrypted in the application layer of the data protocol. Encrypting voice, whether in a cellular radio system or in any voice network, is a relatively complex and expensive task.

Given these benefits, the data user has two options available to him/her. A mobile data system can be installed and operated as a private radio system to be used only by the owner. This has the advantage that the network can be specially tailored to the owners data traffic and requirements. The second option is to use a public mobile data network such as RAM's. In this way, the cost of design, installation, maintenance and operation are distributed among all the users, and the time to get 'on the air' can be greatly reduced. A public system also permits a user to communicate over very wide geographic areas that would be impractical to cover by all but the largest and most expensive private systems.

The remainder of this paper discusses RAM's Mobitex network and some of the radio channel design issues involved in a mobile packet-switched data network, including the waveform design, roaming, channel access and low power portable operation.

RAM's Mobitex Network

RAM Mobile Data, Inc. (RAM) is installing a nationwide mobile data network in the United States. It became operational on 1 October 1990 in ten cities and now operates 160 base stations covering 13 of the largest metropolitan areas. In 1989, RAM obtained licenses from the FCC and 10 to 30 channel pairs in each of the top 50 metropolitan areas in the 900 MHz SMR band.

RAM selected the Mobitex® system supplied by Ericsson after an extensive review of offerings from around the world. The Ericsson system was developed in conjunction with the Swedish PTT. Public Mobitex systems have been operating in Sweden, Norway and Finland for several years, more recently in Canada, and now in the United States. RAM is also installing a Mobitex network in the United Kingdom. Two of the more important reasons for selecting Mobitex was its state-of-the-art technology and its open architecture. The air interface between the RAM network and the mobile radios is defined by an interface specification that is available to any interested manufacturer. This specification is controlled by the Mobitex Operators Association, a group made up of representatives from each of the companies or countries that are (or will be) using the Mobitex system. Therefore, it is impossible for any manufacturer or system operator to unilaterally change the specification.

The Mobitex system is designed as a hierarchical network as depicted in Figure 1. At the top of the network is a network control center (NCC) from which the network is managed. The top level of switching is a national switch (MHX1) that routes traffic between regions. At the next level are regional switches (MHX2s). Below that are the local switches (MOXs) that handle traffic within a given service area. Finally, at the lowest level are the radio base stations (BAS) that communicate with the mobile and portable data sets. Messages are handled at the lowest node in the network that is common to the origination and destination addresses.

The radio base stations are laid out over a service area in a grid pattern using the same engineering rules as for cellular telephony, relative to interference management, frequency reuse, cell splitting, etc. In fact the system is much like a cellular telephone system, except that there is no need for handoff during the packet transmission. When a change from one base station to a better one is required, that decision is made by the mobile set, not the land network computer as in cellular telephony.

From the customer's perspective, the network can appear to operate as either a public or private network. A customer subscribes for service for one or more mobile terminal subscriptions and one or more fixed terminal subscriptions, each with an associated subscription number or address. The network can accommodate up to 16 million separate addresses. Alternatively, a person can subscribe for service via a personal subscription in which the person has an address. The person can then log onto the system at any Mobitex terminal and his/her messages will be addressed to that terminal until he/she logs off. There are also group subscriptions that permit a dispatcher to address a given message to all members in the group. A subscriber can belong to more than one group at a time. There are also closed user groups that permit messages to be exchanged only between members of the same group.

Radio/Modem Design Issues

The mobile and portable radio/modems perform a number of functions in order to operate on the Mobitex network. Several of these functions are discussed below.

In order to stay in good radio contact with the network, the mobile (or portable) radio/modems must continuously monitor the system channel associated with the current base station as well as all neighboring base station system channels. A list of 'neighbors' to be monitored in this fashion is transmitted by each base station on the system channel. The mobiles sample the Received Signal Strength Indicator (RSSI) from the radio at 1000 samples per second to determine the best/stongest neighbor at any time. A base station change will occur if this neighboring base station's signal strength is greater than that of the current base station by a specified amount. After listening to this new channel to determine the base station ID, the mobile terminal will then send a roam/registration packet to the new base. This registration information is distributed within the network to update the routing tables.

The radio channel between base stations and mobile terminals is a difficult propagation media due to multipath, terrain and motion. Reflections off of buildings, hills and moving vehicles produces Ricean or Rayleigh fading (depending on whether a direct path exists) with the fade rate a function of the speed of the mobile terminal and, to a lesser extent, the reflectors. To operate in this environment, the network and data protocol has been implemented containing a number of robust features.

The base station cells are laid out in such a way as to achieve a -113 dBm signal strength at the cell edge. This corresponds to a 10% block error rate (or 1% bit error rate) at the mobile terminals under static (non-fading) conditions.

The modulation is a non-coherent GMSK which is relatively immune to the sudden phase changes that can cause problems to a coherent demodulation system, but is still quite bandwidth efficient.

The 8-bit characters are grouped into blocks of 18 and, for error detection, the CCITT standard 16 bit Cyclic Redundancy Check (CRC) is appended to each block.

Each character or byte of data is encoded using a shortened [12,8] Hamming code capable of correcting any single bit error in the codeword.

Each 20 by 12 bit block is interleaved before transmission so that a fade induced burst of up to 20 bit errors is evenly distributed among the codewords after de-interleaving; these single bit errors can be corrected by the Hamming code.

A selective repeat ARQ scheme is used so that only the blocks with detected errors are retransmitted in the next packet.

If the packet is not successfully acknowledged, it is retransmitted a specified number of times to increase the chance of successful delivery.

To permit timely access to the radio channel by many half-duplex users and achieve efficient channel usage, a new channel access algorithm was designed based on principles of Slotted ALOHA and Carrier Sense Multiple Access (CSMA). The base stations indicate the availability of their channels by sending free signals containing the number and length of random and free slots in the free cycle (see Figure 2). Mobile traffic initiated before the beginning of the free cycle is distributed at random with the mobile selecting one of the random slots. Traffic initiated during a free cycle is sent at the beginning of the next free slot. Once the base station detects a valid packet header, it immediately sends a silence signal on the associated downlink channel to prevent other users from transmitting in subsequent slots. Once the base station acknowledges a successfully received message, it sends another free signal allowing other mobiles to transmit.

A separate low power protocol is provided for portable terminals. The portable radio remains in a low power, standby mode and wakes periodically (every 10 to 20 seconds) to listen for base station signals. These signals include information for timing, roaming and a list of the portable terminals with messages waiting to be sent to them by the base station to which they are registered. If a message is pending, then the portable stays in the operational mode for this period or until the message is successfully received and acknowledged.

Radio/Terminal Opportunities

The open architecture of RAM's Mobitex offering presents a number of business opportunities for companies to design and supply radio/terminal equipment to the customers of the RAM network. It is important to note that a common design can be sold in Canada as well as the United States. In other countries, the only design variation required is to accommodate the radio channel allocations peculiar to a given country. In North America, 200 channel pairs are allocated in the 900 MHz SMR band. In Europe, the channels are in the 400/450 MHz bands; 30 channel pairs are allocated in the UK. In all cases the channel width is 12.5 kHz. The channel data rate is 8000 bps and the data modulation is GMSK0.3. The mobile transmitter power is dynamically variable up to 10 W and the portable power output is variable up to 2 to 4 W. A manufacturer can choose to provide a radio, a data modem, a terminal, or any combination. They can be mobile or portable, plug-in boards to PCs or tiny acknowledgment pagers. RAM has no desire to be in the radio/terminal business, but will help manufacturers during their design, and will test and certify products as suitable for use on its networks.

Manufacturers interested in obtaining a copy of the interface specification, more details of the RAM service offering, or information on the market in the United States, Canada, or the UK, can contact the authors.

Summary

Mobile data is emerging as an important and rapidly growing means of communication for people on the move. There are and will be many alternative solutions to the mobile data needs of a wide spectrum of present and potential mobile data users. There is no single mobile data system that will satisfy all user needs. The RAM Mobile Data implementation of the Ericsson Mobitex system in the US and the UK, has been described here as one solution to these needs.

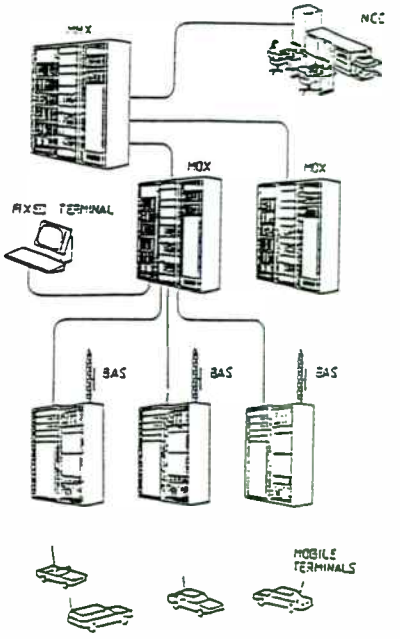

Figure 1
Mobitex Network
Structure

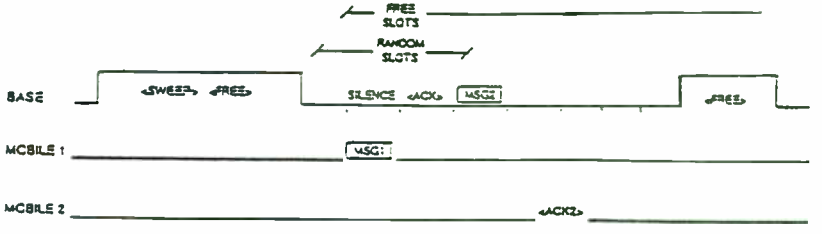

Figure 2
Channel Access
Signaling Diagram

MAKING IT IN THE U.S.A.

A CASE HISTORY

by Albert D. Helfrick, Ph.D., P.E., K2BLA
Consulting Engineer
Helfrick and Associates, Inc.

INTRODUCTION

This paper describes the design of a high-volume consumer RF product for manufacture in the United States. Discussed in this paper are the design techniques employed, and the experiences and results of the design effort. The item was to compete with established products being produced in the Pacific rim.

The subject of this paper is a video cassette recorder accessory device that allows the broadcast of television signals over a short range. This device is for the purpose of transmitting program material from one source, typically a video cassette recorder, to one or more television receivers within a home. The product operates within the frequency range of 902 MHz to 928 MHz and is approved under the provisions of part 15 of the FCC rules and regulations.

Other than those imposed by part 15 of the FCC rules and regulations, there were no restrictions placed on any part of the design. Cabinets, features, packaging, performance; any aspect of the product was to be considered in the design. The electrical design probably had more effect on the overall cost and competitiveness than any other facet of the project. This paper deals with the electrical design of this product.

The product consists of a transmitter and one or more receivers. Usually, a consumer purchases one transmitter and receiver. All reference throughout this paper to the "video broadcaster" refers to the usual configuration of a set of one transmitter and one receiver.

EARLY PLANNING AND INVESTIGATION

One of the first tasks undertaken in the design of this item was to evaluate current competing products to establish areas where improvements could be made and competition could be established. Similar products were purchased and their performance evaluated. The units were dissected, parts counted and costed, the number of internal adjustments were counted and rough schematics traced.

It was determined, and to no one's surprise, that not even one of our potential competitor's units could be copied and made in the United States, and be cost competitive with imports. What was required was a superior design.

In the case of some competitive products, making a superior design would be simple. These were, primarily, designs employing labor-intensive techniques such as hand-mounted components, intricate shielded enclosures, many tuning adjustments and so on. Interestingly, these units were those with the lower retail prices.

The more sophisticated video broadcasters used modern techniques such as surface-mount components, simpler shields, fewer adjustments and offered more features. These more sophisticated units provided the benchmark for our design.

From the design team's experience with off-shore factories, we knew that many imported items have an extremely high labor content. There also is a widely accepted opinion that RF circuits require labor-intensive construction such as shields, hand-wound coils and a large number of trick adjustments. Because of the significantly lower labor costs in some Pacific-rim countries, many products employing even this high-labor content construction are profitable.

SETTING THE GOALS FOR A SUCCESSFUL DESIGN

The design criteria for the video broadcaster involved the following goals, in their order of importance:

1. Minimum assembly labor
2. Minimum test time
3. Maximum yield
4. Minimum parts count
5. Minimum parts cost

The order of importance will tend to vary depending on the product involved. As an example, an item that would have a high material cost rather than labor cost would not benefit from a further reduction in labor. The list shown represents an order of importance for a typical electronic product. As technology provides more complex integrated circuits, the number of active component parts would decrease while the labor either remains the same or increases. This would have an effect on the order of importance.

Although there has been phenomenal advances in integrated circuits in the RF region, a lot of RF tasks are still done in the classic way. One excellent example of this is filters. Most RF filtering is done with discrete inductors and capacitors, with either element being variable for critical filters. The existence of a filter in a design implies considerable labor. The parts are often not machine inserted, and the variable parts require some sort of test procedure to be adjusted.

Although there may be some valid arguments to re-order items 3, 4, and 5 in the list, it is well established that items 1 and 2 are at the top of the list for RF devices.

MINIMIZE ASSEMBLY LABOR

To meet the first criterion, assembly labor can be minimized through the following techniques:

1. Designing the electronics so that the vast majority of components are machine assembled;
2. Reducing the number of sheet-metal parts;
3. Reducing the number of screws, clips and other fasteners; and
4. Reducing the number of hand soldering operations.

1. MACHINE ASSEMBLY

Item 1 is a very large factor. Not only can a machine place parts at a rate far exceeding that of an assembler, many modern surface-mount machines are capable of pretesting the components for orientation, electrical parameters, and placement accuracy.

In the early stages of the design, there was some study to evaluate relative cost of surface-mount vs. through-hole technology. It was found and verified by some recent articles in the trade journals, that the cost of surface-mount technology may be slightly higher than through-hole technology mainly due to the high cost of surface-mount placement machines. There is some cost disadvantage for some surface-mount components while, on the other hand, there is a significant advantage for many.

Not all components were available in surface- mount packages at the time of the design of the video broadcaster. The number of parts being added to the surface-mount list grows daily but there will always be some parts not available as surface-mount components.

There may be a cost premium for a surface- mount part relative to through-hole parts and the temptation to save cost by using a through-hole part must be considered very carefully.

A situation arose in the design of this device involving a quartz crystal. As it turned out, the surface-mount crystal was significantly more expensive than the conventional HC/18 can with wire leads. It was decided to provide a surface mount pad layout on the printed circuit board and to surface solder the conventional HC/18 crystal in anticipation of a more affordable surface-mount crystal becoming available.

The more generic surface-mount parts such as 74HC logic, and standard linear ICs such as op-amps, tend to have the lowest prices due to the greater amount of industry competition. In many cases it is more economical to perform a task using a larger number of generic parts rather than one unique part.

The frequency synthesis of the video broadcaster's oscillators is an example of a larger number of generic ICs being less expensive than a smaller number of unique chips. The frequency synthesizer could have been reduced to a total of three chips using a sole-sourced synthesizer chip. However, this part was not available in a surface- mount version and was not multiple sourced. Therefore, it was deemed prudent to use a design with generic parts in spite of the fact that seven chips were required. The cost of the seven chips, after careful shopping, was less than the cost of the three-chip design. This is in addition to the peace of mind from having a practically inexhaustible supply of parts.

Because the video broadcaster operated in the 915 MHz region, the use of chip components was a significant advantage. The video broadcaster used microstrip techniques and the surface-mount chip components are especially suited for this frequency range. No special microwave parts were used but great precautions were taken to insure that components were evaluated for specific circuit locations and that new vendors would be evaluated before loading their parts onto the surface-mount assembly machine.

The estimated average cost of assembly for a surface-mount component is $0.03 per part which is about the same as for a conventional through-hole part. However, when the suitability of the chip components to the 915 MHz range is considered, the advantage of the surface-mount technology was overwhelming and was chosen as the basis of this design.

Most likely, for some applications, the older through-hole, wave-soldered assembly technique would prove to be more cost effective and would be the obvious method of choice. Each application requires it's own analysis.

2. REDUCING SHEET METAL PARTS

Sheet metal parts, the subject of Item 2 of the list of priorities, are notoriously expensive. It is not so much the expense of a fabricated part but the expense of handling those parts after they are received. Sheet metal parts are such items as brackets, cases, and, particularly for RF devices, shields. They must either be soldered in place, screwed down, tabs bent, clipped, or some other type of hand operation employed. Thus, sheet metal parts add to the tasks under items 3 and 4.

Some sheet metal parts are unavoidable, such as shields. However, the amount of shielding can be kept to a minimum by lowering signal levels to prevent radiation, decreasing sensitivity to minimize the effects of signal ingress, and making tight, compact circuits. In the video broadcaster, microstrip techniques were used with a very large ground plane area to contain the RF fields and minimize undesired radiation.

When shields are required, they should be as small as possible and made from one piece of stock. Also, remember that shields need not be made from brass or copper and do not need to be thick. In the video broadcaster, the shields were fabricated from .005" tin-plated steel with solder tabs which were inserted into the board like a component. The shields had small holes to allow access to the enclosed circuits for tuning.

3. REDUCING FASTENERS

In addition to being applied to sheet metal parts, fasteners are found on plastic parts, machined parts, purchased components, etc.

The expense of fasteners is the labor required to apply these fasteners. Clips and speed nuts are preferable to screws and nuts but the use of minimal fasteners is the ideal.

When applied to product cases, fasteners can be minimized by using cases that dovetail, have slots for mounting printed circuit boards and other parts, etc.

The video broadcaster uses a two-piece, injection-molded plastic case with a rear panel that fits into slots on the upper and lower halves of the case. The printed circuit board nests into four bosses and the entire assembly is fastened with four self-tapping screws. The decorative front panel is fastened with an adhesive backing. Although the circuits are quite different, the video broadcaster transmitter and receiver use the same case but with different graphics on the front and rear panels.

Another very useful technique for reducing the number of fasteners is the use of printed-circuit-board-mounted controls, connectors and switches. There are two significant advantages to this; first, the controls, connectors and switches may be wave soldered and save labor and fasteners. Second, the electronics assembly may be wholly contained on one PC board and thus fully tested before it is installed in the case.

4. REDUCE HAND SOLDERING

Reducing hand soldering is a matter of choosing the right components. Hand soldering is usually associated with the larger components of an electronic circuit board. In many cases, items that were hand soldered may be replaced with items that may be wave soldered. Some really clever component designs are allowing more of the larger components to be surface mounted which opens up the possibility of complex assemblies requiring neither hand soldering nor wave soldering.

One of the more common hand soldering tasks is the connection of wires to a printed circuit board to connect to power supplies, front panel components or other externally mounted parts. Ideally, wires should be eliminated. In addition to an expensive manual soldering job, the wires must be cut, stripped and tinned before soldering.

REDUCE TEST TIME

Immediately following assembly labor in the list of design goals; test time is a significant cost factor for two reasons. First, not only is labor involved, it is at a higher skill level than assembly and, thus, is more costly. More employee training is required in addition to a test fixture and test equipment. These last two items, fixturing and test equipment, can be particularly expensive when RF is involved.

Test procedures usually imply that something must be adjusted. A variable circuit element is generally much more expensive than a fixed element. As an example, a variable resistor, i.e. a potentiometer, costs about as much as 25 fixed resistors. Furthermore, to the component cost must be added the expense of a test technician and all the needed equipment to set the adjustment to the correct setting.

In the case of the video broadcaster, the oscillators were synthesized for the three operating channels using a phase-locked loop. This required the inclusion of seven ICs in the receiver and another seven in the transmitter. This was offered as a feature to the consumer and some of the cost was justified by that. In the competitive unit in which the frequency was set by a varactor voltage, three potentiometers were provided to set the three operating frequencies. The cost of the three potentiometers was about one-third the cost of the ICs required to implement the phase-locked loop. When the cost of setting those three potentiometers to the correct frequency is considered, the cost of the phase-locked loop becomes much less significant.

Automatic test equipment is another method of reducing test time. Providing test points that allow internal measurements while the unit is in a test fixture greatly reduces test time.

Some tests, particularly those required of RF systems, are notoriously expensive. On such test is any sort of swept-frequency test. In one competition video broadcaster, RF amplifiers were made from transistor and matching networks, whereas, in the domestic design, MMICs were used without tuning. Expensive sweep testing was required to adjust the coils of the matching network to provide the necessary gain. From a parts cost viewpoint, the transistor amplifiers with their impedance-matching networks were less expensive. However, from an overall cost standpoint, once the hand inserted coils and the swept-frequency RF tuning were considered, the transistor amplifiers were much more expensive.

To design an electronic circuit that requires less testing and, ideally, no adjustments, implies a design that is tolerant of normal variations in component values.

Typical design techniques to achieve this is to design circuits where the gain is set by feedback rather than device gain, operating circuits in saturation where the signal level is a function of power supply voltage rather than device gain, etc.

It is important to perform extensive analysis whenever a circuit cannot be adjusted for component parameter variation. Computer analysis such as Monte-Carlo analysis is very important in high volume designs. It is necessary to operate at such narrow profit margins that even a small number of rejects could prove disastrous.

MAXIMIZE YIELDS

If any subassembly or final assembly fails to meet the acceptance specifications, that part must be either repaired or discarded. The further along the production process the item is, the more costly the repair or discarding will be. Thus, it is necessary to perform as much evaluation as possible early in the assembly process.

Repair is to be avoided at all cost. If a subassembly has to be discarded, it is best if the subassembly has the minimum amount of parts installed. If repair has to be performed, it is most easily done when the circuit is of minimum complexity.

However, as it was explained previously, the test time should be minimized as it is expensive. The least expensive and very effective test is performed by the surface-mount assembly machine before a component is installed. As an example, consider a resistor that is discarded for an out-of-tolerance value before being installed. The cost of this part is less than one cent. Consider now if the resistor were installed but was caught at a subassembly test. The test technician may take one minute at a cost of about $0.75 plus the penny for the resistor. But, if the first test that identifies the out-of-tolerance resistor is the final test, it may take a test technician 5 minutes to locate and replace the bad part and now the cost is $3.75 plus the penny for the resistor.

Testing can be enhanced by the use of test points which may be provided for a bed-of-nails check for low frequency or DC checks. Certainly for the 915 MHz frequencies involved in the video broadcaster, the bed-of-nails will not provide an accurate result.

The DC parameters of RF circuits, while operating, may be measured through a test point if a series resistor is provided to offer isolation from the test pin to the high frequencies. The addition of a resistor results in an unused component under normal operating circumstances. However, the cost of the resistor and it's placement is of the order of $0.037 which means that 135 resistors cost as much as one 5 minute repair job.

MINIMUM PARTS COUNT

One requirement of a successful product is a clever design. A clever design is one that performs the maximum functions from the minimum components, is easy to assemble, requires very little or no testing or adjustment, and so on. How clever a design is, is not measurable and is an intangible. However, sufficient engineering talent along with ample time and support must be provided if there is to be any hope of a clever design.

There are several good reasons to design electronic circuits that use a minimum of parts. First, the fewer parts the less the parts cost. This statement is not always true. Obviously an expensive part that replaces a few very inexpensive parts does not support a lower parts cost. When the parts being minimized are similar parts such as resistors or ceramic capacitors, then making a reduction in component parts has a significant effect. There is a lot of overhead associated with component parts. They must be purchased, stocked, loaded on to the surface-mount assembly machine, tested and finally placed on the printed circuit board.

Below is a tabulation of the parts count in the video broadcaster compared to that of the competition:

	Imported Unit	Domestic Unit
RECEIVER		
Capacitors	45	50
Resistors	26	49
Potentiometers	2	0
Inductors	28	7
Transistors	6	4
ICs	2	11
Diodes	5	7
Crystals	0	1

TRANSMITTER		
Capacitors	48	51
Resistors	32	46
Potentiometers	5	0
Inductors	15	3
Transistors	7	4
ICs	2	12
Diodes	5	5
Ceramic Filters	1	1
TOTALS	229	251

One of the first observations is that the domestic units have more parts by about 10 percent. Although this is true, further investigation is necessary. First, the domestic unit offers more features and performance. This means that the unit does more with only a ten percent increase in components. One significant difference is that the transmitter and receiver local oscillators are synthesized. This saves some test time as the receiver local oscillator and transmitter oscillator do not have to be adjusted using an expensive spectrum analyzer to spot the oscillator frequency. The phase-locked loop is most evident in the integrated circuit count of the two units and the existence of two quartz crystals in the component count. When a standard crystal is used such as a watch crystal, or color-burst crystal the cost can be low. Notice, also, the domestic unit has no potentiometers as compared to a total of seven for the pair in the imported design. As previously explained, these are usually expensive parts.

One very important observation is the significant number of inductors used in the imported unit. Many of these are hand-wound air-core inductors that must be tuned by spreading the turns. It is not the cost of the inductor that is significant, but the fact that it must be tuned. The imported unit had more than four times the number of inductors that the domestic unit has. Not every inductor was tuned, on either the domestic or imported units. But, the difference in adjustments -- either inductors or other adjustments -- on the new design is one-fourth that of the competition. A printed filter using microstrip techniques was used on the domestic unit while a lumped filter was used on the imported unit as one example of saving inductors.

If the component list of the product includes a large number of different parts, many more purchases must be made of smaller quantities. In addition, it is necessary to load more parts on to the surface-mount machine. The goal for cost effective parts requirements is to use the minimum number of parts and to use as many common parts as practical.

In the video broadcaster, every bypass capacitor is of one value. Furthermore, the same value is used for coupling, even in applications where this common value is much larger than necessary. The use of a smaller capacitor may save a small amount but would be more than wiped out by the increased cost of introducing a new part.

PARTS PROCUREMENT

When designing for low cost, engineers must be involved with the early parts procurement process. If the product has potential for very large volume, such as a consumer item, the purchasing process must be very aggressive. Those engineers who have not been involved with high-quantity production, particularly those whose experience is primarily involved with high-rel, low-quantity RF circuits, will be absolutely amazed at the real cost of some familiar items when the quantity is over a million pieces.

First, always design around multiple-sourced components. In the design of the video broadcaster, the phase-locked-loop synthesizer was originally designed around a single-chip synthesizer which was sole sourced. The design was extremely compact and elegant. However, the manufacturer could name its price for the chip and should the chip supplier ever develop a production glitch the broadcaster would be doomed. Although the new synthesizer design used seven chips, three were the same, and the chips were common 74HC items.

The new synthesizer design resulted in two strong bargaining tools when shopping for low prices, common parts and high quantity. What resulted was a circuit with almost four times as many ICs but no worries about price or an available supply.

There was one basic rule followed in the design of the video broadcaster. Whatever the quoted price of a component part, it was never low enough. The quantities involved in the video broadcaster were sufficiently high that quotes could be made directly from the factory at very competitive prices.

CONCLUSION

There is an unfortunate irony in the chronicle of the video broadcaster. Although it was our sincere desire to manufacture a consumer item in the United States, many of the internal components are of foreign origin. Even the components bearing U.S. manufacturer's logos are assembled in foreign lands. Many major items are of domestic origin such as the plastic cases, panels, and the printed circuit board. However, there is even strong competition in this area from foreign suppliers. All those involved in this project would like to see competitive domestic components available, particularly in surface-mount components. On the other hand, the most value added was from domestic sources.

There were no new, unexplored techniques used in the design of the video broadcaster. All of the techniques discussed in this paper have been available for some time. Being competitive is a matter of using modern techniques, a clever design,
and a good deal of common sense.

SPREAD SPECTRUM CELLULAR COMMUNICATIONS: BENCHMARKS FOR COST, POWER AND SPECTRAL PERFORMANCE

Steven A. Morley
Director, VLSI Products Division

QUALCOMM, Inc.
10555 Sorrento Valley Road
San Diego, CA 92121

INTRODUCTION AND BACKGROUND

Since the day when the first two-way radio was installed in a police car during the 1930's, the demand for the ability to communicate wherever you go has steadily increased. High equipment costs, expensive maintenance, and that ever limiting factor of available bandwidth have kept wireless communications limited to small capacity, costly networks, or overloaded hobbyist channels. However, the need for large capacity, low cost, high quality wireless communication networks is increasing throughout the world today.

In industrialized nations the demands for efficient use of time in busy everyday life combined with our "mobile" society pushes for such communication capabilities. In developing nations, the simple need to offer even basic telephone communications in areas where laying cable is either not practical or where maintaining that wired network is very difficult also demands low cost, highly reliable wireless communications.

The communications industry is pushing ahead to develop new technology to meet these increasing demands. A major area of growth in telecommunications is the technology and infrastructure to support high-quality, low cost, easy to use, readily available "personal" wireless telephone service to a mobile user, whether vehicular or pedestrian. Before the advent of cellular phone service in the United States in 1983, such wireless, mobile voice communication was limited to hobbyist bands, public service, military systems, or expensive, small capacity commercial services. In the few short years since cellular service was introduced the "need" to communicate without being located next to a stationary tethered telephone has grown exponentially. Today more than five million people in the United States are subscribers of cellular phone service. The demand for increased capacity, seamless operation over nationwide or worldwide coverage areas, and expanded services increases constantly.

The advancement of technology that allows people to "stay in touch no matter where they are" is the next step in the historical progression of communications. Before the late 1800's, it had been necessary for a person to be in the same location as another person with whom he or she wished to communicate in "real time." The advent of radio communications and telephone service just over a century ago allowed people to communicate with each other remotely. However, the two communicators were required to be physically near a fixed station, either telephone or radio setup. The introduction of cellular service, and the various follow-on services now in development, whetted the appetite of large numbers of people to "take communications with them" no matter where they should go. This demand for "personal" communication capability, and the profit advantage to those who provide it, is now pushing technology to develop new capacity and capabilities in wireless networks. The result will be a large scale system that no longer identifies the called party by the station (e.g., telephone) at which they are located, but by the person for whom the communication is intended.

The ideal system for such a capability would allow huge populations to use the limited bandwidth of the RF spectrum that is available. Such a system should allow a basic design to adapt to the differing requirements for the communications needs in a

domestic home, a large business, a pedestrian network, a vehicular mobile system, and, ultimately to an air-to-ground communications ability. Ideally, one communication terminal, small enough to travel with a person wherever he or she goes, will provide for all these differing requirements. Perhaps, eventually, the distinctions between the different services will fade and a person will be interconnected to one large public network wherever he or she goes. The eventual realization of such a network has become more an issue of regulatory, logistic, and business considerations, rather than a technology limitation.

WHY DIGITAL WIRELESS TRANSMISSION TECHNOLOGY?

Until recently, almost all wireless voice communications have used analog modulation (frequency or amplitude) for transmissions. However, the advent of commercial communication satellite systems, such as Satellite Business Systems, GTE Spacenet, and INTELSAT IBS and IDR services in the 1980's has led to an increasing number of large-scale digital wireless transmission services, especially over satellite communication channels. Digital transmission technology offers a range of characteristics that provide new techniques and options to the communication systems engineer as he or she strives to optimize the transmissions to meet the requirements of individual services and channels. Digital modulation technology is now being applied to wireless terrestrial communication systems, such as cellular telephone networks. The advantages of digital communication systems include:

New techniques for optimizing the quality of the transmission in the channel: A wireless communication channel exhibits various noise, fading, and interference effects due to physical phenomenon. In addition, these systems are typically limited in transmitted power and bandwidth due to regulatory restrictions. Besides the greater flexibility in the selection of the actual modulation technique, digital transmissions can take advantage of forward error correction (FEC) techniques to balance the combined limitations of power and bandwidth to achieve the highest system performance. FEC involves the encoding of information bits before transmission, resulting in the formation of additional redundancy bits that are also transmitted. In some codes the actual information itself is not even transmitted. Only encoded bits from which the original information is transmitted and decoded are sent to the receiving station to generate the original information.

While FEC increases the number of "bits" transmitted (i.e., increases the required bandwidth), the power required for transmission of these bits to decode the correct original data stream at the receiver is decreased. A class of codes known as "convolutional codes" is commonly used in digital wireless communication systems. These codes are often decoded using an algorithm known as the Viterbi decoding algorithm. This decoding technique for convolutional codes was invented by Dr. Andrew J. Viterbi in the late 1960's [1]. The additional redundancy bits added by the FEC process are not to be confused with the overlaid "bits" used in the code division multiple access (CDMA) process described below. However, the use of FEC techniques exhibits special advantages when operating with CDMA systems [2] which make the use of such coding even more valuable in these systems. Convolutional encoding with Viterbi decoding is the specified FEC technique used in all the proposed digital cellular systems around the world, although the exact code used in each system differs.

New techniques for channel access: With analog modulation systems, channels are normally defined by the frequency at which they are transmitted. Digital transmission channels can also be identified by unique frequencies using Frequency Division Multiple Access (FDMA). However, an alternative channelization approach identifies channels by the time at which the transmission occurs. This is known as Time Division Multiple Access (TDMA). Most existing or proposed wireless telecommunication systems use some form of FDMA or TDMA. A third technique for channel identification is known as Code Division Multiple Access (CDMA). CDMA will be further described later in

this paper. Each technique for channel access offers different advantages in different types of systems. However, for the environment and system parameters found in terrestrial wireless digital communication systems such as cellular systems, CDMA technology offers unique advantages that will be described throughout this paper.

Support of new services: An ever increasing range of services that extend beyond basic voice communications is being required of existing and future communication systems. The phenomenal increase in the use of facsimile machines and laptop or notebook computers is being extended to the mobile environment. The need to connect these digital devices through a wireless communication network is growing. In addition, special services such as location reporting, navigation, and telemetry transmissions of various types are expanding. A digital wireless transmission system can support these services directly without the requirement to convert the digital bitstreams to analog waveforms, providing higher data rates and better quality for these types of transmissions.

Consistent data and speech quality: Analog transmission systems typically degrade in quality with even a slight increase in noise. Digital transmission systems can be designed to maintain consistently high quality of the demodulated information under a range of changing channel conditions. This high quality is maintained up to the point where the capability of the receiver and the error correction system are exceeded. Typically this degradation occurs at signal levels much lower than those which can be supported with an analog system. In addition, digital transmission systems can use a wide range of diversity techniques to enhance the ability of the system to operate in less than ideal conditions. The CDMA system discussed in this paper uses several diversity techniques to achieve maximum signal quality, as well as increased system capacity, from the mobile environment.

Privacy: An important advantage to the user of a digital transmission system is the ability to add any level of security or privacy required. An eavesdropping station may be able to detect a transmission, but the ability to demodulate and interpret the information can be made virtually impossible by data encryption techniques. This security is possible without signal degradation to the intended receiver.

VLSI implementation: Factors such as low cost, small size, and high levels of reliability are being demanded from systems that also require ever-increasing circuit sophistication. The advances made in the past two decades in the area of digital logic circuitry and signal processing implementations in single-device Very Large Scale Integrated circuitry (VLSI) has direct application in the implementation of modern digital communication systems. In spite of computing power requirements that exceed the capability of a room-sized computer of just 15 years ago, today a hand-held battery operated communication terminal can be purchased for a low cost. Increased levels of circuit integration in low-power CMOS devices will only expand the capabilities of future terminals while providing for lower powered, less costly implementations.

In addition, the reliability of a terminal constructed of only a few devices is inherently increased, especially in the rugged environment in which a portable unit operates. As circuit density and speed of integrated circuits increase, signal processing and communication sciences find new ways to implement an increasing percentage of the terminal functionality in the digital circuits. The amount of analog circuitry in a digital cellular phone will be minimal. The digital demodulation circuitry in a properly designed digital terminal will perform well with low cost analog components. An important aspect of any system being planned or designed today is to realize that this remarkable increase in digital technology has not peaked. The rate of technology advancement seems to continually increase. A well-planned system will meet the needs of today's requirements, but will also remain flexible to take advantage of future advances.

Lower transmit power: As previously described, the application of FEC techniques to digital wireless communication systems allows these systems to operate with lower transmit power than equivalent analog systems. This decreases the overall power requirements of a digital communication terminal. Low power

transmission is an important attribute for a portable battery-operated system where the cost of batteries or the limited time between battery recharges becomes the limiting factor in user convenience.

WHAT ARE THE CHOICES IN A DIGITAL WIRELESS COMMUNICATIONS SCHEME?

The selection of a digital transmission system includes two fundamental decisions: the choice of the modulation technique and the selection of the access technique. Modulation can be one of many forms of frequency shift keying (FSK), amplitude shift keying (ASK), or phase shift keying (PSK). In addition, any number of combinations of these basic modulation techniques is possible. Most proposed digital cellular systems use some type of PSK modulation. The CDMA system discussed in this paper uses a special form of PSK modulation that is optimized to work well with the particular characteristics of the CDMA access method. The choice of the access method usually involves partitioning channels by frequency location (FDMA), a position in time (TDMA), or a combination of the two. Refer to Figures 1 and 2.

A third technique is the partitioning of channels by assigning a unique "overlaid" binary sequence that is linearly combined (using modulo-2 addition) with the data before transmission. This overlaid "channel code" sequence has two fundamental properties: 1) the baud rate (referred to as the "chip rate") of the channel sequence must be higher than the data bit rate, and 2) the chip sequence of the code should be orthogonal, or nearly orthogonal, to other sequences used by other channels operating in the same frequency, time, and geographical area. This is referred to as Code Division Multiple Access (CDMA). Refer to Figure 3.

HOW DOES CDMA WORK?

The basic operation of a CDMA channel is described in the previous section. The fundamental concept is that unique channels can operate at the same time, using the same frequency band, and in the same geographic area as long as the transmissions of a unique station can be detected and demodulated by the intended receiver without catastrophic interference from other transmitters that are also operating. This is possible by the way in which the receiver operates. The receiver is a demodulator that receives symbols at the chip rate. The demodulator then combines the received chips with a time-synchronized duplicate of the code sequence used at the transmitter using the same modulo-2 addition process. In a noise free transmission environment the cascaded double combination of the code sequence with the information bits (once at the transmitter and once at the receiver) results in exactly the original information bit sequence. The demodulator at the receiver integrates this code-combined received stream over an entire bit time. Without the presence of noise or interference the output of the integration process will be the original bit stream. Of course, as there will normally be other transmitted streams co-existent with the desired channel, the receiver will also process the information from these other transmitters. If the chip streams used by the different channels are orthogonal or nearly so, when the received chips are integrated of the bit time, the effects of the other channels average out to a random interference. This random interference can be treated as any other source of random noise and can be corrected by powerful FEC techniques discussed earlier. The result is the ability to receive only the intended transmission.

An example will further explain these techniques. Say that a digitized voice signal at a data rate of 10 Kbps is to be transmitted using a CDMA system. Each bit (lasting 100 microseconds) is first encoded using a rate 1/2 convolutional code. That

is, for each information bit in the digitized speech, two encoded bits are generated. Only these encoded bits, now at a rate of 20 Kbps, are to be transmitted. This 20 Kbps stream is combined with a higher rate (say 1 Mchip/second) spreading sequence using a modulo-2 addition process. That is, 50 time-sequential outputs of a code generator circuit operating at a 1 MHz rate are combined with each bit of the FEC encoded data stream in a sequential manner. The bandwidth of the resulting digital stream is, of course, expanded by this frequency "spreading" caused by the combination of the data with the 1 Mchip/second code stream. If the transmission system supports modulation at the rate of one "bit" per Hertz of bandwidth, the resulting transmitted signal will require 1 MHz of bandwidth. At first this seems to be a great waste of precious bandwidth to require a full Megahertz of bandwidth to send a single 10 Kbps information stream. However, the entire concept of the CDMA system is that multiple channels are being co-transmitted using this frequency band at the same time. Rather than becoming terribly wasteful of frequencies, the actual cellular system can provide network capacities 15 to 20 times higher than the current American FM-based analog cellular system [3].

Three fundamental channel characteristics affect the ability of a system based on CDMA techniques to operate correctly. First, the signal power received by a station must be balanced so that the level of the desired transmitted channel is equal to the level of any other transmitters in that region of operation. In the case of a base-to-many-mobiles scheme such as used in cellular systems, this is easily achieved in the "forward" channel (from base to mobile) by assuring that all channels from the base station are equal powered at the transmitter. However, in the reverse channel (from base to mobile) the transmit path from each mobile to the base station varies greatly due to differing distances between the base and mobile stations and other environmental effects. The result is the need to implement a wide dynamic range and quickly variable power control scheme for the transmissions from the mobile to the base station.

The second characteristic for correct operation is that the timing between the CDMA code generators at the base and mobile stations must be synchronized in order for the timing of the code combination at the transmitter to be in line with the code combination at the receiver. This can be achieved by slaving the mobile unit to master timing from the base station, but involves special synchronization techniques.

The third characteristic for a good CDMA scheme is the correct selection of code sequences. The code generation technique must be flexible enough to allow for a large population of users without interference caused by code correlation.

The CDMA cellular system proposed by QUALCOMM, Inc., provides solutions to each of these concerns. In addition to the special issues mentioned in the previous paragraphs, a cellular system based on CDMA techniques must consider the effects of transmissions in adjoining cells and allow a mobile user to move from cell to cell without losing the ability to continue communication. The special considerations of the fading channel environment and multi-path signal reception place additional requirements on a correctly designed CDMA system. All these considerations have been included in the QUALCOMM system design and carefully modeled using analytical techniques, computer simulations, and actual field operation of a breadboard system in 1989. As the system definition has progressed, a number of additional benefits of CDMA technology have been included. These are described in the next section.

WHY IS CDMA THE RIGHT SOLUTION FOR CELLULAR COMMUNICATIONS?

CDMA technology offers several advantages to the implementation of cellular systems when compared to FDMA or TDMA systems. These advantages benefit not only the end-user, but actually simplify the network engineering tasks. Some of the advantages are described in the following paragraphs.

Robust Channel Performance

Some of the major considerations in the mobile environment that limit the performance of a communication system include:

- weak areas of reception due to shadowing, fading (fast and slow), and multipath;
- even in strong reception areas, multi-path can be a major source of interference;
- moving mobiles require communications that must adaptively match the best performance for a dynamically changing environment over a range of fast/slow movement effects.

CDMA provides a powerful and efficient solution to these concerns through the inherent ability to provide the following:

- diversity of various types to maximize signal reception,
- powerful use of FEC techniques.

The use of FEC techniques has been previously discussed. The types of diversity used in the QUALCOMM-proposed CDMA system include:

Frequency diversity: The frequency "spreading" of a CDMA signal improves the reception of that signal by avoiding major signal loss due to frequency-specific fading effects.

Path diversity: In analog, FDMA, and TDMA systems the effects of multi-path appear as noise to the intended signal. However, if properly used, the multi-path signal can enhance the reception. A multi-path signal is simply a delayed version of the intended signal that has followed a different (reflective) path compared to the direct signal. If the receiving station is able to combine this signal energy with the direct path signal the result will be a higher quality signal for demodulation.

Because the multi-path signal follows a different path to the receiver, the effects of fading and path interference effects differ between the two signals and the strength of one signal can offset the weak receptions of the other. Also, there is no fundamental reason to restrict the additional energy to only one multi-path signal. In actual systems there may be several multi-path signals, especially in urban environments. In some cases of severe shadowing the multi-path signal may be stronger than the direct path. The CDMA system makes use of the multi-path signals by use of an architecture known as a "rake receiver."

A rake receiver is a type of demodulation system in which the received signal is simultaneously demodulated by several demodulation circuits, each operating on a signal that is slightly offset in time from the other demodulator "tines." The combined output of the multiple path receiver is used to determine the correct demodulated information.

Antenna Diversity: Many analog cellular systems today use antenna diversity at the base station to maximize receive signal energy. Two or more receive antennas are spaced a certain distance apart so that if one antenna is receiving a weak signal the receive energy at the other antenna(s) is stronger. Even some

mobile analog cellular units are able to take advantage of two spatially diverse antennas mounted in two locations on the mobile unit. The QUALCOMM CDMA cellular system will use similar receive antenna diversity to enhance signal reception.

Spatial diversity: The CDMA cellular system offers a very special capability to enhance receive signal quality at the point where the communication quality between the base and mobile stations is typically the weakest. This is when the mobile unit is transversing between two base stations and is approximately equidistant between the two bases. At this point the received signal energy from the base station is weakest at the mobile unit due to the distance between the two. The received energy from the mobile unit at the base station is also weak at this point. The QUALCOMM CDMA cellular system provides a special capability during this transition period known as "soft handoff." Refer to Figure 4.

This is a special operation wherein the system establishes communication between two base stations and the mobile station as long as the mobile unit is within transmission capability to each, as defined by a signal strength measurement. As the mobile unit moves between one cell and the next, that unit is able to detect the ability to communicate with the new base station (see Figure 4). The network establishes a second communication link from the central switch office to this new base station. The same information received from the switch office is sent to both base stations which transmit the same information to the mobile unit.

Although these transmissions use different codes, the frequency band is the same so that only a single RF chain is required in the mobile unit. The mobile unit uses the additional "tines" of the rake receiver to operate with this new code for as long as the soft-handoff is established. During this transition period the mobile unit is receiving energy from two very diverse locations and the combined energy at the mobile receiver provides improved reception. The transmissions from the mobile unit are also demodulated by both base stations and the demodulated signals are then combined back at the central network switch office. As the mobile unit moves away from the first base station, the link with that station is dropped and the mobile unit operates only with the new base station.

A special result of this soft-handoff technique is that the transition from base station to base station is typically transparent to the communicating parties. When a handoff occurs in today's cellular system the transmission is first stopped while the mobile unit retunes to a different frequency channel in order to operate with the new base station. Communications then continue once the radio is retuned. Although this outage lasts typically for only a fraction of a second it can occur several times in only a short period. During field trials of the CDMA cellular system in 1990 in Manhattan, the FM cellular phone that was being used for comparison performed a handoff five times while the mobile unit was stopped for a traffic light. The capability to perform soft-handoff is a special feature of a cellular system that operates adjacent base stations using the same frequency band and is not possible in an FM or TDMA/FDMA system unless multiple radio circuits are provided in the mobile units. Although it would seem that soft-handoff operation would decrease system capacity (because during a soft handoff the single mobile unit is operating on multiple base station channels), the fact is that this process increases network capacity.

In the CDMA cellular system the limit on capacity is determined by the interference caused by other users. When a mobile unit is in the soft-handoff operation it is not required to transmit as much power as it would if only communicating with a single base station. This results in less interference to other users and thus the number of users supportable by the system increases by as much as 20 percent over a system that does not implement soft handoff.

Dynamic Channelization

"Noise" as perceived by the receiver at a base or mobile station in a CDMA system is largely a function of interference from other users. The more bits being transmitted by all units in a system the higher the interference (noise) level to any one

unit. By choosing codes that are nearly orthogonal to each other the interference appears as Gaussian noise that is mitigated with FEC techniques.

The level of this interference is a function of how many other users are transmitting at any given moment and (in the case of reception at the base station) the ability of the mobiles to control their transmit power so that the base station receives equal power from all mobiles. Even in the event that a single mobile is transmitting with higher power than it should, the contribution by that mobile is only a small component of the overall interference level. Also, given that some mobiles may be transmitting "too loud," others (statistically) will be transmitting "too quiet" and the average will be balanced. If all mobiles transmit "too loud," then this is back to the optimal situation where we desired to have equal receive power.

To maximize capacity (in terms of the number of simultaneous users) we desire to restrict the bit rate of any given user to that required to achieve an acceptable level of quality. Since most cellular users are transmitting speech, we want to find the most efficient method of encoding that speech. A characteristic of speech information is that certain sounds are more dynamically complex, requiring a certain bit rate to accurately represent them. Other sounds can be accurately encoded with fewer bits. In addition, during normal telephone conversation one party or the other is typically not talking approximately half of the time. A system that can rapidly change the transmission rate to adjust to these varying requirements for accurate speech encoding and periods of silence allows us to maximize our overall network use of the bandwidth available.

The QUALCOMM CDMA Cellular system uses a vocoder algorithm known as the QUALCOMM Code Excited Linear Predictive coding system (QCELP) which accounts for these changing bit rate requirements. This algorithm dynamically determines the number of bits required on a frame-by-frame basis (i.e., 20 msec.) for a given speech segment. If fewer bits are required to accurately represent the speech for a given segment, the vocoder outputs fewer bits and the transmitter sends less energy for that speech segment. Listening tests have shown that the QCELP algorithm provides speech quality equal to vocoders operating at 8 Kbps or higher. The maximum output bit rate of the QCELP vocoder is about 8 Kbps. However, the average bit rate for the QCELP system during continuous talk operation is less than 7000 bps and the average rate during normal phone conversations is less than 3200 bps. While most systems are unable to dynamically adjust channelization fast enough to take advantage of this available capacity, the CDMA system adjusts automatically. The capacity, as measured by the number of simultaneous users which can be supported with a given level of quality, is thus directly increased by the ratio of the average vocoder bit rate compared to the maximum, for a capacity increase of more than 2 to 1.

The "soft capacity" of CDMA is also advantageous during peak operation hours. While a high quality of speech is available during normal times, in the event of unusually high traffic times, such as perhaps when an accident slows traffic on a normally fast-moving highway, the network will still allow connectivity to the increased user population. However, each user will hear a slightly higher noise level caused by the additional interference of the extra users.

Another feature of the soft capacity of a CDMA cellular system is the ability to simultaneously support communication links at different bit rates. For example, perhaps one user establishes a call to transmit a facsimile at 9600 bps rate and a second user is holding a voice conversation with the QCELP vocoder at 3200 bps average. The network can support both without a major re-structuring of the channels and without inefficiency. In addition, if future vocoders provide good speech quality at

lower data rates the CDMA system can automatically provide optimal channelization at the lower rate.

Ease of Network Engineering

In today's FM cellular system different base stations operate with different sets of frequency channels. This requires a complex network engineering task to balance the assignment of RF channels. Each radio in each base station must be tuned to the unique channel. When additional base stations are added, the frequency channel allocation process must be repeated and the radios must be re-tuned. Every base station in a CDMA network can operate with the same radio channel. Thus the network engineering is simplified and the addition of new base stations in the network does not require additional extensive frequency planning.

Low Power Operation

The average transmit power of the mobile CDMA cellular unit is quite low compared to FM or TDMA units. This is due to the advantages of the wide signal bandwidth and powerful error correction. In addition, the majority of the functions required to modulate and demodulate the CDMA signals are easily implemented in low power CMOS VLSI devices. The first generation CDMA cellular unit implements all the modulation/demodulation functions in three VLSI circuits. The second generation equipment will implement these functions in a single VLSI device. The result is a very low power implementation required for the portable units. The major power consumption in a handheld CDMA unit is the DSP processor required for the vocoder. Of course, this vocoder circuit is only used when the unit is in use so that "standby" power consumption is very low. These combined low power considerations result in a handheld cellular unit requiring less than half the power of today's FM units. This directly relates to increased battery operation time, without consideration for more powerful battery technology.

SUMMARY AND CONCLUSION

Will CDMA technology solve all the issues for a complete cellular system for the next two decades? The CDMA architecture is certainly flexible to take advantage of new technology as it becomes available. New technology will result in lower rate vocoders, new kinds of transmitted information and higher densities in VLSI. In addition, if capacity demands increase, even the first generation CDMA cellular architecture can be expanded: more base stations can be easily added to the network; the CDMA base unit can be "sectorized" to almost an unlimited number of sectors; and additional frequency channels can be added. There isn't a technology today which can match the dynamic ability of CDMA to adjust to varying channel conditions, traffic loads and services provided. Because of the ability of CDMA systems to grow and remain flexible in a number of applications as well as the implementation in cost efficient VLSI circuits, this technology could become the major transmission technique for many years to come.

In addition, the technology developed during the design of the CDMA cellular system can be used to solve a number of additional communication system requirements throughout the next decade. The first of these will be a PCN network based on the design of the CDMA cellular system, but using smaller geographic cells. Wireless PBX and advanced cordless telephones will also benefit through the use of CDMA technology. A major advantage to the CDMA solution versus various other systems is that one phone can be designed to operate with all these networks.

Although a basic understanding of CDMA technology has existed since the same timeframe as that first police car radio of the 1930's, its advantages have been largely restricted to complex military systems. Even though CDMA technology is only now gaining popularity for large scale commercial systems, the potential and promise of CDMA technology require further exploration and exploitation of this elegant and powerful communication science. The 1990's and beyond will see an explosive use of CDMA methods in voice communication systems as well as wireless data networks and other digital communication applications.

References:

[1] A. J. Viterbi, "Convolutional Codes and Their Performance in Communication Systems," *IEEE Trans. Commun. Technol.*, vol. COM-19, pp. 751-752, 1971.

[2] A. J. Viterbi, "Spread Spectrum Communications - Myths and Realities," *IEEE Commun. Mag.*, pp. 11-18, May 1979.

[3] K. S. Gilhousen, I. M. Jacobs, R. Padovani, A. J. Viterbi, L. A. Weaver, Jr., C. E. Wheatley III, "On the Capacity of a CDMA System," *IEEE Trans. Veh. Technol.*, vol. 40, no. 2, pp. 303-312, May 1991.

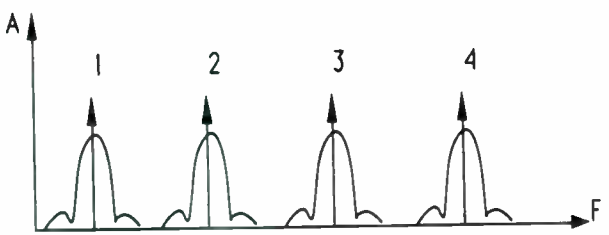

Figure 1. Frequency Division Multiple Access (FDMA)

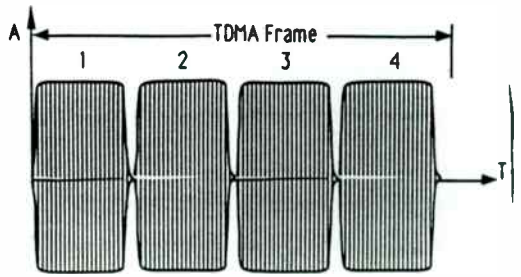

Figure 2. Time Division Multiple Access (TDMA)

Figure 3. Code Division Multiple Access (CDMA)

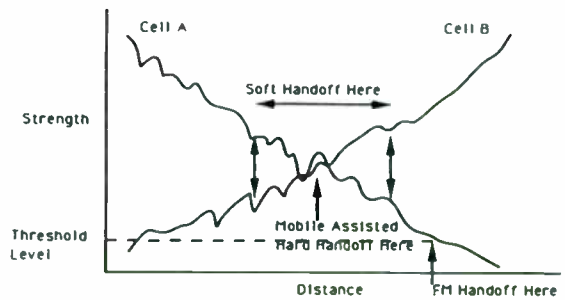

Figure 4. Soft Handoff Operation in the CDMA Cellular System

An Adaptive Technique For Improving Spread Spectrum Interference Rejection

John F. Doherty
Department of Electrical Engineering and Computer Engineering
Iowa State University

Abstract

An adaptive technique is presented that utilizes the known characteristics of the pseudo-noise spread spectrum sequence to enhance the detection capabilities diminished by interference excision. The new technique uses a constrained excision to decrease the bit error rate. The formation of constraint surfaces is the basis of the projection technique used in the adaptive update of the excsision filter. The constrained updating of the filter coefficeints retains the interference rejection properties of the excision filter while decreasing the variance of the decision variable. filter operates without training bits and requires little additional computational processing cost over a standard adaptive excision filter. Simulation results demonstrate the bit error rate improvement by using the constrained excision filter.

1 Introduction

The theory of spread spectrum communications for interference immunity is well founded [1]. The excision of narrowband interferences to improve the performance of direct sequence spread spectrum (DS-SS) systems has also received much attention [2, 3]. The role of the excision filter is to remove the interference prior to despreading of the received chip sequence. However, the nulling of the interference also induces distortion of the chip sequence resulting in a reduced correlation peak and reduced immunity to noise. The properties and performance of various adaptive algorithms for implementing the excision filter have been extensively researched [4, 5, 6]. However, these techniques only use the psuedo-white correlation property of the pseudo-noise (PN) sequence to extract it from the correlated interference. The PN sequence has additional structure that can be exploited to directly improve the estimate of the chip sequence and indirectly improve the decision variable.

The technique presented in this paper uses a constrained excision filter (CEF) at the output of the recieve filter. The constrained excision filter is able to selectively enhance the chip sequence while retaining the nulling properties of an uncaonstrained excision filter. This is accomplished by using projections onto constraint surfaces to adaptively update the excision filter. The constraint surfaces represent sets of solutions for the excision filter which force its output to satisfy certain known properties of the PN sequence. This type of projection updating is used extensively in image processing with excellent results [7].

2 Adaptive Excision Algorithm

The goal of the constrained excision filter (CEF) is to recover, as much as possible, the known properties of the original PN code. Thus, the objective is to enhance the input of the decision device

$$U = \sum_{k=1}^{L} \tilde{y}_k c_k \tag{1}$$

where $\tilde{y}_k$ is the output of the CEF. It has been shown that the adaptation process for discrete time filters can be formulated as a solution to a set of linear equations [8]. The adaptive excision filter output can be constrained to satisfy the linear constraint equation by using the projection update

$$\mathbf{h}_{k+1} = \mathbf{h}_k + \mu \left[d_k - \mathbf{h}_k^T \mathbf{v}_k \right] \mathbf{v}_k \Big/ \|\mathbf{v}_k\|^2 \tag{2}$$

where $\mathbf{v}_k$ are the filter state vectors and d_k represent the output constraint conditions. The step size μ determines the degree of agreement with the constraint. The filter can be made to satisfy various output constraints by appropriately choosing d_k and $\mathbf{v}_k$ in (2). The update equation (2) is identical in form to the normalized LMS (NLMS) update procedure. However, the interpretation is no longer restricted to reducing the correlation between a primary signal, d, and a reference signal, v. The removal of this restriction allows greater flexibility in adjusting the filter coefficients to produce the desired results. We may also apply the update equation (2) for any time instant $k \geq n$ by retaining the input vector $\mathbf{v}_n$. We will now discuss further choices for d_k and $\mathbf{v}_k$.

The primary goal of the CEF algorithm is the minimization of the output power, since this serves to remove the correlated interfence. This goal can be achieved by using an algorithm such as the LMS algorithm or the RLS adaptive algorithm to update the weights of a transversal (FIR) excision filter. The desired signal for the adaptive algorithm is taken as the value of the center tap of the transversal filter [4]. This implies a unity gain for the center tap coefficient. The RLS and LMS updates are optimal only for reducing the output power, which is analogous to removing self correlation of the signal. We will introduce other updates based upon constraining the output to conform to known properties of the PN sequence.

An auxiliary constraint used in the CEF algorithm is the one that maximizes the output of the despreading operation,

$$U = \sum_{k=1}^{L} \hat{c}_k p_k \tag{3a}$$

$$\hat{c}_k = \mathbf{h}^T \mathbf{x}_k = \tilde{A} p_k + e_k \tag{3b}$$

where the CEF state vector is comprised of the channel output,

$$\mathbf{x}_k = [r_{k-M}, \ldots, r_{k-1}, r_k, r_{k+1}, \ldots, r_{k+M}]^T$$

Rearranging (3a) we obtain

$$U = \tilde{A} \mathbf{h}^T \sum_{k=1}^{L} p_k \mathbf{x}_k \tag{4}$$

where $\tilde{A}$ equals the CEF estimate of the information bit. Defining, $\mathbf{u}^{(1)} = \sum_{k=1}^{L} p_k \mathbf{x}_k$, (4) becomes

$$U = \pm \mathbf{h}^T \mathbf{u}^{(1)} \tag{5}$$

The decision variable U is passed through a hard-limiter for the final decision on the information bit $\mathcal{A}$. In an ideal situation, $U = \pm L$ which leads to the following linear constraint,

$$\mathbf{h}_{k+1} = \mathbf{h}_k + \mu \left[L\mathcal{A} - \mathbf{h}_k^T \mathbf{u}^{(1)} \right] \mathbf{u}^{(1)} \Big/ \left\| \mathbf{u}^{(1)} \right\|^2 \tag{6}$$

The update in (6) causes the CEF coefficient vector $\mathbf{h}$ to produce a correlation peak that approaches L, the ideal correlation peak.

A second constraint equation arises from the partial sum conditions

$$s_m = \mathcal{A} \sum_{k=1}^{m} p_k \tag{7}$$

where $c_k = \mathcal{A} p_k$. A special case of (7) is $s_L = \pm 1$, that is, all the chips must sum to either ± 1, depending upon the information bit. This property can be applied to form a constraint on the excision filter output.

$$\mathcal{A} s_k = \mathbf{h}^T \mathbf{u}_k^{(2)} \tag{8}$$

where $\mathbf{u}_k^{(2)} = \sum_{n=1}^{k} \mathbf{x}_k$. Substituting (8) into (2) leads to the update equation

$$\mathbf{h}_{k+1} = \mathbf{h}_k + \mu \left[\mathcal{A} s_k - \mathbf{h}_k^T \mathbf{u}_k^{(2)} \right] \mathbf{u}_k^{(2)} \Big/ \left\| \mathbf{u}_k^{(2)} \right\|^2 \tag{9}$$

A third constraint is the one that forces the output of the CEF to equal the transmitted chip sequence

$$\mathcal{A} p_k = \mathbf{h}^T \mathbf{x}_k \tag{10}$$

An estimate of the information bit, $\mathcal{A}'$, can be obtained from the output of the excision filter

$$\mathcal{A}' = sgn \left(U = \sum_{k=1}^{L} y_k p_k \right) \tag{11}$$

where $sgn(\cdot)$ is the usual signum function and y_k is the output of the excision filter based upon the previous update interval.

3 Simulations

The CEF algorithm is simulated using the model of Figure 1. The discrete time input signal is taken as

$$r_k = c_k + i_k + n_k \tag{12}$$

where c_k is the chip sequence, i_k is the correlated interference, and n_k is the wideband noise. The interference is either narrowband or wideband and is uncorrelated with either the chip sequence or the random noise. The excision filter is the optimal linear filter obtained by using the recursive least-squares (RLS) algorithm to solve the discrete-time Weiner-Hopf equations [4]. The excision filter is a linear phase FIR filter and uses the center tap as a reference signal. The excision filter has 9 coefficients for the narrowband case and 21 coefficients for the wideband case. The PN code lengths used are 31 and 63.

Narrowband Simulations

The narrowband interference takes the form,

$$i_k = B\cos(\omega_s k + \theta) \tag{13}$$

where ω_s respresents the deviation from the carrier, θ is uniformly distributed over $(0, 2\pi]$. The frequency deviation of the interference chosen for simulations is $\omega_s = 0.2\pi$. The excision filter is configured with 9 taps and CEF algorithm operates with a step size of $\mu = 0.1$. The output mean square error (MSE) is shown in Figure 2.

The performance gain of the CEF is not predominant until the SNR reaches approximately 10dB. This is caused by the poor estimates of the information bits provided by the excision filter for low SNR.

3.1 Wideband Simulations

The wideband interference takes the form,

$$i_k = B\sum_{n=1}^{N} h_n \cos\left([\omega_s + \omega_0(n/N)]k + \theta_n\right) \tag{14}$$

where ω_0 is the spread of the wideband interference and h_n is the discrete Hamming window. The parameters of this simulation are $\omega_s = 0.2\pi$ and $\omega_0 = 0.05\pi$, so that the correlated interference occupies 10% of the signal bandwidth. The excision filter has 21 taps and CEF algorithm operates with a step size of $\mu = 0.1$. The MSE performance is shown in Figure 3 for a processing gain of 31 and in Figure 4 for a processing gain of 63. The average correlation with the PN sequence for the processing gain of 31 is shown in Figure 5. The CEF improves the correlation properties of the excision filter output.

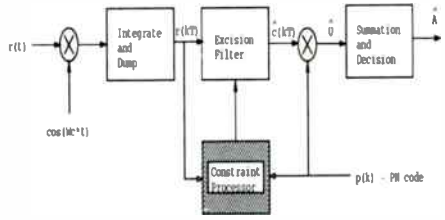

Figure 1: A block diagram of the direct sequence spread spectrum receiver. A typical configuration does not include the constraint processor. (shaded region). The constraint processor works in conjuction with the excision filter to reduce the output mean-square error.

4 Summary

An adaptive algorithm was presented that incorporated deterministic properties of spread spectrum direct sequences to improve interference rejection performance. The improved performance was demonstrated as a reduction in the mean square error at the output of the excision filter. The excision filter output correlation with the direct sequence was also shown to improve with the use of the new technique.

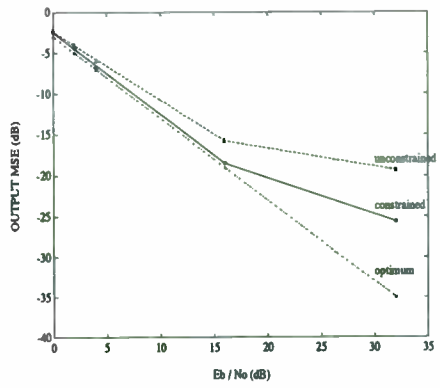

Figure 2: The mean square error performance curves for a tonal interference at $\omega_s = 0.2\pi$. The CEF (-o-) is compared to the standard excision filter (- - x - -) and to no interference (· — · * · — ·). SIR= -15dB. Processing gain : 31.

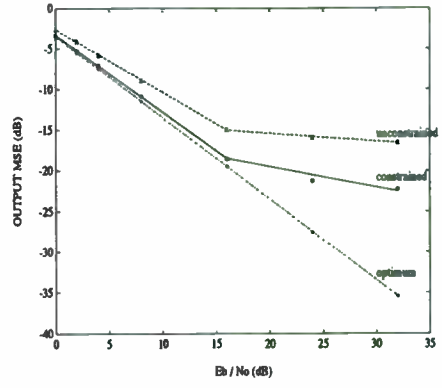

Figure 3: The mean square error performance curves for a wideband interference centered at $\omega_s = 0.225\pi$ and bandwidth $\omega_0 = 0.05\pi$. The CEF (-o-) is compared to the standard excision filter (- - x - -) and to no interference (· — · * · — ·). SIR = -15dB. Processing gain = 31.

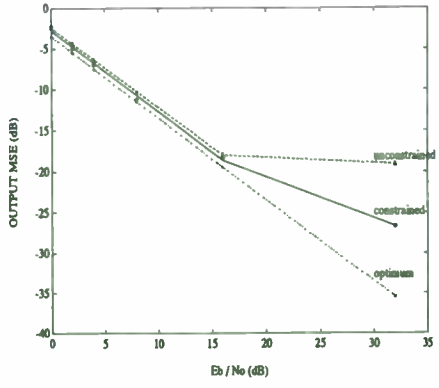

Figure 4: The mean square error performance curves for a wideband interference centered at $\omega_s = 0.225\pi$ and bandwidth $\omega_0 = 0.05\pi$. The CEF (-o-) is compared to the excision filter (- - x - -) and to no interference (· — · * · — ·). SIR = -15dB. Processing gain = 63.

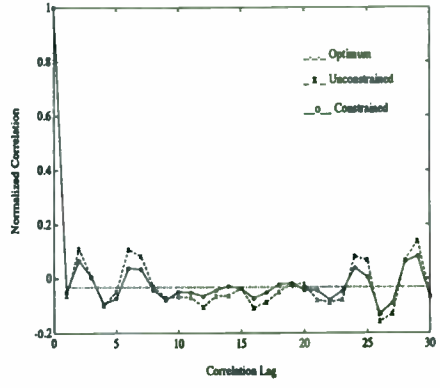

Figure 5: The average correlation of the filter output with the PN sequence for a wideband interference centered at $\omega_s = 0.225\pi$ and bandwidth $\omega_0 = 0.05\pi$. The CEF (-o-) is compared to the standard excision filter (- - x - -) and to no interference (· — · — ·). SIR = -15dB. Eb/No = 16 dB. Processing gain = 31.

References

[1] R. Pickholtz, D. Schilling, and L. Milstein, "Theory of spread-spectrum communications–a tutorial," *IEEE Transactions on Communications*, vol. COM-30, pp. 855–884, May 1982.

[2] S. Davidovici and E. Kanterakis, "Radiometric detection of direct sequence spread spectrum signals using interference rejection," *IEEE Transactions on Communications*, May 1989.

[3] L. Milstein, "Interference suppression to aid acquisition in direct-sequence spread-spectrum communication," *IEEE Transactions on Communications*, vol. 36, pp. 1200–1207, November 1988.

[4] L. Milstein and R. Iltis, "Signal processing for interference rejection in spread spectrum communications," *IEEE Acoustics, Speech, and Signal Processing Magazine*, vol. 3, pp. 18–31, April 1986.

[5] L. Milstein and P. Das, "An analysis of real-time transform domain filtering digital communication system, part i: Narrowband interference rejection," *IEEE Transactions on Communications*, vol. COM-28, pp. 816–824, June 1980.

[6] J. Ketchum and J. Proakis, "Adaptive algorithms for estimating and supressing narrowband interference in PN spread spectrum systems," *IEEE Transactions on Communications*, vol. COM-30, pp. 913–923, May 1982.

[7] C. Podilchuk and R. Mammone, "A comparison of projection techniques for image restoration," in *SPIE Proceedings on Electron Microscopy and Video Processing*, (Los Angeles, CA), January 1989.

[8] J. Doherty and R. Mammone, "A row-action projection algorithm for adaptive filtering," in *IEEE International Conference on Acoustics, Speech, and Signal Processing*, p. 20.D5.4, April 1990.

Simulation of Millimeter-Wave High-Power CW Frequency Doubling using Multi-Junction Varactors[1]

S.P.A. Bren, N.S. Dogan

Department of Electrical Engineering
and Computer Science
Washington State University
Pullman, WA 99163
Tel. No. 509-335-6602
Fax No. 509-335-3818

Abstract

Improved epitaxial growth techniques have allowed single-crystal growth of multiple *p-n* junctions with high precision. *N*-stacking of *p-n* junctions has been applied to varactor diodes to extend their maximum power handling capabilities. Theoretical large-signal and thermal models have been developed which simulate performance of these devices. The models have been implemented using FORTRAN and are user-interactive. Derivations of the models are briefly discussed. CW performance of a diode reported in the literature has been simulated and the results found in good agreement with experimental data. Theoretical performance of two diodes developed in our work are simulated and the results presented.

1. Introduction

Multi-watt power generation in the millimeter-wave frequency range has been dominated by IMPATT diodes. They are compact and simple solid-state sources of power. However,

1. This work was supported by the Boeing High Technology Center

their operation is noisy; matching problems arise continuously; and their high-temperature operation reduces usable life span. An alternative technique is to use a more efficient, lower frequency source coupled to a high efficiency frequency multiplier. Varactors are highly suitable for such a purpose.

Varactors are very efficient frequency multipliers. However, *p-n* junction characteristics have limited the maximum output power attainable by limiting the maximum voltage which may be applied. In the past, this constraint has been circumvented by stacking the diodes, or by bonding the diodes, in series. In recent years, high-precision epitaxial growth techniques have been developed which allow a simpler method of extending the maximum output power of these devices. Using the latest epitaxial techniques, impurity concentration and layer thickness can be controlled down to atomic dimensions and thus high-precision epitaxial layers may be grown and uniform impurity profiles achieved. In essence, *N*-diode stacking can be accomplished at the epitaxial level.

The varactor is a nonlinear device. In a restricted range of operation total capacitance of the diode is defined by the depletion-layer width which is a function of voltage. This nonlinear relationship between voltage and reactance is utilized in several ways. Parametric amplifiers and signal modulators are common applications of varactors. The nonlinear reactance can also be used to generate harmonics of a signal which, through appropriate filtering, results in frequency multiplication.

In order that varactor reactance be completely specified by the depletion-region, the applied voltage must be restricted. This range usually lies between forward contact potential ϕ and reverse breakdown voltage V_B and is determined by the impurity concentration and profile of the semiconductor. Thus, for a given doping density, the maximum power output

is severely bounded. Engineering development through the late 50's and 60's was able to overcome this hurdle through N-stacking of encapsulated diodes, or bonding of individual diodes, in series.

N-stacking of diodes in their individual encapsulations is a straightforward way of extending the voltage range of the varactor [1]; each diode then having its own casing and heatsink. This method is still commonly used for high-power applications. In the late 60's, Irvin and Swan [2] were able to stack individual diodes together through thermocompression bonding and the assembly then encapsulated. This method is most suitable for pulsed applications where high peak power but low average power is desired. The principle advantage of the new Integrated Series IMPATT Structure (ISIS) varactor over existing methods is that the series integration is accomplished at the epitaxial level.

ISIS techniques have been applied to IMPATT diodes as well [3,4], however significant difficulties are encountered in their design. The avalanche process used in IMPATTs is highly sensitive to temperature. Temperature differentials will exist among the diodes of the N-junction IMPATT. These temperature differential lead to nonuniform power generation among the diodes of the structure. Extra care must be taken when designing N-junction IMPATT diodes with respect to doping concentration and layer thickness's so that power generation among the diodes is uniform and oscillation frequencies are equal and in phase. These problems are avoided in N-junction varactor design.

The goal of our work has been straightforward: by increasing the number of junctions and the junction area by some integer N the power handling capability is theoretically increased by N^2 [1,5,6,7]. Accomplishing this task at the epitaxial level has a a number of advantages. Parasitics are reduced since single-junction encapsulations may still be used.

Enhanced thermal performance is achieved allowing both CW and pulsed applications. To examine the efficacy of this procedure a model was developed which simulates the device large-signal and thermal behavior. This model was then used to probe device operating characteristics. The model developed in our work was useful as a tool for analyzing diode potential before fabrication, thus minimizing costs and conserving efforts.

2. Large-signal ISIS Varactor Model

The frequency doubler is the simplest frequency multiplier circuit since no idlers are required. For the abrupt junction approximation closed form solutions are possible. Analysis of the varactor diode begins with the large-signal equation which is obtained by inspection of figure 1:

$$v(t) = Ri(t) + \int NS(t)i(t)dt \tag{1}$$

where N is the number of junctions and

$$R = NR_s + R_p \tag{2}$$

where R_s is the varactor series resistance and R_p is parasitic resistance. This equation is nonlinear since elastance is dependent on the stored charge of the depletion-region which is function of voltage. For CW operation, an input voltage signal of the form

$$v(t) = V_0 + V_s cos(\omega_0 t), \tag{3}$$

is assumed, where V_0 is the bias voltage and V_s is the signal voltage magnitude and the phase has been chosen without loss of generality. Using the one-sided abrupt-junction approximation, an expression is obtained relating elastance to applied voltage:

$$S(t) = S_{max}\left(\frac{\phi + v(t)}{\phi + V_B}\right)^{1/2} \tag{4}$$

where S_{max} is the elastance at forward contact potential ϕ. The Fourier coefficients of elastance are then found as

$$S_k = S_{max}\left(\frac{V_0+\phi}{V_B+\phi}\right)^{1/2}\frac{1}{\pi}\int_0^{\pi}\left(1+\left(\frac{V_s}{\phi+V_0}\right)cos(\omega_0 t)\right)^{1/2}cos(k\omega_0 t)d(\omega_0 t) \quad (5)$$

where $k = 0, 1, 2$.

Transforming equation (1) into the frequency domain and applying the appropriate boundary conditions (band pass filters at ω_0 and $2\omega_0$; see figure 2) obtains two coupled algebraic equations

$$\begin{bmatrix} V_1 \\ V_2 \end{bmatrix} = \begin{bmatrix} NS_2/j\omega_0 & R+NS_0/j\omega_0 & S_1^*/j\omega_0 \\ 0 & NS_1/j2\omega_0 & R+NS_0/j\omega_0 \end{bmatrix} \quad (6)$$

where "*" denotes the complex conjugate. From these equations, expressions for all the important quantities can be obtained. For example, for input and load impedance we obtain

$$Z_1 = R + NS_0/j\omega_0 + NS_2e^{-j\theta}/\omega_0 \quad (7)$$

and

$$Z_2 = -R - NS_0/j2\omega_0 + N^2S_1^2e^{j\theta}/2\omega_0 2NS_2 \quad (8)$$

respectively, and for input and output power we obtain

$$P_{in} = \frac{1}{2}\left|\frac{V_s^2}{Z_1}\right|cos(\angle Z_1) \quad (9)$$

and

$$P_{out} = \frac{1}{2}\left|2\frac{S_2}{S_1}\frac{V_s}{Z_1}\right|^2|Z_2|cos(\angle Z_2) \quad (10)$$

To calculate these quantities the simulation program first prompts for the necessary input parameters. Once the input parameters have been obtained, the first three fourier coefficients of elastance can then be found. Using the elastance coefficients and drive voltage parameters all the important varactor performance quantities can then be calculated.

3. ISIS Varactor Thermal Model

Other than breakdown voltage and frequency matching considerations, the primary limitations on varactor CW performance are thermal. Heat energy is generated in the diode as a result of series resistance in the active regions and substrate and is dissipated at a finite rate. This rate is determined by material parameters of the semiconductor device and its encapsulation.

Varactors are typically operated in the temperature range from 300 to $500K$. At higher temperatures ($500K$ and above) device performance becomes complicated by the increased intrinsic carrier concentration becoming appreciable to the impurity concentration. Leakage currents may increase to such a point that they contribute significantly to dissipation, and ultimately leading to thermal runaway. At still higher temperatures, eutetic points between metal-semiconductor contacts may be reached leading to permanent device degradation. In this work, maximum "safe" operating temperature was limited to $500K$.

Restricting the maximum operating temperature ultimately limits the maximum drive voltage at a particular frequency. This limitation is imposed on the large-signal model through integration with a second, thermal model.

Power dissipation is assumed to occur along a plane centered in the n-layer. The location of this plane along the diode axis defines a heat generation "node" (figure 3). The N-junction stack is assumed joined to a semi-infinite heatsink of gold or diamond (figure 4).

The rate of heat flow per unit time between two isothermal surfaces T_{i+1} and T_i is given by

$$T_{i+1} = T_i + P_i\theta_i \quad (11)$$

where P_i is the power flowing through the ith lamina and θ_i is the thermal resistance of the

ith lamina. The N-junction diode is divided into a series of lamina and N "nodes" (figure 5). Nodal temperatures are obtained iteratively.

The large-signal and thermal models have been implemented using MicroSoft FORTRAN and are user-interactive. The simulation program can be run from any PC. The user enters diode and drive voltage parameters and the program then simulates CW performance, such as input and output power, efficiency, etc.

4. Simulation Results

A diode reported by Williamson [8] was analyzed by the model. Diode epitaxial layer specifications are shown in table 1. The diode was assumed fully driven. Frequency doubler circuit ports were assumed matched to their complex conjugates. Series resistance was assumed to be $1.5 ohms$ which is typical of varactor frequency doublers using epitaxially grown diodes [9] and gave the best fit with our results. Williamson was able to achieve $2W$ at $44GHz$ at greater than 45% efficiency. Simulated performance by the model gave $2.4W$ at $44GHz$ at an efficiency of 46%.

We have also simulated 3- and 4-junction diodes with the profiles shown in tables 2 and 3, respectively. During fabrication of these diodes the substrate is completely removed, eliminating all substrate series resistance and improving thermal performance.

Thermal limitations are imposed upon the large-signal model through integration with the thermal model. As input frequency is increased input resistance decreases, thus boosting input power. However, efficiency declines, leading to increased power dissipation in the diode and elevating its CW temperature. When the hottest part of the diode, the junction most distant from the heatsink, reaches $500K$ then further increases in input frequency must be accompanied by a reduction in drive voltage amplitude so as not to exceed this temperature.

Mismatch at the output port also reduces efficiency, causing greater power dissipation in the diode. The effects of all these factors on varactor output power can be seen in figures 6 and 7 for the 3- and 4-junction diodes, respectively.

For each diode, the load was matched to a center frequency at the output of $40GHz$. Input frequency was then swept from $5GHz$ to $30GHz$ in $500MHz$ increments. The diodes were fully driven and series resistances were assumed to be $1.0 ohm$ for each diode.

The results suggest that given junction number, epitaxial layer specifications, and input frequency, an optimum junction diameter will exist.

In general, CW performance of the simulated diodes was found to be sensitive to varactor series resistance, effecting the efficiency by more than 10% for each $0.5 ohm$ change. Output power was less sensitive to variations in series resistance, assuming that input power could be varied as desired.

5. Conclusion

We have presented a model which simulates N-junction varactor CW performance. The simulation program developed in our work has proven useful as a tool for analyzing diode potential before fabrication, thus minimizing costs and conserving efforts.

Derivation of the model was briefly outlined. A diode reported in the literature [8] was analyzed by the program and simulated performance was found in good agreement with experimental data. Theoretical performances of two diodes with three and four junctions were presented.

Acknowledgements

The authors thank Dr. R. Shimoda of Boeing High Technology for the support of this work.

References

1 A. Uhlir Jr., "The Potential of Semiconductor Diodes in High Frequency Communications," Proc. IRE, **46**, 1958.

2 J.C. Irvine, C.B. Swan, "A Composite Varactor for Simultaneous High Power and High Efficiency Harmonic Generation," IEEE Trans. **ED-13**, 1966.

3 A. Christou, N.A. Papaniclou, "MBE GaAs Integrated IMPATT Structure," J. Vac. Sci. Tech. B, **3**, 1985.

4 N. Lam, "Analysis and Design of GaAs Integrated Series IMPATT Structures," M.S. Thesis, WSU, Pullman, WA 1988.

5 P.W. Staecker, M.E. Hines, F. Occhiuti, J.F. Cushman, "Multi-watt Power Generation at Millimeter Wave Frequencies using Epitaxially Stacked Varactor Diodes," IEEE MTT-S Digest, 1987.

6 P. Penfield Jr., R.P. Rafuse, *Varactor Applications*, M.I.T. Press, MA, 1962.

7 A.H. Watson, *Semiconductor Applications*, McGraw Hill, 1969.

8 I.M.H Williamson, J. Bowen, L. Koh, W. Gulloch, "High Power MM-Wave Frequency Multiplier Incorporating Multi-Junction GaAs Varactor Diodes," IEE Coll. Sol. State Micro. Gen., 10(1986).

9 D. Peterson, "The Varactor Power Frequency Multiplier," Microwave J., May 1990.

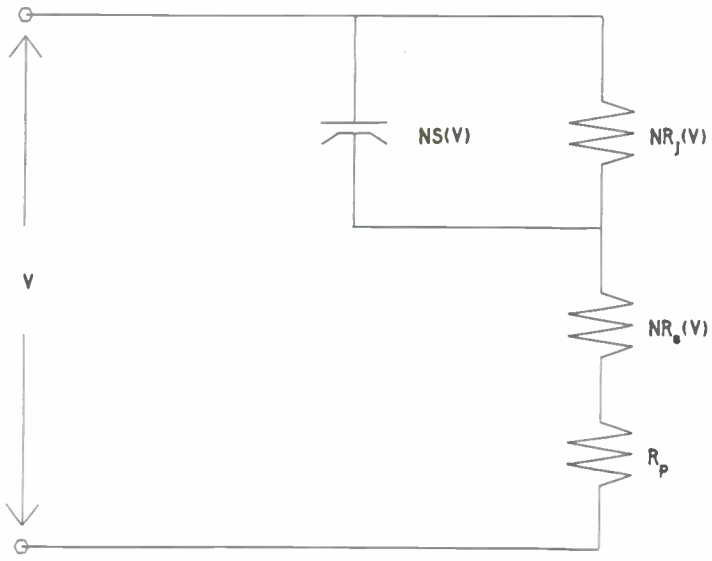

Figure 1. Large-signal model of the varactor and its encapsulation.

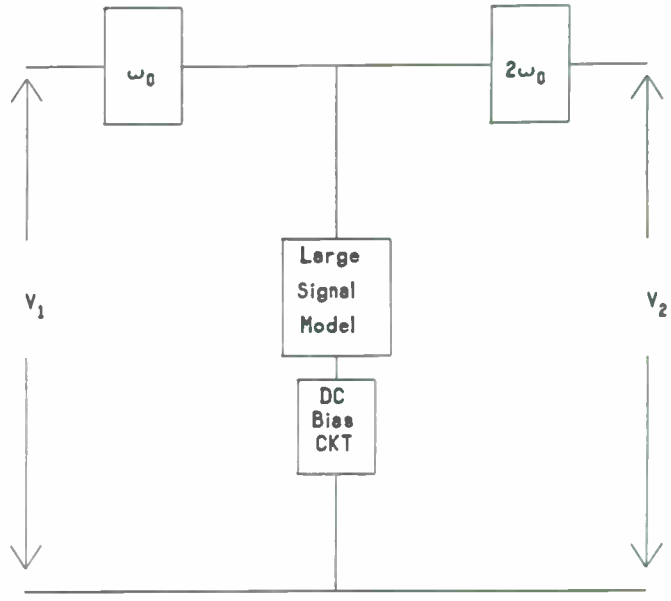

Figure 2. Frequency doubler circuit model with bandpass filters at ω_0 and $2\omega_0$.

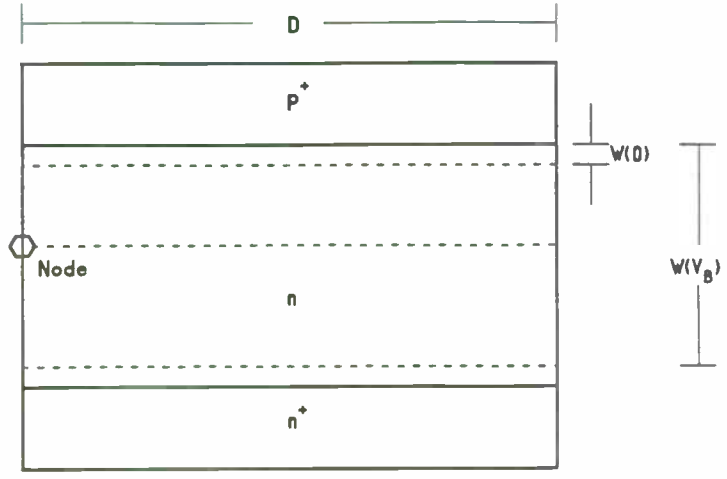

Figure 3. Location of average power dissipation in p-n junction diode. Width of depletion region, W, at V = 0 and V = V_B shown.

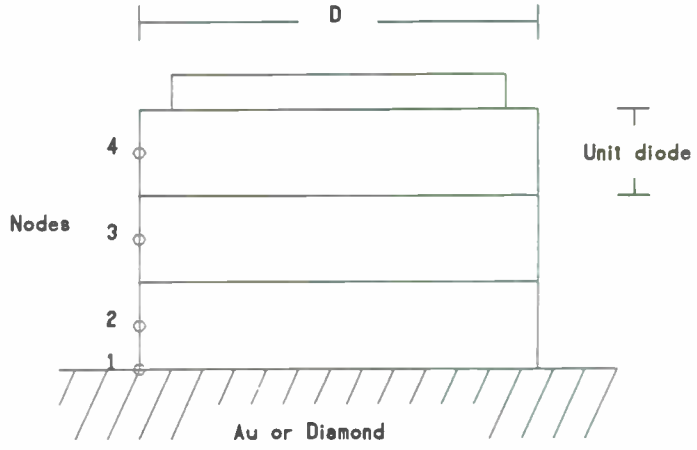

Figure 4. Thermal model of N-junction diode and heatsink.

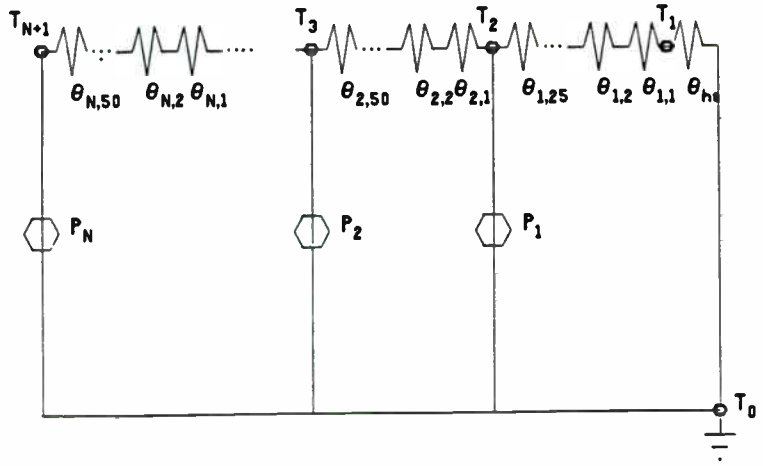

Figure 5. Electrical circuit analog of thermal model.

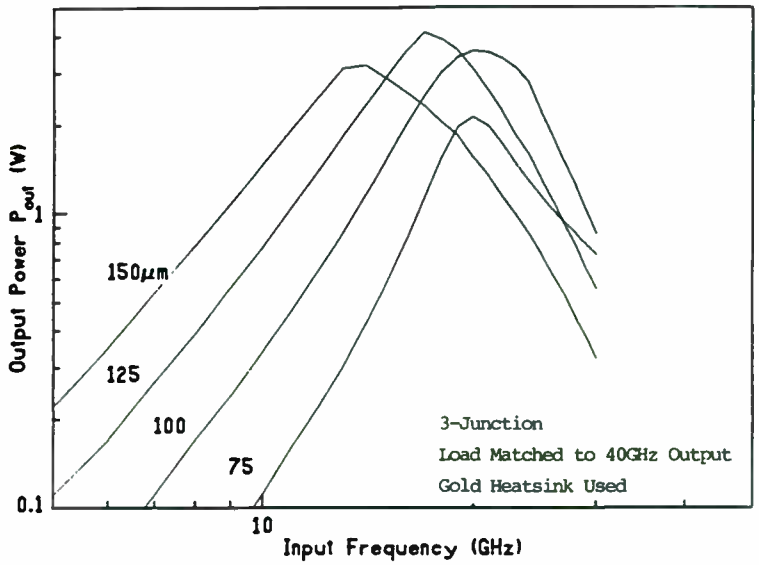

Figure 6. Effect of thermal limitations on output power P_{out} versus input frequency. 3-junction case. Center frequency: 20GHz.

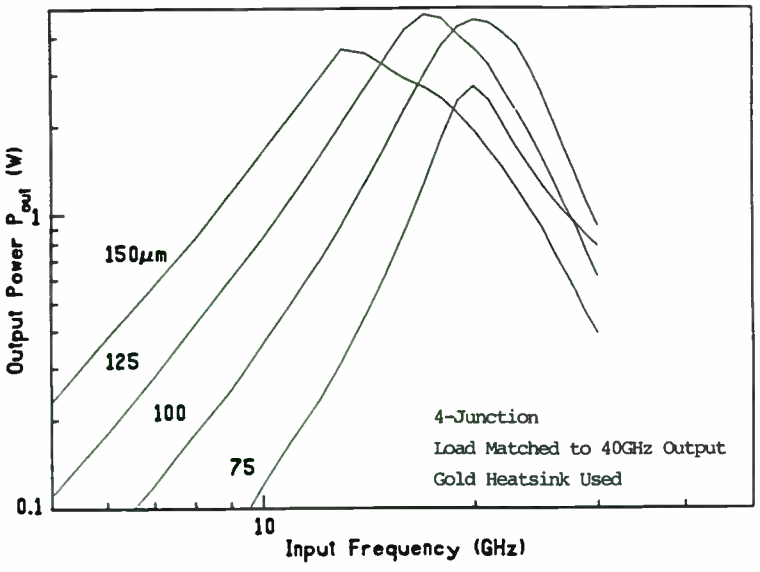

Figure 7. Effect of thermal limitations on output power P_{out} versus input frequency. 4-junction case. Center frequency: 20GHz

Table 1

2-Junction Stacked Varactor Diode IS21*

Epitaxial Layer Specifications

Layer	Type	um	cm^{-3}
6	n^+	1.2**	$1.1X10^{18}$
5	n	1.5	$2.1X10^{16}$
4	p^+	1.6	10^{19}
3	n^+	1.6	$1.1X10^{18}$
2	n	1.5	$2.1X10^{16}$
1	p^+	0.5	10^{19}

* Reported by Williamson

** Target value used

Table 2

3-Junction Stacked Varactor Diode

Epitaxial Layer Specifications

Layer	Type	um	cm^{-3}
9	n^+	0.6	$5X10^{18}$
8	n	1.5	$35X10^{15}$
7	p^+	0.6	$1X10^{19}$
6	n^+	0.6	$5X10^{18}$
5	n	1.5	$35X10^{15}$
4	p^+	0.6	$1X10^{19}$
3	n^+	0.6	$5X10^{18}$
2	n	1.5	$35X10^{15}$
1	p^+	0.6	$1X10^{19}$

Table 3

4-Junction Stacked Varactor Diode

Epitaxial Layer Specifications

Layer	Type	um	cm^{-3}
12	n^+	0.5	$5X10^{18}$
11	n	1.1	$40X10^{15}$
10	p^+	0.25	$1X10^{19}$
9	n^+	0.25	$5X10^{18}$
8	n	1.1	$40X10^{15}$
7	p^+	0.25	$1X10^{19}$
6	n^+	0.25	$5X10^{18}$
5	n	1.1	$40X10^{15}$
4	p^+	0.25	$1X10^{19}$
3	n^+	0.25	$5X10^{18}$
2	n	1.1	$40X10^{15}$
1	p^+	0.5	$1X10^{19}$

STUDIES OF THE CROSS ANTENNA

R. P. Haviland

MiniLab Instruments

P. O. Box 21086

Daytona Beach, FL 32121-1086

Abstract

The Cross antenna was developed by Antoine G. Roederer, French patent 85 10463. It is made of N straight-sided symmetrically arranged U-shaped elements in a plane, pointed to a common center, with adjacent element ends connected, mounted above a ground plane. The sides of the U are 180 degrees long, the ends 360/N degrees. As designed, one short side is interrupted, one end being fed against ground, the other loaded with a resistance to ground, to give a traveling wave feed. Because of the phase differences introduced by side lengths, the antenna produces a circularly polarized pattern, at right angles to the antenna plane. Typical pattern and performance data are given for the 4 arm Cross, with some data for thee 3 arm type. An alternate form, fed by series interruption of a side to give a standing wave antenna is described, and 4 arm performance shown.

INTRODUCTION

The common method of creating a circularly polarized signal uses two dipoles at right angles to each other, fed by signals of equal magnitude but at 90 degrees phase difference. There is, however, a radiator which produces essentially circular polarization from a single signal. This is the Helix antenna, which can be designed to produce nearly ideal circular polarization over an appreciable frequency range.

THE CROSS ANTENNA

Another method of producing circular polarization with a single feed has been developed by Antoine G. Roederer, and is described in French patent 85 10463, and in the reference. The concept involves N straight sided U shaped sections with the open ends facing a center point, and with the ends of adjacent U's connected. As seen from the basic four arm type shown in Fig. 1, a cross is formed, now the name of the antenna.

The conditions for circular polarization are threefold:

- the long sides of the arm are 180 electrical degrees in length,
- the end of the arms are 360/N degrees in length, N being the number of arms;
- the ensemble is fed as a traveling wave antenna.

The feed method suggested by the developer is to open one of the short side arms, and bend the two parts downward towards a ground plane. Feed is then between one end and the ground plane, with a load resistor between the other end and the ground.

As in the Beverage and other traveling wave antennas, the resistor absorbs the incident wave. Because of the geometry, there are now two half-wave elements at right angles, then a 90 degree phase shift, followed by another pair of half-wave radiators, etc.

CURRENT DISTRIBUTION

The current pattern can be seen in the Mininec derived plot of Fig. 2. This is for a frequency somewhat higher than that precisely meeting the three relations above. This and following data is for a 4 arm cross with long arms being 1/2 wave physical length at 300 MHZ, and 0.2 wavelength above an idea infinite ground plane. Conductor diameter is .006 meter.

The double sawtooth at the zero line is a coded representation of the position of the Mininec current pulses along the cross arms. Note that there is only one current pulse at the short arms. In the following, patterns should have the best accuracy. Drive impedance accuracy, especially for reactance, is likely to be relatively poor. This is a computer limitation, and a much larger computer would be required to get better simulation.

The current magnitude varies from 8 to about 1.5 amperes per kilovolt of drive. The least squares line is superimposed, showing that the current is composed of a component which decreases linearly with distance along the cross elements, plus a small standing wave component. Note that the connection between the cross and the ground plane is acting as a short section line transformer. Power input is 3.99 KW, with 2.96 KW being lost in the load resistor.

Comparison of the phase, the large sawtooth, and the connection codes shows that the requirement of 90 degree phase shift between arm sections is not exactly met at the frequency of analysis. This, plus the presence of a standing wave of current, means that the radiation will not be exactly circularly polarized at this frequency.

AXIAL RATIO

Fig. 3 shows the axial ratio as magnitude and phase angle for the on-axis radiation components. The exact degree of circular polarization in a function of the magnitude of the load resistance, and of operating frequency. Perfectly circular polarization is obtained at 306 MHZ with a load of 155 ohms. Axial ratio magnitude is not highly sensitive to frequency, and phase is insensitive to load resistance.

DRIVE IMPEDANCE

Drive impedance as a function of frequency and load resistance is

shown in Figs. 4 and 5. Note that there is a valus of load which makes the drive impedance essentially independent of frequency. The possibility of moving this to the value needed for best polarization circularity by choice of conductor size or by changing the spacing between the connections to the ground plane has not investigated.

PATTERNS

The H component patterns for 0 and 90 degrees is shown in Figs. 6 and 7, and the V component at 0 degrees in Fig. 8 The total component at 90 degrees is shown in Fig. 9. In all, the cross is horizontal and the zenith at the top of the charts. These are for a frequency of 305 MHZ, with a load of 150 ohms, very nearly conditions for ideal circular polarization.

Some of the minor lobe component is due to the connections from the arm to the ground plane. Since these are separated by one quarter wavelength, they are acting as short vertical radiators.

The main lobe gain against a linear antenna varies from about 7 to 10 DB.

OTHER CROSSES

Of the many other possible cross designs, only the three arm type was investigated for this study. A typical pattern is shown in Fig. 10. This is at a frequency of 300 MHZ, with a load resistance of 220 ohms.

As expected from the fact that there are fewer radiating sections, the gain is lower. It appears that the fawer radiators also means poorer cancellation of side lobes. These are sizeable in this example, partly because the load resistance is above the the value for best axial ratio.

The reference describes multi-turn and multi-arm types. Some of the multi-turn types use log-periodic values of arm width and length. The purpose is to increase the bandwidth of good axial ratio. Additionally, the multi-arm types should show slightly increased gain, since the occupied area is more nearly filled with radiators.

Because of computer limitations, these variations have not been investigated.

THE RESONANT CROSS

Instead of feeding the cross to produce a travelling wave pattern, resonant feed can be used. This can be done by breaking the cross of Fig. 1 at any convenient place, and connecting a two- wire feed.

Fig. 11 shows the total component gain of such a 4 arm cross spaced 0.2 wavelengths above an infinite perfect ground plane at 300 MHZ, the arms being 1/2 and 1/4 wavelength at this frequency. For analysis, feed was placed at the junction of a long and short arm.

This resonant cross gives a main lobe gain of 12 DB or more over a range of some 40 MHZ, good bandwidth for this degree of directivity. Lobe splitting occurs for frequencies about 25 MHZ removed from the nominal design frequency.

A point of interest is that the main lobe gain is a respectable 7.5 DB for a frequency range of at least 75 to 250 MHZ. In this range the antenna is operating as a form of Quad loop.

The ability to use this wide frequency range will depend on the system sensitivity to drive impedance. As shown in Figs. 12 and 13, both drive resistance and reactance vary widely. With a narrow band signal, automatic or manual "antenna match" will serve to compensate for the variation. For a wideband signal, a compensating network may be needed.

CONCLUSIONS

The cross antenna has good properties in both the traveling wave and standing wave versions. The first gives reasonable gain and good to perfect circular polarization. The second gives good gain over a reasonable bandwidth, and also reasonable gain over a wide bandwidth. Matching to standard line impedances will be easy for narrow band operation, but will require special steps if wide signal bandwidth is to be used in the wideband range.

There are possibilities for improvement in performance by such techniques as log-periodic spaced multiple turn designs.

It is recommended that large computer analysis of the basic design and variations be made for critical applications. The data presented here should be adequate for normal preliminary design.

REFERENCE: The Cross Antenna: A New Low-Profile Circulary Polarized Radiator, Antoine G. Roederer, IEEE Trans. Antennas and Propagation 38, 5, May 1990.

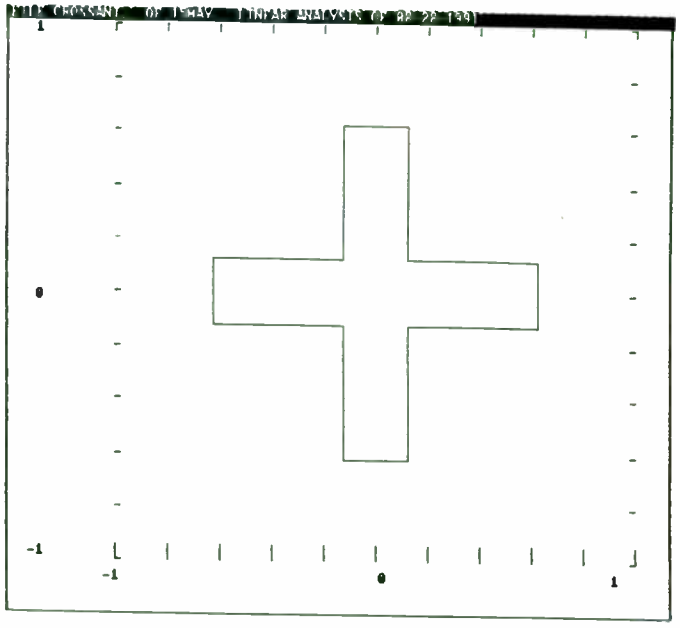

Fig. 1. Four arm cross, dimensions in meters for a nominal frequency of 300 MHz.

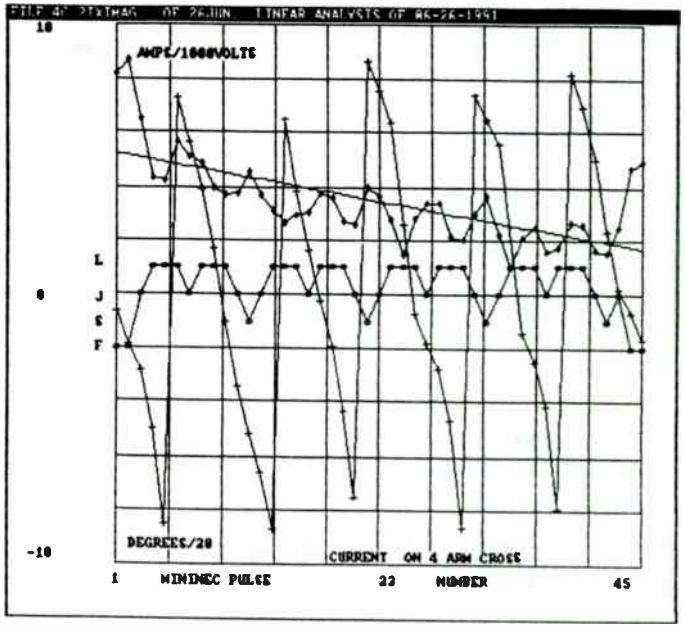

Fig. 2. Current distribution on the arms of a 4 arm cross. See text.

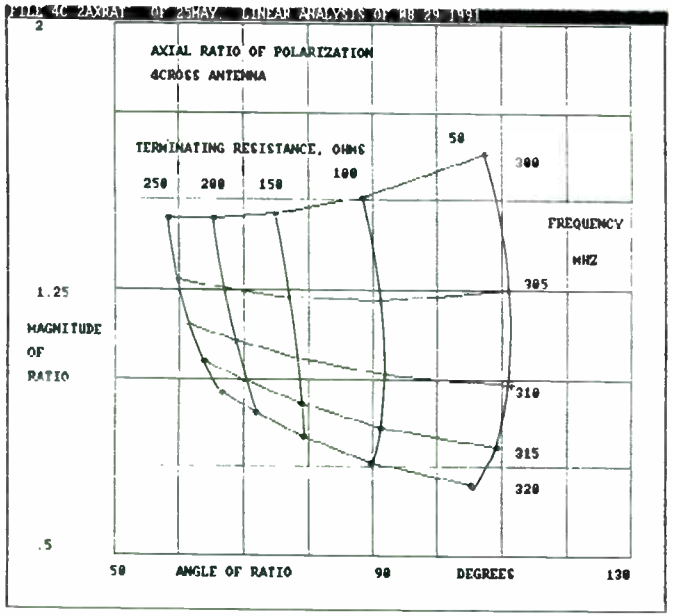

Fig. 3. Polarization axial ratio of a 4 arm cross as a function of frequency and terminating load resistance.

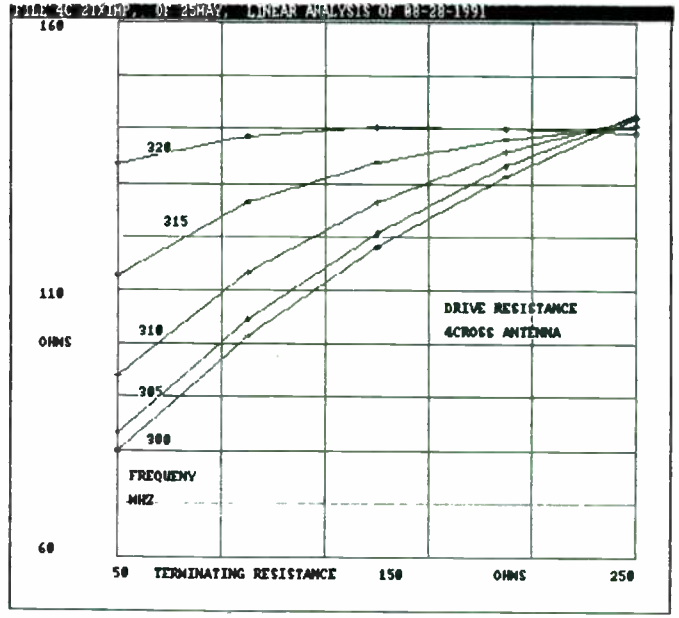

Fig. 4. Drive resistance of a 4 arm cross as a function of frequency and terminating load resistance.

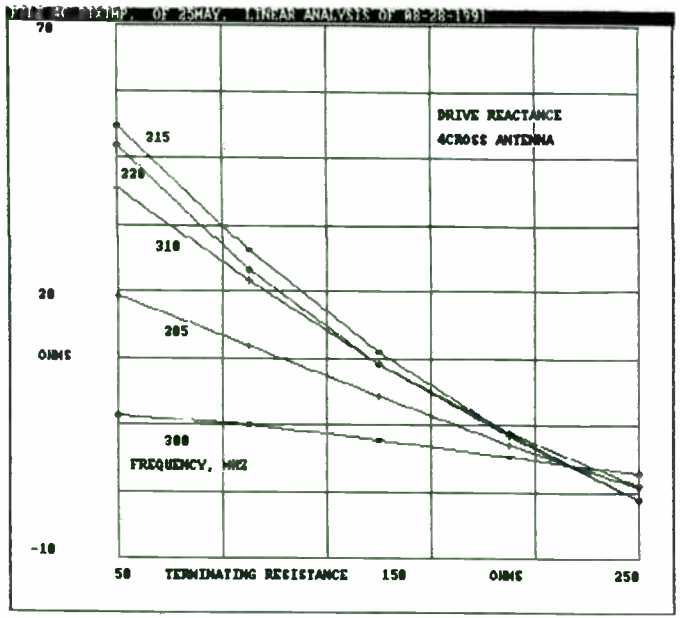

Fig. 5. Drive reactance of a 4 arm cross as a function of frequency and terminating load resistance.

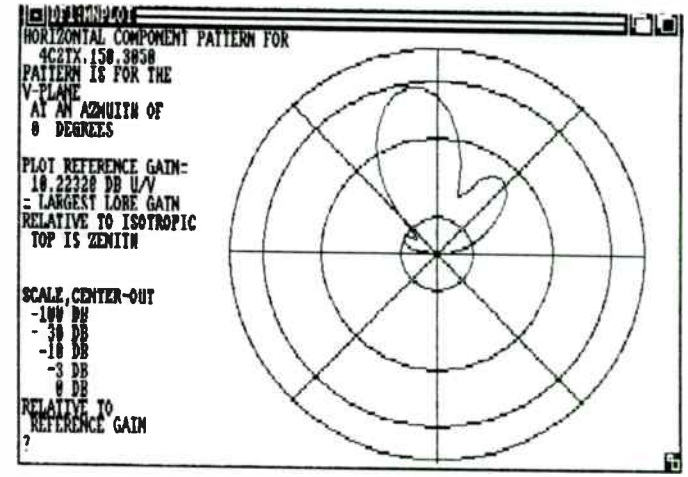

Fig. 6. Pattern for a 4 arm cross, for the "H" component in the plane intersecting the fed arm.

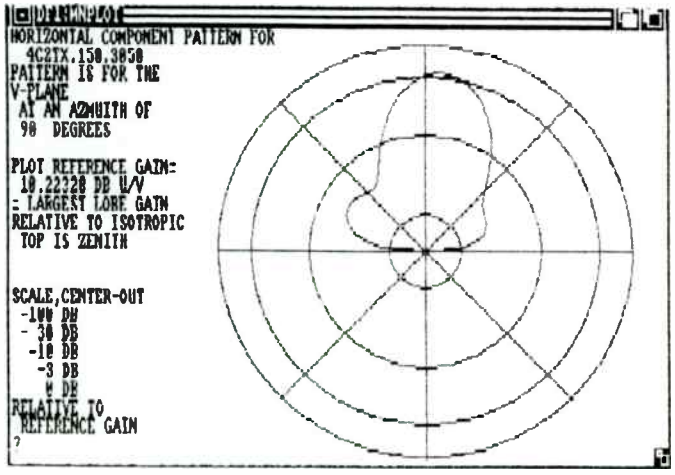

Fig. 7. Pattern for a 4 arm cross, for the "H" component in the plane parallel to the fed arm.

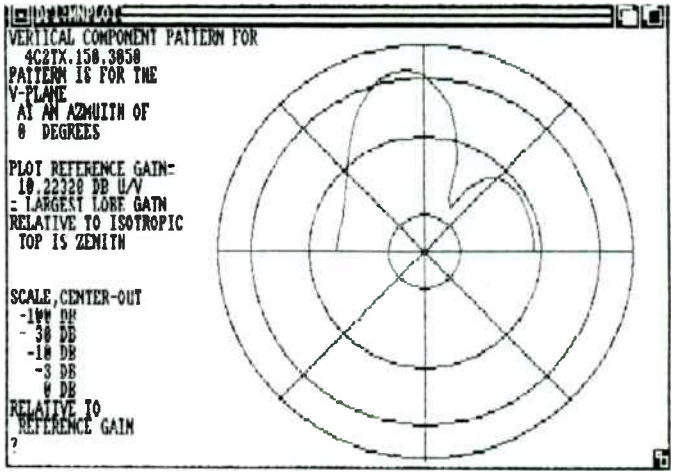

Fig. 8. Pattern for a 4 arm cross, for the "V" component in the plane intersecting the feed arm.

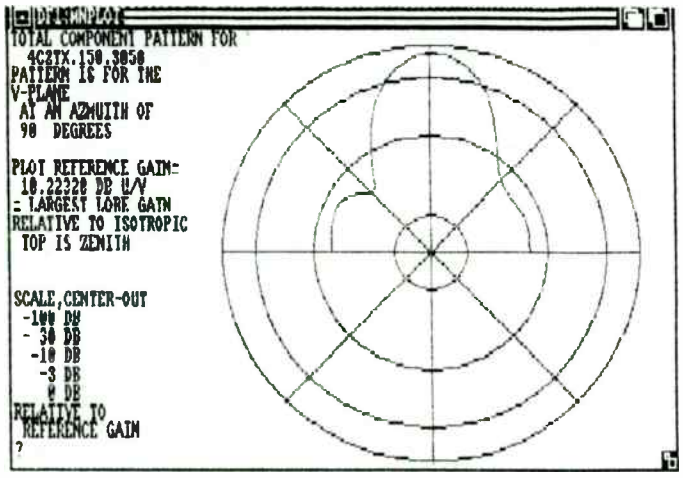

Fig. 9. Pattern for a 4 arm cross, for the total component in the plane parallel to the feed arm.

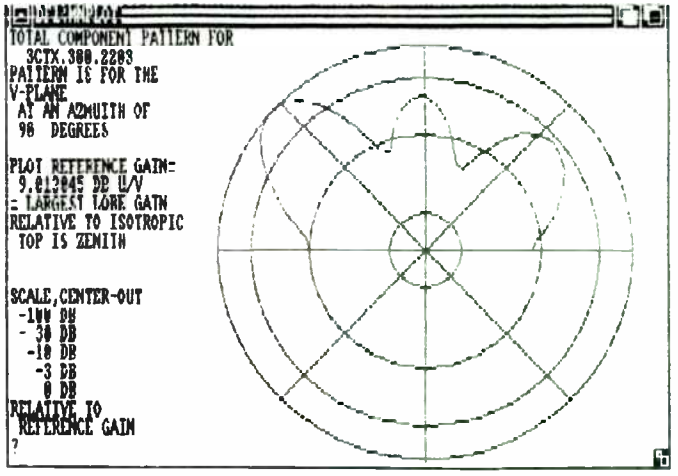

Fig. 10. Pattern for a 3 arm cross, for the total component in the plane parallel to the feed arm.

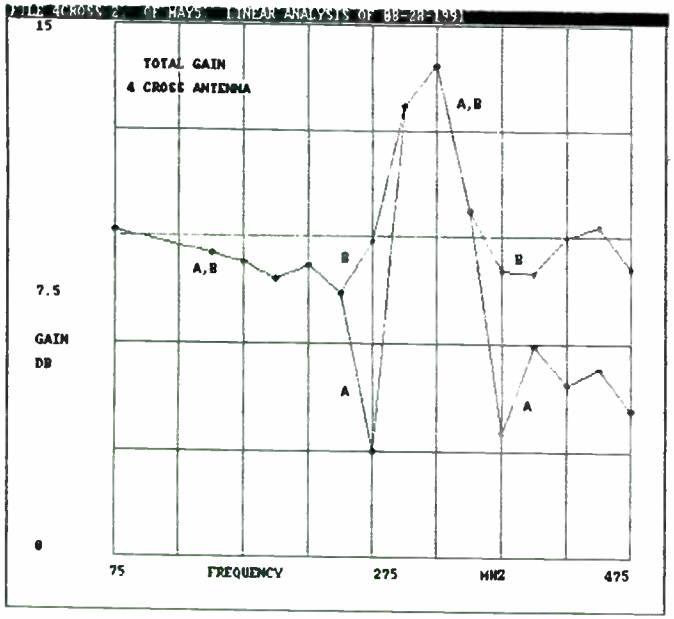

Fig. 11. Total gain of a standing wave 4 arm cross, for the lobe normal to the plane of the cross, and for the maximum lobe, for the frequency range 75-475 MHz.

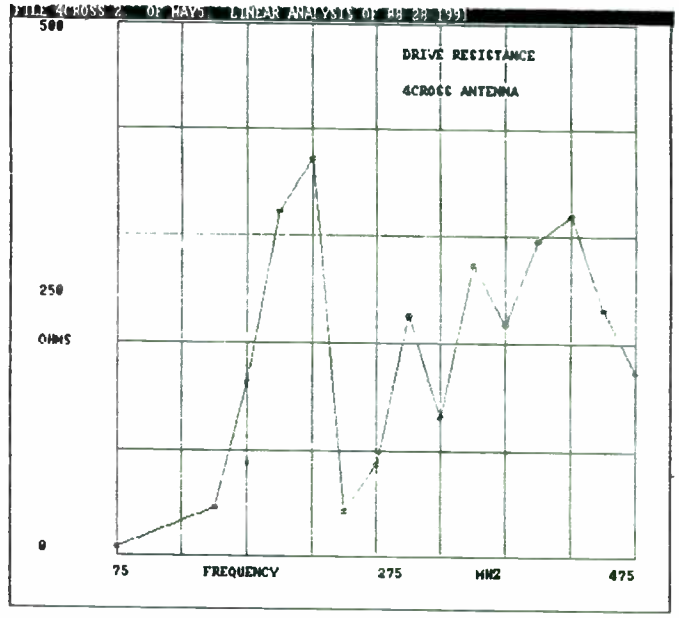

Fig. 12. Drive resistance of a standing wave 4 arm cross, for the frequency range 75-475 MHz.

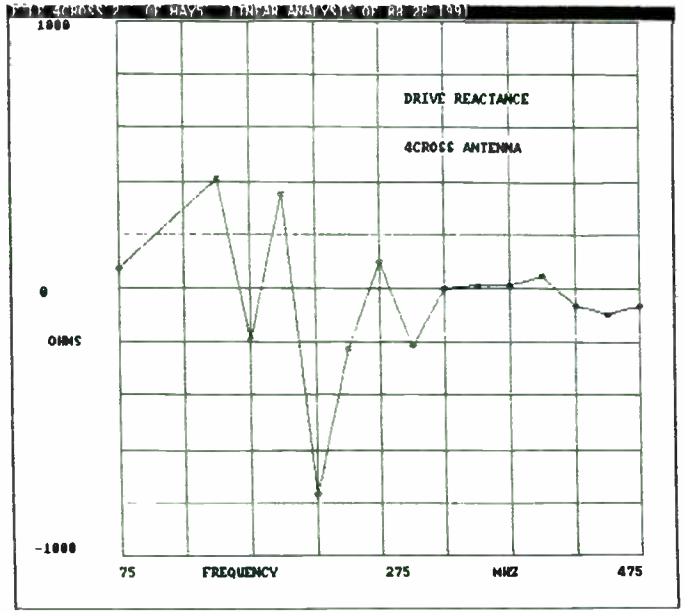

Fig. 13. Drive reactance of a standing wave 4 arm cross, for the frequency range 75-475 MHz.

A SIMPLE EXPRESSION FOR THE MUTUAL INDUCTANCE OF A WIRE CURRENT SOURCE AND A NON-COPLANAR, PARALLEL, RECTANGULAR LOOP

Byron D. Berman

Westinghouse Electric Corporation
P. O. Box 746, MS 504
Baltimore, Maryland 21203

ABSTRACT

A simple expression for the low frequency mutual inductance between an infinite straight wire and a non-coplanar, parallel, rectangular loop (both exhibiting negligible conductor cross-sections) is derived in terms of geometrical parameters. This expression is verified empirically by an indirect measurement. Several characteristics of the mutual inductance are identified and found comparable to mutual inductance features of a similar circuit geometry with the thin, source wire replaced by a finite length linear track (with small, rectangular cross-section). From the simple expression, a known formula for the mutual inductance of a straight wire and a coplanar, parallel, rectangular loop was derived as a special case.

1.0 BACKROUND

Previous efforts [1] to arrive at the mutual inductance between a linear current source, with a rectangular cross-section, and a non-coplanar, parallel, rectangular loop, with negligible cross-section, have yielded a double integral [1, equation (16)] with a lengthy integrand [1, equation (16A)]. Even when simplified with appropriate geometrical assumptions, the result still requires the numerical evaluation of a double integral [1, equations (16) and (16B)] to yield readily identifiable results. For the "front-line" design engineer, this kind of model can be an unwieldy tool, when used for gaining insight into the solution of multiple parasitic magnetic coupling problems. Under such circumstances, model simplicity may be paramount to model accuracy, provided that the predicted parasitic coupling trends are correct.

Clearly, it would be beneficial if a reasonably accurate, simple model of the mutual inductance were derived. Such a model is the purpose of this paper.

2.0 MUTUAL INDUCTANCE DERIVATIONS

Section 2.1 provides a derivation of the mutual inductance between a theoretical infinite length straight wire, and a non-coplanar, parallel rectangular wire loop, each of negligible conductor cross-section. A closed-form mathematical formula for the mutual inductance (equation 13) is presented. The formula is graphically presented in Section 2.2. Finally, in section 2.3, a familiar mutual inductance formula is derived as a special case of equation (13).

2.1 Derivation of Mutual Inductance

The mutual inductance associated with the flux lines sourced at circuit #1 linking circuit #2 is given by:

$$M = \Phi / I \quad \text{(Henries)} \qquad (1)$$

where: Φ = magnetic flux, in Webers, linking circuit #1 current to circuit #2

I = current , in Amperes, of circuit #1

In order to compute the mutual inductance using equation (1), the magnetic flux at circuit #2 must be computed in terms of the current in circuit #1. In order to do this, a description of both circuits in an appropriate coordinate system is required.

Figure 1 depicts circuit #1 as a straight wire of infinite length parallel to the z-axis and laying in the x-z plane at x = 0. A rectangular wire loop representing circuit #2 is located in a different plane, parallel to the x-z plane, but displaced the distance y = T. Hence, two sides of the loop are assumed parallel to the x-axis and the remaining two sides of the loop are assumed parallel to the z-axis. The size and shape of each wire cross-section is assumed to be negligible for the purposes of this derivation. The centerline of the loop is displaced relative to the straight wire of circuit #1 by a distance X, along the x-axis.

The origin of the coordinate system is located at the straight wire. The definition of the magnetic flux is given [3, page 8] by:

$$\Phi = \int \int \bar{B} \cdot \bar{n} \, dz \, dx \qquad (2)$$

where: n = unit vector, normal to loop area

B = magnetic flux density, in Teslas

$= \mu_o H$

μ_o = permeability of free-space,

$= 4\pi * 10^{-7}$ Henries/meter

$dx\, dz$ = differential area, (variable of integration)

The dot product between H and n is of the form:

$$\bar{H} \cdot \bar{n} = H \cdot \cos(\theta) \qquad (3)$$

where: θ = angle between H and n

= angle between radius vector r, and x-axis, (see Figure 2)

From the analytic geometry, cos (θ) becomes:

$$\cos(\theta) = \frac{x}{\sqrt{x^2 + T^2}} \qquad (4)$$

For the analytical representation of the magnetic field, the infinite length straight-wire model is used.

$$H = \frac{I}{2 \cdot \pi \cdot r} \qquad (5)$$

where: r = radial distance, in meters, from the wire source and some point of observation.

I = current flowing in + Z direction.

For this problem, the points of observation are within both the plane and area of the loop of circuit #2. Recomputing r:

$$r = \sqrt{x^2 + T^2} \qquad (6)$$

Substituting equations (4), (5), and (6) into equation (3), we get:

$$\bar{H} \cdot \bar{n} = \frac{I \cdot x}{2 \cdot \pi \cdot \left[x^2 + T^2\right]} \qquad (7)$$

The direction of H is determined from the direction of I, using the right-hand rule.

The limits of integration in the x-direction are determined from Figure 2. The x-variable begins at Xo-L and ends at Xo. From Figure 1, the domain of integration in the z-direction begins at -W/2 and ends at +W/2. Substituting these limits and equation (7) into the integral of equation (2), we obtain:

$$\Phi = \int_{Xo - L}^{Xo} \int_{\frac{-W}{2}}^{\frac{W}{2}} \mu o \cdot \frac{I \cdot x}{2 \cdot \pi \cdot \left[x^2 + T^2\right]} \, dz \, dx \qquad (8)$$

This definite integral becomes:

$$\Phi = \frac{\mu o \cdot I}{2 \cdot \pi} \cdot W \cdot \ln \sqrt{\frac{Xo^2 + T^2}{(Xo - L)^2 + T^2}} \qquad (9)$$

where: ln is the natural logarithm.

If we re-express Xo in terms of the offset (in the x-direction) of the centerline of the loop, X and the straight wire using the change of variables:

$$X = Xo - \frac{L}{2} \qquad (10)$$

and substitute equation (10) into the expression for the flux Φ:

$$\Phi = \frac{\mu o \cdot I}{2 \cdot \pi} \cdot W \cdot \ln \sqrt{\frac{\left[X + \frac{L}{2}\right]^2 + T^2}{\left[X - \frac{L}{2}\right]^2 + T^2}} \qquad (11)$$

Substituting equation (11) into equation (1), the expression for the mutual inductance becomes:

$$M = \frac{\mu o}{2 \cdot \pi} \cdot W \cdot \ln \sqrt{\frac{\left[X + \frac{L}{2}\right]^2 + T^2}{\left[X - \frac{L}{2}\right]^2 + T^2}} \qquad (12)$$

where: X = offset between loop circuit centerline and straight track, in meters

L = length of loop circuit, in meters

W = width of loop circuit, in meters

T = planar displacement, in meters, of circuits # and #2

2.2 Graphical Presentation of Mutual Inductance

Prior to plotting the mutual inductance , using the circuit geometrical parameters as independant variables, it is beneficial to reduce the expression of equation (12) to a form commonly found in the literature. It is worthy to note that the parameters within the radical may be any units of length, provided that the units are all the same. The natural logarithm function (ln) may be replaced by the common logarithm function (log) by using the identity:

$$\ln(N) = \log(N)/\log(e)$$

where: e = 2.718....

N = any real number greater than zero.

Also, incorporating the variables of the coefficient so that W is now in units of inches, we get the final result in μHenries:

$$M = 0.00508 \cdot W \cdot \left[2.303 \cdot \log \left[\sqrt{\frac{\left[X + \frac{L}{2}\right]^2 + T^2}{\left[X - \frac{L}{2}\right]^2 + T^2}}\right]\right] \qquad (13)$$

where: X = offset between loop circuit centerline and straight track, in inches

L = length of loop circuit, in inches

W = width of loop circuit, in inches

T = planar separation, in inches, of circuits #1 and #2

Equation (13) may be used as a basis for graphical presentation by normalizing the mutual inductance to the loop width W, and by normalizing both the offset X and the planar separation T to the loop length L. Figure 3 shows the normalized mutual inductance plotted against the normalized offset.The normalized planar separation is treated as a second independant variable.

Several conclusions may be determined from Figure 3. One characteristic is that for T < L/2, the inductance has a maximum value when the offset position is approximately one-half the loop length. Physically, this places one end of the loop almost directly over the straight wire. This effectively maximizes the flux linking the wire to the loop. As the offset is decreased, the normal component of the wire magnetic field has contributions in both directions, thereby reducing the total linking flux. As the offset approaches zero, the normal magnetic field components are equal and opposite, reducing the flux contribution to zero. Hence, the mutual inductance is minimized when the loop is symetrically placed over the straight wire. As the offset is increased beyond the half loop-length position, the inductan again begins to drop as the flux reduces with increasing distance from the straight wire.

These characteristics are qualitatively similar to those of the mutual inductance of a straight, finite length track (with rectangular cross-section) and a non-coplanar, parallel rectangular wire loop (with negligible cross-section) as shown in Figure 4 and [1, Figure 4]. Although the model of equation (13) may predict mutual inductance values approximately 3 to 10 times larger than the model of Reference [1], the basic trends in the relationship between geometrical parameters and mutual inductance are preserved. It is asserted, without proof, that the variance of mutual inductance values between the two models has its origin in the reduced contribution to the linked magnetic flux from the finite length current source (assuming very small conductor cross-section, compared to the geometrical offset and separation).

By computing the derivative of (13) with respect to X/L, and setting it equal to zero , the value of normalized offset which maximizes the mutual inductance is computed as:

$$\frac{X}{L} = \sqrt{\left[\frac{T}{L}\right]^2 + 0.25}$$

When the normalized mutual inductance is plotted as a function of normalized planar separation, using this value of normalized offset, the characteristic of the maximum normalized mutual inductance is displayed. See Figure 5.

2.3 Coplanar Loop Mutual Inductance

In order to analytically check the results of equation (13), the mutual inductance of a linear current source and a coplanar, parallel, rectangular loop, for which there is a published result [2, page 3] should be derivable as a special case of equation (13).

To accomplish this derivation, some modified definitions and a change of variables are required.

Let: A = length of finite wire (here, all end effects are ignored)

B = distance from source to farthest parallel conductor of loop, in inches, measured in the plane containing the loop

C = distance from source to nearest parallel conductor of loop, in inches, measured in the plane containing the loop

Then:

$$X = (B + C)/2 \quad . \qquad (14)$$

For values of offset X > L/2 (a requirement which prevents shorting the current source to the loop), let us assume that T = 0 (coplanar). Let the loop width W equal the wire length A. The loop length L becomes:

$$L = B - C \quad . \qquad (15)$$

Substituting these values for X, L, and T into equation (13), we get:

$$M = .00508 \cdot A \cdot \left[2.303 \cdot \log \left[\frac{\sqrt{\left[\frac{B + C}{2} + \frac{B - C}{2} \right]^2 + 0}}{\sqrt{\left[\frac{B + C}{2} - \frac{B - C}{2} \right]^2 + 0}} \right] \right]$$

This expression simplifies to:

$$M = .00508 \cdot A \cdot \left[2.303 \cdot \log \left[\sqrt{\frac{B^2}{C^2}} \right] \right]$$

yielding a final result of:

$$M = 0.00508 \cdot A \cdot \left[2.303 \cdot \log \left[\frac{B}{C} \right] \right] \quad \mu H.$$

This is expression is identical to the formula of [2]. Hence, the new analytical result is consistant with a previously established formula.

3.0 MEASUREMENT OF MUTUAL INDUCTANCE

Section 3.1 describes a test setup used to indirectly measure the mutual inductance of a straight wire and a rectangular loop. Sections 3.2 and 3.3 presents the test results and error analysis, respectively. Finally, Section 3.4 compares the empirical data with the theoretical predictions.

3.1 Description of Test

Figure 6 shows a schematic representation of the test setup. An HP 3325A Synthesizer is used as a 4 KHz. signal source for a Solar 6552-1A Audio Amplifier. The amplifier, in turn, drives 10.5

Amperes, peak-peak, of sinosoidal current through a 1 Ω resistor in series with 36" x 44.75" (vertical) rectangular loop of # 14 wire, which establishes the source magnetic field. The source loop size and geometry is selected in order to approximate the magnetic field from a single straight wire current source, for positions of observation at the upper 36" horizontal leg. (See Section 3.3 for further discussion concerning errors due to stray magnetic field contributions.)

The current through the source wire is measured using a Stoddart Model 91197-1 Current Probe. The probe output (designed to drive a 50 Ω load impedance) is connected via coaxial cable to a 50 Ω input channel of the Tektronix (TEK) Model 2465 oscilloscope. The calibrated probe factor at 4 KHz. is -10.35 dBΩ. The probe is positioned at the lower 36" horizontal leg of the source loop to minimize interactions with the source magnetic field (44.75 inches above).

The magnetic source loop is supported by a wooden laboratory bench-top and eight inches of stiff foam rubber. The 36" upper leg of the source loop is aligned with a horizontal "source loop" positioning grid. The perpendicular centerline of that leg is marked on that grid. Offset positions at 2.5", 4.0", 5.0", 6.0", and 7.0" from the wire are marked along that centerline, in the horizontal plane.

The magnetic pickup device, emulating an ideal rectangular loop circuit, is a 10" x 55/64" rectangular loop of # 14 wire with twisted leads, terminating in a BNC adaptor. A coaxial cable from the BNC adaptor connects to a 1 M Ω channel of the TEK 2465 scope, where the magnetically-induced open-circuit loop voltage is constantly measured.

The magnetic pickup loop is mounted to the underside of a masonite board for rigidity. The pickup loop is also aligned with a horizontal "pickup loop" positioning grid. The centerline of the loop at the 5" point along the length is marked. Dielectric shims are used to establish the loop separation from the magnetic source wire.

Positioning of the pickup loop is accomplished by first aligning the short side of the pickup loop parallel with the source wire, using the centerline and grids. The pickup loop is parallel displaced until the desired offset is achieved. The shims are then installed to provide the desired separation. The pickup loop orientation and offset are then checked before the position is fixed.

Once the pickup loop position is fixed relative to the 36" upper leg, the drive current level of 10.5 Amperes, peak-peak is monitored using the Stoddart 91197-1 Current Probe and the TEK 2465 Oscilloscope. For each fixed pickup loop position, the current probe voltage, the pickup loop voltage, the pickup loop offset distance and separation distance are recorded.

The selection of 4 KHz. as a test frequency was based on several requirements: to develop sufficient pickup loop voltage which is measurable on the TEK 2465 scope, to use the current probe at a specific calibrated frequency (rather than use the probe at an interpolated frequency), and to maintain an upper limit on source loop inductive reactance.

3.2 Test Results

Table 1 contains the raw voltage data taken during the test, for the various separations and offsets shown. In order to reduce this data, an additional formula needs to be derived.

The voltage developed at the pickup loop due to the current in the source wire is computed from:

$$V_{loop} = M \cdot 2 \cdot \pi \cdot f \cdot I_{wire}$$

where: M = mutual inductance

V_{loop} = sinosoidal peak-peak pickup loop output voltage

I = sinosoidal peak-peak source wire current

f = frequency, in Hertz.

Solving the equation for M yields:

$$M = \frac{V_{loop}}{2 \cdot \pi \cdot f \cdot I_{wire}} \qquad (16)$$

The Stoddart Current Probe output voltage and the wire current are related by the current probe factor T_{probe} (dBΩ) as shown in equation (17).

$$V_{probe} = I_{wire} \cdot 10^{\left[\frac{T_{probe}}{20}\right]} \qquad (17)$$

Solving equation (17) for I_{wire} and substituting the results into equation (16):

$$M = \frac{V_{loop}}{2 \cdot \pi \cdot f \cdot V_{probe}} \cdot 10^{\left[\frac{T_{probe}}{20}\right]} \qquad (18)$$

Substituting the probe factor and frequency into equation (18), the mutual inductance is calculated as:

$$M = \frac{V_{loop}}{V_{probe}} \cdot 12.09 \quad \mu H \qquad (19)$$

Application of the results of equation (19) to the raw data contained in Table 1 yields the values of mutual inductance (nH) in Table 2. See Figure 7 for a plot of the measured mutual inductance.

3.3 Error Analysis

3.3.1 Measurement Errors

The significant measurement errors are introduced in the loop voltage measurement, the probe voltage measurement, and the current probe factor measurement (performed as a calibration activity, independant of this author and this measurement effort). Using equation (18) as a starting point for the error analysis, the total differential of the mutual inductance is computed in terms of the partial derivatives:

$$dM = \frac{\delta M}{\delta V_{loop}} \cdot dV_{loop} + \frac{\delta M}{\delta V_{probe}} \cdot dV_{probe} + \frac{\delta M}{\delta T_{probe}} \cdot dT_{probe} \qquad (20)$$

After performing the differential calculus indicated in equation (20), and simplifying the expression:

$$dM = M \cdot \left[\frac{dV_{loop}}{V_{loop}} - \frac{dV_{probe}}{V_{probe}} + \frac{\ln(10)}{20} \cdot dT_{probe} \right] \qquad (21)$$

Each one of the error contributions are assessible. The current probe factor is measured to within +/- 0.5 dB at the calibration laboratory. The current probe voltage measurement error is constant at +/- 0.1 volt, peak-peak. The pickup loop voltage errors vary with the measurement, and are presented in Table 3. By applying the various error contributions to equation (21), the peak error (+/- dM), in nanohenries, is calculated. The errors are compared to the mutual inductance (M) in Table 4.

3.3.2 Stray Magnetic Field Contributions

The measurement site at the upper horizontal leg of the large current loop is intentionally located at the midpoint to maximize the distance (18 ") from the vertical legs. The magnetic field components from the vertical legs should not induce any significant voltages in the pickup loop since they are mostly coplanar with the pickup loop area. The field components from the lower horizontal leg is 44.75 inches away from the measurement site. Their strengths vary from 33 dB to 51 dB down from the magnetic field strength levels of interest at the measurement site, depending on the pickup loop separation. Hence, induced pickup loop voltages due to stray fields are insignificant.

To further minimize stray magnetic field contributions from external sources, the test was performed within a shielded enclosure.

3.3.3 Wire Separation Errors

The separation of the pickup loop and the source loop, as previously stated, is established by shimming the masonite board supporting the pickup loop above the surface supporting the source wire. Three separations are used: 0.125 ", 0.5 ", and 1.0 ". These values do not account for the finite thickness of the wires, 3/32 inch. Furthermore, the analysis of section 2 implies that the conductors are infinitesimally thin. Hence, the correct separation values for the measurement corresponds to the distance from wire-center to wire-center. These calculated separation values are: 0.031 ", 0.406 ", and 0.906 ", respectively.

3.3.4 Finite Length Source Wire

To minimize the effects of reduced flux contributions from a finite length source wire, the length of the upper (and lower) leg of the source was selected to be 36 inches, which is better than 40 times the pickup loop width.

3.4 Comparison of Empirical and Theoretical Data

Figure 8 shows the theoretical mutual inductances for the pickup loop dimension, offsets, and calculated separations used in the measurement. Figures 9, 10, and 11 show the empirical and theoretical mutual inductances for calculated separations 0.031 ", 0.406 ", and 0.906 " respectively, along with the associated errors.

The theoretical mutual inductances and the empirical mutual inductances agree within the accuracy of the measurement, except at two points. In Figure 10, the empirical curve is low for the 2.5 inch offset. In Figure 11, the empirical curve is high for the 5 inch offset.

4.0 CONCLUSIONS

A closed-form, simple analytical expression (equation 13) for the low frequency mutual inductance between an infinite length, linear current source and a non-coplanar, parallel, rectangular loop (both exhibiting negligible conductor cross-sections) has been derived in terms of the wire-to-loop planar separation, the loop dimensions, and the wire-to-loop lateral offset. From this expression, the more familiar expression for the mutual inductance of a straight wire and a coplanar, parallel, rectangular loop was derived as a special case. Equation (13) has been verified empirically by an indirect measurement for all but two of the fifteen data points taken.

Mutual inductance values computed when using equation (13) will be larger than the values predicted by the model of [1] for finite source circuit lengths that are equal to the pickup loop width. However, the qualitative relationships between mutual inductance and the circuit offset and planar separation are preserved in equation (13). Finally, equation (13) provides an easy-to-calculate upper bound on the mutual inductance values for the finite source length case.

REFERENCES

[1] Berman, Byron D., "The Mutual Inductance of a Linear Current Source and a Non-Coplanar, Parallel, Rectangular Loop", Symposium Record, 1989 IEEE National Symposium on Electromagnetic Compatibility, May 1989, pages 309-314.

[2] Condon, G. P., Printed Circuit Board and Wiring Design for EMI Control, R & B Enterprises, Washington, 1985

FIGURE 1 CIRCUIT GEOMETRY

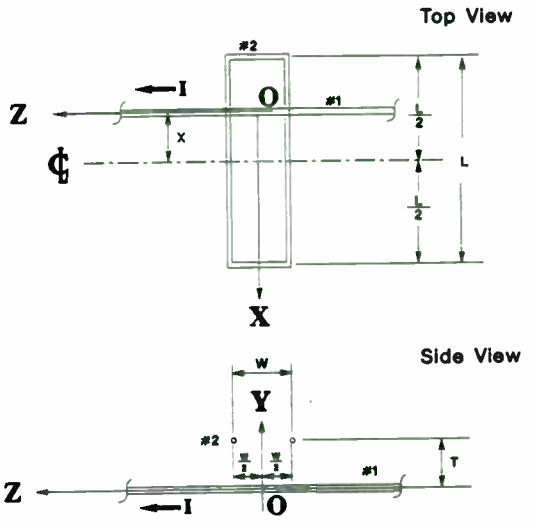

FIGURE 2 ORIENTATION OF FIELD VECTORS

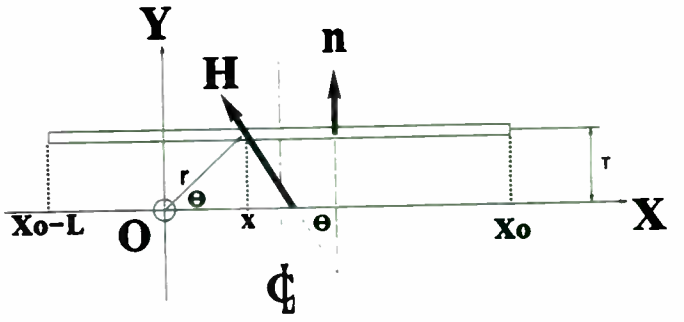

FIGURE 3 NORMALIZED MUTUAL INDUCTANCE

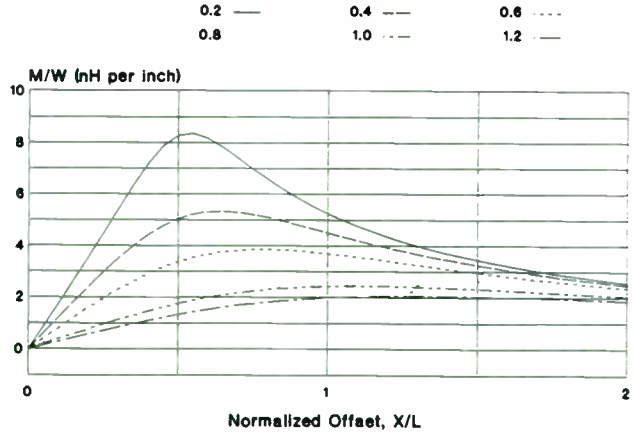

FIGURE 4 MUTUAL INDUCTANCE, FINITE LENGTH SOURC
WITH RECTANGULAR CROSS-SECTION (BASED ON REF [1] MOD

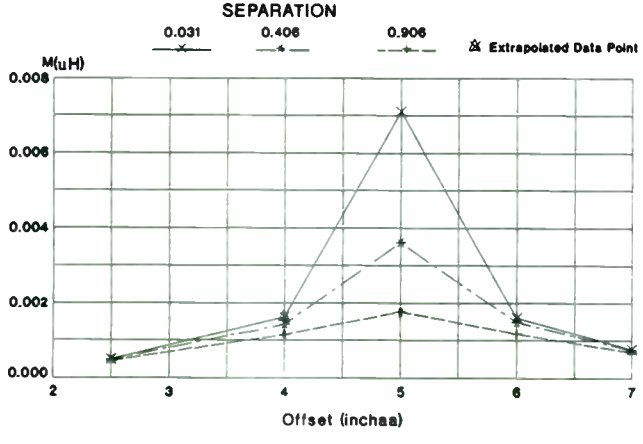

FIGURE 5 NORMALIZED MUTUAL INDUCTANCE, MAXIMIZED

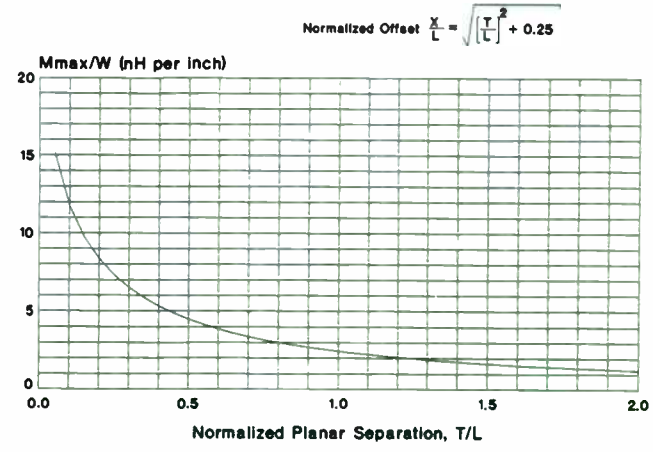

FIGURE 6 SCHEMATIC OF TEST SETUP

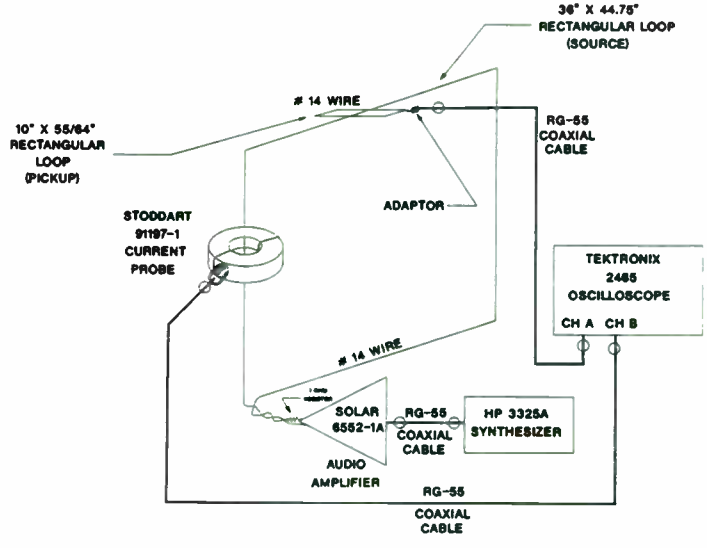

FIGURE 7 MEASURED MUTUAL INDUCTANCE

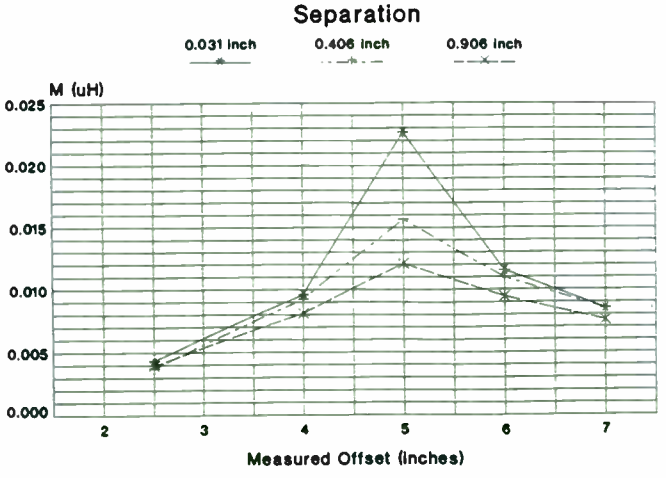

FIGURE 8 THEORETICAL MUTUAL INDUCTANCE

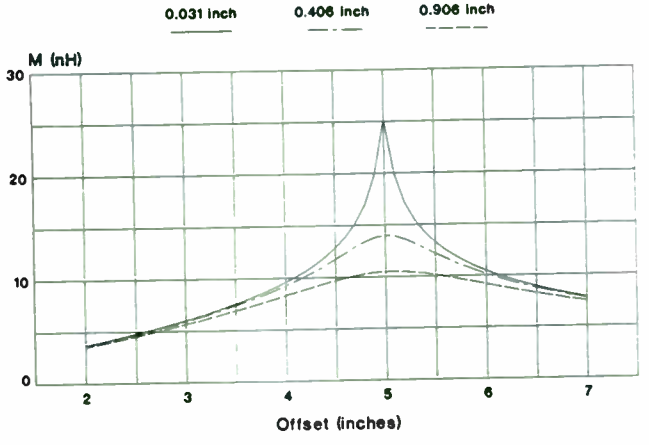

FIGURE 9 COMPARISON OF EMPIRICAL AND THEORETICAL MUTUAL INDUCTANCE (Separation = 0.031 inch)

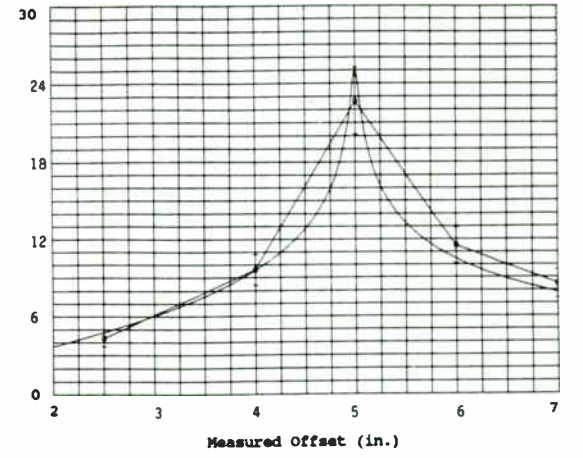

FIGURE 10 COMPARISON OF EMPIRICAL AND THEORETICAL MUTUAL INDUCTANCE (Separation = 0.406 inch)

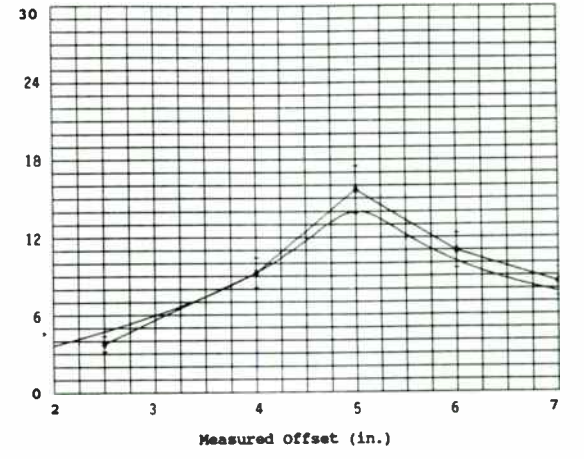

FIGURE 11 COMPARISON OF EMPIRICAL AND THEORETICAL MUTUAL INDUCTANCE (Separation = 0.906 inch)

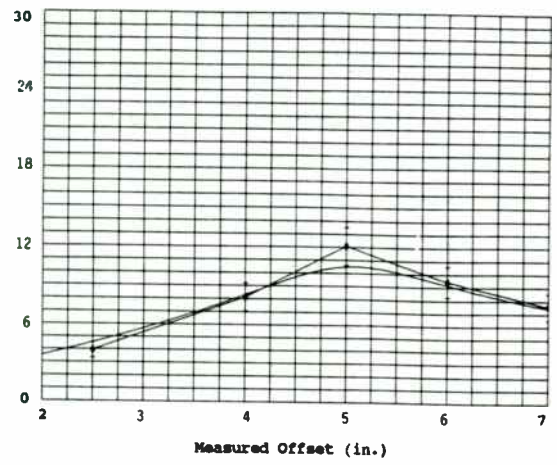

TABLE 1 RAW TEST DATA

MEASURED SEPARATION (Inches)	TEST PARAMETER (Units)	MEASURED OFFSET (Inches) 2.5	4.0	5.0	6.0	7.0
0.125	Vprobe (Vp-p)	3.2	3.2	3.2	3.2	3.2
	Vloop (mVp-p)	1.15	2.55	6.0	3.05	2.25
0.5	Vprobe (Vp-p)	3.2	3.2	3.2	3.2	3.2
	Vloop (mVp-p)	1.00	2.45	4.15	2.90	2.25
1.0	Vprobe (Vp-p)	3.2	3.2	3.2	3.2	3.2
	Vloop (mVp-p)	1.05	2.15	3.2	2.5	2.0

TABLE 2 MUTUAL INDUCTANCE (nH)

MEASURED SEPARATION (Inches)	MEASURED OFFSET (Inches) 2.5	4.0	5.0	6.0	7.0
0.125	4.343	9.631	22.66	11.52	8.498
0.5	3.777	9.253	15.67	10.95	8.498
1.0	3.966	8.120	12.08	9.442	7.553

TABLE 3

PICKUP LOOP
VOLTAGE MEASUREMENT
ERRORS (+/- mVolt, peak-peak)

MEASURED SEPARATION (Inches)	MEASURED OFFSET (Inches)				
	2.5	4.0	5.0	6.0	7.0
0.125	0.07	0.09	0.14	0.10	0.09
0.5	0.07	0.09	0.11	0.10	0.09
1.0	0.07	0.09	0.10	0.09	0.09

TABLE 4

PEAK ERRORS COMPARED
TO MUTUAL INDUCTANCE

MEASURED SEPARATION (Inches)	Mutual Inductance//Errors (nH)	MEASURED OFFSET (Inches)				
		2.5	4.0	5.0	6.0	7.0
0.125	M	4.343	9.631	22.66	11.52	8.498
	+/- dM	0.650	1.195	2.541	1.401	1.095
0.5	M	3.777	9.253	15.67	10.95	8.498
	+/- dM	0.600	1.162	1.807	1.350	1.095
1.0	M	3.966	8.120	12.08	9.442	7.553
	+/- dM	0.617	1.061	1.451	1.178	1.011

TRANSCEIVER CHARACTERISTICS AND THEIR IMPACT ON BATTERY LIFE PERFORMANCE IN LAND MOBILE AND CELLULAR PORTABLE RADIOS

MASOOD GHADAKSAZ

GTE Laboratories
Systems Technology Laboratory
40 Sylvan Road
Waltham, MA 02254

ABSTRACT

The technology of land mobile and cellular portable radio equipment has grown over the years. Technological advances in semiconductor devices and state-of-the-art circuit design techniques have led to considerable size reduction but only modest efficiency in power consumption. Portable radio operation relies on battery power as the primary source. A major challenge still posed to the portable radio designer is to achieve a sufficiently long battery life for higher transmitter power. Obtaining sufficient amount of transmitter power without excessive battery drain is a problem on all frequency bands. The public services which make considerable use of portable radios require long battery life (at least 8 hours) for their portable units at the rated antenna power. To conserve battery life in portable radios, a common practice is to limit the transmitter power. However, low transmitter power in portable radio operation is a handicap and can limit the ability of the operator to communicate over the desired range particularly in heavily built-up areas and in today's congested spectrum. There are many factors such as PA efficiency, receive current drain, transmitter circuit loss, standby current, duty cycle,...ctc. which combine to drain the battery system of the portable radio. Because these factors place limits on the battery life and hence on the performance of the portable communication system, it is necessary to provide accurate information about the battery life performance as a function of RF transceiver parameters which gives a clear insight into the impact of portable transceiver design on the battery life performance. This paper descibes a method of battery life performance characterization in terms of RF transceiver parameters of the land mobile and cellular portable radio equipment and gives measured and analytical results of the studies conducted to determine the impact of these parameters on the battery life performance.

Introduction

There are a number of controllable parameters in the design and operation schemes of the portable radio transceivers that have direct influence on the battery life performance of the portable power system. These include RF power amplifier (PA) efficiency, receive current drain, transmitter circuit loss, standby current drain, duty cycle,..etc. which combine to drain the battery system. Ideally the DC current drain of the portable radio should be as small as possible and the RF PA efficiency should be as high as possible. The DC current drain in the portable radio transceiver is primarily due to the need to DC bias and drive various active circuits in the transmitter and receiver chains such as RF and IF amplifiers, mixers, T/R switch, frequency synthesizers; audio circuits, control and logic circuits...etc. The RF transceiver design has a strong influence over the current drain control under transmit, receive, and standby conditions and if they are not carefully administered early in the design with regard to selection of active components and devices and the performance of individual circuits can indeed cause rapid battery drain. In practice however, for reasons of hardware economy and size reduction the importance of battery life performance is either ignored or overlooked in the product design and development. It is always a good design practice to assign a budget for DC current drain just as it has been done for other parameters such as noise, bandwidth,..etc.

There are a number of ways by which battery life can be conserved such as selectable RF power output (also known as battery saving mode), shorter talk time to maintain a reasonable duty cycle, use of high capacity batteries...etc. But it is generally conceded that, provided certain conditions are met, these solutions can in fact cause a serious handicap in the operation of the portable radio. For instance, limiting the transmitter RF

power can seriously limit the ability of the user to communicate over the desired range particularly in heavily built-up urban areas and in the presence of other transmitters operating within the coverage area. Similarly shorter talk time is not always a viable solution specially for public services where emergencies are frequent. Furthermore high capacity rechargeable nickel-cadmium (NiCad) batteries have bulky and heavy weight packages which make them cumbersome for the portable radio user.

It is also desired to use higher capacity rechargeable batteries in small light weight packages to achieve longer battery life for portable radio operation. Almost all rechargeable batteries used in portable radio products use NiCad cells. NiCad cells continue to dominate the rechargeable portable battery market. Developments in recent years to improve battery performane in terms of capacity, cost, size, and weight have only made little progress. Compact portable land mobile and cellular radio design poses new challenges to the portable rechargeable battery industry. The demand for more RF power and longer battery life in portable radio system although contradictory is on the rise. Portable rechargeable batteries with higher capacity in small light weight packages can provide a partial solution to accommodate the growing need for higher power portables with longer battery life.

In order to design portable radio transceivers with optimum compromise between performance, battery life, and cost some knowledge of battery life performance as a function of transceiver design parameters is required. In this paper using parametric characterization the impact of parameters associated with the RF transceiver design and operation on the battery life performane will be discussed.

Parametric Characterization

To conduct parametric characterization of the battery life performance, mean values for major parameters influencing battery drain must be established. These parameters include total receive current drain, total standby current drain, total transmit current drain, transmitter insertion loss, power amplifier efficincy, battery capacity and voltage, power at antenna output, and duty cycle. Table 1 lists the mean values used for each parameter. These values are based on actual measurements and are used in a life performance model for the portable battery system. The battery life performance model is used in a computer program to make accurate predictions of the battery life as a function of one or several variables.

Transmitter Impact on Battery Life Performance

In the transmitter circuit of a portable radio the major factors that contribute the most to the battery drain are; (i) RF power amplifier efficiency, and (ii) transmit path loss. Figure 1 shows simplified system block diagram of a modern portable radio transceiver. The total current drain in the transmit mode is largely a function of the PA efficiency but it is a sum of the PA current,T/R switch current, transmit synthesizer current, standby current,..etc. Path loss in both transmitter and receiver circuits strongly influence battery life performance. In the transmitter circuit ,for example, a harmonic lowpass filter while needed to suppress harmonic and spurious emissions if it is too lossy can lead to rapid battery drain. Insertion loss due to a harmonic filter, directional coupler, T/R switch, antenna connector,..etc. in the transmitter circuit reduce power transfer to the antenna. As a result more RF power must be generated to compensate for such losses in order to achieve the desired power output at the antenna port. The additional power that must be generated to compensate for the transmit path loss will require the amplifier stages to draw more current thus resulting in faster battery discharge and hence shorter battery life. Figure 2 shows the effect of increasing insertion loss on transmit current drain for two values of antenna power. It is evident that at high transmit power level this effect is more pronounced. The impact of transmitter insertion loss on battery life performance has been studied and sample results are shown in Figure 3 at 5-5-90 duty cycle and for 1200 mAH and 800 mAH batteries where one dB reduction in insertion loss can improve the battery life by as much as 55 minutes at 6 W and 35 minutes at 750 mW at 5-5-90 duty cycle. Sample results for battery life performance as a function of power amplifier efficiency are shown in Figures 4 and 5. It is evident that at 45% efficiency and at 5-5-90 duty cycle only with high capacity batteries (1500 mAH and 1700 mAH) will be able to achieve 8 hours of battery life for given mean values. These batteries as was discussed earlier are bulky and heavy and are considered to be unwieldy. If however, the duty cycle is

increased to 10-10-80, 8 hours of battery life can only be achieved if PA efficiency can exceed 80% and using 1700 mAH battery. In practice the efficiency of power amplifiers used in portable radio transmitters whether hybrid or discrete is typically between 40 to 45%. Figures 6, 7, and 8 show the impact of PA efficiency on battery life as a function of antenna power. At 5-5-90 duty cycle for the mean values and using a 1200 mAH battery 8 hours of battery life can only be met if antenna power is reduced to less than 4.5 W. If either the duty cycle is increased to 10-10-80 or battery capacity is reduced to 800 mAH this power must further be reduced to about 1.5 W to achieve 8 hours of battery life.

Receiver Impact on Battery Life Performance

The major factors in the receiver circuit responsible for the battery drain are; (i) receive current and (ii) standby current. Figure 9(a) and (b) show the effect of varying receive and standby current drain on battery life. Although both clearly demonstrate this effect the stanby current drain has the highest degree of impact on the battery life performance and this is more pronounced at 5-5-90 duty cycle for an obvious reason. At 5-5-90 duty cycle the radio is in the standby mode for 90% of the time and as a result the degree of impact by the standby current drain on the battery life performance despite its magnitude (60 mA) is remakable. For example at 5-5-90 duty cycle 50% reduction in the standby current drain corresponds to a battery life saving of as much as 1 hour and 10 minutes while battery life saving for 50% reduction in receive current drain only amounts to 27 minutes. The effect of the variation in the magnitude of each current for 800 mAH battery at 5-5-90 and 10-10-80 duty cycles has also been computed and sample plots are shown in Figures 10(a) and (b). The impact of standby current drain variation on the battery life performance with 800 mAH battery at 5-5-90 duty cycle is reduced but remains significant. Under these conditions 50% reduction in standby current drain will amount to a saving of about 44 minutes while the saving for 50% reduction in receive current drain is less than 8 minutes. A comparison of the battery life performance as a function of receive and standby current drain is shown in Figure 11. It is evident that if effort is to be made to improve battery life performance it has to be concentrated on components, devices, and circuits that control the standby current.

Conclusions

Of all the parameters examined in this paper RF power amplifier efficiency demonstrates the highest degree of impact on the battery life performance. Figures 12(a) and (b) clearly testify to this fact. The degree of impact on the battery life performance by the RF amplifier efficiency varies markedly with duty cycle compared to other parameters considered in this study.

Table 1
Parametric assumptions for battery life predictions

Parameter	Symbol	Mean Value	Unit
Receive current	I_{rx}	200	mA
Standby current	I_{sy}	60	mA
Transmit current	I_{tx}	2.37	A
Transmitter insertion loss	L_{tx}	1.25	dB
Power amplifier efficiency	η	45	%
Battery voltage	V_b	7.5	V
Power at antenna output	P_{ant}	6	W

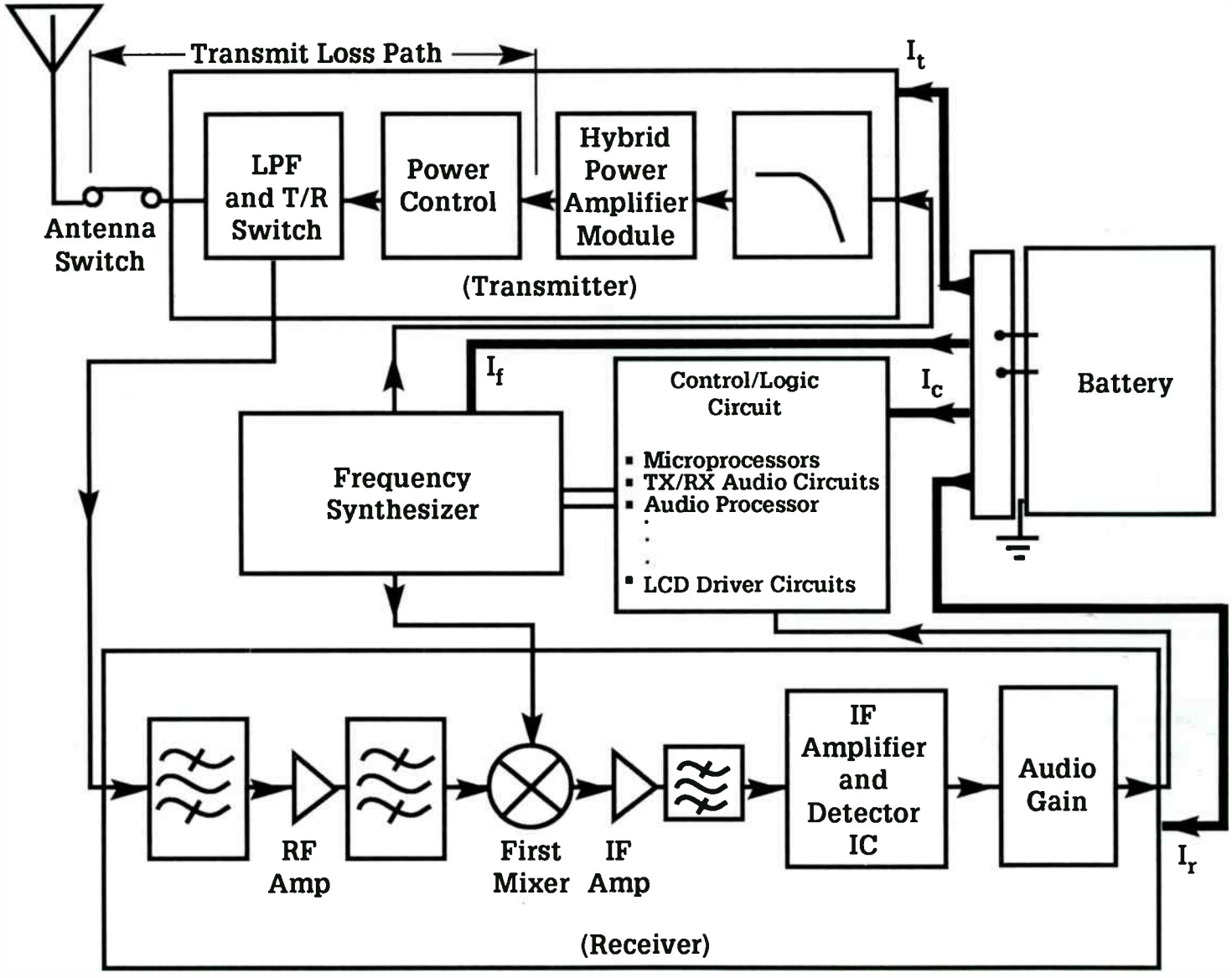

Figure 1. Simplified system block diagram of modern portable radio and its major DC current drain paths.

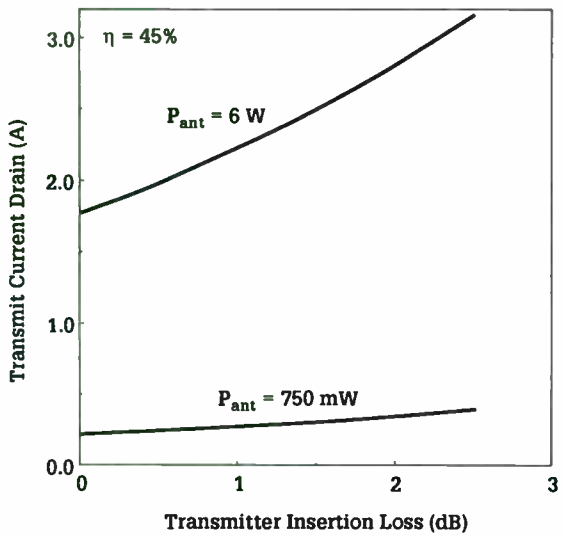

Figure 2. Current drain variation as a function of insertion loss in the transmitter circuit.

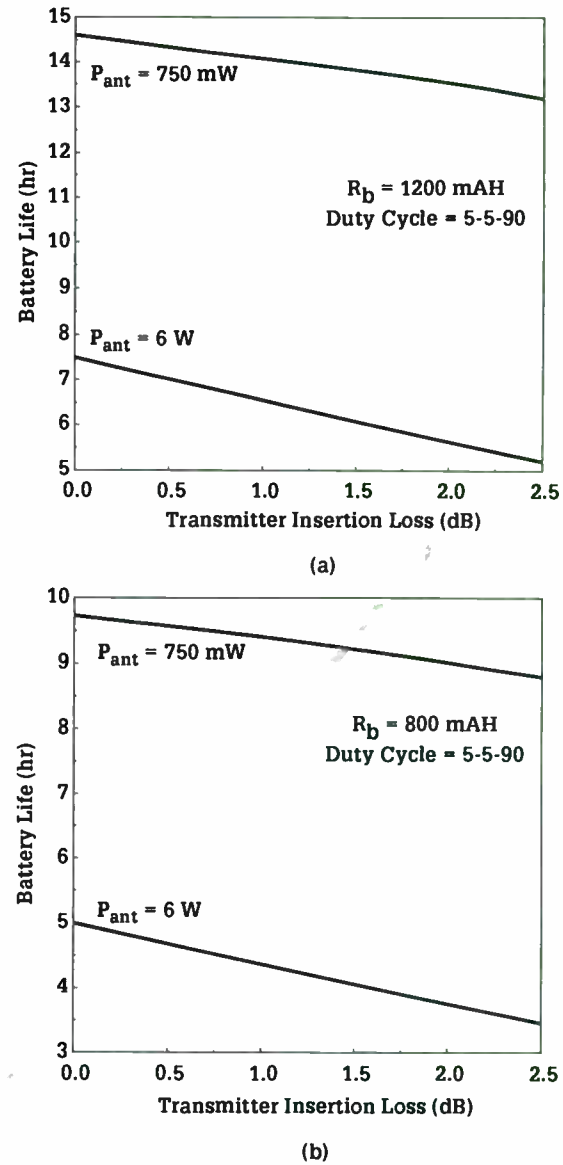

Figure 3. (a) Battery Life Performance as a Function of transmitter insertion loss at 5-5-90 duty cycle for 1200 mAH battery and (b) battery life performance as a function of transmitter insertion loss at 5-5-90 duty cycle for 800 mAH battery.

1552A 03

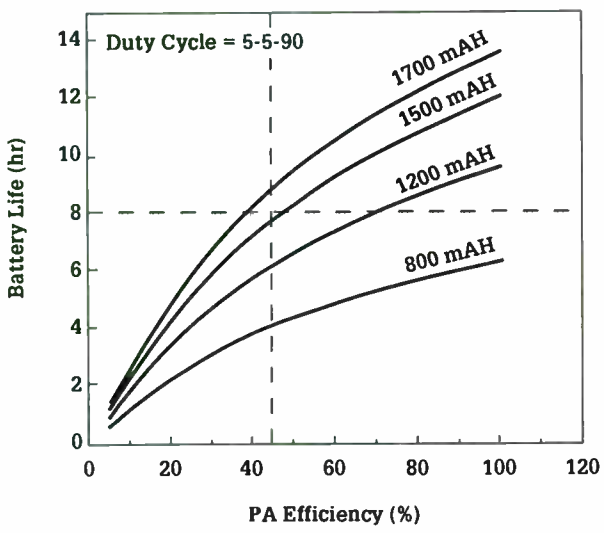

Figure 4. Battery life prediction as a function of PA efficiency for different values of battery capacity at 5-5-90.

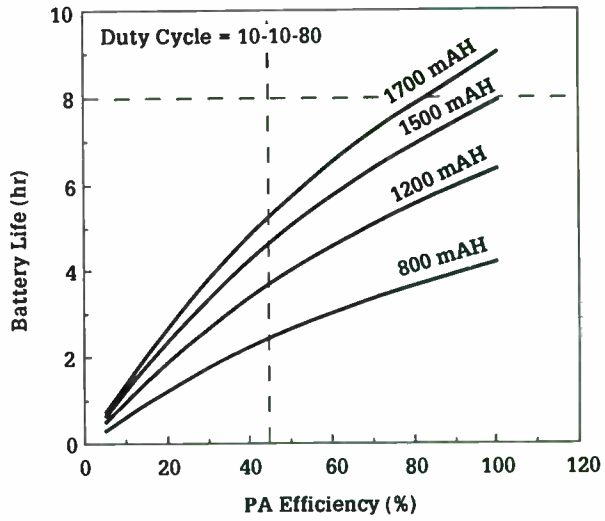

Figure 5. Battery life performance as a function of PA efficiency for different values of of battery capacity at 10-10-80 duty cycle.

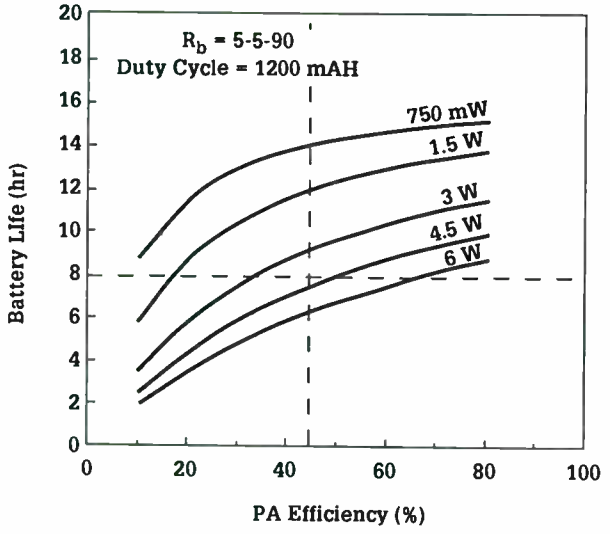

Figure 6. Battery life performance as a function of PA efficiency for different values of power output at 5-5-90 for 1200 mAH battery.

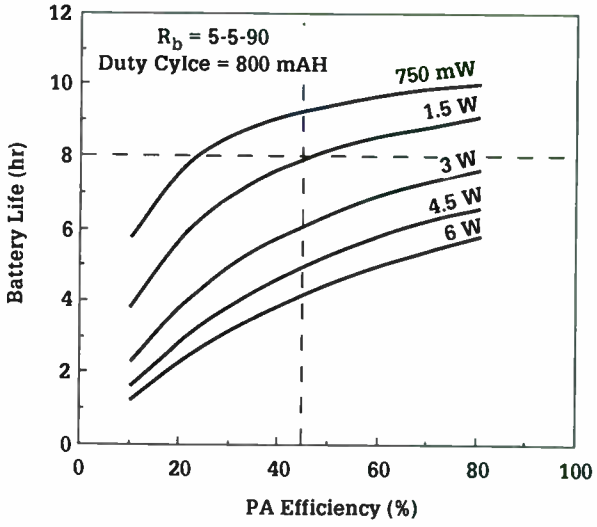

Figure 7. Battery life performance as a function of PA efficiency for different values of power output at 5-5-90 for 800 mAH battery.

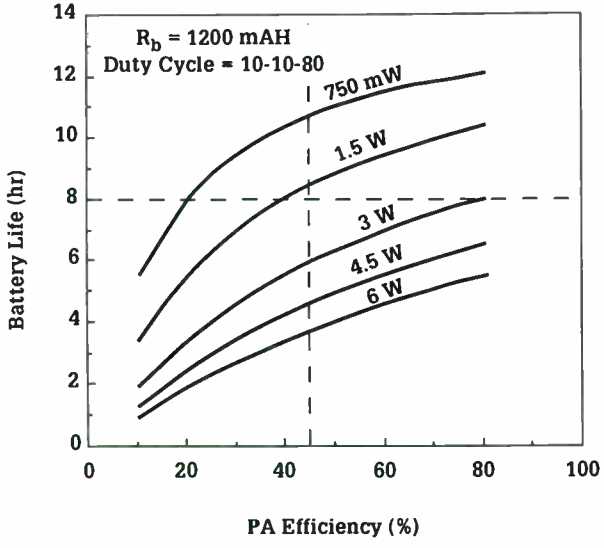

Figure 8. Battery life performance as a function of PA efficiency for different values of power output at 10-10-80 for 1200 mAH battery.

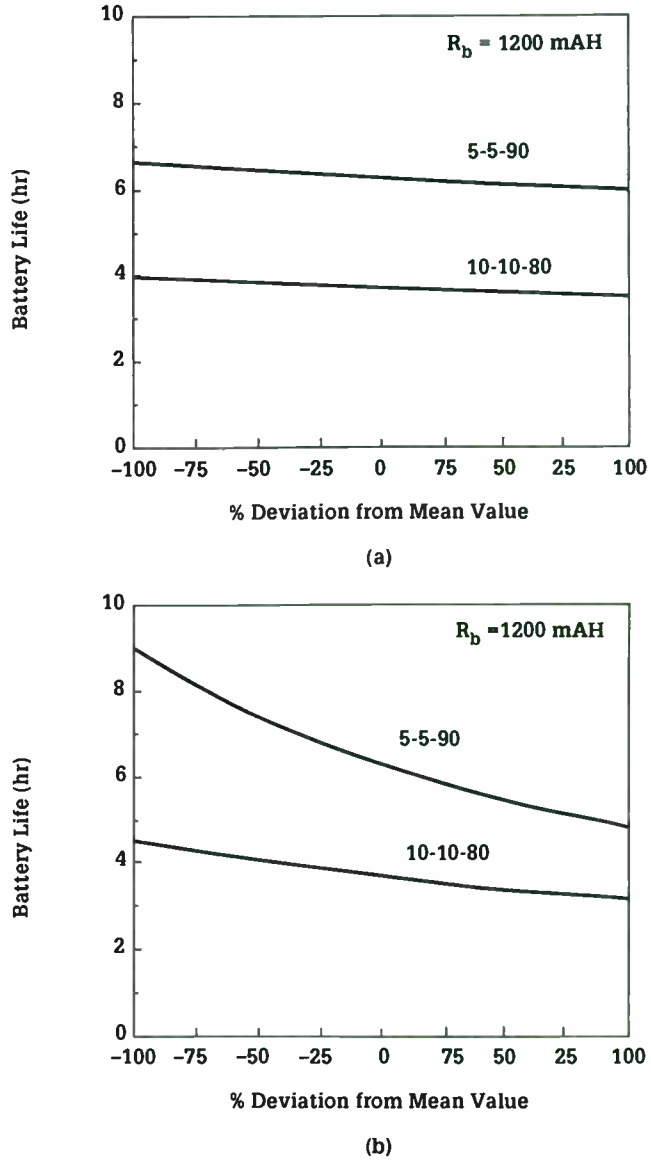

Figure 9. (a) Battery life performance as a function of receive current drain and (b) battery life performance as a function of standby current drain.

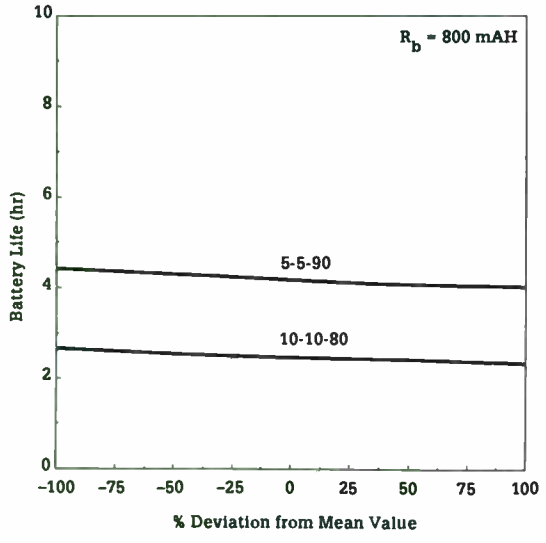

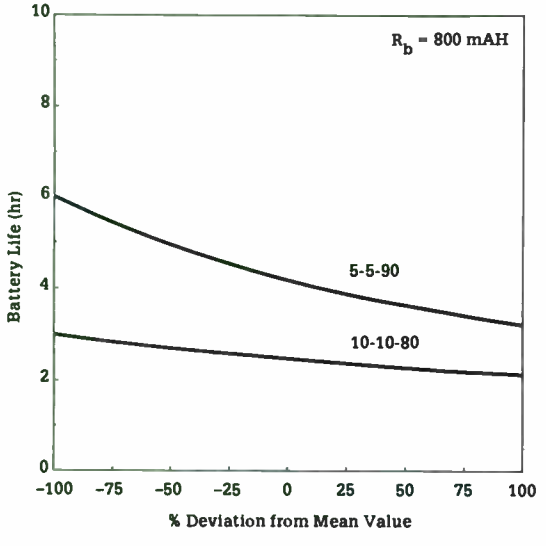

Figure 10. (a) Battery life performance as a function of receive current drain and (b) battery life performance as a function of standby current drain.

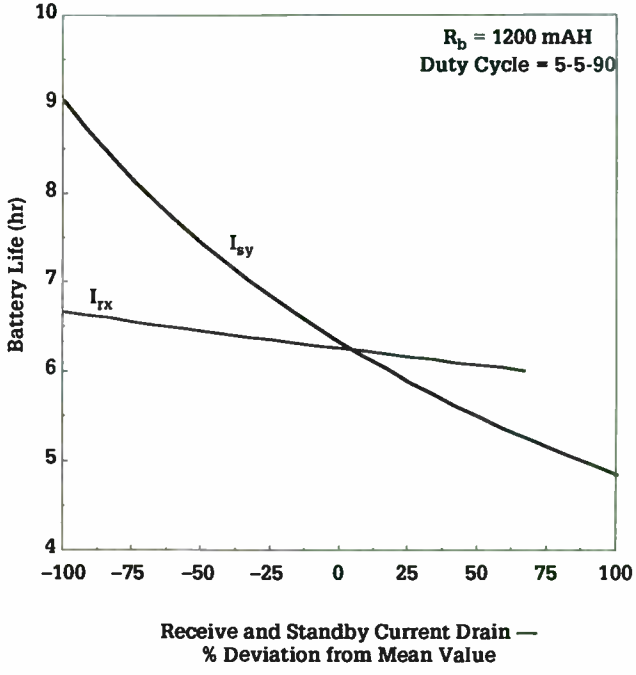

Figure 11. Battery life performance as a function of standby and receive current drain at 5-5-90 duty cycle for 1200 mAH battery.

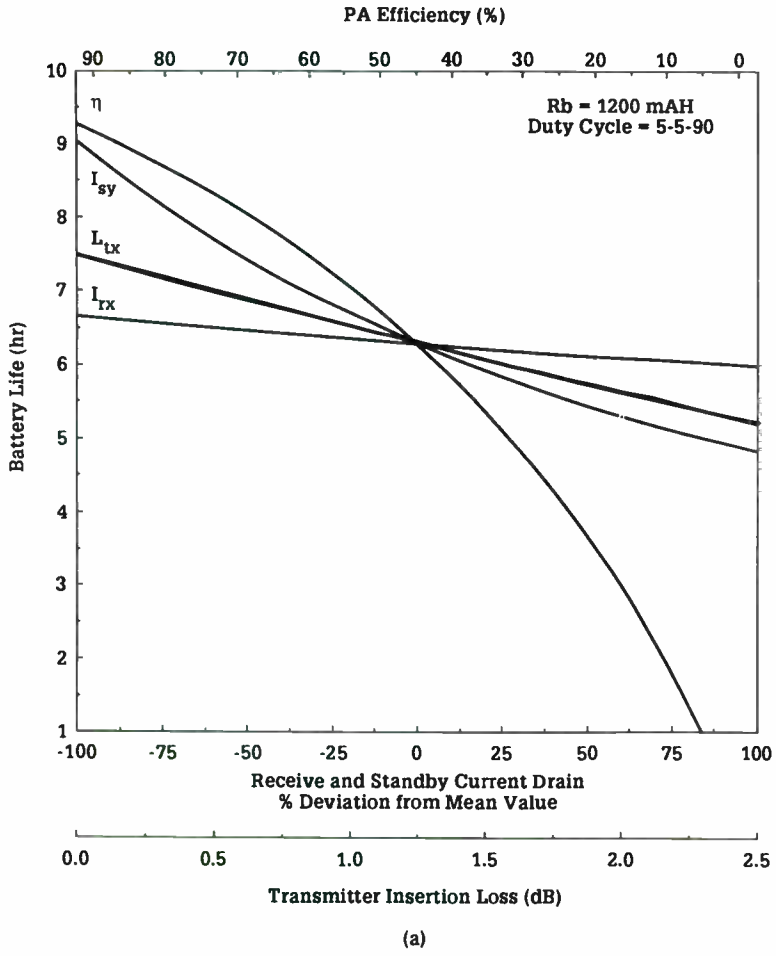

Figure 12.(a) Battery life performance comparison as a function of transceiver parameters.

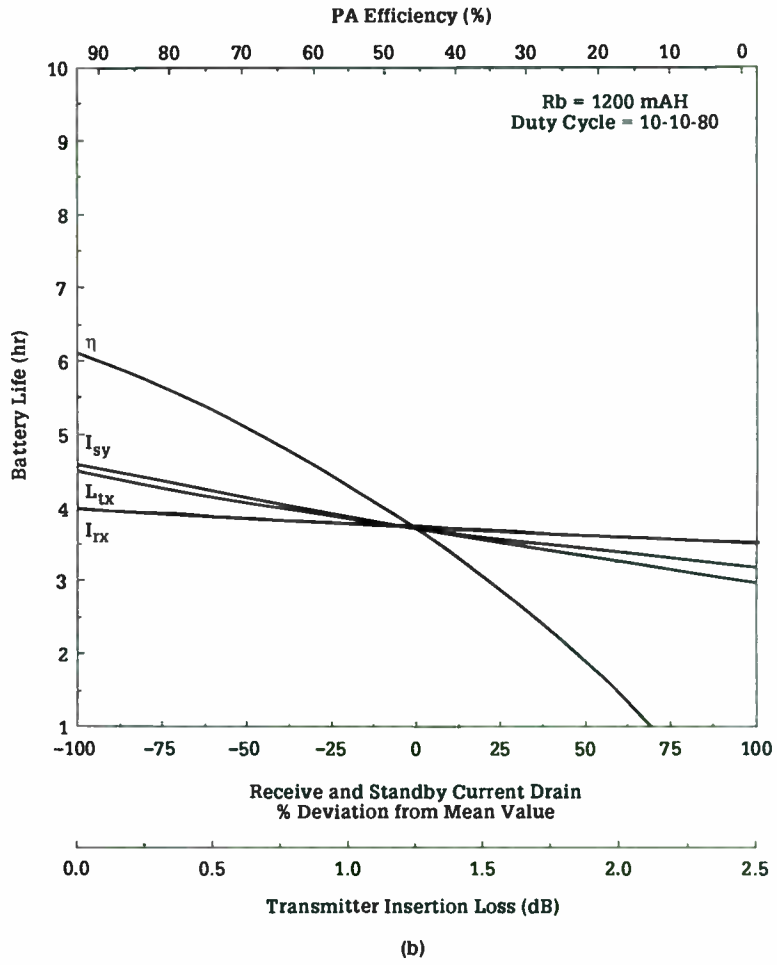

Figure 12. (b) Battery life performance comparison as a function of transceiver parameters.

DESIGN AND PERFORMANCE OF HIGH POWER PIN DIODE T/R SWITCHES FOR VHF AND UHF LAND MOBILE VOICE AND DATA COMMUNICATION SYSTEMS

MASOOD GHADAKSAZ

GTE Laboratories
Systems Technology Laboratory
40 Sylvan Road
Waltham, MA 02254

ABSTRACT

There is a growing demand for data transmission over VHF and UHF land mobile radio channels. At present it is possible to use a half-duplex or a simplex channel using VHF and UHF portable and low and medium power land mobile radio units for data communication. However, the time taken for high power (110 W) land mobile and base station units to switch from receive to transmit and back to receive exceeds the time required for the transmission of a data block for maximum throughput. This slow switching time is primarily due to the electro-mechanical switch separating the transmitter and the receiver. To accommodate both data and voice communications in high power land mobile radio systems high power T/R switches with faster switching time are required. This paper describes design and performance of several resonant high power PIN diode T/R switches with emphasis on the development of a novel dual function T/R network for use in 110 W VHF and UHF land mobile voice and data communications systems.

Introduction

PIN diodes have long been used as RF switching elements in the design of low power solid state antenna switches in radio transceivers. The main function of the PIN diode antenna switch in radio transceivers is to provide low-loss connection between the antenna and the transmitter in the transmit mode with the receiver isolated from the transmit path and between the antenna and the receiver in the receive mode with the off transmitter isolated from the antenna. In two way land mobile radio equipment transmit-receive (T/R) PIN diode switches are used in portable and low and medium power (40 W) radio units. While electro-mechanical relays are still widely used as antenna switches in the design of modern high power (110 W) land mobile and base station radio equipment. Electro-mechanical relay type antenna switches exhibit high isolation, low insertion loss, and low distortion characteristics. However, these switches inherently have slow switching time and their long term reliability is undermined by the deterioration of their moving parts.

In recent years, developments in high power PIN diode technology have led to significant improvements in the characteristics of high power packaged PIN diodes such as low forward bias resistance and high impedance at zero bias, increased RF power handling capability, higher reliability, improved mechnical ruggedness, and faster switching speed. These characteristics make these diode ideally suited for RF switching in large signal applications where low loss, high isolation, low distortion, and fast switching time antenna switch performance is required. Because of these characteristics high power PIN diode T/R switches have significant advantages over the electro-mechnical relay type switches particularly in applications requiring fast antenna switching on the order of several microseconds. One such application is in land mobile radio equipment where there is a growing need for high speed data transmission capability. To provide high power land mobile equipment with this capability the switching time of the antenna switch to switch from receive to transmit and back to receive must be less than the time required for the transmission of a data block for maximum throughput.

In this paper after a brief review of the basic PIN diode T/R switch design and its limitations, design methods to improve the performance of the PIN diode T/R switch with emphasis on the design and performance of a novel dual function T/R switch network are discussed.

Basic PIN Diode T/R Switch

The basic T/R switch network comprises a series PIN diode placed in the transmit path and a shunt PIN diode connected across the receiver and separated by a quarter-wavelength transmission line from the series diode and the antenna as shown in Figure 1. In the transmit mode with both diodes forward biased the series diode provides a low-ioss low impedance connection between the transmitter and the antenna while the low impedance presented by the shunt diode shorts the receiver terminals. The quarter wavelength transmission line transforms this nearly short circuit impedance to a nearly open circuit impedance at the antenna. In practice due to the parasitic inductance associated with the diode package the transmit-receive isolation is frequency dependent and typically is limited to about 25 dB up to about 500 MHz. Although considered a disadvantage it will be shown later in this paper that the parasitic inductance can offer an advantage. In many practical applications specially where high power transmitters are used 25 dB isolation is obviously inadequate. To increase transmit-receive isolation another quarter wavelength stage is added as shown in Figure 2. The isolation added by the second stage is also limited to about 25 dB because of the package parasitics. Therefore the total isolation is often limited to about 50 dB at UHF. Adding more stages will increase isolation but it also increases insertion ioss, current drain, cost, and size.

An important operating characteristic of the T/R switch is the distortion caused by the PIN diodes. The distortion level typically varies as a function of the RF signal level and the forward bias current or the reverse bias voltage depending on the diode state. In the transmit mode the forward biased series PIN diode is normally the major contributor to the distortion in the transmitted signal. For most large RF signal applications the distortion caused by the T/R switch is a serious concern specially if its level is high compared to the desired signal level. In the transmit mode which the series PIN diode is subjected to high RF signal level the distortion can be reduced by adding another series PIN diode in a back to back configuration as shown in Figure 2. It is also extremely important that the two diodes be placed physically as ciose as possible to each other.

Resonant Lowpass T/R Switch

At VHF and UHF distributed quarter wavelength transmission line is considered to be impractical for most applications requiring compact design. However, in practice a quarter wavelength line can be simulated at VHF and UHF using lumped elements. Two lumped element topologies can effectively simulate a quater wave line. Figure 3 shows a lowpass and a highpass equivalent circuit of a quarter wavelength transmission line. Figure 4 shows a iowpass lumped element implementation of the T/R switch circuit in Figure 2. The degradation caused by the package inductance in the transmit-receive isolation can effectively be overcome by tuning out the parasitic inductance of each diode using an external capacitor. Placing an external capacitor in series with each shunt diode forms a PIN diode switched capacitor as shown in Figure 5. Figures 4(b) and (c) clearly demontrate the improvement in the transmit-receive isolation which amounts to an increase of at least 30 dB in the 400 to 500 MHz range. Despite the bandwidth limitation caused by the two diode notch resonators this improvement is significant over the desired frequency range.

Resonant Highpass T/R Switch

Figure 6(a) shows a highpass lumped element version of the two stage T/R switch circuit in Figure 2. The performance of this switch has been simulated and is shown in Figure 6(b). The iowpass network topology is almost always used to simulate quarter wavelength transmission line in the T/R switch design. However, the highpass equivalent network of the quarter wavelength transmission line can offer many advantages. For example in practice a lowpass filter placed ahead of the T/R switch and shared by both the transmitter as well as the receiver can form a bandpass filter network as shown in Figures 7(a) (b).

Resonant Bandpass T/R Switch

A resonant bandpass T/R switch can be formed by using both lowpass and highpass equivalent networks of the quarter wavelength transmission line simultaneously in the design of a two stage T/R switch circuit as shown in Figures 8(a) and (b). In a way the lowpass and the highpass filter networks complement each other in this T/R switch to form a bandpass filter network in the receive mode.

A Novel Selective Dual Function T/R Switch

It was shown that lowpass and highpass equivalent network topologies for quarter wavelength transmission line offer attractive practical possibilities for the simultaneous design of VHF and UHF PIN diode T/R switches and receiver front-end filters. However the need for selective bandpass filtering in the receiver front-end created the stimulus to develop a PIN diode T/R switch network that can either eliminate the need for a separate bandpass filter or minimize the filtering function and thus help reduce the size and cost in the receiver. Figure 9(a) shows such a novel T/R switch network topology that has been developed for the design of high power VHF and UHF PIN diode T/R switches for use in land mobile radio equipment. This dual function T/R network when forward biased presents a low-loss low distortion path in the transmit mode and at zero bias state presents a selective bandpass filter response in the receive mode. Figure 9(b) shows a sample computer simulation at UHF. Figure 9(c) shows the measured performance of a UHF switch. Figures 10-14 show measured harmonic distortion at VHF and UHF for two dual function PIN diode T/R switches as a function of forward bias current for the transmit mode at 110 W and 150 W and as a function input power for the receive mode at zero bias. The switching time including the drive circuit for both the VHF and UHF PIN diode T/R switch circuits was measured and found to be less than 8 microseconds.

Conclusions

It was shown that both lowpass and highpass equivalent network topologies for quarter wavelength transmission line combined with the resonant switch design approach offer attractive practical possibilities for the design of high performance RF PIN diode T/R switch which led to the development of a novel dual function PIN diode T/R switch network. This dual function T/R network while serving as a high performance, high power, and fast switch also functions as a selective bandpass filter in the receive mode. The selective receive mode bandpass filter response is an important characteristic which is inherent in this novel T/R switch design and can offer many advantages including either eliminating or minimizing the need for a separate bandpass filter in the receiver front-end, size reduction, cost reduction...etc.

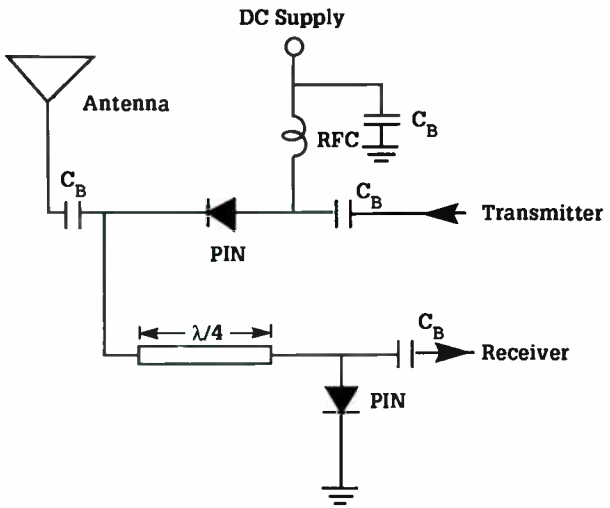

Figure 1. (a) Basic λ/4 transmission line T/R switch.

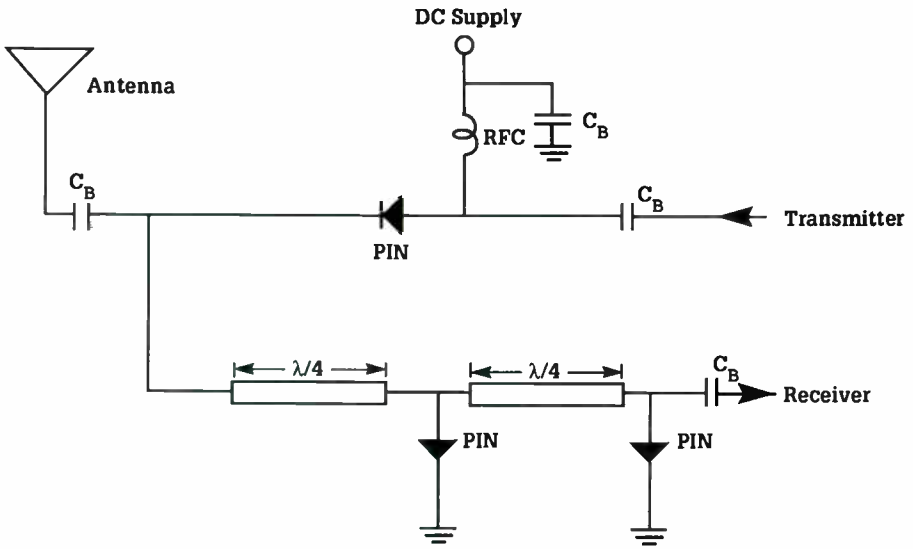

Figure 1. (b) Two-section λ/4 transmission line T/R switch.

1552-01

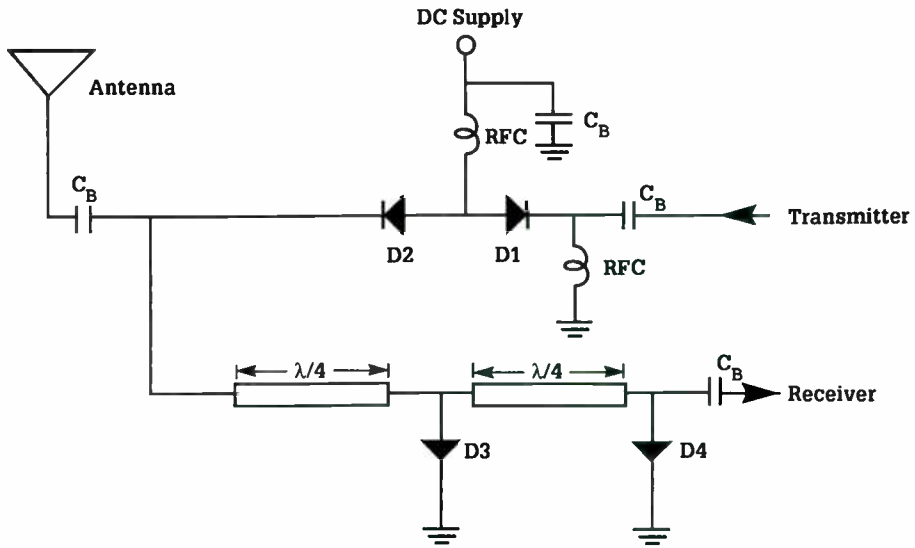

Figure 2. Two-section λ/4 transmission line T/R switch for low distortion performance.

1552-02

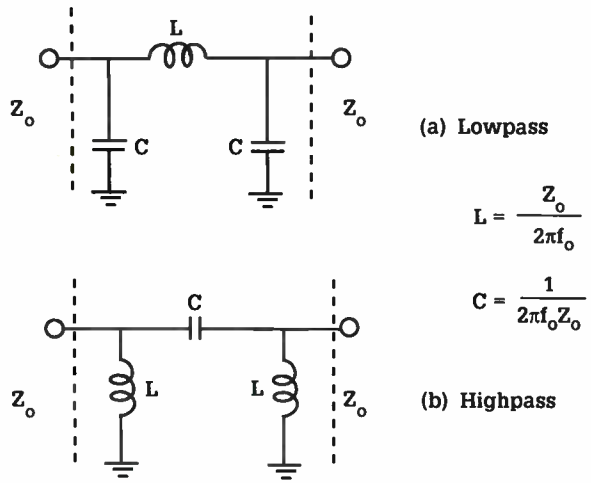

Figure 3. Lumped element equivalent circuits of λ/4 transmission line.

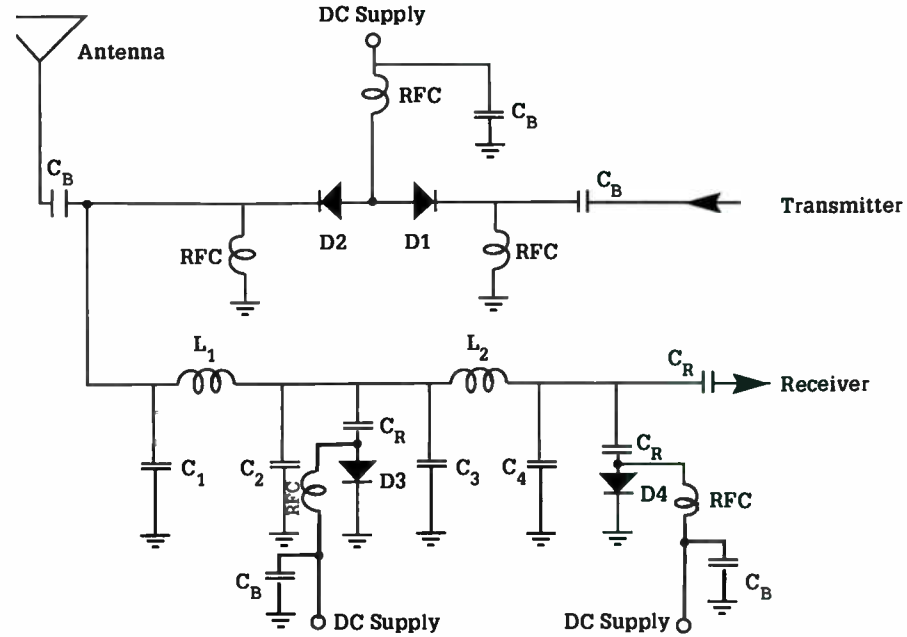

Figure 4. (a) Lowpass lumped element implementation of two-section λ/4 T/R switch for increased isolation and low distortion performance.

1552-03

1552-04

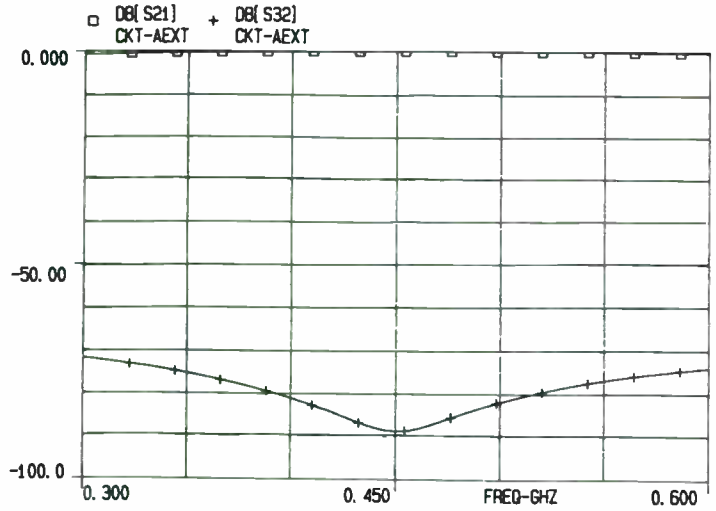

Figure 4. (b) Simulated transmit-receive isolation with package parasitic inductance tuned-out.

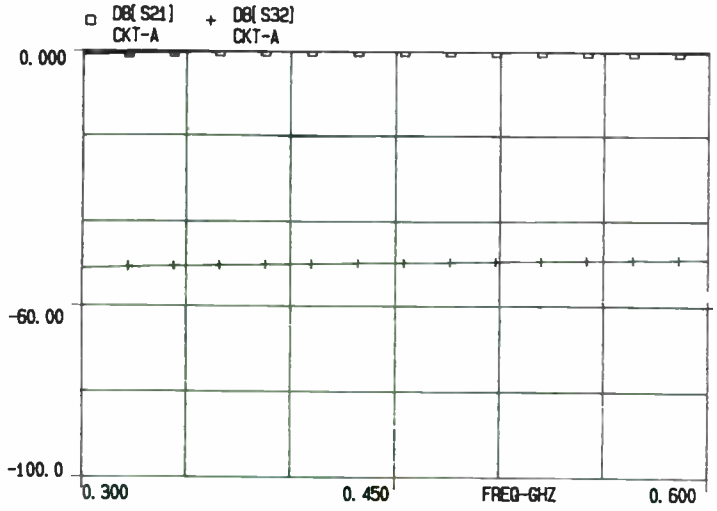

Figure 4. (c) Simulated transmit-receive isolation including the effects of package parasitics.

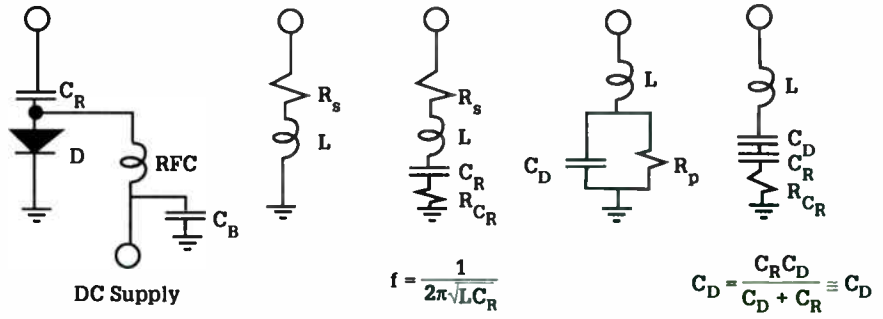

Figure 5. (a) PIN diode switched capacitor; (b) simplified PIN diode model under foward bias condition; (c) forward bias model for PIN diode notch resonator, (d) PIN diode model under zero bias condition, and (e) zero bias PIN diode switched capacitor.

1552-05

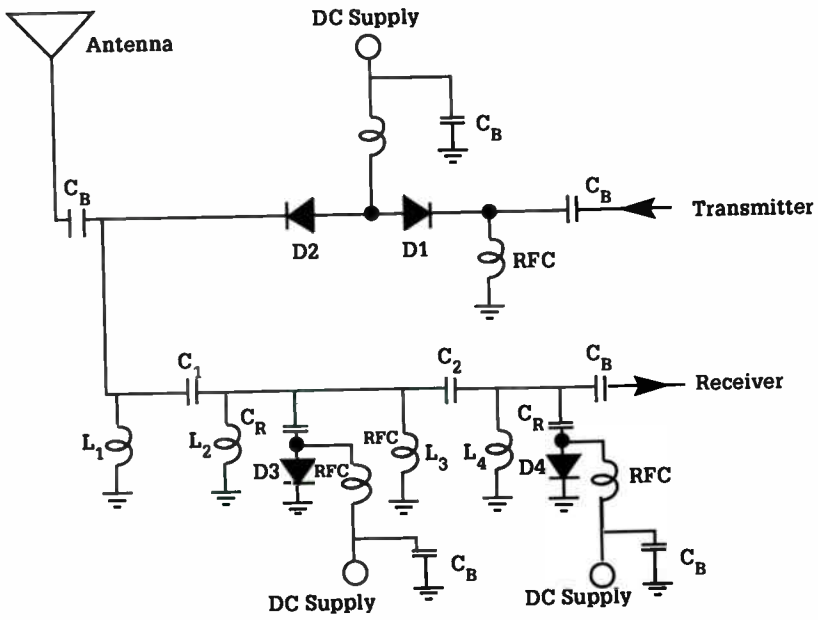

Figure 6. (a) Highpass lumped element implementation of two-section λ/4 T/R switch for increased isolation and low distortion performance.

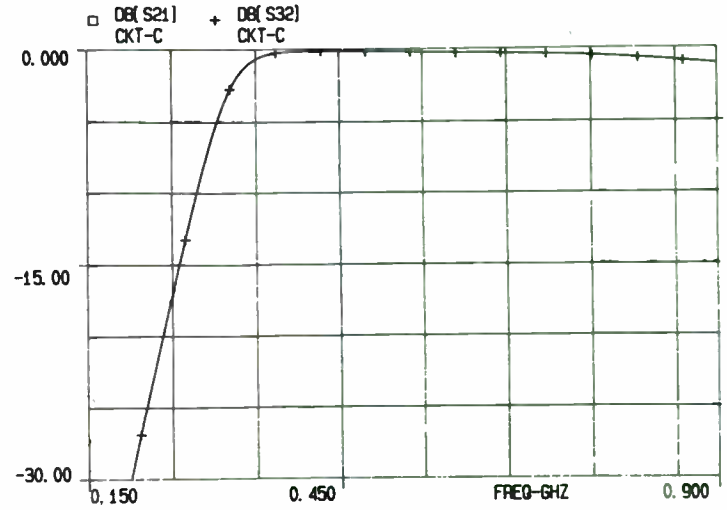

Figure 6. (b) Simulated receive mode response of the highpass T/R switch network at UHF.

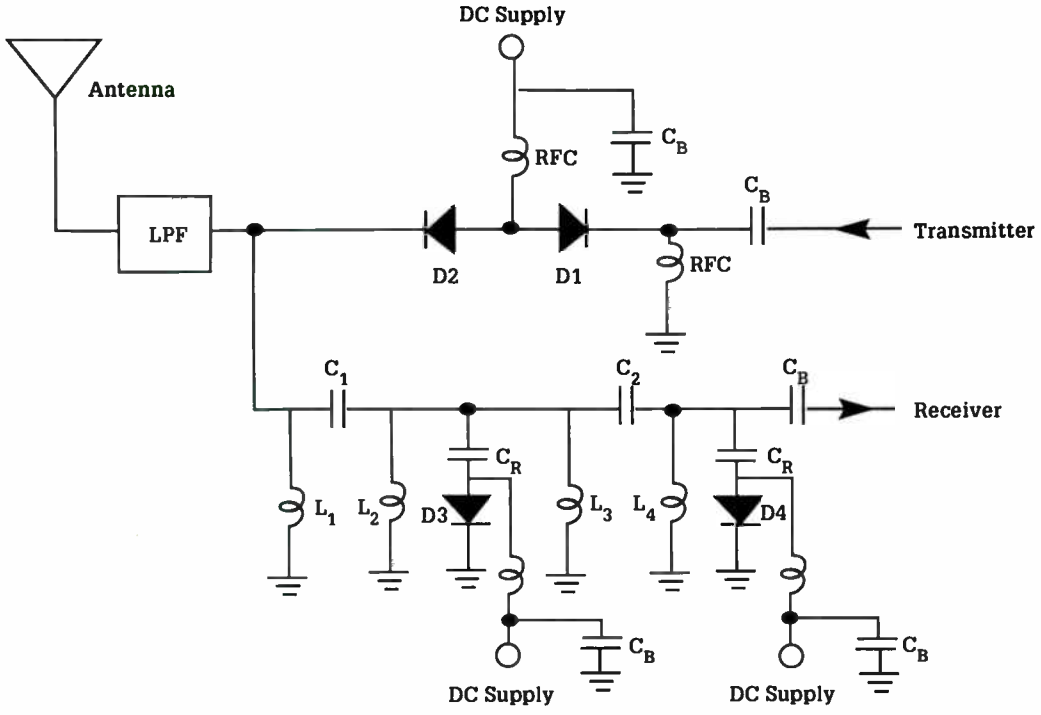

Figure 7. In the receive mode combination of a lowpass filter and a highpass T/R switch produces a bandpass filter network in the receiver front-end.

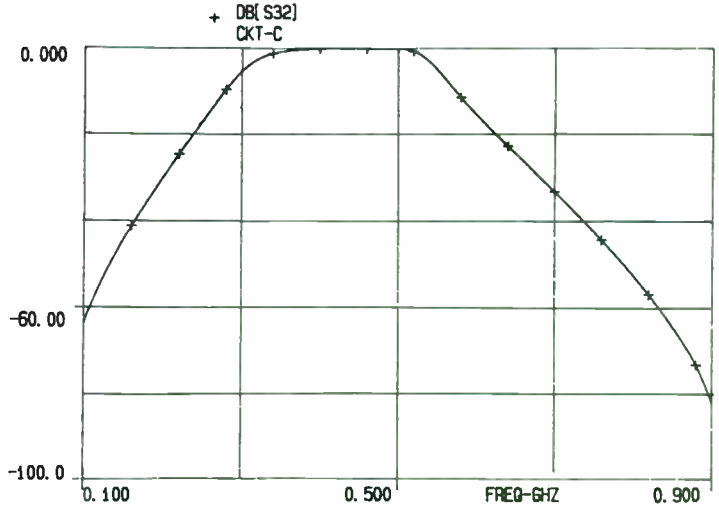

Figure 7. (b) Combined simulated receive mode response of the resonant highpass T/R switch and a lowpass harmonic filter.

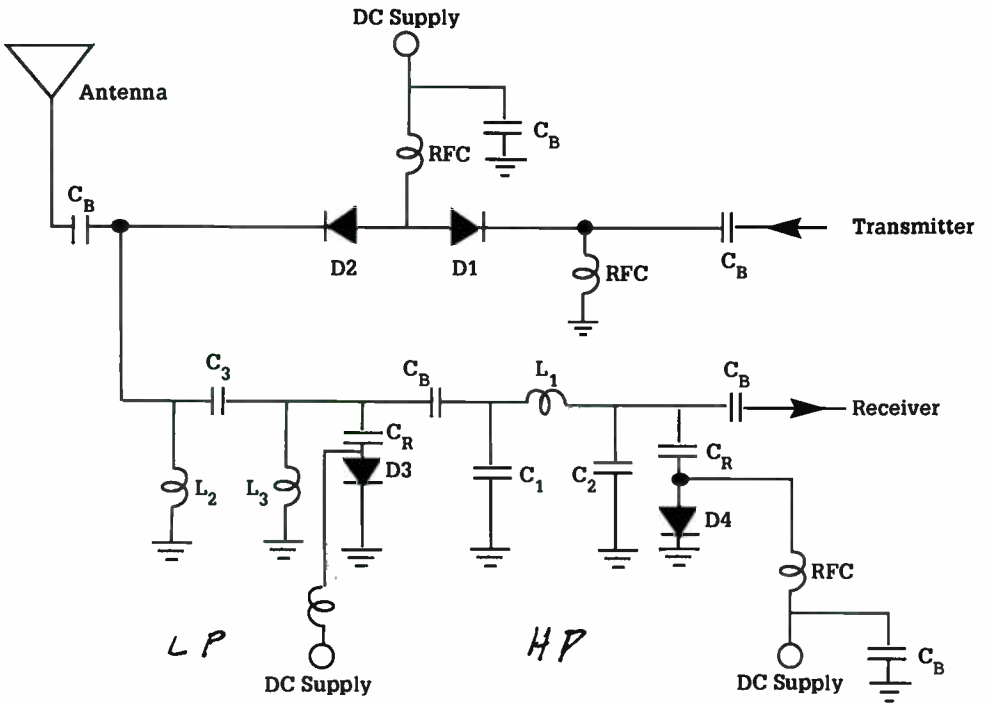

Figure 8. (a) Bandpass lumped element implementation of two-section λ/4 T/R switch for increased isolation and low distortion performance.

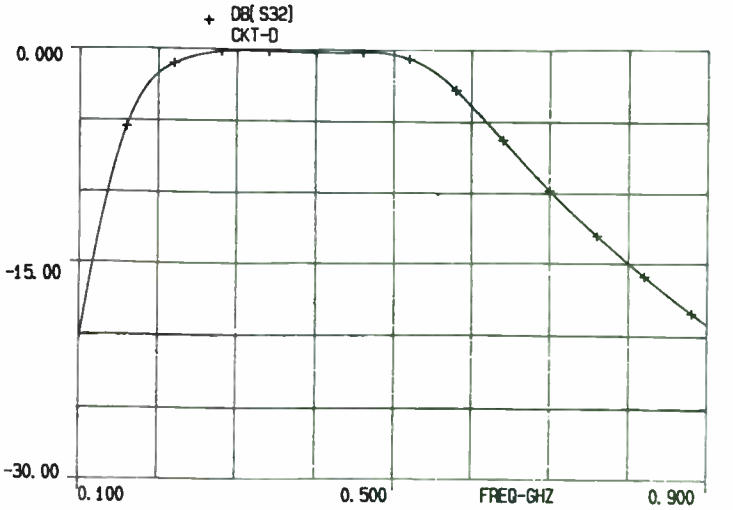

Figure 8. (b) Simulated receive mode response of the resonant bandpass T/R switch network at UHF.

C_R resonates PIN inductance.

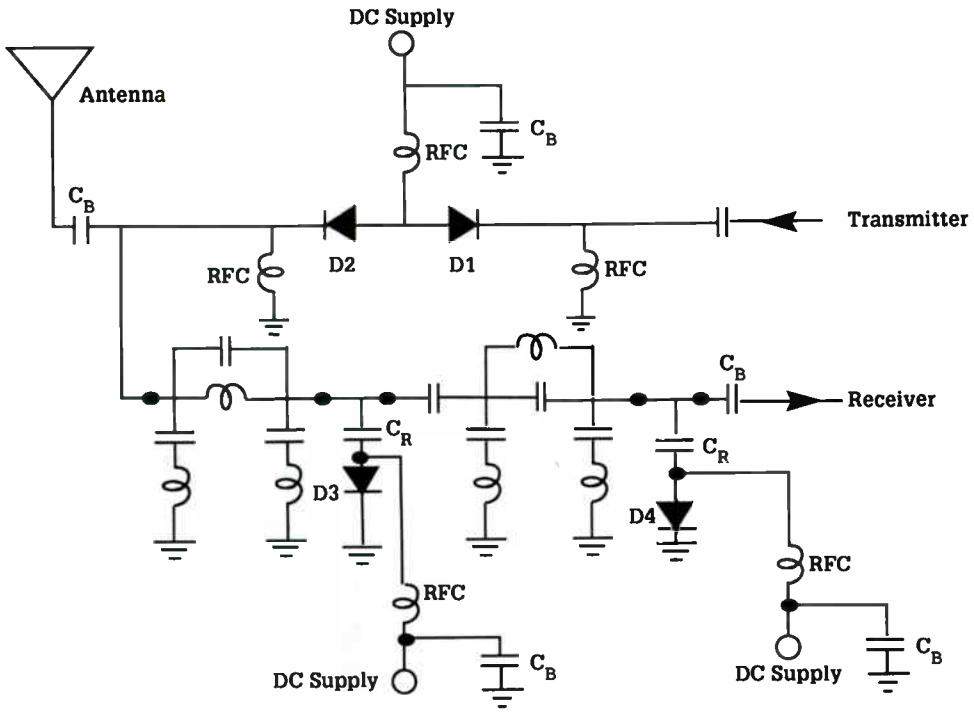

Figure 9. (a) Selective dual function T/R switch network.

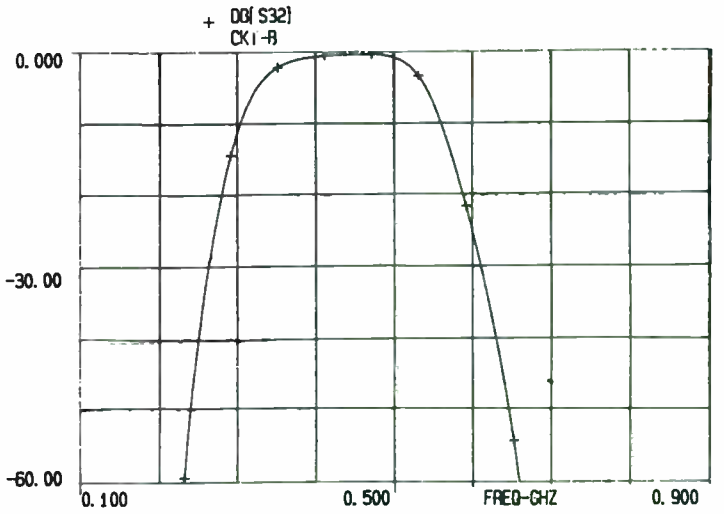

Figure 9. (b) Simulated receive mode response of the dual function T/R network at UHF.

Forms BPF in receive.

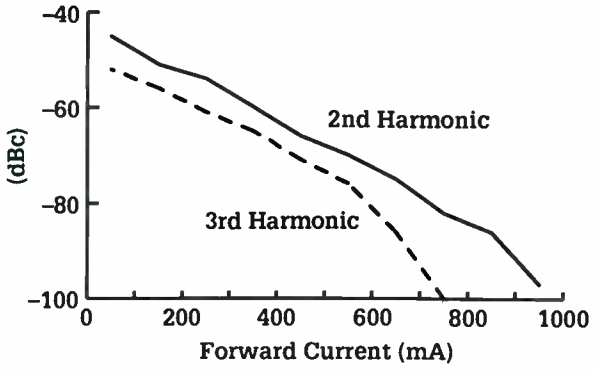

Figure 10. Harmonic distortion as a function of forward bias current at 150 MHz and P_{in} = 150 W.

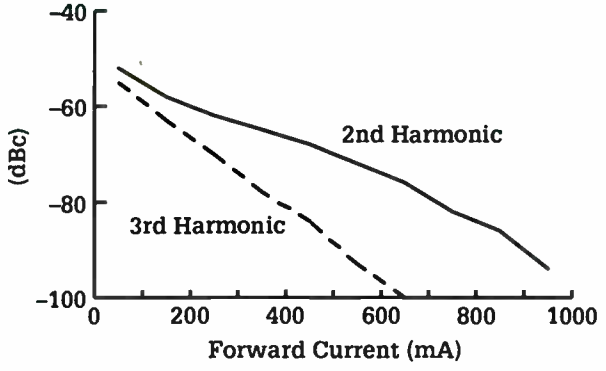

Figure 11. Harmonic distortion as a function of forward bias current at 450 MHz and P_{in} = 150 W.

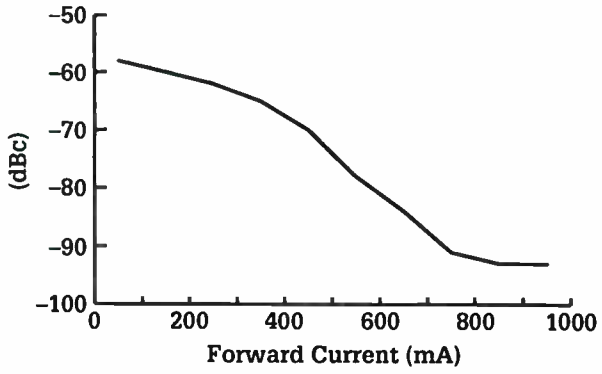

Figure 12. Forward bias third order intermodulation distortion as a function of forward current at P_{in} = 110 W per channel, F_1 = 449 MHz, F_2 = 450 MHz.

1552-12

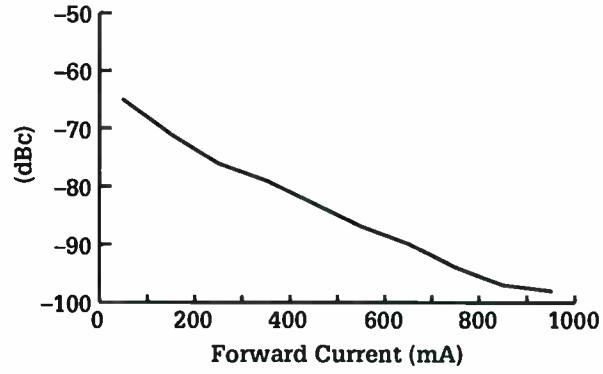

Figure 13. Forward bias third order intermodulation distortion as a function of forward current at P_{in} = 110 W per channel, F_1 = 149 MHz, F_2 = 148 MHz.

1552-13

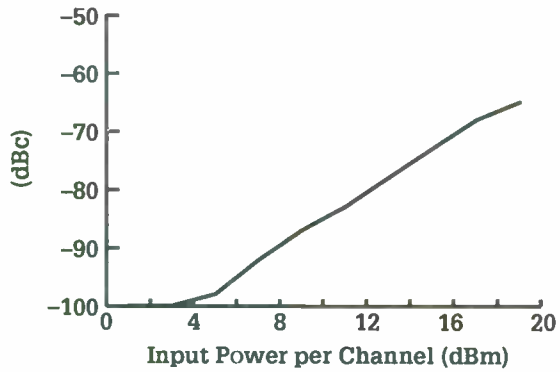

Figure 14. Zero bias third order intermodulation distortion as a function of input power, F_1 = 449 MHz, F_2 = 450 MHz.

1552-14

Design and performance of a 16-way combiner using 1/16 wavelength microstrip transmission lines

M. Abdollahian, R. Gage, P. Palermo & B. Hazen

GTE Laboratories Incorporated

40 Sylvan Road

Waltham, MA 02254

Abstract

One of the challenging tasks for rf engineers and system designers is efficient and low-cost combining of high-power amplifiers. Communication and jamming systems, typically, require combining multiple amplifier modules to achieve the desired power levels. At present, combining networks usually consist of multiple stages of 1/4 wavelength transmission line sections and high power isolation resistors. These 1/4 wavelength combiners pose serious disadvantages to modern system design and integration due to their increased size and weight requirements, specifically, at radio frequencies. Size reduction techniques using high-dielectric constant materials can be costly, moreover, the use of high-dielectric substrates results in increased insertion loss due to the reduced line-widths.

This paper describes a novel technique of combining 16 power amplifiers to achieve high cw power at UHF and microwave frequencies. The design consists of four stages of 1/16 wavelength transmission lines to combine the power and at the same time accomplish any necessary impedance transformation(ie ; the input and output impedance of the amplifier modules can be other than 50 Ω). This combiner exhibits excellent performance and is compact in size.

Introduction

In many applications, RF power levels are required that far exceed the capability of any single device or amplifier. Thus several devices or amplifiers must be combined to generate this power. Divider/combiner technology over the past several years has allowed combining several amplifiers to provide multi-kilowatt modules. However these combiners are usually large in size and typically have high insertion losses.

Combining schemes generally fall into two categories, chain (serial, non-binary) and corporate (parallel,tree or binary) [1], and are shown in Figures 1a & 1b. In this paper combiners of the corporate structure are discussed. The corporate combining scheme can be categorized into tree or parallel structures. Tree or binary structures are advantageous when the number of devices involved are few, since the combining efficiency degrades with the addition of each adder. Parallel combiners (also referred to as n-way), on the other hand, operate with better combining efficiencies due to their single step combining feature. A novel combiner design which takes advantage of characteristics of a binary combiner and at the same time maintains the small physical size and low insertion loss behavior associated with n-way combiners, is discussed in this paper. This paper also discusses the various combiner/divider approaches that will allow combining several transistor chips or power amplifiers. One of the concepts presented is believed to be a unique solution to the size and weight constraints imposed on many power amplifier designs.

Considerations In Designing Power Combiners / Dividers

Although lumped element reactive components and coaxial transformers are used extensively in solid-state RF power circuit designs, in many cases superior performance can be achieved with distributed transmission-line elements. This is particularly true at VHF, UHF and most certainly in the microwave region, where stripline techniques contribute greatly to

predictability, reproducibility and low losses.

Some of the questions in the design of a power combiner / divider that should be answered by the designer are listed below:

*What degree of isolation is required?

* How many amplifiers are combined?

* How much loss can be tolerated?

* What bandwidth is required?

* How would the combiner react to mismatch ?

Two of the considerations that will always require a compromise are isolation Vs loss. If the application requires a very low loss combiner a very solid building block is a must.

2.0 The Wilkinson Combiner

A two way Wilkinson combiner is shown in Figure 2, while its frequency response characteristics are illustrated in Figure 3. A Wilkinson consists of two quarter-wave transmission line transformers which transform each of the source impedances of Z_s to a load impedance Z_L. It is shown that for a quarter-wave transformer the characteristic impedance is;

$$Z_0 = \sqrt{Z_s \cdot Z_L}$$

Therefore, for a Wilkinson with source and load terminating impedances of 50 Ω, the characteristic impedance of the line is equal to 70.7 Ω. By looking into the load port of the combiner we see $2Z_L \| 2Z_L = Z_L$. The same applies for each of the source ports; looking into either source port with the other ports properly terminated, we see $2Z_s \| 2Z_s = Z_s$. The combiner is designed so that two signals of equal magnitude and phase incident on the source ports will combine at the load and under these condition there will be no power dissipated by the resistor. By the same token, power incident on one of the two ports will split equally between the transmission line and the resistor (each path presents an impedance of $2Z_s$ to ground)

A 2-way Wilkinson provides a simple and straight forward method of combining the power with excellent performance characteristics. However a Wilkinson structure for combining more than two amplifiers becomes physically large or non-planar due to the topology of its isolation resistors. If the isolation resistors are totally eliminated from the circuit, The input port will see heavy mismatch when one of the component amplifier fails. Figure 4 shows a 16-way implementation of the Wilkinson in a parallel configuration. As seen in this figure, due to topology of the isolation resistors, the layout of the combiner can not be planar. Figure 5 illustrates a 16-way binary Wilkinson. Although this combiner can be implemented, it is physically large and it will be lossy since the overall length of the combiner is one wavelength long.

Four-way Combiner Design Using 1/8 Wavelength Transmission Lines.

As discussed in the previous section, the networks used to combine and impedance match several chips/transistors to some load impedance consists of multiple stages of λ/4 transmission-line sections. Networks with λ/4 lines, however, are large, especially at VHF & UHF frequencies. To reduce the size, high-dielectric constant substrates are normally used for the transmission-line network. The use of the high dielectric constant substrate, on the other hand, results in a decreased line-width and corresponding increase in insertion loss. A design for a four-way combiner/impedance matching network which can also accommodate the impedance transformation is discussed in this section.

The example design discussed here consists of two stages of λ/8 transmission lines to combine the power while, at the same time, accomplishing the necessary impedance transformation. Figure 6 shows the schematic representation of a 1:4 divider/combiner network. As seen in this figure, two stages of λ/8 microstrip transmission line are used to form the combiner/impedance transformer, thus providing a total path length of λ/4 (from point 1 to point 5) between each of the source impedance (Z_s) ports and the load impedance (Z_L). The impedance at point 3 will be 1/2 of the impedance at point 2 and similarly the

impedance at point 5 will be 1/2 of the impedance at point 4. So to facilitate a simple transformation from Z_s to Z_L, the characteristic impedance of the first λ/8 transmission line section should be twice the characteristic impedance of the second section.

Let us consider the transmission path from Z_s to Z_L.
For a λ/4 line;

$$Z_0 = \sqrt{Z_s \cdot Z_L}$$

The characteristic impedances of each stage of λ/8 (Z_{01} and Z_{02}), Therefore, can be expressed by:

$$Z_{01} = 2\sqrt{Z_s \cdot Z_L}$$
$$Z_{02} = \sqrt{Z_s \cdot Z_L}$$

Figure 7 shows an example in which a source impedance Z_s = 10 Ω is transformed to a load impedance Z_L = 50 Ω. As seen in this figure the source impedance of 10 Ω is first transformed to a normalized impedance of 0.44 + j0.9 Ω (impedance at point 2) via a λ/8 transmission line with a 44.6 Ω characteristic impedance. The parallel combination of the 2A and 2B impedances combined at point 3 results in the normalized impedance of 0.22 + j0.45 Ω . At this point, since the characteristic impedance of the second transmission line section (Z_{02}) is 1/2 of the characteristic impedance of the previous section (Z_{01}), the normalized value of the impedance becomes 0.44 + j0.9 Ω . This impedance is then transformed by the λ/8 line with the characteristic impedance of 22.3 Ω to a real normalized value of 4.46 Ω (impedance at point 4) which translates to a impedance value of 100 Ω. The resulting net impedance at the output of the combiner, when two 100 Ω impedances are paralleled, is then 50 Ω real providing the optimum match. Note that the characteristic impedances chosen above only simplifies the analysis, transmission lines with other characteristic impedance values can also be used to accomplish this task. Figure 8 illustrates the fractional bandwidth of the combiner as a function of the port impedance ratio (Z_L/Z_s) for a VSWR of less than 1.5:1.

Sixteen-way Combiner Design Using λ/16 Wavelength Transmission Lines

A similar method as shown above can be employed to combine 16 chips, or transistors using λ/16 wavelength transmission lines. This design is comprised of four stages of 1/16 wavelength transmission lines paired and cascaded to form the 16-way combiner/impedance transformer. Figure 9 shows the schematic representation of the 1:16 way divider/combiner network. As seen in this figure, four sections of 1/16 λ microstrip transmission lines are used to form the combiner, providing a total path length of λ/4 (from point 1 to point 9) between each of the source impedance, Z_s, ports and the load impedance, Z_L. The impedance at point 3 will be 1/2 of the impedance at point 2 and so on. To facilitate a simple impedance transformation from Z_s to Z_L, the characteristic impedance of the first λ/16 transmission line section should be twice of characteristic impedance of the second section and so forth.

The characteristic impedances of each stage of 1/16 λ transmission lines (Z_{01}, Z_{02}, Z_{03} and Z_{04}) can be expressed by:

$$Z_{01} = 4\sqrt{Z_s \cdot Z_L}$$
$$Z_{02} = 2\sqrt{Z_s \cdot Z_L}$$
$$Z_{03} = 1\sqrt{Z_s \cdot Z_L}$$
$$Z_{04} = 1/2\sqrt{Z_s \cdot Z_L}$$

Figure 10 is an example in which the source impedance Z_s = 10 Ω is transformed to Z_L = 50 Ω. A detailed CAD simulation was performed to demonstrate the feasibility of this approach. Figure 11 shows the return loss for a 16 way UHF (800 MHz to 900 MHz)

combiner/impedance matching transformer with a source impedance of 10 Ω, while Figure 12 illustrates the insertion loss of two combiners in a back to back configuration. As shown in these figures, the combiner /impedance transformer has a return loss of less than -20 dB and insertion loss of less than 0.15 db over the entire 100 MHz of bandwidth.

Results

Since the ultimate goal of this work was to develop low-loss, compact combiners for high power applications, a 16-way combiner / impedance transformer was designed and fabricated. This combiner will permit combining of 16 amplifiers with output impedances of 25Ω, over a bandwidth of 12 %, at a center frequency of 425 MHz. Figure 13 is a layout of the 16-way combiner. The combiner is fabricated on a soft-dielectric substrate (E_R=2.55) and is small (3.6 inches by 4.2 inches). This combiner was tested with each port properly terminated, Figure 14 shows the return loss of the combiner, while Figure 15 illustrates the insertion loss of two combiners in a back to back configuration. As shown in these figures the combiner exhibits excellent characteristics over the required band.

References

1. Ha, T. T., "Solid-state Microwave Amplifier Design," *John Wiley & Sons, New York* (1981).

2. Mathaei, G., Young, L., Jones, E. M., "Microwave Filters, Impedance Matching Networks, and Coupling Structures," *Mc Graw-Hill, New York* (1964).

3. Howe, H., "Stripline Circuit Design," *Artech House, Dedham, Mass* (1974).

4. Gilmore, R. P. , "Applications of Power Combining in Communications Systems" *Proc. RF Technology Expo East* (1986).

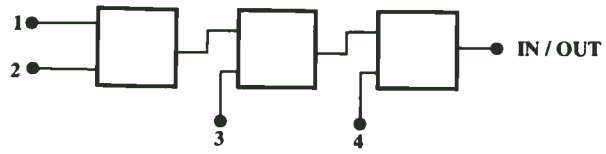

Figure 1a. A chain (series) combining structure

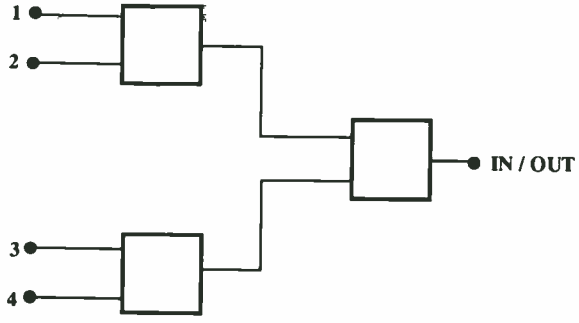

Figure 1b. A corporate (parallel) combining structure

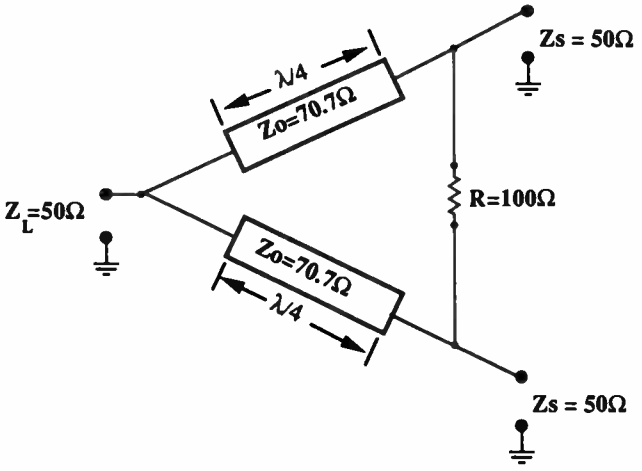

Figure 2. A 2-way in phase (Wilkinson) combiner

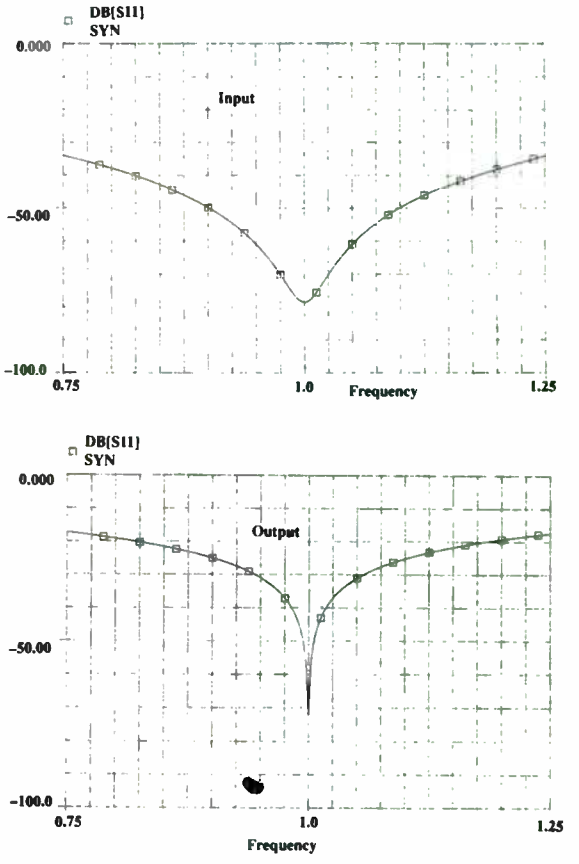

Figure 3. Return loss vs normalized frequency for a two-way equal phase, equal amplitude Wilkinson combiner.

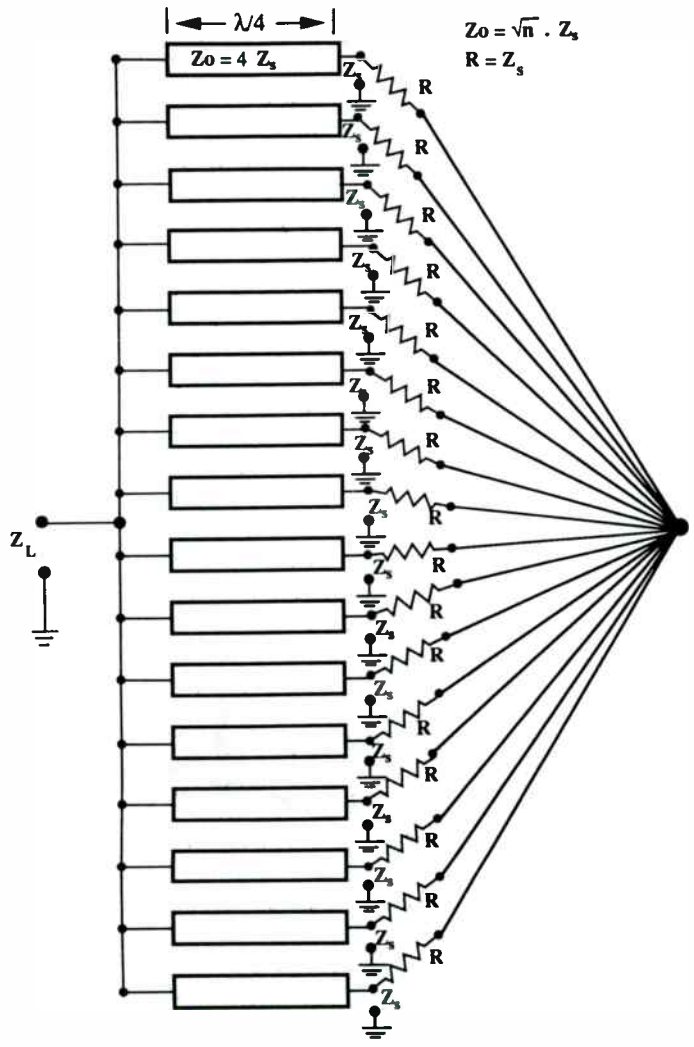

Figure 4. A 16-way in-phase, equal amplitude parallel combiner

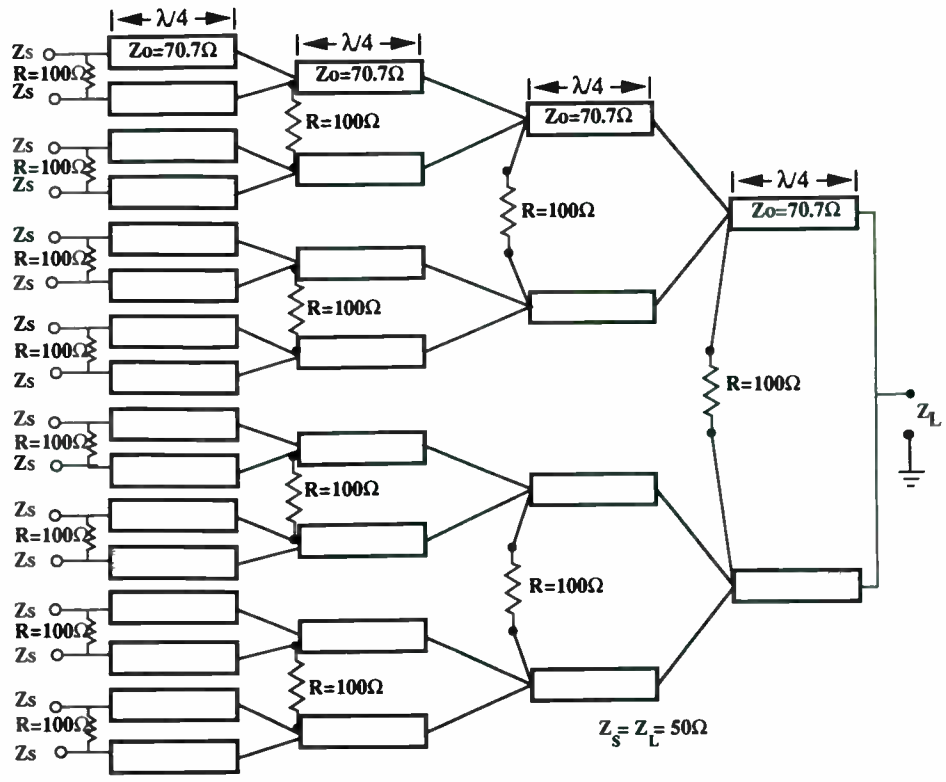

Figure 5. A 16-way equal phase, equal amplitude binary combiner

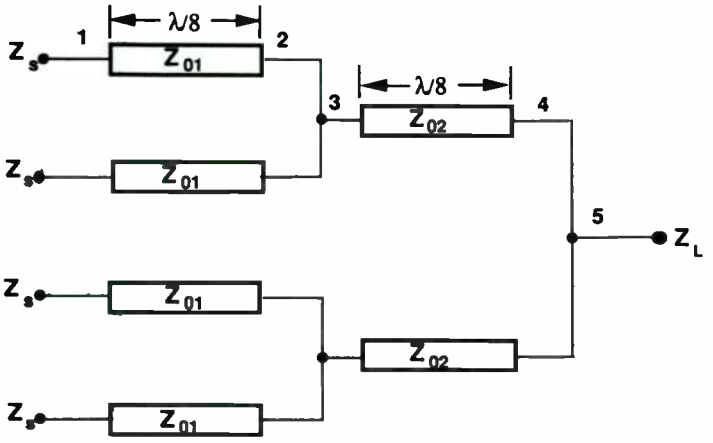

Figure 6. A 4-way equal phase, equal amplitude combiner

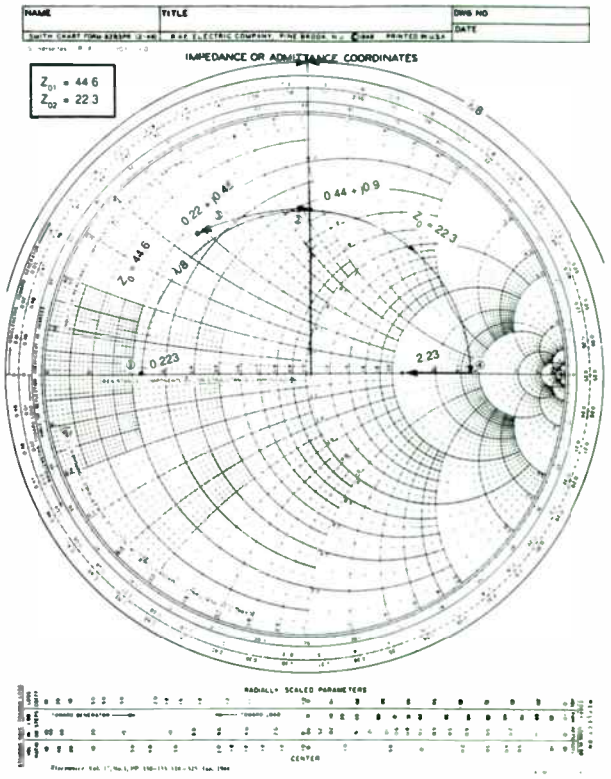

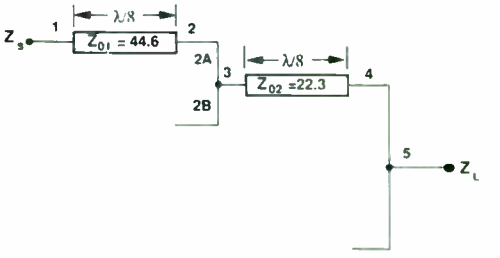

Figure 7. 10 Ω to 50 Ω impedance transformation through 1:4 way combiner.

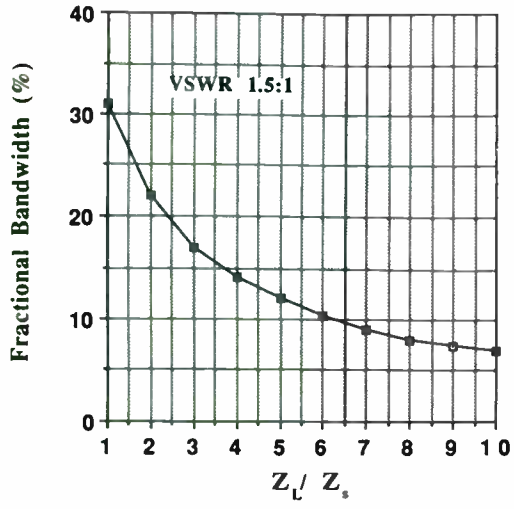

Figure 8. Fractional bandwidth Vs the load to source impedance ratio

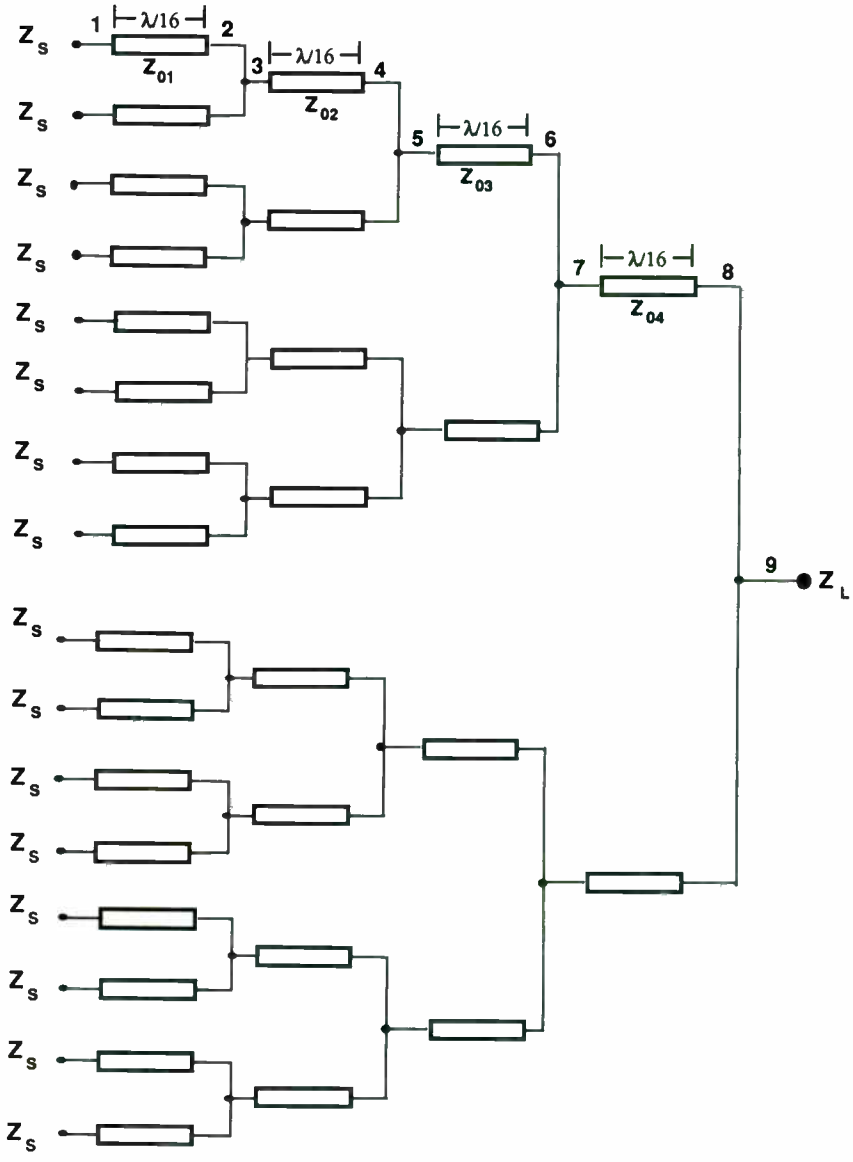

Figure 9. A 16-way equal phase, equal amplitude combiner

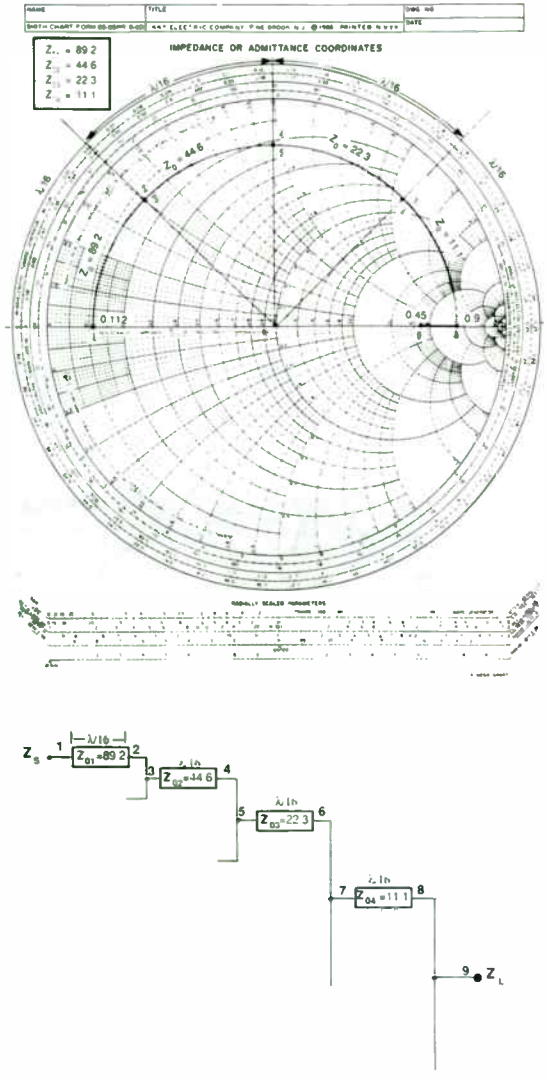

Figure 10. 10 Ω to 50 Ω impedance transformation through 1:16 way combiner.

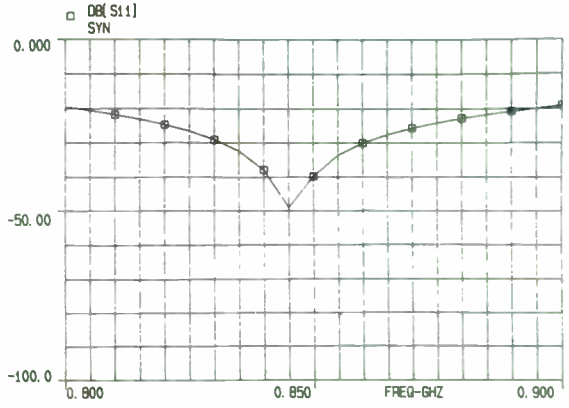

Figure 11. Return loss of the 16-way combiner with Z_s = 10 Ω.

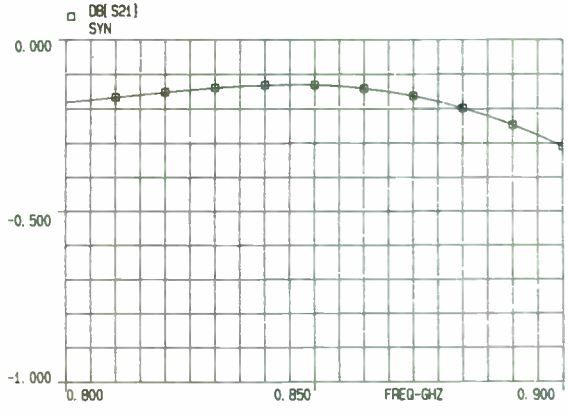

Figure 12. Back-to-back insertion loss for two 16-way combiners.

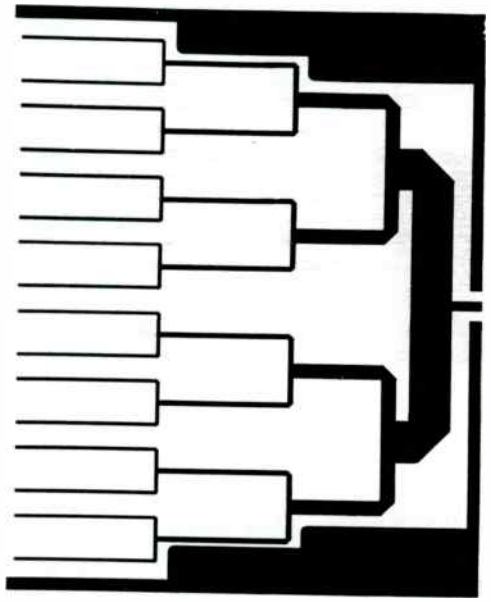

Figure 13 . Layout of a 16-way equal phase, equal amplitude UHF combiner

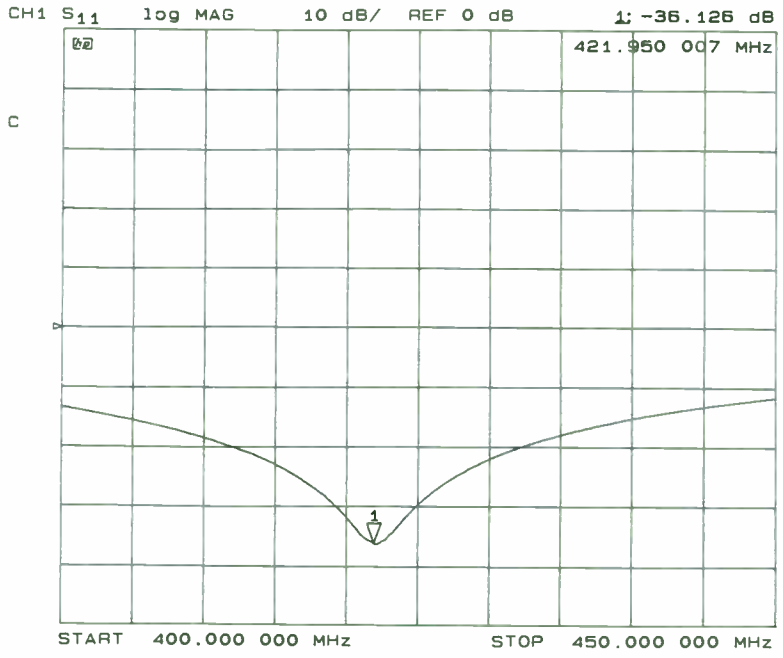

Figure 14 . Measured return loss of the 16-way equal phase, equal amplitude UHF combiner

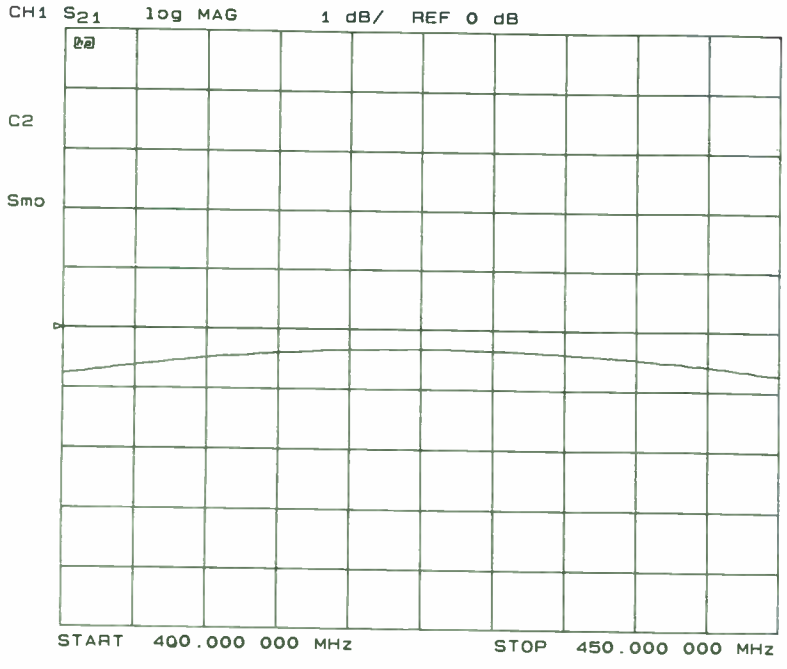

Figure 15 . Measured insertion loss of two 16-way equal phase, equal amplitude UHF combiners in a back to back configuration.

A VERSATILE UHF DATA/TELEMETRY TRANSMITTER

HARRY J. SWANSON

Motorola Semiconductor Products Sector
Linear RF/Telecom Applications
Linear Analog IC Division
2100 East Elliot Road, EL340
Tempe, AZ 85284

ABSTRACT

This paper details the design of a UHF AM/FM transmitter featuring a monolithic UHF transmitter IC, MC13176. The IC contains a Colpitts reference oscillator, divide by 8 or divide by 32 prescalar, UHF current control oscillator and phase detector forming a versatile PLL system. A complete UHF data/telemetry subsystem incorporating few external components, power down functions, lithium battery power and AM and FM modulation is demonstrated. The system application is complete with PCB layout and housing and antenna interface circuitry.

INTRODUCTION

RF communication in the UHF and 900 MHz bands constitute a new and growing industry covered by the FCC regulations Title 47; Part 15. This section covers unlicensed security systems, keyless entry, and RF local area networks (LAN'S) in the 260 to 470 MHz band. The 902 to 928 MHz band is also covered by Part 15 where frequency hopping and direct digital sequence spread spectrum techniques are employed to increase frequency spectrum capability and to provide secured communications. Discretes and some IC components

are available to the system designer but until now there heve been very few system components that offer a low cost , sophisticated solution.

Data transmission systems used in consumer applications are simple inexpensive and often mediocre in performance. Two common circuit designs that are currently used are:

1). Frequency Multiplier system where a reference crystal is used with cascaded multiplier stages to achieve the desired carrier frequency.

2). A SAW Resonator plus a simple Colpitts oscillator network is used in Amplitude Shift Key (ASK) applications where On-Off Keying is required.

The shortcomings of the current systems include:

- expensive 5th or 7th overtone crystals
- high manufacturing cost due to sophisticated alignment procedures
- lack of frequency stability
- high current consumption in receiver to provide needed IF bandwidth
- Compromised reliability due to large number of critically tuned components
- Little or no FM possibilties.

Many more complex applications including cellular, CT2 and SMR can also benefit from a fully integrated system that employs a PLL structure.This paper demonstrates a complete system with functional performance suitable for a low cost solution to data/telemetry and voice applications. Cost and size restraints are met by the simplicity of the supporting circuitry. Total system reliability and performance are vastly improved with a single chip PLL approach. The MC13175 and MC13176 offer the following features:

- UHF Oscillator Current Controlled
- Uses Easily Available 3rd Overtone or Fundamental Crystals

- Output Frequency Set by 8x Reference Frequency for MC13175 and 32x Reference Frequency for MC13176
- Low Number of External Parts Required
- Low Operating Supply Voltage (1.8-5.0 Vdc)
- Low Supply Drain Currents
- Power Output Adjustable (Up to +10 dbm)
- Differential Output for Loop Antenna or Balun Transformer Networks
- Power Down Feature
- ASK Modulated by Switching Output On and Off
- Easily FM Voice or FSK Modulated
- Surface Mount 16 Pin SOIC

PLL SYSTEM DESCRIPTION

The MC13175 and MC13176 are one chip FM/AM transmitter subsystems designed for AM/FM communcation systems operating in VHF, UHF or 900 MHz bands. The system consists of a Colpitts reference crystal oscillator, UHF oscillator, divide by 8 (MC13175) or divide by 32 (MC13176) prescalar, and phase detector forming a versatile fully integrated PLL system

Figure 1 is the component block diagram of the MC1317XD PLL system in which the loop characteristics are described by the gain constants. Access to individual components of this PLL system is limited, inasmuch as the loop is only pinned out at the phase detector output and the frequency control input for the CCO. However, this allows for characterization of the gain constants of these loop components. The gain constants K_p,K_o and K_n are derived and specified in the MC13176 data sheet. A detailed discussion of the characteristics of the IC with a pin by pin description and a discussion of the

PLL fundamentals and how they apply to this PLL system component is also included in the data sheet (1). For the benefit of the reader, the pin by pin description is included in Appendix A of this paper.

LOOP FILTERING

The Fundamental loop characteristics , such as capture range, loop bandwidth, lock-up time and transient response are controlled externally by loop filtering. The loop filter may take the form of a simple low pass filter or a lag-lead filter which creates an additional pole at origin in the loop transfer function. This additional pole along with that of the CCO provides two pure integrators ($1/s^2$). With two poles at the origin, a type 2 second order response yields a zero phase error to a step input of phase or frequency. The natural frequency, w_n and damping factor, ∂ are important in the transient response to a step input of phase or frequency. For a given ∂ and lock time, w_n can be determined from the output response of a type 2 second order system shown in Figure 2a (2).

In the lag-lead low pass network shown in Figure 3, the values of the low pass filtering parameters R1, R2 and C determine the loop constants w_n and ∂. The following equations show this relationship (2,3,4):

$$w_n^2 = (K_pK_oK_n) / (R_1C) = K_pK_o / R_1CN$$

$$\partial = KpKoKnR_2 / 2w_nR_1 = K_pK_oR_2 / 2w_nR_1N$$

Rewriting in terms of R_2 and R_1C:

$$R_1C = K_pK_o/w_n^2N$$

$R_2 = 2\partial w_n R_1 N / K_p K_o = 2\partial / C w_n$

FIGURE 3 - LAG-LEAD LOW PASS FILTER

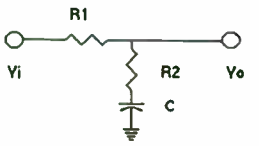

DEMONSTRATION TRANSMITTER

The demonstration transmitter is discussed in the following sections and is built on a double sided PCB defined in the data sheet. The center section of the board provides an area for attaching all SMT components to the circuit side and radial leaded components to the component ground side of the PCB. Additionally, the peripheral area surrounding the RF core provides pads to add supporting and interface circuitry.

FM MODULATION

The demonstration transmitter is FM modulated with voice and data via a summing amplifier to pin 6 as shown in Figure 4. In FM voice and low data rate applications, the loop bandwidth must be narrow enough so that the loop will not cancel out the modulation frequency components. The loop bandwidth is related to the natural frequency, w_n as shown in the table in Figure 2b. For a loop bandwidth of 1kHz, the natural frequency , w_n is 3.05 krad/sec for a damping factor, ∂ of 0.707 (3).

In the example below, R_1, R_2, and C are calculated for the second order, type 2 system described above

$K_p K_o K_n = (30)(0.91 \times 10^6)(1/32) = 0.853 \times 10^6$

$R_1 = K_p K_o K_n / w_n^2\ C = 0.853 \times 10^6 / (9.30 \times 10^6)\ (C)$

$R_2 = 2\partial / w_n C = (2)(.707)/(3.05 \times 10^3)\ (C)$

For C= 1.0μ; then R_1 = 91.6k and R_2 = 464

In the above example the following standard value components are used

C = 1.0 μ; R_2 = 470 and R'_1 = 91.7k - 53k ~ 39k

(R'_1 is defined as R_1- 53k, the output impedance of the phase detector)

Since the output of the phase detector is high impedance and serves as a current source, and the input to the frequency control, pin 6 is low impedance (impedance of the two diode to ground is approximately 500Ω), it is imperative that the second order low pass filter design above be modified. In order to minimize loading of the R_2C shunt network, a higher impedance must be established to pin 6. A simple solution is achieved by adding a low pass network between the passive second order network and the input to pin 6 (see Figure 5). This helps to minimize the loading effects on the second order low pass while further suppressing the sideband spurs of the crystal oscillator. A low pass filter with R3 = 1k and C2 = 1500p has a corner frequency, f_c of 106 kHz; the reference sideband spurs are down greater than - 60 dBc.

FIGURE 5 - MODIFIED LOW PASS LOOP FILTER

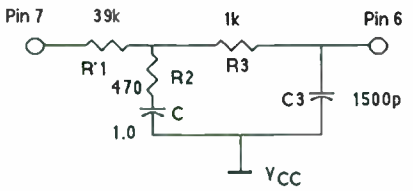

HOLD-IN RANGE

The hold-in range, also called the lock range, tracking range and synchronization range, is the ability of the CCO frequency, f_o to track the input signal, f_{REF} x N as it gradually shifted away from the free running frequency, f_f. Assuming that the CCO is capable of sufficient frequency deviation and that the internal loop amplifier and filter are not overdriven, the CCO will track until the phase error, Θ_e approaches $\pm \pi/2$ radians. Since sin Θ_e cannot exceed $\pm$ 1, as Θ_e approaches $\pm \pi/2$ the hold-in range is equal to the dc loop gain, K_V x N.

$$\pm \Delta w_H = \pm K_V \times N$$

where $K_V = K_P K_O K_n$

In the above example, $\pm\Delta w_H = \pm 27.6$ Mradians/sec; $\pm\Delta f_H = \pm 4.40$ MHz. (4)

EXTENDED HOLD-IN RANGE

The hold-in range of about 3.0 % could cause problems over temperature in cases where the free running oscillator drifts more than 2 to 3 % because of relatively high temperature coefficients of the ferrite tuned CCO inductor. This problem might be worse for lower frequency applications where the external tuning coil is large compared to internal capacitance at pins 1 and 4. The hold-in range can be increased to approximately 10 % by addition of an external loop amplifier with an external current source at pin 6 that extends the operating range of the CCO (1).

In the demo transmitter, the external loop amplifier in Figure 6 is used. An external resistor (R5) of 15k to VCC (3Vdc) provides approximately 100 µA boost to supplement the existing 50 µA internal source current. R4 (1k) is selected for approximately 0.1 Vdc across it with 100 µA. R1,R2 and R3 are selected to set the potential at pin 7 and the base of 2N4402 at approximately 0.9 Vdc and the emitter at 1.55 Vdc when the error current to pin 6 is approximately zero µA. C1 is chosen to reduce the level of the crystal sidebands. The impedance at this node now is the parallel resistances of 68k and 33k with (HFE + 1)(RE) which is >150k.; the equivalent impedance seen by pin 7 is approximately 20k. The lead-lag loop filter described in Figure 3 is added to provide zero phase and frequency errors to transient inputs.

Figure 7 shows the improved hold-in range of the loop. The Δf_{REF} is moved 950 kHz with over 200 µA swing of control current for an improved hold-in range of ±15.2 MHz or ±95.46 Mradians/sec.

VIDEO MODULATOR

The demo transmitter is also capable of AM modulation. Analog AM bandwidth using a sinusoidal waveform is typically 25 MHz. Figure 8 is the circuit used to amplitude modulate with a NTSC composite video signal. It is necessary to invert the negative going sync of composite video before applying the signal to pin 16 of the IC. As in the analog AM example in the data sheet , the modulating signal rides on a positive dc offset ; however, in this case the video sync is clamped by the diode, MPN3401. The gain in the amplifier and the linearity of the AM modulation is adjusted by the 500 ohm pot in the emitter of the 2N4401.

FIGURE 8 - NTSC VIDEO MODULATOR

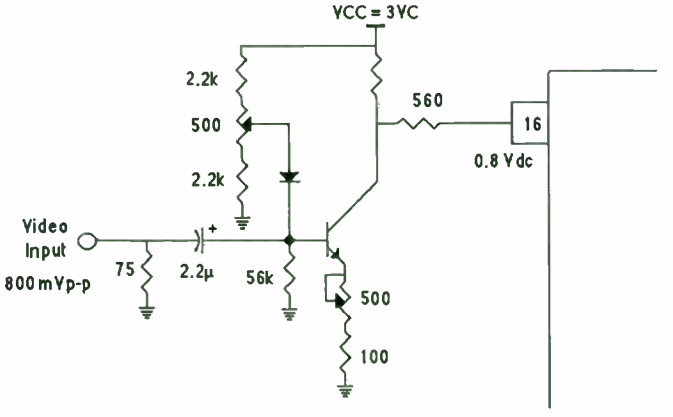

PCB LAYOUT CONSIDERATIONS

In the PCB layout, the VCC trace must be kept as wide as possible to minimize inductive reactance along the trace; it is best that VCC (RF ground) completely fills around the surface mounted components and interconnect traces on the circuit side of the board. This technique is demonstrated in the demo transmitter PC board.

The ground pins (also applies to pins 10 & 15) are connected directly to chassis ground. Decoupling capacitors to V_{CC} are placed directly at the ground returns.

BATTERY - SELECTION - LITHIUM TYPES

The operating supply voltage range is from 1.8 Vdc to 5.0 Vdc. The demo transmitter is operated from a 3 volt lithium battery. Selection of a suitable battery is important. Because one of the major problems for long life battery powered equipment is oxidation of the battery terminals, a battery mounted in a clip-in socket is not advised. The battery leads or contact post should be isolated from the air to eliminate oxide build-up. The battery should have PC board mounting tabs which can be soldered to the PCB. Consideration should be given for the peak current capability of the battery. Lithium batteries have current handling capabilities based on the composition of the lithium compound, construction and the battery size. A 1300 mA-hr rating can be achieved in the cylindrical cell battery. The Rayovac CR2/3A Lithium-Manganese Dioxide battery is a crimp sealed, spiral wound 3 volt 1300 mAhr cylindrical cell with PC board mounting tabs. It is an excellent choice based on capacity and size (1.358 inches long by .665 inches in diameter).

DIFFERENTIAL OUTPUT (PINS 13 & 14)

The availability of micro-coaxial cable and small BALUNS in surface mount and radial-leaded components allows for simple interface to the output ports. A loop antenna may be directly connected with bias via RFC or 50 ohm resistors. Antenna configuration will vary depending on the space available and the frequency of operation.

MATCHING TO ANTENNA

When using an antenna having 50 ohms impedance, a quarter wave BALUN with a Zo = 50 ohms would present a 50 ohm load to the IC. However, if the antenna is not actually 50 ohms, then the complex impedance presented to the device would be transformed by the BALUN as shown in the following formula

$$Z_S = Z_O{}^2 / Z_{load}$$

where Z_{load} is the complex impedance of the antenna

Z_S is the load presented to the device

Z_O is 50 ohms

For instance, if the antenna radiation resistance is low (when its electrical length is less than 1/10 wavelength), Zs would be transformed to a relatively high impedance. Thus, the energy delivered to the antenna is reduced because of a severe mismatch of the antenna to the IC. Therefore, the 1/4 wavelength BALUN is intended in systems where the load impedance is near 50 ohms..

SIZE AND TYPE ANTENNA

The size and type of antenna is an important consideration. At 320 MHz, a quarter wavelength antenna is 0.234 meters or 9.2 inches. This is likely to be too long for practical systems. However, when the antenna is on the order of 1/25 wavelength, the radiation efficiency of the antenna is very low (< 1 %). The radiation and loss resistances of an antenna determine the radiation efficiency. The loss resistance of a short loop is generally much larger than its radiation resistance. To increase the radiation efficiency (increased radiation resistance), multiturn loops are often employed, but the spacing between loops must be maintained. For close spacing between turns, the contribution to the loss resistance due to proximity effects can be larger than that due to the skin effect. In other words, a multiturn loop antenna which has the turns touching or with spacing between turns less than 3 times the wire diameter will increase the ohmic resistance exponentially with decreasing distance between turns. Therefore, a multiturn loop antenna requires adequate space for proper distance between the turns and for the necessary ratio of loop circumference to the wavelength.

Radiation resistance equation can be written as

$$R_r = 20\pi^2(C/\lambda)^4$$

where $C = 2\pi a$ is the circumference of the loop (5). At 320 MHz, if the radius of a single turn loop in free space equals 1/10 wavelength or approximately 3.6 inches, then the radiation resistance is 29.4 ohms. For a loop with a radius of 1/25 wavelength or 1.5 inches, the radiation resistance falls to less than one ohm. To accommodate the size constraints placed on a system, resonant loops

and folded monopoles are sometimes employed. A resonant loop may be configured as a parallel resonant circuit of a single turn loop and small series loop radiation resistance with a shunt capacitor in which high loop energy is developed at the carrier frequency. This loop should be printed on the PCB as an airline (i.e. no ground plane on either side of the board under or around the loop). In a hand held portable transmitter the coupling effects of the hand must be considered.

In most cases these designs are a compromise in which either the receiver is counted on to have excellent sensitivity or the transmitter requires relatively excessive power to make up for the lack of efficiency in the antenna. The size and design of the antenna system is important to its radiation capability; this area should not be overlooked in terms of the total transmitter system. It is not the scope of this paper to propose the ultimate solution or profess that one exists.

CONCLUSIONS

This paper has detailed the design of a monolithic UHF transmitter IC and its interface circuitry. The demonstration transmitter shows the versatile aspects of this basic PLL building block in both AM and FM applications. It offers the following advantages:

1. Uses low cost surface mounted and low profile insertion mounted components
2. On a double sided PCB a finished product takes up little space.
3. With the extended hold-in range circutry, the transmitter functions from -40 ^{o}C to +85 ^{o}C.
4. Excellent frequency stability
5. Low manufacturing cost due to simple tuning procedures.

The issues left open by this paper and the data sheet, such as temperature characterization are important and will likely be addressed as the product matures. The benefits of using this single chip PLL in other more complex applications are yet to be realized. Being the first of its kind opens the way to scrutiny on one hand, but paves the way to new horizons on the other hand.

REFERENCES

1. MC13175D and MC13176D Technical Data Sheet, Motorola, Inc., 1991.
2. AN553, A New Generation of integrated Avionics Synthesizers, Motorola, Inc., 1971, p. 6.
3. AN535, Phase-Locked Loop Design Fundamentals, Motorola, Inc.
4. Herbert L. Krauss, Charles W. Bostian, and Frederick H. Raab, *Solid State Radio Engineering*, Wiley, New York, 1980, pp. 164-185.
5. Constantine A. Balanis, *Antenna Theory: Analysis and Design*, Wiley, New York, 1982, pp. 169- 184.

FIGURE 1 - MC1317XD PLL BLOCK DIAGRAM

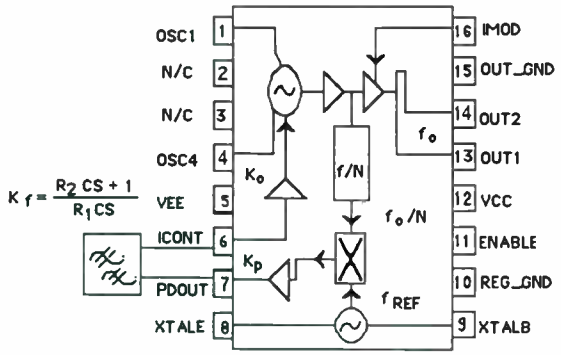

where

K_p is Phase detector gain constant in μA per radian; K_p = 30 μA/rad

K_f is Filter transfer function, F(s)

K_n is 1/N; N= 8 for MC13175 and N = 32 for the MC13176

K_o is CCO gain constant in radians per second per μA; K_o = 9.1 x 10^5 radians/sec/μA.

FIGURE 2a - TYPE 2 SECOND ORDER RESPONSE

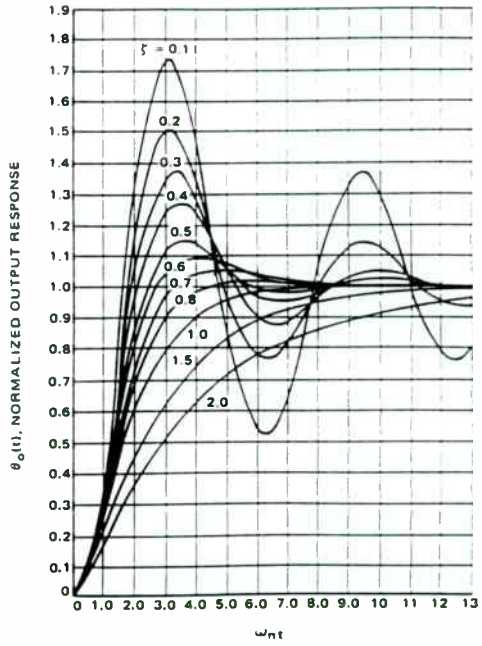

FIGURE 2b - LOOP BANDWIDTH

Bandwidth as a Function of Damping Ratio	
ζ	$\omega_{-3\ dB}$
0.5	1.82 ω_n
0.7	2.06 ω_n
1.0	2.48 ω_n

FIGURE 4 - MICROPHONE/DATA AMPLIFIER

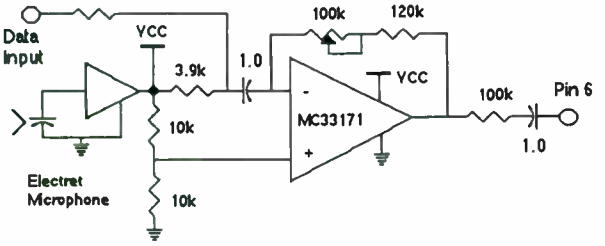

FIGURE 6- EXTERNAL LOOP AMPLIFIER

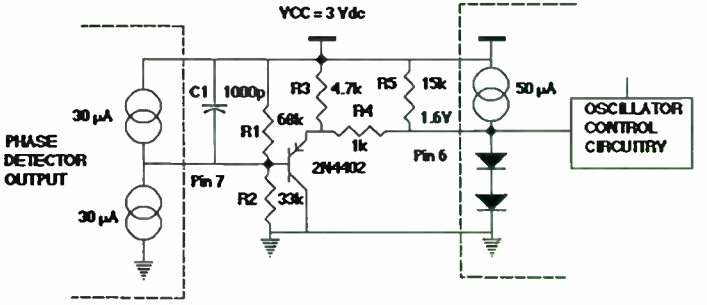

FIGURE 7 - MC13176D REFERENCE OSCILLATOR FREQUENCY versus OSCILLATOR CONTROL CURRENT

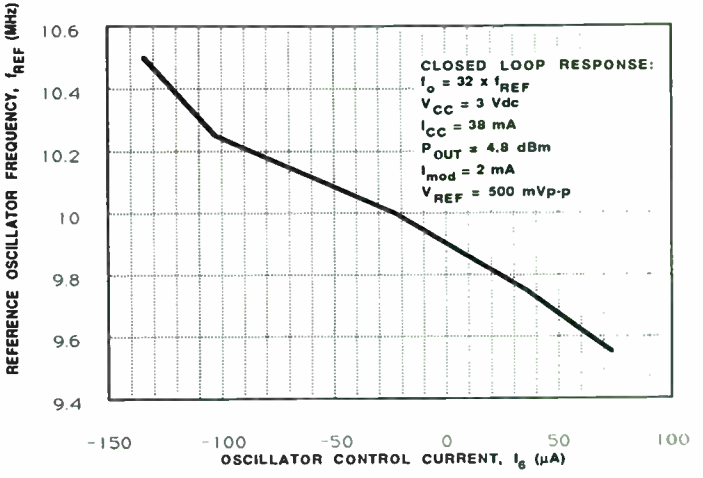

APPENDIX A

PIN BY PIN DESCRIPTION AND INTERNAL CIRCUITS

CCO Inputs (Pins 1 & 4)

The oscillator is a current controlled type. An external oscillator coil is connected to Pins 1 and 4 which forms a parallel resonance LC tank circuit with the internal capacitance of the IC and with parasitic capacitance of the PC board.Three base - emitter capacitances in series configuration form the capacitance for the parallel tank. These are the base - emitter at pins 1 and 4 and the base - emitter of the differential amplifier. The equivalent series capacitance in the differential ampifier is varied by the modulating current from the frequency control circuit (see pin 6 internal circuit).

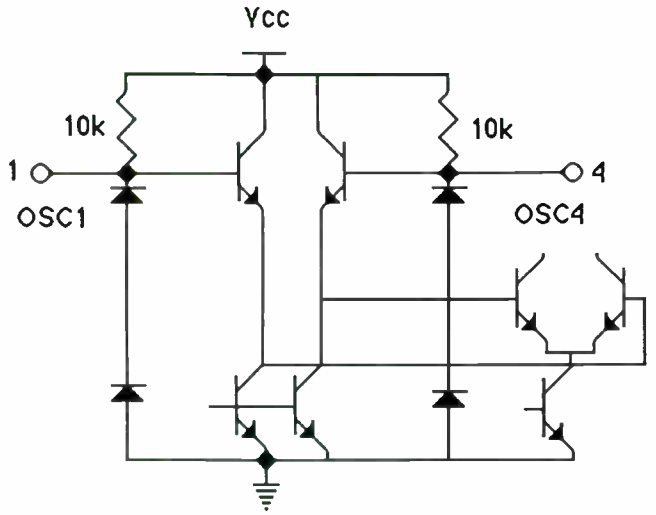

Frequency Control (Pin 6)

The voltage at pin 6 is approximately 1.55 Vdc. With +/- 30 µA of control current, the free running oscillator frequency will swing +/- 1.7 % in the MC13176 (see Figure A1). The oscillator is current controlled by the error current from the phase detector. This current is amplified to drive the current source in the oscillator section which controls the frequency of the oscillator.

The CCO may be FM modulated as shown in the MC13176D Demo Transmitter. A detailed discussion of the specific application shows how to extend the hold-in range

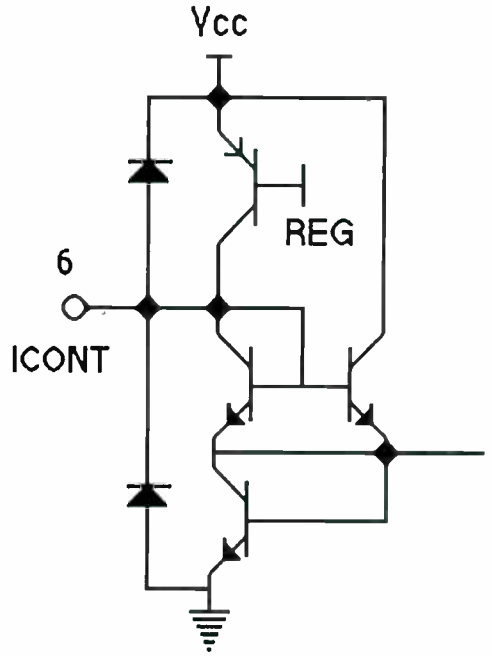

Phase Detector Output (Pin 7)

The phase detector provides +/- 30 µA to keep the CCO locked at the desired carrier frequency. It is a sinusoidal type detector derived from a four quadrant multiplier which receives its inputs from the internal divider network and from the Colpitts reference oscillator. The phase detector output circuit is in an npn/pnp push-pull configuration and has an output impedance of approximately 53kΩ. Under closed loop conditions, there is a DC voltage which is dependent upon the free running oscillator and the reference oscillator frequencies. The circuitry between pins 7 and 6 should be selected for adequate loop filtering necessary to stabilize and filter the loop response. Low pass filtering between pin 7 and 6 is needed so that the corner frequency is well below the sum of the divider and the reference oscillator frequencies, but high enough to allow for fast response to keep the loop locked.

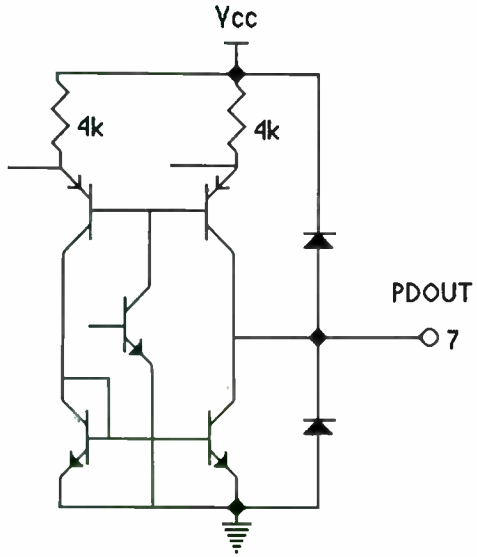

Crystal Oscillator Inputs (Pins 8 & 9)

The internal reference oscillator is configured as a common emitter Colpitts. It may be operated with either a fundamental or overtone crystal depending on the carrier frequency and the internal prescalar. Crystal used in the application is a fundamental 10 MHz.

With Vcc= 3 Vdc, the voltage at pin 8 is approximately 1.85Vdc and at pin 9 is approximately 2.3Vdc. 500 to 1000 mVp-p should be present at pin 9. The Colpitts is biased at 200 µA; additional drive may be acquired by increasing the bias to approximtely 500 µA. Use 6.2k from pin 8 to ground.

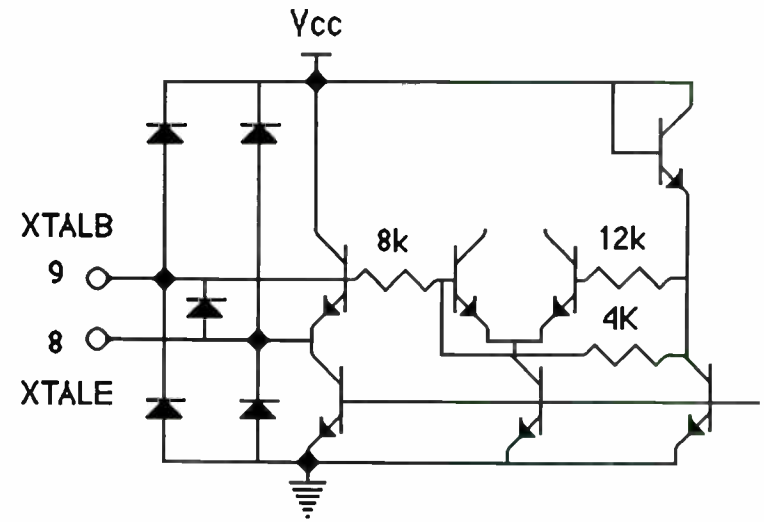

Regulator Ground (Pin 10)

An additional ground pin is provided to enhance the stability of the system. Decoupling to the VCC (RF ground) is essential; it should be done at the ground return for pin 10.

Device Enable (Pin 11)

The potential at pin 11 is approximately 1.25 Vdc. When pin 11 is open, the transmitter is disabled in a power down mode and draws less than 1 µA I_{CC} if the MOD, pin16 is also open (i.e. it has no current driving it). To enable the transmitter a current source of 10 to 90 µA is provided Figures A2 & A3 show the relationship between I_{CC}, V_{CC} and $I_{REG\text{-}ENABLE}$; note that I_{CC} is flat at approximately 10 mA for $I_{REG\text{-}ENABLE}$ = 5 to 100 µA (I_{mod}= 0).

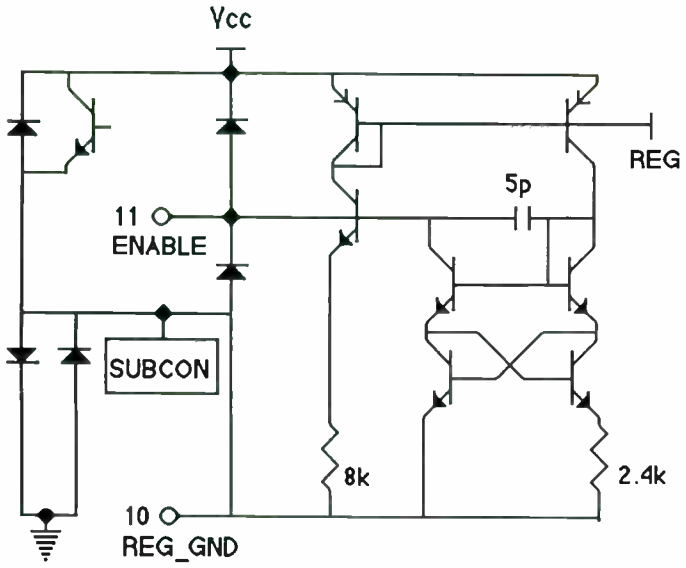

Differential Output (Pins 13 & 14)

The output is configured differentially to easily drive a loop antenna. By using a transformer or BALUN, as shown in the application schematic, the device may then drive an unbalanced low impedance load.

Output Ground (Pin 15)

This additional ground pin provides direct access for the output ground to the circuit board VEE.

AM Modulation / Power Output Level (Pin 16)

The DC voltage at this pin is 0.8 Vdc with the current source active. An external resistor is chosen to provide a source current of 1 to 3 mA, depending on the desired output power level at a given Vcc. Figure A4 shows the relationship of Power Output to Modulation Current, Imod. At Vcc = 3.0 Vdc , 3.5 dBm power output can be acquired with about 35mA Icc.

For FM modulation , pin 16 is used to set the desired output power level as described above.

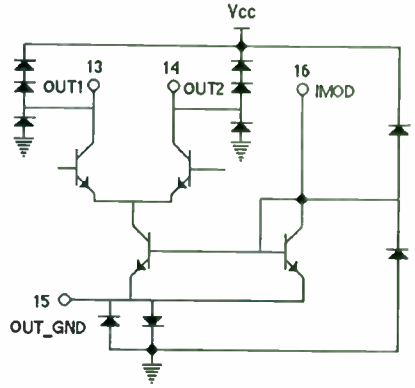

FIGURE A1 - MC13176D REFERENCE OSCILLATOR FREQUENCY versus PHASE DETECTOR CURRENT

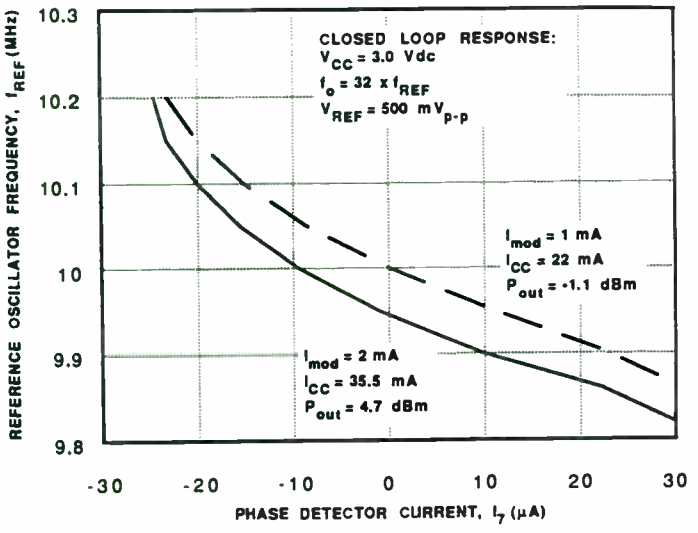

FIGURE A2 - SUPPLY CURRENT versus SUPPLY VOLTAGE

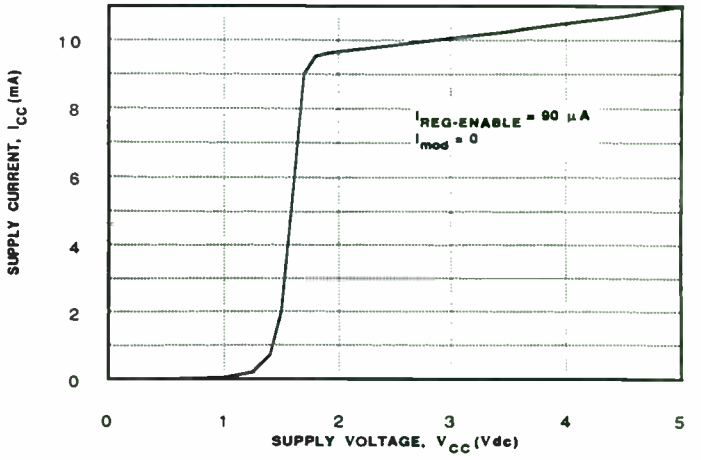

FIGURE A3 - SUPPLY CURRENT versus REGULATOR ENABLE CURRENT

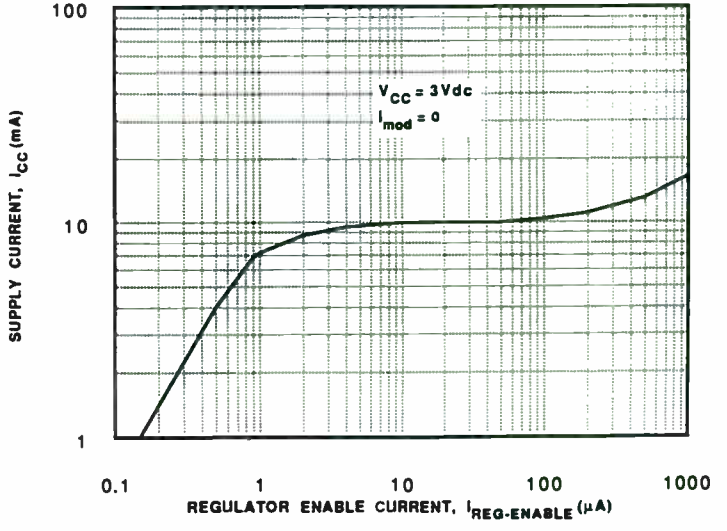

FIGURE A4 - POWER OUTPUT versus
MODULATION CURRENT

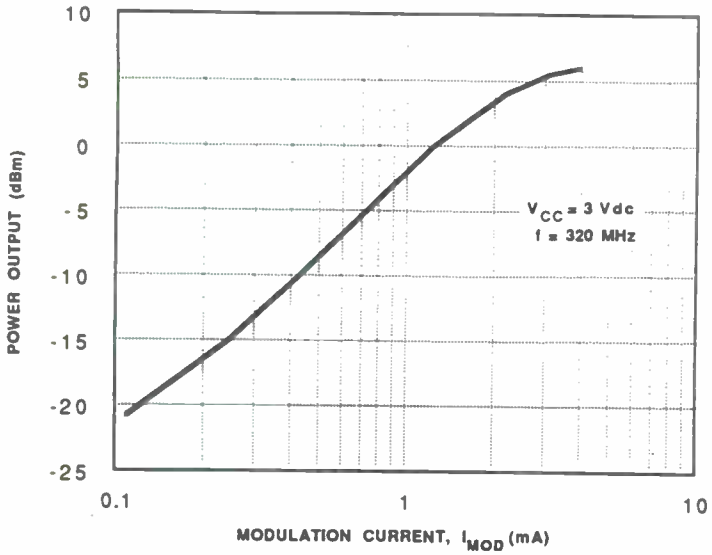

SIXTH ANNUAL

RF expo EAST

October 29-31, 1991
Stouffer Orlando Resort
Orlando, Florida

RF Expo East Sponsored by *RF Design* Magazine

Good Sines & Bad Signs

Looking for a low-noise, fast-switching signal source?

Good Sines

Whether it's automatic test equipment, satellite uplinks, EW communications or imaging systems, **Programmed Test Sources** has a frequency synthesizer to fit your needs. GE MRI units, Teradyne Testers, Varian Spectrometers . . . all use **PTS** synthesizers.

Bad Signs $$$

And while other manufacturers have big dollar signs, PTS synthesizers start as low as $2,010.

PTS manufactures a complete line of precision synthesizers covering the 100 KHz to 1 GHz frequency range with switching times as fast as 1μ second for our ***direct digital*** models. And plenty of other options as well, like resolution down to .1 hertz (millihertz available as special order), GPIB and digital phase rotation.

Just as important, along with every **PTS** synthesizer comes our "absolutely everything covered" **2-year warranty.** At the end of two years comes our flat $350* service charge for any repair up to the year 2001! **PTS** has a commitment to quality you won't find anywhere else.

Find out how **PTS** synthesizers used the world over can help you in your application today. Call for our complete catalog, or to talk to an applications engineer.

*$500.00 for **PTS** 1000.

Call (508) 486-3008 *Fax* (508) 486-4495

PTS

PROGRAMMED TEST SOURCES, Inc.
9 Beaver Brook Road, P.O. Box 517, Littleton, MA 01460

WELCOME

Welcome to the largest, most exciting RF Expo East in our history. This year's exhibit hall was SOLD OUT months prior to the Expo, and pre-registered attendance has continued strong. Why? Because there is so much going on in the exciting area of radio frequency. Remember when people actually thought that RF only covered beepers and pagers, or hobby communications? The truth is that the RF industry is a 300+ billion-dollar industry, covering everything from sophisticated radar and weapons systems to every form of communication. This has made our industry one of the few bright spots in electronics...and its broad base of application areas grows everyday with the addition of technologies like CTII, wireless office products, and Personal Communications Networks.

It's true: information is power, and there is simply no other event that provides so much hands-on, useful information on RF technologies in one place, at one time. New products, new design techniques, new regulations, and new application areas can be researched at RF Expo East 1991. Experts from around the world have accepted our invitation to speak to RF Expo attendees, and manufacturers representing virtually every product category and configuration are on hand in the exhibit hall to answer your questions. We know how much there is to see and hear over three days...and have worked to develop a program that will allow you to spend time in both the sessions and the exhibit hall.

And while we are all here to learn more about the technology and meet with other professionals, don't forget to enjoy yourselves as well. Back by overwhelming demand is the Ham Radio Reception, deli lunch in the exhibit hall for attendees, prize give-a-ways, and more. This year we have even planned a little Halloween fun for Thursday!

Lastly, the staff of *RF Design* magazine and the RF Expo Show Department wish to sincerely thank our hundreds of exhibiting companies for supporting this event and the RF industry, and to thank the more than 50 speakers and moderators who have volunteered to share their expertise and experience with all of us. And thank you to YOU, our RF Expo East attendees, for helping to make this the most exciting RF Expo East in history.

Kathi Walsh
Publisher

Kathy Kriner
Vice President

Kristin Hohn
Convention Manager

TABLE OF CONTENTS

The 48 cent solution.

Wideband Amplifiers – From $.48 each

UPC1653 To 1300MHz 18dB G_P	**UPC1654** To 1100MHz 19dB G_P	**UPC1655** To 900MHz 18dB G_P	**UPC1656** To 850MHz 19dB G_P	**UPC1658** To 1100MHz 17dB G_P 2.0dB NF	
UPC1659 600MHz to 2300MHz 23dB G_P	**UPC1675** To 2100MHz 12dB G_P	**UPC1676** To 1300MHz 20dB G_P 4.0dB NF	**UPC1677** To 1700MHz 24dB G_P P_{out} = 19.5dBm	**UPC1678** Up to 1900MHz 23dB G_P P_{out} = 18dBm	**UPC1688** Up to 1000MHz 21dB G_P 4.0dB NF

Prescalers – From $2.20 each

UPB581 ÷ 2 500MHz to 2.8GHz	**UPB582** ÷4 500MHz to 2.8GHz	**UPB584** ÷2 500MHz to 2.5GHz	**UPB585** ÷ 4 500MHz to 2.5GHz	**UPB586** ÷ 512/256 500MHz to 2.5GHz	**UPB587** ÷ 2/4/8 50MHz to 1.0GHz V_{CC}=2.2 to 3.5V	**UPB588** ÷64/128 500MHz to 2.5GHz

Freq. Convertors – From $1.58 each

UPC1685 DC to 890MHz 14dB GAIN Double Balanced Mixer Applications	**UPC1686** DC to 890MHz 22dB GAIN	**UPC1687** DC to 890MHz 28dB GAIN I_{CC} of 38mA

IF Amplifiers – From $3.50 each

UPC1668 10 to 170MHz G_L=14.5dB 60dB Isolation	**UPC1669** 10 to 180MHz G_L=10.5dB 55dB Isolation	**UPC1670** 10 to 150MHz IM_3 of 56dBc 60dB Isolation

Transistor Arrays From $2.40 each

UPA101 F_T=9GHz Double Balanced Mixer Applications	**UPA102** F_T=9GHz Differental Amplifier
UPA103 F_T=9GHz Differental Amplifier	**UPA104** F_T=9GHz OR/NOR Functions

Special Function M IICs From $1.08 each

UPC1684 LED DRIVER 150mA Drive Current 300 Mbits NRZ	**UPC1663** VIDEO AMPLIFIER 170MHz @ A_{VOL}=100 1.6ns Propagation Delay

Note: MMIC prices based on 25K quantities

NEC®

Want to make life simpler? Reduce the parts count in your design with silicon MMICs from NEC. They're the low cost, no-hassle way to achieve your design goals.

But be aware of the side effects!

Reducing your parts count can also make your QC easier. Your overall circuit more reliable. And your assembly, whether manual or automated, faster and more efficient.

NEC MMICs come in chips and a variety of packages, including hermetic, low cost plastic, surface mount and tape and reel. So they're ideal for high volume automated assembly.

And their quality and reliability is proven: With a production rate of *7 million a month,* no one knows MMICs like NEC.

Our **Silicon MMIC Product Selection Guide** lists specifications for dozens of parts. Chances are good it has just what you need. To get a copy, call your nearest CEL Sales Office or circle the number below.

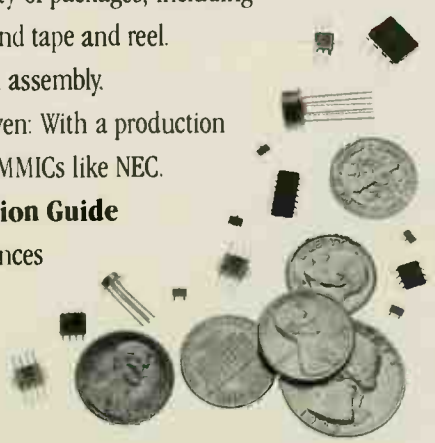

California Eastern Laboratories

CEL Headquarters, 4590 Patrick Henry Drive, Santa Clara, CA 95056-0964; (408) 988-3500 FAX (408) 988-0279 ☐ Santa Clara, CA (408) 988-7846 ☐ Los Angeles, CA (213) 645-0985 Bellevue, WA (206) 455-1101 ☐ Scottsdale, AZ (602) 945-1381 ☐ Richardson, TX (214) 437-5487 ☐ Shawnee, KS (913) 962-2161 ☐ Woodridge, IL (708) 241-3040 ☐ Cockeysville, MD (410) 667-1310 Peabody, MA (508) 535-2885 ☐ Hackensack, NJ (201) 487-1155 or 487-1160 ☐ Palm Bay, FL (407) 727-8045 ☐ Snellville, GA (404) 978-4443 ☐ Nepean, Ontario, Canada (613) 726-0626

Please see us at RF Expo East, Booth #416.

PROGRAM AT A GLANCE

TUESDAY, OCTOBER 29

A-1:	**Using CAD in RF Engineering** Yellowtail Room	8:30-11:30 a.m.	• State of the Art Nonlinear CAD for Microwave/RF	J. Gerber, L. Mah and C. Chang, *Compact Software, Inc.*
			• New Nonlinear Noise Model for MESFETS Including MM-Wave Applications	R. Pengelly and U. Rohde, *Compact Software, Inc.*
			• Design Desensitization	T. Zhang and M. Eron, *Compact Software, Inc.*
			• Microwave/RF System Simulation	Raymond S. Pengelly and R. Hicks, *Compact Software, Inc.*
			• E-M Theory-Based Simulations of Passive Microstrip RF Components on Single and Multiple Metalization Layers	A. Hill, J. Burke and K. Kottapalli, *Compact Software, Inc.*
A-2:	**RF System Performance** Wedgwood Room	8:30 a.m.	• A Unified Look at Spurious Performance of Multiple Conversion Receiving and Transmitting Systems	R. Webb, *Webb Laboratories*
		9:30 a.m.	• Specifying Local Oscillator Phase Noise Performance: How Good is Good Enough	R. Gilmore, *QUALCOMM, INC.*
		10:30 a.m.	• Receiving Subsystem RF/IF Design Methodology	J. Summerville, *Eaton Corporation*
A-3:	**Design & Manufacturing** Coral Ballroom A/B	8:30 a.m.	• RS-232 Communication for Turn-Key Test Stations	W. Walls, *Erbtec Engineering*
		9:30 a.m.	• Chemical Vapor Deposited Diamond Heat Carriers Cooling High Temperature Electronic Components	T. Tuma, *Deptartment of the Navy*
		10:30 a.m.	• Transceiver Characteristics and Their Impact on Battery Life Performance in Land Mobile/Cellular Portable Phones	M. Ghadaksaz, *GTE Laboratories, Inc.*
A-4:	**Test and Measurement** Crystal Ballroom E	8:30 a.m.	• Optimize Mixer Performance Through Swept-Frequency and Power Characterization	B. Brown and J. Dunsmore, *Hewlett-Packard*
		9:30 a.m.	• Testing Dual Mode North American Cellular, Japan Digital Cellular Transceivers	D. Hoover, *Hewlett-Packard*
		10:30 a.m.	• Power Triode Tube Curve Tracer	L. Erb and W. Walls, *Erbtec Engineering*
B-1:	**Filter Design Techniques** Yellowtail Room	1:30 p.m.	• Filters With Improved Delay Characteristics	W. Lurie
		2:30 p.m.	• Design of Filters with Unsymmetrical Stopbands	W. Lurie
		3:30 p.m.	• Approximation of Filters with Shaped Passbands	G. Szentirmai, *DGS Associates, Inc.*
B-2:	**Oscillators** Wedgwood Room	1:30 p.m.	• The MCXO, Characteristics and Applications	B. Rose, *Q-Tech Corporation*
		2:30 p.m.	• Defining VCO Tuning Linearity	A. Coon, *RF Monolithics, Inc.*
		3:30 p.m.	• Microwave Oscillators	R. Weber, *Electrical Engineering*
B-3:	**RF Power** Coral Ballroom A/B	1:30 p.m.	• Class-E Power Amplifier Output Power, Efficiency, and Output Impedance vs. Loaded Q and Component Parasitic Losses	N. Sokal, I. Novak and L. Drimusz, *Design Automation, Inc.*
		2:30 p.m.	• Design and Performance of High Power Pin Diode T/R Switches for VHF and UHF Land Mobile Voice and Data Communications Systems	M. Ghadaksaz, *GTE Laboratories Incorporated*
		3:30 p.m.	• Directions and Developments in Very High Power RF at LAMPF	R. Cliff, M. Parsons and H. Ward Harris, *Los Alamos Labs*
B-4:	**Special Open Session** Crystal Ballroom E	1:30 p.m.	• Low Frequency Circulator/Isolator Uses No Ferrite or Magnet	C. Wenzel, *Wenzel Associates*
		2:30 p.m.	• A Comprehensive Filter Design Program	M. Ellis

WEDNESDAY, OCTOBER 30

C-1:	**Low Noise Amplifier Tutorial** Yellowtail Room	8:30-11:30 a.m.	• Design of Low Noise RF and Microwave Amplifiers	R. Webb, *Webb Laboratories*
C-2:	**Application of MMICs** Wedgwood Room	8:30 a.m.	• Microwave EW System Enhancements Using MMIC Technology	J. Summerville, *Eaton Corporation*
		9:30 a.m.	• Effective MMIC Testing Strategies for Engineers (dBm)	J. Sheinwald, *AIL Systems, Inc.*
		10:30 a.m.	• Silicon MMIC Amplifier Hits the 20/20 Gain/Power Mark at UHF	D. Osika and R. Green, *SGS-Thomson*
C-3:	**Receivers** Coral Ballroom A/B	8:30 a.m.	• Distribution of Gain and Selectivity in Receivers	W. Vogel, *MATE Electronics*
		9:30 a.m.	• Tunable Notch Filter for Interference Rejections	E. Adler and E. Viveiros, *Harry Diamond Laboratories*
		10:30 a.m.	• Spurious Analysis of Superhetrodyne Receivers and Frequency Synthesizers	S. Vincent, *Raytheon Company*
C-4:	**New RF Applications I** Coral Ballroom C	9:30 a.m.	• Survey of Component Technologies for 900, 2400 and 5700 MHz Unlicensed Spread Spectrum Transceivers	A. Ward, *Avantek*
		10:30 a.m.	• Integrated RF Interfaces for Rural Central Offices	M. Pitke, *Computer Systems & Communications Group*
D-1:	**Power Amplifier Tutorial** Yellowtail Room	1:30-4:30 p.m.	• Classes of RF Power Amplifiers A Through S, How They Operate, and When to Use Each	N. Sokal, I. Novak and J. Donahue, *Design Automation, Inc.*
D-2:	**Spread Spectrum/Mobile Radio** Wedgwood Room	1:30 p.m.	• Upper Limits of a Phase Multiplexed Correlator in a Multiple Access Spread Spectrum System	M. Belkerdid and G. Koller, *University of Central Florida*
		2:30 p.m.	• Mobile Data Packet Networks	J. Kilpatrick and J. Troe, *RAM Mobile Data, Inc.*
		3:30 p.m.	• The Development of an 8 kbps GMSK-Like Modem for Mobitex	J. Seymour, *Gandalf Mobile Systems Inc.*
D-3:	**New RF Applications II** Coral Ballroom A/B	1:30 p.m.	• Making It In The USA	A. Helfrick
		2:30 p.m.	• A Versatile UHF Data/Telemetry FM Transmitter	H. Swanson, *Motorola, Inc.*
D-4	**CDMA Spread Spectrum** Coral Ballroom C	1:30 p.m.	• Spread Spectrum Cellular Communications: Benchmarks for Cost, Power and Spectral Performance	S. Morley, *QUALCOMM Inc.*
		2:30 p.m.	• Field Test Experiments Using Broadband Code Division Multiple Access	D. Schilling, *City College*
		3:30 p.m.	• An Adaptive Technique for Improving Spread Spectrum Interference Rejection	J. Doherty, *Iowa State University*

THURSDAY, OCTOBER 31

E-2:	**Microwave & Military Applications** Wedgwood Room	8:30 a.m.	• Design and Performance of a Novel Broadband Combiner/Impedance Transformer Using 1/16 Wavelength Microstrip Transmission Lines	M. Abdollahian and R. Gage *GTE Laboratories Incorporated*
		9:30 a.m.	• Simulation of Millimeter-Range High-Power CW Frequency Doubling Using Multi-Junction Variable Reactance Diodes	S. Bren and N. Dogan, *Department of Electrical Engineering*
E-3:	**Antennas and Electromagnetics** Coral Ballroom A/B	8:30 a.m.	• Studies of the Cross Antenna	R. Haviland
		9:30 a.m.	• A Simple Expression for the Mutual Inductance of a Wire Current Source and a Non-Coplanar, Parallel, Rectangular Loop	B. Berman

GENERAL INFORMATION

Registration
Location: Stouffer Orlando Resort, Convention Center Lobby
Phone: (407) 351-5555
Hours:

Monday, October 28	7:00a.m.- 6:00p.m.
Tuesday, October 29	7:00a.m.- 6:00p.m.
Wednesday, October 30	7:00a.m. - 6:00p.m.
Thursday, October 31	8:00a.m. - 2:00p.m.

Exposition
Location: Stouffer Orlando Resort, Convention Center Ballroom
Hours:

Tuesday, October 29	11:00a.m. - 6:00p.m.
Sponsored Cocktail Party	5:00p.m. - 6:00p.m.
Wednesday, October 30	11:00a.m. - 6:00p.m.
Sponsored Cocktail Party	5:00p.m. - 6:00p.m.
Thursday, October 31	10:00a.m. - 2:00p.m.

Special Courses
Monday, October 28
Fundamentals of RF Circuit Design: Part I
8:00a.m. - 5:00p.m.
Crystal Ballroom, Section D

Filter and Matching Network Design
8:00a.m. - 5:00p.m.
Crystal Ballroom, Section B

Tuesday, October 29
Fundamentals of RF Circuit Design: Part II
8:00a.m. - 5:00p.m.
Crystal Ballroom, Section D

Wednesday, October 30
Oscillator Design Principles
8:00a.m. - 5:00p.m.
Crystal Ballroom, Section D

Pre-registration for these courses is mandatory. No registrations will be accepted on-site. Badges and tickets need to be called for at the RF Expo East registration counter at 7:00a.m. on Monday, October 28, Tuesday, October 29 and Wednesday, October 30.

Conference Proceedings
Location: Stouffer Orlando Resort
Registration Counter

Proceedings of the RF Expo East are printed and available for purchase at the registration area. The cost to attendees is $65.00. The cost for non-participants is $135.00.

Message Center
Location: Stouffer Orlando Resort, Registration Area
Phone: (407) 352-5791

Any message received for attendees or exhibitors during the show will be posted at the message center. If you want to leave a number with someone back at the office, they can call in and leave a message for you. Messages will be posted alphabetically by last name. Please check daily for messages.

Speaker Ready Room
Location: Fantail Room, Second Floor

Convention Badges

Attendees	Red
Exhibitors	Blue

Hotel
Stouffer Orlando Resort
6677 Sea Harbor Drive
Orlando, FL 32821
(407) 351-5555

Future Shows

RF Expo East September 22-24, 1992 Tampa Convention Center Tampa, Florida	RF Expo East August 17-19, 1993 Baltimore Convention Center Baltimore, Maryland
RF Expo West March 18-20, 1992 San Diego Convention Center San Diego, California	RF Expo West March 17-19, 1993 San Jose Convention Center San Jose, California
RF Expo West March 22-24, 1994 San Jose Convention Center San Jose, California	RF Expo West February 22-24, 1995 Long Beach Convention Center Long Beach, California

SCHEDULE OF EVENTS

TUESDAY, OCTOBER 29

7:00a.m.-6:00p.m.
Registration Open
Stouffer Orlando Resort
Convention Center Lobby

8:00a.m.-5:00p.m.
Fundamentals of RF Circuit Design: Part II
Stouffer Orlando Resort
Crystal Ballroom, Section D

8:30a.m.-4:30p.m.
Technical Program Sessions

11:00a.m. -6:00p.m.
EXHIBITS OPEN
Stouffer Orlando Resort
Convention Center Ballroom

11:30a.m.-1:30p.m.
Deli Lunch, Exhibit Hall Floor

5:00p.m.-6:00p.m.
Sponsored Cocktail Party
Exhibit Hall Floor

WEDNESDAY, OCTOBER 30

7:00a.m.-6:00p.m.
Registration Open
Stouffer Orlando Resort
Convention Center Lobby

8:00a.m.-5:00p.m.
Oscillator Design Principles
Stouffer Orlando Resort
Crystal Ballroom, Section D

8:30a.m.-4:30p.m.
Technical Program Sessions

11:00a.m.-6:00p.m.
EXHIBITS OPEN
Stouffer Orlando Resort
Convention Center Ballroom

5:00p.m.-6:00p.m.
Sponsored Cocktail Party
Exhibit Hall Floor

5:30p.m.
Winners of Best Booth Contest Announced
Exhibit Hall Floor

6:00p.m.-7:30p.m.
Ham Radio Reception
Stouffer Orlando Resort, Wedgwood Room

THURSDAY, OCTOBER 31

8:00a.m.-2:00p.m.
Registration Open
Stouffer Orlando Resort
Convention Center Lobby

8:30a.m.-11:30a.m.
Technical Program Sessions

10:00a.m.-2:00p.m.
EXHIBITS OPEN
Stouffer Orlando Resort
Convention Center Ballroom

1:30p.m.
Grand Prize Giveaways Drawn
Exhibit Hall-Cardiff Booth #326

EXHIBITOR GIVEAWAYS

Stop by these booths and enter your name for the following giveaways:

Eagleware Corporation in booth 209 will be drawing for a SuperStar professional (valued at $995) on Thursday, October 31 at 12:15p.m. Stop by the booth to register.

Webb Laboratories in booth 702 will be giving away the SysCad Version 5.0 Software for Complex Spurious Analysis & System Engineering, on Wednesday, October 30 at 5:00p.m.

Loral Microwave-FSI Semiconductor in booth 518 will be holding a drawing for a golf putter on Tuesday, October 29 and Wednesday, October 30 at 4:00p.m. and also on Thursday, October 31 at 12:30p.m. You must register at the booth.

Thomson-ICS in booth 621 will be giving away a bottle of French cognac on Wednesday, October 30 at 12:30p.m.

Brennan Associates in booths 722 & 724 will be giving away a one-of-a-kind puzzle on Thursday, October 31 at 11:30a.m. Drop your business card off at the booth in order to win.

Signetics in booth 106 & 108 will be holding a drawing for a compact disc player on both Tuesday, October 29 and Wednesday, October 30 at 5:15p.m. Stop by the booth to enter in the drawing.

Applied Specialties Inc. in booth 711 will be holding three separate drawings. On Tuesday, October 29 at 12:15p.m. and Wednesday, October 30 at 12:15p.m. three Avantek Designer Kits will be given away. On Thursday, October 31 the drawing will be held at 11:00a.m. and three more Avantek kits will be given away and also Windows Software. Stop by the booth to register.

Applied Microwave Magazine in booth 725 will be holding a drawing for 1989-1990 hardcover books on Thursday, October 31 at 10:30a.m. Participants must fill out a reader reply card to qualify.

Hewlett-Packard in booths 309,311,410 & 412 will be giving away E2373A, E2377A and E2378A multimeters. One will be given away per day. The drawings will be held on Tuesday, October 29 at 5:30p.m., Wednesday, October 30 at 5:30p.m. and Thursday, October 31 at 12:00 noon.

Proxim Inc. in booth 126 will be giving away a bottle of California wine on Tuesday, October 29 at 12 noon and 3:00p.m., Wednesday, October 30 at 12 noon and 3:00p.m. and on Thursday, October 31 at 11:45a.m.

Fotofabrication Corp. in booth 618 will be drawing for an RF shield prototype kit on Wednesday, October 30 at 4:45p.m. Stop by the booth to see the prize on display and to enter in the drawing.

GRAND PRIZE GIVEAWAYS

The following prizes will be given away at 1:30p.m. on Thursday, October 31 at the Cardiff Publishing Company booth, 326. In order to qualify, attendees must have a validated punch card dropped in the ballot box.

Stouffer Orlando Resort will be giving away a goody bag full of surprises.

Cardiff Publishing and **RF Design Magazine** will be giving away a complete library of RF Expo East Proceedings.

Motorola will be giving away a carousel CD player.

BOARD OF ADVISORS

The Board of Advisors actively contributes to the success of both RF Expo East and RF Expo West by sharing exhibitor and attendee needs with Show Management. We encourage you to contact them with your input during the show.

Malcom Levy
Racal-Dana Instruments

Tony Ramsden
Merrimac Industries

Jim Reeve
Wavetek Corporation

Earl Olsen
John Fluke Manufacturing

Frank Perkins
RF Monolithics

Don Davis
American Technical Ceramics

David Herron
Avantek, Inc.
(photo not available)

PRESENTATION BRIEFS


Pengelly


Hicks


Webb


Walls


Ghadaksaz


Brown

TUESDAY, OCTOBER 29, 8:30-11:30 a.m.

Session A-1: Using CAD in RF Engineering
Yellowtail Room

8:30-11:30 - State of the Art Nonlinear CAD for Microwave/RF
J. Gerber, L. Mah and C. Chang, Compact Software

A review of the various approaches to nonlinear CAD are presented, covering pure time domain to pure frequency domain techniques.

Jason Gerber received his MSEE from the University of Massachusetts in 1989. Since 1988 he has worked for Compact Software developing nonlinear simulation and parameter extraction tools. Leong F. Mah received his BSEE and MSEE from Washington University in 1986 and 1988 respectively. His interests are in the area of nonlinear circuit analysis and parameter extraction. Chao-Ren Cheng received his BS from National Cheng Kung University in 1971 and his MS and Ph.D. from North Carolina State University in 1980 and 1990, all in electrical engineering.

New Nonlinear Noise Model for MESFETS Including MM-Wave Applications
Raymond S. Pengelly and Ulrich L. Rohde, Compact Software

This paper shows a linearized time-domain approach for calculating the dynamic elements of the hybrid Pi, MesFET model. A novel enhancement to the basic equivalent circuit guarantees its use into the MM-wave area.

Raymond Pengelly has authored over 70 papers and has written and edited three books on FETs and MMICs. He is the Vice President of Marketing and Sales at Compact Software.

Design Desensitization
T. Zhang, Compact Software and Murat Eron, M/A-COM

Methods for estimating and maximizing design yields of mass produced circuits can also be used to reduce the sensitivity of circuits to parameter variations and uncertainties.

Tianrong Zhang received her Ph.D. from the Center of Relativity, at the University of Texas at Austin in 1985. She has been with Compact Software since 1989 as a Senior Engineer, working on the analysis, optimization, statistical and noise analysis, and yield optimization of microwave circuits. Murat Eron received his MS and Ph.D. from Drexel University in 1980 and 1984 both in electrical engineering. From 1988 to 1991 he was employed at Compact Software where he was manager of MMIC program tasks, involved in device modeling, parameter extraction and laboratory activities. He recently joined M/A-COM GMIC operations as the Applications Manager.

Microwave/RF System Simulation
Raymond S. Pengelly and Ross G. Hicks, Compact Software

This paper will refer specifically to two available simulators, Microwave Success from Compact Software and OmniSys from EEsof. After a discussion of requirements for and computations available from such simulators, two design examples are given.

Ross Hicks received his BE and Ph.D. in 1976 and 1984 from the University of Queensland, Australia. He then took up a two-year postdoctoral study fellowship at NASA Goddard Institute for Space Studies where he studied superconducting receivers. He is currently Vice President of Engineering at Compact Software.

E-M Theory-Based Simulations of Passive Microstrip RF Components on Single and Multiple Metallization Layers
A. Hill, J. Burke and K. Kottapalli, Compact Software

It will be demonstrated that E-M theory-based simulation tools have become practical and friendly enough to exploit unique passive structures in the design of high performance circuits.

Achim Hill received his MS and Ph.D. degree in electrical engineering and microwave engineering in 1986 and 1989. His area of interest included equivalent circuit modeling of passive microwave structures such as microstrip discontinuities and interconnects. He has been with Compact Software since 1989 where he is responsible for electromagnetic and other program development.

Session A-2: RF System Performance
Wedgwood Room

8:30 - A Unified Look at Spurious Performance of Multiple Conversion Receiving and Transmitting Systems
Dick Webb, Webb Laboratories

While spurious behavior of mixers is generally well-understood, system architectures, especially those involving multiple frequency conversions, are often defined without full anticipation of undesired tuned and coincident responses. A nomenclature is proposed for quick identification of spurious product type and origin.

Richard Webb is president of Webb Laboratories whose primary business involves the development and support of computer-aided-engineering tools for system simulation, lumped and distributed network synthesis, and high frequency circuit analysis and optimization. Prior to founding Webb Labs, he led the high frequency development effort for the GE Magnetic Resonance Imaging Program.

9:30 - Specifying Local Oscillator Phase Noise Performance: How Good is Good Enough?
Robert Gilmore, Qualcomm

Under- or over-specifying local oscillator phase noise requirements can result in unsatisfactory performance, or unnecessarily high cost. This paper examines the factors to be considered in determining the required performance of a local oscillator.

Robert Gilmore is the Engineering Director for Qualcomm. He holds a BSEE and MSEE from M.I.T. in 1977. He is a member of Tau Beta Pi, Eta Kappa Nu and Sigma X.

10:30 - Receiving Subsystem RF/IF Design Methodology
John D. Summerville, AIL Systems

A systematic approach to microwave multi-octave receiving subsystem design and implementation is presented. The major factors that must be considered in selecting a cost-effective, reproducible RF input to IF output are addressed.

John Summerville is a Section Head in the RF Engineering Department at AIL Systems Inc. He is a member of the AIL MMIC Technology Committee and the editor of the AIL MMIC Newsletter. He is also a Senior Member of the IEEE and MTT-S and a member of the AOC.

Session A-3: Design & Manufacturing
Coral Ballroom A/B

8:30 - RS-232 Communication for Turn-Key Test Stations
Warren Walls, Erbtec Engineering

PRESENTATION BRIEFS


Dunsmore


Hoover


Erb


Lurie


Szentirmai


Rose

Many PC-based automated test stations use a combination of GPIB and RS-232 communication formats to control test equipment and interface with the device under test. The different formats of RS-232 communication hardware were investigated and a couple of C libraries were generated in order to produce a reliable test station.

Warren Walls is an electrical engineer at Erbtec Engineering. He holds a BSEE from the University of Colorado and is a member of IEEE. For the past seven years his company, Femtosecond Systems, has produced a variety of phase noise and signal characterization equipment.

9:30 - Chemical Vapor Deposited Diamond Heat Carriers for Cooling High Temperature Electronic Components
Thomas N. Tuma, U.S. Army CECOM Center for Signals Warfare

This paper describes a plasma-enhanced chemical vapor deposition techniques for creation of diamond films. The improved thermal conductivity and low electrical conductivity of diamond makes this process attractive for heat-generating semiconductors.

10:30 - Transceiver Characteristics and Their Impact on Battery Life Performance in Land Mobile and Cellular Portable Phones
Masood Ghadaksaz, GTE Laboratories

This paper presents a method of characterizing battery life performance in terms of RF transceiver parameters, giving measured and analytical results of the studies conducted.

Masood Ghadaksaz received his B.A.Sc. degree in electrical engineering from the University of Ottawa and his M.Eng. degree in microwave electronics from Carleton university. He is a senior member of technical staff at GTE Laboratories and is currently involved in the design and development of advanced RF subsystem technology for mobile and cellular communications systems.

Session A-4: Test and Measurement
Crystal Ballroom E

8:30 - Optimize Mixer Performance Through Swept-Frequency and Power Characterization
Barry Brown and Joel Dunsmore, Hewlett-Packard Co.

The mixer is a key element in frequency conversion systems. This paper discusses the basics of non-linear mixer behavior, and presents measurement techniques to view this behavior directly using a vector network analyzer.

Barry Brown is a Hardware Design Engineer for HP's Network Measurements Division. He received his BSEE from Purdue University and his MSEE from Stanford University. He has done analog and RF circuit design for the HP8510 and HP8753 network analyzers, along with evaluation of these products. Joel Dunsmore is an RF Design Engineer for HP's Network Measurements Division. He received his BSEE and MSEE degrees from Oregon State University. He has authored several articles and papers on RF measurements and design, and has received patents for the HP83420 Lightwave Test Set and for RF component design in the HP 8752.

9:30 - Testing Dual Mode North American Cellular, Japan Digital Cellular Transceivers
Dave Hoover, Hewlett-Packard Co.

A method for generating and testing accuracy of PI/4 DQPSK modulated signals is presented, along with a test system for the North American Digital Cellular system.

Dave Hoover received his BSEE and MSEE in 1980 and 1981 respectively from the University of Washington. He holds a patent for a synthesis techniques used in the HP 8645A Signal Generator and has a patent pending for the HP11846A generator's filter technique.

10:30 - Power Triode Tube Curve Tracer
Lee Erb and Warren Walls, Erbtec Engineering

Power triodes remain an economical choice for high power RF systems. This paper presents a general purpose curve tracer for incoming test and engineering characterization of power triodes.

Lee Erb is the founder and president of Erbtec Engineering. He holds a BSEE from the University of Colorado and is a member of the IEEE. He worked for the University of Colorado Nuclear Physics Laboratory before starting Erbtec.

TUESDAY, OCTOBER 29, 1:30-3:30 p.m.

Session B-1: Filter Design Techniques
Yellowtail Room

1:30 - Filters With Improved Delay Characteristics
William B. Lurie, Consultant

Amplitude characteristics are no longer sufficient for defining filter performance. This paper presents a variety of methods for predicting or controlling phase or delay parameters in filters.

William Lurie holds BS degrees in Mathematics and Physics from Yale University as well as an MA in Education from Columbia University. He is a Life Senior Member of the IEEE and holds numerous patents. Since 1969 he has been a consultant on filter design synthesis and analysis problems.

2:30 - Design of Filters with Unsymmetrical Stopbands
William B. Lurie, Consultant

The most common filter design techniques result in filters with symmetrical stopbands. For some applications, unsymmetrical stopbands are desirable. A relatively simple technique for designing filters with desired stopband shape is presented.

3:30 - Approximation of Filters with Shaped Passbands
George Szentirmai, DGS Associates

An optimization procedure is described that was developed for the approximation of filter transfer functions to provide arbitrary passband loss (and possibly delay) shapes. The method is implemented on an interactive program running on a personal computer.

Dr. George Szentirmai has worked for companies such as Bell Laboratories, Rockwell International, and COMSAT and has taught at Cornell, UCLA and Santa Clara University. He has published approximately 40 papers on filters and CAD techniques. He is a member of the IEE and a Fellow of the IEEE.

Session B-2: Oscillators
Wedgwood Room

1:30 - The MCXO, Characteristics and Applications
Brian Rose, Q-Tech

The new aspects of the design of a Microprocessor Controlled Crystal Oscillator (MCXO) are presented, including crystal self-temperature sensing and external compensation.

Brian Rose has 30 years experience in the field of solid state RF circuits, oscillator

PRESENTATION BRIEFS


Weber


Sokal


Novak


Ellis


Sheinwald


Summerville

design, subsystems and system design. He received his BS and MS degrees in Engineering from the University of California at Los Angeles.

2:30 - Defining VCO Tuning Linearity
Allan Coon, RF Monolithics

Tuning linearity of a VCO is often poorly defined, leading to misunderstandings. The various definitions of VCO linearity are presented and defined in sufficient detail to be unambiguous.

Allan Coon has worked as Senior Applications Engineer at RF Monolithics for the part five and a half years. Prior to joining RFM he worked for Del Norte Technology, Decibel Products and Motorola. He is a member of the IEEE, Eta Kappa Nu and Tau Beta Pi.

3:30 - Microwave Oscillators
Robert Weber, Iowa State University

Robert Weber is an associate professor of electrical engineering at Iowa State University doing teaching and research in microwave devices and circuits and in semiconductor device research and fabrication. Dr. Weber received his Ph.D. in electrical engineering from Iowa State in 1967.

Session B-3: RF Power
Coral Ballroom A/B

1:30 - Class-E Power Amplifier Output Power, Efficiency, and Output Impedance vs. Loaded Q and Component Parasitic Losses
Nathan O. Sokal, Istvan Novak and Laszlo Drimusz

Design equations are presented to calculate the output power, efficiency and output impedance of nominally tuned Class E amplifiers.

Nathan Sokal is a Fellow of the IEEE. He received his BS and MS degrees in Electrical Engineering from MIT in 1950. He holds seven patents in power electronics and has published one book and more than a hundred technical papers. Dr. Istvan Novak teaches graduate and undergraduate courses in electronics, microwaves and RF, radio-communications technology, and digital and pulse techniques. He has developed RF and microwave transmitters, receivers, oscillators, and modulators, high-resolution MF spectrum analyzers and switching mode DC power supplies. Dr. Laszlo Drimusz has been working at Design Automation since 1988 developing digital hardware and software for industrial machine control. He was the programmer for the HEPA-PLUS computer program for designing, simulating, and optimizing high-efficiency RF power amplifiers.

2:30 - Design and Performance of High Power Pin Diode T/R Switches for VHF and UHF Land Mobile Voice and Data Communications Systems
Masood Ghadaksaz, GTE Laboratories

This paper describes a PIN diode switch that replaces an electromechanical design used in a 110 watt land mobile radio used for data communications.

3:30 - Directions and Developments in Very High Power RF at LAMPF
Richard Cliff, Mark Parsons and Harlan Ward Harris, Los Alamos National Laboratory

The RF power sections of the LAMPF 800 MEV linear accelerator are described, including four 2.5 megawatt, 201.25 MHz sections, and forty four 805 MHz, 1.2 megawatt sections.

Session B-4: Special Open Session -- 1991 Contest Winners
Crystal Ballroom E

1:30 - Low Frequency Circulator/Isolator Uses No Ferrite or Magnet
Charles Wenzel, Wenzel Associates

An active structure using high-speed current-feedback operational amplifiers performs the same functions as the ferrite or magnet-type circulators common at microwave frequencies.

Charles Wenzel is president of Wenzel Associates, a manufacturer of specialty crystal oscillator products for high purity, high stability applications. He holds a BSEE from the University of Texas.

2:30 - A Comprehensive Filter Design Program
Michael Ellis, U.S. Army Corps of Engineers

This paper discusses the theoretical basis and software writing techniques used in the development of a major filter synthesis and analysis program.

Michael Ellis received his BSEE and MSEE degrees from Vanderbilt University in 1974 and 1976 respectively, and is currently a Ph.D. candidate in electrical engineering at Mississippi State University. Since 1987 his has been employed by the Army Corps. of Engineers in Vicksburg, MS, and is involved in fiber optic technology, computer networking, and data compression.

WEDNESDAY, OCTOBER 30, 8:30-11:30 a.m.

Session C-1: Low Noise Amplifier Tutorial
Yellowtail Room

8:30 - 11:30 - Design of Low Noise RF and Microwave Amplifiers
Dick Webb, Webb Laboratories

A comprehensive tutorial beginning with a discussion of system noise contributions, proceeding to RF and microwave small-signal amplifier design considerations of gain, VSWR, stability and noise performance. Theory and practice of noise measurement is included, as well.

Session C-2: Application of MMICs
Wedgwood Room

8:30 - Microwave EW System Enhancements Using MMIC Technology
John D. Summerville, AIL Systems

The small, reliable and cost-effective designs required by the military market can be met with GaAs MMIC technology. This paper discusses how both MIMIC program results and commercial GaAs chips can be utilized in EW systems.

9:30 - Effective MMIC Testing Strategies for Engineers
Jesse D. Sheinwald, AIL Systems

Testing MMICs can be done at the chip level and substrate (carrier) level. The conditions under which each of these must be done are described, as well as the operational requirements of the necessary test stations.

Jesse Sheinwald is a Staff Engineer at AIL Systems working primarily on the implementation of MMIC's into custom EW subsystems. He has extensive design and development experience at AIL and other companies in PIN diode control components, filters and active devices.

10:30 - Silicon MMIC Amplifier Hits the 20/20 Gain/Power (dBm) Mark at UHF
David M. Osika and Ronald Green, SGS-Thomson Microelectronics

PRESENTATION BRIEFS


Green


Osika


Viveiros


Vincent


Donohue


Koller

This paper introduces a medium power 50 ohm silicon MMIC, producing 20 dBm power output with 20 dB gain, using a 9.0 VDC supply.

David Osika has worked on transient and steady state temperature modeling, automated testing, life testing and power device design of BJTs and Static Induction Transistors. He received his BSEE degree from Drexel University in 1985 with concentration in semiconductor device physics and computers. Ron Green received his BSEE from the University of British Columbia in 1985 with specialization in RF and semiconductor physics. While at U.B.C he worked in the CATV and Satellite receiving industries. In 1985 he joined the RF power amplifier group at Novatel Cellular Communications which culminated in two patents on RF power detectors for AGC circuits.

Session C-3: Receivers
Coral Ballroom A/B

8:30 - Distribution of Gain and Selectivity in Receivers
W.J. Vogel, MATE Electronics

Optimum gain distribution and selectivity in receiver circuitry is investigated in this paper, with considerations for noise, linearity and intermodulation. Practical design rules for receivers are presented.

W.J. Vogel received his Masters at Delft Technical University in 1979 after which he worked for Philips Consumer Electronics until 1988. Since then he has worked as a senior consultant for several organizations as well as a freelance teacher in electronic engineering for private and public schools.

9:30 - Tunable Notch Filter for Interference Rejections
Eric D. Adler and Edward Viveiros, Harry Diamond Laboratories

Wideband receiving systems are constantly plagued by the effects of overpowering narrowband interferers. This paper presents the design of a fixed notch filter with additional frequency tuning hardware that is capable of reducing such interfering signals.

Edward Viveiros received his BSEE from Rutgers University in 1984 and his MSEE from Johns Hopkins University in 1990. He is currently a senior design engineer at Harry Diamond Laboratory, Signal Processing Systems Branch. He has worked on several radar and COMINT systems in receiver, exciter, frequency synthesizer and system design.

10:30 - Spurious Analysis of Superhetrodyne Receivers and Frequency Synthesizers
Sherman Vincent, Raytheon Company

Determining optimum system architecture can be time consuming. This paper presents spurious signal considerations, and a novel computer program to help speed the analysis of a typical receiver.

Sherman Vincent received his BSEE from the Milwaukee School of Engineering in 1967 and his MSEE from the University of California in 1976. he has been Section Manager of Receiver Design and Development at Raytheon Electromagnetic Systems Division since 1984.

Session C-4: New RF Applications I
Coral Ballroom C

9:30 - Survey of Component Technologies for 900, 2400 and 5700 MHz Unlicensed Spread Spectrum Transceivers
Al Ward, Avantek

This paper surveys the device technologies available on the market today for use in unlicensed spread spectrum transceivers in UHF and microwave bands. Comparisons of performance, frequency and cost are presented, along with specific circuit examples.

10:30 - Integrated RF Interfaces for Rural Central Offices
M.V. Pitke, Tata Institute of Fundamental Research

RF interfaces for rural central offices can provide a cost-effective solution to rural communications. Implementation of such a system is discussed in this paper.

M.V. Pitke is presently a professor in the computer systems and communications group at Tata Institute. His interests are in parallel processing, new switch architectures, wireless networks, education and training, and technology development and transfer.

WEDNESDAY, OCTOBER 30, 1:30-4:30 p.m.

Session D-1: Power Amplifier Tutorial
Yellowtail Room

1:30 - 4:30 - Classes of RF Power Amplifiers A Through S, How They Operate, and When to Use Each
Nathan O. Sokal, Istvan Novak and John E. Donohue, Design Automation

With at least ten lettered classes of RF power amplifiers, confusion is an common result. This tutorial presents a review of the various classes of power amplifier and the behavior of the devices as switches, current sources, or as a combination of both.

John Donohue received a BSEE from MIT in 1978. He has been with Design Automation since 1979 involved in a wide range of analog design areas, including switching mode power conversion, linear and RF power, precision measurement and control, data conversion, and circuit simulation.

Session D-2: Spread Spectrum/Mobile Radio
Wedgwood Room

1:30 - Upper Limits of a Phase Multiplexed Correlator in a Multiple Access Spread Spectrum System
Madjid A. Belkerdid and Glen G. Koller, University of Central Florida

The relatively new concept of Phase Modulated Correlation (PMC) is applied to the CDMA DSSS environment to determine coarse acquisition advantages. Simulation results graphically illustrate performance trends.

Glen Koller received his BSEE and MSEE degrees from the University of Wisconsin -Milwaukee in 1987 and 1989. He spent two years at GE as a Process Engineer and is currently pursuing a Ph.D. in Electrical Engineering at the University of Central Florida.

2:30 - Mobile Data Packet Networks
John Kilpatrick, James L. Troe, RAM Mobile Data

Mobile data is here, and this paper presents an overview of one option available to users, the Mobitex network, and includes some details of its over-the-air protocols.

John Kilpatrick is a systems engineer specializing in digital communication modems and radio networks. He received his BA in Applied Mathematics from Gordon College in 1978 and his MS in Systems Engineering from the University of Lowell in 1982.

3:30 - The Development of an 8 kbps GMSK-Like Modem for Mobitex
D. Peter Noel, George Dew, Sasi Kumar,

PRESENTATION BRIEFS


Helfrick


Morley

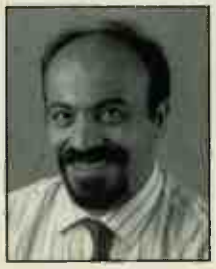
Abdollahian


Bren


Dogan


Berman

Marie Fiala-Timlin and Karl Mann

Presentation of the design and development of a modem for the 1200 bps/8000 bps land mobile data communications system commonly known as Mobitex.

Session D-3: New RF Applications II
Coral Ballroom A/B

1:30 - Making It In The USA
Albert Helfrick, Consulting Engineer

This paper describes the design of a high-volume consumer RF product for manufacture in the United States. Design techniques and experiences derived from the design effort are presented.

Albert Helfrick is the president of Helfrick and Associates. He has been involved with various design projects involving both RF and other disciplines for sophisticated low-volume systems to simpler, consumer items. He is a senior member of the IEEE.

2:30 - A Versatile UHF Data/Telemetry FM Transmitter
Harry J. Swanson, Motorola Bipolar Analog IC Division

A UHF FM transmitter featuring the MC13175 is presented, demonstrating the use of the ICs divide-by-8 or divide-by-32 prescaled PLL configuration.

Session D-4: CDMA Spread Spectrum
Coral Ballroom C

1:30 - Spread Spectrum Cellular Communications: Benchmarks for Cost, Power and Spectral Performance
Steve Morley, Qualcomm

Steven Morley is the Director of VLSI Products for Qualcomm. He holds a patent in the area of radiotelephone networks and has published papers in the areas of cryptography and forward error correction for satellite networks.

2:30 - Field Test Experiments Using Broadband Code Division Multiple Access
D. Schilling, L. Milstein, R. Pickholtz, F. Bruno, E. Kanterakis, W. Biederman, D. Fishman, D. Salerno, City University of New York

3:30 - An Adaptive Technique for Improving Spread Spectrum Interference Rejection
John Doherty, Iowa State University

THURSDAY, OCTOBER 31, 8:30-11:30 a.m.

Session E-2: Microwave and Military Applications
Wedgwood Room

8:30 - Design and Performance of a Novel Broadband Combiner/Impedance Transformer Using 1/16 Wavelength Microstrip Transmission Lines
M. Abdollahian and R. Gage

Combining high power amplifiers is usually accomplished using multiple stages of 1/4 wavelength sections and isolation resistors. This paper presents a four-stage, 1/16 wavelength per stage combiner that can also achieve necessary impedance transformation.

Mehdy Abdollahian is a member of technical staff in the Electronic Applications Department at the Systems Technology Laboratory. He is currently responsible for projects involving RF/microwave device characterization, RF and microwave subsystem design and development.

9:30 - Simulation of Millimeter-Range High-Power CW Frequency Doubling Using Multi-Junction Variable Reactance Diodes
Stephen Bren and Numan S. Dogan, Washington State University

Improved epitaxial growth techniques have allowed single-crystal growth of multiple p-n junctions with high precision. Theoretical performances and test results for two diodes are presented in this paper.

Stephen Bren received his BS degree in physics from the University of Washing in 1986 and received his MS in electrical engineering from Washington State University in 1990. His graduate research was in the area of solid-state device modeling. Numan Dogan received his Ph.D. from the University of Michigan in 1986 in electrical engineering. His technical area of interests include semiconductor device modeling and fabrication for microwave and millimeter wave applications, circuit design, high temperature electronics and recently biosensors.

Session E-3: Antennas and Electromagnetics
Coral Ballroom A/B

8:30 - Studies of the Cross Antenna
R. P. Haviland, Mini Lab Instruments

The cross antenna developed by Antoine G. Roedere is an alternative for radiating circularly polarized signals. The radiation patterns and driving impedances for this type of antenna are presented.

Robert Haviland is a partially retired electrical engineer, with extensive experience in communications and electronics mostly in the fields of space communications. For the past ten years he has specialized in studies of antennas for practical use.

9:30 - A Simple Expression for the Mutual Inductance of a Wire Current Source and a Non-Coplanar, Parallel, Rectangular Loop
Byron D. Berman

A simple expression for the low frequency mutual inductance between an infinite straight wire and a rectangular loop is derived by geometrical means and verified empirically by indirect measurement. A known formula for this configuration is then derived as a special case.

Byron Berman received his BSEE from the University of Maryland in 1972 and his MS in applied physics from Johns Hopkins in 1985. Since 1976, he has been with the Product Qualification Laboratory of the Westinghouse Electric Corporation working on the electromagnetic compatibility design and test of both military and commercial systems.

EXHIBITOR LIST

ADVANTEST

Advantest
300 Knightsbridge Parkway
Lincolnshire, IL 60069
708-634-2552
Booth: 110, 112
Products: The R3271 Microwave Spectrum Analyzer covers 100Hz to 26.5GHz and provides 100dB or greater dynamic range permitting highly accurate measurement.

Alan Industries, Inc.
745 Greenway Drive
Columbus, IN 47201
812-372-8869
Booth: 417
Products: Attenuators: programmable, continuously variable, rotary, fixed cam actuated, toggle switch, rocker switch, push button; also terminations, directional couplers, RF fuses, resistive dividers, impedance matching pads.

american technical ceramics CORP.

American Technical Ceramics
One Norden Lane
Huntington Station, NY 11746-2102
516-547-5700
Booth: 608
Products: ATC is exhibiting several new products: the 180 Series capacitors designed for mobile telephone applications at 1.8 GHz; and, ATC's new QUIK DESIGN™ kits.

Amphenol RF/Microwave Operations
One Kennedy Avenue
Danbury, CT 06810
203-796-2030
Booth: 601
Products: RF/microwave coaxial, twinaxial, triaxial connectors and cable assemblies.

AMPLIDYNE, INC.

Amplidyne, Inc.
Units 9 & 10, Bldg. 7
Ilene Ct.
Belle Mead, NJ 08502
908-359-6710
Booth: 719
Products: Solid state low noise and power amplifiers for cellular, PCN and GSM applications. Telecom amplifiers for radio links in the 1.7-2.3 GHz frequency range.

AMPLIFIER RESEARCH

Amplifier Research
160 School House Road
Souderton, PA 18964
215-723-8181
Booth: 305, 307
Products: Broadband, high power amplifiers and accessories for general RF and RFI susceptibility testing. Amplifiers from 10 kHz to 1000 MHz frequency range and 1 to 10,000 watt power output. Accessories include tem cells, antennas, field-strength monitors and leveling preamplifiers.

Anritsu America, Inc.
15 Thornton Rd.
Oakland, NJ 07436
201-337-1111
Booth: 322, 324
Products: RF and microwave spectrum analyzers.

Antenna Research Associates, Inc.
11317 Frederick Avenue
Beltsville, MD 20705-2088
301-937-8888
Booth: 708
Products: Individually calibrated antennas for EMI/tempest testing and HF/VHF/microwave antennas for transmit/receive applications.

Apex Systems, Inc.
2400 Central Ave.
Suite A
Boulder, CO 80301
303-443-3393
Booth: 419
Products: Apex Systems is a design engineering consulting firm specializing in RF, analog and control systems design. Previous products include pagers, animal tracking systems and wireless print sharers.

Applied Engineering Products
104 John W. Murphy Dr.
P.O. Box 510
New Haven, CT 06513
203-776-2813
Booth: 521
Products: Subminiature coaxial connectors and cable assemblies.

Applied Microwave Magazine
52 Waltham St.
Lexington, MA 02173
617-863-9603
Booth: 725
Products: Applied Microwave is a quarterly magazine written for the microwave professional. Articles are presented in whole page units edited for easy, informative reading. Special reports detail the important microwave conferences as well as the state of the art.

Applied Specialties Inc.
10101F Bacon Drive
Beltsville, MD 20705
301-595-5396
Booth: 711
Products: RF coaxial connectors, microwave components and cable assemblies.

Arrowsmith Shelburne, Inc.
2085 Shelburne Road
Shelburne, VT 05482
802-985-8621
Booth: 123
Products: RF/microwave switches, RF/microwave cables and electrical interconnect systems.

AT & T Microelectronics
Dept. 52AL040400, 555 Union Blvd.
Allentown, PA 18103
800-372-2447
Booth: 202
Products: AT&T will feature the new T1 frequency translator: PLXO, and display crystal oscillators, timing recovery units, SAW filters, hybrid IC and multichip module capabilities.

Avantek, Inc.
481 Cottonwood Dr.
Milpitas, CA 95035
408-432-3080
Booth: 606
Products: High-frequency ICs, RF and microwave products including transistors, MMIC amplifiers and frequency converters for spread spectrum, DBS, fiber-optic and other communications applications.

Balo Hermetics Company
45 Carey Avenue
Butler, NJ 07405
201-492-2256
Booth: 623
Products: Hi-Rel packages for microwave, hybrid and power applications. Glass-to-metal and ceramic-to-metal construction. Surface mount high frequency RF packages...all metal designs. Also, laser weldable micro "D" aluminum flange multi-pin connectors. In-house machining, sealing and plating capabilities meeting all MIL specs.

Bipolarics Inc.
108 Albright Way
Los Gatos, CA 95030
408-438-0806
Booth: 317
Products: Silicon bipolar RF/microwave transistors - SS low noise to 25 W, MMIC gain blocks, matched transistors, semi-custom, custom and foundry service with transistors to ft 15 GHz.

Boonton Electronics Corporation
791 Route 10
Randolph, NJ 07869-1980
201-584-1077
Booth: 319
Products: Designs and manufactures RF and Microwave: CW and peak powermeters, voltmeters, sweep and signal generators, and scalar network analyzers. Plus modulation meters and analyzers.

BRENNAN ASSOCIATES

Brennan Associates
211 Ewing Avenue
P.O. Box 5006
Clearwater, FL 35618-34616
813-446-5006
Booth: 722, 724
Products: AGCs, amplifiers (IF, Limiting, Log, RF), attenuators, chip capacitors, comparitors, couplers, crystal devices, detectors, discriminators, hybrids, modulators, shielded enclosures, splitters, switches, switch matrices, subsystems and VCAs.

BWS Microwave Marketing
1290 Hwy A1A
Suite 206
Satellite Beach, FL 32937
407-773-6170
Booth: 705, 707
Products: Manufacturers rep firm specializing in IF and RF microwave components and sub-systems.

Cal Crystal Lab, Inc./Comclok Inc.
1142 N. Gilbert St.
Anaheim, CA 92801
800-333-9825
Booth: 224
Products: Manufacturer and distributor of quartz crystals and clock oscillators.

CEL

California Eastern Labs
4590 Patrick Henry Drive
Santa Clara, CA 95056-0964
408-988-3500
Booth: 416
Products: Exclusive North American source for NEC RF and microwave semiconductors including small signal and power bipolars, low noise and power GaAs FETs, silicon and GaAs MMICs, silicon and GaAs prescalers, diodes and surface mount devices.

Cascade Microtech
14255 S.W. Brigadoon Ct.
Beaverton, OR 97005
503-626-9227
Booth: 423
Products: High-frequency probing equipment and microstrip testing products. Featuring: Summit 9300 analytical probe station, MTF26 microstrip test station, and a variety of microprobes.

Ceramic Devices, Inc.
8145 Ronson Road
San Diego, CA 92111
619-560-7575
Booth: 625, 627
Products: EMI/RFI filters and feed-thru capacitors. QPL source to MIL-F-28861 and MIL-F-15733. Custom filters and assemblies are our specialty.

Compac Development Corporation
1320-13 Lincoln Avenue
Holbrook, NY 11741
516-585-3400
Booth: 508
Products: RFI/EMI shielded enclosures standard sizes off the shelf, custom enclosures to customer specifications gasketing, connectors and coaxial attenuator.

EXHIBITOR LIST

Compact Software
483 McLean Blvd. & Corner of 18th Avenue
Paterson, NJ 07504
201-881-1200
Booth: 510, 512
Products: Products include serenade PC and WS schematic captive and layout software. Super Compact and Microwave Harmonica RF linear and nonlinear simulators; Microwave Success - system simulator.

Compex Corporation
238 Taunton Blvd.
Medford, NJ 08055
609-596-9388
Booth: 320
Products: Single layer ceramic parallel plate microwave chip capacitors. Gold or tin metalization. Split electrode, binary, arrays and custom electrode configuration available in Class I and II dielectrics.

Component Distributors, Inc. - CDI Hightek
1320 Clearmont St. N.E.
Palm Bay, FL 32905
407-724-9910
Booth: 704
Products: Leading edge technology RF and microwave components and sub-systems of all types, plus power supplies and electromechanical components used in RF/microwave systems.

Croven Crystals Limited
500 Beech Street
Whitby, Ontario L1N 5S5
Canada
Booth: 727
416-668-3324
Products: Piezo-electric quartz crystals, crystal oscillators, crystal filters, crystal and component ovens.

CTS Corporation - Frequency Control Division
400 Reimann Ave.
Sandwich, IL 60548
815-769-8411
Booth: 315
Products: Manufacturer of quartz crystals, oscillators, precision TCXO's, OCXO's and VCXO's. Also offering a contractual surface mount assembly service.

Dynawave, Inc.
94 Searle Street
Georgetown, MA 01833
508-352-7800
Booth: 705, 707
Products: Connectors - SMA, SSMA, field replacable blindmate handformable cable and cable assemblies.

Eagleware/Circuit Busters
1750 Mountain Glen
Stone Mountain, GA 30087
404-939-0156
Booth: 209
Products: High frequency design software for IBM and compatible personal computers. New program for SUN, HP, Apollo and DEC workstations.

E.D.S.I.
320 Riggs Ave.
Melbourne Beach, FL 32951
407-952-1240
Booth: 708
Products: Manufacturers' representative RF and microwave products.

EDSI/RF PRIME
11305 D Sunrise Gold Circle
Rancho Cordova, CA 95742
800-878-4669
Booth: 708
Products: Manufacturer of RF and microwave components, including mixers, power splitters/combiners and transformers all available in metal can, plastic and surface mount packages.

EEsof, Inc.
5601 Lindero Canyon Rd.
Westlake Village, CA 91362
818-991-7530
Booth: 715, 717
Products: EEsof, Inc. is dedicated to the development of high-frequency analog design automation software with applications in RF and microwave system and circuit design engineering.

E.F. Johnson
299 Johnson Ave.
Waseca, MN 56093
800-247-8256
Booth: 221, 223
Products: RF coaxial connectors, RF cable assemblies, electronic circuit interconnect hardware, spacers, air variable capacitors, data telemetry equipment, two-way radios.

EG&G Frequency Products, Inc.
4914 Gray Road
Cincinnati, OH 45232
513-542-5555
Booth: 424
Products: Design and manufacture of crystals, oscillators, filters and assembly of electronic modules.

ENI
100 Highpower Road
Rochester, NY 14623
716-427-8300
Booth: 507
Products: Solid state RF power amplifiers from 1 to 5000 watts: 9 kHz to 1 GHz.

Erbtec Engineering, Inc.
2760 29th St.
Boulder, CO 80301
303-447-8750
Booth: 222
Products: High powered RF amplifiers, currently being utilized in the MRI field. Adaptable to other applications.

Filtronetics, Inc.
6010 Parretta Dr.
Kansas City, MO 64120
816-231-7375
Booth: 101
Products: Filtronetics manufacturers custom crystal filters from 5 kHz to 150 MHz, LC (discrete and lumped) filters from 5 kHz to 1 GHz, phase match, linear phase, and anti-alias type.

Florida RF Labs
P.O. Box 2643
Stuart, FL 34995
407-286-9300
Booth: 418
Products: Custom RF cable assemblies: Standard RG cables, semi-rigid cable and coaxial delay lines. Resistor products: flange and pill termination, stud mounted resistors and terminations, high power chip termination and high power attenuators.

Fotofabrication Corp.
3758 Belmont
Chicago, IL 60618
312-463-6211
Booth: 618
Products: See our RF shield prototype kit with 54 potential sizes of RF shields for one low price! Custom RF shields made to your design. Very low tooling costs! Also see our standard shields.

Getelec, Inc.
6487 A. Calle Real
Goleta, CA 93117
805-964-4499
Booth: 625, 627
Products: Manufacturer of Conductive/Shielding products for the military, aerospace and industrial markets. Conductive elastomers and compounds, innovative anti-corrosion gaskets, molded, die-cut, precision laser cut, and extruded gaskets, both standard and custom.

Harris Semiconductor
1301 Woody Burke Rd.
Melbourne, FL 32919
800-4-Harris
Booth: 316, 318
Products: Harris Semiconductor is focused on high speed signal processing and power control applications that demand high reliability integrated circuits and discrete semiconductors.

Hewlett-Packard
1400 Fountaingrove Parkway
Santa Rosa, CA 95403
707-577-1400
Booth: 309, 311, 410, 412
Products: The leaders in RF design software and test equipment present their latest network analyzers, communication test equipment and circuit simulation software.

Hewlett-Packard
5301 Stevens Creek Blvd.
Santa Clara, CA 95052
800-452-4844
Booth: 309, 311, 410, 412
Products: Featuring three instruments: HP8751A vector network analyzer, 5 Hz - 500 MHz; HP4195A combination network/spectrum/impedance analyzer, 10 Hz - 500 MHz; HP4285A precision LCR meter, 75 kHz - 30 MHz.

Hewlett-Packard
1620 Signal Drive
Spokane, WA 99220
509-921-3331
Booth: 309, 311, 410, 412
Products: The HP 8920A RF Communications Test Set is a portable service monitor containing over 22 functions to solve radio and system problems faster. It also includes a high performance spectrum analyzer and software for testing cellular radios.

Hittite Microwave Corporation
21 Cabot Road
Woburn, MA 01801
617-933-7267
Booth: 701
Products: Hittite Microwave Corporation is a designer and supplier of MMIC chips and RF assemblies containing MMICs. Hittite specializes in multi-function integration and multi-chip packaging.

Huber & Suhner Inc.
One Allen Martin Drive
Essex, VT 05451
802-878-0555
Booth: 413
Products: RF and microwave connectors, cable assemblies, lightning and EMP protectors, microwave passive components, fiber optic cable assemblies and sub systems.

IFR Systems, Inc.
10200 W. York St.
Wichita, KS 67215
316-522-4981
Booth: 604
Products: RF spectrum analyzers, microwave spectrum analyzers, communications service monitors.

Inter-Continental Microwave
1515 Wyatt Drive
Santa Clara, CA
408-727-1596
Booth: 625, 627
Products: DC, RF, microwave and high speed digital test fixtures are featured from DC to 50 GHz to test chip, MMIC and packaged devices of all types.

Integrated Microwave Corporation
3422 Tripp Court
San Diego, CA 92121-1009
619-259-2600
Booth: 620
Products: Integrated microwave produces a wide range of high-quality microminiature lumped-element, suspended substrate, combline, interdigital and cavity filters and multifunction modules in the DC to 26.5 GHz range.

JFW Industries, Inc.
5134 Commerce Square Drive
Indianapolis, IN 46237
317-887-1340
Booth: 107
Products: Manufacturer of RF attenuators, switches, programmables, fixed attenuators, terminations and switching systems.

EXHIBITOR LIST

FLUKE®

John Fluke Mfg. Co. Inc.
6920 Seaway Blvd.
Everett, WA 98203
206-347-6100
Booth: 404, 406
Products: Test and measurement equipment, including a full line of high purity and general purpose RF signal generators, frequency counters, and digital storage oscilloscopes covering the frequency spectrum up to 2,000 MHz.

Kurt Whitlock Associates, Inc.
4103 Neptune Rd.
St. Cloud, FL 34769
407-892-9876
Booth: 517
Products: SMD rework/repair soldering/desoldering equipment, coaxial wire stripping equipment, wire stripping equipment.

LCF Enterprises
621 Barrington Court
Newbury Park, CA 91320
805-388-8454
Booth: 519
Products: High performance RF power amplifiers, 1 MHz to 2 GHz, output powers 1W to 1KW in a small package. High performance RF power devices with low variation and high repeatability.

Locus, Inc.
P.O. Box 740
State College, PA 16804
814-466-6275
Booth: 705, 707
Products: Microwave and RF products. Amplifiers, converters, mixers quadrature networks, modulation/demodulation.

Loral Microwave - FSI Semiconductor Div.
16 Maple Road
Chelmsford, MA 01824
508-256-4113
Booth: 518
Products: Silicon abrupt junction tuning varactors, VHF/UHF tuning varactors, frequency linear tuning varactors, GaAs tuning varactors, pin and nip diodes, limiter diodes, mesa and planar beam leads, UHF/VHF pin diodes, chip capacitors, planar spiral inductors, step recovery diodes, harmonic generator varactors, multi-chip high power generator varactors, noise diodes, power generation multiplier varactors.

Lorch Electronics, Inc.
2801 72nd St.
St. Petersburg, FL 33710
813-347-2181
Booth: 705, 707
Products: RF and IF signal processing components. Filters, attenuators, phase shifters, couplers, mixers, power splitters, modulators, switches, surface mts. and package tech available.

M/A-COM, Inc.
63 South Avenue
Bldg. 2
Burlington, MA 01803
617-272-3000
Booth: 403, 405, 407
Products: M/A-COM is a broad based manufacturer of DC thru millimeterwave semiconductors, transistors, devices, components, connectors and cable assemblies for the communication and defense industries.

M/A-Com Control Components
2100 Continental Blvd.
Merrimack, NH 03054
603-424-4111
Booth: 418
Products: Attenuators, terminations, couplers/hybrids, waveguide adapters, detectors, monitor tee's, DC blocks, power dividers/combiners, phase shifters, and electromechnical switches.

M/A-Com Omni Spectra
140 Fourth Avenue
Waltham, MA 02254
603-424-4111
Booth: 418
Products: RF connectors per: MIL-C-39012; series SSMA, SMA, SMB, SMC, BNC, TNC, N, SC, OSP, 2.4mm, blind mate, and adapters per MIL-A-55339.

Marconi Instruments
3 Pearl Court
Allendale, NJ 07401
201-934-9050
Booth: 603, 605
Products: RF signal generators and sweepers, power meters, modulation meters, microwave sweepers, scalars and counters.

Megacity Tool & Mfg.
349 Progress Rd.
Dayton, OH 45449
513-859-8251
Booth: 708
Products: MIL-45208 qualified and commercial stampings. Large and short run items. Satellite dish stampings. Tooling, dies, jigs and fixtures.

MEL Microwave
18718 Geraci Road
Lutz, FL 33549
813-888-9055
Booth: 125
Products: Manufacturers' representative of microwave components.

Merrimac Industries, Inc.
41 Fairfield Place
West Caldwell, NJ 07006
201-575-1300
Booth: 503, 505
Products: IF and microwave devices, components, and subsystems; using lumped element and stripline designs, IF integrated assemblies and Hi-Rel networks.

Metelics Corp.
975 Stewart Dr.
Sunnyvale, CA 94086
408-737-8181
Booth: 625, 627
Products: Microwave semiconductors and components. Schottky barrier diodes, pin diodes, SRD's, silicon tuning diodes, drop-in sub-assemblies, tunnel diodes and MNOS capacitors, chips and beam leads.

Micro-Coax Components, Inc.
245 West Fifth Avenue
Collegeville, PA 19426
215-489-3700
Booth: 422
Products: Semi-rigid cable and cable assemblies, coaxial delay lines, low-, band-, and high-pass patented "In-A-Cable" coaxial filter assemblies. "In-A-Cable" coaxial attenuators/amplifiers/impedance transformers and rectangular and double ridge aluminum waveguide. Also, high-performance flexible microwave cable assemblies to 40 GHz.

Micro-Dynamics, Inc.
10 Sonar Drive
Woburn, MA 01801
617-729-9450
Booth: 524
Products: Low and high power RF switches, digital and analog attenuators, phase shifters, limiters, switch filter banks, integrated subassemblies, waveguide TRL's and switches.

Micronics
7 Alexander Place
Glen Cove, NY 11542
516-759-5600
Booth: 708
Products: Synthesizers, oscillators and custom sub-systems.

Microsonics Incorporated
Weymouth, MA
617-337-4200
Booth: 723
Products: 1 kHz - 1 GHz frequency coverage, oscillators, TCXO, OCXO, VCXO, crystal and lumped element filters, acoustic memories and delay devices and frequency synthesizer products.

Microwave Components, Inc.
3171 SE Dominica Terrace
Unit 5
Stuart, FL 34997-5994
407-286-4455
Booth: 418
Products: RF connectors, resistive products, cable assemblies, attenuators, couplers, power dividers, termination, coaxial cable, IDC connectors, air coils and EMI filters.

Microwave Engineering Corporation
1429 Osgood Street
N. Andover, MA 01845
508-685-2776
Booth: 708
Products: Rectangular, double ridge and flexible waveguides. Millimeter waveguides and waveguide components. 1 GHz and up. Custom waveguide assemblies.

Microwave Journal
685 Canton St.
Norwood, MA 02062
617-769-9750
Booth: 726
Products: Trade journal covering electronic design and news from RF through lightwaves.

Microwave Product Digest
167 South Broadway
Hastings on Hudson, NY 10706
914-478-0909
Booth: 124
Products: Microwave product tabloid.

MwT
MICROWAVE TECHNOLOGY

Microwave Technology
4268 Solar Way
Fremont, CA 94538
415-651-6700
Booth: 706
Products: GaAs FETs to 20 GHz; silcon power FETs to 1 GHz and 120 watts; microwave hybrid gain modules 2 to 20 GHz; and microwave amplifiers and integrated assemblies.

Microwaves & RF
611 Rte. 46 West
Hasbrouck Heights, NJ 07604
201-393-6289
Booth: 624
Products: Microwaves & RF serves engineers and engineering management involved with RF, microwave and optical devices across a broad spectrum of applications.

Mini-E-Con
3160 Pullman
Costa Mesa, CA 92626
714-434-7312
Booth: 625, 627
Products: Micro miniature connectors and multi-connector harness assemblies M83513 qualified. PC board mounts available.

Motorola
5005 E. McDowell Road
Phoenix, AZ 85008
602-244-3818
Booth: 203, 205, 304, 306
Products: Motorola offers the broadest line of RF products in the industry and is constantly adding new discrete transistor, amplifier assemblies, linear, and microwave transistor to maintain the title of the industry's 1 supplier.

Nedrud Data Systems
P.O. Box 27020
Las Vegas, NV 89126
702-254-2045
Booth: 612
Products: Full featured RF circuit design software for Macintosh computers includes schematic entry, optimization, spectacular graphics, complete element library. Independently evaluated best value on any platform.

Olektron Corporation
61 Sutton Road
Webster, MA 01570

EXHIBITOR LIST

508-943-7440
Booth: 723
Products: 10 kHz - 2 GHz frequency coverage, couplers, hybrids, power dividers, mixers, phase shifters/attenuators, RF switches, digital attenuators, integrated RF packages and complex phase modulators and detectors.

Philips Components Discrete Products Division
2001 W. Blue Heron Blvd.
Riviera Beach, FL 33404
407-881-3308
Booth: 102, 104
Products: Categories exhibited include CATV, video and RF modules, RF small signal transistors, RF and microwave power transistors, and circulators and isolators.

Philips Components-Signetics
811 E. Argues
P.O. Box 3409, M/S 60
Sunnyvale, CA 94088-3409
408-991-2000
Booth: 106, 108
Products: Signetics is a world leader in RF integrated circuits. Product line includes: RF amplifiers, compandors, FM IF systems, audio and data processors, mixers, frequency synthesizers, pagers and data receivers.

Piezo Technology, Inc.
2525 Shader Road
Orlando, FL 32804
407-298-2000
Booth: 105
Products: Frequency control products including: TCXO's, OCXO's, VCXO's, monolithic and discrete crystal filters, LC, interdigital combline, and cavity filters, sub-assemblies and hybrid circuits.

POLY CIRCUITS, INC.

Poly Circuits, Inc.
215 Park Street
Bensenville, IL 60106
708-860-3560
Booth: 219
Products: Flexlink, a patented process for bonding of PTFE circuits to heatsinks and various metal ground planes. Teflon and polyimide doublesided and multilayer circuit boards.

Polyflon Company
35 River Street
New Rochelle, NY 10801
914-636-7222
Booth: 204
Products: High voltage, high Q, nonmagnetic fixed, variable and trimmer capacitors, CuFlon® low loss substrate and circuit boards, custom manufacture MRI probes, coils and antennas.

Power Systems Technology
63 Oser Avenue
Hauppauge, NY 11788
516-435-8597
Booth: 705, 707
Products: A complete line of solid state RF power amplifiers and sub-systems 1 MHz - 4,000 MHz, 2 watt-2,000 watts.

proxim

Proxim, Inc.
295 North Bernardo Avenue
Mountain View, CA 94043
415-960-1630
Booth: 126
Products: Direct digital synthesis components and complete synthesizer boards. Spread spectrum RF data communication products including FCC-certified RF modem for wireless connectivity.

Q-bit Corporation
2575 Pacific Ave., N.E.
Palm Bay, FL 32905-2699
407-727-1838
Booth: 103
Products: RF amplifiers covering a frequency of .1 MHz to 3 GHz. Limiters, voltage-controlled amplifiers and attenuators and integrated sub-assemblies for the military and commercial markets. Hybrid and coaxial packaging available.

RACAL-DANA Instruments Inc.

Racal-Dana Instruments Inc.
4 Goodyear Street
Irvine, CA 92718
714-859-8999
Booth: 120
Products: RF instruments (signal generators, level meters) and RF chassis, RF development module and new RF instruments in VXI.

Republic Electronics Corp.
Ceramic Capacitors for over 45 years

Republic Electronics Corporation
476 Blackman St.
Wilkes-Barre, PA 18702
717-823-9900
Booth: 622
Products: Manufacture ceramic multilayer capacitors, microwave capacitors, mil-approved to MIL-C-55681, single layer capacitors with operating frequencies to 50 GHz.

RF Associates, Inc.
5840 Auvers Blvd.
Suite 108
Orlando, FL 32807
407-657-7332
Booth: 625, 627
Products: Manufactures representatives for the following manufacturers: Ceramic Devices, Inc., Getelec, Inc., Inter-Continental Microwave, Metelics Corp., Min-E-Con, Tele-Tech, Teledyne Microwave, TRX and Valbar.

RF Components, Inc.
Beverly, MA
508-922-0019
Booth: 723
Products: 10 MHz - 2 GHz frequency coverage, log amplifiers, constant phase log amplifiers, constant phase limiting amplifiers, integrated phase/amplitude detection subsystems, phase detector modules, frequency discriminators and signal generation products.

RFdesign

RF Design
6300 S. Syracuse Way, 650
Englewood, CO 80111
303-220-0600
Booth: 326
Products: Sponsor of both RF Expo East and RF Expo West. The only magazine exclusively dedicated to RF engineers and engineering managers.

RFM

RF Monolithics, Inc.
4441 Sigma Road
Dallas, TX 75244
214-233-2903
Booth: 310, 312
Products: SAW resonators, low-loss SAW filters and delay lines, SAW-stablized frequency sources, high-frequency digital clocks, low-power UHF radio transmitters and receivers.

Sawtek Incorporated
P.O. Box 609501
Orlando, FL 32860-9501
407-886-8860
Booth: 215, 217
Products: Sawtek produces SAW low-loss and bandpass filters, oscillators, delay lines, frequency control components, and custom subsystems. These SAW products are used in LANs, cellular telephones, radar systems, CATV, satellite communications, GPS, and spread spectrum applications with frequency ranges from 10 MHz to 2 GHz.

SGS-Thomson Microelectronics
211 Commerce Dr.
Montgomeryville, PA 18936
215-361-6400
Booth: 511, 513
Products: Silicon RF/microwave power transistors; silicon MMIC's; RF hybrid power modules; RF/microwave power amplifiers and HPA subsystems; solid-state noise generators.

Sierra Microwave Technology
11295-A Sunrise Gold Circle
Rancho Cordova, CA 95742
916-638-2002
Booth: 225
Products: Manufacturer of microwave components up to 50 GHz including isolators, circulators, filters, switches, equalizers, integrates components, and amplifiers.

Signal Technology Corporation
955 Benecia Ave.
Sunnyvale, CA 94086
408-730-6300
Booth: 723
Products: Signal Technology Corporation is represented at this years RF Expo East by the following divisions: Olektron Corporation, Microsonics Incorported and RF Components.

Sprague-Goodman Electronics Inc.
134 Fulton Ave.
Garden City Park, NY 11040
516-746-1385
Booth: 607
Products: Trimmer capacitors (air, ceramic, film, glass, mica, quartz and sapphire dielectric); precision inductors; surface mounted trimmer capacitors and inductors, and Radiocer high power-RF ceramic capacitors.

Stetco Inc.
3344 Schierhorn Ct.
Franklin Park, IL 60131
708-671-4208
Booth: 520
Products: Electronic component manufacturer offering a line of surface mount and leaded inductors, capacitors and chip LED's. Also filter connectors and customer specific RFI filtering devices.

Synergy Microwave Corporation
483 McLean Boulevard
Paterson, NJ 07504
201-881-8800
Booth: 411
Products: Mixers, power dividers, directional and bi-directional couplers, filters, phase shifters, attenuators, 90 degree hybrids, 180 degree hybrids, phase detectors, modulators, amplifiers, switches, and subsystems.

Tampa Microwave Lab, Inc.
8742 North Mobley Road
Odessa, FL 33556
813-920-8822
Booth: 709
Products: TML manufactures phase locked oscillators and related products such as: phase locked down converters, up converters, frequency translators, Ku antenna phasing systems and crystal heaters.

Technical Systems Associates, Inc.
730 Central Florida Pkwy.
Orlando, FL 32824
407-857-3235
Booth: 226
Products: Technical Systems Associates' unique design, development, and manufacturing capabilities allow us to specifically meet our customer requirements for microwave antennas, components and systems.

Tektronix®
COMMITTED TO EXCELLENCE

Tektronix Inc.
P.O. Box 500

Beaverton, OR 97077
503-627-1557
Booth: 227
Products: High-performance bipolar ASIC technology. Semicustom and full custom design methods are offered with exceptional CAD tools and support services. Also, very high speed data converter products.

Teledyne Microwave
1290 Terra Bella Avenue
Mountain View, CA 94043
415-960-2211
Booth: 625, 627
Products: Isolators and circulators. Filters and multiplexers. Electromechanical coaxial switches, bulk acoustic wave delay devices. Amplifiers, oscillators, DLVA's and subsystems.

Tele-Tech
2050 Fairway Drive
P.O. Box 790
Bozeman, MT 59715
Booth: 625, 627
Products: Broad-band signal processing components for both military and commercial applications, from VLE to microwave frequencies.

THOMSON-CSF

THOMSON-ICS
104 Feeding Mills Rd.
P.O. Box 1088
Southwick, MA 01077
413-569-0575
Booth: 621
Products: SAW, BAW, AO and integrated optic components and modules: low loss filters, bandpass filters, dispersive and non-dispersive delay lines, BAW microwave delay lines, pulse compression subsystems.

TRAK Microwave Corporation
4726 Eisenhower Blvd.
Tampa, FL 33634
813-884-1411
Booth: 321, 323
Products: Synthesizers, multi-function assemblies, oscillators phase locked, dielectrically stablized, voltage controlled, XCO, TCXO, VCXO - frequency multipliers, comb generators, IF amplifiers, isolators, circulators, GPS station clocks.

Trilithic, Inc.
9202 E. 33rd St.
Indianapolis, IN 46236
800-344-2412
Booth: 208
Products: RF and microwave components including miniature, surface mount, and coaxial filters; rotary and fixed attenuators; terminations; switches; oscillators; sweep generators.

TRONTECH INC

Trontech, Inc.
38 Industrial Way East
Eatontown, NJ 07724
908-542-1133
Booth: 614
Products: RF and microwave amplifiers from 1 kHz to 6 GHz; product types include LNA's; broadband medium power and high power to 500 watts, Class AB.

TRX
1326 Mechanic Street
Attleboro, MA 02763
508-226-3350
Booth: 625, 627
Products: Thick film chip resistors, terminations, attenuators for surface mount applications: (Rated from 750-50W). Approved to MIL-R-55342.

TTE®

TTE, Incorporated
2251 Barry Avenue
Los Angeles, CA 90064-1400
213-478-8224
Booth: 504, 506
Products: Active and passive electrical wave filters, including anti-aliasing, delay equalized video filters, programmable filters, filter systems, duplexers and diplexers covering the frequency range of 0.1Hz to 500MHz.

Valbar
1326 Mechanic Street
Attleboro, MA 02763
508-226-3350
Booth: 625, 627
Products: Complete microwave and RF circuit board fabrication on PTFE materials such as "DUROID."

Vanguard Electronics Co., Inc.
1480 W. 178th St.
Gardena, CA 90248
213-323-4100
Booth: 523
Products: Wide range of RF and microwave inductive components for hi rel military and telecommunication applications. Also, configured in leadless surface mount as well as leaded.

Vcc
VCO COMMUNICATION CORPORATION

VCO Communications Corporation
10242 NW 47th Street
Suite 17
Ft. Lauderdale, FL 33351
305-746-9003
Booth: 420
Products: Low cost voltage controlled oscillators in the frequency range of 100 MHz to 3.0 GHz pin or surface mount. Small size, 0.75 x 0.75 x 0.3 for commercial applications.

VECTRON
The Crystal Oscillator Company

Vectron Laboratories, Inc.
166 Glover Avenue
Norwalk, CT 06850
203-853-4433
Booth: 206
Products: Crystal and non-crystal controlled oscillators from 0.1 Hz to 2 GHz, sinewave, TTL, CMOS, HCMOS, ACMOS, ECL, ECLIPS, including XOs, TCXOs, OCXOs, TC/VCXOs, VCXO and VCOs.

Voltronics Corporation
West Street
P.O. Box 476
East Hanover, NJ 07936
201-887-1517
Booth: 211
Products: Precision trimmer capacitors - glass, quartz, sapphire, teflon and air dielectrics. MIL QPL. Non-magnetic versions. Tuners for DRO's and microwave cavities.

Wavetek
9145 Balboa Ave.
San Diego, CA 92123
619-450-9971
Booth: 116, 118
Products: Wavetek is a worldwide manufacture and distributor of test and measurement software, instruments and systems. Our product areas include: Signal and sweep generators from RF to microwave. RF and microwave scalar network analyzers. RF and microwave components.

Wayne Kerr/Farnell
600 W. Cummings Park
Woburn, MA 01801
800-933-9319
Booth: 121
Products: RF spectrum analyzer 1 GHz. RF signal generators 10 kHz to 2 GHz. Modulation meyers to 2.4 GHz. DC power supplied 60w, 500w, 1KW and 3KW.

WEBB LABORATORIES

Webb Laboratories
139 E. Capitol Drive
Suite 4
Hartland, WI 53029
414-367-6823
Booth: 702
Products: PC-based CAE tools for system simulation, complex spurious analysis, coupler and filter synthesis, and network analysis and optimization.

W.L. Gore & Associates
1505 N. 4th St.
Flagstaff, AZ 86004
602-526-1290
Booth: 703
Products: EMI gasket and shielding materials, flexible microwave cable; D.C. through 40 GHz, precision digital coaxial cable.

SPEAKERS AND CHAIRMEN

M. Abdollahian
GTE Laboratories Inc.
40 Sylvan Road
Waltham, MA 02254
617-466-2565

Eric D. Adler
Harry Diamond Laboratories
2800 Powder Mill Road
Adelphi, MD 20783-1197
301-394-2520

Madjid A. Belkerdid
Electrical Engineering Department
University of Central Florida
Orlando, FL 32816
407-823-5793

Byron D. Berman
6301 Benhurst Road
Baltimore, MD 21209
301-993-6626

Les Besser
Besser Associates
4600 El Camino Real
Los Altos, CA 94022
415-949-3300

Stephen Bren
Department of Electrical Engineering
and Computer Science
Washington State University
Pullman, WA 99163
509-335-6373

Barry Brown
Hewlett-Packard
Network Measurements Division
1400 Fountaingrove Parkway
Santa Rosa, CA 95403-1799
707-577-4749

J. Burke
Compact Software, Inc.
483 McLean Blvd. & 18th Avenue
Paterson, NJ 07504
201-881-1200

C. Chang
Compact Software, Inc.
483 McLean Blvd. & 18th Avenue
Paterson, NJ 07504
201-881-1200

Richard Cliff
Los Alamos Meson Physics Facility
Los Alamos National Laboratory,
M/S H826
Los Alamos, NM 87545
505-665-5686

Allan Coon
RF Monolithics, Inc.
4441 Sigma Road
Dallas, TX 75244
214-233-2903

Numan Dogan
Department of Electrical Engineering
and Computer Science
Washington State University
Pullman, WA 99163
509-335-6373

John Doherty
Iowa State University
330 Coover, EECPE
Ames, IA 50011
515-294-9957

John Donohue
Design Automation, Inc.
809 Massachusetts Avenue
Lexington, MA 02173-3992
617-862-8998

Laszlo Drimusz
Design Automation, Inc.
809 Massachusetts Avenue
Lexington, MA 02173-3992
617-862-8998

Joel Dunsmore
Hewlett-Packard
Network Measurements Division
1400 Fountaingrove Parkway
Santa Rosa, CA 95403-1799
707-577-4749

Michael Ellis
412 Elmwood
Vicksburg, MS 39180
601-638-0670

Lee Erb
Erbtec Engineering
2760 29th Street
Boulder, CO 80301
303-447-8750

Murat Eron
M/A-COM
80 Cambridge Street
Burlington, MA 01803-4107
617-273-3333

R. Gage
GTE Laboratories Inc.
40 Sylvan Road
Waltham, MA 02254
617-466-2992

J. Gerber
Compact Software, Inc.
483 McLean Blvd. & 18th Avenue
Paterson, NJ 07504
201-881-1200

Masood Ghadaksaz
GTE Laboratories Inc.
40 Sylvan Road
Waltham, MA 02254
617-466-2992

Robert Gilmore
QUALCOMM, Inc.
10555 Sorrento Valley Road
San Diego, CA 92121
619-587-1121

Ronald Green
SGS-Thomson Microelectronics
211 Commerce Drive
Montgomeryville, PA 18936-1002
215-361-6400

Harlan Ward Harris
Los Alamos Meson Physics Facility
Los Alamos National Laboratory,
M/S H826
Los Alamos, NM 87545
505-665-5686

R. P. Haviland
1035 Green Acres Circle North
Daytona Beach, FL 32119

Albert Helfrick
5 Banta Road
Kinnelon, NJ 07405
201-492-8363

Ross G. Hicks
Compact Software, Inc.
483 McLean Blvd. & 18th Avenue
Paterson, NJ 07504
201-881-1200

A. Hill
Compact Software, Inc.
483 McLean Blvd. & 18th Avenue
Paterson, NJ 07504
201-881-1200

Dave Hoover
Hewlett-Packard Corporation
Spokane Division
1620 Signal Drive
Spokane, WA 99220
509-921-4001

John Kilpatrick
RAM Mobile Data, Inc.
10 Woodbridge Center Drive
Woodbridge, NJ 07095
201-602-5538

Glen Koller
Electrical Engineering Department
University of Central Florida
Orlando, FL 32816
407-823-5793

K. Kottapalli
Compact Software, Inc.
483 McLean Blvd. & 18th Avenue
Paterson, NJ 07504
201-881-1200

William Lurie
8503 Heather Place
Boynton Beach, FL 33437
407-369-4218

L. Mah
Compact Software, Inc.
483 McLean Blvd. & 18th Avenue
Paterson, NJ 07504
201-881-1200

Steve Morley
QUALCOMM, Inc.
10555 Sorrento Valley Road
San Diego, CA 92121-1617
619-597-5218

Istvan Novak
Design Automation, Inc.
809 Massachusetts Avenue
Lexington, MA 02173-3992
617-862-8998

David Osika
SGS-Thomson Microelectronics
211 Commerce Drive
Montgomeryville, PA 18936-1002
215-361-6400

Mark Parsons
Los Alamos Meson Physics Facility
Los Alamos National Laboratory,
M/S H826
Los Alamos, NM 87545
505-665-5686

Raymond S. Pengelly
Compact Software, Inc.
483 McLean Blvd. & 18th Avenue
Paterson, NJ 07504
201-881-1200

M. V. Pitke
Computer Systems &
Communications Group
Tata Institute of Fundamental
Research
Homi Bhabha Road
Bombay, India 400 005
91-22-215-2971

Randy Rhea
Eagleware
1750 Mountain Glen
Stone Mountain, GA 30087
404-939-0156

Ulrich L. Rohde
Compact Software, Inc.
483 McLean Blvd. & 18th Avenue
Paterson, NJ 07504
201-881-1200

Brian Rose
Q-Tech Corporation
10150 W. Jefferson Blvd.
Culver City, CA 90232-3510
213-836-7900

Donald Schilling
Department of Electrical Engineering
City College
The City University of New York
New York, NY 10031
516-883-0760

John Seymour
Gandalf Mobile Systems
2 Gurdwara Rd.
Ste. 500
Nepean, Ontario, Canada K2E 1A2
613-723-6500

Jesse Sheinwald
AIL Systems, Inc.
Walt Whitman Road
Melville, NY 11747
516-595-4619

Nathan Sokal
Design Automation, Inc.
809 Massachusetts Avenue
Lexington, MA 02173-3992
617-862-8998

John Summerville
Eaton Corporation
AIL Systems, Inc.
Walt Whitman Road
Melville, NY 11747
516-595-4377

SPEAKERS AND CHAIRMEN

Harry Swanson
Motorola Inc.
Bipolar Analog IC Division, M/S EL340
Linear Applications Engineering
2100 East Elliot Road
Tempe, AZ 85284
602-897-3842

George Szentirmai
DGS Associates, Inc.
1353 Sarita Way
Santa Clara, CA 95051
408-554-1469

James Troe
RAM Mobile Data, Inc.
10 Woodbridge Center Drive
Woodbridge, NJ 07095
201-602-5538

Thomas Tuma
Department of the Navy
U.S. Army Communications
Electronics Command
Center for Signals Warfare
Vint Hill Farms Station
Warrenton, VA 22186-5100
703-349-6914

Sherman Vincent
Raytheon Company
6380 Holister Avenue
Goleta, CA 93117
805-967-5511

Edward Viveiros
Harry Diamond Laboratories
2800 Powder Mill Road
Adelphi, MD 20783-1197
301-394-2520

Warren Walls
Erbtec Engineering
2760 29th Street
Boulder, CO 80301
303-447-8750

Al Ward
Avantek
101 W. Renner Road, Suite 180
Richardson, TX 75081
214-437-5694

Dick Webb
Webb Laboratories
139 East Capitol Drive, Unit 4
Hartland, WI 53029
414-367-6823

Robert Weber
Electrical Engineering
Iowa State University
333 Coover, EECPE
Ames, IA 50011
515-294-8432

Charles Wenzel
Wenzel Associates
14050 Summit Drive, Suite 119
Austin, TX 78728
512-244-7741

T. Zhang
Compact Software, Inc.
483 McLean Blvd. & 18th Avenue
Paterson, NJ 07504
201-881-1200

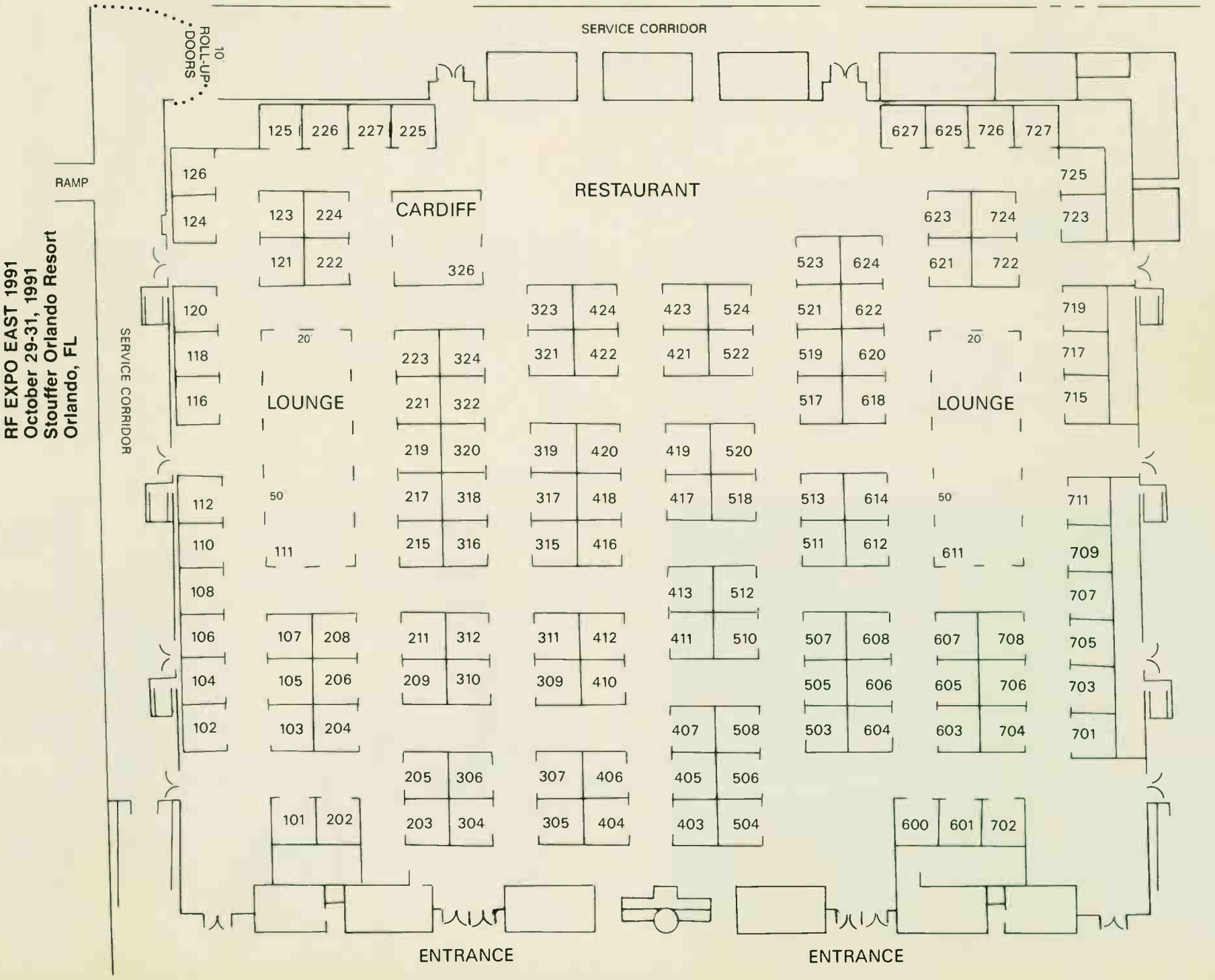

F I R S T F L O O R

Stouffer Orlando Resort

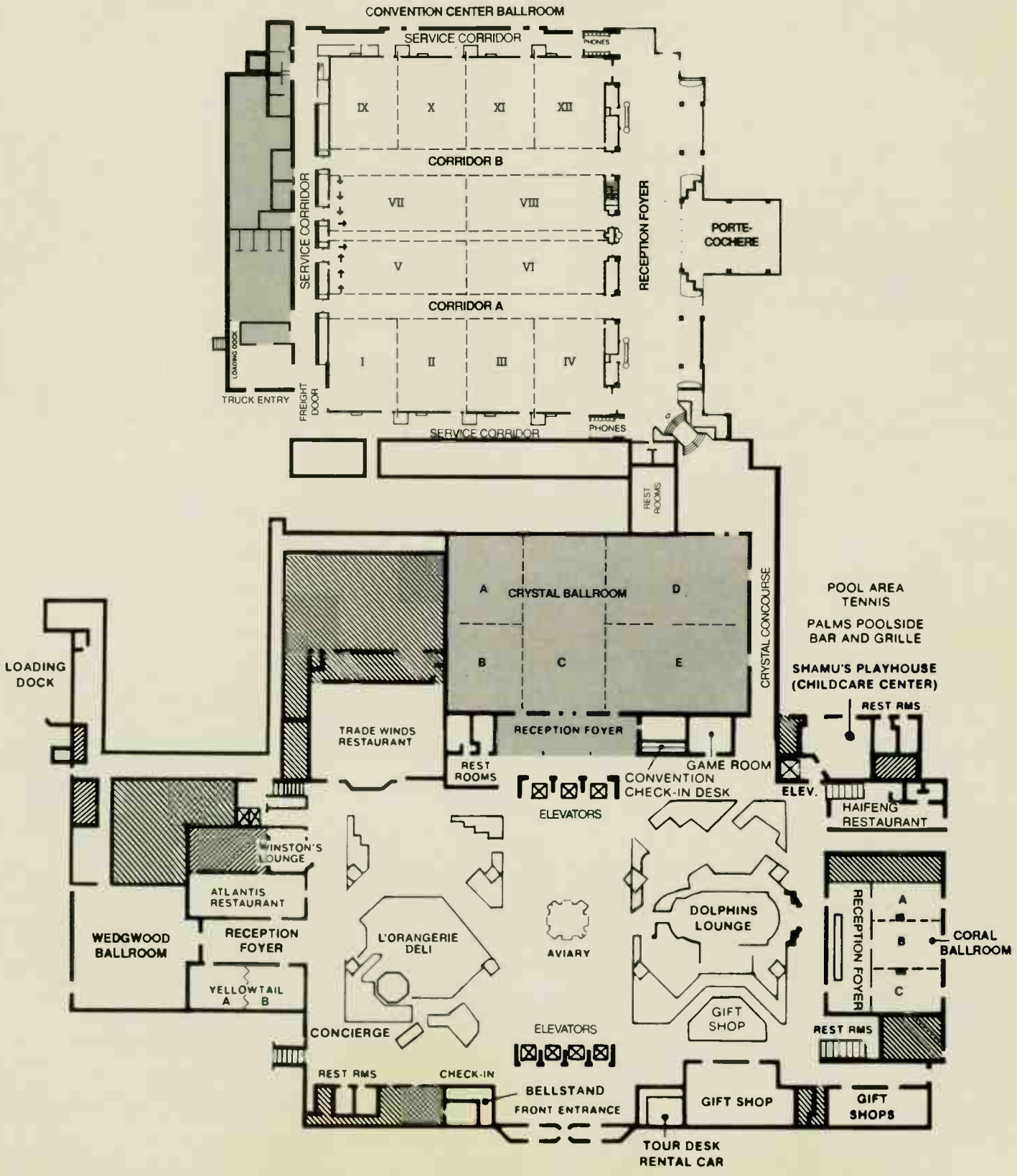

NEW PRODUCTS

Ceramic Water-Cooled 20 kV Capacitor
Sprague-Goodman Electronics, Inc.
Booth 607
Sprague-Goodman Electronics, Inc. has announced the addition of a new model, No. 40601, to the HWS Series of Radiocer™ power capacitors. These devices combine a 10,000 pF capacity and a 20 kV rating, and are designed for use in high frequency induction heating generators operating in the frequency range of 200 to 500 kHz. Other specifications include a nominal reactive power of 4000 kVAr, a nominal RMS current rating of 350 A, and an operating temperature range of 0 to 100 degrees C. The dimensions of the capacitor are 13.7 cm maximum diameter and 28.6 cm high. The tubular design offers the advantage of internal cooling. The HWS Series capacitors are coated with an elastomer for applications which may subject them to harsh environments. Prices start at under $1,600 (up to 4 pieces).

Power JFET
Microwave Technology
Booth 706
A silicon power JFET series capable of providing 10 dB gain with power outputs from 15 to 120 Watts has been introduced by Microwave Technology. These new devices offer excellent linearity and efficiency for mobile communications base stations.

4.5 GHz Prescaler
John Fluke Mfg. Co., Inc.
Booth 404, 406
Fluke will introduce a 4.5 GHz prescaler for the PM 6680 timer/counter. With this option, the PM 6680 provides complete timer/counter functionability plus microwave counting. The PM 6680 has 19 measuring modes, 500 ps resolution, 2,000 readings per second, built-in math and statistics, and advanced arming capabilities.

CMOS Oscillator
CTS Corp./Frequency Control Division
Booth 315
The CXO-HG Series of tri-state CMOS oscillators has been extended up to 70.0 MHz and offers CMOS or TTL output drive capability. The tri-state output is perfect for automated testing or frequency switching applications. Choose the CXO63HG for a 14 DIP package or the CXO23HG for a 8 pin DIP package.

GaAs FET
California Eastern Laboratories
Booth 416
New silicon bipolar and GaAs hetero junction FETs have been introduced by NEC. The NE46134 Si bipolar has a 1.5 dB noise figure, and 1/2 watt power output, while the NE32400 and NE24200 are GaAs FETs for C to Ka-band applications with 0.6 noise figure at 12 GHz.

I and Q Modulator
Synergy Microwave Corporation
Booth 411
Synergy Microwave Corporation has announced an off-the-shelf 34:1 bandwidth, I & Q modulator (SSB modulator), quad IF mixer and QPSK modulator. Typical conversion loss is 9 dB, amplitude balance is ±0.5 dB, phase balance is ±10 degrees and VSWR is 1.5:1.

Microwave Power Transistor
Motorola Inc.
Booth 203, 205, 304, 306
Motorola has introduced a high-gain, one watt microwave power transistor for use in large-signal output and driver amplifier stages operating in the frequency range of 1.0 to 4.0 GHz. The MRW54602 power transistor is designed with all-gold metallization for improved reliability.

Precision Trimmer Capacitors
Voltronics Corporation
Booth 211
Voltronics has produced a new line of sealed precision trimmer capacitors with Teflon replacing air as the dielectric. The voltage rating is 1,000 DC working volts and 2,000 DC withstanding volts. The capacitance range is 1 to 9 pF with a high Q.

Parallel Plate Capacitors
Compex Corporation
Booth 320
Compex parallel plate capacitors are designed with bare ceramic borders on the top side for use in applications where conductive epoxy shorting is a problem. They are also useful where image recognition equipment requires a distinction between the capacitor and any gold surface that it is mounted on.

FM IF System
Signetics Company
Booth 106, 108
Signetics has introduced the NE/SA 606/607 FM receiver devices designed to dramatically shrink the size and power consumption of portable communication systems such as cellular and cordless phones, wireless LANs and other communication systems.

Peak Power Meter
Boonton Electronics Corporation
Booth 319
The Boonton 4400 peak power meter covers a frequency range of 30 MHz to 40 GHz and its dynamic range extends from -40 to +20 dBm. Measurements are made at a rate of 40 to 70 measurements per second, and waveforms are digitized at a 1 MHz rate.

Substrate Test Fixture
Inter-Continental Microwave
Booth 625, 627
Inter-Continental Microwave has introduced a universal substrate test fixture for testing hybrid substrates separately or on carriers, DC to 50 GHz. It features moveable RF launches and DC probes, and ground contact is always maintained under the launch.

Switching Matrices
Lorch Electronics
Booth 705, 707
A 19 inch rack mount IEEE-488 controllable RF switching matrices have been announced by Lorch Electronics. The units have up to 30 inputs by 30 outputs and an internal regulated power supply. Typical specifications are a 10 dB gain, 4 dB noise figure, 1.2:1 VSWR, and greater than 70 dB of isolation.

Serenade PC and Microwave Harmonica PC
Compact Software, Inc.
Booth 510, 512
Compact Software, Inc. has introduced a new schematic editor for Super Compact, Microwave Harmonica and Success Simulators. Also shown is the new version of their linear/nonlinear simulator operating under DOS, Windows 3.0 or OS/2.

Spectrum Analyzers
Anritsu America Inc.
Booth 322, 324
The MS2601B/K series of advanced spectrum analyzers has the following features: accurate measurement of frequencies and levels; high speed measurement using the zone marker and zone sweep; EMI measurement functions; new analysis display functions and PTA.

New Products
Tele-Tech Corp.
Booth 625, 627
Tele-Tech Corp. will be showing a host of new products including I-Q assemblies, frequency discriminators, power dividers and quadrature hybrids.

Phase Locked Oscillators
Tampa Microwave Lab, Inc.
Booth 709
TML is offering phase locked oscillators from .4 GHz to 14 GHz utilizing surface mount construction techniques to reduce production costs. Proprietary sampling techniques offer wide temperature and frequency ranges.

Power Amplifiers
Power Systems Technology, Inc.
Booth 705, 707
Power Systems Technology, Inc. has announced the development of solid state high power amplifier Model BHE4819-1000. The amplifier delivers 1000 watts CW output power in the frequency range of 400 to 1000 MHz, with an instantaneous bandwidth of 600 MHz.

Bonding PTFE Circuits to Heat Sinks
Poly Circuits
Booth 219
Poly Circuits has developed a new technology for bonding PTFE circuits to heat sinks and various ground planes called FLEXLINK™ using an elastic electrically conductive bonding adhesive. This patented process is less costly and more reliable than prebonded or 'sweating' process.

Conduction Cooled Resistors
Florida RF Labs, Inc.
Booth 722, 724
Florida RF Labs is offering a broad selection of high power conduction cooled resistors and terminations with power handling capabilities to 800 watts and a frequency range to 6.0 GHz.

Network Analyzers
Hewlett-Packard Company
Booth 309, 311, 410, 412
The HP8751A vector network analyzer combines high speed and accuracy with advanced features to meet demanding requirements from 5 Hz to 500 MHz. The HP 8711A is fully integrated 300 kHz to 1300 MHz component test system. Key features include a fast, synthesized source with 50 ms sweeps and 1 Hz resolution, 90 dB dynamic range, built-in disk drive and instrument BASIC.

Multi-Pin Connector
Balo Hermetics Company
Booth 623
A new hermetic multi-pin connector that can be laser welded to any aluminum package/module has been announced by Balo Hermetics Company. The connector assembly features a flange that is weld compatible. It complies with MIL-C-83513 connector specifications and is available with 9, 15, 21 and 31 pins.

RF Circuit Simulation
EEsof, Inc.
Booth 715, 717
jOMEGA features a wide range of RF models for passive and active elements and includes a full set of microwave transmission line models. Other features include interactive tuning, and performance and yield optimization.

Inductors and Transformers
Vanguard Electronics Company, Inc.
Booth 523
Vanguard Electronics is offering surface mount leadless power inductors and transformers to meet MIL-T-27/356 military specifications. Features include a compact low profile, surface mountable package having tin plated phosphor bronze terminations, and a frequency range of 100 kHz to 300 MHz.

Crystal Oscillator
AT&T Microelectronics
Booth 202
The phase-locked crystal oscillator (PLXO) is a 16-pin, ceramic packaged device that provides frequency translation between telephone standard reference clocks associated with the DS-1, DS-1C, and CEPT-1 transmission rates.

Amplifiers, Mixers, Converters
Locus, Inc.
Booth 705, 707
Locus, Inc. will be showing many new products with an operating frequency of base band through 18 GHz. These

products include image reject mixers, quadrature hybrids, low noise amplifiers, solid state power amplifiers and redundant amplifier systems.

Cellular Direct I/Q Modulators
M/A-COM, Inc.
Booth 403, 405, 407
Anzac has announced the new EQKR8 Series I and Q modulators that offer direct modulation/demodulation at carrier frequencies of up to 1 GHz. These units, available in standard 8 pin relay headers, provide quadrature input and cover 25 MHz bandwidths.

Low Frequency Amplifier
ENI
Booth 507
ENI's Model 1140LA RF power amplifier produces up to 1100 watts of linear Class B output over the frequency range of 9 kHz to 250 kHz. Up to 1600 watts is available from 11 to 75 kHz; extended range performance is possible with somewhat reduced output power and linearity.

Four Channel Preselector Switch
Sierra Microwave Technology
Booth 225
Sierra Microwave Technology has introduced a four channel preselector capable of selecting lumped element filters with bandwidths from 10 percent to 100 percent in the 0.5 to 6 GHz frequency range. Passband insertion loss is typically less than 5 dB at a maximum VSWR of 1.5:1. Rejection is greater than 60 dB at all frequencies from DC to 12 GHz.

Spectrum Analyzer
Advantest
Booth 110, 112
The R3265 microwave spectrum analyzer covers the range 100 Hz to 8 GHz. It has user defined menus, 50 microsecond sweep, noise levels in high sensitivity mode as low as -140 dBm and a variety of user oriented features.

Cable Bending Tool
Applied Specialties Inc.
Booth 711
Applied Specialties Inc. has introduced a new cable bending fixture for construction of semi-rigid coaxial assemblies.

Linear Amplifier
Trontech
Booth 614
Part number PF880-39 is a 8 watt, Class A, linear amplifier covering the 869 to 896 MHz range. This amplifier features 40 dB of gain over 27 MHz of band width, power output at the 1 dB compression point is 39 dBm.

Low Noise OXCOs
Vectron Laboratories, Inc.
Booth 206
Series CO-724SI2 OCXO provides a low noise +7 dBm output at any frequency in the 25 through 140 MHz range in a 2 x 2 x 1 inch package. Temperature stability is $\pm 5 \times 10^{-9}$ over 0 C to +50 C and $\pm 5 \times 10^{-8}$ over -55 C to +85 C. Aging is 2×10^{-9} per day, 5×10^{-7} per year. Phase noise at 100 Hz is -130 dBc/Hz and at 50 kHz is -157 dBc/Hz.

Oven Controlled Crystal Oscillator
Piezo Technology, Inc.
Booth 105
Piezo Technology, Inc. has developed a new miniature oven controlled crystal oscillator. PTI Model XO5002C offers a standard +/-.02 ppm stability over the temperature range of -30 to +70 C. The standard frequency is 10.0 MHz with optional frequencies available between 9.0 and 16.0 MHz.

Integrated Switching Subassemblies
JFW Industries, Inc.
Booth 107
JFW Industries' current attention has been focused upon the design, development and manufacturing of integrated switching subassemblies. Each unit is available with operating software. P.C.,RS-232 or IEEE-488 are control options, and DC or AC powered versions are available.

Surface Mount Mixer
EDSI/RF Prime
Booth 708
EDSI/RF Prime has introduced a small 3 GHz surface mount mixer with a conversion loss of 9 dB at a low input of 7 dBm.

RF Modem
Proxim, Inc.
Booth 126
RF Modem is a 'plug-and-play' unit that provides wireless data communication between microprocessor-based devices. The RF Modem, which does not require any FCC site license, is fully compatible with most hardware communication interfaces, providing high speed, multi-node, or point-to-point local network of distances up to 500 feet.

Tunable Bandpass Filter
Integrated Microwave Corporation
Booth 620
Integrated Microwave Corporation has introduced a 5-Band, micrometer tunable bandpass filter. Features include a tuning range of ±8 percent, a 1.5 dB bandwidth of 8 MHz min., 20 dB bandwidth of 60 MHz max., 50 dB bandwidth of 200 MHz max., and VSWR of 1.5:1.

Low Noise, Power Amplifiers
Amplidyne, Inc.
Booth 719
Amplidyne, Inc. has introduced cellular low noise and power amplifiers for radio links in the 1.7, 2.3 GHz frequency range. The solid state LNA's and power amplifiers are used for PCN and GSM applications.

Low Pass Filters
Sawtek Incorporated
Booth 215, 217
Sawtek has developed a series of low-loss filter for use in both cellular site and subscriber GSM/PCN applications. Features include small size, single level fabrication, quartz temperature stability, standard fixed value component matching and low cost. The center frequency can be placed anywhere from 20 MHz to 400 MHz.

Standard Waveguide Horns
Antenna Research Associates, Inc.
Booth 708
A complete range of standard waveguide horns, double ridge multi-lloctave band horns and dual polarized horns has been announced by Antenna Research Associates, Inc.

High Power, Low Pass Filters
TTE, Incorporated
Booth 504, 506
TTE has introduced miniature 9 pole Chebyshev low pass filters covering the range of 250 kHz to 100 MHz. Features include power levels up to 250 watts CW and a small size of 2 x 4 x .25 inches high.

Synthesized Pulse/Function Generator
Wavetek San Diego, Inc.
Booth 116, 118
Wavetek has announced a new 20 MHz synthesized pulse/function generator. Its pulse capability generates pulses to 50 MHz and square waves to 100 MHz. The Model 91 provides a source of sine, triangle and square waveforms with 15 volts peak-to-peak output into 50 ohms.

Ultra Low Noise Transistors
Avantek
Booth 606
The ATF-35 family of ultra-low-noise GaAs pseudomorphic high-electron-mobility transistors offer noise figures as low as 0.75 dB at 12 GHz with 11 dB associated gain. These transistors are provided in a new commercial-grade 0.070 inch metal/ceramic microstrip surface-mount package.

Solid State Amplifier
Amplifier Research
Booth 305, 307
The new Model 300A100 all solid state broadband amplifier delivers 300 watts minimum linear (less than 1 dB compression) over its 10 kHz to 100 MHz bandwidth. Typical applications are RF susceptibility testing, antenna and component testing, and wattmeter calibration.

Test Cable Assemblies
Applied Engineering Products
Booth 521
Rugged, multi-use, phase stable cable assemblies offered by Applied Engineering Products are manufactured in standard three foot lengths. AEP cable assemblies utilize high quality, heavy duty low loss cable and are fabricated with captive contact, passivated SMA plugs per MIL-C-39012.

High Bandwidth CATV Modules
Philips Semiconductors
Booth 102, 104
New CATV modules from Philips Semiconductors have sufficient bandwidth to carry 110 TV channels. BGY600 series amplifier modules and BGD600 series power doubler modules have a bandwidth of 40 to 600 MHz, while BGY700 and BGD700 series devices

offer bandwidth extension to 750 MHz.

Simulation and Analysis Software
Eagleware
Booth 209
LINMIC+ is a suite of modules integrating simulation, optimization, global noise analysis, parameter extraction and layout generation. Developed by Jansen Microwave and distributed and supported by Eagleware.

Interference Tracker
Trilithic, Inc.
Booth 208
The PLI-150 is an instrument designed to find AC power distribution sources of radiated RF interference. The system includes a hand-held receiver, antennas, mounts, and carrying case.

PC-Mount Attenuator
Alan Industries, Inc.
Booth 417
Alan Industries' 50CAL( ) PCB is a continuously variable attenuator available in 10, 15 and 25 dB ranges for operation up to 400 MHz. Average power handling is 0.5 watt.

SAW-Stabilized Receiver
RF Monolithics
Booth 310, 312
RF Monolithics will demonstrate an advanced version of their SAW-stabilized superregenerative receiver, the RB1018. This 418 MHz receiver features -105 dBm sensitivity, 500 kHz bandwidth, and low reradiation to allow certification to FCC, DOT and DTI requirements.

1-Watt Amplifier
LCF Enterprises
Booth 519
A high-gain medium power amplifier with greater than 1 watt output over 100-400 MHz with 32 dB gain is introduced. Packaged in 1.0 x 2.0 x 0.75 inch case, the unit draws less than 0.5 amp from a 12 VDC supply.

15 kW MRI Amplifier
Erbtec Engineering
Booth 222
NMR-4, a 15 kW solid-state RF amplifier for NMR and MRI is announced by Erbtec Engineering. Self-protection circuitry is included to monitor operation. Current models cover 40-80 MHz and 155-180 MHz.

BNC Connectors
Amphenol Corporation
Booth 601
Amphenol introduces a new right angle bulkhead BNC receptacle isolated from ground. This model is designed for printed circuit board applications.

Ultra-Broadband Isolators
Teledyne Microwave
Booth 625, 627
Teledyne Microwave has introduced a new, ultra-broadband isolator that covers the 2-18 GHz frequency range. The unit exhibits 11 dB minimum isolation, 2.5 dB (max) insertion loss and 2.00:1 maximum VSWR.

Portable Microwave Spectrum Analyzer
IFR Systems, Inc.
Booth 604
The AN930 portable microwave spectrum analyzer features: 9 kHz to 22 GHz frequency range, 3 Hz to 25 MHz resolution bandwidth, high speed triggered sweep, 1 Hz resolution frequency counter, RS-232 and IEEE-488 interfaces, and AC or DC operation.

Saw Filters
Thomson-ICS Corporation
Booth 621
A low loss SAW filter, Thomson model FBN069, designed for GSM applications. Insertion loss)10 dB, very small package, 14 pin DIP. Nominal center frequency 71 MHz, minimum 3 dB BW, 130 kHz.

Hybrid Amplifiers
Q-bit Corporation
Booth 103
The QBH-816 thin-film TO-3 hybrid amplifier operates in the frequency range of 10 to 2000 MHz. The amplifier has 10.2 dB of gain with a gain flatness of less than 1 dB pp. A high output compression point of 21 dBm is achieved while maintaining noise figure of less than 8.0 dB over the entire frequency range.

Capacitors
American Technical Ceramics
Booth 608
The ATC 180 series capacitors designed for mobile telephone applications at 1.8 GHz and ATC Quick Design™ kits containing RF/microwave surface mount MLCs for circuit design.

RF expo WEST

March 18-20, 1992
San Diego Convention Center
San Diego, California

Here are a few of the reasons you should make plans to attend RF Expo West:

SESSION TOPICS AND PAPERS (As of October 15, 1991)

Session: RF Power Circuits	• Predict Temperature Rise in Reverse Biased PIN Diodes at High Power Levels • The Engineering Development of Low Cost GaAs Power Module for Cellular Telephones
Session: RF and Computers	• Building a Network System for an Engineering/Manufacturing Company: Keeping Your Engineers Happy Without Giving Away the Farm • Modeling Surface Mount Components • Power MOSFET Modeling
Session: High Performance Circuits	• The Design of a Monolithic Hybrid Integrated Circuit RF Package for Space Application • The Photistor: An Innovative, Optoelectronic RF Switch/Attenuator
Session: RF Integrated Circuits	• Design of High Density, High Yield MMIC Devices for Low Cost Applications • Characterization of a Silicon Bipolar Process for RF ASIC Development • GaAs MMIC Control Devices: Theory of Operation & Fabrication
Session: Antennas	• Shaped Beam Microstrip Antennas Applied to Personal Communication Networks • Development of Microstrip Antennas • Miniature Narrowband Radiator for UHF Application
Session: Thermionic Power Devices	• High Power RF Amplifiers, TWTs, Klystrons, Magnetrons
Session: Frequency Synthesis	• Dividerless Phase Locked Loops • Design Considerations for a Low Cost Wideband RF Synthesized Source • A Monolithic 12-Bit 100MSPS Digital to Analog Converter for Frequency Synthesis
Session: Low Cost Design	• Receiver Mixers and LOs • Los Cost SMD Power Limiters • Practical Variable Gain Amplifiers
Session: Space-Based Radar	• Space-Based Angle-Tracking Radar System Design • RF Electronics Design for Space Flight Applications • Spurious Noise Prediction and Reduction in Direct Digital Synthesizers • Electrical Performance of a GaAs DDS System for Space Applications • Signal Processing for a Space-Based Monopulse Radar • Thermal Distortion Analysis for Space-Based Monopulse Radar Antenna Array
Session: Special Open Session	• Three Contest Prize Winners — Software and Design
Session: Communications Systems	• A Satellite Based Radio Tag System • Own Jamming Excision — Changing the Way Communication Systems Are Jammed • One Technique for Increasing Compression Ratio for Facsimile Picture Transmission Over Mobile Radio
Session: Transmission Systems	• Analysis of Dielectric Materials in Waveguide and Feedhorn • High Power Filter for Broadcasting
Session: Receiver Circuits	• Various Mixer Types Used in Cellular Radios • Direct IF to Digital Conversion Using New Monolithic RF Track and Holds
Session: RF Filters	• Tunable Bandpass Filters for VHF-UHF Receivers as a Preselector Applications • GaAs Technology Opens New Frontiers in Electronically Tunable Filters
Session: Power Amplifier Design	• The Design of RF Modules Intended for Combining High Power • High Power VHF Power Dividing and Combining Techniques • Monitoring, Control and Diagnostics of an RF Amplifier Over a Modem Link

Early registration discount now available.
For complete details: (800) 525-9154; (303) 220-0600; Fax (303) 770-0253.
RF Expo West 1992; 6300 S. Syracuse Way, Suite 650; Englewood, CO 80111.

The industry's foremost RF technology conference.

Sponsored by *RF Design* magazine, RF Expo West will be in San Diego March 18-20 at the San Diego Convention Center. And special rates are being offered for early registration.

SEE demonstrations of the newest equipment the industry has to offer.

HEAR top industry professionals share their knowledge on today's most important topics.

JOIN electronics engineers, engineering managers, engineering service professionals, owners and consultants at the Ham Radio Reception.

PROFIT by choosing from among more than 50 technical sessions.

MEET more than 200 industry exhibitors with the latest and best in electronic design services and equipment.

LEARN new skills or reinforce present knowledge by signing up for one or more of the four full-day special courses. (Fundamentals of RF Circuit Design: Parts I and II; Filter and Matching Network Design: L-C and Distributed Circuits—HF to Microwaves; Oscillator Design Principles.)

DISCOVER new sources for answering questions about your particular needs.

WIN one of several big prizes being awarded by sponsors of the Ham Radio Reception.

COME to RF Expo West '92 sponsored by *RF Design* magazine.

The best minds in RF Design are yours for three days, March 18-20, at the San Diego Convention Center. Register now by calling (800) 525-9154.

STAFF

Kathy Kriner
Vice President

Kathi Walsh
Publisher

Gary Breed
Editor

Kristin Hohn
Convention
Manager

Liane Pomfret
Associate Editor

Bill Pettit
Associate
Sales Manager

Cindy Wieland
Account
Executive

Maryanne Averill
Account
Executive

Barb Binge
Exhibit
Coordinator

LeAnn Nowacki
Trade Show
Account Executive

Dawn Keith
Registration
Coordinator

Kirsten Gisle
Exhibit
Coordinator

Dick Purcell
Marketing Manager

Staying power.

Reliable solid-state power. When we designed our new 300-watt Model 300A100 rf amplifier, we knew it would answer the needs of many kinds of people.

People seeking a stable, economical way to drive an antenna to deliver at least 50 volts per meter for susceptibility testing. People who *must* trust an amplifier's ability to keep operating into a severe load mismatch—even shorted or open output terminals—without damage, oscillation, or foldback. People who expect the full bandwidth—10 kHz to 100 MHz—to be there instantly for sweep testing, with no need for tuning or bandswitching. People who have to monitor both forward and reflected power. People who want automatic leveling. People who regularly perform both pulsed and cw procedures. People who demand remote-control interfacing.

The 300A100 is the latest all-solid-state member of a family of AR amplifiers covering a power range from one watt up to 10 kilowatts, and the rf range from 10 kHz up to 1 GHz. Their staying power is rated very conservatively—output stated as minimum, not nominal or peak. Chat with one of our applications engineers, who'll

pick up the phone himself when you call, toll-free,

1-800-933-8181

AMPLIFIER RESEARCH

160 School House Road
Souderton, PA 18964-9990 USA
215-723-8181 • Fax 215-723-5688

For engineering assistance and service throughout Europe, call
EMV GmbH • Munich • 89-612-8054
EMV Ltd. • London • 908-566-556
EMV S.A.R.L. • Paris • 1-64-61-63-29

1677

Please see us at RF Expo East, Booths #305, 307.

RF/Microwave Surface Mount MLCs Within Arm's Reach

$499.95
each kit

Order Before January 1, 1992 and receive a BONUS refill offer

New ATC RF/Microwave Capacitor Kits

American Technical Ceramics new **Quik Design Kits**™ provide everything you need for circuit design within arm's reach. Each Kit contains a wide range of consecutive values stocked in **100**-piece quantites in convenient matrix packs (Cap-Pacs®), along with a **Tuning Stick**® for each value.

The **QK3000 Kit** is stocked with over **5000** A-Case Capacitors with capacitance values ranging from 0.2 pF to .01 MFd, and tolerances B, C, J, K and M. The **QK4000 Kit** contains over **4000** B-Case Capacitors with values of 0.3 pF to .039 MFd and B,C, K and M tolerances. All capacitors are laser marked with value and tolerance.

All kit values are available in solder plate (nickel barrier) on tape and reel for high volume, automated pick and place applications. Solder dipped nickel barrier capacitors are available in matrix packaging or tape and reel on special order.

For Complete Information and Catalog
Call our **APPLICATIONS HOTLINE**
(516) 547-5708
Available in stock through ATC's **QUIK-PICK 48 HOUR SYSTEM**™

american technical ceramics CORP.
one norden lane, huntington station, n.y. 11746-2102 usa
phone 516-547-5700 • telex 825707 • fax 516-547-5748

Please see us at RF Expo East, Booth #608.